NASA CONTRACTOR REPORT

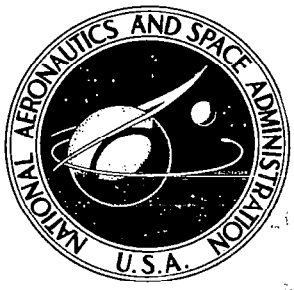

NASA CR-761

LIFT FAN TECHNOLOGY STUDIES

by Zygmunt J. Przedpelski

Prepared by
GENERAL ELECTRIC COMPANY
Cincinnati, Ohio
for Ames Research Center

NATIONAL AERONAUTICS AND SPACE ADMINISTRATION • WASHINGTON, D. C. • APRIL 1967

NASA CR-761

LIFT FAN TECHNOLOGY STUDIES

By Zygmunt J. Przedpelski

Prepared under Contract No. NAS 2-3077 by
GENERAL ELECTRIC COMPANY
Cincinnati, Ohio

for Ames Research Center

NATIONAL AERONAUTICS AND SPACE ADMINISTRATION

For sale by the Clearinghouse for Federal Scientific and Technical Information
Springfield, Virginia 22151 – CFSTI price $3.00

LIFT FAN TECHNOLOGY STUDIES

By Zygmunt J. Przedpelski
General Electric Company

SUMMARY

The existing lift fan hardware is a proven V/STOL propulsion system. The challenging aerodynamic, mechanical, and system problems created by the non-uniform fan inflow conditions have been successfully solved.

High pressure ratio lift fans, powered by the high specific energy gas generators currently under development, show a three-fold increase in lift to weight ratios over the existing lift fans. The lift to volume and lift to installed area improvements are of the same magnitude.

Extensive thermodynamic, aerodynamic, mechanical and systems studies defined the interrelationships among the various engine and fan design parameters. With this knowledge, an optimum fan design can be identified for any given requirement. Fan installation thickness reduction was stressed throughout the study; new mechanical and aerodynamic designs evolved to satisfy the requirements of supersonic fan-in-wing installations. An inlet guide vane (IGV) and rotor fan stage shows promise where minimum thickness is desired, at some penalty in system efficiency. Test programs to identify means of improving fan inflow conditions during cross flow were conducted. Inlet performance, as a function of inlet lip geometry and cross flow velocity, was obtained for a range of variables applicable to high pressure ratio lift fans operating in highly loaded wings. An extensive analysis of fan rotor performance in a shallow inlet installation was performed. Good correlation with existing lift fan data was obtained, and prediction of high pressure ratio fan performance was made.

Five lift fans of 1.18 to 1.28 pressure ratio were preliminarily designed based on the results of this study and the extensive lift fan design experience. Three of these fans (13,650 pounds lift each) were designed for minimum thickness, compatible with a supersonic fan-in-wing fighter aircraft installation. The other two fans (26,000 pounds lift each) were designed for a V/STOL transport, with primary emphasis on low weight. Lift to weight ratios of over 20 to 1 were achieved with four of the five designs. Data is provided for scaling each fan, plus-or-minus 30 percent of its nominal lift.

All of the thermodynamic, aerodynamic, and system studies results are reported in their entirety in this part of the research report. The summaries of the mechanical studies and of the preliminary designs are also included in this part, while the details are reported in Part II of the research report.

CONTENTS

ILLUSTRATIONS

TABLES

INTRODUCTION

The potential of fan-in-wing propulsion systems for V/STOL applications has been demonstrated by the XV-5A fan-in-wing research aircraft. However, it was recognized that the level of technology in the X353-5 fans was inadequate for an efficient aircraft system. The extensive testing and studies conducted in support of the XV-5A aircraft program and the flight test itself identified several areas of lift fan design improvement. System and mission studies and hardware designs conducted in support of future fan-in-wing V/STOL aircraft provided additional insight into the effects of various fan design parameters on fan and overall aircraft performance.

This contract consisted of advanced lift fan technology studies and procurement of full scale fan inlet and exit hardware, which was identified in previous scale model tests as beneficial to cross flow fan performance. The objectives of the study program were to define mechanical, thermodynamic and aerodynamic designs of lift fans compatible with 1968-1972 technology core engines. Emphasis was placed on:

1. Reduction of installed fan dimensions to the point of virtually eliminating the wing size penalty previously associated with fan-in-wing designs.

2. Achievement of a lift-to-weight ratio of at least 20:1.

3. Compatibility of fan hardware with drive gas temperatures of 1400°F to 1600°F.

4. Improvements in cross flow performance.

To achieve these objectives, refinements of the existing rotor-stator design were made and new design concepts including the IGV-rotor and rotor only (statorless) were investigated. The study was conducted in four phases:

I Identify new fan design concepts and parametrically define fan dimensional, weight and performance trends as influenced by fan pressure ratio, engine cycle selection and fan design concept.

II Provide test verification of some of the design approaches identified in Phase I.

III Using results of Phases I and II, define two fan designs for a transport-type aircraft and three fan designs for a fighter-type aircraft.

IV Define a fan design to be used in static and cross flow tests to further substantiate and verify the results of this study.

Phase I - Parametric Studies

The flow chart of parametric studies is shown in Chart 1. In order to provide the most useful output, the individual studies were guided by the preliminary results of the system studies and by the extensive background accumulated in preceeding studies, designs and tests relating to lift fans. A continuous exchange between the four major sub-groups was also maintained to insure that the studies complement each other. The results of the parametric studies were used to define the starting points for the conceptual fan designs, and to identify areas to be investigated further by testing.

Phase II - Test Programs and Fan Stall Predictions

Thin fan-in-wing installation axiomatically means short inlets, low radius ratio bellmouth and inlet flow distortion during transition. It is readily apparent that success of a thin fan installation is greatly dependent on the inlet performance. Two test programs were defined to provide data on inlet performance statically (hover) and in cross flow (transition).

The inlet scoop tests defined possible gains in cross flow performance, and the penalties if any, of a scoop inlet closure during static (hover) operation. The results of these tests were also helpful in designing the full scale inlet scoop hardware required by this contract.

The inlet suck down tests provided static and cross flow inlet performance as a function of bellmouth lip radius ratio and IGV presence. The data were obtained at varying cross flow ratios and axial velocities to determine the effects of compressibility. The results of these tests were used in stall prediction studies and fan conceptual designs.

Phase III - Fan Conceptual Designs

Two specific V/STOL aircraft configurations were defined and five different fans were designed to best meet these aircraft requirements. The first aircraft configuration was a high-speed attack-type aircraft with single fan in each wing. The basic configuration was similar to the XV-5A but the greatly reduced fan thickness made a supersonic delta wing design feasible. For this aircraft an IGV-rotor, rotor-stator and statorless fans were preliminarily defined based on results of the parametric studies. Further optimizations were made by varying the major fan design parameters to obtain the smallest, lightest and thinnest designs, all providing the required lift of 13,650 pounds, with a fixed size medium energy core engine.

The second aircraft configuration chosen was a subsonic transport with either multiple fan-in-wing installation, folding fans or podded fans. An IGV-rotor and a rotor-stator fan were preliminarily defined based on the results of parametric studies. Further optimizations were made by varying the major fan design parameters to obtain the smallest and lightest fans to provide the required lift of 26,000 pounds with a fixed size high energy core engine.

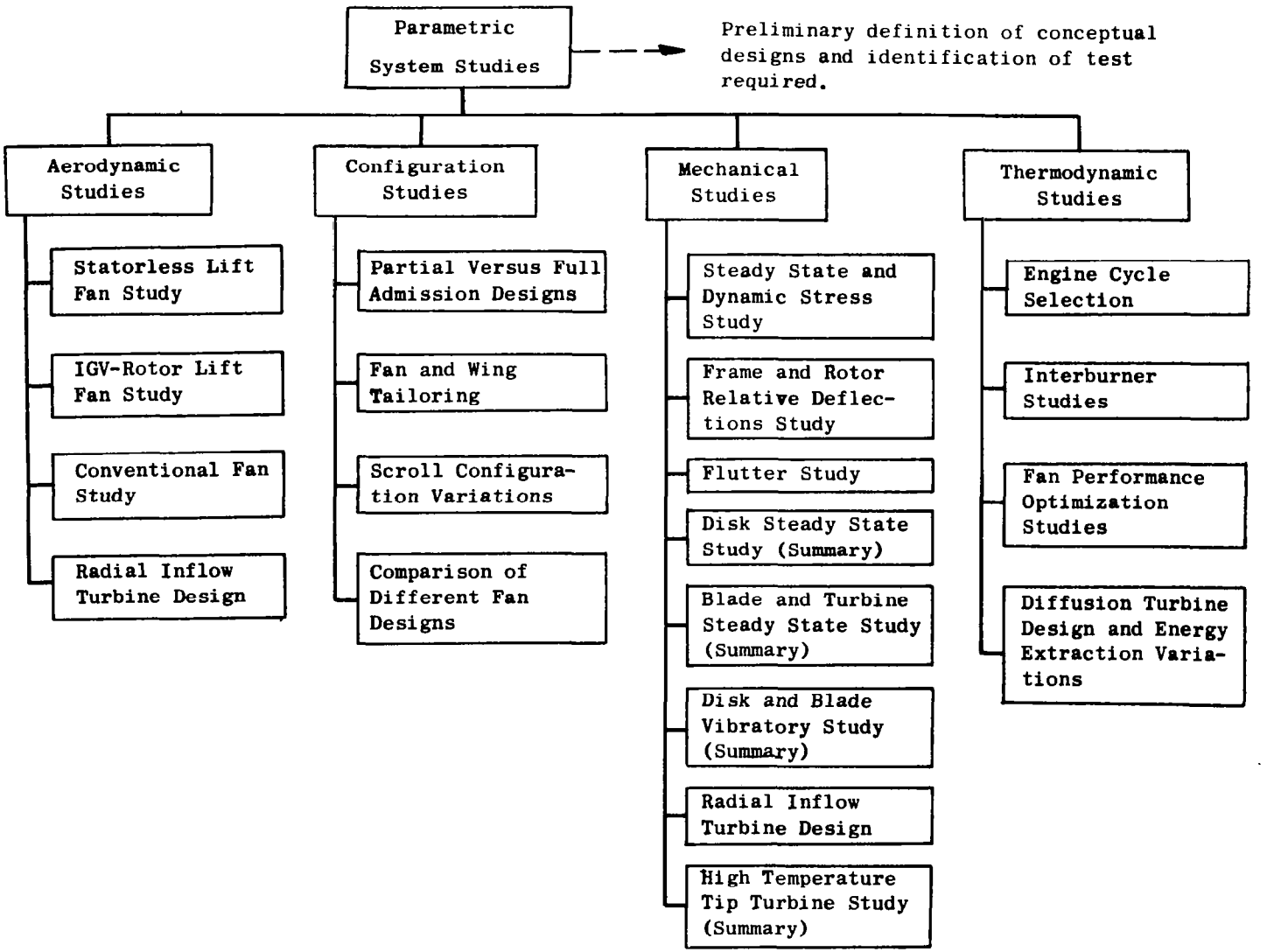
Parametric System Studies
Preliminary definition of conceptual designs and identification of test required.
Aerodynamic Studies
Statorless Lift Fan Study
IGV-Rotor Lift Fan Study
Conventional Fan Study
Radial Inflow Turbine Design
Configuration Studies
Partial Versus Full Admission Designs
Fan and Wing Tailoring
Scroll Configuration Variations
Comparison of Different Fan Designs
Mechanical Studies
Steady State and Dynamic Stress Study
Frame and Rotor Relative Deflections Study
Flutter Study
Disk Steady State Study (Summary)
Blade and Turbine Steady State Study (Summary)
Disk and Blade Vibratory Study (Summary)
Radial Inflow Turbine Design
High Temperature Tip Turbine Study (Summary)
Thermodynamic Studies
Engine Cycle Selection
Interburner Studies
Fan Performance Optimization Studies
Diffusion Turbine Design and Energy Extraction Variations

Chart 1

Because of the great interdependence between fan shape and wing loading and/or thickness, the conceptual fan designs are tailored to utilize the available area and volume most efficiently.

Phase IV - Test Fan Definition

A small tip turbine fan of approximately 36 inch fan tip diameter and 1.3 pressure ratio was defined for future research testing. The fan could be powered by a variety of existing gas generators and by gas generators which will be available in 1970.

This study identified several areas of fan design improvements. Some of these improvements will be realized through material and manufacturing advancements which are coming with the new generation of core engines. However, the largest portion of lift fan improvements will come about from the solution of problems which are unique to lift fans. The area needing immediate attention in the form of further theoretical studies, component designs, and testing is: aerodynamic and mechanical performance of highly loaded, high aspect ratio stage in nonuniform inflow and back pressure conditions typical of submerged lift fan installations.

SYMBOLS

A	area - $inches^2$ or $feet^2$
AR	aspect ratio - non-dimensional
C	velocity - feet/second
c	chord - inches or feet
D	diameter - inches and drag - pounds
EGT	exhaust gas temperature - °F or °R
F	thrust - pounds
f	frequency - cycles/second
g	gravity field - non-dimensional
h	height - inches or feet
HP	horsepower
I	area moment of inertia - $(inches)^4$
i	incidence angle - degrees
K	spring constant - pounds/inch
L	lift - pounds
l	length - inches
M	moment - inch-pounds and Mach number - non-dimensional
N	speed - percent
n	exponent
P	total pressure - psia
p	static pressure - psia
P/P	fan pressure ratio - between stage exit and stage inlet P_{11}/P_{10} - does not include inlet or exit losses
R	radius - inches
r	radius - inches

T	total temperature - °R or °F, torque - inch-pounds or foot-pounds
t	static temperature - °R or °F
Tm/C	airfoil thickness to chord ratio
U	wheel rotational velocity - feet/second
W	weight flow - pounds/second
WT	weight - pounds
V	velocity - feet/second
V_{U1}	tangential component of turbine nozzle spouting velocity
α	angle of attack - degrees
β	relative air angle - degrees
β_V	exit louver angle - degrees - measured from vertical
γ	ratio of specific heats - non-dimensional
Δ	change, difference
δ	pressure correction - $P_{BAR}/29.92$ - deviation angle - degrees
η	efficiency - percent or ratio
θ	angle - degrees and temperature correction - $T_{AMB}/518.688$
ρ	density - pounds-second^2/feet^4
σ	solidity - chord/spacing - non-dimensional
Ψ	pressure coefficient - $2\Delta P_T/\rho(V_{TIP})^2$ - non-dimensional
Ω	gyroscopic precession rate - radians/second
ω	angular velocity - radians/second
$\bar{\omega}$	loss coefficient - $\Delta P/P$ - non-dimensional

stagger angle (orientation angle) - angle between axis and mean chord line

camber angle - difference between blade angles at leading and trailing edges

static pressure rise coefficient - $\dfrac{\Delta p}{p_2\left[\left(1+\frac{\gamma-1}{2}M_{REL}^2\right)^{\frac{\gamma}{\gamma-1}}-1\right]}$

Subscripts

A	air
a	axial
AMB	ambient
AVG	average
c	critical
d	pertaining to disk
FR	fan root
FT	fan tip
MAX	maximum
MIN	minimum
N	net, nozzle
REF	reference
REL	relative
S	static
T	total
TR	turbine root
TT	turbine tip
U	tangential
X	horizontal
Y	vertical
Z	axial
0	free stream
2	compressor inlet
3	compressor exit

4	turbine inlet
5	turbine exit (before cooling air mixing)
5.1	turbine exit (after cooling air mixing)
5.5	tip turbine rotor inlet
5.8	tip turbine nozzle exit
8	turbojet nozzle exit
9	fan inlet
10	fan rotor inlet
11	fan exit
13	fan nozzle exit

THERMODYNAMIC STUDIES

Engine Cycle Selections

Introduction.- Previous studies indicate that engine cycle selection affects the fan performance, size and weight. Ten specific engine cycles with turbine inlet temperatures of 2160, 2460 and 2760 degrees Rankine and compressor pressure ratios between 7 and 20 are used in this study and are shown in Table I. Turbine inlet temperature and compressor pressure ratio are the primary variables considered in any engine cycle analysis. The secondary variables of compressor and turbine efficiencies, combustor pressure drop, combustor efficiency, and turbine cooling flow are also considered. For this study it is assumed that compressor efficiency varies with compressor pressure ratio; turbine efficiency is set at a constant 90 percent; combustor pressure drop is set as a function of compressor pressure ratio and combustor temperature rise; turbine cooling flow varies with turbine inlet temperature, and combustor efficiency is constant for all cycles. These cycle efficiency assumptions are made based on 1967 to 1970 state of the art technology.

Specific horsepower.- A well known performance parameter for evaluating turbojet engines is specific thrust or thrust per pound of engine airflow. For fan analysis a more meaningful parameter is the gas generator exhaust specific horsepower. Specific horsepower is the total ideal exhaust output horsepower divided by the gas flow. Specific horsepower is calculated by complete isentropic expansion of the core engine exhaust gases to ambient pressure, and it is proportional to the square root of the specific thrust.

Fan thrust for a fixed fan pressure ratio is nearly proportional to specific horsepower. This characteristic will be shown in later paragraphs. Small variations are caused by tip turbine efficiency changes with changes in nozzle spouting velocity.

Within the range of engine turbine inlet temperatures (T_4) and compressor pressure ratios (P_3/P_2) considered, the specific horsepower is almost entirely a function of T_4; changes in compressor pressure ratio result in less than ± 2 percent change in specific horsepower at fixed T_4. The variation in specific horsepower versus T_4 is shown in Figure 1. The increase is almost linear with T_4, the derivative ΔSpecific Horsepower/ΔT_4 is 0.167 hp/lb/sec/°R. While the overall level of specific horsepower is unaffected by compressor pressure ratio, the form of the gas energy changes as indicated in Figure 2. The high compressor pressure ratio results in higher nozzle pressure ratios but lower temperatures.

Effect of engine cycle on ducting size and loss.- In all lift fan installations ducting is an integral part of the lift system. Even in close-coupled arrangements the turbine scroll constitutes a ducting system. The size and losses in ducting vary considerably with engine discharge conditions. Total

pressure losses in ducting vary with duct geometry, length, number of turns, turn radius ratio, and duct Mach number. In the range of Mach number considered practical for ducting (0.2 to 0.5) the loss coefficient ($\Delta P_T/P_T-P_S$) is a function of geometry only, and the total pressure loss, $\Delta P_T/P_T$, is proportional to (Mach number)^2. The energy loss in the ducting is proportional to the total pressure loss and inversely proportional to the total pressure level; in other words a ducting system operating at constant Mach number will have a higher energy loss if operated with a low cycle pressure ratio gas generator.

Figure 3 indicates the duct Mach number, diameter, and cross-sectional area changes required to maintain a constant percentage of energy loss in the ducting. The reference engine cycle has a T_4 of 2460 degrees Rankine and a compressor pressure ratio of 12:1. The available energy loss level is set at 5 percent, which is representative for the XV-5A-type ducting geometry. Combining the results from Figure 3 and the available energy levels from Figure 1, the horsepower density in the ducting for constant level of energy loss can be determined. The results are shown in Figure 4 and indicate that the ducting cross-sectional area varies by a factor of three from the lowest turbine inlet temperature and compressor pressure ratio engine to the highest. The actual horsepower densities can be varied depending on the level of acceptable losses, however the ratios will remain virtually unchanged. The ducting diameter, volume and weight is not included in further lift fan studies and comparisons since it is so much a function of aircraft mission, configuration, etc., however the effect shown in Figure 4 must be qualitatively evaluated in parametric studies to identify possible problem areas, and must be fully evaluated in specific configuration.

Effect of engine cycle on fan characteristics.- Performance and weights of the lift fans described in this section are based on a minimum fan tip speed necessary to achieve the desired pressure ratio. This results in reduced centrifugal stresses in the blades and turbine segments, and also results in high fan efficiencies because friction and Mach number losses are held to a minimum. The schedule of fan tip speed, radius ratio, pressure ratio and fan efficiency assumptions is shown in Table II. Fan performance levels are based on analytical studies verified with full and scale model tests conducted in support of the XV-5A programs. The performance levels, therefore, are applicable to the fan-in-wing fan installations of the rotor-stator design. Other designs as well as refinements of the rotor-stator design are described in other sections of this report.

Fan performance can be expressed in terms of specific horsepower and fan pressure ratio. Within the range of engine cycle variables studied, the turbine inlet temperature (T_4) level determines the specific horsepower level and therefore fan performance can be expressed as a function of fan pressure ratio and T_4.

The term augmentation ratio is used in describing fan performance, and is defined as the fan lift/ideal gas generator thrust based on isentropic expansion of the gases, at core engine turbine discharge station, to ambient pressure.

Nominal fan pressure ratio is defined from ambient to stator discharge. The actual fan pressure ratio is less by the amount of exit louver losses.

The augmentation ratio versus turbine inlet temperature and fan pressure ratio for a full admission fan is shown in Figure 5. The performance for a partial admission fan is generally 1 to 2 percent lower because of partial admission turbine losses. Fan performance can be fully described with fan pressure ratio and T_4; however the overall system, which includes the engine, is affected by the compressor pressure ratio. Figure 6 shows the variation in system specific fuel consumption as a function of fan and compressor pressure ratio. The T_4 level has an almost negligible effect on system specific fuel consumption; small variations are caused by changes in fan turbine efficiency as the nozzle spouting velocity changes. The width of lines on Figure 6 indicates the spread caused by the turbine efficiency changes.

The fan lift-to-weight ratio variation as a function of engine cycle parameters and fan pressure ratio is shown in Figure 7. The drop-off in lift/weight at the high T_4 and low compressor pressure ratio is caused by the increase in gas temperature (see Figure 2). The decrease in turbine bucket and scroll size which occurs at the higher T_4 (higher specific horsepower) partially offsets the increase in stock thickness required with the higher temperatures, resulting in small changes in lift/weight ratios at the higher compressor pressure ratios. The lift/weight ratios shown in Figure 7 are for fans of 13,650 pounds lift. For other lift values, corrections shown in Figure 8 should be applied. The overall effect of augmentation and fan weight is indicated in Figure 9 for a 1.3 pressure ratio lift fan. The reference engine is assigned a thrust/weight of 9, which is representative of 1967 cruise engine technology. All system lifts and weights are made equal by adjusting the engine and fan sizes and the engine thrust/weight. Figure 9 indicates the required engine lift/weight to make all systems equal weight. The main conclusion is that low T_4 (2160°R) engines need considerably higher thrust/weight ratios to be competitive with the reference engine. This is not likely, since higher engine thrust/weight ratios are a result of higher T_4. Increase in T_4 to 2760 degrees Rankine shows some improvements, especially when accompanied with improvement in engine thrust/weight. The higher gas temperatures, however, cause increase in ducting wall thickness, insulation, and may require tip turbine cooling. The temperature at which tip turbine cooling is required is defined in later sections. The system improvements which occur with increases in compressor pressure ratio at constant T_4 are the result of increased horsepower density and decreased T_5 (Figures 2 and 4).

Comparison of system performance after 5 minute hover indicates a similar trend but the influence of compressor pressure ratio is more pronounced because the fuel weight (specific fuel consumption) is included (Figure 10). High P_3/P_2 is desirable as far as system performance is concerned, but there will be a penalty in engine weight and volume since additional compressor stages are required. This penalty will be minimized with use of transonic and supersonic compressor stages. For details of required engine lift/weight calculations, see Appendix A.

The reference engine is near optimum for the existing state of the art of lift fan and engine technology. Further technology advancements in higher temperature materials, tip turbine cooling, dual wall ducts and transonic compressor stages, will result in shifting the optimum engine toward higher T_4 and higher compressor pressure ratios.

Interburner Studies

Interburner can be used to augment the lift during hot day and/or elevated altitude operation, for overload operation, and for control. Figures 11 and 12 show the results of interburning the low and medium energy engine exhaust at two levels of interburner dry loss. The increase in available energy is approximately equal to 20 percent for a 400-degrees Fahrenheit increase in exhaust gas temperature. The fuel flow increase is larger than the increase in available energy. This can be proven in the following manner: Energy available in the nozzle is proportional to total temperature, T. The energy ratio, therefore, is equal to $(\Delta T \text{ Interburner} + T_{5.1})/T_{5.1}$. The fuel flow of the main combustor is proportional to $T_{5.1}-T_0$, while the fuel flow of the interburner is proportional to ΔT Interburner, and the ratio of fuel flows is equal to $(\Delta T \text{ Interburner} + T_{5.1}-T_0)/(T_{5.1}-T_0)$. It can be proven that for all values of T_0 larger than zero degrees Rankine the fuel flow ratio is larger than the energy ratio, resulting in a specific fuel consumption increase as interburning is introduced. In more rigorous calculation the additional pressure losses of the interburner and the variations in specific heat values of the gases have to be considered, as was done in calculating the results shown in Figures 11, 12, and 13.

Comparison of two means of increasing available energy for driving the fan is made in Figure 13. In both cases the starting (nominal) point is the engine cycle Number 6 described in Table I. In one case the increase in energy is obtained by an increase in main combustor fuel flow (T_4); in the other case it is obtained by interburning.

The line representing the main combustor fuel addition in Figure 13 represents different engines. For any given engine, interburning can be used effectively to increase gas energy for control, engine out condition, or during adverse ambient conditions of high altitude and/or high temperature.

Fan Performance Optimization Studies

Fan-turbine efficiency optimization.- The conventional fan designs are based on the minimum fan tip speed required to produce the desired pressure ratio. This results in low tip turbine efficiency for the low pressure ratio fans powered by medium and high energy gas generators. The turbine efficiency is a function of bucket solidity, aspect ratio, clearance (leakage), partial admission losses and the ratio of turbine wheel speed to the tangential component of the nozzle spouting velocity (U/V_{U1}). The wheel speed is fixed by the allowable fan tip speed, and the tangential component of spouting velocity is a function of gas generator exhaust gas energy level, and the level of energy extraction. The turbine rotor efficiency variation versus U/V_{U1} is shown in Figure 14. This efficiency, when modified by nozzle, stator, leakage, and partial admission losses, if any, becomes the overall turbine efficiency. Figure 15 shows the variation of U/V_{U1} with fan pressure ratio for high, medium, and low energy engines when the fans are designed for minimum tip-speed. (Tip speed versus fan pressure ratio schedule is given in Table II.) From results shown in Figures 14 and 15 it becomes apparent that the fan designs operate at wheel speeds below optimum for high turbine efficiency. The modified tip speed schedule shown in the tabulation below results in improved turbine efficiency.

Modified Conventional Fan

P/P	V_{TIP} ft/sec	R_{HUB}/R_{TIP}
1.10	900	0.4
1.15	912	0.4
1.20	925	0.4
1.25	937	0.4
1.30	950	0.479

The gains in performance are shown in Figure 15.

In conclusion, the fan tip speed schedule versus fan pressure ratio will be adjusted upward for the medium and high energy gas generators. The final optimum schedule will be a trade-off between efficiency, size and weight, and will be determined in the conceptual design studies. The full gains inherent in the high energy gas generators cannot be realized unless fan tip speeds of 1000-1100 feet per second can be achieved without large fan weight penalties.

Diffusion Turbine Design and Energy Extraction Variations

In large diameter thin lift fan installations, the static and rotating components are "limber" when compared to conventional turbomachinery. This results in relatively large clearances and potential leakage problems. The most critical area is between the turbine and fan flow paths, just ahead of the rotor. The leakage penalty is two-fold:

1. The loss of available turbine inlet energy.

2. The effect of the low density leakage air on the fan performance.

The calculation of the first is relatively straightforward; knowing the static pressure difference across the seal, the average seal clearance and the turbine gas conditions, the weight flow across the seal can be calculated.

The effect of this leakage on the fan performance is more complex. The effect is minor in a deep inlet installation like the fan in fuselage. In a shallow installation like the fan-in-wing, the leakage causes blade tip unloading, inlet flow separation and a resultant fan overspeed and lift loss. In the XV-5A lift fan design this loss was reduced by installation of a circular vane which reduced the diffusion rate on the bellmouth. Similar results can be obtained by increasing the inlet depth and bellmouth radius ratio.

The most direct means to reduce the turbine leakage is by reducing the static pressure difference across the seal. The turbine designs used with lift fans are pure impulse with the static pressure ahead of the turbine rotor equal to ambient pressure. (Static pressure in the fan inlet is 2.5 to 3.5 pounds per square inch below ambient, depending on fan pressure ratio.) Reduction of turbine inlet pressure can be accomplished by a negative reaction design, however the turbine efficiency decreases rapidly and there is no gain in system performance.

Another means of reducing the turbine inlet static pressure is by decreasing bucket height, increasing turbine discharge Mach number ($M_{5.5}$) and diffusing downstream. The results of this study are shown in Figure 16. The higher total lift ratio with diffusion, shown in Figure 16, reflects an increase in energy extraction but not the improvements in fan performance caused by reduction in leakage. In the conventional fan designs there is sufficient depth below the rotor to accomplish the diffusion efficiently; in IGV and statorless designs, the available depth may be critical. The diffuser efficiency assumptions used in this study are described in Appendix A. Higher diffuser efficiencies result in lower values of static pressure in the turbine rotor and further reduction in hot gas leakage into the fan stream.

The potential advantages of this approach are: (at constant lift)

1. Better fan efficiency and higher flow coefficient (smaller fan for the same lift)

2. Shorter turbine buckets (lower rotor weight and polar moment of inertia, especially on partial admission fans, lower height of scroll above the rotor, and smaller rotor diameters)

3. Potentially lower radius ratio inlets (less depth required above the rotor)

4. Overall turbine efficiency, including diffuser, bucket, partial admission, and leakage losses unchanged.

In designs where it is impractical to diffuse in turbine discharge, fan weight and installed area are reduced appreciably by increasing the residual turbine energy ($M_{5.5}$). The effect of $M_{5.5}$ variation on fan lift and weight and installed area is shown in Figure 17. Further application of this method of fan size and weight reduction is contained in the conceptual design studies section.

AERODYNAMIC STUDIES

Statorless Lift Fan Study

Introduction.- The practical application of wing-installed lift fans to high speed aircraft requires that fans be made as thin as possible so as to cause the least amount of disturbance to the ideal wing cross section. Elimination of the fan stator vanes can make substantial reductions of fan thickness and weight. The question then arises as to whether or not the performance penalties associated with removal of the fan stators can be tolerated.

For a given power input and desired lift (augmentation ratio) the fan pressure ratio required depends upon its efficiency. Thus, a fan with a low efficiency and low pressure ratio can be made to generate the same lift from the same power as a fan with a higher efficiency and higher pressure ratio. The low efficiency, low pressure ratio fan, however, must pass more airflow and will therefore be larger in diameter. Thus, for a given power input and lift requirement, a loss in fan efficiency is reflected as an increase in fan diameter. The effect of fan stator removal might then be considered as a trade-off between fan thickness and fan diameter.

With a conventional rotor-stator fan design, a substantial part of the static pressure rise at the hub occurs across the stator vanes, whereas most of the static pressure rise at the tip usually occurs across the rotor blades. In a statorless fan the rotor hub sustains a much larger static pressure rise than the hub of a comparable rotor-stator design. In order to sustain this higher static pressure rise without stalling, the hub of a statorless fan must be designed with higher wheel speed, although increased rotor blade solidity and decreased aspect ratio can also help. The increased hub speed can be obtained by increasing wheel speed and/or hub diameter.

Since variations in fan diameter, tip speed, and radius ratio may affect the performance and weight of the driving tip turbine, these factors must also be included in any study of a statorless fan system. In order to gain as clear an understanding as possible from this study, it is completed in three different steps.

The first step is to study the effects of removing the stator on the fan alone. This first phase is not encumbered with considerations of turbine performance variations, inlet or exit losses, variations in drive gas conditions, or fan weights. The purpose is to establish the performance levels attainable with statorless fans and to establish design parameters such as radius ratio, tip speed, blade solidity and aspect ratio.

The second phase of the study uses the results of the first phase to compute the installed performance and dimensions of a complete tip turbine driven statorless fan system, using two different core engine cycles. For comparison, comparable rotor-stator lift fans are also evaluated using the same two core engine cycles.

The third phase of the study is then to use the design parameters and sizes determined in phases one and two to compute comparative weights of the various systems.

Analysis.- Eight statorless fan designs are made covering a pressure ratio range from 1.1 to 1.3 and rotor tip speeds of 1000 and 1100 feet per second. These tip speeds are selected because it is felt that the highest possible tip speeds will turn out to be the most desirable and these are about as high as mechanically practical for a tip turbine driven rotor. In the design of these fans it is assumed that there is no cross flow velocity and no inlet or exit louver loss. It is assumed that the velocity at the rotor inlet plane is axial and uniform and that the discharge static pressure is ambient. The inlet velocity is assumed to be equal to the average exit axial velocity. This results in some convergency of the flow path due to the density increase across the rotor.

With the above assumptions the hub static pressure rise coefficient is found to depend only on the fan pressure ratio and hub wheel speed. The hub wheel speed depends in turn on the rotor tip speed and hub radius ratio. Figure 18 shows the relation between tip speed, radius ratio and fan pressure ratio required to give a hub static pressure rise coefficient of 0.45. The choice of the static pressure rise coefficient is important in that it has a strong influence on the stall margin and distortion tolerance of the fan. By comparison, the X353-5 lift fan has a static pressure rise coefficient at the rotor hub of 0.43. If the statorless fan is to operate in cross flow and exit louver vectoring influences, it probably cannot differ appreciably from this value. Figure 18 shows then, that once a tip speed and pressure ratio are chosen for a fan, the minimum radius ratio is fixed by the limiting value of hub static pressure rise coefficient. In this study, the radius ratio of all statorless fans is chosen as being this minimum value with a hub static pressure rise coefficient of 0.45.

In statorless fans it becomes desirable to vary the energy addition along the radius in order to unload the hub while loading up the tip. A uniform energy addition along the radius results in excessive losses in swirl energy at the hub. This loss must be balanced against the thrust loss due to a non-uniform jet velocity. In order to determine an optimum energy variation with radius it is assumed that the axial component of fan discharge velocity varies with radius ratio as follows:

$$V_{a2} = V_{a2_{TIP}} \left(\frac{r}{R}\right)^n$$

Thus, n = 0 represents a uniform leaving axial velocity; n = 1 represents a leaving axial velocity proportional to radius. Figure 19 shows how the fan thrust varies with the value of n and hub radius ratio for a constant integrated value of leaving jet kinetic energy. For several of the statorless fan designs the value of n was varied between 0 and 1, and it was found that n = 0.4 was about optimum in that it resulted in the most thrust for a given amount of power

input to the fan. However, fairly large variations from the optimum do not seriously affect the fan performance. Also, n = 0.4 results in roughly uniform tangential leaving velocities. Thus a value of n = 0.4 is chosen for the remainder of the designs.

All the statorless fans in this study have rotor blade tip sections operating in the transonic region, and it becomes necessary to allow for shock losses in estimating rotor blade loss coefficients. Figure 20 shows the assumed values of profile and shock loss coefficients as functions of diffusion factor and blade relative Mach number respectively. Diffusion factor and relative Mach number are defined on Page 20. These two loss coefficients are then added to determine the total blade element loss. A fan efficiency is then calculated based on these loss coefficients and the assumption that none of the leaving swirl velocity is recovered. A rotor efficiency is also calculated which takes credit for all the leaving swirl kinetic energy. The difference in rotor efficiency and fan efficiency is then the fraction of input energy which is contained in the exit swirl kinetic energy. The shock loss coefficient used is typical for circular arc blade sections. Improvements in the rotor efficiency on the order of 2 percent for the 1000 feet per second V_{TIP} fan at 1.175 fan pressure ratio can be made by using transonic blade designs with the lower shock losses shown in Figure 20.

In addition to the blade element losses explained above, it is necessary to account for the end wall losses and the loss induced by hot gas leakage into the fan at the rotor tip. Based on previous experience, the fan efficiency is reduced by two points to account for these effects.

Rotor blade tip solidities are selected on the basis of tip relative Mach numbers so as to be consistent with the shock losses shown in Figure 20. Rotor blade aspect ratios must be selected low enough to enable the rotor blades to sustain the required static pressure rise. The maximum value of aspect ratio which is used is related to the rotor blade static pressure rise coefficient, the solidity and the blade relative leaving angle. The stalling static pressure rise coefficient has been found to correlate well with a solidity-aspect ratio parameter defined by:

$$\text{solidity-aspect ratio parameter} = \sqrt{\sigma/AR \cos \beta_2}$$

where σ = blade solidity at mean diameter, β_2 = relative leaving angle at mean diameter and AR = blade aspect ratio.

For a stall margin comparable to the X353-5 lift fan and a pressure rise coefficient of 0.45 at the hub, the correlation indicates that a solidity-aspect ratio parameter of 0.6 is required. This then establishes a maximum aspect ratio from aerodynamic considerations.

Results.- Figure 21 shows a plot of relative tip diameter versus relative lift for the statorless fan designs and also for conventional rotor-stator designs. The base point used in the comparison is the 1.3 pressure ratio rotor-stator design. The two lines representing the statorless designs are for fan tip speeds of 1000 and 1100 feet per second with pressure ratio varying

along the lines as shown. The line representing the rotor-stator designs assumes a fan efficiency of 0.85 and pressure ratio again varies along the line. This line assumes that tip speed varies with pressure ratio as required to give a fan efficiency of 0.85.

Figure 22 shows how fan and rotor efficiencies vary with pressure ratio for tip speeds of 1000 and 1100 feet per second. The two efficiencies vary by the amount of swirl. The following tabulation gives a number of additional significant parameters for the eight statorless fan designs:

Tip Speed	1000 (ft/sec)				1100 (ft/sec)			
Pressure Ratio	1.10	1.15	1.20	1.30	1.10	1.15	1.20	1.30
Radius Ratio	.436	.53	.60	.70	.40	.48	.543	.64
Mean Swirl Angle	20.1	23.2	26.3	32.6	19.0	22.3	25.3	32.0
Tip Solidity	.9	.95	1.0	1.1	1.0	1.05	1.1	1.2
Root Solidity	1.65	1.43	1.33	1.25	2.00	1.74	1.62	1.50
Rotor Blade Aspect Ratio	5.4	4.7	4.2	3.8	6.7	5.6	5.1	4.5
Tip Relative Mach Number	.99	1.03	1.07	1.14	1.07	1.11	1.15	1.22

From Figure 21 we see that the statorless fans are larger in diameter and lower in pressure ratio as compared to a rotor-stator fan of the same lift. Also, the statorless fan with a tip speed of 1000 feet per second is larger than the statorless fan with a tip speed of 1100 feet per second, except at the lowest pressure ratio of 1.1. From Figure 22, however, we see that the 1100-feet-per-second tip speed fan is lower in efficiency than the 1000-feet-per-second tip speed fan. The efficiency of the higher speed statorless fan is lower because of higher shock losses at the rotor blade tip. It was expected that the higher tip speed would reduce the exit swirl angle and thus recover most of the additional shock loss, but as shown in the above tabulation, there is very little difference in the average swirl angle between the two tip speeds.

The lift to weight of statorless fans is shown in Figure 23 as a function of admission arc and fan pressure ratio. The reason for the drop in lift to weight ratio above approximately 1.22 pressure ratio is caused by the rapid efficiency decrease above this pressure ratio value. For comparison, conventional fan data are also presented.

IGV-Rotor Lift Fan Study

Introduction.- The IGV fan concept promises a potentially thinner installation than the conventional rotor-stator design without the high efficiency and swirl losses of the rotor-only fan design. The main reason for the potential thickness reduction of the IGV-rotor is apparent from examining Figure 24. There is considerable thickness required above the rotor to accommodate the scroll "gooseneck and the fan inlet bellmouth. The IGV stage can be accommodated in this available depth and a net saving of the entire stator thickness

is theoretically possible. The static structure and scroll bubble diameter and the new rotor thickness have to be considered to determine the actual thickness reduction. This study defines the efficiency, blading geometry, and fan sizing data for IGV fans.

Analysis.- The comparison is given between the conventional rotor-stator fan and the IGV-rotor fan in the sketch below. It will be noticed that the IGV-rotor fan has inlet counterswirl which raises the relative inlet velocity. At design point there is no exit swirl with the IGV-rotor system.

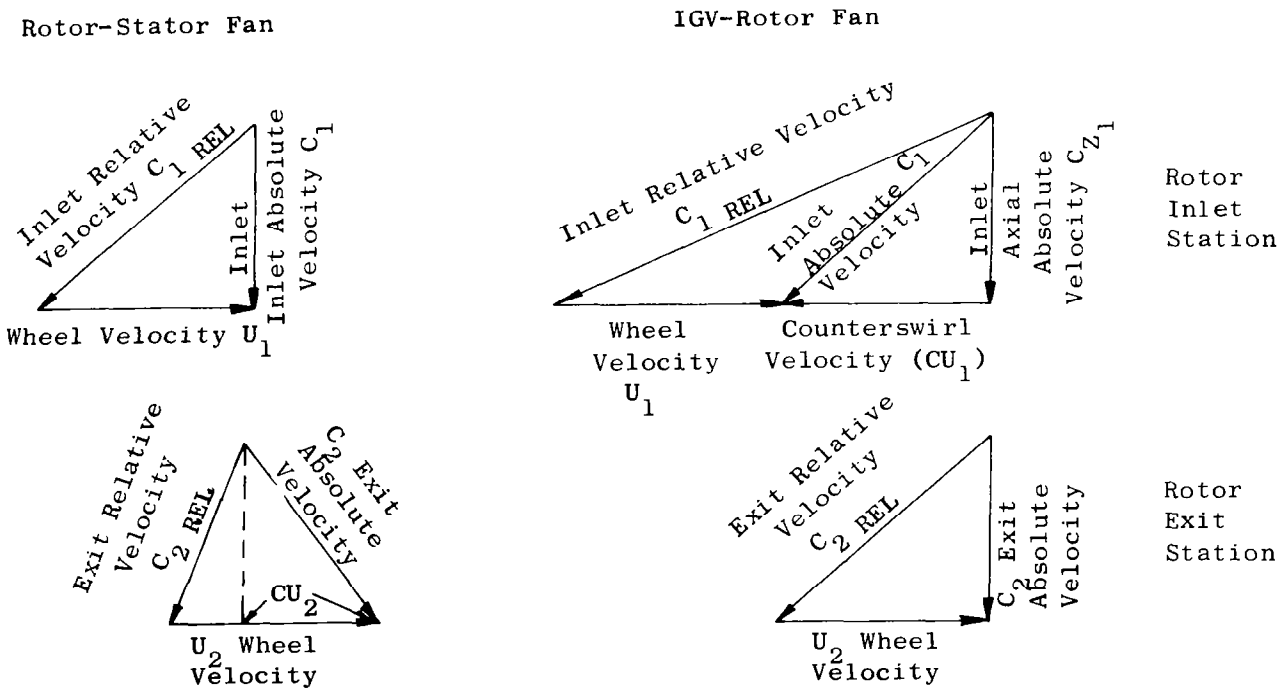

Using the above vector diagrams, relative Mach number and diffusion factor are defined as follows:

$$\text{Relative Mach Number} = M_{REL} = \frac{C_{1\ REL}}{V_{SONIC}}$$

$$\text{Diffusion Factor} = \left(1 - \frac{C_{2\ REL}}{C_{1\ REL}}\right) + \left[\frac{(U_1 - CU_1) - (U_2 - CU_2)}{2\ C_{1\ REL}}\right] \frac{1}{\sigma_R}$$

The bulk of the efficiency calculations was done using the time sharing computer program. When given wheel speed, pressure ratio, efficiency, inlet axial velocity, IGV total pressure loss, and solidity, the program solves each velocity triangle for parameters which include all velocities and components, angles, Mach numbers, diffusion factors, and loss coefficients. The program assumes that fan exit static pressure was equal to ambient pressure, that there was no exit swirl, and that exit louver pressure losses were not considered.

Velocity triangles were calculated for hub, pitch, and tip blade sections. At the hub, wheel speed was made equal to counterswirl velocity (CU_1). A range of pressure ratios from 1.1 to 1.3 were studied. At each pressure ratio and wheel speed a plot (shown in sketch below) was prepared.

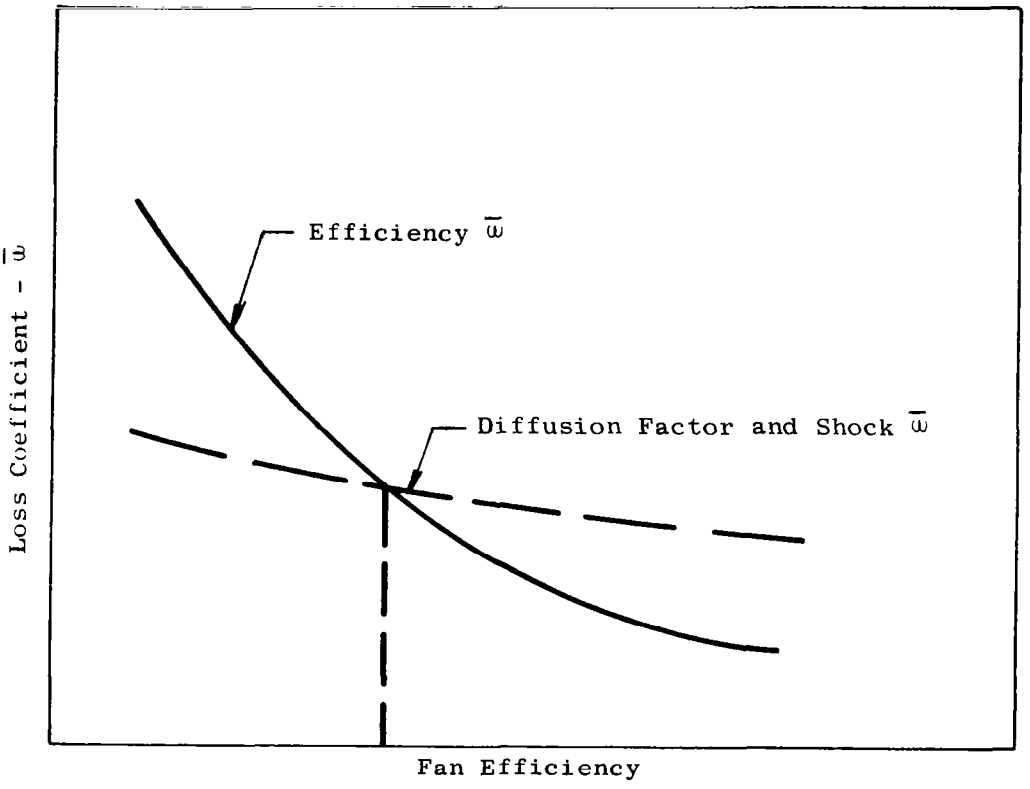

The solid line connects points whose loss coefficients are consistent with the input efficiency, pressure ratio, and wheel speed. The dashed line connects points whose loss coefficients are consistent with the diffusion factor and inlet relative Mach number generated by the velocity triangle calculations. The intersection of the two lines determines the efficiency of the blade section.

Inlet guide vane total pressure losses are based on a nozzle efficiency of 97 percent, where nozzle efficiency is defined as:

$$\eta_N = \frac{V^2}{V^2 \text{ Ideal}}$$

This can be developed into a total pressure loss percentage as a function of rotor inlet absolute Mach number, as shown in Figure 25. IGV loss is found to have only a secondary effect on the fan efficiency determination. The nozzle efficiency of 97 percent correlates well with levels used in existing turbine nozzle vane designs.

Profile loss coefficient is correlated with diffusion factor and rotor inlet relative Mach number. The diffusion factor correlation shown in Figure 26 is based on NACA data. A shock loss increment is added to the diffusion factor loss coefficient to account for Mach number effects. A shock loss level attainable with an arbitrary blade section is used. Figure 27 shows that the arbitrary blade shock loss is more optimistic than that for circular arc blades, but less optimistic than normal shock loss or the shock loss levels in the NACA 1400-feet-per-second tip speed stage (RME55A27).

Axial inlet velocity levels are determined from an axisymmetric streamline calculation. The calculation is done for a fan with an average pressure ratio of 1.25. The IGV fan study results are summarized in Figures 25 through 37.

Results.- Hub, pitch, and tip sections are averaged to give the efficiency results shown in Figure 28. Pitch sections are given twice the weight of the hub or tip sections in the averaging. At 1.1 pressure ratio, hub, pitch and tip sections produce the same pressure ratio. As the average pressure ratio increases, pressure ratio becomes radially nonuniform. At an average pressure ratio of 1.25, the hub section is at 1.18 while the tip section has a pressure ratio of 1.32. It will be noted that efficiency increases as average pressure ratio decreases from 1.3 to 1.18, due to reduced shock losses. As pressure ratio drops from 1.18 to 1.1, efficiency also decreases. This effect results from the fact that the lower pressure ratio stage cannot tolerate as high a loss coefficient as the higher pressure ratio stage. For a given loss level, a greater percentage of the pressure rise is lost in the low pressure ratio stage. In the current IGV-rotor fan calculations, the effect of reduced shock losses is not enough to make up for reduced loss tolerance. The efficiency levels as shown in Figure 28 do not include the effects of hot gas leakage at rotor tip.

Figure 29 shows the effects of average pressure ratio on radius ratio for tip speeds of 877, 1000, and 1100 feet per second. Hub wheel speed is taken as the square root of the enthalpy rise ($C_p \Delta T$) because of the assumed work coefficient of 1.0. The hub wheel speed is therefore independent of rotor tip speed but a function of pressure ratio and efficiency only.

Figure 30 shows the effect of nonuniform exit velocity on thrust. It will be noticed that the greatest thrust loss is 0.65 percent at 1.3 pressure ratio for the assumed radial variation of pressure ratio.

The rotor inlet annulus can be sized using Figures 29, 31a and 31b. Figure 32 is a general curve for axial flow into an annulus. Figures 31a and 31b give limitations on inlet Mach number due to increasing swirl as pressure ratio increases. The "choking" line of Figure 31a accounts only for the swirl effect. The practical limit shown in Figure 31b includes the additional effects of blockage, inlet guide vane loss, and radial equilibrium. The practical limit is influenced by tip speed, but this effect is very minor compared with the effect of pressure ratio. Above the practical limit, difficulty is encountered in analyzing with the axisymmetric computer program. The equivalent axial Mach number of Figures 31a and 31b is the "M" shown on Figure 32, defined as the Mach number which exists through the annulus at the IGV trailing edge with no swirl.

Using the maximum inlet flow and the radius ratio and tip speed correlation versus fan pressure ratio, the maximum lift/inlet area is calculated as shown in Figure 33. For fan pressure ratios below approximately 1.18, the discharge area required to pass the flow becomes larger than the inlet area and the discharge area becomes the ruling factor in determining fan disk loading.

Rotor characteristics which are essential to preliminary mechanical and system design studies are determined for hub, pitch and tip sections. Figures 34a, 34b, 34c and 34d show the fan pressure ratio, rotor inlet Mach number, blade stagger (orientation angle) and camber angles for the hub section as a function of average fan pressure ratio. Figures 35a, 35b, 35c, 36a, 36b, 36c, and 36d show similar data for the pitch and tip sections respectively. Similar data for the inlet guide vanes is shown in Figures 37a, 37b, and 37c.

Conclusions - IGV-rotor fans.- This study describes in a brief, general manner the efficiency, radius ratio, and flow capacity characteristics for IGV-rotor fans as a function of pressure ratio and rotor tip speed. A theoretical indication of the thrust loss due to nonuniform work distribution is also presented.

IGV fan diameters will have to be slightly larger than conventional fans for the same lift, to compensate for the lower (2 to 4 percent) efficiency and the reduced maximum inlet Mach number.

Parametric off-design studies of IGV-rotor concept are beyond the scope of this contract, however, off-design data is presented for the specific conceptual designs in other sections of this report. In addition, extensive static and cross-flow inlet test data were obtained and are presented in the inlet suck down test results section.

Conventional Lift Fan Study

Uniform radial loading.- This study predicts fan radius ratio and efficiency as a function of fan pressure ratio and tip speed. The efficiency levels calculated in this study are consistent with the X353-5 results and the design values for the 80-inch lift/cruise fan, however, hot gas leakage effects are not included. Tip speeds of 877, 950, 1000 and 1100 feet per second, and pressure ratios from 1.15 to 1.30 are evaluated. The conventional fan with uniform loading study results are summarized in Figures 38 through 45.

Hub wheel speed requirements are calculated so that the rotor turns the relative flow to the axial direction. Through-flow velocity components are chosen based on axisymmetric compressor calculations and exhaust velocity considerations. Flow paths are assumed cylindrical at the lower pressure ratios and converging at fan pressure ratios of 1.2 and above.

Efficiencies are calculated at hub, pitch, and tip. Figures 38 and 39 are used to get losses due to wakes, friction, and vorticity. These figures are based on NACA data. Shock loss shown in Figure 20, typical of circular arc blading, are used. In addition, a secondary flow loss coefficient is used.

This additional loss coefficient is 0.02 at hub and tip and is as shown in Figure 40 at the pitch line. End wall effects suggest that these losses are higher at hub and tip. Average stage efficiency is calculated giving the pitch section twice the weight of the hub or tip sections. The pitch wheel speed is taken as the arithmetic average of the hub and tip.

Although it was attempted to make this study as realistic as possible, specific rotor-stator designs which followed this effort may not fall exactly on these trends. Detailed analysis of a specific case may allow optimizations which are not evident in forming the basic assumptions for the parametric study. The preliminary geometry which is given assumes circular arc mean camber lines. Table III gives a summary of input assumptions.

In Figures 41 through 45 fan characteristics are presented as a function of fan tip speed and fan pressure ratio. Figure 41 shows efficiency trends. Radius ratio trends are shown in Figure 42. Hub geometry is given in Figures 43a through 43e. Pitch and tip section parameters are given in Figures 44a and 44b and 45a and 45b respectively.

Efficiency trends shown in Figure 41 differ from those shown in the IGV-rotor parametric study. This is partially due to the loss as a function of diffusion factor. This loss is less for an IGV-rotor system, where high velocities into the rotor keep the diffusion factor low, as compared to conventional fans. The loss system shown in Figures 38 and 39 shows an increase in loss at the highest diffusion factors. The hooking over of the 877 U_{FT} curve in Figure 41 is due to higher diffusion factors. All lines of constant tip speed do not cover the full range of pressure ratio, since fans of less than 0.4 radius ratio were not considered.

The inflections in the curves of Figure 42 are due to the transition from cylindrical to converging flow paths and fan radii being measured at the rotor inlet plane.

Nonuniform radial loading.- In this study, fan radius ratios are kept as close to 0.4 as loading will permit. Fan pressure ratio at the tip is made greater than hub pressure ratio where this reduces the radius ratio closer to 0.4. Tip speeds of 877, 950, 1000 and 1100 are evaluated. Average pressure ratios between 1.15 and 1.3 are studied. The conventional fan with nonuniform loading study results are summarized in Figures 46 through 51.

The amount of increase in tip pressure ratio is limited by considerations of radius ratio and rotor tip diffusion factor. Radius ratios less than 0.4 with tip turbine driven fans are not of interest for mechanical reasons. Increased tip pressure ratios at a given tip speed require increased turning by the rotor, which increases the tip diffusion factor. A tip diffusion factor limit of 0.45 is selected as a balance between good efficiency and radius ratio reduction. Considerations of fan weight and mechanically practical tip chord to hub chord ratios lead to setting the rotor tip solidity limit at 0.9.

Loss assumptions are the same as those for uniform case. Losses are considered to be a function of diffusion factor, inlet relative Mach number, and solidity. Pitch section axial velocity assumptions are the same as for the uniform case. Changing the pressure ratio distribution radially affects rotor exit swirl. Increasing tip pressure ratio at a given tip speed affects radial equilibrium so that tip section axial velocities are reduced and hub axial velocities are increased. Hub and tip axial velocity assumptions are based on axisymmetric radial equilibrium calculations and the predicted velocity distributions for X353-5 and the 80-inch cruise fan.

As in the uniform loading case, hub wheel speed is set so that the exit flow relative to the rotor is axial. Wall slopes are considered to be a function of average pressure ratio.

Efficiencies are calculated at hub, pitch, and tip and then averaged with the pitch section getting twice the weight of the hub and tip. Pitch wheel speed is taken as the arithmetic average of the hub and tip.

Preliminary geometry assumes circular-arc mean camber lines. Table IV gives a summary of input assumptions.

Pitch section pressure ratio is taken equal to the average pressure ratio. Tip pressure ratio minus pitch pressure ratio is equal to pitch pressure ratio minus hub pressure ratio.

Radius ratio is given in Figure 46 as a function of average fan pressure ratio and tip speed. At a tip speed of 877 feet per second, fans having pressure ratio greater than 1.192 must have radius ratios greater than 0.4 due to rotor tip diffusion factor loading. At the other extreme, 0.4 radius ratio may be attained by any fan with 1100 feet per second of tip speed regardless of fan pressure ratio, without exceeding the hub loading design criteria.

The efficiency trends shown in Figure 47 form a rather complex pattern. In general, efficiency slowly decreases as tip speed increases. Between pressure ratios of 1.2 and 1.23 efficiency is nearly constant up to tip speeds of 1025. The effects of reduced loading with increased tip speed are compensated by increased shock loss. Above 1000 feet per second tip speed the shock loss is the dominant effect.

Areas in Figure 47 above pressure ratios of 1.24 and at the combination of low pressure ratio and high tip speed show a different trend. At a given tip speed, efficiency increases with pressure ratio. This is the same trend as seen for the uniformly loaded case, where a given shock loss has a diminishing effect on efficiency as pressure ratio is increased.

Figure 48 shows that for the combinations of fan pressure ratio and nonuniformity considered in Table IV, the thrust loss due to nonuniform exit velocity is less than one percent.

Figures 49a, 49b, 49c, 50a, 50b, 50c, 51a and 51b present rotor inlet relative Mach number, rotor blade orientation angle and camber, stator vane camber, and stator vane orientation angle for hub, pitch, and tip sections.

Table V shows differences between the skewed pressure ratio fans of this study and the flat (constant pressure ratio radially) distribution fans of the previous study. At low tip speeds and low pressure ratios, there is a slight efficiency improvement with the skewed distribution, but there is a slight efficiency penalty elsewhere. The improvement is due to lower pitch line wheel speed and higher tip pressure ratio which is less sensitive to shock losses. The efficiency drops are due to higher rotor tip loading and stator hub loading. In all cases shown in Table V, radius ratio is reduced by the skewed distribution which permits a smaller diameter fan for given weight flow, pressure ratio, and lift.

Conclusions.- Uniform and nonuniform radial loading rotor-stator fans have essentially the same efficiency.

Nonuniform loading results in a smaller fan for a given tip speed; for a fixed size, the nonuniform loading allows a reduction in tip speeds and therefore weight and mechanical risk.

Some modifications in the tip loading will be necessary to account for leakage affects.

Radial Inflow Turbine Design

The aerodynamic studies of the radial inflow tip turbine indicate that it can be mounted in a slightly larger volume than required for the axial tip turbine. The efficiency is expected to be the same as for the axial turbine, however cascade tests are required to define the optimum bucket shapes.

The details of bucket design are given in Appendix A, and the mechanical and installation details are given in the Mechanical Studies section.

MECHANICAL STUDIES

Introduction

Extensive parametric mechanical studies were conducted to determine the effects of varying the basic fan parameters, such as tip speed, radius ratio, blade aspect ratio and admission arc, on fan weights, deflections and susceptibility to vibratory excitations. The purposes of these studies were to define the combination of variables to satisfy the requirements for light weight and thin fan stages, and to provide derivative data to allow refinements in the final designs. The disk and blade studies involve so much data that only the summary is included in this volume, while the complete results and background information are submitted in Part II of the research report.

The over-riding conclusion from the mechanical studies results is that thinning down of rotating stages greatly magnifies the vibratory and deflection problems. The conceptual designs therefore show only a moderate decrease in rotor thickness while the majority of reduction in installation thickness is accomplished by novel static parts design and tailoring the fan structure to fit efficiently into the wing cutout.

IGV Steady State and Dynamic Stress Study

The IGV analysis was conducted based on aerodynamic data on a 1.25 pressure ratio IGV-rotor fan of 62.5 inches diameter. The nominal IGV definition is given in Table VI. Starting with the basic design point defined in Table VI, the aspect ratio was varied from 7.36 to 12.36 and the number of vanes was varied from 52 to 88. The vanes had three longitudinal channel spars for additional stiffness. The skin thickness was assumed to be 0.020, 0.030, and 0.040 inches.

The loads were combined and assumed to act about the I_{MIN} axis, which was oriented at an average stagger angle of 17 degrees. The vanes were assumed to act as uniformly loaded beams with one end built in and the other simply supported. The resulting bending stresses are shown as a function of aspect ratio for a skin thickness of 0.020, 0.030, and 0.040 inches in Figure 52.

An analysis was conducted to determine the effect of varying the aspect ratio on the reduced velocity or tendency to flutter. The first step was to determine the natural frequency in torsion of the vanes. The results show that for a given aspect ratio and skin thickness the ω does not change with material. The analysis was conducted for a cantilevered beam, which is conservative since the vanes are fixed at the ends. The actual result lies somewhere between a cantilevered and built-in case, with the built-in vane having twice the natural frequency (ω) of a cantilevered beam.

The results are shown in Figures 53a and 53b as reduced velocity ratios versus aspect ratio for thickness families of 0.010 to 0.040 inches. The relative velocity is assumed to be 503 feet per second. Unsupported and mid-span shroud cases are compared.

Vane weights are also calculated for steel vanes of varying aspect ratios and skin thickness varying from 0.020 to 0.040. These results are shown in Figure 54.

Frame and Rotor Relative Deflections Study

An analysis was made of the relative deflections of frame and rotor for the conventional four-strutted frame design. The maximum relative deflections occur at the scroll seal under the 3 o'clock (inboard) strut. The reasons for this location are as follows:

1. The frame is relatively stiff fore and aft because the main strut protrudes above the wing surface. The lateral (minor) struts have relatively small depth with corresponding reduction in lateral stiffness.

2. One of the vertical mount restraints is located on the inboard 3 o'clock strut preventing it from following the rotor deflection; the outboard strut, which by necessity is even less stiff than the inboard strut, is free at the end and follows the rotor, resulting in smaller relative deflections.

The sources and magnitudes of each deflection at the 3 o'clock position for a moment caused by a 2 radian/second precession and a design lift load, are shown in Figure 55. The magnitude of the gyroscopic deflections is four times the level of steady state (lift) deflections. To reduce the relative deflection due to gyroscopic precession, it is possible to do one or more of the following:

1. Decrease the rotor polar moment of inertia
2. Increase rotor stiffness
3. Increase the minor strut stiffness
4. Consider alternate designs and mounting arrangements

Rotor polar moment of inertia can be decreased (for a given fan size and pressure ratio) by increasing admission arc, increasing engine cycle pressure ratio and specific energy level, diffusing behind the turbine, reducing tip speed with a corresponding increase in rotor radius ratio, and increasing blade aspect ratio.

Rotor stiffness can be increased by reduction in blade aspect ratio and disk design changes. Minor strut stiffness can be modified by changes in aspect ratio, material changes (beryllium) and wall thickness changes. The effect of aspect ratio and wall thickness on minor strut deflections is shown in Figure 56.

Use of beryllium could reduce deflections by 25 percent for geometrically similar structure, with an appreciable weight savings.

A brief investigation was conducted on configurations other than the 4-strut. These consisted of "H" struts, "Y" strut, and 4-strut with inlet guide vanes. The results indicate that the lowest deflections are obtained with the 4-strut-IGV system, followed very closely by the 4-strut-only system with the struts at right angles to each other.

Other possible design changes are: using an inboard strut both above and below the fan, restricting the fan axially at the outboard position, and changing the IGV mounting arrangement. These studies were conducted during the conceptual design phase.

Blade Flutter Study

Fan blade susceptibility to flutter is a function of aspect ratio and fan pressure ratio. The correlating parameter used is the reduced velocity $(V_{REL}/(c/2)\ \omega)$, where V_{REL} is the air velocity relative to the blade in feet per second, c/2 is blade chord/2 in feet, and ω is the blade first torsional frequency in radians per second.

A safe value of reduced velocity parameter based on extensive test background is 2.0 or less. Higher values have been tested and found acceptable only in limited range of blade incidence angle. The fan-in-wing concept is not compatible with a limited blade incidence range, as cross-flow and exit vectoring cause large swings away from design point. The variation in reduced velocity parameter (RVP) is shown in Figure 57. Two fan designs, the LF2 (an improved lightweight rotor for the lift fan powering the XV-5A aircraft) and the 80-inch cruise fan (a high pressure ratio tip turbine driven fan) are shown as references. Two main factors contribute to the increase in RVP as fan pressure ratio is increased:

1. Increase in blade relative velocity
2. Change in blade airfoil shape and radial thickness distribution

It is apparent from Figure 57 that for high pressure ratio fans an aspect ratio of between 4 and 5 is limiting with the design assumptions used. Analyzing the equation for RVP it can be seen that once the fan size, pressure ratio, and blade aspect ratio are fixed, the only variable that can be changed is the first torsional frequency (ω). There are three possible means of varying ω:

1. Change the blade end restraint
2. Change the effective blade length
3. Change the blade stiffness to density ratio (E/ρ)

In the present tip turbine design, the blade is essentially fixed in torsion on both ends and little or no increase in ω is possible. By adding a midspan shroud, change in effective blade length is possible, however problems in

manufacturing and assembly will be introduced by the requirement of maintaining close tolerances at three points on the blade (tip, dovetail, and midspan). Stiffness to density ratios of conventional materials (steel, titanium and aluminum) are almost the same. Large gains are possible with the introduction of beryllium and boron filament techniques. These materials definitely hold great promise and will be investigated further during the conceptual studies phase. Some small increases in first torsional frequency are possible by using hollow blades. This method does not pay off on small fans where the physical blade thickness is small; it will, however, be considered in the large fan designs.

Disk Steady State Study (Summary)

Thirty different disk geometries were analyzed to determine the affect of changes of the basic disk parameters (Figure 58) and loading conditions on disk deflections, stresses and weights. The largest changes in deflections were caused by changes in bore to web radius ratio (R_1/R_{web}) and web thickness ratio (h_2/h_1).

Blade and Tip Turbine Steady State Study (Summary)

Basic rotor parameters, turbine arc of admission (θ), radius ratio ($\bar{R}$), fan tip velocity, blade aspect ratio (AR), fan blade thickness to chord ratio (Tm/C), and rotor solidity were varied to determine effects on rotor weights, gyroscopic deflections, and blade tip loads.

The study was conducted with 45 and 62 inches D_{FT} to determine size effects. Blade tip deflections were mostly affected by changes in blade aspect ratio and wheel speed (deflection $\approx (AR)^{2.4}$) and $(V_{TIP})^{1.9}$). Rotor weights were mostly influenced by tip speed and admission arc. Blade tip loads were mostly affected by tip speed, arc of admission and blade aspect ratio. These results are shown in Figures 59 through 63.

Disk and Blade Vibratory Study (Summary)

A study was conducted to investigate the effect of varying the disk and blade parameters on the gyroscopic deflections and cosine 2θ and 3θ (four and 6 nodes) wheel vibration modes. As a rule, the changes which reduce rotor thickness also reduce the system spring constants, and therefore lower the critical frequencies. Examples of these trends are shown in Figures 64 and 65. Most likely, potential area of increasing the natural wheel frequencies, while at the same time reducing rotor thickness, is by use of the high density to weight materials like boron filaments and beryllium.

Radial Inflow Turbine Design

Purpose.- A radial inflow turbine design was studied for the thin-fan-trade-off program. The intent of the study was to:

1. Identify the aerodynamic and thermodynamic requirements for a radial turbine design.

2. Compare the installation of the radial turbine with the more conventional axial flow turbine.

3. Evaluate potential problems in manufacturing and design.

4. List the secondary effects which result from using the radial inflow turbine.

Results.- The results of the study described above are as follows:

1. The aerodynamic/thermodynamic design of the radial turbine is described in other sections of this report.

   A full-admission turbine with an engine weight flow of 67 pounds per second was chosen. Two hundred turbine buckets were required and the basic shape of the radial bucket was defined.

2. Utilizing the aerodynamic turbine bucket design and scaling the dimensions to account for a partial admission arc turbine, a layout has been prepared for a direct comparison of the radial turbine and an axial turbine. The layouts are shown in Figures 66a, 66b, 67a, and 67b. During this study the following ground rules were used:

   a) The fan blade design, fan size and clearances were the same for each of the turbines. Dimensions for static parts came from previous studies.

   b) It was assumed that bellmouth curvature could be reduced so that the bellmouth added only slightly to the required installation thickness.

   c) A minimum turning radius in the conventional-scroll "neck" was used as 1.35 bucket length.

   d) Gas flow areas for the scrolls at the sections studied were the same for the two turbines.

   e) Maximum installation radius for the two designs was not allowed to differ by a large amount. (Maximum difference for the two designs was 10 percent of fan tip radius.)

   f) Circular scroll sections were used as far as possible.

For an IGV fan with no rear frame, comparisons were made at a section where the scroll size largely controlled the installation thickness and at a section where the scroll size was not necessarily the controlling factor (Figures 66a and 66b).

In the large scroll-bubble section the radial turbine was to require slightly more depth because of a larger bubble diameter. Utilization of a scroll neck of sufficient area would require a larger installation radius, but could result in a scroll bubble diameter equal to that for the conventional scroll. However, in this region an increased installation radius could reduce the thickness requirements for both designs if noncircular scroll sections were used.

In the smaller scroll-bubble areas, the two designs were shown to have the same thickness with the radial turbine requiring a slightly larger installation radius. The increased depth of the radial turbine bucket took up the reduction in thickness obtained by moving the scroll bubble to the plane of the rotor. The radial turbine thickness might be reduced if detailed design studies indicate that the bucket could be moved forward relative to the fan rotor center line.

For a conventional fan with a front frame and rear frame, two similar comparisons were made. In the large scroll-bubble sections the result was similar to the IGV fan case, where the radial turbine installation was slightly thicker than the conventional turbine installation unless given a larger installation radius. In the smaller scroll-bubble sections the radial turbine showed a reduction in thickness due essentially to the elimination of the front frame and bellmouth. This step then required a rear frame design capable of supporting the fan rotor. However, the penalty of increased installation radius was still present (Figures 67a and 67b).

The layout used percentage of fan tip radius and percentage of blade chord for convenience. The dimensions will not change in proportion to changes in fan radius and blade chord.

3. Manufacturing difficulties are anticipated in:

   a) Forming bucket shapes as defined.

   b. Fabrication of supporting members and buckets into an assembly.

   These problems should not be any more difficult than development problems on new axial designs. Design difficulties are associated mainly with maintaining the bucket shape and holding the outer shroud in the high centrifugal field at the blade tip.

4. The use of the radial turbine changes several conditions which influence the design of other fan components. Fan blade, disk, and bearings are subjected to different loading conditions such as the following:

a) Estimated weight for the radial turbine is 20 percent greater than the axial design.

b) Turbine thrust continuously acting on thrust bearing is 10 to 15 percent of the fan static thrust.

c) An over-turning moment about any diameter is created by the turbine thrust. This moment is about 13 percent of that commonly associated with fan gyroscopic conditions. This moment is felt externally only for a partial admission scroll.

d) Each blade carries a bending moment due to the turbine, which is about the same as the axial design at the tip tang and amounts to about 10 percent of the normal steady state moment at the dovetail.

High Temperature Tip Turbine Study (Summary)

A conceptual design study for the high temperature cruise fan was conducted previously (Reference 1). The present study deals with similar problems, except that a design life of 300 hours is assumed for the lift fans. In addition to the scope covered in Reference 1, the problem of turbine nozzle cooling and the effects of admission arc are investigated. Lift fan component cooling requirements can be divided into three areas: the ducting and scrolls, the turbine nozzle partitions, and the turbine bucket and attachment to the fan blade. All of these areas were investigated with the following conclusions: below 1400 degrees Fahrenheit gas temperatures, fan component construction can remain the same as the present X353-5 fans; between 1400 degrees Fahrenheit and 1600 degrees Fahrenheit, the turbine nozzles require cooling, the ducting and scroll construction may have to be changed to a dual wall construction for duct diameter larger than 10 inches, and special shielding may have to be applied to carrier structure to prevent direct hot gas impingement. The need for this shield depends on fan admission arc (full admission turbines operate at higher temperatures). The material properties used in this study are shown in Figure 68. The cross-over point for dual versus single wall ducts is given in Figure 69, the uncooled nozzle weight penalty in Figure 70, and the relative weights of bucket and carrier assemblies using various methods of cooling in Figure 71.

Curve 1 of Figure 71 is for an uncooled design. This design has no heat shielding over the attachment area and no double seal arrangement. Hot turbine gas is in direct contact with the exterior of the carrier side rails and side plates. Curve 2 is for a carrier with the double seal arrangement, both fore and aft, but with no heat shield protecting the attachment area. Cool air of 110 degrees Fahrenheit flows between the inner and outer seals and cools the bucket side rails and side plates. There is no internal cooling of buckets or carrier. Curve 3 is similar to Curve 2 except that the cooling air has been assumed to be at a temperature midway between the bucket relative temperature and 110 degrees Fahrenheit. Curve 4 is similar to Curve 3, except that shielding has been added to protect the bucket attachment area.

Curve 5 is for a carrier with the forward side cooled as for Curve 4, but with the side cooled by 110 degrees Fahrenheit cooling air. The carrier and bucket are also cooled internally with 110 degrees Fahrenheit cooling air. The heat shield covers only the forward side of the bucket attachment area. Curve 6 is similar to Curve 5, except that there is no double seal on the forward side and hot turbine gas is in direct contact with the forward side rail. Curve 7 is for a carrier which is cooled internally only. Buckets are uncooled and hot gas is in direct contact with the exterior of the carrier side rails and side plates. The attachment area is shielded on both sides but there is no second seal at the outer radius of the carrier. Cooling air temperature is at 140 degrees Fahrenheit. Curve 8 is for a carrier with shields over the side plates and side rails as shown in Figure 72. There is no cooling of any of the carrier components. This method is preferred since it is simple, does not cause performance losses and is relatively light.

CONFIGURATION STUDIES

Partial Versus Full Admission Designs

Full admission fans have the hot gas scroll around the entire fan (360 degrees), while partial admission fans have the scroll around the inboard half of the fan (180 degrees). The basic fan design offers the flexibility of adjusting the admission arc to any value between 180 degrees and 360 degrees. Admission arcs below 180 degrees are also possible. For any given lift fan pressure ratio and gas generator cycle the turbine bucket length varies inversely with admission arc (180 degrees admission arc will result in tip turbine buckets of twice the height of a 360-degree admission bucket). This has the following effects on the fan design:

1. The rotor weights and the overall fan weights are higher for partial admission fans, this effect being more pronounced at the higher fan pressure ratios, which requires higher rotor tip speeds and proportionately larger turbine buckets.

2. The height above the rotor in the active arc is larger in the partial admission fan because scroll height above the rotor is a function of bucket length, as illustrated in Figure 24, while bucket length varies inversely with admission arc. On the outboard half, the fan height above the rotor can be drastically reduced for the partial admission fan while it remains almost constant for the full admission fan. Modifications to reduce thickness of the outboard side of the X353-5 partial admission fan were made under a separate NASA contract.

The thickness of full and partial admission fans on the inboard side is shown in Figure 73. The thickness is calculated as shown in Figure 24 and does not include the scroll bubble but does include the nozzle and scroll gooseneck. The general trend is for the fan thickness for a given lift to be almost independent of fan pressure ratio and gas generator cycle for the full admission fan. The partial admission fan with its inherently larger scroll height (because of the longer turbine buckets) above the rotor is more sensitive to the horsepower density and the increase in energy required to drive the higher pressure ratio fans. In high fan pressure ratio, full admission designs driven by low energy gas generators, the maximum scroll arm diameter is larger than the depth of the basic fan, as shown in Figure 74. In this study it is assumed that the total gas flow required to drive the fan is divided in half upon entry to the scroll, so that each arm carries a maximum of 50 percent of total flow. The scroll buble diameter decreases as the angular distance from the entry point increases, as shown in Figure 75.

For a single fan-in-wing installation, the critical thickness of the scroll can be partially buried in the fuselage. In multiple fan-in-wing designs, scrolls may have to be split by use of multiple entrances. When this becomes necessary, fan thickness can be traded for installation diameter to obtain the optimum configuration. Using the conventional fan design with the medium and high energy engines the scroll arm diameter is not yet critical, however any

considerable reductions in basic fan thickness from alternatives such as radial inflow turbine, statorless fan, and IGV fan, will result in scroll arm diameter determining the installation thickness.

Maximum fan thickness is only one of the indicators of how thin a wing containing a fan can be made. Of equal importance is fan thickness distribution. A study was conducted to define the wing thickness required to contain partial and full admission fans of varying pressure ratio. The wing used was a delta design with a 60-degree sweep of the leading edge, root chord of 330 inches, and semi-span of 171.3 inches. The wing coordinates were NACA 16-00X and wing loading was set at 70 pounds per square foot. The main fans were sized to provide 80 percent of total lift required; the other 20 percent was provided by smaller folding fans ahead of the wing. The lift to weight ratio of the system on a standard day was set at 1.2, which provides for control, acceleration, ground effects and hot day margin.

The results of the study are shown in Figure 76. The results indicate that a partial admission fan will fit into a thinner wing and that there is no difference between a 1.25 and 1.30 pressure ratio fan. Some refinements in fan design, fan tilt, and minor changes in wing thickness distribution can reduce the wing thickness somewhat. The large difference in wing thickness between partial and full admission designs has to be tempered by the knowledge that the full admission fan has an adequate inlet depth to maintain attached flow at static (hover) conditions. The partial admission has a relatively deep inlet on the inboard side, but is not sufficient in depth on the outboard side where a boundary layer control (BLC), or a variable geometry system might have to be used to maintain good static performance. In designs where large amounts of gas transfer are required for aircraft attitude control, the weight and response rate penalties will be larger for a partial admission design, because of the inherently heavier rotor.

In conclusion, it appears that highly swept low aspect ratio wings typical of high speed fighter aircraft can be made thinner with partial admission fans, while high aspect ratio wings with moderate sweep can be made thinner with multiple full admission fan installations.

In either design, careful tailoring of the fan (especially scroll) and wing contour will result in appreciable reduction in overall wing thickness and/or area.

Fan and Wing Tailoring

The installation studies conducted during the first quarter of the contract indicate that partial admission fans fit more efficiently into low aspect ratio wings than full admission fans, and that a 1.25 pressure ratio fan results in a near minimum wing thickness with fixed wing loading and lift to aircraft weight ratio. The studies also reveal that the existing fan envelope is not the most efficient from installation standpoint. While the fan can be comfortable nestled in the wing at one radial and circumferential location, it will protrude at some other point.

This leads to the obvious conclusion that some fan dimensional tailoring can result in an overall wing thickness reduction and/or wing loading increase. This tailoring can and should be done with axial and/or radial dimensions. While it is recognized that the fan can never be made to fit perfectly (with no wasted space) into a wing cutout (without excessively penalizing fan and wing design), it is possible to reduce the installation thickness appreciably by first designing the fan to conform to the general wing thickness distribution and second, by slightly modifying the airfoil coordinates, wing taper and wash-in, and possibly evaluating the effect on wing performance of a small local protrusion, versus a larger and/or thicker wing. In order to obtain a starting point as to what the fan dimension distribution should be, a typical delta wing thickness is plotted versus fan circumferential and radial location (the 1.25 pressure ratio partial admission fan was used for this study). The results are shown in Figure 77 and indicate that the thickness available for the fan varies by a factor of two from the inboard to the outboard fan location. In order to get a feel for what other wing planforms look like, a similar study was made using a Ryan Aeronautical Company wing planform used in the Advanced Lift Fan System Study (LFX - U.S. Army Contract). The results are quite close, as indicated by comparing results in Figure 77 with those in Figure 78. The two wing planforms are considerably different as far as leading edge sweep angle, airfoil coordinates, and aspect ratio are concerned.

Using the partial admission fan as a reference, four areas show up as defining the wing thickness:

1. Minor strut
2. Scroll entrance diameter
3. Scroll gooseneck near the leading and trailing edges of the wing
4. Bulletnose

All of these areas will receive special emphasis in the conceptual design phases. In addition, item 3 can be partially corrected by moving the fans inboard and area ruling the fuselage, as shown in sketch below:

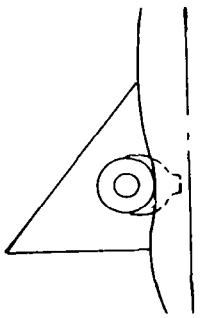

In this arrangement, a large portion of the thick scroll bubble and inlet is located in the fuselage and does not affect the wing thickness.

Scroll Configuration Variations

The scroll is an integral part of any tip turbine fan and its configuration greatly effects the overall fan installation. The scrolls, however, can be designed in various shapes to optimize any given aircraft installation. The major design variables are:

1. Admission arc - also effects the rotor design
2. Gas flow Mach number
3. Number and location of inlets
4. Number and placement of bubbles (arms)
5. Gooseneck height
6. Shape of the bubble cross section

Choice of a particular scroll configuration may be dictated by engine out consideration, ducting arrangement between scroll and engine, or amount of power transfer required. In general, scroll volume and surface area (weight) is reduced as the number of inlets is increased; this is shown in Figure 79. Weight and volume is also decreased as admission arc is decreased, however this is usually offset by increase in rotor diameter (D_{TT}) and rotor weight. The installed dimensions of a typical high pressure ratio fan, as a function of scroll configuration variations, are shown in Table VII. The procedure for calculation of the installed area is given in Appendix A.

In order to minimize scroll weights, the inlet should be located near or in line with the mounting points to eliminate bending stresses in the scroll arms due to piston loads. Cross sections other than circular should be limited only to short arcs in the areas where scroll and wing interference exists, otherwise large weight penalties result. Multi-bubble scrolls are more expensive to manufacture and their use should be limited to cases where appreciable gains in installation dimensions can be realized. Typical aircraft configurations where multi-bubble scrolls would offer large gains are inboard fans on multi-fan-in-wing transports and tandem fan installations.

Comparison of Different Fan Designs

Introduction.- The three basic fan designs (rotor-stator, statorless, and IGV-rotor) are compared parametrically. The primary areas of comparison are the installed size defined by disk loading and relative efficiency defined by augmentation ratio.

Installed disk loading.- The installed disk loading of the lift fan is defined as the total fan lift divided by planform area of the fan, including the scroll. The results are shown in Figures 80 and 81. The maximum effective disk loading of the conventional fans is 40 percent higher than that of the statorless fans, and 10 percent higher than that of the IGV fans. The pressure ratio at which the knee of the curve occurs is 1.20 for the statorless and 1.25 for the

conventional fans. The increase in required fan radius ratio, inlet flow per unit area limit, and the increase in relative scroll size cause the flattening of the installed disk loading at higher fan pressure ratios. The installed disk loading combined with the thickness results shown in Figures 73, 74, and 75 is the best indicator of minimum wing thickness and maximum wing loading potential. It appears from examination of Figures 80 and 81 that the statorless fans will have to be 75 percent of the conventional fan thickness to provide equal lift and installation volume, but IGV fans can be 94 percent of the conventional thickness. IGV fans show promise of increasing lift to volume ratios if the theoretically possible thickness reduction (Figure 24) can be achieved in a final design. Further, more specific comparisons of these designs are made in the conceptual fan design section of this report.

Augmentation ratio.- Fan augmentation ratio is a function of engine specific horsepower, fan design pressure ratio and fan component efficiencies. The effect of engine specific horsepower is shown in Figure 5 and described in the section on engine cycles. The effect of fan pressure ratio and fan efficiency levels is shown in Figure 82 for the conventional, statorless and IGV-rotor fan designs. The modified tip speed conventional design reflects the more optimum combination of fan and turbine efficiencies. The IGV-rotor design assumes the same schedule of pressure ratio and tip speed as the modified conventional design. The IGV-rotor fan is between 3 and 6 percent lower in efficiency than the conventional fan; the statorless fan is still lower in efficiency and has a high amount of discharge swirl at the higher pressure ratios. An approximate comparison of relative sizes of fans is obtained by cross-plotting the results of Figures 80 and 82. This is shown in Figure 83 and indicates that for any desired augmentation ratio, the conventional fan will have a smaller area than the other designs, but may have a larger volume.

TEST PROGRAMS

Inlet Scoop Tests

Introduction.- Inlet scoops have gained considerable acceptance in lift engine installations. The scoop is used as an inlet closure and to reduce flow distortion and losses at the engine inlet.

A test program was conducted to define scoop configuration scale for best lift fan performance throughout the fan operating range from hover to conversion to jet mode.

Previous experience with the X353-5 fan indicates that high inlet recovery does not necessarily improve the overall system performance in cross flow (Reference 4). In order to obtain the most meaningful results (lift and net thrust), it was decided to test the scoop hardware with the existing scale model 26-inch fan used extensively during the X353-5 development program. In addition to defining the design for the full scale hardware for the fan-in-wing installation to be tested in the 40-foot by 80-foot Ames wind tunnel, the scoop tests provide extensive data on various scoop configurations.

Tests were conducted at static (hover) conditions and at two velocity ratios (V_o/V_{inlet}) of 0.36 and 0.46.

Test hardware and instrumentation.- The 26-inch scale model fan was used for all of the inlet scoop tests. The fan is an aerodynamic scale model of the X353-5 lift fan. Overall lift and net thrust, fan revolutions per minute, torque, inlet static pressures, and discharge total pressures were recorded for most of the test points. Pressure instrumentation location is shown in Figure 84. Force data was only taken for points where large changes in flow conditions were not indicated. A cross flow facility capable of adjustment from 0.36 to 0.46 velocity ratio was used. Scoop hardware was manufactured from wood masonite and cardboard. The basic scoop construction is shown in Figure 85. The installation is shown in Figures 86 and 87. Five different scoop configurations were tested and are shown in Figures 88 and 89. The scoop configuration shown in Figure 88 is aerodynamically similar to the full scale hardware delivered to NASA-Ames under this contract, and evolved from the results obtained from the other configurations and from the mechanical performance and installation requirements established for the full scale hardware. In addition to the configuration changes and cross flow variation, the scoop angle and position relative to the wing were adjusted. Scoop position and angle changes are shown in Figure 90. The cross flow conditions at the two velocity ratios are shown in Figures 91 and 92 and indicate that the flow velocity distribution was worse at the high cross flow velocities. This, together with the limited flow area compared to the fan size, makes the absolute values of the results at the maximum cross flow velocity questionable, however the relative performance of the different configurations

is valid. The swept (chevron) exit louvers were used throughout the test; they were fixed at 40 degrees vector for the cross flow test and at 0 degree vector for static tests.

Results and discussion (static).- Table VIII gives a complete summary of static test results. Scoop heights have been normalized by the 26-inch fan diameter to give a scoop height ratio. Lift ratio was based on a reference lift of 101.05 pounds. The reference torque was 42.15 foot-pounds. This reference was taken from a point which had inlet interference predominantly from the scoop supports and shaft, rather than from the scoop.

The four chordwise scoop positions are designated as forward, middle, aft, and far aft positions. In the forward position, the scoop is centered on the shaft.

The static performance of the final scoop configuration as a function of scoop angle and vent hole openings is shown in Figure 93. The results indicate that the scoop can be lowered to 47 degrees with all vent holes opened, with only a 2 percent lift performance loss. This, in conjunction with cross flow results, indicates that a single scoop angle can be used throughout the transition flight.

Figures 94 and 95 show lift ratio and torque ratio as a function of scoop angle and scoop height ratio for the forward scoop position. Figures 96 and 97 show the same trends for the middle scoop chordwise position. Figures 98 and 99 are for the aft and far aft positions.

The scoop shape and size was modified as shown in Figure 89. In configuration A, the forward portion (leading edge side) of the scoop slot was blocked, increasing the scoop area by 41.5 square inches. The slot was completely blocked in configuration B, increasing the area of the scoop by another 36.8 square inches. Tape and cardboard at the aft side of the scoop were used to get configuration C. All holes and slots were blocked to get configuration D. Configurations C and D are attached to the upper surface of the wing at the aft side of the scoop. Tests with the modified scoop configurations were done at a scoop angle of 60 degrees, a scoop height ratio of 1.072, and the aft position. Results are shown below:

Configuration (See Figure 89)	$\Delta A_{forward}$	ΔA_{aft}	$\frac{\Delta \text{ Lift}}{\text{Lift}}$	$\frac{\Delta \text{ Torque}}{\text{Torque}}$
Basic Scoop	0	0	-0.013	+0.009
A	41.5 sq. in.	0	-0.027	+0.010
B	41.5 sq. in.	36.8 sq. in.	-0.033	+0.023
C	41.5 sq. in.	194.0 sq. in.	-0.047	+0.005
D	41.5 sq. in.	399.0 sq. in.	-0.077	-0.006

The area of the basic scoop, which is shown in Figures 85, 86, and 87 is 572.2 square inches.

Several areas of turbulence were noted when checking with tufts was done. The area behind the fan hub is turbulent, as was shown by a tuft on the center exit louver. Tufts on the scoop and inlet static pressure bar were observed

to twitch slowly. Other areas of turbulence are shown in Figure 100. There is an area of separation from the bulletnose, plus two areas of mixing turbulence as the flow comes around the scoop. Tufts at the ends of the exit louvers were also observed to flutter.

Trends in Figures 94 and 95 seem separated into two regions by a scoop height ratio of 0.7. Above h/D = 0.7, the lift ratio varies only slightly and some of the higher scoop angles show less lift loss for a given scoop height. Below h/D = 0.7, lift ratio decreases as scoop angle increases for a given scoop height.

Since both lift and torque are proportional to flow, the main effect of the scoop seems to be a reduction in flow due to decreased inlet pressure. At the higher scoop height ratios this inlet pressure reduction is fairly uniform circumferentially. Turbulence such as is shown in Figure 100 does not usually appear. Lift and torque reduction seem affected by the projection of the scoop area in the plane of the fan, so that there is less lift loss at higher scoop angles.

At lower scoop height ratios there is an increasing amount of turbulence and circumferential distortion as scoop angle is increased. As scoop angle is increased, the scoop trailing edge gets closer to the fan and causes greater flow distortion on the trailing edge side of the fan annulus.

In Figures 98 and 99 (aft and far aft positions), the trends expected at higher scoop height ratios do not appear. In Figures 94 and 95, constant angle lines with steep slopes appear at scoop height ratios less than 0.7, similar to the trends shown in Figures 98 and 99. At the aft and far aft positions shown in Figure 98, the trailing edge of the scoop is closer to the wing surface than at the forward and middle positions at the same scoop height. This means that distortions and turbulence will occur at lower scoop height ratios in the aft and far aft positions than in the forward and middle positions.

In comparing the magnitude of lift reduction and torque requirements, it will be noted that the torque requirement changes only slightly, while there is a pronounced lift loss effect. In some cases the data says that there is a torque increase due to the presence of the scoop. This suggests that an efficiency loss occurs as the scoop distorts the inlet flow. This might be due to secondary losses and churning, or that the blade elements are seeing large incidence changes circumferentially which take them out of their minimum loss range.

Applicability of results of fans of higher pressure ratio.- Turbulence, circumferential distortion, and inlet total pressure loss are responsible for the lift and torque changes in the presence of the scoop. The effects of turbulence and distortion on fans of higher pressure ratio will have to be confirmed by testing at the higher pressure ratios. The inlet total pressure loss, however, can be expressed as the product of a loss coefficient and a dynamic head. By assuming a variation of inlet Mach number with fan pressure ratio, the variation of thrust per horsepower with inlet loss coefficient can be calculated.

Lift fan flow paths are either cylindrical or converging. At pressure ratios up to 1.2, fan axial velocity is nearly constant and equal to velocity attained by expanding from the fan discharge pressure to ambient. This allows the inlet dynamic head to be predicted. At higher pressure ratios, an upper limit on axial inlet velocity is set by consideration of Mach number effects and inlet distortion effects, so that inlet dynamic head can be anticipated. Using these inlet dynamic head assumptions, pressure losses can be calculated for each loss coefficient. The loss in total pressure will reduce both flow and exit velocity of the fan. The resulting changes in lift and power can be calculated for each fan pressure ratio.

At a given fan pressure ratio, horsepower required per pound of lift increases as loss coefficient is increased. A ratio between the zero inlet loss case and horsepower per pound of lift with a given inlet loss coefficient can be formed. Other test results have shown this ratio to be essentially constant at all lift fan pressure ratios as long as axial Mach number is .6 or below, indicating that low speed scale model data of lift loss as a function of loss coefficient is applicable at higher pressure ratios.

Inlet loss coefficient may be affected by installation, scale effects, turbulence, distortion, Mach number, and fan design loading at higher pressure ratios, however if the low speed scale model setup is truly representative of the full-scale design and the data is carefully interpreted, the results should be applicable in all respects.

Results (low cross flow).- Table IX gives a complete summary of the low cross flow test results and static test results with the final scoop configuration. Lift and forward thrust improvement are comparisons with the performance of the fan-in-wing rig without a scoop. Runs 139 to 161 are referenced to the average lift and forward thrust of runs 157 and 158. Runs 162 to 168 are compared with the average lift of runs 169 and 170. Scoop heights were measured between the leading edge of the fixed fan inlet vanes and the intersection of the surface of the scoop with the fan shaft axis. Scoop angles are measured between the planes of the fans and scoop. It will be noticed that none of the cross flow runs showed improvement in forward thrust with the scoop. Only runs 146 and 147 showed a small lift improvement (2.44 percent for run 147).

Results (high cross flow).- Table X shows that the scoop does not improve forward thrust at this cross flow ratio. A scoop angle of 50 degrees was less detrimental, with the 60-degree scoop angle next best, and a 30-degree angle third best.

Some improvement in lift due to the scoop was noted. With the basic "A" scoop, runs 102 and 105 showed the most improvement. With the scoop shape "D" shown in Figure 89, a higher lift improvement was seen at scoop angles of 50 degrees and 30 degrees. Improvement was based on comparison with the average of no-scoop runs 114 and 115.

The experiment of runs 128 to 138, where the scoop angle on the advancing side was lowered, showed some lift improvement but none in forward thrust. Run 134 showed the highest lift, but run 133 was very close to it and had less forward thrust loss. Run 121, where side curtains were used, did not look as good in forward thrust and lift as run 119, without side curtains.

The cross flow results indicate that in the range of velocity ratios (V_o/V_{inlet}) of interest for a lift fan system (up to 0.5 V_o/V_{inlet}), the scoop inlet does not improve the system performance. Apparently any increase in ram recovery is offset by the additional drag of the device. Further refinements in shape of the scoop may result in small overall gains in performance, and the effect on mechanical performance may be beneficial.

Fan internal performance.- The overall performance of the fan in cross flow did not show appeciable change when the scoop was installed. The internal performance, as identified by fan discharge total pressure coefficients, it also almost unaffected by the scoop presence. Comparison of three data points; no scoop, scoop set for maximum thrust, and scoop set for maximum lift, is shown in Figure 101. The data is at highest cross flow ratio tested ($V_o/V_{inlet} = 0.46$) and it shows the characteristic fan performance in cross flow, however changes due to scoop presence are insignificant. This substantiates the overall force data which indicate some small loss in overall performance with the scoop. This loss is apparently caused by additional drag of the scoop and not by any change in fan performance. The loss due to the scoop has to be compared to the loss of any other closure device before final decision on scoop merits can be made. At less than optimum scoop positions, where the overall lift and/or thrust performance was substantially reduced by the scoop, the internal performance showed a corresponding decrement.

Conclusions.-

1. The final scoop configuration can be fixed at a constant angle of 47 degrees throughout the fan operating range, with only a 2 percent loss at hover, and near optimum performance near conversion speeds.

2. The scoop does not improve the system performance in cross flow up to the maximum cross flow velocity ratio of interest in lift fan systems.

3. Final decision on the advisability of a scoop closure for lift fans must be based on factors other than performance in the lift mode. Weight, complexity, and drag in conventional flight mode should be criteria for comparison with other closure systems.

Inlet Suck Down Tests

Introduction.- The higher wing loadings and thinner wing sections which will be used on fan-in-wing aircraft of the future magnify the inlet flow distortion problems. In addition, the high pressure ratio fans are designed with considerably higher axial inflow Mach number (up to M = 0.6 versus M = 0.4 for the X353-5 low pressure ratio fan) with the accompanying compressibility effects. The experience with the X353-5 fans has shown that up to inflow Mach number of 0.4, and cross flow to inflow velocity ratio of 0.5, the inlet and the resulting fan performance can be expressed in non-dimensional form as a function of cross flow only. It is expected that the inlet performance for the high pressure ratio fans, due to the higher axial velocities and possibly lower inlet lip

radii, will differ from the X353-5 inlet performance. In order to obtain order of magnitude effects, a test was conducted in which average inlet velocity was varied from 0 to 0.6 Mach number. The inlet velocity ratio was varied from 0 to 0.5. Inlet lip radius to inlet diameter ratios of 0.03, 0.06 and 0.12 were tested with and without an IGV.

Model assembly.- Photographs of the model assembly are shown in Figures 102 through 105. The basic assembly consists of the model with the inlet lip surrounded by a flat plate. Figures 104 and 105 illustrate the relation of the cross flow duct to the suck down model with and without inlet guide vanes respectively.

The inlet guide vanes used during this test have a constant 30-degree camber from hub to tip, and are not an optimum design for the high velocity testing because of the blunt leading edges and the constant T/C. The IGV is shown in the sketch below:

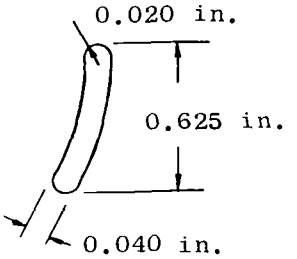

Instrumentation.- Total and static pressure and flow angle were measured by means of a four-parameter probe, which was traversed in a plane at the trailing edge of the IGV. A fifteen-element wake rake was also traversed, and readings were taken at the centers of five equal annulus areas.

The center body had 27 static taps located as shown in Figure 106. Each inlet lip had static taps located 180 degrees apart, and spaced axially around the lip. The number of static taps varied from 18 to 30 taps per lip, depending on the lip radius ratio.

Other instrumentation included a Kiel head and pitot probe in the cross flow duct (station 1), a suck down plenum static (station 4), a pitot probe and thermocouple (station 3), a model boundary layer rake (station 2), and a wing boundary layer rake (Figure 107). There was no direct measurement of total flow. Total flow was calculated by integration of local flow values obtained from the four-parameter traverse.

Test procedure.- The three lip radii were tested with and without cross flow, and with and without an IGV. During each cross flow test, the model was rotated on its axis in order to obtain a circumferential range of data.

At each circumferential position, the four-parameter probe and wake rake were traversed. Each reading was taken at a constant static to total pressure ratio in the cross flow duct (approximately 270 feet per second) and a constant (P_{S4}/P_0) ratio across the model. This resulted in some variation in the actual velocity ratio for the different configurations. For direct comparisons, all

data were corrected to a constant inflow of 18.75 pounds per second, which is equivalent to a no inlet loss one-dimensional inflow Mach number of 0.55, and an equivalent velocity ratio of 0.44. The 0.05 r/D inlet lip was tested at various velocity ratios and at one-half value of the inlet velocity.

During the testing of the IGV configuration, a series of photographs were taken of tufts located on the flat plate as well as above the inlet. Relative to the cross flow velocity direction, tufts were located on wires 7.0 inches above the model leading edge, 5.1 inches above the center body, and 2.4 inches above the trailing edge of the model, as illustrated in Figure 108. The camera was located directly above the center body, and photographs were taken with the IGV at the various velocity ratios.

Discussion.- The most critical area for a fan operating in cross flow is in the region of the leading edge tip. The ability to turn the cross flow into the inlet with little or no lip separation is required for efficient fan operation. The leading edge lip separation is carried circumferentially by the rotor blades in the direction of rotation, with resultant poor performance in the entire retreating blade tip area. A complete discussion of this phenomena is given in the following section on Fan Stall Investigation.

During static operation the separation of the boundary layer from the bellmouth wall occurs before any other loss phenomena are experienced. This separation can affect as much as 20 percent of the fan annulus area. For these reasons, the tip performance is stressed throughout the discussion.

Total pressure recovery.- The total pressure recovery data at cross flow conditions is presented in contour map form in Figures 109 through 114, for the three lip radius ratios, with and without the IGV. The pressure ratio is expressed as the local divided by the free stream total pressure. In other words, a value of 1.0 indicates full recovery of velocity head. The inlet losses with inlet guide vanes are higher than without inlet guide vanes because of the additional losses of the cascade. The comparison of the different configurations is shown in Figure 115, which indicates approximately 2 percent higher losses with the inlet guide vanes. The loss in inlet dynamic pressure is proportional to inlet dynamic head, therefore the data with 300 ft per second inlet flow show smaller losses than at 600 ft per second. It should be noted that the IGV is normally considered a part of the fan and its loss is included in the fan efficiency calculation. The simple inlet pressure recovery is symmetrical about the cross flow axis, as expected. What was not expected is the near symmetry with the IGV configuration. The advancing and retreating blade relationship is shown in Figure 116 and it would be expected to have considerably higher losses on the retreating side of the inlet. Local changes in the orientation angle of the IGV should improve the cross flow performance of the advancing and retreating sides of the fan, with a minimum loss during static operation. Since the through flow was constant for all configurations, the local velocities for the lower lip radii cases were higher because of reduction in effective area. This resulted in an appreciable increase in the IGV losses, as can be seen by comparing the static data in Figure 117. The IGV losses at mid-annulus where the wall effects should be at a minimum are; 1 percent, 1.5 percent and 2.5 percent for the 12, 6 and 3 percent inlet lips respectively. This is more loss increase than would be

predicted for an efficient cascade with the small Mach number changes at mid-annulus associated with the various lip radia. This indicates a very steep loss coefficient for the inlet guide vanes as Mach number 0.6 is approached.

All inlet geometries indicate that the loss area is concentrated in the leading edge area of the inlet. This loss area increases as radius ratio of the lip is decreased. The presence of the IGV slows down this spreading, as can be seen by comparing the 3 percent inlet results in Figures 111 and 114. The presence of a fan in the inlet biases the summetry about the cross flow direction by increasing the recoveries on the advancing side and decreasing the recoveries on the retreating side. This can be explained by the fact that the flow on the advancing side increases, resulting in lower effective values of V_o/V_{inlet} and therefore, lower distortion and pressure losses. The converse occurs on the retreating side.

Inlet total pressure losses are summarized in Figures 115 and 118. The losses expressed in Figure 118 are presented as a fraction of fan through flow velocity head and indicate that for each configuration the loss increases 15 to 20 percent of inlet velocity head between the static point and the maximum velocity ratio of 0.45 V_o/V_{inlet}. The loss coefficient is not a function of absolute velocity level, which is an encouraging situation. This does not imply, however, that the submerged fan performance itself can be extrapolated from low to high pressure ratio fan data. The total pressure losses are only part of overall inlet performance description; the velocity and flow distribution and flow angles are of equal importance in predicting fan performance.

Flow and Mach number distribution.- The flow distribution in cross flow is shown in Figures 119 through 124 and the Mach number distribution is shown in Figures 125 through 130. Flow and Mach number distributions during static operations are shown in Figures 131 and 132. The advancing side of the IGV configurations pumps up to 10 percent more flow per unit area than the retreating side. The inlet guide vane in general improves the flow and Mach number distribution for the 3 and 6 percent inlets. However, the actual values of local Mach numbers are as high or higher for the corresponding IGV configurations, because of the nearly constant 30-degree swirl angle. The IGV increases flow distortion in the 12 percent configuration.

Flow angle variations.- The most pronounced effect of the IGV is on the flow angle distribution at the simulated rotor inlet plane. The flow angle is defined as positive when it produces swirl opposing the rotor velocity. The assumed rotor rotation is counterclockwise. The cross flow angle data is shown in Figures 133 through 138. The flow angle leaving the IGV is close to the design camber angle of 30 degrees, except near the leading edge, where there is essentially no flow. The flow angle without the IGV varies up to ±24 degrees with the 3 percent inlet, and up to ±18 degrees with the 12 percent inlet, between the advancing and retreating side of the inlet. The results of the tuft studies are shown in Figure 139. The plan view shows the streamlines along the wing surface for two velocity ratios (V_o/V_{inlet} = 0.45 and 0.23). The section view shows the flow direction above the inlet along the center line.

Conclusions.-

1. The IGV causes an additional total pressure loss above the simple inlet which is greater than any beneficial affects in the tip region. This loss can be substantially reduced by a more optimum IGV geometry.

2. The IGV improves tip performance of the 3 percent inlet under static conditions, suggesting that a partial IGV in the tip region only may be beneficial in very shallow installations.

3. IGV effectively removes the cross flow horizontal velocity component and results in a near uniform swirl angle entering the rotor.

4. The variation of loss coefficient with velocity ratio (V_o/V_{inlet}) from low pressure ratio fan data can be used to estimate inlet performance for high pressure ratio fans, but internal fan performance may not be extrapolated from low to high pressure ratio fans because of supercritical internal velocities.

5. Additional inlet loss due to cross flow is almost constant with and without inlet guide vanes and is between 15 percent and 20 percent of the inlet velocity head, at a cross flow ratio V_o/V_{inlet} of 0.45.

LIFT FAN STALL PREDICTION

Objective

To evolve an analytic procedure for predicting the stall of a lift fan operating in a cross-flow with throttling effects caused by exit louvers.

To make a qualitative comparison of the probable stall sensitivity of three lift fans: low pressure ratio, X353-5; high pressure ratio, LFX (rotor-stator fans); and an IGV-rotor type lift fan.

Introduction

The study is concerned with the broader problem of performance deterioration rather than being restricted to stall in the usual sense. Cross-flow and the resultant inlet flow distortion are considered from the viewpoint of their effect upon fan performance. A computerized radial equalibrium calculation is applied to show the effects of measured inlet flow data.

Analysis of the Measured Performance of the X353-5 Lift Fan Operating in Transition

Basic approach.- As a result of the cross-flow the flow in a lift fan differs considerably from the axisymetric model normally assumed to facilitate radial equalibrium type calculations. Despite a lack of axial symmetry a radial equalibrium calculation can be applied to describe the flow at any particular section. Certain differences from the axisymetric model must be reflected in the computation.

Firstly, the effect of a flow distribution at the inlet in a given circumferential position is felt at another circumferential location on the same streamline. Put in other words an input to a blade passage is seen as an output at an absolute location at some distance circumferentially as dictated by the rotational and the axial velocities of the fluid. The input to a radial equilibrium type calculation must be selected appropriately to compensate for this phenomena. This concept is described in Appendix A.

The fan performance is computed at several sections. At the inlet computation station the appropriate flow pattern for that section must be described in terms compatible with the radial equilibrium calculation procedure. This requires that inlet cross-flow angle be described in terms of two components. A component of the inlet angle in the meridinal plane, φ and, a second component β in the swirl or circumferential direction is required. Thusly, the cross-flow can be input as a ficticious inlet guide vane in a fictitious annulus section located just upstream of the fan inlet. Figure 140 describes this cross flow model.

The same method is applied to describe the exit louver flow pattern. This is shown in the sketch below, where the air angle caused by the louver is described in terms of two angles, ϕ and β:

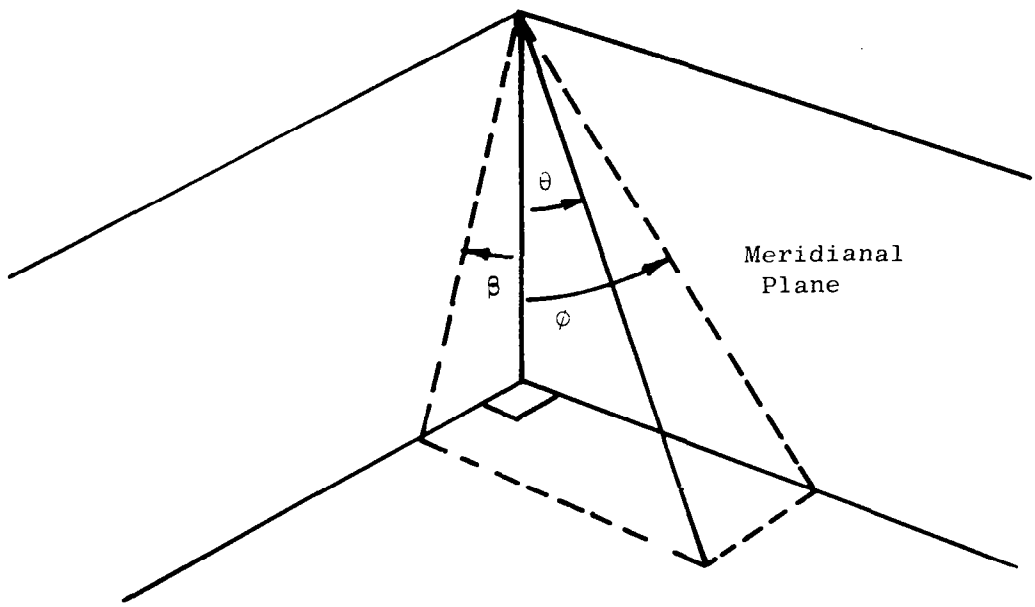

β = fictitious blade angle

ϕ = angle projection in meridianal plane

θ = louver angle

It is assumed that a correct cross-flow inlet flow description is a prerequisite for an accurate performance prediction. Thus far two methods of obtaining an inlet flow description have been identified.

The method used in this analysis for obtaining inlet angle data rests upon the assumption that results collected with a model may be applied to any fan provided that the ratio C_Z/V_P, i.e., the average axial velocity divided by the cross flow velocity, is equal for the fans. The validity of this assumption has, to some extent, been demonstrated by a comparison of results obtained by J.R. Switzer (reference 5) with results obtained in recent inlet tests described in the previous section. Switzer's data describes the inlet angles in a plane normal to the inlet and parallel to the cross flow direction. The more complete data required for this performance study was obtained from the recent tests, which consisted of rotating a four-parameter probe about the inlet. This probe was traversed from the inlet lip to the hub at many circumferential locations, thus providing a good picture of the β component of the inlet flow angle, as well as a description of the shadow or separation at the forward region of the inlets tested. Unfortunately, this data does not reflect the response of the inlet flow to the performance of the lift fan, as is possible by the application of the Laplace type calculation. Furthermore, the data contained no indications of the ϕ angle as required for the meridianal description of the radial equilibrium

calculation. Nevertheless, for study the available β angles appear to be a most significant influence upon performance. The lack of ϕ angle data is compensated for by approximations.

Several radial equilibrium calculations may be required at each section. This is necessitated for example, where excessively high incidence angles indicate stall over some portion of the blade height. Assuming that the stall does occur as expected, performance over the remainder of the blade will be influenced. The radial equilibrium calculation that indicates that stall will occur does not reflect its effect upon the operating portion of the fan. To complete this performance picture, a second radial equilibrium calculation must be made in which the stalled fluid in the rotor undergoes very little turning and is subjected to very high losses. Truly, when the stalled, choked or turbining regions are detected through the radial equilibrium calculation, the entire cross flow inlet pattern should be recomputed for the next set of radial equilibrium calculations.

Application of the performance study to the X353-5 lift fan.- A complete design point description of the X353-5 fan will be found in reference 6. Measured cross flow performance data of the X353-5 lift fan is used to evaluate the performance prediction method as described. The measured data, reference 4, are the result of wind tunnel tests of a full scale wing mounted fan. The study is based upon operation in a 94-knot cross flow at design speed. Four sections are studied in the same locations as the measured data has been obtained, as is shown in Figure 141. This figure is a top view of the suck down test inlet, showing the β components of the inlet air angles relative to the rotor In addition, the calculation sections are indicated as solid radial lines. The dashed lines represent the input locations which have been computed to compensate for the input-output displacement previously described. The X353-5 measured data appears in Figure 142, which is obtained from reference 4, page 240. Here, actual rotor discharge pressure coefficient, Ψ, versus percent annulus area is shown for the four sections indicated in Figure 141. Sections B and D are considered advancing, i.e., the rotor is moving into the cross flow. As a result, their incidence angles, and consequently loading, are higher than design. Advancing sections, especially those approaching the forward region of the inlet, are susceptible to stall, as shown by the sudden collapse of the pressure coefficient in Section B (Figure 142). At Sections F and H, which are referred to as retreating, the rotor moves away from the cross flow. In these sections the incidence angles are likely to be small or negative, and the pressure coefficients will be lower than design. Referring to Figure 142, the pressure coefficient versus percent annulus area curves at $V_o/V_{tip} = 0.22$ are appropriate for this comparison study. These curves are converted to total pressure ratio versus radius ratio for ease of comparison with computed results. Figure 143 is a schematic diagram of the station locations for the radial equilibrium calculation. The input of Station 0 contains meridianal angles, ϕ, describing the inlet flow. Station 1 is a fictitious stator with blade angles describing the β component of the inlet flow. Stations 2, 3, and 4 are free stations at which angular momentum is preserved. The rotor exit is at Station 5; Station 6 is a free station; and Station 7 is the stator exit. The louvers are described at Station 8 in terms of ϕ and β angles. Station 9 is a dummy station included for calculation purposes.

The following analysis, based on flow angle measurements obtained from suck down tests, has the following limitation. The inflow induced by a uniform sink, as in the suck down tests, is symmetrical about an axis parallel to the cross flow velocity. The presence of a rotor in the inlet alters this symmetry. The flow on the side where the blade is advancing is increased due to higher blade loading, resulting in a decrease in effective velocity ratio (V_o/V_{inlet}). The flow on the side where the blade is retreating is reduced, due to lower blade loading, resulting in an increase in effective velocity ratio (V_o/V_{inlet}). As a result, the test data with a fan shows slightly better performance on the advancing side and considerably poorer performance on the retreating side than can be predicted from the simple suck down tests. The inlet-fan interaction on the retreating side has a snow-balling effect; any deterioration in fan performance causes an increase in inlet velocity ratio with the consequent higher inlet losses, flow separation, and further fan performance deterioration.

The X353-5 calculations performed at Stations B, D, F and H are of considerable value in analyzing the measured results. The blade loadings at 7 radii at the four sections are computed in terms of $\Delta P/q$ and diffusion factor. If $\Delta P/q$ exceeds 0.65 and the diffusion factor is greater than 0.6, stall is considered probable. The results of these calculations and comparison with the measured results are shown in Figures 144 through 147. The sharp drop in total pressure ratio appearing at the tip region of the Section B measured data is attributable to stall indicated by excessive incidence angles, as verified by the radial equilibrium calculation. At the tip region of input Section B, Figure 141, there is a rapid increase in β. This is reflected in the sudden increase of slope of the measured data at a radius ratio of about 0.8. The β angle increases rapidly with the radius becoming large enough to cause stall at a radius ratio of about 0.87. Section D is advancing, but has lower total pressure ratios than B because of the lower β angles it encounters in the aft region of the inlet. The computed results do not show high loadings at the tip, consequently some phenomena other than stall induced by cross flow air angles must account for the rather sudden drop in pressure ratio in the region. Separation of the flow impinging upon the circular vane appears to be a reasonable explanation. Based upon suck down model data, the incidence angle i, of the flow upon the vane would be in the order of minus 50 degrees. This is illustrated in Figure 148.

Calculations performed at the retreating Sections F and H indicate that the decay of performance in these tip regions is the result of the shadow or separation through which the rotor passes in the forward part of the inlet. At H, a reasonable estimate of performance can be made at the hub region, and the extent of the stalled portion of the section can be estimated from suck down model test data, Figure 149. From the radial equilibrium calculations, performance should be acceptable from the hub to the tip; however, measured data indicated poor performance from the pitch to the tip of the rotor. This poor performance can be accounted for by consideration of the effects of the forward shadowed region of the inlet. The rotor emerges from the shadow, stalled from the pitch to the tip. Because there is little or no axial velocity in the blade passage, good performance does not resume as might be expected; the incidence angles remain high, and the stall persists. Fortunately, with little or no suck down, the air impinges upon more of the inlet in the retreating region at higher angles, finally

enabling the tip to recover. But, the higher cross flow angles which help the tip to recover, further reduce the loading in the hub region. The poor performance initiated by the shadow and preserved through the slow recovery and secondary effects on the hub accounts for performance losses over two-thirds of the annulus. The low work input in this region leads to over-speed and low efficiency. Furthermore, computed results suggest that the rotor tip never does fully recover. Because of this "snow-balling" effect, the benefits from reduction, or even better, elimination of the shadow at the inlet, appears worth consideration in future designs.

Through application of the radial equilibrium method, the weight flow at any section can be estimated. This is accomplished by altering the weight flow of a calculation at a given section until the static pressure at the louver exit is approximately equal to atmospheric pressure. This, of course, assumes that the static pressure is approximately atmospheric at the louver exit region of the wing pressure surface. This assumption is probably somewhat in error, but must suffice until a further study can include this part of the flow.

Through the computational method referred to as radial equilibrium, a two-dimensional compressible flow solution in cylindrical coordinates is obtained. The basic relationships involved are the equation of continuity,

$$\frac{\partial \rho}{\partial t} + \nabla \cdot (\rho \bar{V}) = 0$$

and the Navier-Stokes equation,

$$\rho \frac{D\bar{V}}{D_t} = \rho \bar{F} - \nabla_P + \mu \nabla^2 \bar{V} + \frac{\mu}{3} \nabla (\nabla \cdot \bar{V}) +$$

$$2 \left[(\nabla_\mu) \cdot \nabla \right] \bar{V} + (\nabla_\mu) \times (\nabla \times \bar{V}) - \frac{2}{3} (\nabla \cdot \bar{V}) (\nabla_\mu)$$

where $\bar{F}$ is the external force exerted on unit mass of gas.

The components of these equations in the radial direction in terms of cylindrical coordinates are simplified through the assumption of an ideal non-viscous gas and axial symmetry. Solution of the simplified equations requires numerical methods in which successive approximations are made until a solution of the entire flow field is found which satisfies the laws of conservation of matter and momentum.

Prediction of the Performance of the LFX Fan in a 135-Knot Cross Flow

The LFX fan was designed for a weight flow of 493 pounds per second, at a total pressure ratio of 1.252. Figure 150 is a schematic diagram of the meridianal plane, showing the calculation stations. Some computed design point data is shown in Table XI.

The LFX performance in a 135-knot cross flow was evaluated, using four sections in the same locations used for the X353-5 study. At Section B, stall is indicated at the rotor tip. The incidence angles in this region were excessively high, as a result of cross flow. This problem is illustrated in Figure 151, in terms of a comparison of the design rotor inlet air angles, and the computed rotor inlet air angles under cross flow conditions. Two radial equilibrium calculations were performed at Section B. The first, A, established the presence of high incidence angles leading to the tip stall. A second calculation, B, was required in which the stalled tip was unloaded, enabling computation of the performance in the unstalled region (Figure 152). Section H, Figure 152, reflects the detrimental effects of the effects of the shadow. The computation indicates that a complete elimination of the lip separation would permit acceptable performance over the entire blade height. From the X353-5 study, it should be recalled that the primary detriment of this tip stall is its lasting effects. Further effects of the tip stall are seen at Section F.

Comments on the Sensitivity of an IGV-Rotor Lift Fan to Cross Flow

According to recent suck down tests, inlet guide vanes operate satisfactorily over a wide range of incidence angles. Cross flows, causing large negative incidences, can be turned on the normally suction surfaces of the vanes. Of course, the losses through inlet guide vanes operating under these conditions are quite high. The transonic rotor following the IGV will require a narrow variation of inlet angles in its supersonic tip region because of its narrow stall margin and pinched loss buckets. The inlet guide vane may provide sufficient control of these inlet angles, especially when considering the reduced effect of deviation angle change has upon the rotor incidence angle. This is typified in the velocity triangle of Figure 153. Here, a deviation angle increase, $\Delta\delta$ = 3 degrees, is seen to cause an incidence angle change, Δi, of only 1 degree. This multiplying effect of the IGV air angle control seems quite promising.

IGV and Conventional Fan Static Performance

Estimated static performance of the inlet guide vane rotor and conventional rotor-stator fans is shown in Figures 154 and 155. The maps are shown for a 1.23 pressure ratio inlet guide vane, and a 1.25 pressure ratio conventional fan. The results are applicable to a range of pressure ratios from 1.2 to 1.3, as long as the same aerodynamic loading criteria are used.

The maps can be scaled within these ground rules by using the following relationships:

$$\left(\frac{(P/P-1)_{\text{new fan design point}}}{(P/P-1)_{\text{map design point}}}\right)\left(P/P_{\text{map}}-1\right)+1 = \text{new fan pressure ratio}$$

$$\left(\frac{\eta_{\text{new fan design point}}}{\eta_{\text{map design point}}}\right)\left(\eta_{\text{map}}\right) = \text{new fan efficiency}$$

Weight flow does not require scaling, since it is presented as percent of design value.

In general, the inlet guide vane fan has a much narrower range of efficient operation because of the high blade relative Mach numbers and resultant rapid increases in blade losses as incidence angle is changed. This is shown in Figure 156, where the blade loss coefficient is plotted as a function of blade incidence angle and design speed (blade relative Mach number). Based on the inlet tests reported in the previous section, it is expected that off-design performance in cross flow will be adequately handled by the inlet guide vane-rotor fan, since the inlet guide vane discharge flow angle remains essentially constant (Figure 137). The inlet guide vane fan will, however, have limited tolerance to discharge throttling. This may be acceptable in aircraft configurations where the fans can be slightly tilted, or where there are additional lift/cruise engines on board. In an XV-5A type installation, either a low throttling louver system, a variable camber inlet guide vane or a power transfer system between the fan and jet nozzle must be used with an inlet guide vane fan for efficient transition operation.

Conclusions

The stall prediction method presented in this report provides reasonably accurate results, when compared to measured lift fan data. Probable stalls can be predicted and an approximation of the weight flow can be made. Further work will improve this method. A new computer program will be required to alter inlet angles according to load weight flow, and more test data would be of value in improving the method.

The study clearly indicates the extent of the poor tip performance caused by forward lip separation. Considerable improvements in performance can be expected through shadow elimination or reduction.

Using this radial equilibrium analysis, fan efficiency can be determined on a blade element basis where the pressure loss coefficients on each streamline can be evaluated in terms of incidence angles, Mach numbers, and radial flows induced by the cross flow. A mass averaged efficiency can then be computed by integrating the results from all calculation sections. These integrated results can be used to estimate fan work and thrust. If turbine performance is considered further, inlet air angle and radial equilibrium calculations can be performed to predict the degree of overspeed in a given cross flow.

CONCEPTUAL DESIGNS

Introduction

The parametric studies conducted in the beginning of the program showed trends and narrowed down the area for further fan design optimization. As the area of investigation was narrowed for the conceptual designs, more design factors were considered, and many new innovations were incorporated into the designs; therefore it is unlikely that any of the point designs exactly match the parametric data. This fact does not invalidate the parametric study conclusions, but it does point out that parametric studies are only a design tool and not a final product.

The conceptual fan designs are sufficiently detailed so that one can expect that final hardware would closely resemble the preliminary designs. Stresses and deflections of all major components were calculated, temperatures in the critical areas were determined and cooling requirements, if any, identified. The performance calculations were based on component efficiencies and loss coefficients consistent with the turbomachine state of the art and modified to account for some of the adverse conditions existing in the lift fan installations. It is of course expected that further testing would be conducted, especially with IGV fans, to verify the performance levels prior to flight hardware procurement.

Two separate requirements for the preliminary designs were established:

1. A single fan-in-wing configuration, similar in concept to the XV-5A, to result in the thinnest wing contour possible for a tactical aircraft in the 20,000 to 35,000 pound gross weight class.

2. A multiple fan-in-wing configuration, also adaptable to folding fan or podded fan concept, to result in a lightweight, compact installation for a transport aircraft in the 60,000 to 200,000 pound gross weight class.

The major objective of the first requirement was wing thickness, therefore the partial admission was chosen (see parameter studies for comparison of full and partial admission). Three fan designs, conventional (rotor-stator), IGV-rotor, and statorless (rotor only) were chosen for comparison. The base point was the rotor-stator design. A pressure ratio was set at 1.25, which, based on parametric studies, results in thinnest, highest lift/weight ratio installation. The medium energy engine with 2460 degrees Rankine T_4 and 12:1 compressor pressure ratio was chosen. Required fan lift was 13,650 pounds, based on the delta wing size and loading used in installation studies. Engine airflow was set at 61.2 pounds (61.8 pounds turbine discharge flow), giving the required fan lift. The engine discharge conditions were maintained for the IGV-rotor and statorless fan designs and the fan cycle parameters were varied to obtain the desired lift of 13,650 pounds. The three fan designs are therefore directly comparable as to weights, installed sizes, and resulting wing thicknesses. Each design was individually optimized within the ground rules set above.

The major objectives of the second requirements were; compact installation, high lift to weight ratios, and a design compatible with a transport wing installation. A high energy engine with 2760 degrees Rankine T_4 and 16:1 compressor pressure ratio was chosen. The reason for choosing the higher energy engine was that, in this type of installation, the engine is used for the lift portion of the mission only, and would most likely operate at higher temperatures than a basically cruise engine of the type used in the first requirement. Since light weight was one of the prime objectives, full admission was picked for this design. Two fan designs, conventional (rotor-stator) and IGV-rotor were chosen for comparison. The conventional (rotor-stator) design, with a pressure ratio of 1.28, was the base point. The fan lift was set at 26,000 pounds which, when scaled ±30 percent, covers the range of CX6 and smaller transport requirements. Engine airflow was set at 103.4 pounds (104.4 pounds turbine discharge flow), giving the desired lift. An IGV fan with the same engine discharge conditions was also designed to 26,000 pounds of lift. The two designs are therefore directly comparable. Each design was individually optimized within the ground rules set above.

Figures 157 through 161 are layouts of the five fans. More detailed full-scale layouts can be requested from the Full-Scale and Systems Research Division at Ames Research Center, Moffett Field, California.

Description of Each Design

The detailed description of each fan design is given in Part II of the research report.

The sizing and performance, the weights and the bearing load summaries for all fans are given in Tables XII through XIV, respectively. The details of blading geometry are given in Tables XV through XVIII for each fan. The dimensional data to determine wing cutouts required are shown in the respective drawings for each fan. A brief description of each fan design follows:

Large inlet guide vane fan.- The large inlet guide vane fan drawing is shown in Figure 157. The design used a multi-strutted front frame, with no projections above the wing upper surface. The struts double up as inlet guide vanes. The front frame and scroll are tied in together and act as a composite structure to resist air and maneuver loads. The rotor blades are hollow titanium construction, which reduces the rotor and, consequently, frame weights over the solid blade design. This, and the fact that the fan is a full admission design, results in overall lift to weight ratio comparable to that of the smaller fans. (As a rule, lift to weight ratio decreases as fan size is increased, as shown in Figure 8.) Since there are no exit stators, a rear frame is not used in this design.

Because of the high temperature of the driving gases (1613 degrees Fahrenheit), the scroll is of dual wall construction, the scroll nozzles are cooled, and the turbine carriers are shielded.

Large conventional fan.- The large conventional fan drawing is shown in Figure 158. The design uses the conventional four-strutted front frame with the major strut running fore and aft, protruding above the wing upper surface. This fan design uses a rear frame to house the exit stators. The hot parts design and rotor design are similar to the large inlet guide vane fan.

Small inlet guide vane fan.- The small inlet guide vane fan drawing is shown in Figure 159. The fan uses a three-strutted front frame. The inlet guide vanes are mounted in the front frame, however their limited depth does not contribute substantially to the load carrying capability. The major strut protrudes above the wing surface, while the minor (inboard) strut folds down to reduce the installation thickness. There is no outboard strut, but the exit louvers support the outboard bellmouth. This is reflected in an increase in the louver weights and a different mounting arrangement. There is no need to cool any of the components using the medium energy engine with exhaust gas temperature of 1447 degrees Fahrenheit. This design does not use a rear frame. The rotor blade aspect ratio, Tm/C, and relative Mach number are such that a midspan shroud had to be added to eliminate the possibility of flutter. Solid titanium fan blades are used on this design. With this rotor size, and the relatively high turbine loads (because of partial admission), the weight savings using hollow blades would be nominal unless a considerably higher Tm/C were used; in that case, however, fan efficiency would be lowered.

Small conventional fan.- The small conventional fan drawing is shown in Figure 160. This fan uses a four-strutted front frame similar to the large conventional fan, but of lower depth. The required thinness necessitates relatively thick and heavy minor inboard and outboard struts. As an alternate, a frame similar to the small inlet guide vane fan frame could be used. The scroll and rotor construction are similar to the small inlet guide vane fan structures.

Small statorless fan.- The small statorless fan drawing is shown in Figure 161. This fan uses a front frame similar to the one used in a small inlet guide vane fan, except that the inboard minor strut rotates rather than folds when not required. Either minor strut mechanism could be used in this design. The rotating strut stores next to the major (fore and aft) strut when not in use, and is actuated with a hydraulic motor mounted in the fan hub. The scroll and rotor are similar to the other two small fan designs. An overall saving in weight of about five percent could be realized in this design with the use of hollow fan blades.

Scaling Data

The conceptual fan designs are based on specific inlet gas flow conditions as well as fixed fan pressure ratios, turbine energy extractions, and other fan design parameters. It is recognized that these selections of design parameters may not be desirable for all lift fan installations. The basic designs are optimized for the selected choice of design variables, however, some changes in fan pressure ratio, and gas generator cycle variables can be made and new fan weight, lift, and size can be determined. To define fans powered by other than

specified gas generator size, discharge gas conditions, and fan pressure ratio, the following procedure is recommended:

1. Identify fan design concept, i.e., small, large, IGV, conventional, statorless.

2. Identify gas generator size and discharge flow conditions.

3. Obtain the lift per pound of gas generator flow from Figure 162 or 163.

4. Multiply results of Item 3 by gas generator discharge flow to obtain the total lift of the fan.

5. Obtain the percentage of base fan design lift by dividing Item 4 by either 13,650 pounds or 26,000 pounds.

6. Obtain the weight and diameter percentages of the fan from Figure 164 or 165.

7. If the desired fan pressure ratio differs from the base fan designs, obtain the lift, weight, and diameter percentages from Figures 166 through 170 as appropriate.

8. To obtain the final values of lift, weight, and diameter, multiply the percentages obtained in Item 6 by the percentages obtained in Item 7, and by corresponding values of base fan design point.

9. It is recommended that the cumulative effect of all the changes not exceed ±30% in fan lift. In other words, small fans obtained in Item 8 should have lift between 9500 and 17,700 pounds, and large fans between 18,200 and 33,800 pounds.

10. Overall installation dimensions can be determined from installation drawings in Figures 157 through 161 and the scaled fan radius (FTR).

The following example is used to illustrate the scaling procedure:

1. Desired fan is large and of conventional design.

2. Gas generator discharge conditions are:

$$W_{5.1} = 110 \text{ lbs/sec}$$

$$T_{5.1} = 2000^{\circ}R$$

$$P_{5.1} = 55 \text{ psia}$$

3. From Figure 162, specific lift = 219 lb/lb/sec

4. Total lift = 219 x 110 = 24,100 lbs

5. Percentage of base fan design lift = 24,100/26,000 = 92.7

6. From Figure 165 at 92.7 design lift percentage

   Diameter percentage = .96

   Weight percentage = .925

7. Desired fan pressure ratio is 1.32 from Figure 167

   Diameter percentage = 97.5

   Lift percentage = 95.0

   Weight percentage = 94.5

8. Final lift = 26,000 x .927 x .950 = 22,900 lbs

   Final weight = 1235 x .925 x .945 = 1080 lbs

   Final fan tip diameter (D_{FT}) = 80.17 x .96 x .975 = 74.9 in

   Final fan tip radius (FTR) = 37.45 in

9. Check lift ratio = $\frac{22,900}{26,000}$ = .871

   13% less than base fan design point - valid

10. Obtain installation dimensions from Figure 158.

    a) Thickness at the outboard position = .37 (37.45) = 13.9 in

    b) Thickness at the inboard position = .47 (37.45) = 17.6 in

    c) Installation diameter from inboard to outboard point = 1.44 + 1.30 (37.45) = 102.6 in.

Selection of Fan Cycle Parameters

Studies were conducted on each of the fans to evaluate the effects of six fan cycle parameters on fan lift, weight and area. The purpose of the study was to determine the combination of numerical values of these six parameters which would minimize fan weight and area (maximize fan lift to weight ratio and fan lift to area ratio) for a fan having a given lift and powered by a given gas generator.

The following fan cycle parameters were investigated:

Fan pressure ratio, FPR

Fan tip speed, V_{TIP}

Scroll inlet Mach number, M_S

Fan inlet Mach number, M_{10}

Turbine discharge Mach number, $M_{5.5}$

Turbine exhaust diffusion

The effect of these six fan cycle parameters on the fan lift, weight and area were determined by varying each parameter over a range of numerical values while holding the remaining five parameters constant.

The lift is defined as the fan total uninstalled lift, the weight is defined as the fan total uninstalled weight including exit louvers, and the area is defined as the fan planform area of the fan and scroll. Appendix A contains a derivation of the expressions for fan area.

The existing digital computer programs for fan cycle analysis and fan weight estimation were used to generate the data. Curves of normalized lift, weight and area were plotted versus each cycle parameter. From these curves, the partial derivatives of lift with respect to weight ($\partial L/\partial W$) and lift with respect to area ($\partial L/\partial A$) were calculated.

The combination of fan cycle parameters which results in a fan of minimum weight (or size) is shown in Appendix A to be that combination for which the partial derivative $\partial L/\partial W$ (or $\partial L/\partial A$) is constant, i.e., the value of this derivative is the same for each cycle parameter. For minimum weight,

$$\left(\frac{\partial L}{\partial W}\right)_{FPR} = \left(\frac{\partial L}{\partial W}\right)_{V_{TIP}} = \left(\frac{\partial L}{\partial W}\right)_{M_S} = \left(\frac{\partial L}{\partial W}\right)_{M_{10}} = \left(\frac{\partial L}{\partial W}\right)_{M_{5.5}}$$

and for minimum area,

$$\left(\frac{\partial L}{\partial A}\right)_{FPR} = \left(\frac{\partial L}{\partial A}\right)_{V_{TIP}} = \left(\frac{\partial L}{\partial A}\right)_{M_S} = \left(\frac{\partial L}{\partial A}\right)_{M_{10}} = \left(\frac{\partial L}{\partial A}\right)_{M_{5.5}}$$

The studies conducted on each of the fans were similar. The study for the small conventional fan is considered typical and will be discussed in detail to illustrate the method.

Fifty-two data points for the small conventional fan were run on the computer programs; these are listed in Table XIX. For runs 1-27, the fan tip speed was varied between 877 and 1100 feet per second, for four values of fan pressure ratio between 1.20 and 1.30. Values of fan efficiency and fan radius ratio were selected for each combination of tip speed and fan pressure ratio using the data obtained from the aerodynamic studies. The normalized lift, weight, and area are shown in Figures 171, 172, and 173; the partial derivatives are shown in Figure 174. All data are normalized to the data of run 9.

For runs 28-31, the scroll Mach number was varied between 0.45 and 0.71. The normalized lift, weight, and area are shown in Figure 175 and the partial derivatives are shown in Figure 176.

For runs 32-36, the fan inlet Mach number was varied between 0.4 and 0.7. The normalized lift, weight, and area are shown in Figure 177 and the partial derivatives are shown in Figure 178.

For runs 37-44, the turbine discharge Mach number was varied between 0.40 and 0.75. The normalized lift, weight, and area are shown in Figure 179 and the partial derivatives are shown in Figure 180.

Runs 45-52 are repeats of runs 37-44, with diffusion of the turbine discharge. The diffusion rate was defined by assigning the turbine discharge static pressure coefficient ($\Delta P_s/q$) a value of 0.30. The selection of this coefficient is discussed in Appendix A. The normalized lift, weight, and area are shown in Figure 181 and the partial derivatives are shown in Figure 182.

Table XX compares the initial and final values of the fan cycle parameters for the small conventional fan.

The final values of fan cycle parameters were selected as follows. The partial derivative of lift with respect to weight was noted to be a weak function of fan pressure ratio for fan pressure ratios between 1.2 and 1.25 (Figure 170), so it was decided to choose the numerical value of fan pressure ratio last. Two parameters having strong lift to weight derivative functions were fan inlet Mach number and turbine discharge Mach number. Practical upper limits on these parameters are 0.60 for the fan inlet Mach number (85 percent of choke), and 0.70 for the turbine discharge Mach number (increasing the turbine discharge Mach number decreases the bucket camber. A bucket with too low camber will be stress-limited). Values of 0.60 for fan inlet Mach number and 0.70 for turbine discharge Mach number, with diffusion, were chosen. These values yield almost identical values of the lift to weight derivatives. The values of the lift to area derivatives are not quite equal. It is not possible to minimize both weight and area simultaneously. The particular combination of cycle parameters

which minimizes weight will not also minimize area (and conversely). Therefore, a compromise must always be made between weight and size.

The scroll Mach number was chosen as 0.325, a compromise between the values required to match the lift to area derivatives of the fan inlet Mach number and the turbine discharge Mach number. Matching the lift to weight derivative of scroll Mach number to that for the fan inlet Mach number and turbine discharge Mach number would result in too low a scroll Mach number. Therefore, scroll Mach number was selected to reduce size. The fan pressure ratio was chosen to be 1.223 to hold the lift at the desired value. The fan tip speed was chosen as 900 feet per second to provide a weight reduction at this pressure ratio.

Table XXI presents the results of this study for the small conventional fan.

This procedure resulted in the selection of cycle parameters which yielded a fan having reduced weight and size while providing constant lift. As shown in Table XXI, the weight was decreased 13.2 percent and the area was reduced 7.1 percent. However, this procedure did not define a so-called "optimum" fan. A further refinement of this study could be made by generating a new set of curves using the final selected values of cycle parameters, and then selecting a new combination of cycle parameters. This should yield nearly equal derivative values. However, it is expected that this additional effort would result in only small corrections to the weight and area reductions already achieved.

There is a second reason why this procedure did not result in an "optimum" fan. The constraints of constant lift and specified gas generator precluded the selection of a fan having a maximum ratio of lift to weight (or lift to area), because it forced the selection of certain of the variables so as to maintain the lift rather than to reduce weight and size. This is a realistic approach, for in most applications for which the lift fan is considered, the choice of the gas generator is dictated by availability and the fan lift is dictated by the required aircraft size. The fan designer must therefore design the fan within these constraints.

Non-Conventional Design Approaches

The fan designs incorporate some features which are departures from what is presently conventional lift fan design practice. These features are:

1. All of the fan designs use tab locks as blade retainers. These tab locks replace bolts, thus reduce fan axial depth at the blade root and provide a small reduction in rotor weight.

2. All of the fan designs use diffusion bonding to join the disk halves. Diffusion bonding eliminates the disk bolts and provides a small weight reduction.

3. The two large fan designs use hollow fan blades, which result in a significant rotor weight reduction.

4. To reduce the fan axial depth, the small conventional fan design uses a large number of high aspect ratio blades stiffened with a midspan shroud, and a large number of high aspect ratio stator vanes stiffened with two concentric rings.

5. The large IGV fan design uses the inlet guide vanes as load carrying members. This eliminates the front frame major and minor struts, reducing the front frame weight.

6. The statorless fan design has a 3 o'clock minor strut which is hinged to the major strut and which folds against the major strut when the fan is not running. This adds some complexity to the design, but reduces the thickness and weight of this strut.

7. The small IGV fan design uses the three longest exit louvers to support the outboard bellmouth loads. These louvers replace the 9 o'clock minor strut, reducing the front frame weight, and allowing a thinner installation on the outboard side of the fan.

8. The small IGV fan design uses a 3 o'clock minor strut which is hinged along the major axis and which folds down into the fan when the fan is not in operation. This feature adds some complexity to the design, but reduces the thickness and weight of this strut.

Three other design features not used in these fan designs but which should be considered in future design studies are:

1. Figure 183 shows a suggested design using fan airfoils made of wound boron filaments. The blade dovetail is made of titanium and has a cap into which the airfoil is bonded. The blade tangs and pins which join the bucket carriers to the blades have been eliminated. The blade tip is bonded into a cap which is part of the bucket carrier. This technique reduces the carrier length, thus reducing the maximum fan diameter and reducing the rotor weight. An estimated rotor weight reduction of 20 percent can be achieved using this design.

2. Fan axial thickness can be reduced by using scroll "strozzles". A strozzle is a combined strut and nozzle in the scroll which removes the tangential component of gas flow from the scroll gooseneck. The scroll gooseneck axial depth can be reduced 50 percent by using these so-called strozzles. This design has an additional estimated total pressure drop in the scroll of 2 percent. The scroll bubble diameter must be increased to carry the tangential flow previously carried in the gooseneck, but this diameter increase is very small because this flow is only a small percentage of the total flow.

3. If the exit louver airfoils are pinned at approximately the quarter-chord point instead of at the tips, the louvers can be aerodynamically balanced, and the louver loads can be reduced. However, this technique requires additional axial clearance between the rear frame and the exit louver system, and therefore increases the fan axial depth.

CONCLUSIONS

The parametric studies, test programs, and conceptual designs indicate that large reductions in fan weight, volume, thickness, and area are possible compared to the X353-5 fans powering the XV-5A research aircraft. These reductions are a result of several changes; the most important one being the increase in fan pressure ratios, which is made possible by the use of high specific energy gas generators currently under development. A 1.23 pressure ratio conventional lift fan, powered by a gas generator with a turbine inlet temperature of 2460 degrees Rankine, produces twice the lift of the X353-5 fan, while maintaining the same lift augmentation and installed diameter. Increasing the gas generator energy by increasing turbine inlet temperature to 2760 degrees Rankine results in further increase in lift, while maintaining lift augmentation and installation diameter constant. Further substantial reductions in fan installation dimensions and weight can be realized by optimizing the fan design parameters, and by tailoring the fan scroll and front frame to use the available area and volume most efficiently. The tailoring can only be made after a specific installation is identified, but it can produce a substantial reduction in wing thickness with almost no weight or performance penalties.

In addition to the conventional rotor-stator lift fan, two other fan design concepts were studied: the inlet guide vane-rotor fan and the statorless, rotor only fan. Both of these new designs result in larger fans than the conventional design because of their lower efficiency. The IGV-rotor fan can be built thinner and slightly lighter than the conventional fan, and may be attractive for some installations requiring minimum thickness, however additional testing is required to establish its performance levels, especially under off-design conditions caused by cross flow and exhaust throttling.

The specific conclusions follow:

1. Efficient lift fans can be installed in 5 to 6 percent thickness to chord ratio delta wings with 70 pounds per square foot wing loading.

2. Partial admission fans result in a thinner wing for a low aspect ratio, single fan per wing configuration; full admission fans result in thinner wing for a high aspect ratio multi-fan-per-wing installation.

3. Fan designs powered by the medium energy gas generators with turbine inlet temperatures of 2460 degrees Fahrenheit will not require cooling or any changes in the design or materials of the fan components. Fans powered by the high energy gas generators with turbine inlet temperatures of 2760 degrees Fahrenheit will require scroll nozzle cooling, double wall scroll construction and changes in the tip turbine design.

4. Inlet scoop which doubles up as fan closure can be installed with no lift penalty at hover, but does not improve the fan performance in cross flow. The scoop can be set at one fixed angle, throughout the

range of flight speed in fan mode, with small performance penalty compared to the optimum scoop angle versus flight speed setting.

5. Fan inlet pressure losses up to an average axial Mach number of 0.6 are a function of inlet geometry and cross flow to through flow velocity ratio only. Based on this, it can be concluded that thrust loss due to inlet loss will be of the same magnitude for high and low pressure ratio fans.

6. An inlet guide vane cascade can be used to delay flow separation along low radius ratio inlet bellmouth.

7. Analyses indicate that high pressure ratio lift fans will have cross flow performance characteristics similar to the low pressure ratio X353-5 lift fan. Elimination of the flow separation region at the upstream side of the fan bellmouth would eliminate fan overspeed in cross flow and provide more lift and thrust in transition.

8. Large fans of up to 30,000 pounds lift, having lift-to-weight ratios above 21 to 1, can be built using existing state of the art methods and materials. Slightly higher lift-to-weight ratios are possible with extremely thin fans in the 10,000 to 15,000 pound lift class. New materials, such as Boron filaments for blades and Beryllium for cold static parts, will further reduce fan weights.

TABLE I

ENGINE CYCLE CONDITIONS - CYCLE VARIATION STUDY

Cycle	Compressor Pressure Ratio P_3/P_2	T_4 (°R)	$T_{5.1}$ (°R)	$P_{5.1}$ (psia)	$W_{5.1}$ (lb/sec)	Specific Horsepower (HP-sec/lb)
1	9	2460	2001	49.5	136.8	203.34
2	12	2460	1907	53.5	136.0	205.46
3	16	2460	1842	56.8	135.6	205.99
4	7	2160	1771	40.2	179.8	153.26
5	9	2160	1686	42.7	179.2	153.34
6	12	2160	1618	45.2	178.6	153.77
7	12	2760	2159	59.9	115.2	250.87
8	16	2760	2073	64.2	115.2	250.44
9	20	2760	2038	67.5	115.0	253.00
10	8	2760	2260	51.0	121.8	237.09

TABLE II

CONVENTIONAL FAN EFFICIENCY LEVELS

P/P	V_{TIP} ft/sec.	R_{HUB}/R_{TIP}	% Fan Efficiency	% Total Pressure Duct Loss	% of Fan Inlet Loss	% Fan & Turbine Discharge Loss	Thrust Coefficient	Turbine Efficiency
1.10	708	.4	85.0	8	10	7	0.99	Variable - Depends on velocity ratio
1.15	753	.4	85.0	8	10	7	0.99	
1.20	810	.4	84.7	8	10	7	0.99	
1.25	877	.4	84.3	8	10	7	0.99	
1.30	950	.479	84.0	8	10	7	0.99	

TABLE III

INPUT DATA[1]

Fan Pressure Ratio	Section	C_{Z_1}	C_{Z_2}	U_2/U_1	σ_R*	σ_S**
1.10	Hub	450	405	1.0	1.4	1.69
	Pitch	450	405	1.0	0.768	0.914
	Tip	450	405	1.0	0.6	0.71
1.15	Hub	468	422	1.0	1.4	1.6
	Pitch	468	450	1.0	1.08	1.0
	Tip	468	468	1.0	0.75	0.75
1.20	Hub	500	477	1.021	1.4	1.5
	Pitch	530	510	1.0	1.08	1.0
	Tip	510	530	0.99	0.75	0.75
1.25	Hub	492	547	1.092	1.4	1.24
	Pitch	595	591	1.0	1.08	1.0
	Tip	539	580	0.965	0.75	0.8
1.30	Hub	475	557	1.1	1.4	1.24
	Pitch	600	570	1.0	1.1	1.0
	Tip	548	600	0.96	0.9	0.8

* σ_R - Rotor Solidity

** σ_S - Stator Solidity

[1]See Table IV for definition of Nomenclature

TABLE IV

INPUT DATA

P/P	Sec-tion	V_{TIP}	PR	U_1	C_{Z_1}	C_{Z_2}	σ_R	σ_S	U_2/U_1
1.15	Tip	877	1.175	877	440	451	0.75	0.75	1.0
	Pitch		1.15	614	468	445	1.08	1.2	1.0
	Hub		1.125	350.8	468	507	1.4	1.6	1.0
1.15	Tip	950	1.15	950	468	468	0.75	0.75	1.0
	Pitch		1.15	665	468	450	1.08	1.0	1.0
	Hub		1.15	380	468	422	1.4	1.6	1.0
1.18	Tip	877	1.235	877	463	476	0.75	0.75	0.997
	Pitch		1.18	614	500	475	1.08	1.2	1.0
	Hub		1.125	350.8	510	555	1.4	1.6	1.002
1.18	Tip	950	1.21	950	485	493	0.75	0.75	0.997
	Pitch		1.18	665	500	475	1.08	1.2	1.0
	Hub		1.15	380	500	505	1.4	1.6	1.002
1.18	Tip	1000	1.195	1000	486	500	0.75	0.75	0.997
	Pitch		1.18	700	500	475	1.08	1.2	1.0
	Hub		1.165	400	495	462	1.4	1.6	1.002
1.20	Tip	877	1.265	877	480	496	0.9	0.75	0.99
	Pitch		1.2	617	530	504	1.08	1.2	1.0
	Hub		1.135	357	530	581	1.4	1.6	1.021
1.20	Tip	950	1.25	950	497	510	0.75	0.75	0.99
	Pitch		1.2	665	530	504	1.08	1.2	1.0
	Hub		1.15	380	520	557	1.4	1.6	1.021
1.20	Tip	1000	1.23	1000	500	520	0.75	0.75	0.99
	Pitch		1.2	700	530	504	1.08	1.2	1.0
	Hub		1.17	400	495	507	1.4	1.6	1.021
1.23	Tip	877	1.28	877	503	530	0.9	0.8	0.98
	Pitch		1.23	632	577	548	1.15	1.2	1.0
	Hub		1.18	387	547	606	1.4	1.6	1.07
1.23	Tip	950	1.29	950	512	535	0.9	0.75	0.98
	Pitch		1.23	665	577	548	1.15	1.2	1.0
	Hub		1.17	380	563	620	1.4	1.6	1.07
1.23	Tip	1000	1.27	1000	517	540	0.75	0.75	0.98
	Pitch		1.23	700	577	548	1.08	1.2	1.0
	Hub		1.19	400	530	580	1.4	1.6	1.07
1.25	Tip	877	1.285	877	525	562	0.9	0.8	0.965
	Pitch		1.25	646	595	565	1.15	1.2	1.0
	Hub		1.215	410	538	595	1.4	1.6	1.092
1.25	Tip	950	1.3	950	519	546	0.9	0.8	0.965
	Pitch		1.25	674	595	565	1.15	1.2	1.0
	Hub		1.2	397	565	625	1.4	1.6	1.092

TABLE IV (Continued)

INPUT DATA

P/P	Sec-tion	U_T	PR	U_1	C_{Z_1}	C_{Z_2}	σ_R	σ_S	U_2/U_1
1.25	Tip	1000	1.3	1000	519	546	0.9	0.75	0.965
	Pitch		1.25	700	595	565	1.15	1.2	1.0
	Hub		1.2	400	565	625	1.4	1.6	1.092
1.25	Tip	1100	1.25	1100	539	580	0.75	0.8	0.965
	Pitch		1.25	770	595	591	1.08	1.0	1.0
	Hub		1.25	440	492	547	1.4	1.24	1.092
1.28	Tip	877	1.295	877	538	592	0.9	0.8	0.962
	Pitch		1.28	661	600	570	1.15	1.2	1.0
	Hub		1.265	445	502	564	1.4	1.6	1.097
1.28	Tip	950	1.317	950	535	590	0.9	0.75	0.962
	Pitch		1.28	689	600	570	1.15	1.2	1.0
	Hub		1.243	428	540	594	1.4	1.6	1.097
1.28	Tip	1000	1.325	1000	535	588	0.9	0.75	0.962
	Pitch		1.28	713	600	570	1.15	1.2	1.0
	Hub		1.235	425	558	615	1.4	1.6	1.097
1.28	Tip	1100	1.3	1100	536	585	0.9	0.75	0.962
	Pitch		1.28	770	600	570	1.15	1.2	1.0
	Hub		1.26	440	536	574	1.4	1.6	1.097
1.30	Tip	877	1.3	877	544	600	0.9	0.8	0.96
	Pitch		1.3	674	600	544	1.15	1.0	1.0
	Hub		1.3	470	475	557	1.4	1.4	1.1
1.30	Tip	950	1.32	950	535	586	0.9	0.8	0.96
	Pitch		1.3	703	600	570	1.15	1.2	1.0
	Hub		1.28	455	513	570	1.4	1.6	1.1
1.30	Tip	1000	1.33	1000	532	576	0.9	0.8	0.96
	Pitch		1.3	725	600	570	1.15	1.2	1.0
	Hub		1.27	450	531	591	1.4	1.6	1.1
1.30	Tip	1100	1.35	1100	524	533	0.9	0.8	0.96
	Pitch		1.3	764	600	570	1.15	1.2	1.0
			1.25	440	567	627	1.4	1.6	1.1

P/P = Average Pressure Ratio

V_{TIP} = Tip Wheel Speed (ft/sec)

PR = Element Pressure Ratio

U_1 = Rotor Inlet Wheel Speed (ft/sec)

C_{Z_1} = Inlet Axial Velocity (ft/sec)

C_{Z_2} = Rotor Exit Axial Velocity (ft/sec)

σ_R = Rotor Solidity

σ_S = Stator Solidity

U_2 = Rotor Exit Wheel Speed (ft/sec)

TABLE V

COMPARISON OF FANS WITH UNIFORM AND NON-UNIFORM PRESSURE RATIO

Fan Pressure Ratio	Tip Wheel Speed	Uniform Fan Pressure Ratio Efficiency	Non-Uniform Fan Pressure Ratio Efficiency	Uniform R_{HUB}/T_{TIP}	Non-Uniform R_{HUB}/R_{TIP}	Δ Efficiency
1.15	877	0.872	0.882	0.438	0.4	+0.01
1.20	877	0.879	0.870	0.485	0.407	-0.009
1.20	950	0.875	0.871	0.447	0.4	-0.004
1.20	1000	0.869	0.871	0.425	0.4	+0.002
1.25	877	0.882	0.876	0.495	0.468	-0.006
1.25	950	0.879	0.867	0.456	0.417	-0.012
1.25	1000	0.874	0.863	0.434	0.4	-0.011
1.30	950	0.882	0.875	0.495	0.48	-0.007
1.30	1000	0.875	0.869	0.47	0.451	-0.006
1.30	1100	0.861	0.852	0.427	0.4	-0.009

TABLE VI

INLET GUIDE VANE DEFINITION

Chord = 2.94 inches

52 vanes

Tangential force = 2,955 lbs

Axial force = 1,274 lbs

Double circular arc airfoils

Fixed inlet guide vane (IGV)

Parameter	Hub	Pitch	Tip
Radius (inches)	10.82	21.64	32.45
Stagger angle (degrees)	19.4	16.0	15.4
Camber (degrees)	37.5	38.4	43.5
Solidity	2.25	1.125	0.75

TABLE VII

SUMMARY OF CRITICAL DIMENSIONS

Configuration	R_1	R_2	R_3	R_4	R_1+R_3	R_2+R_4	$A_{INST}/\pi D_{TT}^2/4$
I	70	53	63	67	133	120	1.63
II	53	63	53	63	106	126	1.43
III	67	63	53	63	120	126	1.55
IV	67	63	53	63	120	126	1.54

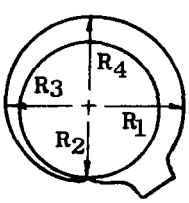

Configuration I

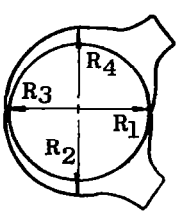

Configuration II

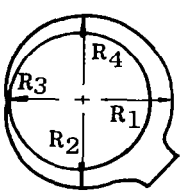

Configuration III

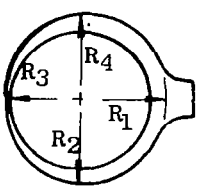

Configuration IV

TABLE VIII

SUMMARY OF STATIC TESTING

Run	Scoop Height (in)	Scoop Angle (deg)	Scoop Position	Corrected Lift $L\frac{\theta}{\delta}$ (lbs)	Corrected Torque $T\frac{\theta}{\delta}$ (ft-lbs)	Lift Improvement (lbs)	Configuration and Remarks
1	19.5	30	Forward	97.76	41.56	-3.27	Unless otherwise noted, all runs were done with the scoop shown in Figure 89a.
2	19.38	40	Forward	98.45	42.48	-2.58	
3	18.75	50	Forward	99.36	42.60	-1.67	
4	18.00	60	Forward	101.15	42.76	+0.12	
5	19.63	0	Forward	99.60	42.31	-1.43	
6	19.69	10	Forward	98.37	42.20	-2.66	
7	19.63	20	Forward	98.29	41.87	-2.74	
8	24.50	30	Forward	99.33	41.95	-1.70	
9	24.38	40	Forward	99.48	42.26	-1.55	
10	24.63	0	Forward	98.60	41.52	-2.43	
11	14.63	0	Forward	97.05	42.06	-3.98	
12	14.69	10	Forward	95.55	41.90	-5.48	
13	14.63	20	Forward	93.24	41.48	-7.79	
14	14.50	30	Forward	95.18	41.24	-5.85	
15	14.38	40	Forward	93.94	41.43	-7.09	
16	13.75	50	Forward	94.86	41.64	-6.17	
17	12.00	30	Forward	89.31	40.96	-11.72	
18	12.13	20	Forward	89.19	40.77	-11.84	
19	12.06	10	Forward	92.27	40.73	-8.76	
20	12.13	0	Forward	89.91	40.99	-11.12	
21	9.63	0	Forward	91.63	40.25	-9.40	
22	9.69	10	Forward	86.52	40.34	-14.51	
23	9.63	20	Forward	82.31	39.83	-18.72	
24	7.13	0	Forward	79.11	37.96	-21.92	
25	7.19	10	Forward	73.38	38.02	-27.65	
26	19.56	0	Middle	99.23	41.92	-1.80	
27	20.00	10	Middle	99.83	41.97	-1.15	
28	20.25	20	Middle	99.10	41.86	-1.93	
29	20.50	30	Middle	98.83	41.98	-2.20	
30	20.69	40	Middle	98.39	42.28	-2.64	
31	20.88	50	Middle	98.74	42.47	-2.29	
32	21.00	60	Middle	99.46	42.02	-1.57	
33	15.88	50	Middle	95.03	41.67	-6.00	
34	15.69	40	Middle	93.52	41.98	-7.51	
35	15.69	40	Middle	95.71	41.87	-5.32	

TABLE VIII (Continued)

SUMMARY OF STATIC TESTING

Run	Scoop Height (in)	Scoop Angle (deg)	Scoop Position	Corrected Thrust $F\frac{\theta}{\delta}$ (lbs)	Corrected Torque $T\frac{\theta}{\delta}$ (ft-lbs)	Lift Improvement (lbs)	Configuration and Remarks
36	15.50	30	Middle	94.40	41.37	-6.63	
37	15.25	20	Middle	95.12	41.32	-5.91	
38	15.00	10	Middle	97.29	41.49	-3.74	
39	14.56	0	Middle	98.99	41.81	-2.04	
40	12.06	0	Middle	93.73	41.40	-7.30	
41	12.50	10	Middle	97.01	41.20	-4.02	
42	12.75	20	Middle	90.71	40.40	-10.32	
43	13.00	30	Middle	89.58	41.01	-11.45	
44	13.19	40	Middle	90.25	41.08	-10.78	
45	9.69	0	Middle	89.24	40.32	-11.79	
46	10.00	10	Middle	91.52	40.53	-9.51	
47	10.25	20	Middle	84.62	39.96	-16.41	
48	10.25	20	Middle	82.32	40.25	-18.71	
49	12.13	0	Forward	96.48	41.16	-4.55	Repeat of run 20
50	9.63	0	Forward	90.87	40.18	-10.16	Repeat of run 21
51	12.00	30	Forward	90.68	41.37	-10.35	Repeat of run 17
52	14.38	40	Forward	95.47	42.22	-5.56	Repeat of run 15
53	18.75	50	Forward	99.80	42.74	-1.23	Repeat of run 3
54	15.69	40	Middle	96.40	42.30	-4.63	Run 54 is a repeat of runs 34 and 35
55	15.00	10	Middle	97.32	41.62	-3.71	Repeat of run 38
56	14.69	0	Middle	97.88	41.64	-3.15	Repeat of run 39
57	12.06	0	Middle	95.90	40.90	-5.13	Repeat of run 40
58	13.19	40	Middle	89.47	41.26	-11.56	Repeat of run 44
59	12.50	10	Middle	96.08	41.62	-4.95	Repeat of run 41
60	12.75	20	Middle	90.90	40.96	-10.13	Repeat of run 42
61	10.25	20	Middle	85.25	40.44	-15.78	Repeat of run 48
62	24.56	0	Middle	100.66	41.68	-0.37	
63	0.0	0	See Remarks	101.05	42.15	+0.02	This run was done with the scoop mounted outboard of motor in order to establish the effect of the scoop supports on thrust
64	23.88	40	Aft	98.37	42.32	-2.66	
65	23.88	40	Aft	98.27	42.87	-2.76	Repeat of run 64
66	25.38	50	Aft	97.62	42.55	-3.41	
67	27.88	60	Aft	99.73	42.81	-1.30	
68	22.63	30	Af	98.87	42.10	-2.16	
69	17.63	30	Af	95.93	41.60	-5.10	
70	18.88	40	Aft	94.54	42.18	-6.49	

TABLE VIII (Continued)

SUMMARY OF STATIC TESTING

Run	Scoop Height (in)	Scoop Angle (deg)	Scoop Position	Corrected Thrust $F\frac{\theta}{\delta}$ (lbs)	Corrected Torque $T\frac{\theta}{\delta}$ (ft-lbs)	Lift Improvement (lbs)	Configuration and Remarks
71	20.38	50	Aft	94.97	42.63	-6.06	
72	22.88	60	Aft	95.40	42.10	-5.63	
73	15.125	30	Aft	91.70	41.59	-9.33	
74	16.38	40	Aft	91.52	41.75	-9.51	
75	27.88	60	Aft	101.25	42.19	+0.22	Runs 75 to 78 were done on a very rainy day. Run 75 is a repeat of run 67
76	27.88	60	Aft	99.85	42.74	-1.18	Blockage is shown in Figure 89d
77	27.88	60	Aft	99.20	42.03	-1.83	Blockage is shown in Figure 89d
78	27.88	60	Aft	98.05	41.99	-2.98	Blockage is shown in Figure 89d was attained with cardboard on the forward side and tape from the rear side to the wing
79	27.88	60	Aft	95.49	42.01	-5.54	Run 79 is a repeat of run 78 on another day with the tape on the rear side backed up with cardboard
80	27.88	60	Aft	92.47	41.54	-8.56	Blockage is shown in Figure 89d
81	27.88	60	Aft	93.20	42.30	-7.83	Runs 81, 82 and 83 are repeats of run 67
82	27.88	60	Aft	98.83	42.50	-2.20	
83	27.88	60	Aft	96.67	42.36	-4.36	
84	30.25	60	Far Aft	97.54	42.32	-3.49	On runs 84 and 85, part of the flow on the fan side of the scoop comes around the motor supports
85	28.75	50	Far Aft	98.51	42.25	-2.52	
86	27.06	40	Far Aft	96.80	42.20	-4.23	
87	23.75	50	Far Aft	93.59	42.03	-7.44	
88	25.25	60	Far Aft	93.70	41.76	-7.33	
89	22.06	40	Far Aft	94.62	42.11	-6.41	
90	19.56	40	Far Aft	92.65	41.69	-8.38	
91	0.0	0	See Remarks	98.30	42.30	-2.73	Runs 91 and 92 are repeats of run 63
92	0.0	0	See Remarks	100.33	41.76	-0.70	Runs 91 and 92 are repeats of run 63
93	27.06	40	Far Aft	98.43	42.52	-2.60	Repeat of run 86
94	28.75	50	Far Aft	98.72	42.73	-2.31	Run 94 is a repeat of run 85. Probing with a tuft was done observing the turbulence shown in Figure 100
95	27.06	40	Far Aft	99.16	42.54	-1.87	The turbulence was in a slightly different place from run 94
96	27.06	40	Far Aft	98.54	42.57	-2.49	The edge radius of the leading edge region of the scoop was increased to 0.75 inch
97	27.88	60	Aft	99.34	43.11	-1.69	Repeat of run 67

TABLE VIII (Continued)

SUMMARY OF STATIC TESTING

Run	Scoop Height (in)	Scoop Angle (deg)	Scoop Position	Corrected Thrust $F\frac{\theta}{\delta}$ (lbs)	Corrected Torque $T\frac{\theta}{\delta}$ (ft-lbs)	Lift Improvement (lbs)	Configuration and Remarks
162	27.0	55.22	Middle	99.56	41.40	- 1.47	Final scoop with lower holes open, no cross flow, and louvers positioned at 0°
163	14.75	38.19	Middle	96.32	40.71	- 4.71	Final scoop with lower holes open, no cross flow, and louvers positioned at 0°
164	6.625	19.46	Middle	80.56	37.81	-20.47	Final scoop with lower holes open, no cross flow, and louvers positioned at 0°
165	6.625	19.46	Middle	89.03	39.74	-12.00	Final scoop with all holes open, no cross flow, and louvers positioned at 0°
166	14.75	38.19	Middle	98.03	41.39	- 3.00	Final scoop with all holes open, no cross flow, and louvers positioned at 0°
167	27.0	55.22	Middle	99.61	41.25	- 1.42	Final scoop with all holes open, no cross flow, and louvers positioned at 0°
168	0.0	90.00	90°	100.60	41.35	- 0.43	Scoop tapped to 2 x 4 braces
169	0.0	0.0	No Scoop	101.51	41.24	-	No Scoop
170	0.0	0.0	No Scoop	100.54	41.01	-	No Scoop

TABLE IX

SUMMARY OF LOW CROSS FLOW TESTING

Run	Scoop Height (in)	Scoop Angle (deg)	Scoop Position	Corrected Lift $L\frac{\theta}{\delta}$ (lb)	Corrected Thrust $F\frac{\theta}{\delta}$ (lb)	Corrected Torque $T\frac{\theta}{\delta}$ (in-lb)	Lift Improvement (lb)	Thrust Improvement (lb)	Configuration and Remarks
139	15.69	40	Middle	66.86	15.82	42.71	- 3.66	- 6.73	Basic scoop
140	13.19	40	Middle	65.56	16.97	42.56	- 4.96	- 5.58	Basic scoop
141	13.0	30	Middle	69.00	18.08	42.02	- 1.52	- 4.47	Basic scoop
142	15.125	30	Aft	69.81	19.75	42.46	- .71	- 2.80	Basic scoop
143	16.38	40	Aft	69.15	19.76	42.11	- 1.37	- 2.79	Basic scoop
144	20.375	50	Aft	69.15	19.26	42.35	- 1.37	- 3.29	Basic scoop
145	23.75	50	Far Aft	70.51	17.53	42.47	- .01	- 5.02	Basic scoop
146	30.25	60	Far Aft	70.65	18.06	42.67	.13	- 4.49	Basic scoop
147	30.25	60	Far Aft	72.78	17.16	42.41	2.26	- 5.39	"B" Configuration
148	23.75	50	Far Aft	68.62	18.00	42.64	- 1.90	- 4.55	"B" Configuration
149	16.375	40	Aft	68.65	18.87	42.47	- 1.87	- 3.68	"B" Configuration
150	15.125	30	Aft	68.58	18.28	42.49	- 1.92	- 4.27	"B" Configuration
151	20.375	50	Aft	69.39	17.22	41.70	- 1.13	- 5.33	"B" Configuration
152	20.375	50	Aft	68.20	16.55	41.51	- 2.32	- 6.00	"D" Configuration
153	30.27	60	Far Aft	69.23	14.78	41.78	- 1.29	- 7.77	"D" Configuration
154	13.19	40	Middle	65.73	13.25	42.17	- 4.79	- 9.30	"D" Configuration
155	13.0	30	Middle	66.85	15.1	42.74	- 3.67	- 7.45	"D" Configuration
156	13.0	30	Middle	51.44	4.58	40.11	-19.08	-17.97	"D" plus side curtains
157	0	0	No Scoop	71.11	22.34	42.72	-	-	No scoop
158	0	0	No Scoop	69.92	22.76	42.74	-	-	No scoop
159	27.0	55.22	Middle	69.96	18.27	42.42	- 0.56	- 4.28	Final scoop with holes covered
160	14.75	38.19	Middle	68.37	18.79	42.53	- 2.15	- 3.76	Final scoop with holes covered
161	6.625	19.46	Middle	44.95	2.61	36.06	-25.57	-19.94	Final scoop with holes covered

TABLE X

SUMMARY OF HIGH CROSS FLOW TESTING

Run	Scoop Height (in)	Scoop Angle (deg)	Scoop Position	Corrected Lift $L\frac{\theta}{\delta}$ (lb)	Corrected Thrust $F\frac{\partial}{\delta}$ (lb)	Corrected Torque $T\frac{\theta}{\delta}$ (lb)	Lift Improvement (lb)	Thrust Improvement (lb)	Configuration and Remarks
99	20.375	50	Aft	68.65	3.51	40.36	2.47	- 2.08	Runs 99 through 110 were done with the basic scoop to obtain an optimum position.
100	16.375	40	Aft	69.57	0.298	40.14	3.39	- 5.30	
101	15.125	30	Aft	67.92	1.59	40.05	1.74	- 4.00	
102	23.75	50	Far Aft	70.39	1.69	39.68	4.21	- 3.90	
103	30.25	60	Far Aft	68.14	2.69	39.97	1.96	- 2.90	The leading edge of the scoop was out of the cross flow stream.
104	15.69	40	Middle	68.29	1.40	40.05	2.11	- 4.19	
105	13.19	40	Middle	70.40	0.20	38.84	4.22	- 5.39	
106	13.0	30	Middle	67.83	2.00	39.46	1.65	- 3.59	
107	10.25	20	Middle	66.43	-2.50	39.38	0.25	- 8.085	
108	9.69	10	Middle	63.40	-3.20	39.36	-2.79	- 8.79	
109	9.63	20	Forward	66.23	-0.70	40.03	0.05	- 6.29	
110	7.19	10	Forward	60.93	-4.99	38.78	-5.26	-10.58	
111				70.72	63.58	40.84			Scoop off static test to check load cell accuracy. Temperature measurement error.
112				69.93	63.34	40.55			Temperature measurement error. Static test with scoop reversed to show effect of scoop supports.
113				75.22	67.67	42.69			Rerun of 112. Trouble with the load cell readout was noted.
114				66.81	5.34	40.84	0.63	- 0.25	Setup of 112, but in cross flow.
115				65.56	5.83	40.79	-0.63	0.25	No scoop in cross flow.
116	20,375	50	Aft	67.53	5.64	40.86	1.35	0.06	It was noticed that the fan windmilled with the scoop in place, but not in the previous runs without the scoop. This was a recheck of 100.
117	30.25	60	Far Aft	63.90	3.57	40.87	2.29	- 2.02	Recheck of 103.
118	13.0	30	Middle	60.61	1.38	40.54	-5.58	- 4.21	Recheck of 106.
119	20.375	50	Aft	71.08	1.59	41.08	4.90	- 4.00	"D" configuration, the fan seemed to windmil faster than with the slot open as in run 116. The LE of the scoop is 1 inch outside the air stream.
120	20.375	50	Aft	68.37	2.09	41.05	2.19	- 3.50	Repeat of 119.
121	20.375	50	Aft	66.23	0.60	40.33	0.05	- 4.99	Side curtains were used. Increased windmilling speed was noticed relative to runs 116 and 119.
122	20.375	50	Aft	67.36	2.00	41.04	1.18	- 3.59	Repeat of 119.
123	20.375	50	Aft	67.99	3.02	40.74	1.81	- 2.57	"B" configuration.
124	20.375	50	Aft	68.28	3.61	40.89	2.10	- 1.98	Repeat of 116.

TABLE X (Continued)

SUMMARY OF HIGH CROSS FLOW TESTING

Run	Scoop Height (in)	Scoop Angle (deg)	Scoop Position	Corrected Lift $L\frac{\theta}{\delta}$ (lb)	Corrected Thrust $F\frac{\theta}{\delta}$ (lb)	Corrected Torque $T\frac{\theta}{\delta}$ (lb)	Lift Improvement (lb)	Thrust Improvement (lb)	Configuration and Remarks
125	30.25	60	Far Aft	64.20	1.25	41.70	- 1.99	- 4.34	"D" configuration.
126	13.19	40	Middle	68.23	-1.67	40.96	2.05	- 7.26	"D" configuration.
127	13.0	30	Middle	70.11	-0.42	40.94	3.93	- 6.001	"D" configuration.
128	14.5	30	Forward	67.70	0.21	41.00	1.52	- 5.38	Basic scoop.
129	14.625	30	Forward	67.36	0.53	41.11	1.18	- 5.06	Basic scoop.
130	14.69	10	Forward	65.77	1.89	41.04	0.42	- 3.70	Basic scoop.
131	14.625	0	Forward	64.25	0.42	40.55	- 1.94	- 5.17	Basic scoop.
132	14.375	40	Forward	69.38	1.27	41.33	3.20	- 4.32	Basic scoop
133	13.75	50	Forward	71.49	4.96	41.65	5.31	- 0.63	Basic scoop. The tip of the scoop was out of the cross flow stream.
134	14.06	50/40	Forward	72.16	2.11	41.53	5.98	- 3.48	Runs 134 to 138 were an experiment to get better incidence on retreating side. The top side of the scoop was held at 50° while the lower half of the scoop was set at a lower angle.
135	14.13	50/30	Forward	69.02	2.54	41.10	2.84	- 3.05	
136	14.19	50/20	Forward	69.76	1.16	41.27	3.58	- 4.43	
137	14.22	50/10	Forward	67.11	0.63	41.01	0.93	- 4.96	
138	14.19	50/0	Forward	66.33	0.42	40.91	0.15	- 5.17	

TABLE XI

DESIGN POINT DATA FOR THE LFX LIFT FAN

Streamline	Tip	Pitch	Hub
Station 0 - Rotor Inlet			
Radius - inches	28.290	22.053	13.449
C_Z - ft/sec	480.449	586.256	500.832
U - ft/sec	949.027	739.778	451.147
β_{REL} - degrees	63.149	51.604	42.012
M_{REL}	0.982	0.871	0.660
Station 1 - Rotor Exit			
Radius - inches	27.419	21.986	14.520
C_Z - ft/sec	556.538	559.103	557.210
U - ft/sec	919.796	737.532	487.095
β_{REL} - degrees	49.476	36.724	1.377
M_{REL}	0.776	0.623	0.521
Station 2 - Stator Inlet			
Radius - inches	27.289	21.966	14.650
C_Z - ft/sec	595.107	570.553	569.040
β_{REL} - degrees	24.404	29.340	39.526
M_{REL}	0.599	0.586	0.681
Station 3 - Stator Exit			
Radius - inches	27.100	21.840	14.791
C_Z - ft/sec	597.338	575.573	615.372
β_{REL} - degrees	-0-	-0-	-0-
M_{REL}	0.530	0.513	0.550

Symbols

C_Z - Axial velocity

U - Wheel speed

M_{REL} - Relative Mach number

β_{REL} - Relative air angle

TABLE XII
CONCEPTUAL FAN DESIGN SIZING AND PERFORMANCE DATA

	Large IGV Fan	Large Conventional Fan	Small IGV Fan	Small Conventional Fan	Small Statorless Fan
Core Engine Discharge Pressure - $P_{5.1}$, psia	64.2	64.2	53.5	53.5	53.5
Core Engine Discharge Temperature - $T_{5.1}$, °R	2073	2073	1907	1907	1907
Core Engine Discharge Flow - $W_{5.1}$, lb/sec	104.4	104.4	61.8	61.8	61.8
System Lift - lbs	26,000	26,000	13,650	13,650	13,650
Fan Lift - lbs	22,400	22,330	11,550	11,750	11,900
Turbine Lift - lbs	3600	3670	2100	1900	1750
Fan Pressure Ratio	1.26	1.28	1.21	1.22	1.175
Fan Airflow - W_{10}, lb/sec	1160	1149	670	685	750
Fan Tip Speed - V_{TIP}, ft/sec	1000	1025	960	900	1000
Fan Efficiency - η_F, percent	81	86	82	87	73
Fan Inlet Loss - ω_{10}, percent	5	10	6	10	10
Fan Exit Loss - ω_{13}, percent	5	5	5	5	5
Fan Nozzle Thrust Coefficient	.985	.985	.986	.985	.985
Inter-turbine Pressure Loss - percent	10.5	9.10	9.5	8.5	8.0
Turbine Efficiency - η_T, percent	83	83.4	83	83.6	83
Turbine Exit Loss - ω_{55}, percent	5	5	5	5	5
Turbine Nozzle Thrust Coefficient	.990	.99	.990	.99	.990
Scroll Mach Number - M_{Scroll}	.40	.35	.38	.325	.30
Fan Inlet Mach Number - M_{10}	.51	.60	.53	.60	.44
Turbine Exit Mach Number - M_{55}	.56	.60	.60	.70	.50

TABLE XII (Continued)

CONCEPTUAL FAN DESIGN SIZING AND PERFORMANCE DATA

	Large IGV Fan	Large Conventional Fan	Small IGV Fan	Small Conventional Fan	Small Statorless Fan
Turbine Diffusion	No	No	No	Yes	No
Fan Radius Ratio - R_{HUB}/R_{TIP}	.45	.412	.44	.42	.57
Fan Tip Diameter - D_{FT}, inches	86.5	80.17	64.6	62.16	79.6
Fan Root Diameter - D_{FR}, inches	38.9	33.03	28.4	26.14	45.4
Turbine Root Diameter - D_{TR}, inches	89.3	83.0	67.9	65.3	83.1
Turbine Tip Diameter - D_{TT}, inches	93.2	86.8	73.2	70.60	88.4
Fan Weight - lbs	1178	1235	604	635	738
Fan Lift/Weight	22.1	21.1	22.6	21.5	18.5
Scroll Admission Arc - degrees	360	360	180	180	180

TABLE XIII

WEIGHT SUMMARY

	Large Inlet Guide Vane Fan	Large Conventional Fan	Small Inlet Guide Vane Fan	Small Conventional Fan	Statorless Fan
Rotor	346	312	192	175	253
Front Frame	383.5	247	179	142.5	202.5
Scroll	229	226	104	99	120.5
Rear Frame	--	243	--	103.5	--
Exit Louvers	219.5	207	129	113	162
Total	1178	1235	604	635	738
Lift	26,000	26,000	13,650	13,650	13,650
Lift/Weight Ratio	22.1	21.1	22.6	21.5	18.5

TABLE XIV

BEARING LOAD TABLE

Maneuver	Condition	Percent Rotor Speed	Percent Time	Load Factor (g's)				Moments	
				Vertical	Horizontal		Combined Horizontal	Percent Cross-flow Moment	Gyroscopic Precession (Rad/Sec)
					Fore/Aft	Side			
Idle	Standing	70	30	0.5	0	0.5	0.5	25	0
	Taxi	100	$\frac{10}{40}$	0.5	1.5	1.5	2.12	50	0.1
Hover	Normal	100	40	3	0.5	0.5	0.707	50	0
Transition	Normal	110	19.95	1	1	1	1.414	100	0.1
	Intermittant	115	$\frac{0.05}{20}$	1	1	1	1.414	100	1
Jet Mode	Static	0	50	10	4	4	5.66	0	0
	Oscillatory	3	50	10	4	4	5.66	0	0

TABLE XV

LARGE INLET GUIDE VANE BLADE GEOMETRIES

	Turbine Buckets	Fan Rotor Blades			Fan Inlet Guide Vanes		
	Pitch	Hub	Pitch	Tip	Hub	Pitch	Tip
Solidity	1.8	1.92	1.21	0.89	2.18	1.11	0.75
Aspect Ratio	3.1	--	3.9	--	--	3.9	--
Length - inches	2.35	--	23.3	--	--	29.4	--
Chord - inches	0.75	6.0	6.0	6.0	7.5	7.5	7.5
Diameter - inches	91.9	39.9	63.2	86.5	30.6	60.0	89.4
Number	680	--	40	--	--	28	--
Orientation Angle - degrees	--	41	49	61	22	18	28
Tm/C - percent	--	7.0	6.5	6.0	6	6	6
Camber - degrees	--	22	12	23	41	40	67
M_{REL} Inlet	--	1.14	1.29	1.30	0.51	0.51	0.51

TABLE XVI

LARGE CONVENTIONAL FAN BLADE GEOMETRIES

	Turbine Buckets	Fan Rotor Blades			Fan Stator Blades		
	Pitch	Hub	Pitch	Tip	Hub	Pitch	Tip
Solidity	1.8	1.80	1.162	0.900	1.58	1.0	0.733
Aspect Ratio	2.17	--	5.478	--	--	6.69	--
Length - inches	1.90	--	23.57	--	--	21	--
Chord - inches	0.876	3.891	4.3025	4.714	--	3.14	--
Pitch - inches	0.486	21.62	3.704	5.247	1.96	3.14	4.35
Diameter - inches	85.51	33.03	56.6	80.17	--	--	--
Number	552	--	48	--	--	56	--
Stagger Angle - degrees	--	13.8	37.8	52.8	13.6	12	11.7
Tm/C (maximum) - degrees	0.15	0.07	0.06	0.05	0.08	0.08	0.08
Camber - degrees	--	42	20.7	17.7	41	35	37
M_{REL} Inlet	--	0.64	0.875	1.06	--	--	--

TABLE XVII

SMALL INLET GUIDE VANE BLADE GEOMETRIES

	Turbine Buckets	Fan Rotor Blades			Fan Inlet Guide Vanes		
	Pitch	Hub	Pitch	Tip	Hub	Pitch	Tip
Solidity	1.8	1.61	1.07	0.84	1.87	1.10	0.77
Aspect Ratio	2.1	--	5.5	--	4.6 to 20*		
Length - inches	2.5	--	18.2	--	--	20	--
Chord - inches	1.2	3.1	3.4	3.7	1.0 to 4.3		
Pitch (spacing) - inches	0.67	1.9	3.2	4.4	Varies		
Diameter - inches	73.2	28.2	46.4	64.6	Varies		
Number	322	--	46	--	--	122	--
Orientation Angle - degrees	--	40	49	61	21	16	23
Tm/C - percent	--	4.3	3.3	2.3	6	6	6
Camber - degrees	--	19	7	18	39	33	55
M_{REL} Inlet	--	1.04	1.22	1.20	0.53	0.53	0.53

* There are four sets of inlet guide vanes used, varying in chord from 1.0 to 4.3 inches.

TABLE XVIII

SMALL CONVENTIONAL FAN BLADE GEOMETRIES

	Turbine Buckets	Fan Rotor Blades			Fan Stator Blades		
	Pitch	Hub	Pitch	Tip	Hub	Pitch	Tip
Solidity	1.80	1.54	1.088	0.90	1.56	0.984	0.716
Aspect Ratio	3.083	--	7.16	--	--	10.87	--
Length - inches	2.629	--	18.01	--	--	16.3	--
Chord - inches	0.8527	2.10	2.51	2.93	1.5	1.5	1.5
Pitch - inches	0.474	1.37	2.31	3.26	1.152	1.623	2.094
Diameter - inches	67.892	26.14	44.15	62.16	27.4	43.7	60
Number	450	--	60	--	--	90	--
Orientation Angle - degrees	--	12.9	35.1	49.6	12.3	11.3	12.1
Tm/C - percent	0.20	0.07	0.06	0.05	0.08	0.08	0.08
Camber - degrees	--	38.8	23.2	20.3	37.3	34.3	36.4
M_{REL} Inlet	--	0.610	0.788	0.937	--	--	--

TABLE XIX

RUNS MADE FOR FAN CYCLE OPTIMIZATION STUDIES
FOR THE SMALL CONVENTIONAL FAN

Run	FPR	V_{TIP}	M_{Scroll}	M_{10}	$M_{5.5}$	Turbine Diffu-sion
1	1.20	877	0.30	0.500	0.500	No
2		900				
3		950				
4		1000				
5		1025				
6		1050				
7	1.25	877	0.30	0.500	0.500	No
8		900				
9		950				
10		1000				
11		1025				
12		1050				
13		1100				
14	1.28	877	0.30	0.500	0.500	No
15		900				
16		950				
17		1000				
18		1025				
19		1050				
20		1100				
21	1.30	877	0.30	0.500	0.500	No
22		900				
23		950				
24		1000				
25		1025				
26		1050				
27		1100				
28	1.25	947	0.2	0.50	0.50	No
29			0.3			
30			0.4			
31			0.5			
32	1.25	947	0.3	0.45	0.50	No
33				0.50		
34				0.53		
35				0.55		
36				0.71		
37	1.25	947	0.3	0.50	0.40	No
38					0.45	
39					0.50	
40					0.55	
41					0.60	
42					0.65	
43					0.70	
44					0.75	
45	1.25	947	0.3	0.50	0.40	Yes
46					0.45	
47					0.50	
48					0.55	
49					0.60	
50					0.65	
51					0.70	
52					0.75	

TABLE XX

COMPARISON OF CYCLE PARAMETERS FOR THE SMALL CONVENTIONAL FAN

Cycle Parameter	Initial Value	Final Value
Fan pressure ratio, FPR	1.25	1.223
Fan tip speed, V_{TIP}	947	900
Scroll Mach number, M_S	0.30	0.325
Fan inlet Mach number, M_{10}	0.50	0.60
Turbine discharge Mach number, $M_{5.5}$	0.50	0.70
Turbine discharge diffusion	No	Yes

TABLE XXI

RESULTS OF THE CYCLE SELECTION STUDY
FOR THE SMALL CONVENTIONAL FAN

	Initial Value	Final Value
Total fan lift, pounds	13,650	13,650
Total fan weight, pounds	714	620
Total fan area, square inches	5708	5301
Lift/weight ratio	19.1	22
Lift/area ratio	2.39	2.57
Decrease in weight, percent	-	13.2
Decrease in area, percent	-	7.1

APPENDIX A

REQUIRED ENGINE LIFT TO WEIGHT RATIO CALCULATION

The overall system lift to weight ratio can be expressed as a function of fan lift/weight, engine thrust/weight, augmentation ratio and engine sfc.

$$\text{System Weight/Lift} = \frac{\text{Fan}_{\text{Weight}} + \text{Engine}_{\text{Weight}} + \text{Fuel}_{\text{Weight}}}{\text{Fan}_{\text{Lift}}}$$

$$= \frac{\text{Fan}_{\text{Weight}}}{\text{Fan}_{\text{Lift}}} + \frac{\text{Engine}_{\text{Weight}}}{\text{Engine}_{\text{Thrust}}\ (\text{Augmentation Ratio})} +$$

$$\frac{\text{SFC (Minutes)}}{\text{Augmentation Ratio (60)}}$$

This expression can be solved for engine weight to thrust ratio:

$$\frac{\text{Engine}_{\text{Weight}}}{\text{Engine}_{\text{Thrust}}} = \text{Augmentation Ratio} \left(\frac{\text{System Weight}}{\text{Lift}}\right) -$$

$$\text{Augmentation Ratio} \left(\frac{\text{Fan}_{\text{Weight}}}{\text{Fan}_{\text{Lift}}}\right) - \text{SFC} \left(\frac{\text{Minutes}}{60}\right)$$

The relative merits of various engines as power sources for the lift fan can be estimated by this method using the parametric fan performance results. This method is useful for optimizing engine and fan cycles for a system where the engine is used in lift mode only, in a XV-5A type configuration other requirements like cruise thrust and SFC may set the engine design point.

DIFFUSION TURBINE DESIGN REQUIREMENTS

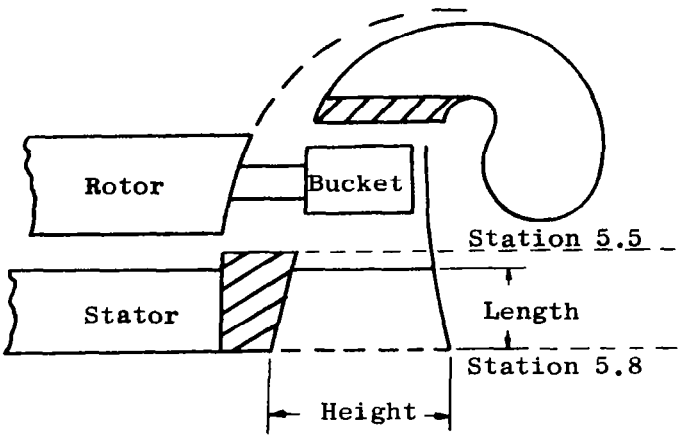

The following assumptions were made in the diffusion turbine design (refer to sketch above).

1. Diffuser static pressure rise coefficient.

$$\frac{P_{s5.8} - P_{s5.5}}{P_{t5.5} - P_{s5.5}} = 0.3$$

2. Impulse bucket design.

3. $P_{s5.8}$ = Ambient.

4. Diffuser loss coefficient.

$$= \frac{P_{t5.5} - P_{t5.8}}{P_{t5.5} - P_{s5.5}} = 0.05$$

5. Diffuser length/height = 1.0.

6. All other turbine calculations and assumptions are the same as for conventional tip turbine designs.

RADIAL INFLOW TURBINE

Table I lists the assumptions used in calculations of the bucket geometries for the radial inflow turbine. Two designs were investigated: (1) a bucket developed from a conical surface, (2) a conventional bucket with an exhaust hood.

Figure 184 shows the side view of the scroll, bucket and fan blade for the conical bucket design. Figure 185 shows the top, side and bottom views of the conical buckets. Figures 186 and 187 are sketches showing how the bucket was developed from the conical surface. The derivation of the surface equation follows using symbols identified in Figures 186 and 187. Figure 188 is a side view of the conventional type bucket with an exhaust hood.

TABLE I

LIFT FAN RADIAL INFLOW TURBINE DESIGN DATA

Turbine tip diameter, in	68.80
Turbine pitch diameter, in	66.80
Turbine root diameter	64.80
Nozzle height, in	2.00
Inlet pressure, psia	49.22
Inlet temperature, $^{\circ}R$	1907
Gas flow, lb/sec	67.32
Discharge pressure, psia	14.97
Turbine pressure ratio	3.290
Nozzle efficiency	.960
Nozzle exit angle, (to tangential), deg:min	18:42
Nozzle exit velocity, ft/sec	2545
Bucket blade velocity, ft/sec	1028
Bucket inlet relative velocity, ft/sec	1605
Bucket inlet angle, β_1, deg:min	30:32
Bucket efficiency	.960
Bucket exit relative velocity, ft/sec	1556
Bucket exit angle, β_2, deg:min	31:55
Exit absolute velocity, ft/sec	872
Exit swirl angle (backward) deg:min	19:35
Turbine shaft output, Btu/lb	103.0
Turbine shaft efficiency	.770
Turbine total efficiency	.850
Admission arc, deg	360

Equations for Conical Blade Surface

Assume a conical surface with vertex at the origin and axis of the cone on the 'μ' axis. Then the equation of the conical surface is:

$$X_1^2 + Z_1^2 = P^2 Y_1^2$$

where the subscript (1) refers to the axis before rotation.

Rotate the cone about the 'x' axis through the angle ϕ in the position 'z' direction. Then rotate the cone about the 'z' axis through the angle θ in the positive 'x' direction.

This rotation of axis gives:

$$X = X_1 \cos\theta + Y_1 \sin\theta \cos\phi - Z_1 \sin\theta \sin\phi$$

$$Y = -X_1 \sin\theta + Y_1 \cos\theta \cos\phi - Z_1 \cos\theta \sin\phi$$

$$Z = Y_1 \sin\phi + Z_1 \cos\phi$$

Assume $\phi = 39^\circ\text{-}3'$

$\theta = 37^\circ\text{-}30'$

Then $X = 0.7933X_1 + 0.4725Y_1 - 0.3835Z_1$

$Y = -0.6087X_1 + 0.6160Y_1 - 0.4995Z_1$

$Z = 0.6300Y_1 + 0.7766Z_1$

Or $X_1 = 0.7933X - 0.6087Y$

$Y_1 = 0.4730X + 0.6160¢ + 0.6300Z$

$Z_1 = -0.3840X - 0.5000Y + 0.7766Z$

Substituting these in

$$X_1^2 + Z_1^2 = P^2 Y_1^2 \quad \text{with } P = 0.811$$

Gives the equation of the blade surface

$$\underline{X^2 + 0.5900Y^2 + 0.5435Z^2 - 1.533\,XY - 1.572XZ - 2.045YZ = 0}$$

INSTALLED AREA CALCULATION PROCEDURE

Installed fan area is: (Refer to sketch below.)

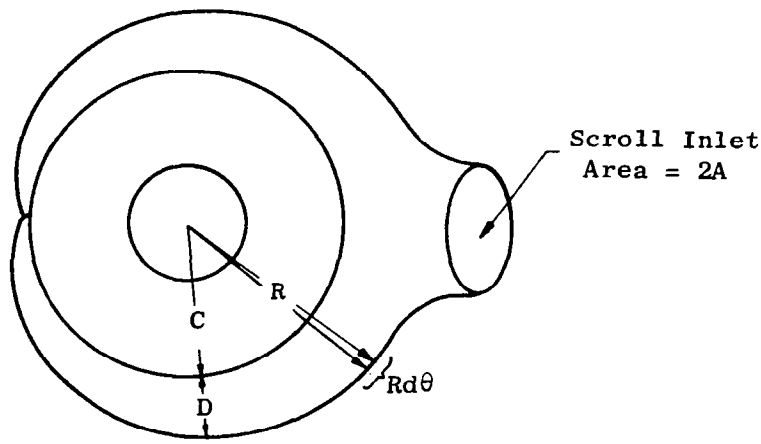

Full Admission Symmetrical Scroll

$$\text{Fan Area} = 2\int_0^{\pi} \frac{R\ (Rd\theta)}{2}$$

$$R = C + D$$

where $C = \dfrac{1.05\ D_{TT}}{2}$

$$D = \frac{\sqrt{4A}\ \sqrt{\pi-\theta}}{\pi}$$

where A is equal to one-half of the inlet duct across the sectional area. Integral becomes:

$$\int_0^{\pi} (C + D)^2\ d\theta$$

$$\int_0^{\pi} \left(C + \frac{\sqrt{4A}}{\pi}\ \sqrt{\pi-\theta}\right)^2 d\theta$$

$$\int_0^{\pi} \left[C^2 + \frac{4C\sqrt{A}}{\pi}\sqrt{\pi-\theta} + \frac{4A}{\pi^2}(\pi-\theta)\right] d\theta$$

integrating

$$\left[C^2\theta - \left[\frac{4C\sqrt{A}}{\pi}\ \frac{2}{3}\ (\pi-\theta)^{3/2}\right] + \frac{-4A}{\pi^2}\frac{(\pi-\theta)^2}{2}\right]_0^{\pi}$$

$$= C^2\pi + 4.72\ C\sqrt{A} + 2A$$

substituting for C

$$\underline{.86(D_{TT})^2 + 2.48(D_{TT})\sqrt{A} + 2A}$$

For a partial admission fan with symmetrical scroll: installed area

$$\underline{.86(D_{TT})^2 + 1.24(D_{TT})\sqrt{A} + A}$$

The procedure can be modified for asymmetrical scroll configurations, it leads to results very close to actual designs and is adequate for parametric comparisons of fan installed areas.

CIRCUMFERENTIAL FLOW DISPLACEMENT CALCULATION

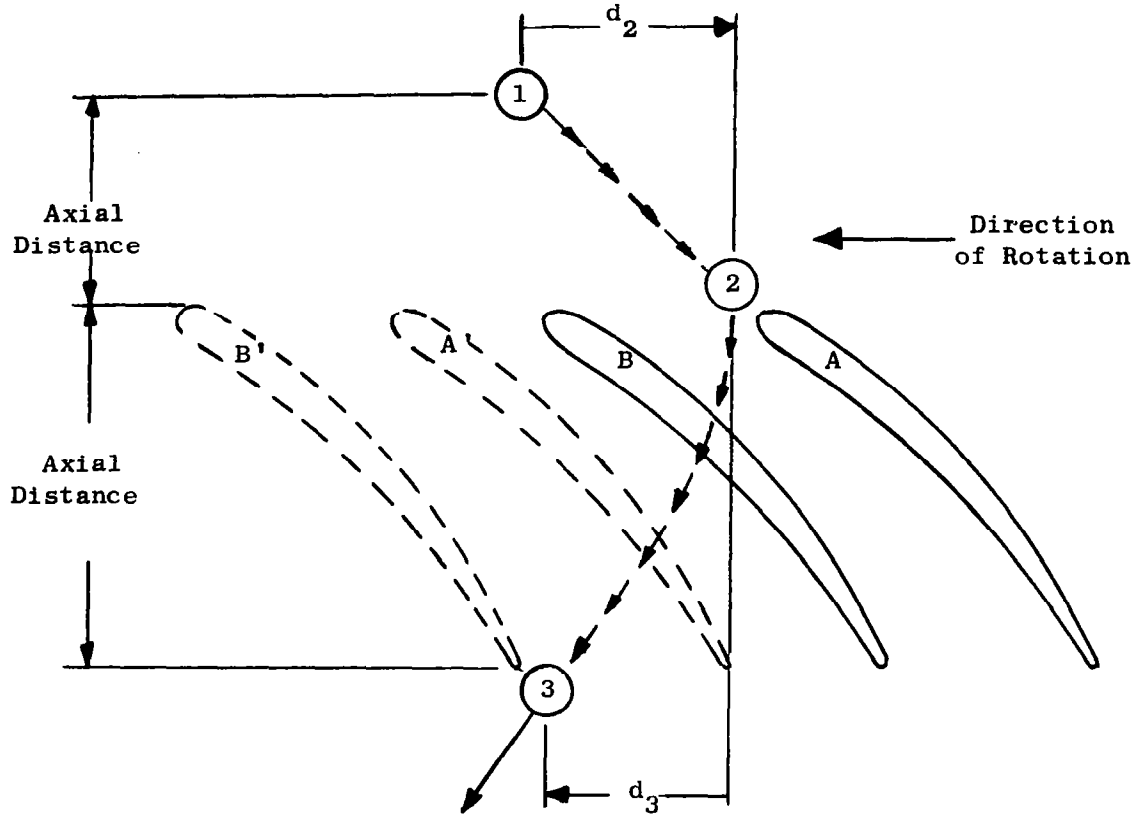

A particle or perturbation entering the blade row at (1) will exit at (3).

$$t = \frac{\text{Axial Distance}}{\bar{C}_Z}$$

where $\bar{C}_Z$ = Axial Velocity

the circumferential displacement, d

$$d_2 \simeq \frac{(V_{u1} + V_{u2})}{2} \times t$$

and $d = d_2 + d_3$

or in terms of angular displacement

$$\phi_d = \frac{d}{R} \text{ radians}$$

where R = radius

Through this sort of process the location of a distortion moving through the fan can be estimated.

SELECTION OF FAN CYCLE PARAMETERS TO MINIMIZE FAN WEIGHT AND SIZE

For a fan having constant lift, the combination of fan cycle parameters which results in a fan of minimum weight (or minimum size) will be shown to be that combination for which the derivative $\partial L/\partial WT$ (or $\partial L/\partial A$) is constant, i.e., the value of this derivative is the same for each fan cycle parameter. This is explained mathematically as follows.

The weight of the fan can be expressed as a function of the selected fan cycle parameters as

$$WT = WT\ (FPR,\ V_{TIP},\ M_S,\ M_{10},\ M_{5.5}) \tag{1}$$

where WT = fan weight
FPR = fan pressure ratio
V_{TIP} = fan tip speed
M_S = scroll Mach number
M_{10} = fan inlet Mach number
$M_{5.5}$ = turbine discharge Mach number

The above relationships may be either analytical or empirical. A necessary condition for minimum weight is that the total derivative of weight must be zero. From equation (1), the total derivative is

$$dWT = \left(\frac{\partial WT}{\partial FPR}\right) dFPR + \left(\frac{\partial WT}{\partial V_{TIP}}\right) dV_{TIP} + \left(\frac{\partial WT}{\partial M_S}\right) dM_S + \left(\frac{\partial WT}{\partial M_{10}}\right) dM_{10} + \left(\frac{\partial WT}{\partial M_{5.5}}\right) dM = 0 \tag{2}$$

This condition must be satisfied subject to the constraint that lift remain constant. The lift L can be expressed as

$$L = L\ (FPR,\ V_{TIP},\ M_S,\ M_{10},\ M_{5.5}) \tag{3}$$

Since lift is constant, the total derivative of lift is zero. From equation (3)

$$dL = \left(\frac{\partial L}{\partial M_{10}}\right) dFPR + \left(\frac{\partial L}{\partial V_{TIP}}\right) dV_{TIP} + \left(\frac{\partial L}{\partial M_S}\right) dM_s + \left(\frac{\partial L}{\partial M_{10}}\right) dM_{10} + \left(\frac{\partial L}{\partial M_{5.5}}\right) dM_{5.5} = 0 \tag{4}$$

The problem is now to find numerical values for each of the cycle parameters which will simultaneously satisfy equations (3) and (4). If equation (4) be multiplied by a constant, say, $-1/\lambda_1$, and the result added to equation (2), there obtains

$$\left(\frac{\partial WT}{\partial FPR} - \frac{1}{\lambda_1}\frac{\partial L}{\partial FPR}\right) dFPR + \left(\frac{\partial WT}{\partial V_{TIP}} - \frac{1}{\lambda_1}\frac{\partial L}{\partial V_{TIP}}\right) dV_{TIP} + \left(\frac{\partial WT}{\partial M_S} - \frac{1}{\lambda_1}\frac{\partial L}{\partial M_S}\right) dM_S$$

$$+ \left(\frac{\partial WT}{\partial M_{10}} - \frac{1}{\lambda_1}\frac{\partial L}{\partial M_{10}}\right) dM_{10} + \left(\frac{\partial WT}{\partial M_{5.5}} - \frac{1}{\lambda_1}\frac{\partial L}{\partial M_{5.5}}\right) dM_{5.5} = 0 \qquad (5)$$

Equation (5) is satisfied if all of the bracketed terms simultaneously are equal to zero. This will occur if λ_1 has the value

$$\lambda_1 = \frac{\partial L/\partial FPR}{\partial WT/\partial FPR} = \frac{\partial L/\partial V_{TIP}}{\partial WT/\partial V_{TIP}} = \frac{\partial L/\partial M_S}{\partial WT/\partial M_S} = \frac{\partial L/\partial M_{10}}{\partial WT/\partial M_{10}} = \frac{\partial L/\partial M_{5.5}}{\partial WT/\partial M_{5.5}} \qquad (6)$$

Simplifying equation (6),

$$\lambda_1 = \left(\frac{\partial L}{\partial WT}\right)_{FPR} = \left(\frac{\partial L}{\partial WT}\right)_{V_{TIP}} = \left(\frac{\partial L}{\partial WT}\right)_{M_S} = \left(\frac{\partial L}{\partial WT}\right)_{M_{10}} = \left(\frac{\partial L}{\partial WT}\right)_{M_{5.5}} \qquad (7)$$

Similarly, it can be shown that area can be minimized if

$$\lambda_1 = \left(\frac{\partial L}{\partial A}\right)_{FPR} = \left(\frac{\partial L}{\partial A}\right)_{V_{TIP}} = \left(\frac{\partial L}{\partial A}\right)_{M_S} = \left(\frac{\partial L}{\partial A}\right)_{M_{10}} = \left(\frac{\partial L}{\partial A}\right)_{M_{5.5}} \qquad (8)$$

REFERENCES

1. Simonson, Marvin R.; General Electric Company, Flight Propulsion Division, Cincinnati, Ohio: Investigation of High Gas Temperature Utilization for Advanced Tip Turbine Fans. USAAVLABS Technical Report No. 66-37, 1966.

2. Tyson, B.I.; Douglas Aircraft Company: Tests to Establish Flow Distortion Criteria for Lift Engines. AIAA Paper No. 64-608, Seattle, Washington, August 10-12, 1964.

3. Cockshutt, E.P.; Schaub, U.W.; National Research Council, Ottawa, Canada: Analytical and Experimental Studies of Normal Inlets With Special Reference to Fan In Wing VTOL Powerplants. AIAA Paper No. 64-572, Paris, France, August 1964.

4. General Electric Company, Flight Propulsion Division, Cincinnati, Ohio: Results of Wind Tunnel Tests of A Full-Scale, Wing Mounted, Tip-Turbine-Driven Lift Fan. TRECOM Technical Report No. 63-21, September 1963.

5. Switzer, J.R.; General Electric Company, Flight Propulsion Division, Cincinnati, Ohio: VTOL Wing-Fan Model Tests. General Electric Company Report No. 58AGT593, 1958.

6. Hess, P.J.; General Electric Company, Flight Propulsion Division, Cincinnati, Ohio: Aerodynamic Design of the Fan for the X353-5 VTOL Engine. General Electric Company Report No. DF59FPD517, July 1959.

7. True, Harris C.; Volk, Lawrence J.; General Electric Company, Flight Propulsion Division, Cincinnati, Ohio: Results From an Advanced Lift Fan (LFX) Systems and Preliminary Design Study (CLASSIFIED). USAAVLABS Technical Report No. 66-51, 1966.

8. Asmus, F.J.; General Electric Company, Flight Propulsion Division, Cincinnati, Ohio: Parametric and Preliminary Design Studies of High-Speed and Low-Speed Cruise Fan Propulsion Systems. USAAVLABS Technical Report No. 65-57, March 1966.

9. Jacklitch, John J. Jr.; Klapproth, John F.; Tuso, Edward R.; National Aeronautics and Space Administration, Lewis Research Center, Cleveland, Ohio: Design and Performance of a 1400 Feet/Second Tip Speed Supersonic Compressor Rotor. NASA-Lewis Report No. RME-55-A27.

10. Rainey, Gerald E.; National Aeronautics and Space Administration, Langley Field, Virginia: Preliminary Study of Some Factors Which Affect The Stall-Flutter Characteristics of Thin Wings. NASA Technical Note No. 3622.

11. Clark, Donald E.; General Electric Company, Flight Propulsion Division, Cincinnati, Ohio: Aerodynamic Design of the Eighty Inch Lift/Cruise Fan. General Electric Company Report No. R65FPD208.

12. General Electric Company, Flight Propulsion Division, Cincinnati, Ohio: Tandem Cascade Thrust Vectoring Research Program. TRECOM Technical Report No. 64-59, November 1964.

13. Przedpelski, Z.J.; General Electric Company, Flight Propulsion Division, Cincinnati, Ohio: Lift Fans for Advanced V/STOL Aircraft. CASI/AIAA Paper No. 65-708, Montreal, Canada, October 18-19, 1965.

14. General Electric Company, Flight Propulsion Division, Cincinnati, Ohio: Results of Static Tests of Full Scale Wing Mounted, Tip-Turbine-Driven Lift Fan. TRECOM Technical Report No. 62-21, March 1962.

15. Kirk, Jerry V.; Hickey, David H.; Hall, Leo P.; National Aeronautics and Space Administration, Ames Research Center, Moffett Field, California: Aerodynamic Characteristics of a Full-Scale Fan-In-Wing Model Including Results in Ground Effect With Nose-Fan Pitch Control. NASA Technical Note No. D-2368.

16. National Aeronautics and Space Administration, Ames Research Center, Moffett Field, California: Conference on V/STOL and STOL Aircraft. NASA-SP-116, April 4-5, 1966.

17. Gregory, N.; Raymer, W.G.; Love, Edna M.; National Physical Laboratory, Aerodynamics Division: The Effect of Forward Speed on the Inlet Flow Distribution and Performance of a Lifting Fan Installed in a Wing. NPL-AERO-REP-1018, June 6, 1962.

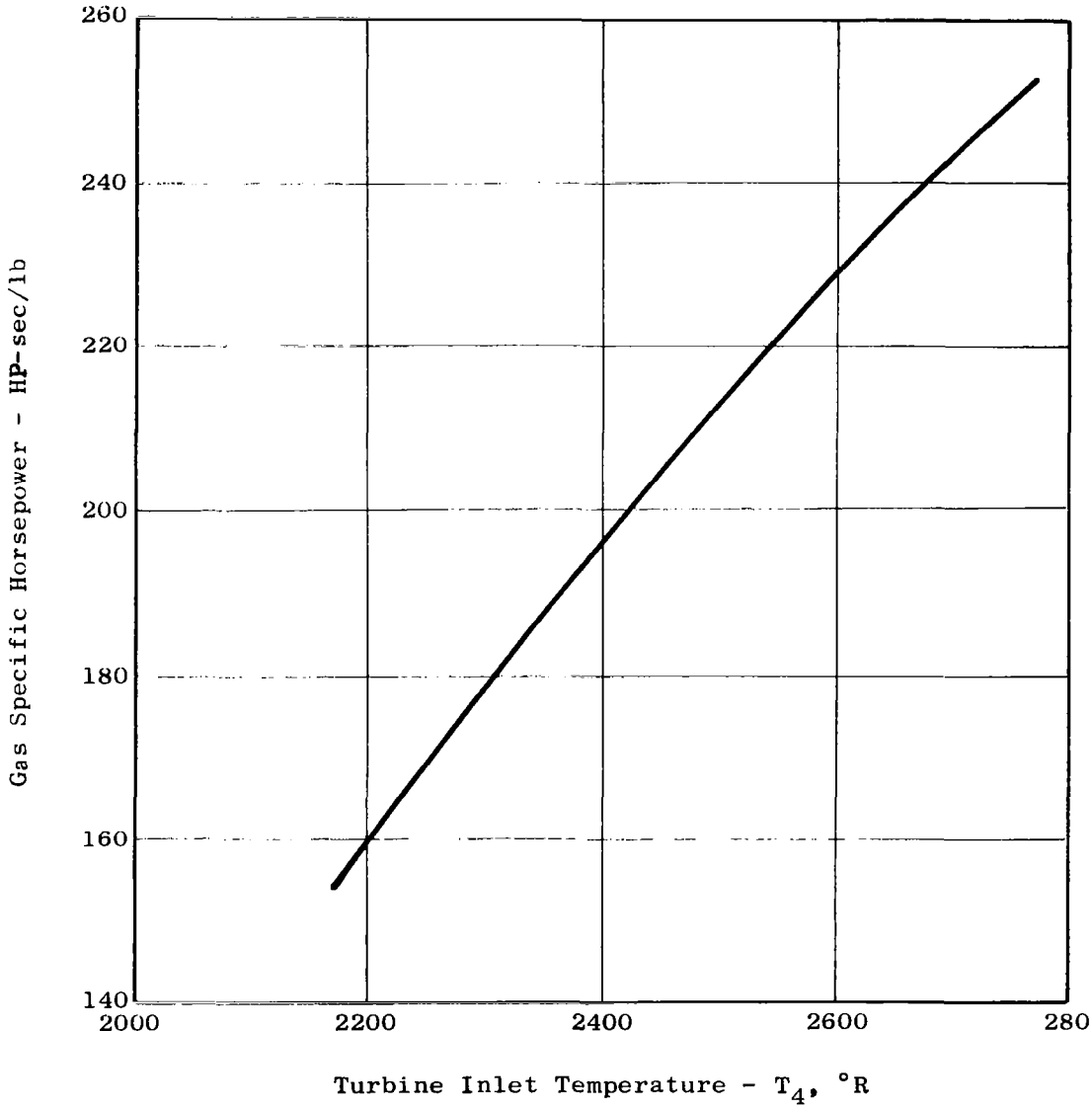

Figure 1. Gas Specific Horsepower Versus Turbine Inlet Temperature.

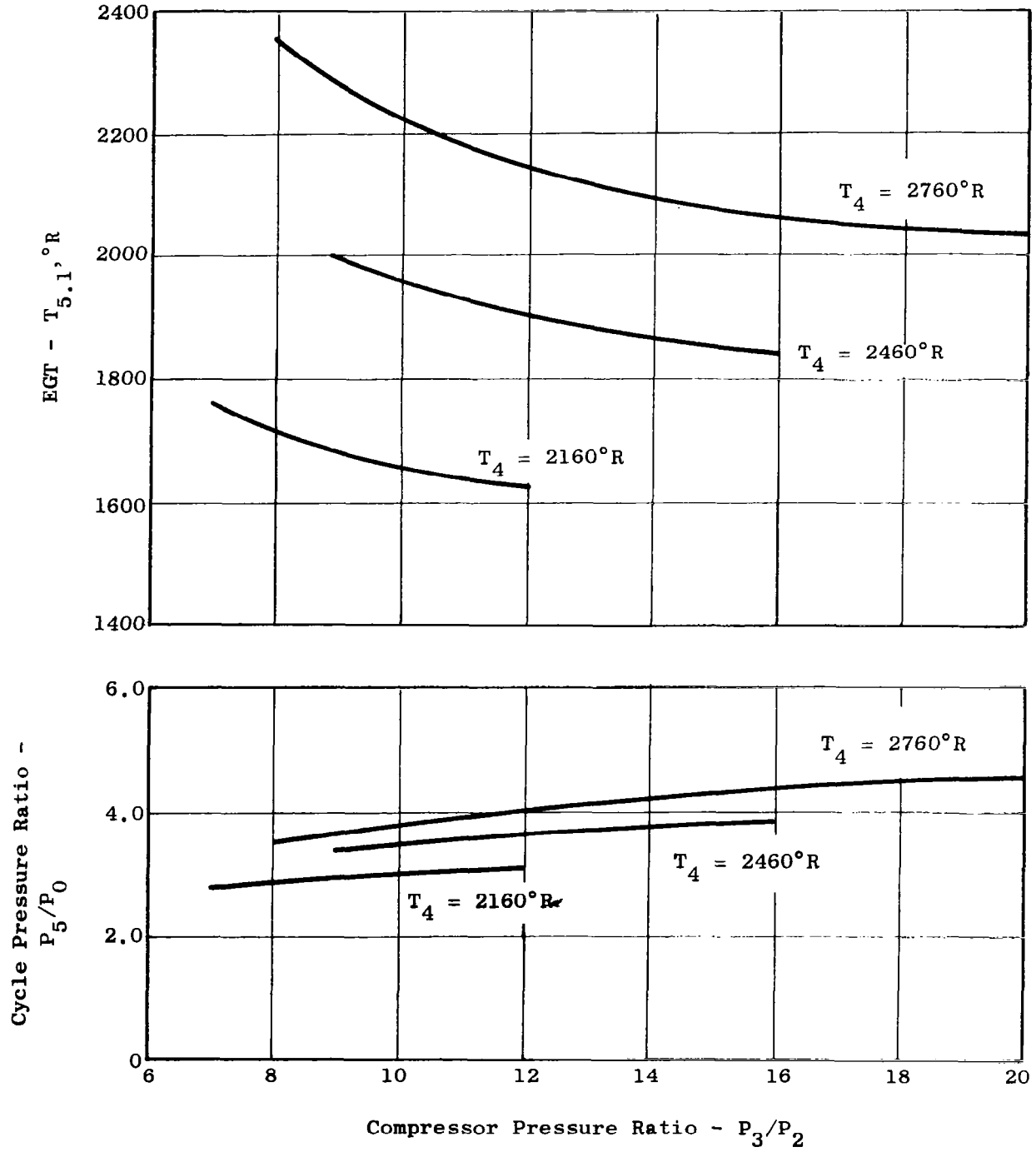

Figure 2. Gas Conditions Versus Engine Cycle Parameters.

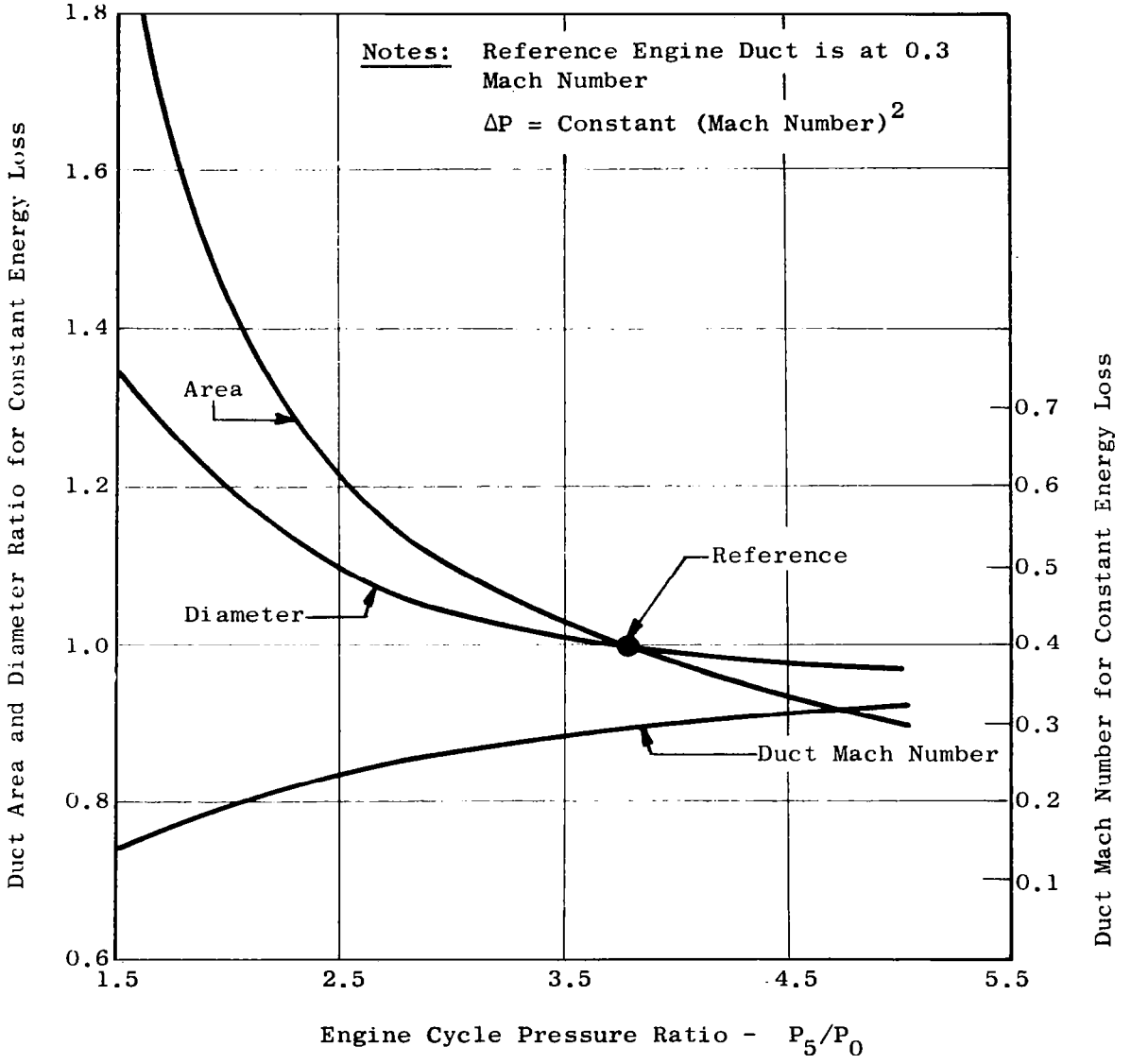

Figure 3. Duct Size Versus Engine Cycle Pressure Ratio.

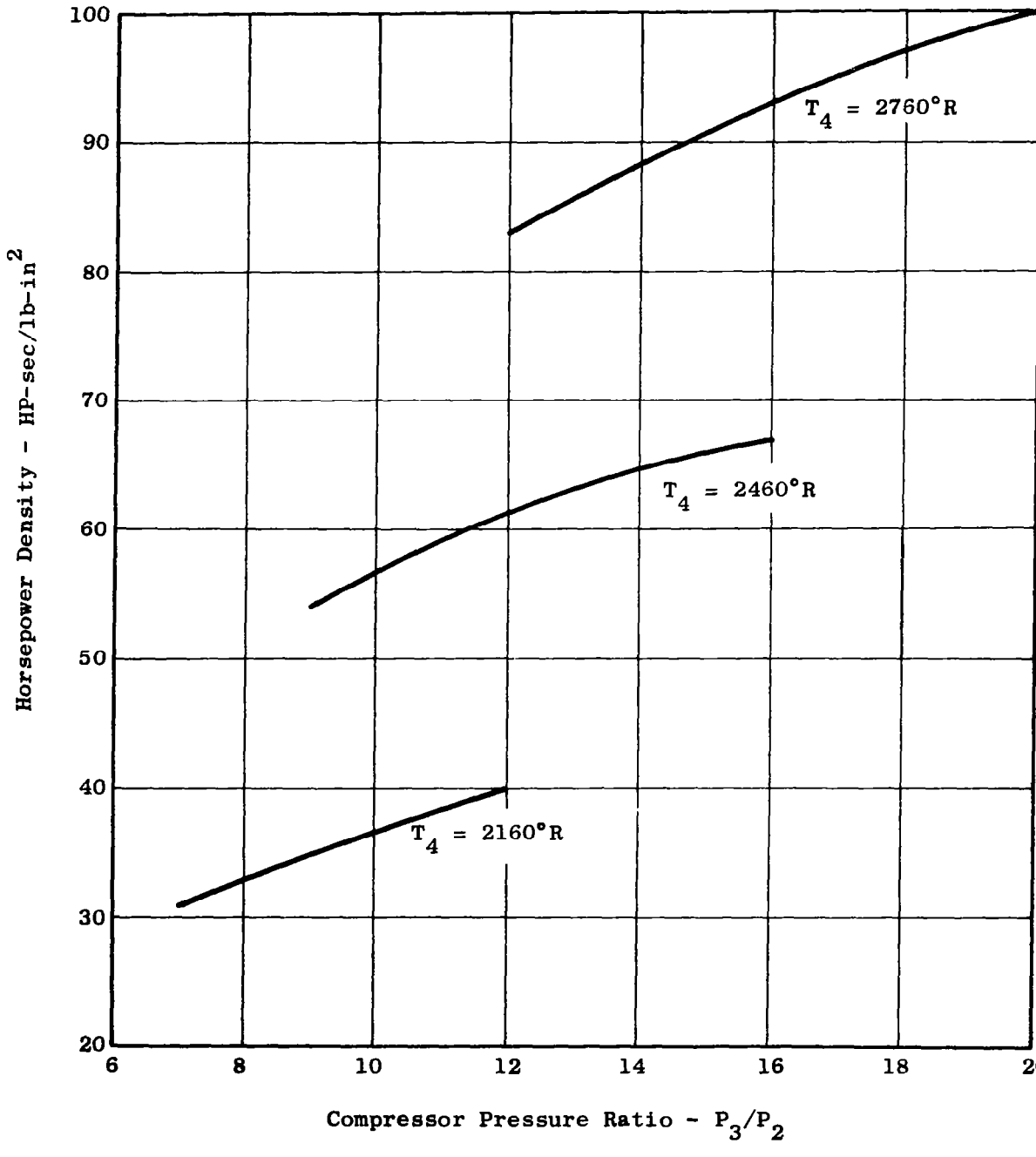

Figure 4. Horsepower Density in Ducts Versus Gas Generator Parameters.

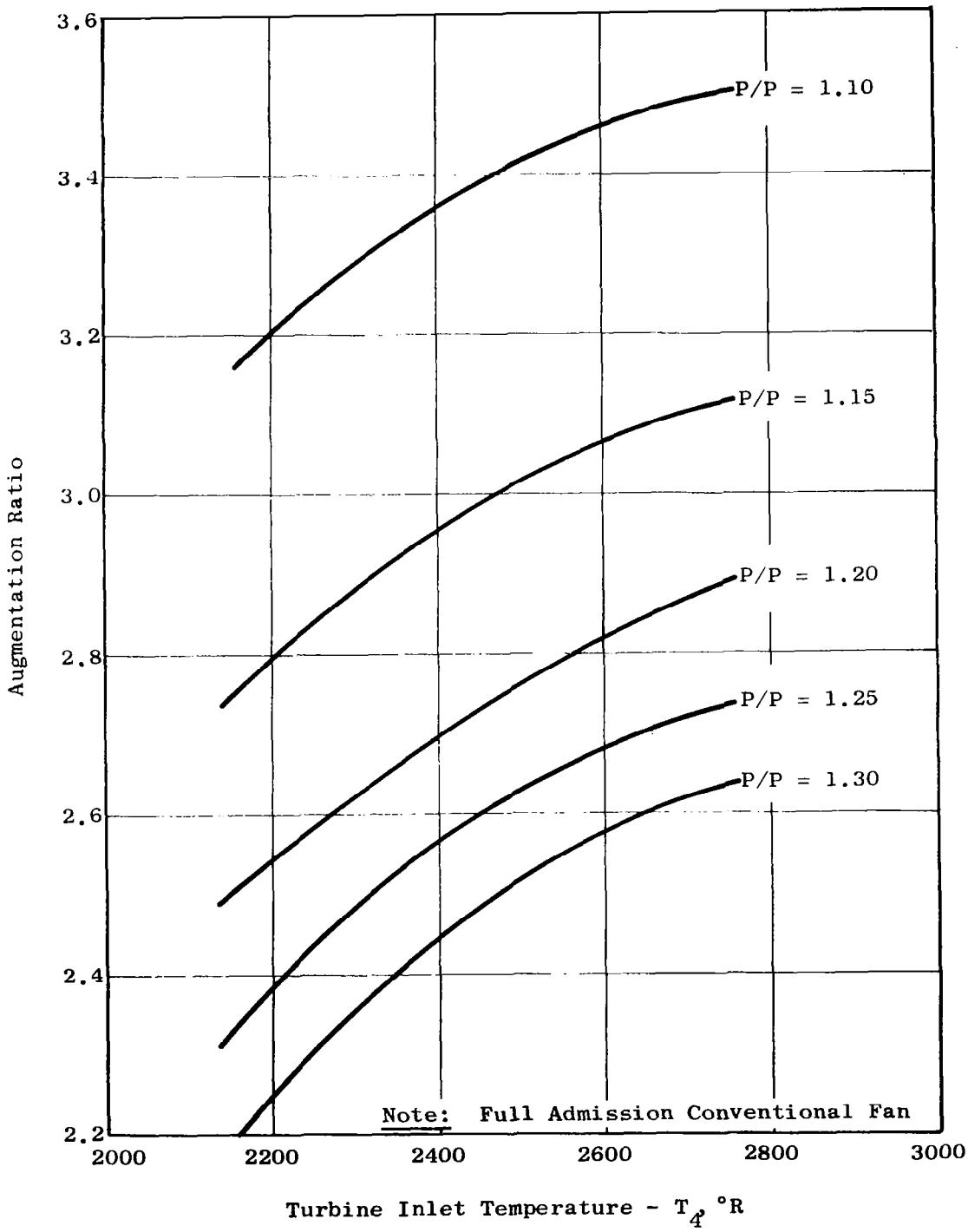

Figure 5. Augmentation Ratio Versus Turbine Inlet Temperature and Fan Pressure Ratio.

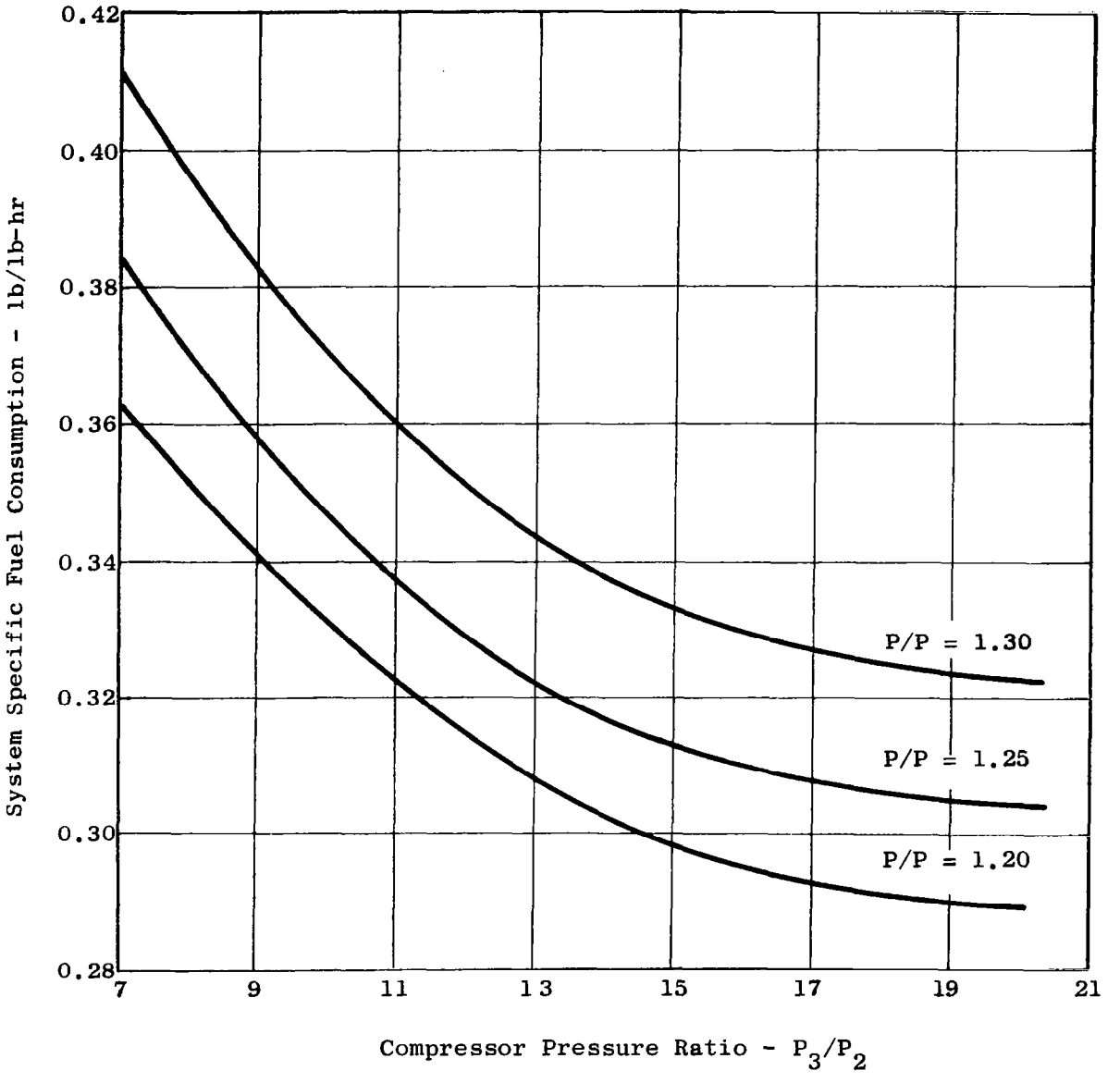

Figure 6. System Specific Fuel Consumption Versus Compressor Pressure Ratio and Fan Pressure Ratio.

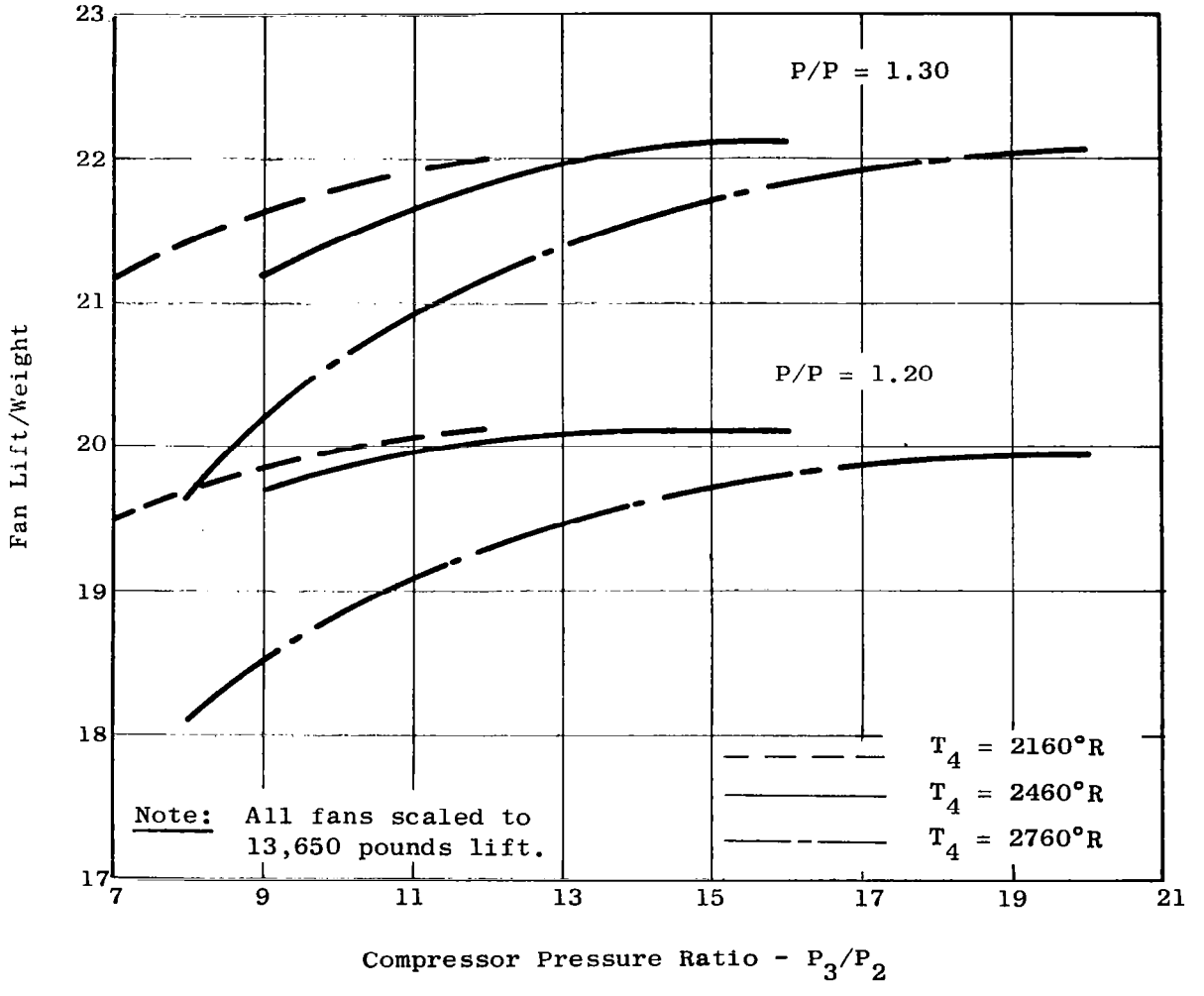

Figure 7. Fan Lift/Weight Versus Fan Pressure Ratio and Engine Cycle Characteristics.

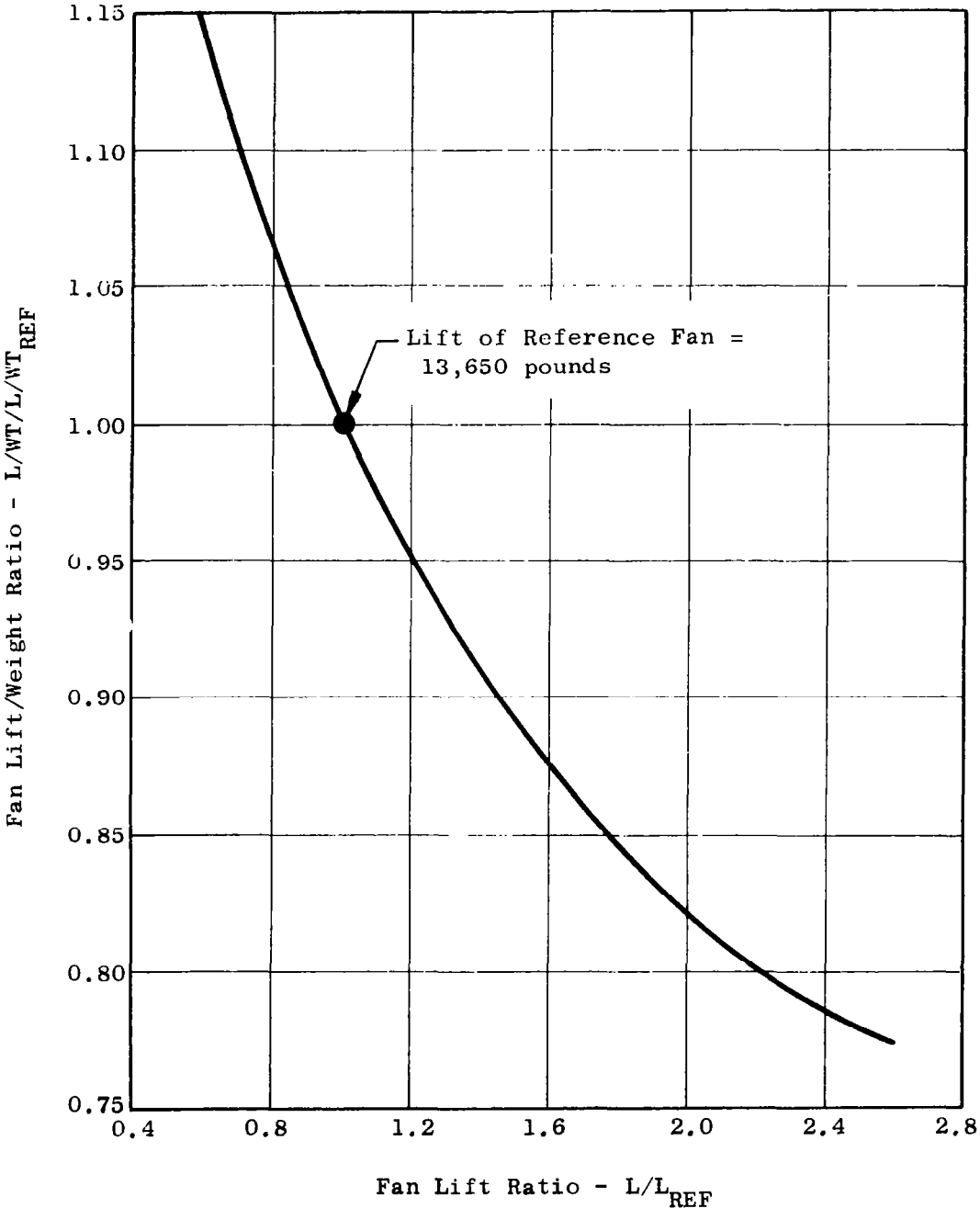

Figure 8. Fan Lift/Weight Ratio Versus Fan Lift Ratio.

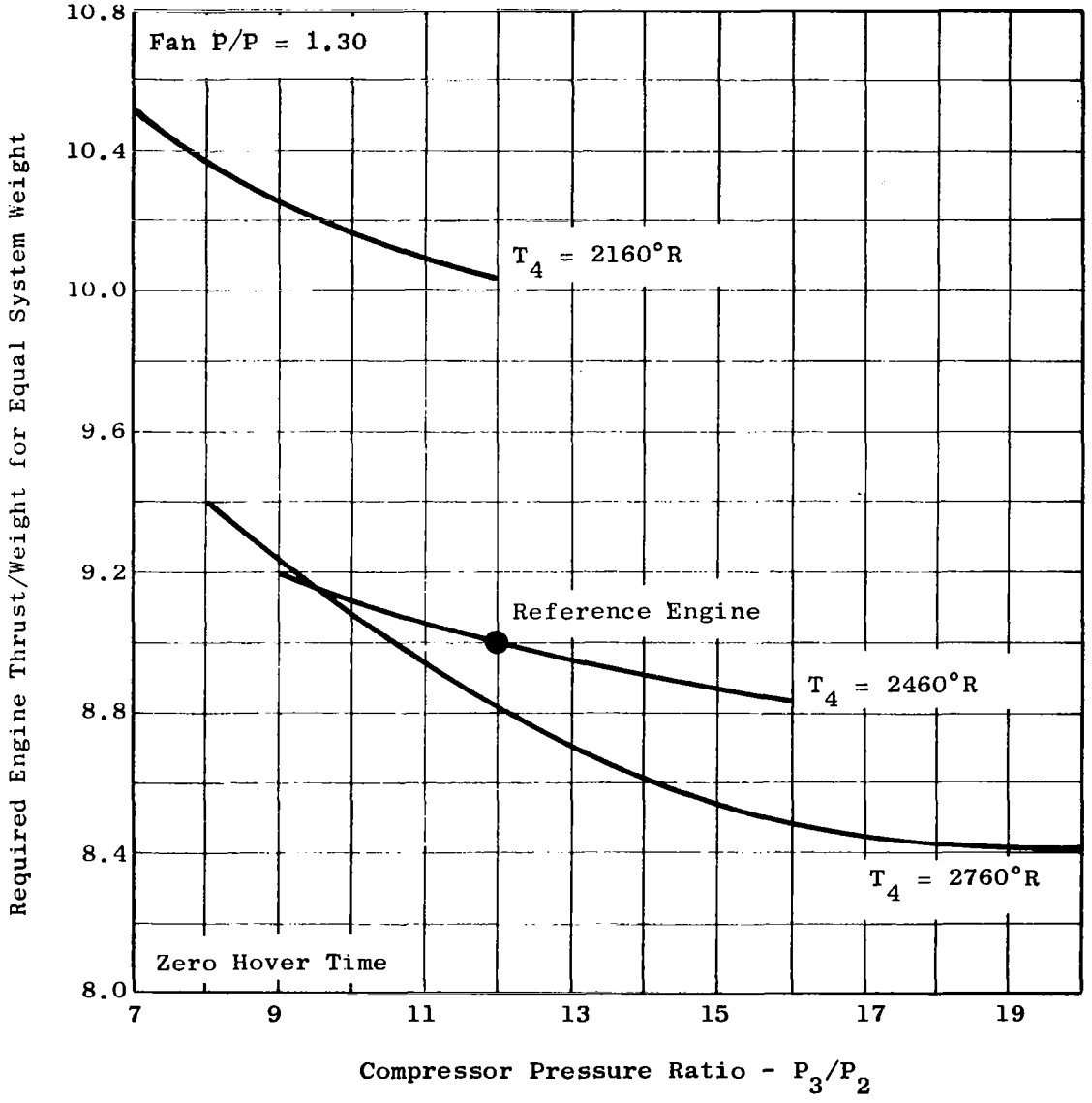

Figure 9. Engine Thrust/Weight for Equal System Weight Versus Compressor Pressure Ratio.

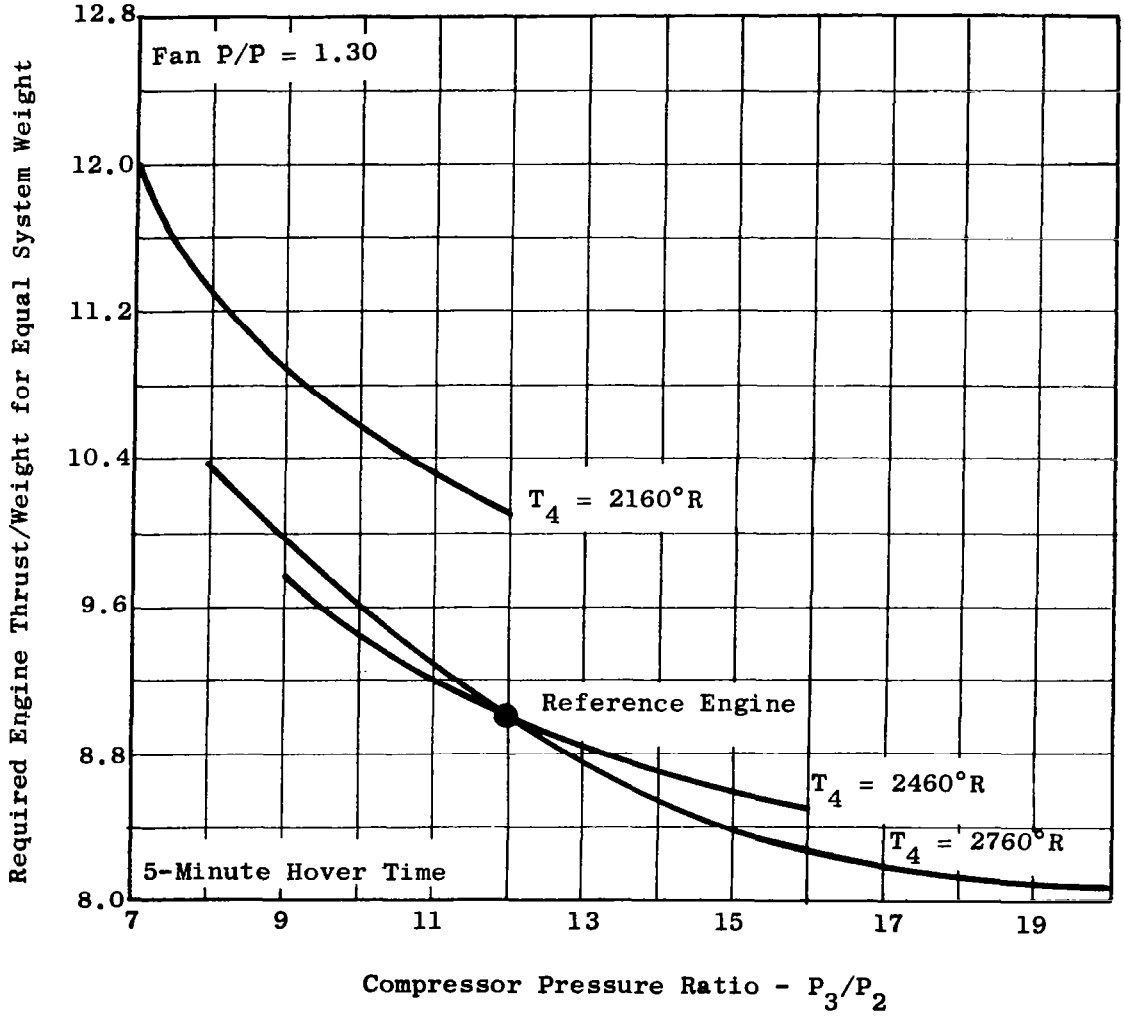

Figure 10. Engine Thrust/Weight for Equal System Weight Versus Compressor Pressure Ratio.

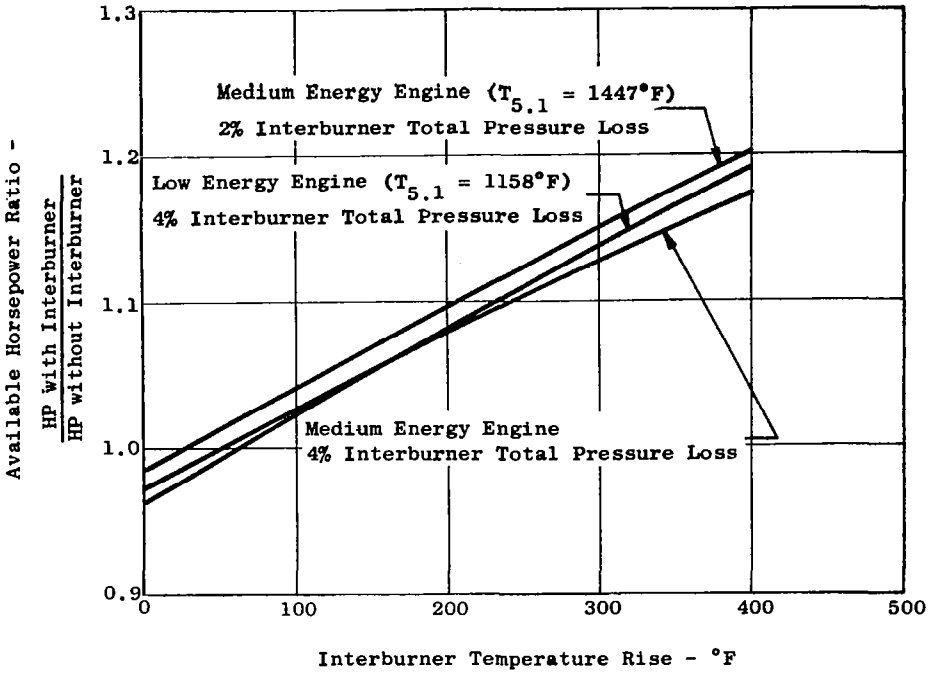

Figure 11. Interburner Performance.

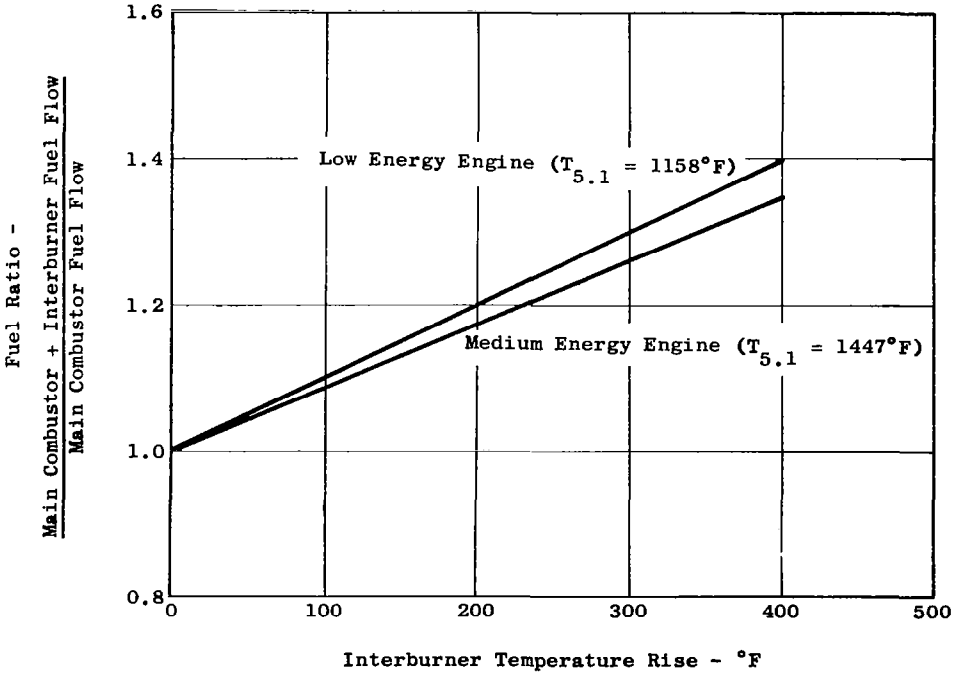

Figure 12. Interburner Performance.

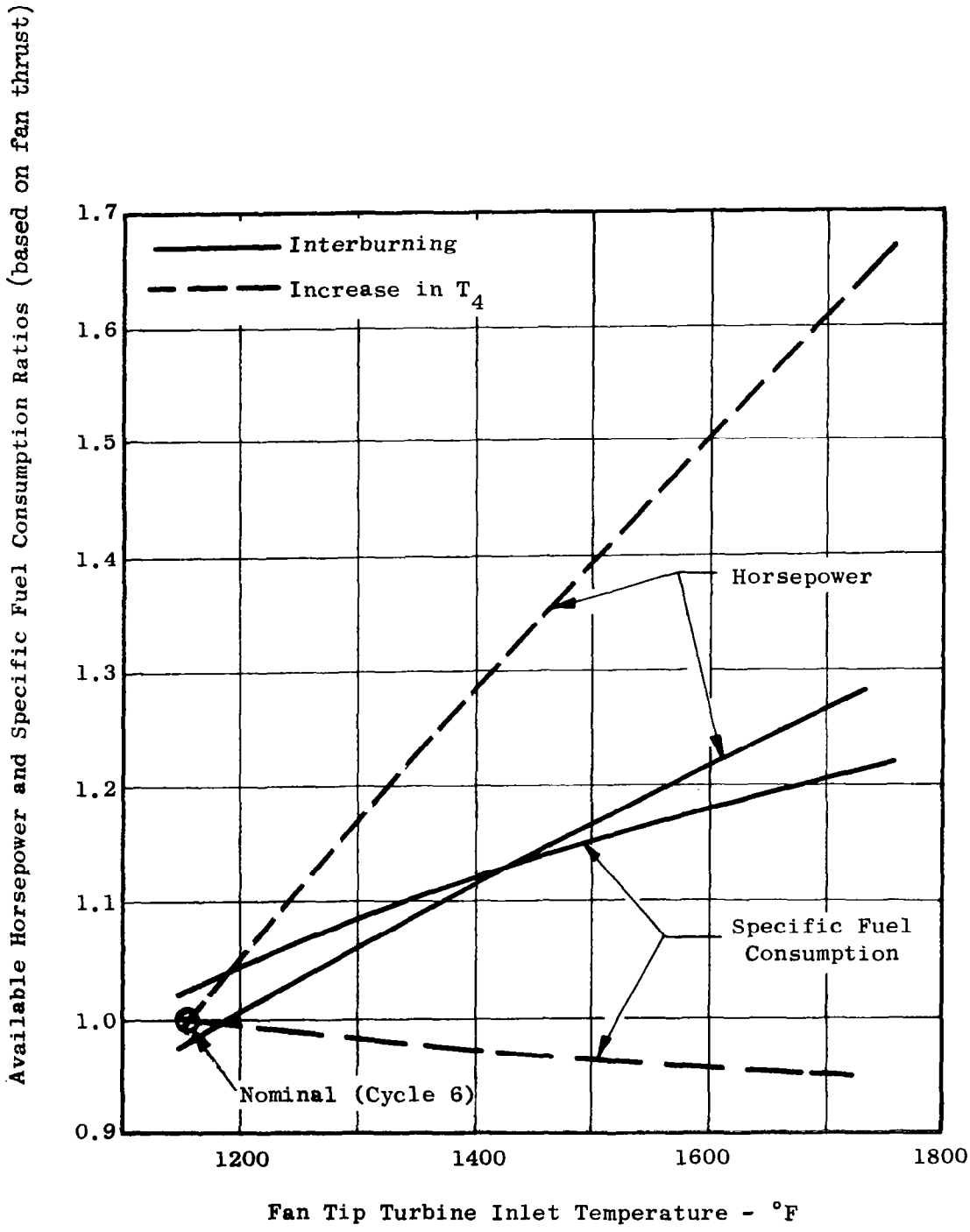

Figure 13. Comparison of Interburner Versus Cycle Temperature Increase.

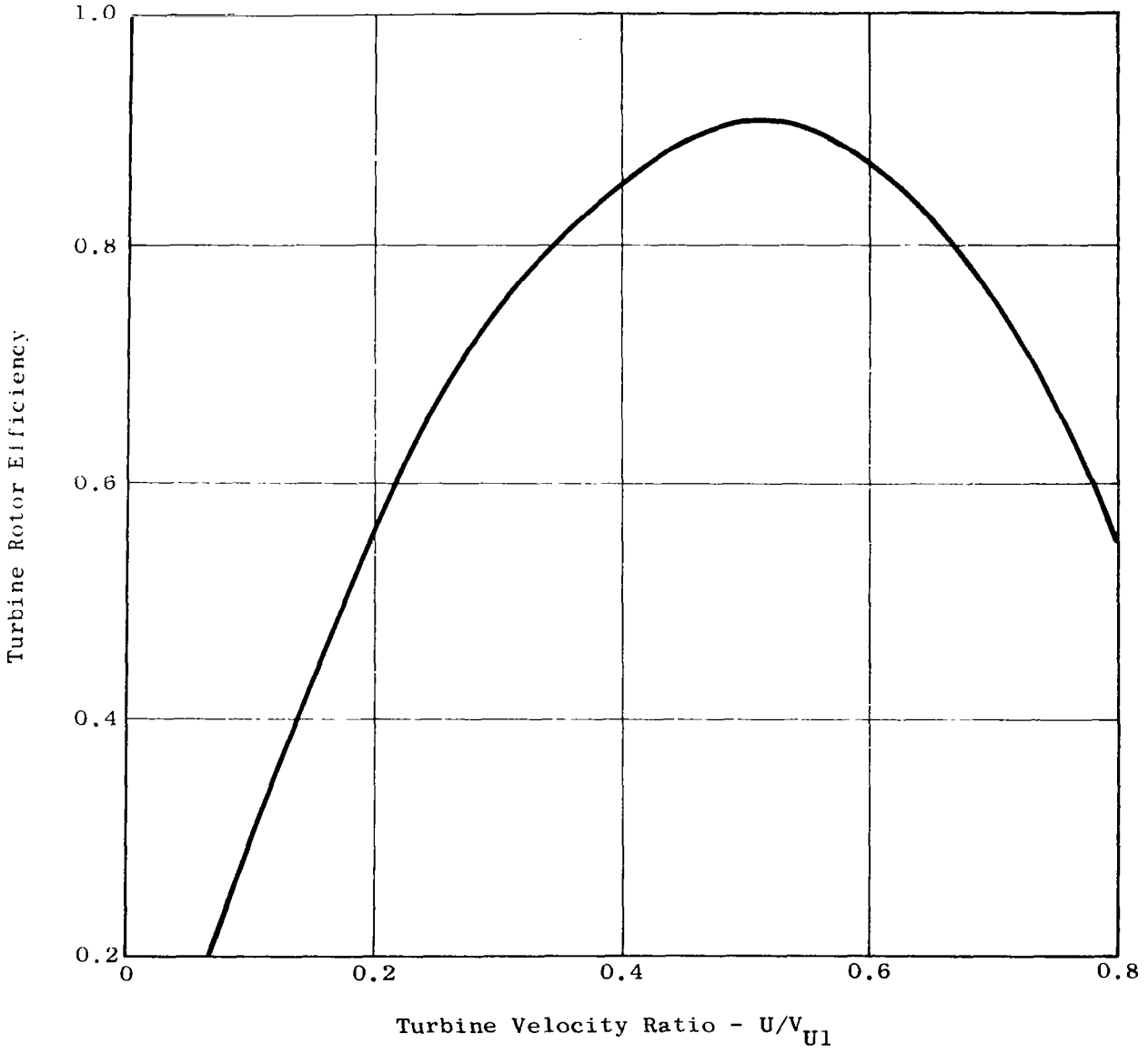

Figure 14. Turbine Rotor Efficiency Versus Velocity Ratio.

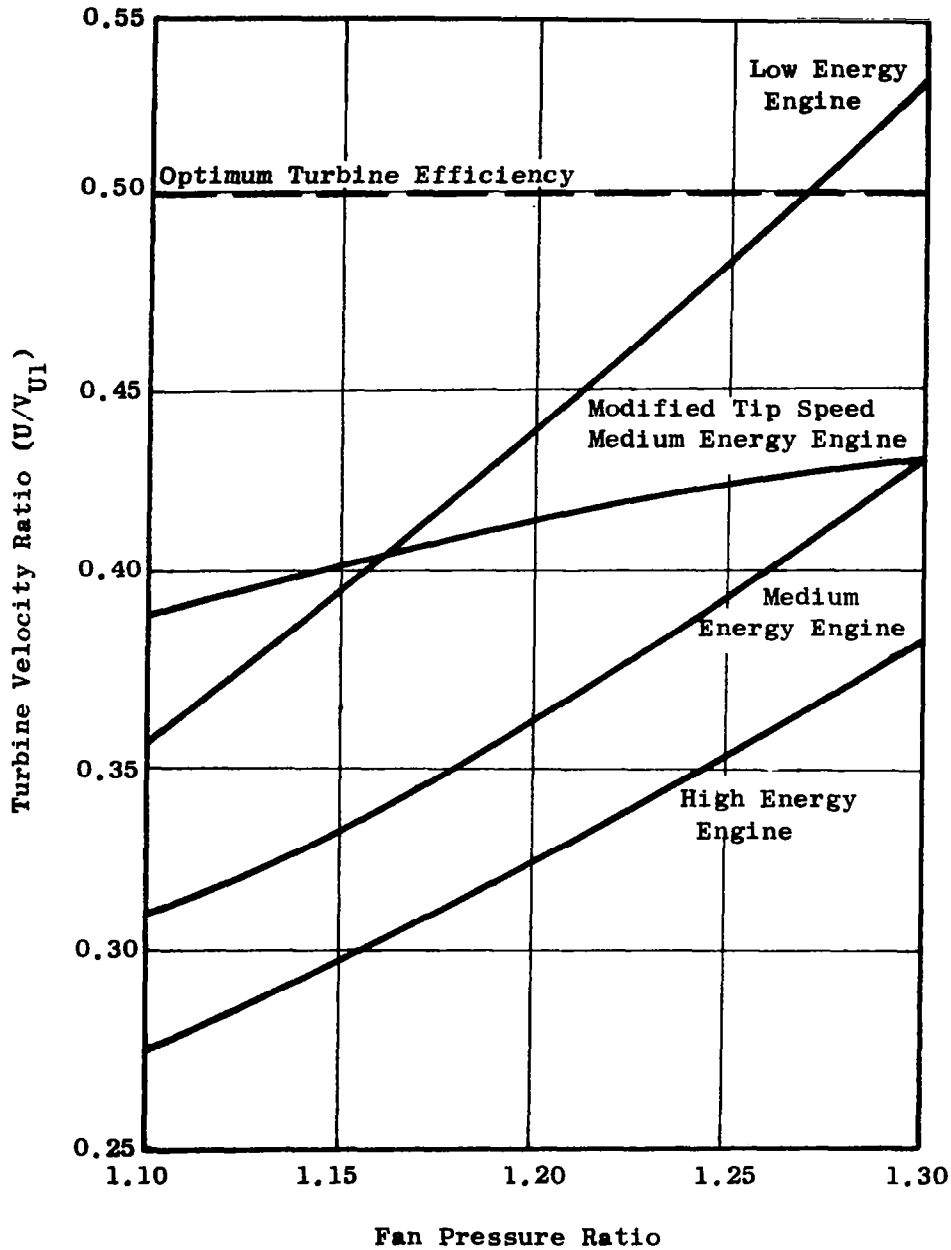

Figure 15. Turbine Velocity Ratio Versus Fan Pressure Ratio and Engine Energy.

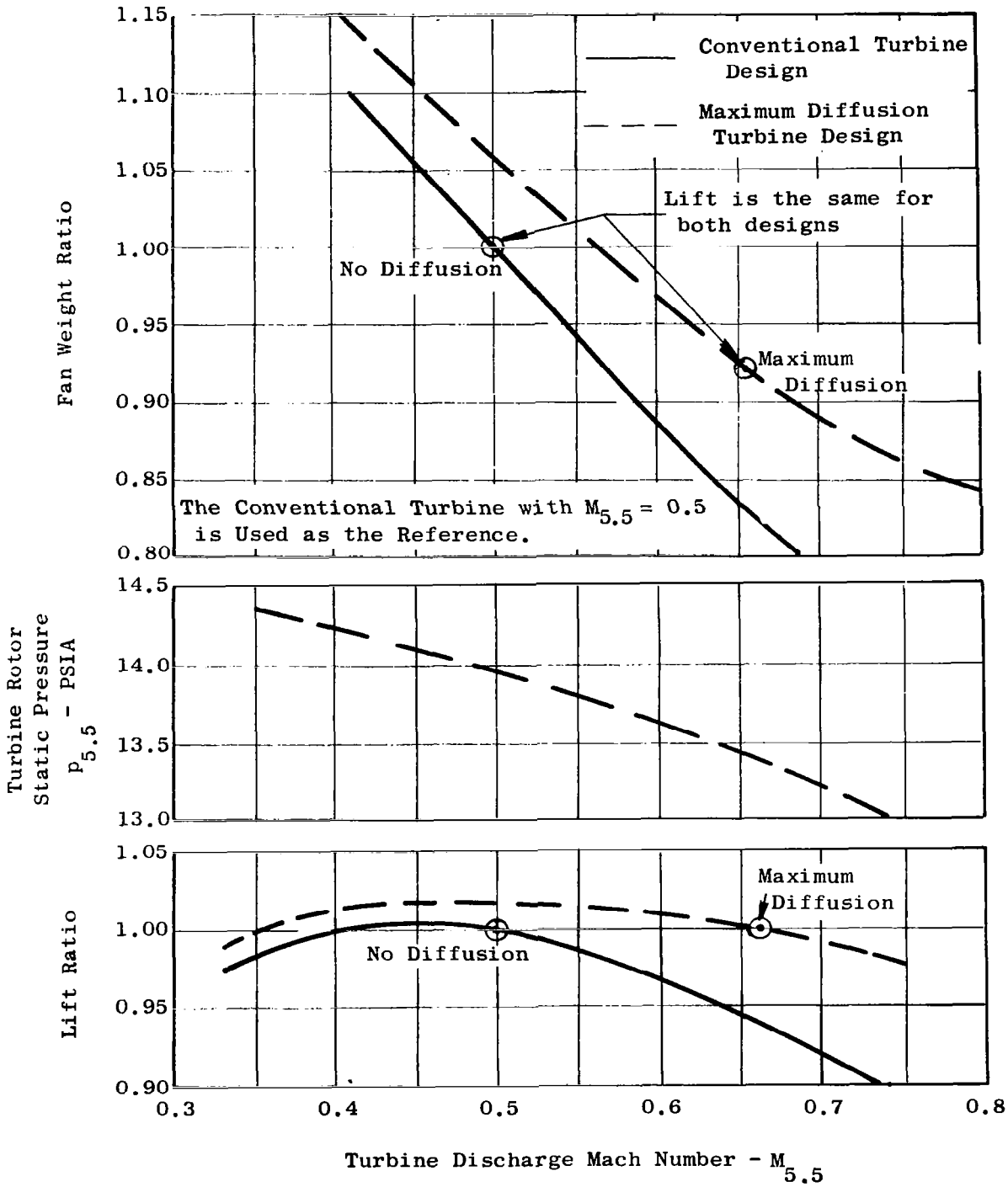

Figure 16. Fan Characteristics as a Function of Turbine Design.

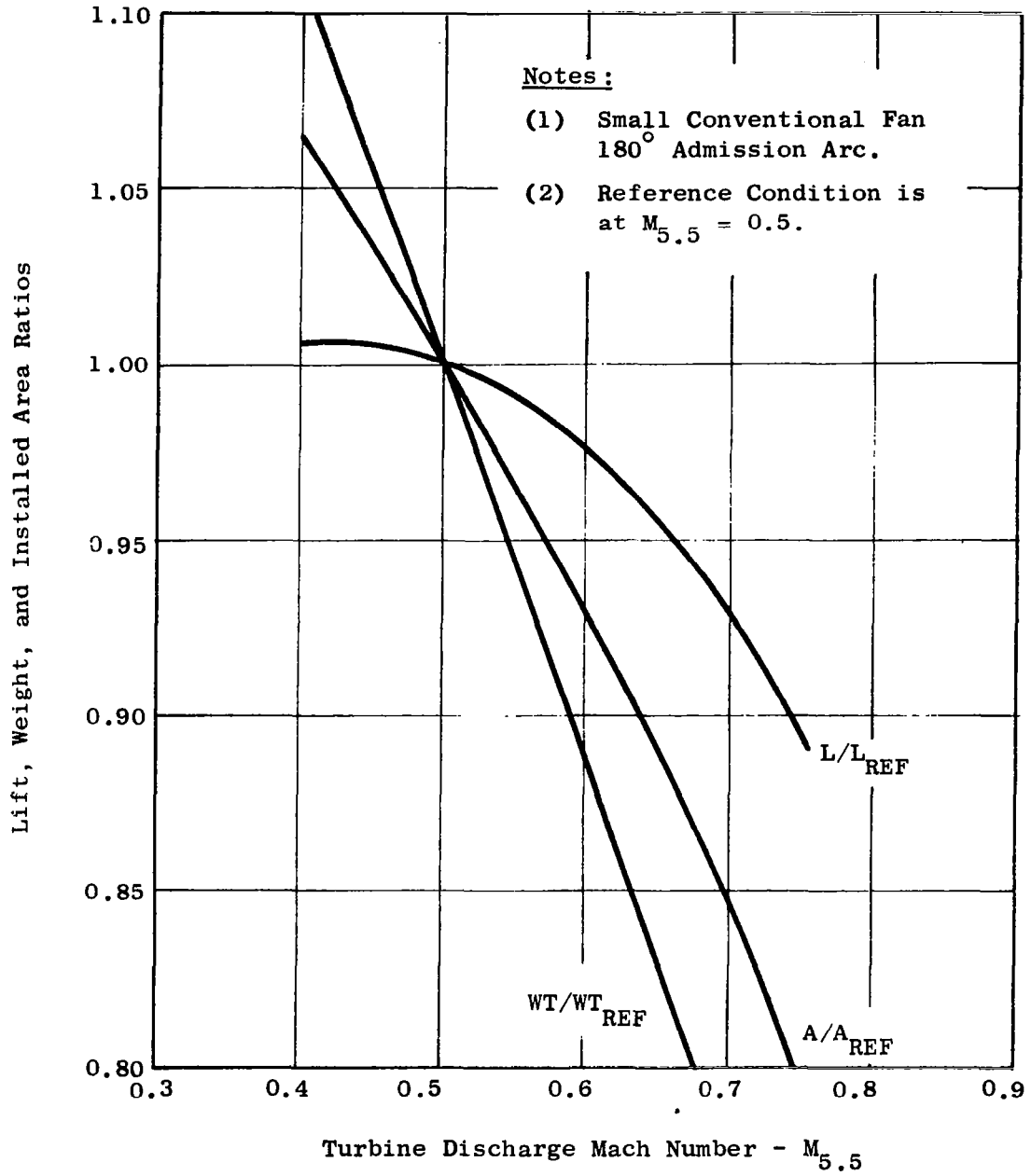

Figure 17. Fan Lift, Weight and Installed Area Versus Turbine Discharge Mach Number, $M_{5.5}$.

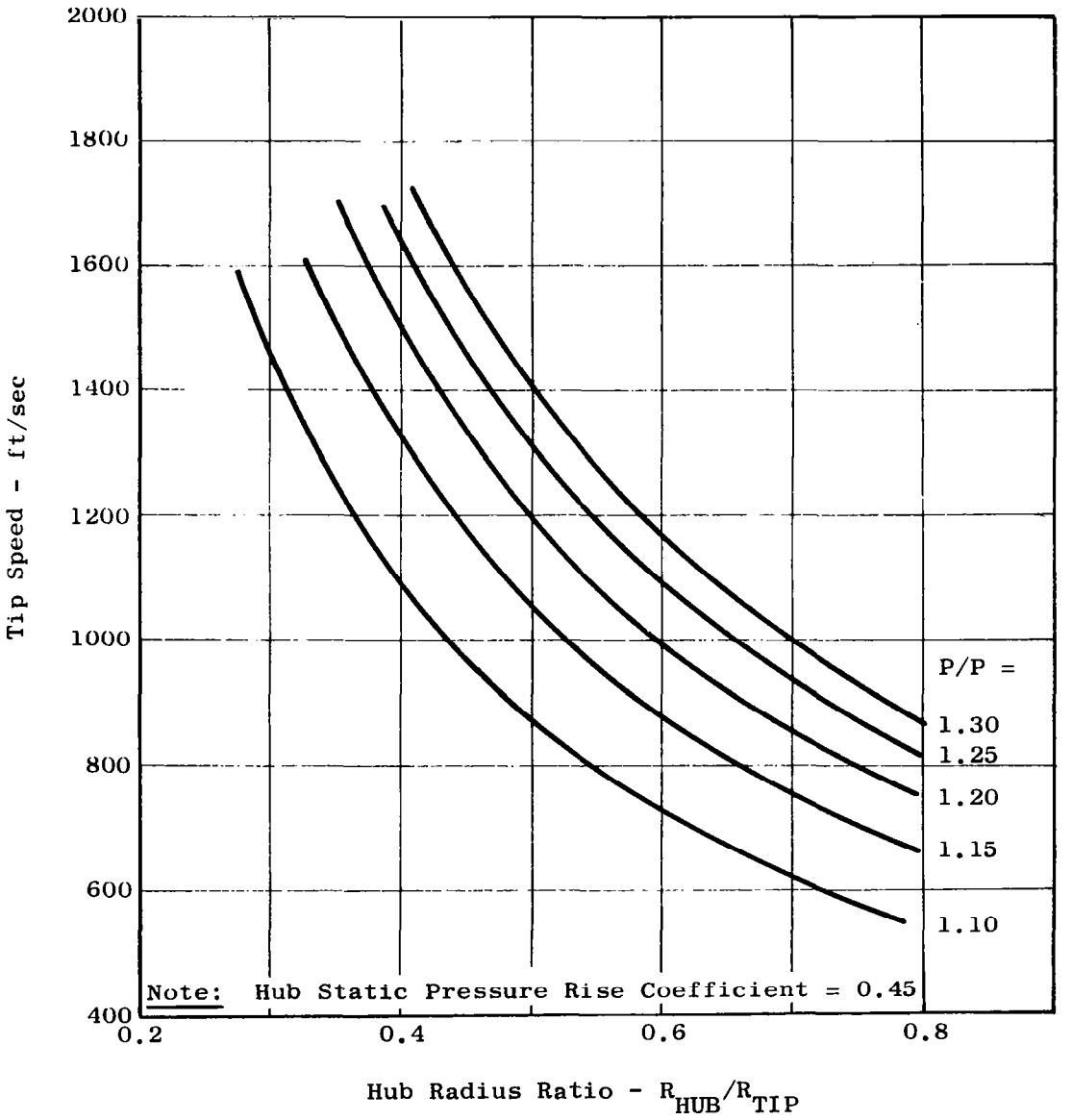

Figure 18. Required Tip Speed Versus Hub Radius Ratio for Statorless Fans.

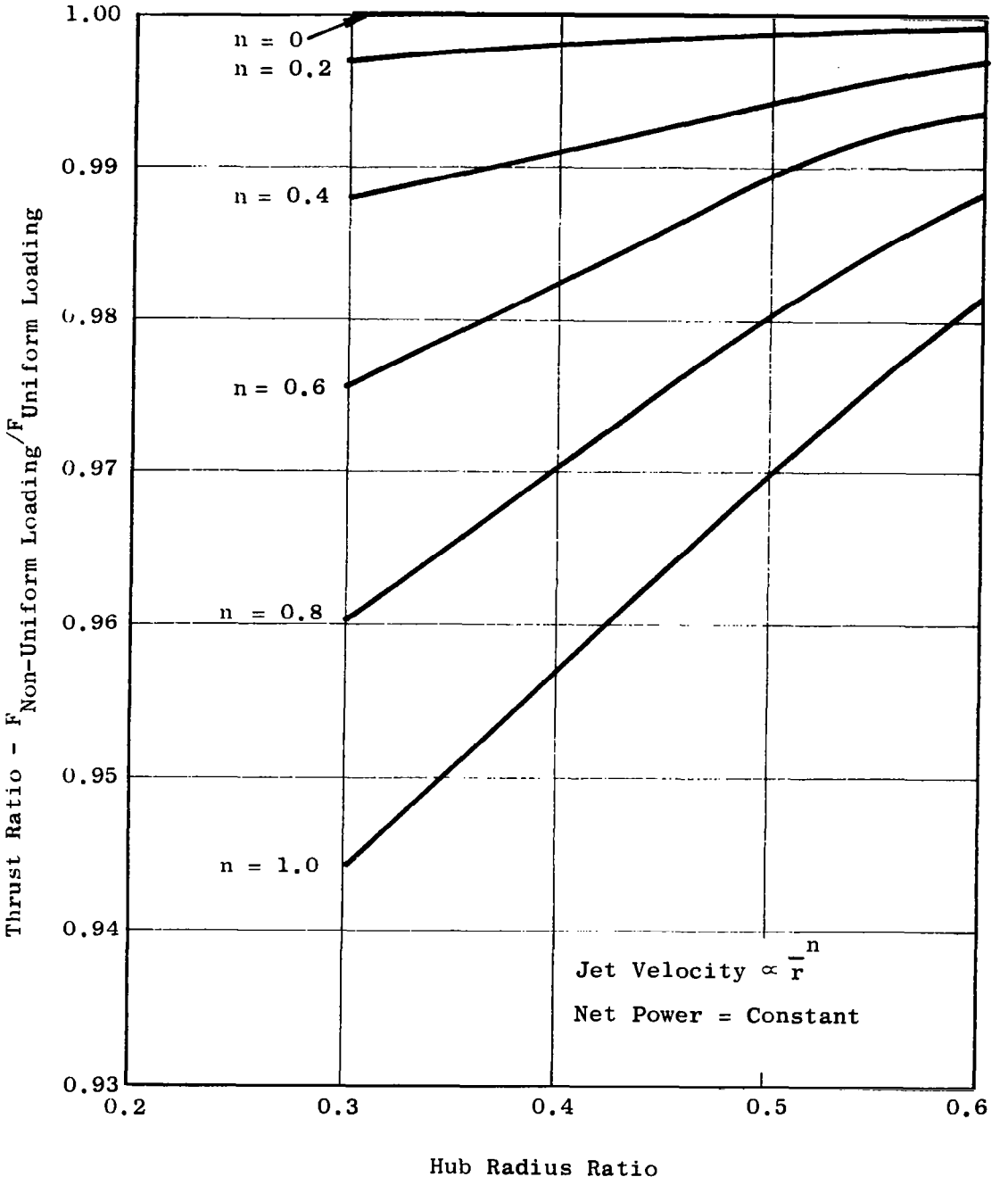

Figure 19. Effect of Radial Variation of Energy on Thrust.

Profile Loss Coefficient Versus Diffusion Factor

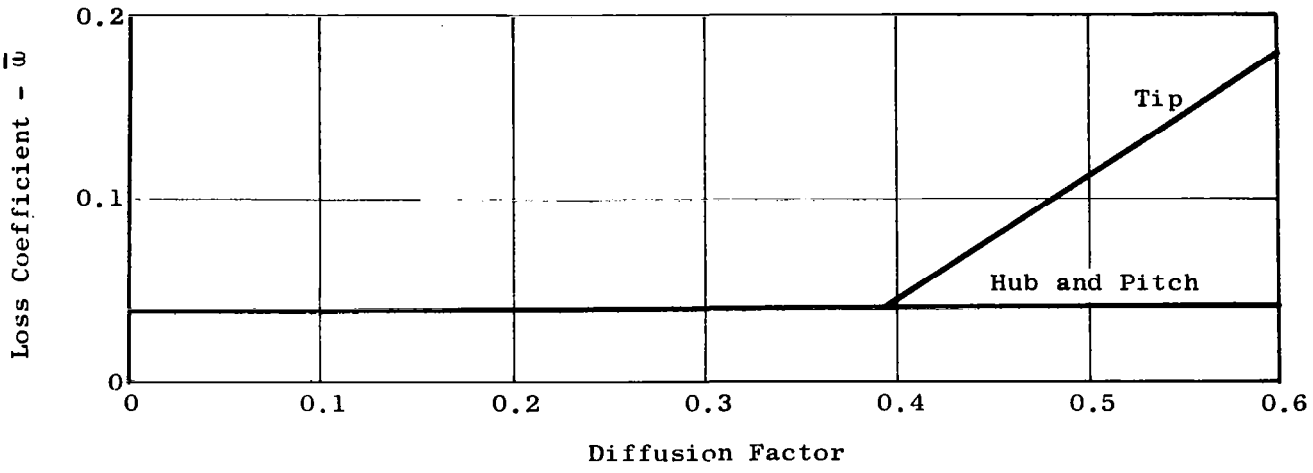

Shock Loss Coefficient Versus Relative Mach Number

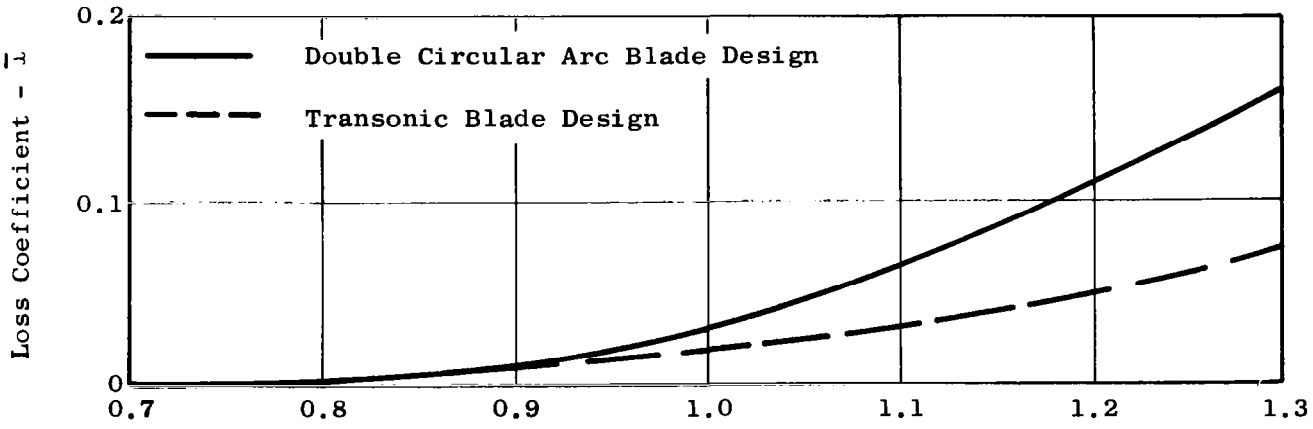

Figure 20. Rotor Losses for Statorless Fan.

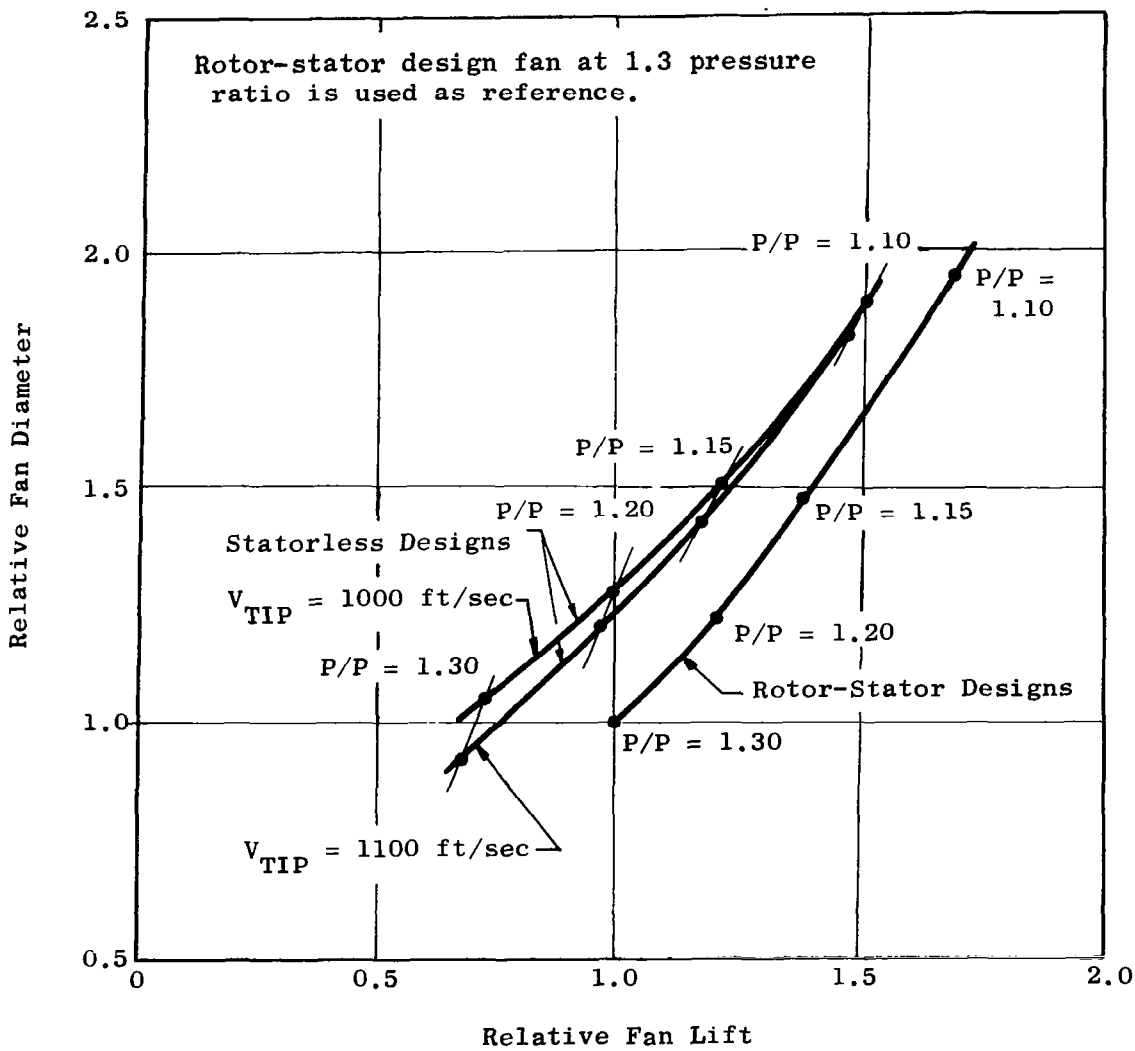

Figure 21. Size and Efficiency Comparison.

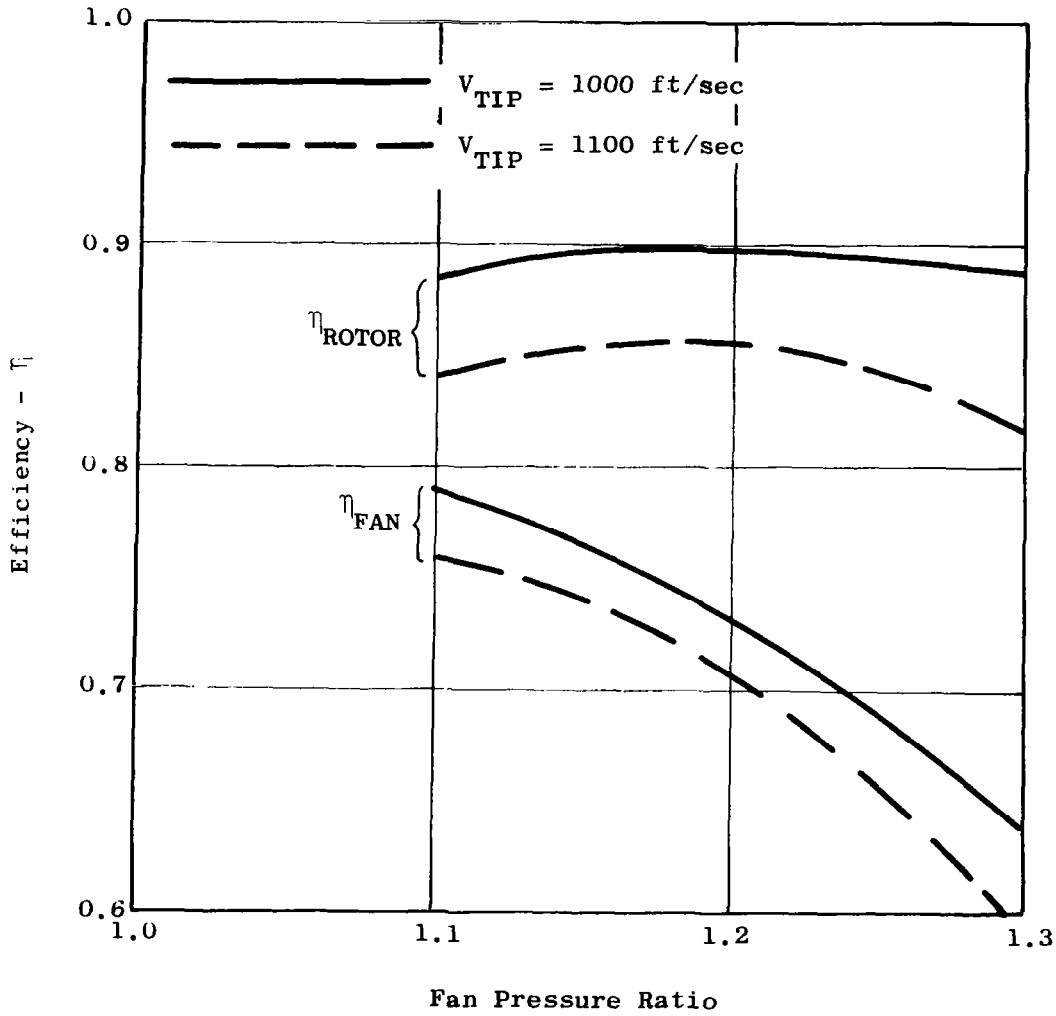

Figure 22. Statorless Fan Efficiency Versus Pressure Ratio.

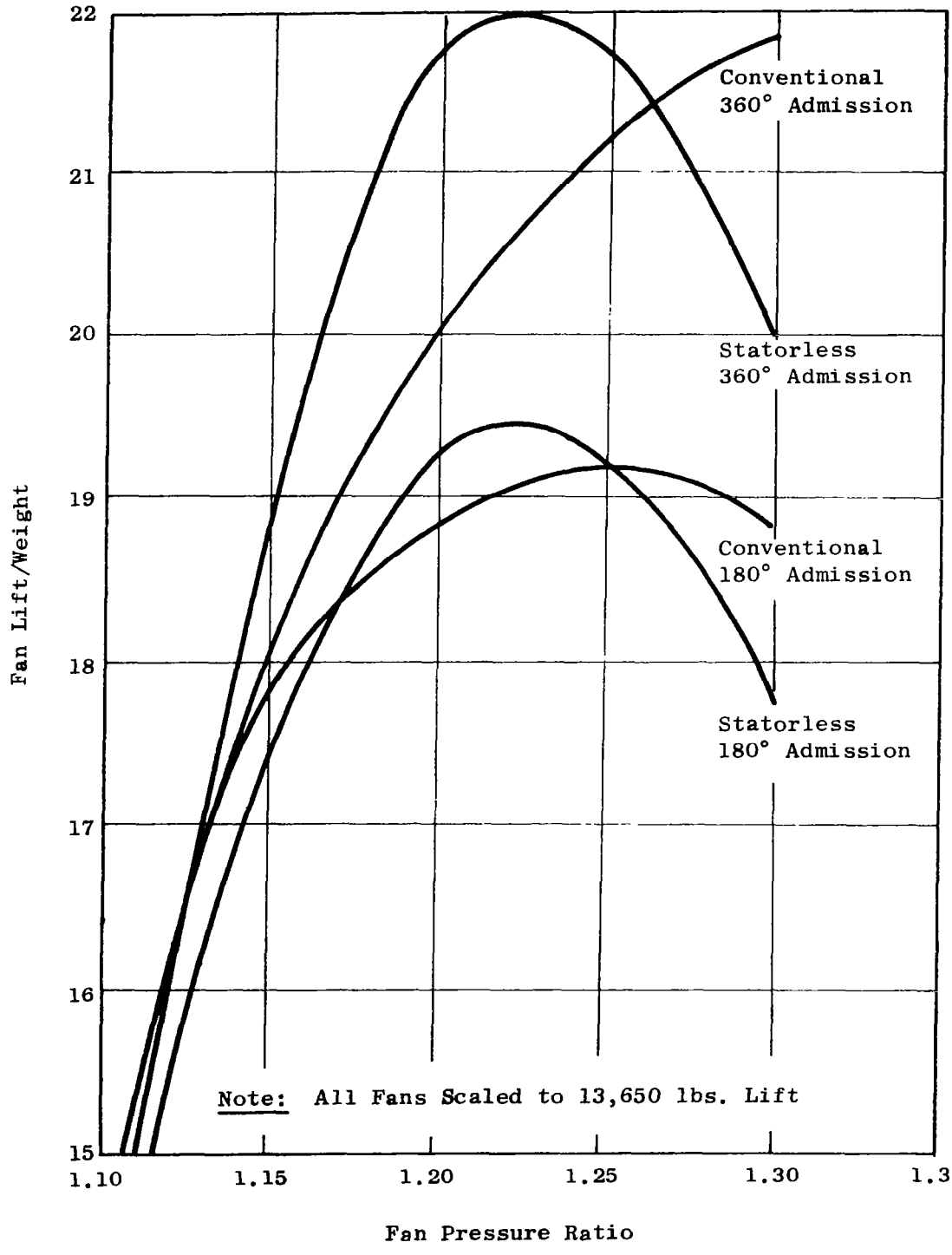

Figure 23. Fan Lift/Weight Versus Fan Pressure Ratio.

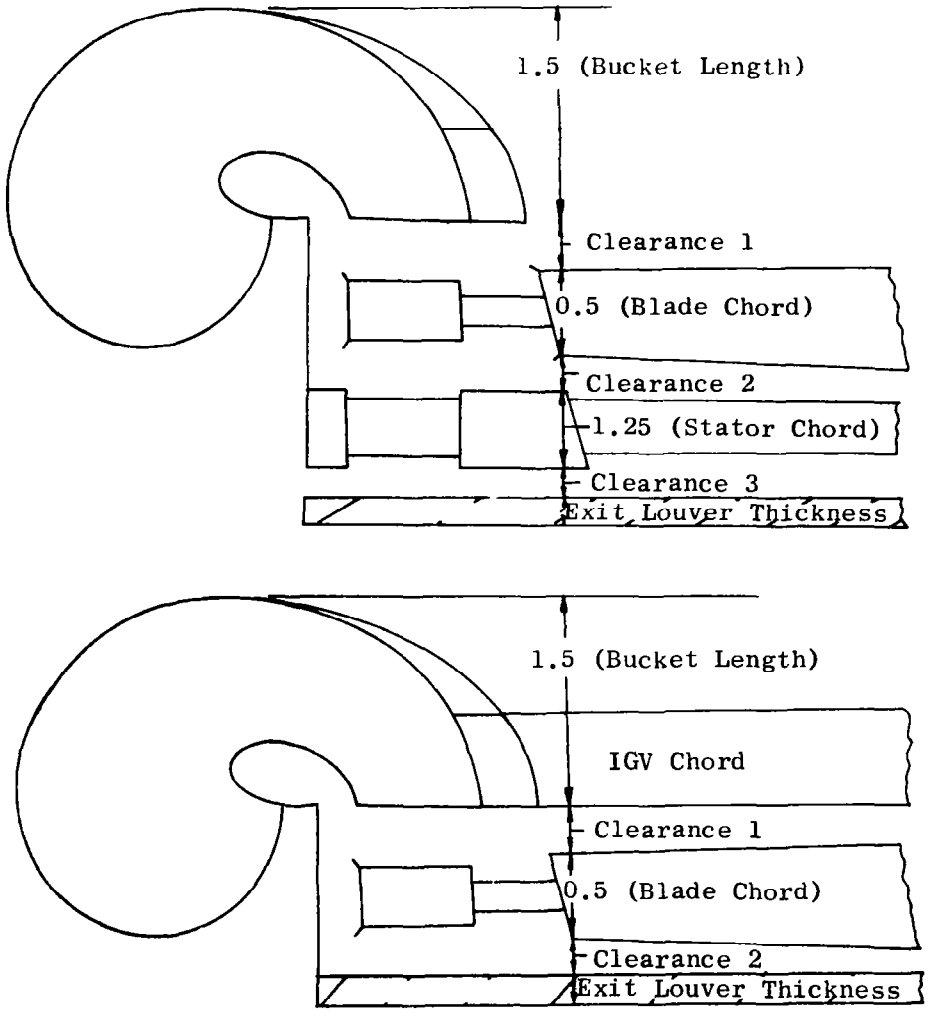

Fan Thickness

Rotor-Stator

1.5 (Bucket Length)
Clearance 1
1.5 (Bucket Chord)
or
0.5 (Blade Chord)
Clearance 2
1.25 (Stator Chord)
Clearance 3
Exit Louver Thickness

IGV-Rotor

1.5 (Bucket Length)
Clearance 1
1.5 (Bucket Chord)
or
0.5 (Blade Chord)
Clearance 2
Exit Louver Thickness

Figure 24. Fan Thickness Dimensions.

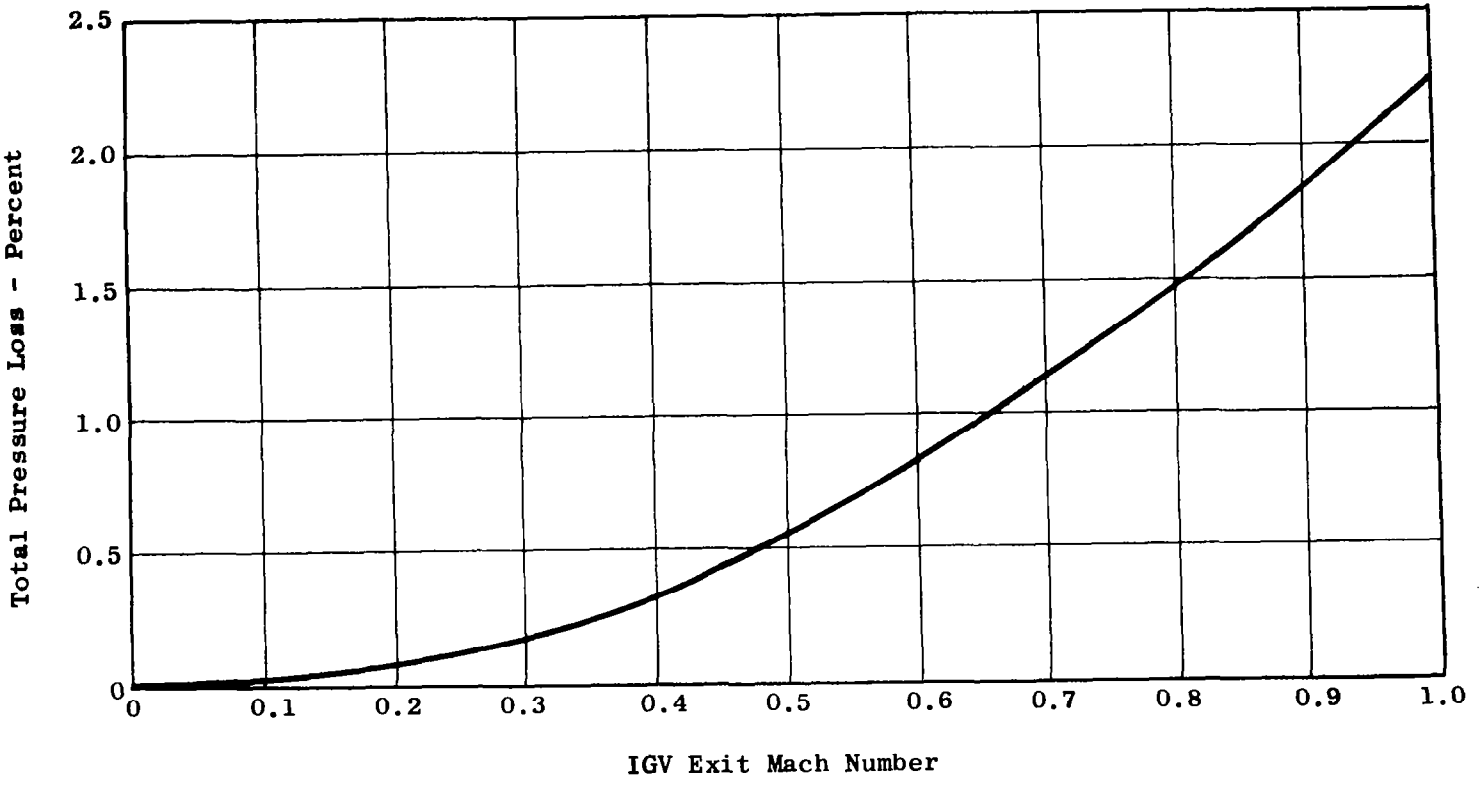

Figure 25. IGV Total Pressure Loss Versus Exit Mach Number (Nozzle Efficiency - $V^2/V^2_{IDEAL} = 0.97$).

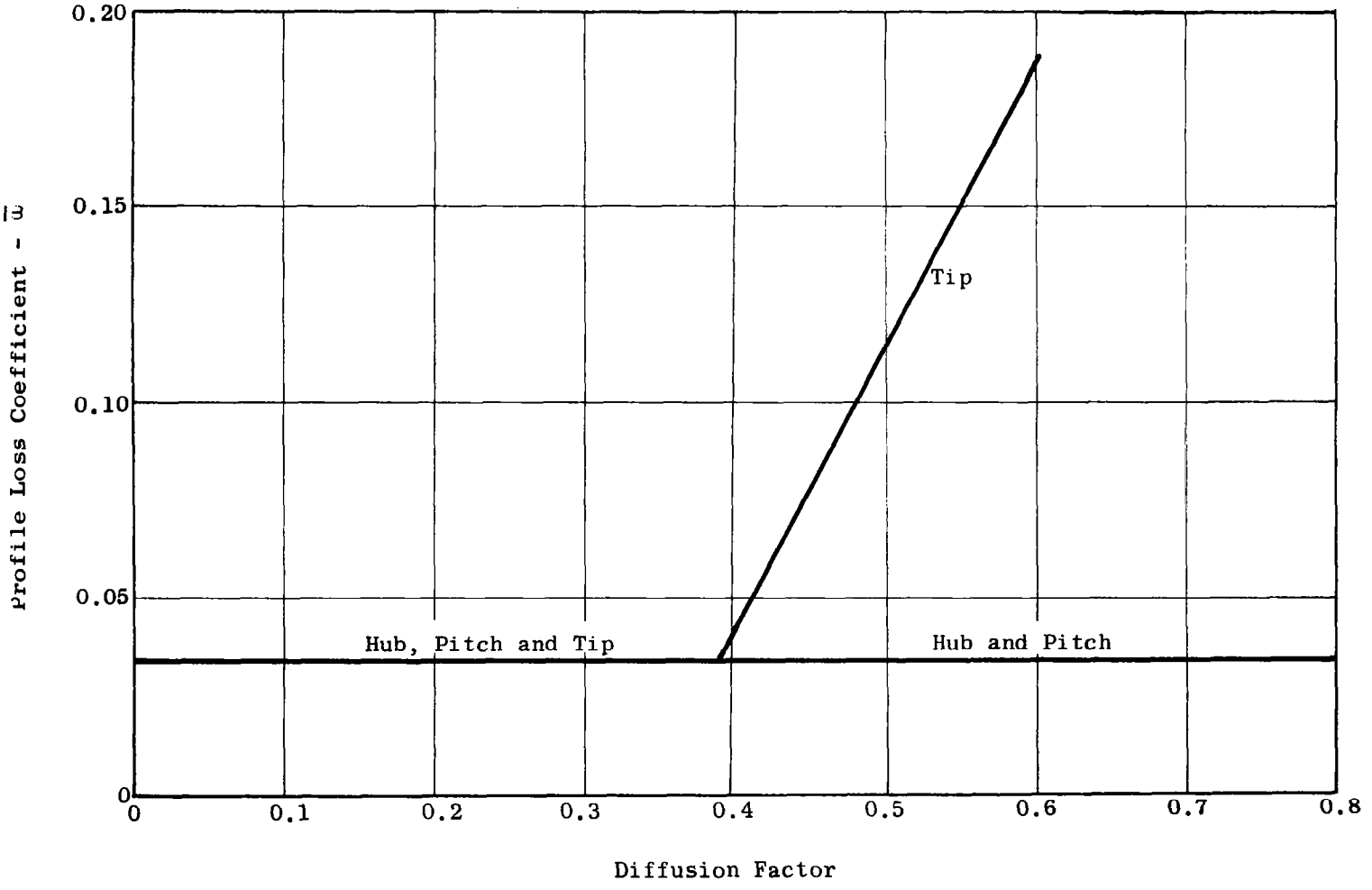

Figure 26. IGV-Rotor Fan Profile Loss Coefficient Versus Diffusion Factor.

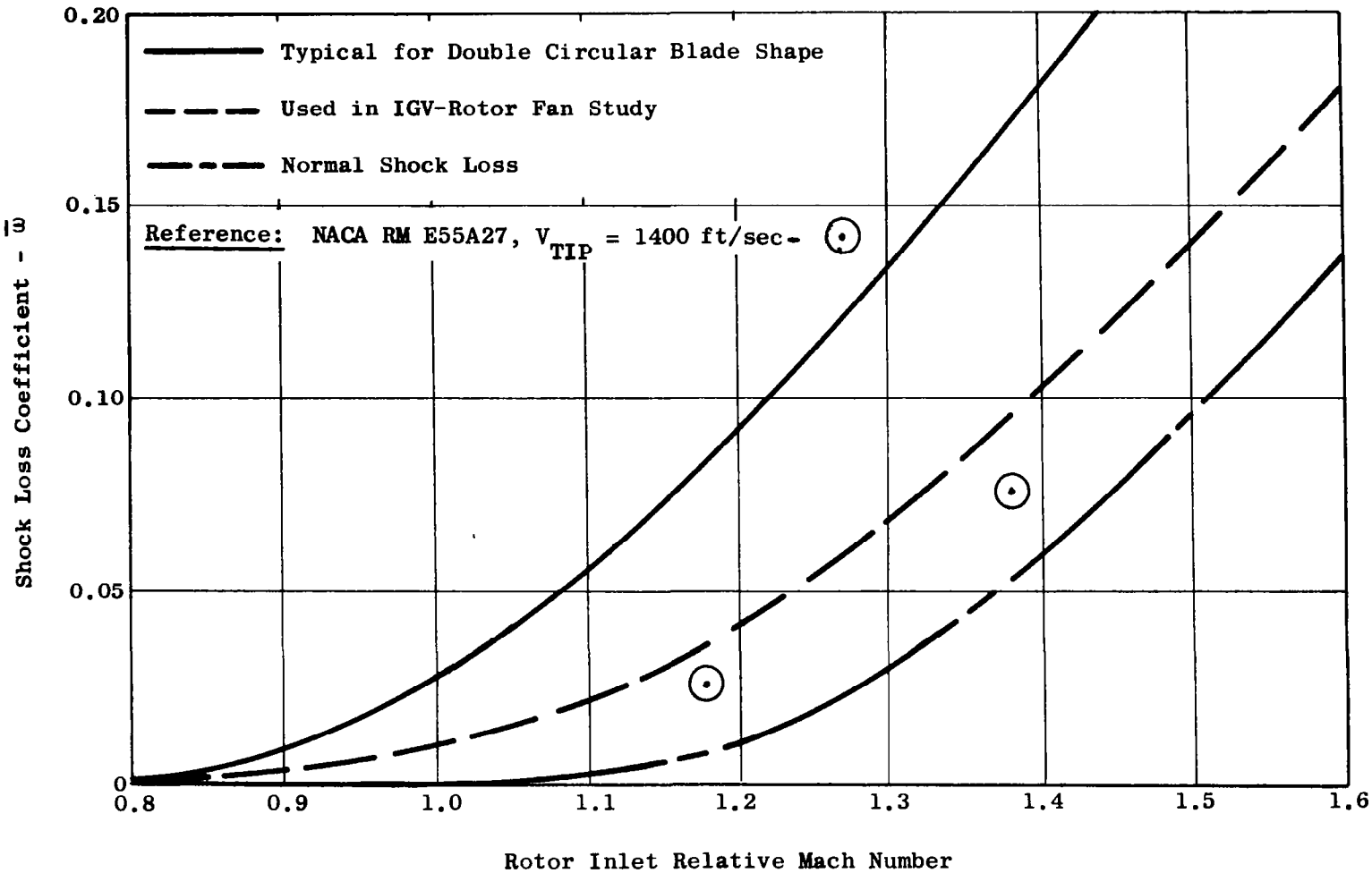

Figure 27. IGV-Rotor Fan Shock Loss Coefficient Versus Rotor Inlet Relative Mach Number.

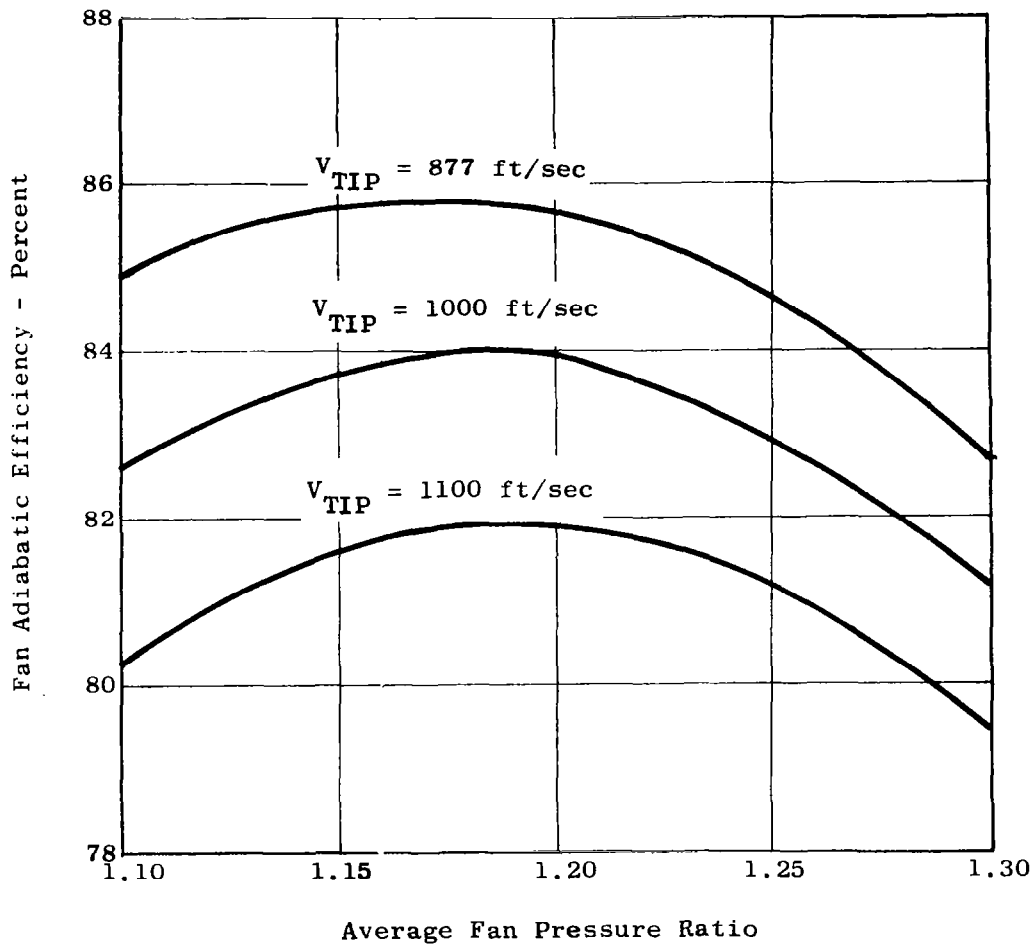

Figure 28. IGV-Rotor Fan Characteristics.

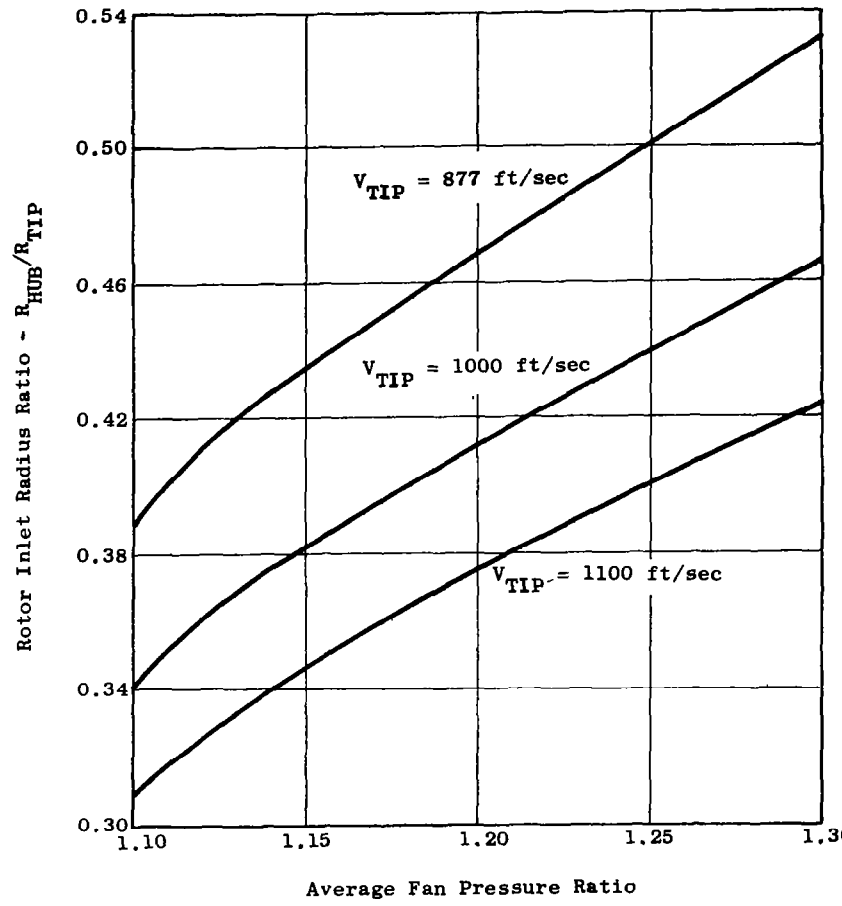

Figure 29. IGV-Rotor Fan Characteristics.

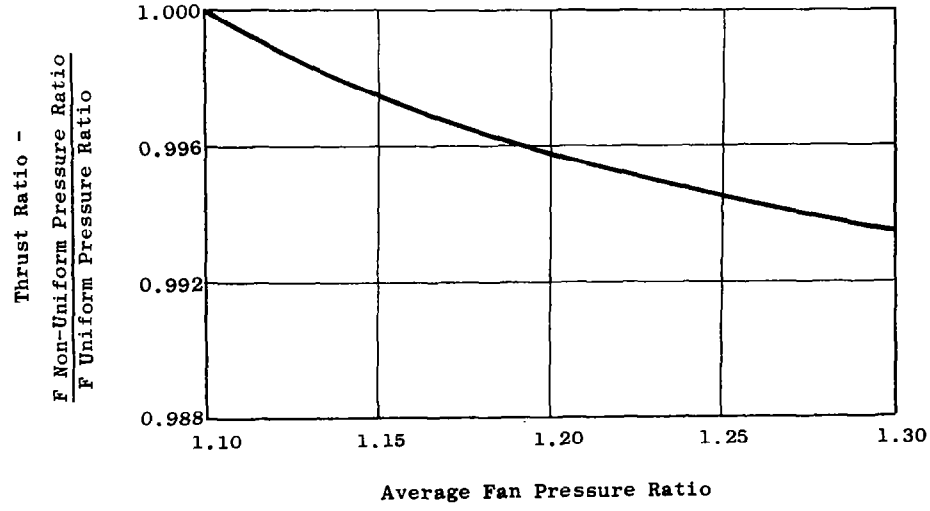

Figure 30. IGV-Rotor Fan Characteristics.

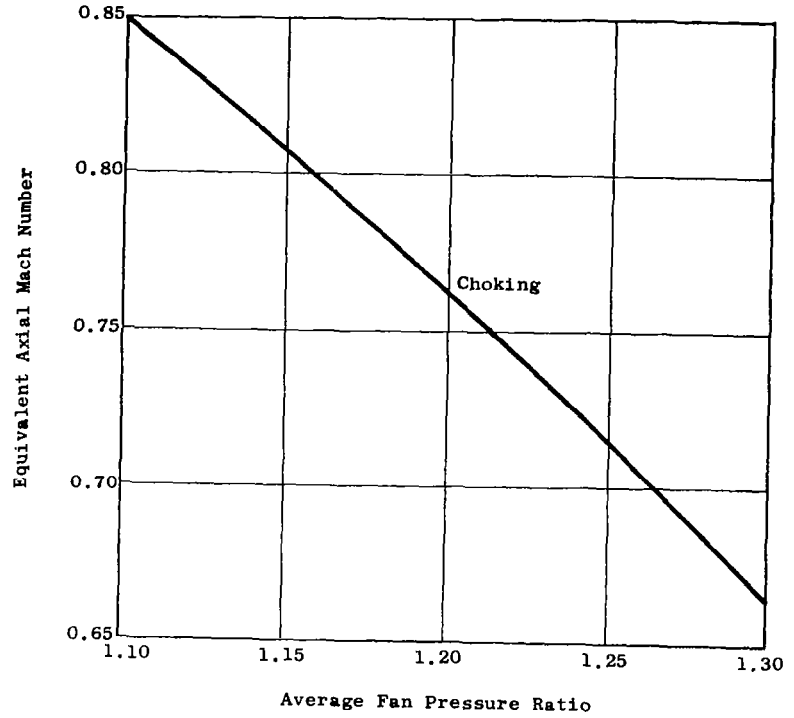

Figure 31a. IGV-Rotor Fan Characteristics.

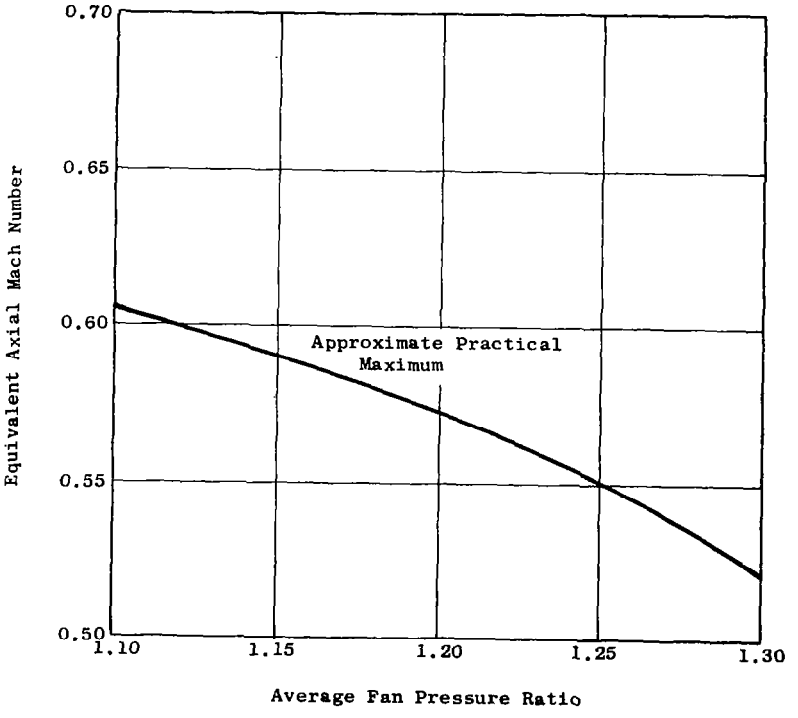

Figure 31b. IGV-Rotor Fan Characteristics.

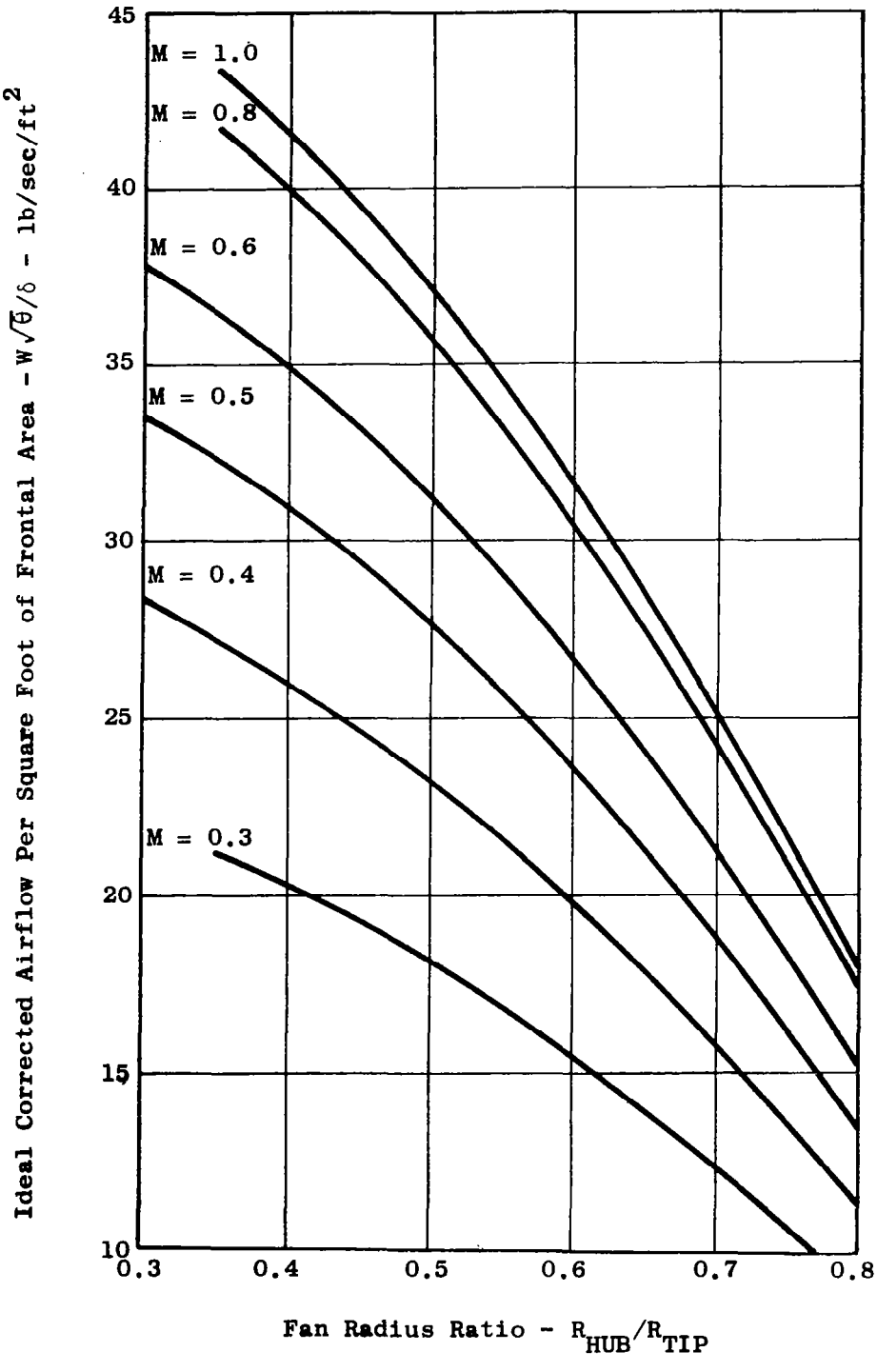

Figure 32. Flow Per Unit Frontal Area Versus Fan Radius Ratio and Axial Mach Number.

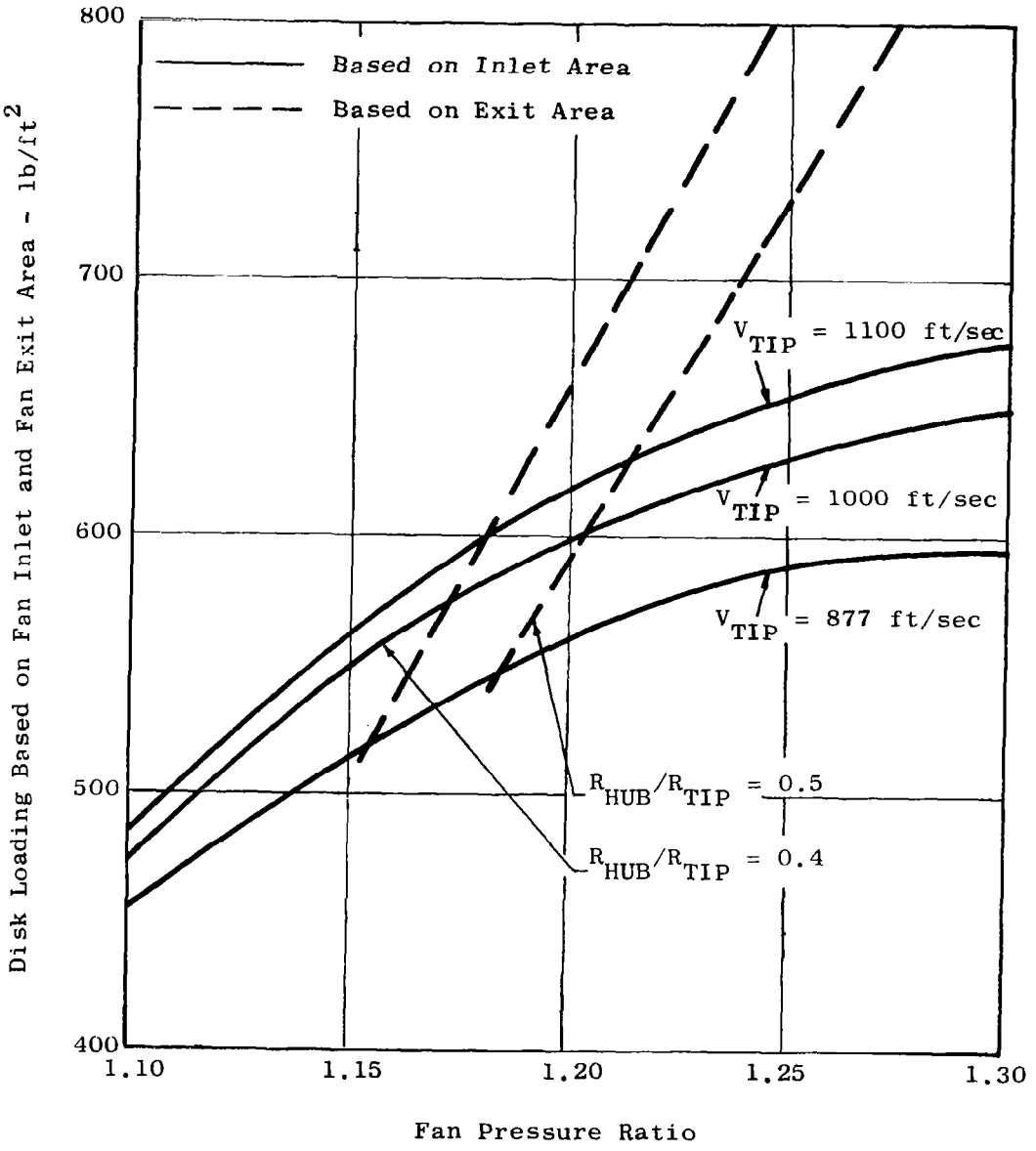

Figure 33. Disk Loading Versus Fan Pressure Ratio.

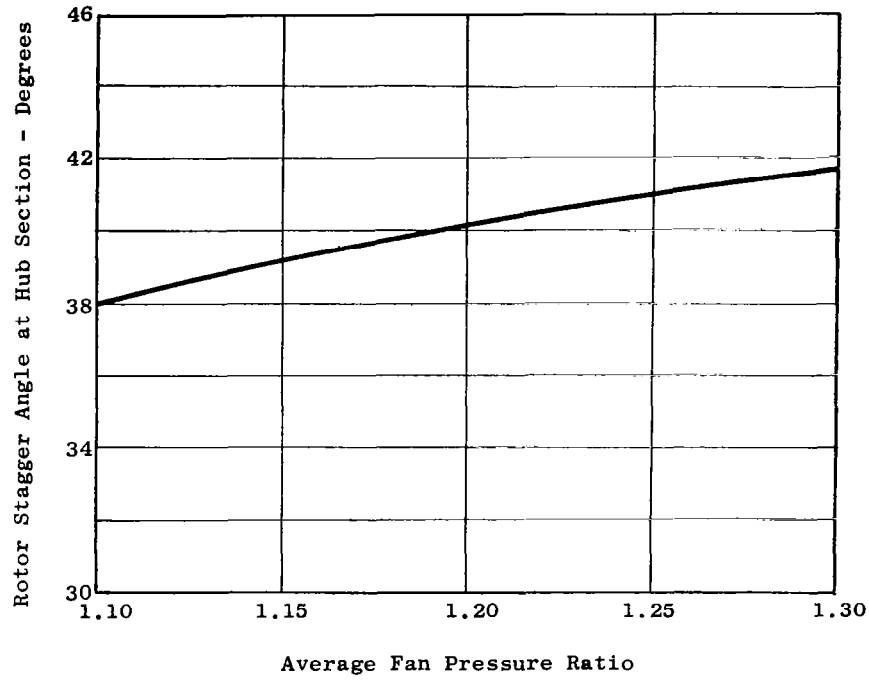

Figure 34a. IGV-Rotor Fan Characteristics - Hub Section.

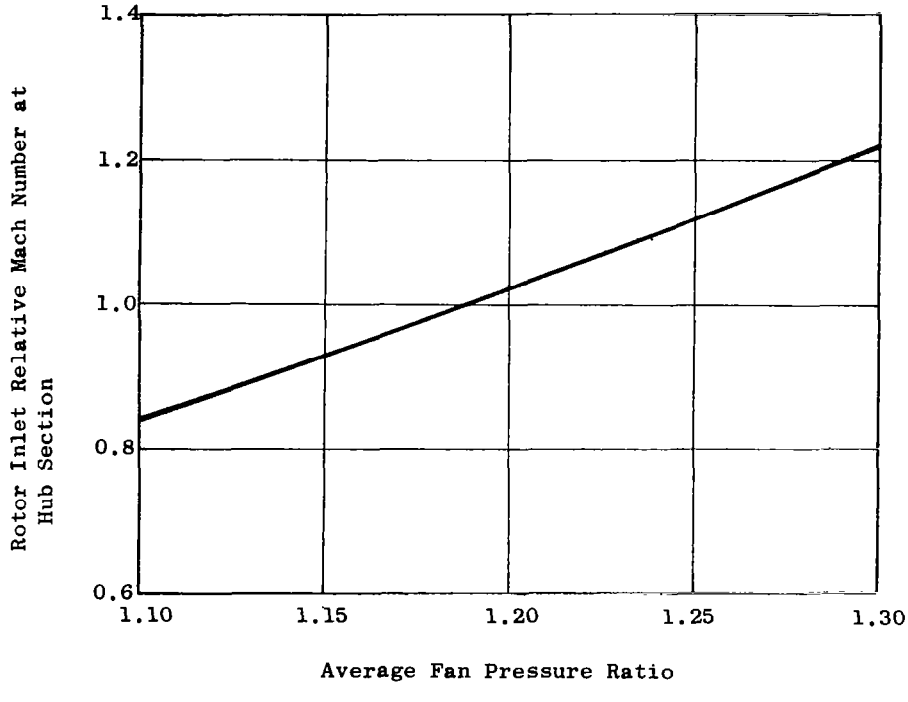

Figure 34b. IGV-Rotor Fan Characteristics - Hub Section.

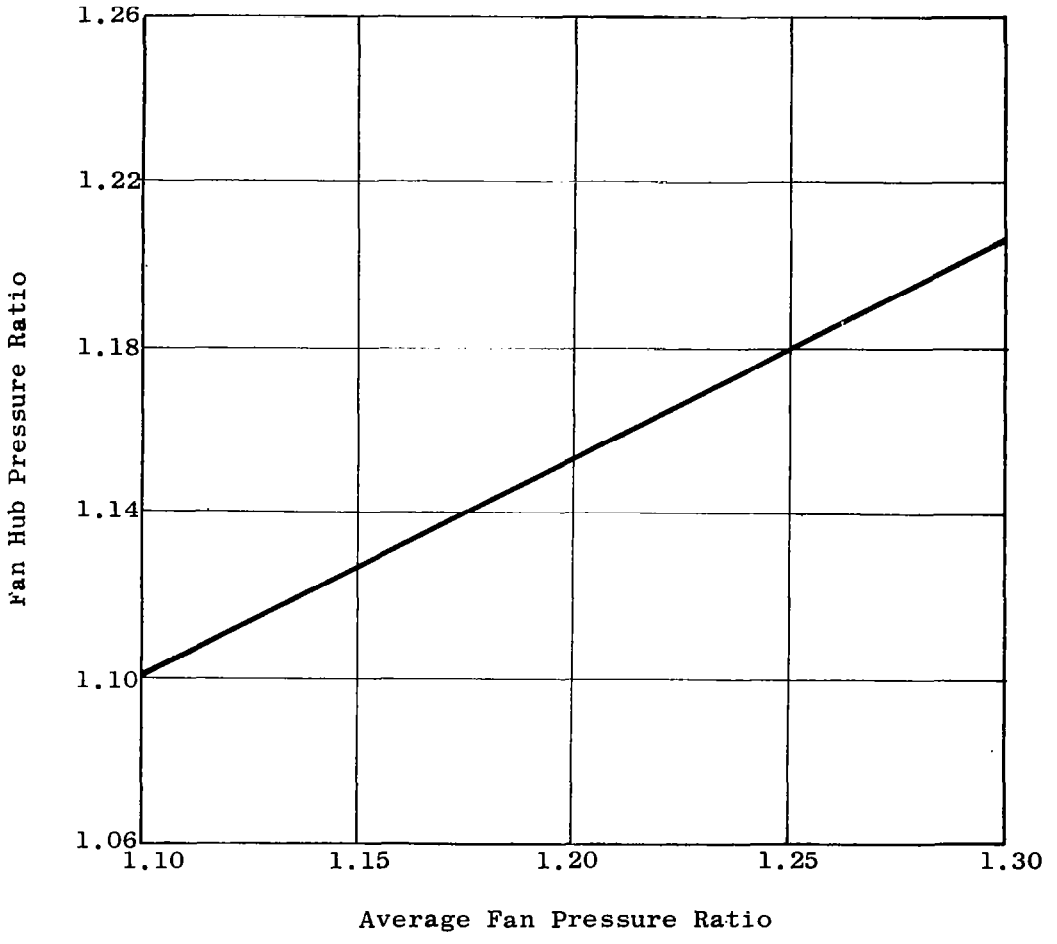

Figure 34c. IGV-Rotor Fan Characteristics - Hub Section.

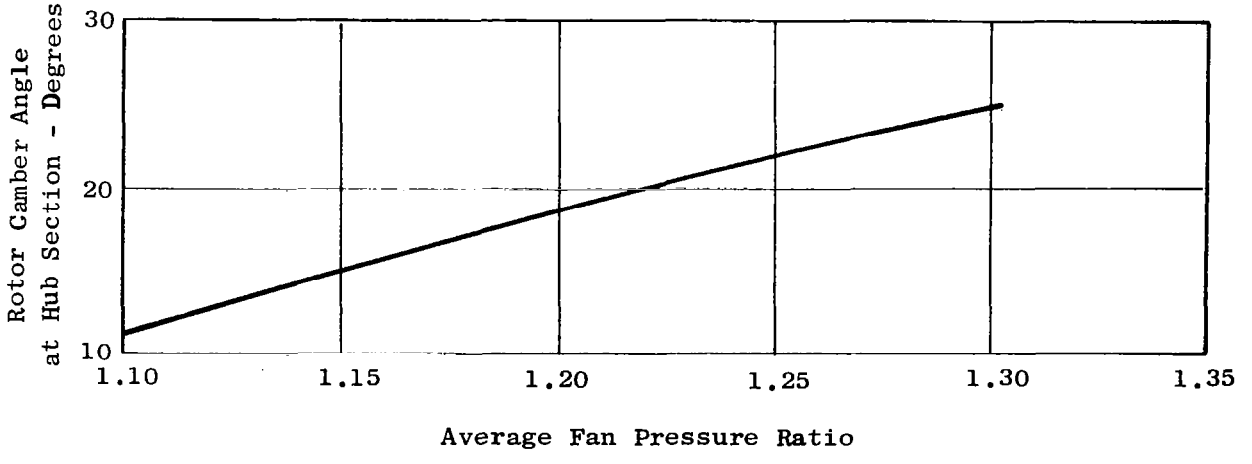

Figure 34d. IGV-Rotor Fan Characteristics - Hub Section.

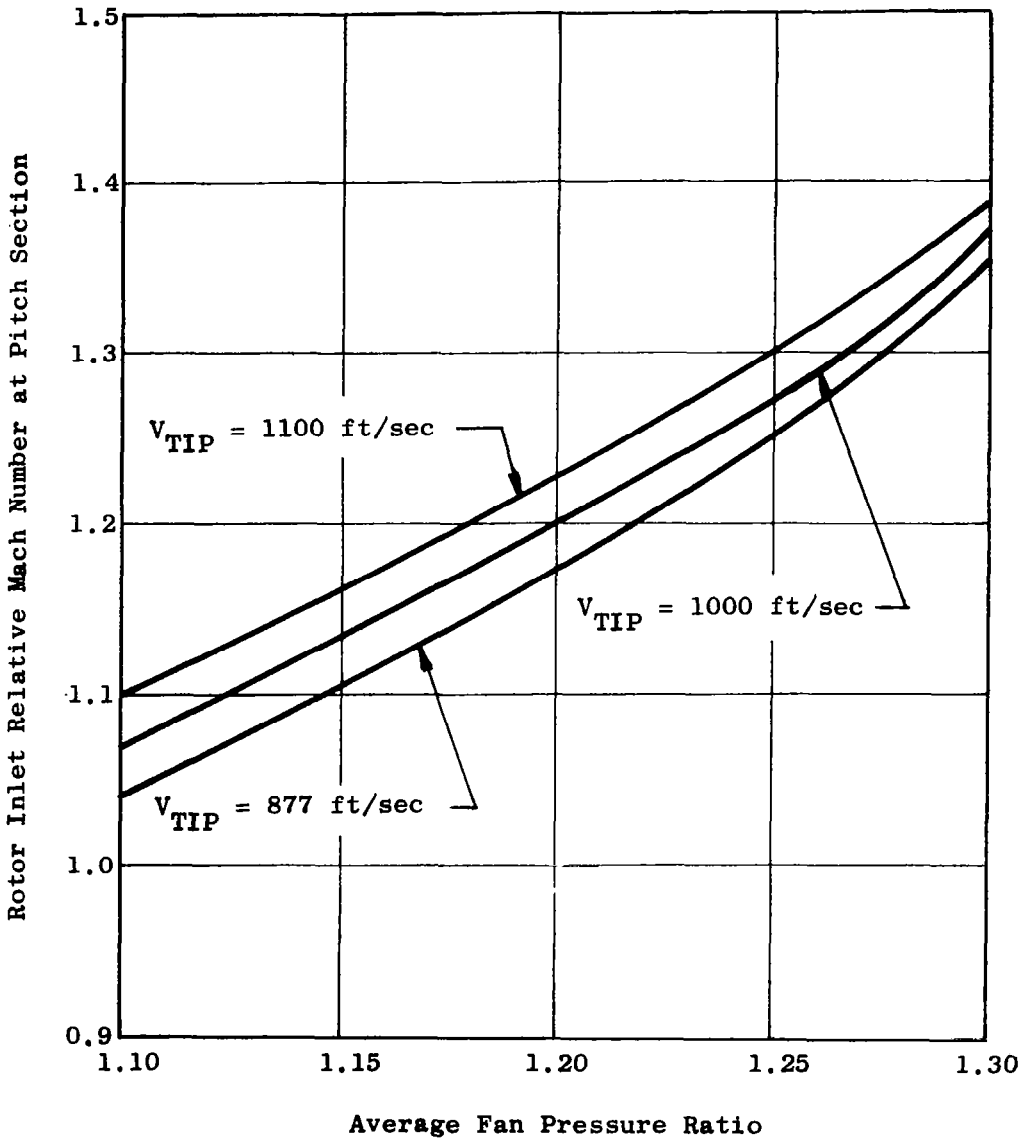

Figure 35a. IGV-Rotor Fan Characteristics - Pitch Section.

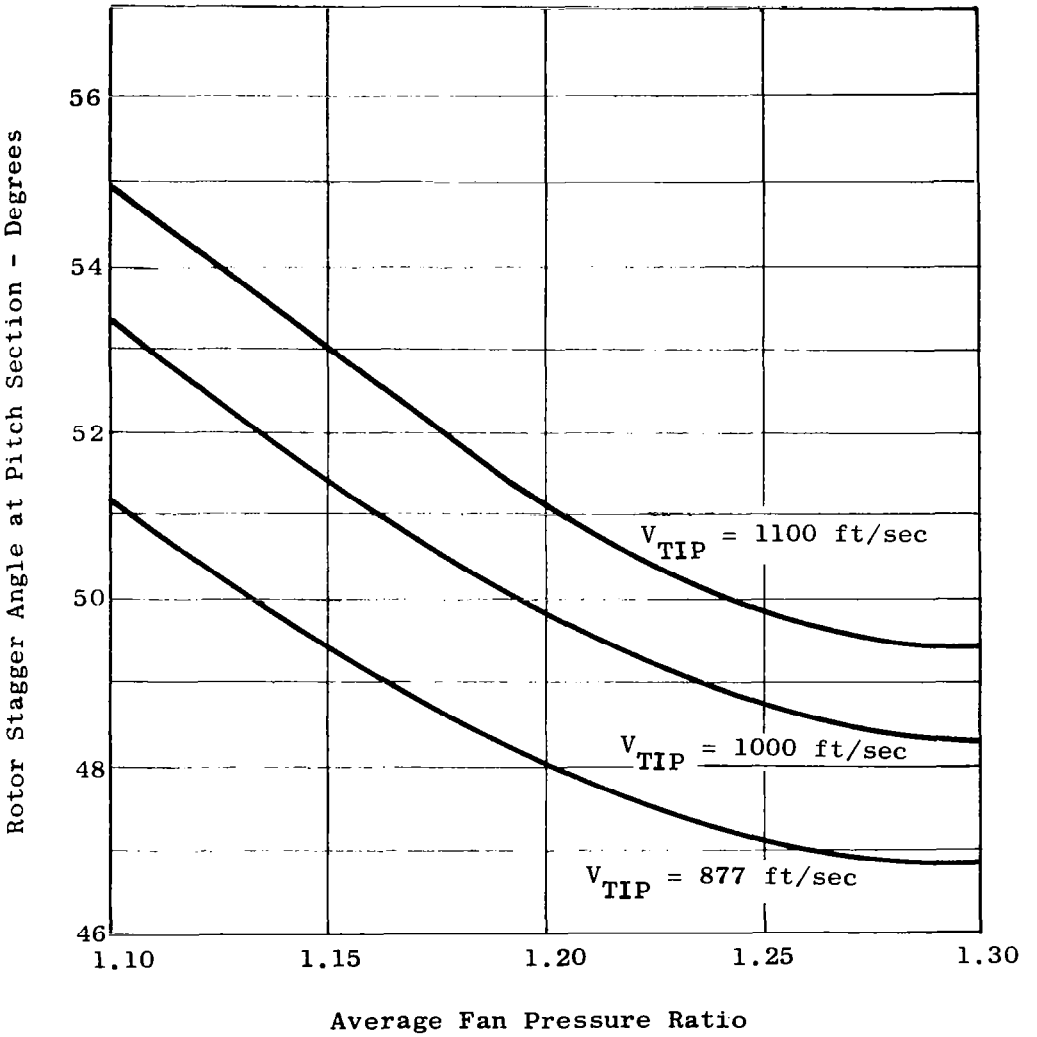

Figure 35b. IGV-Rotor Fan Characteristics - Pitch Section.

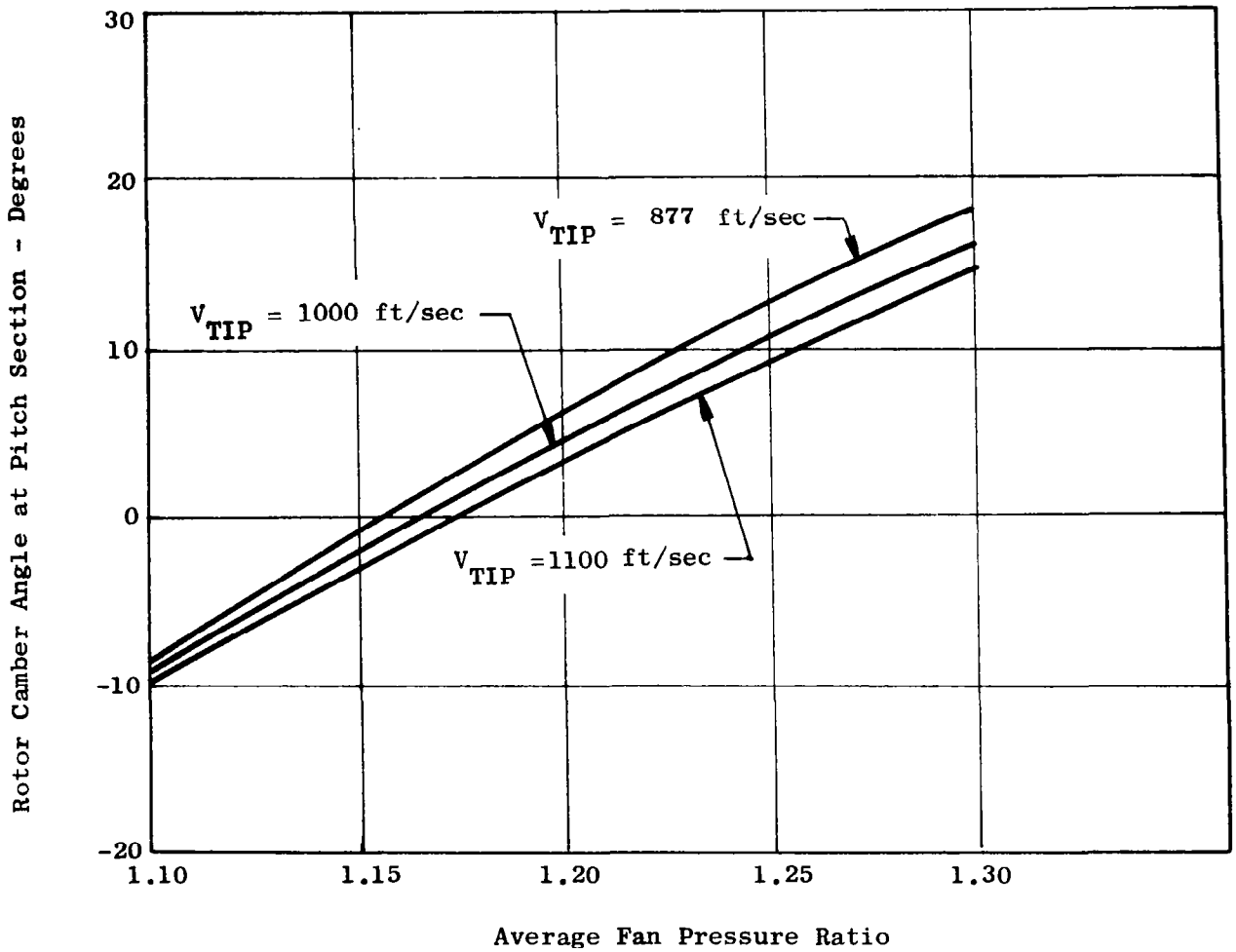

Figure 35c. IGV-Rotor Fan Characteristics - Pitch Section.

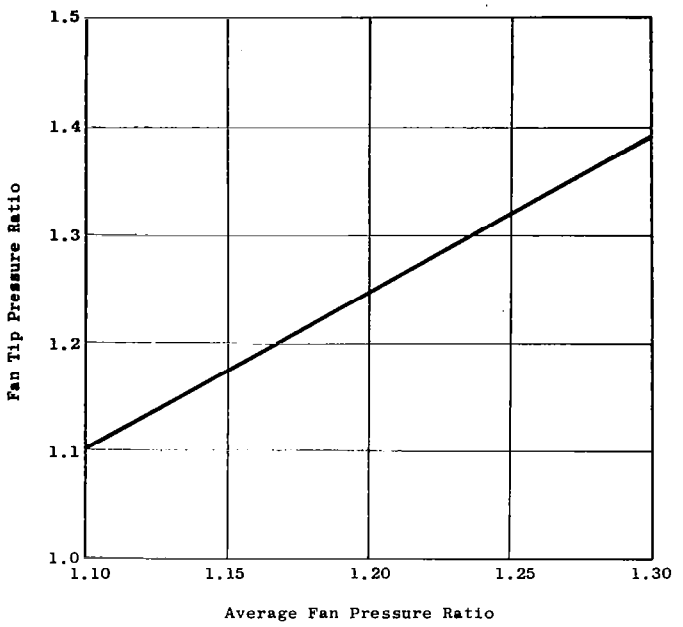

36a. IGV-Rotor Fan Characteristics - Tip Section.

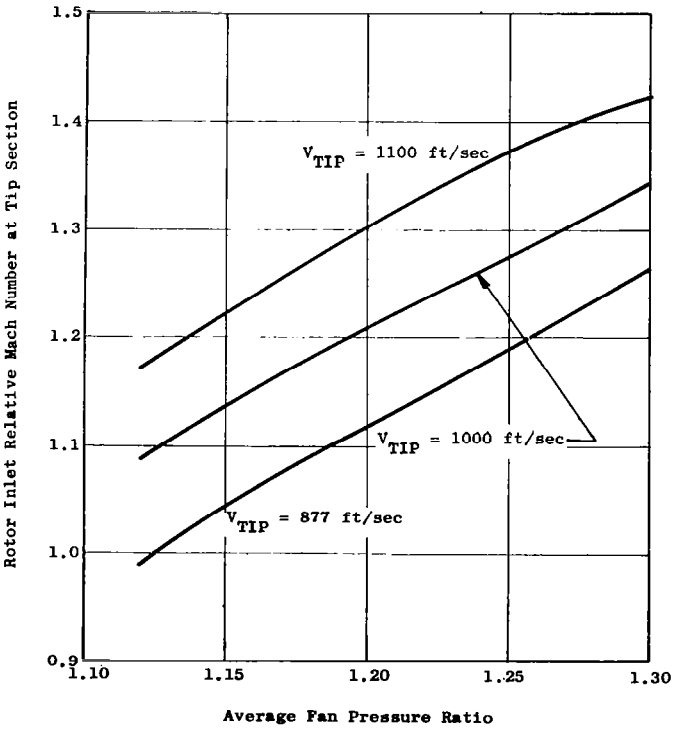

36b. IGV-Rotor Fan Characteristics - Tip Section.

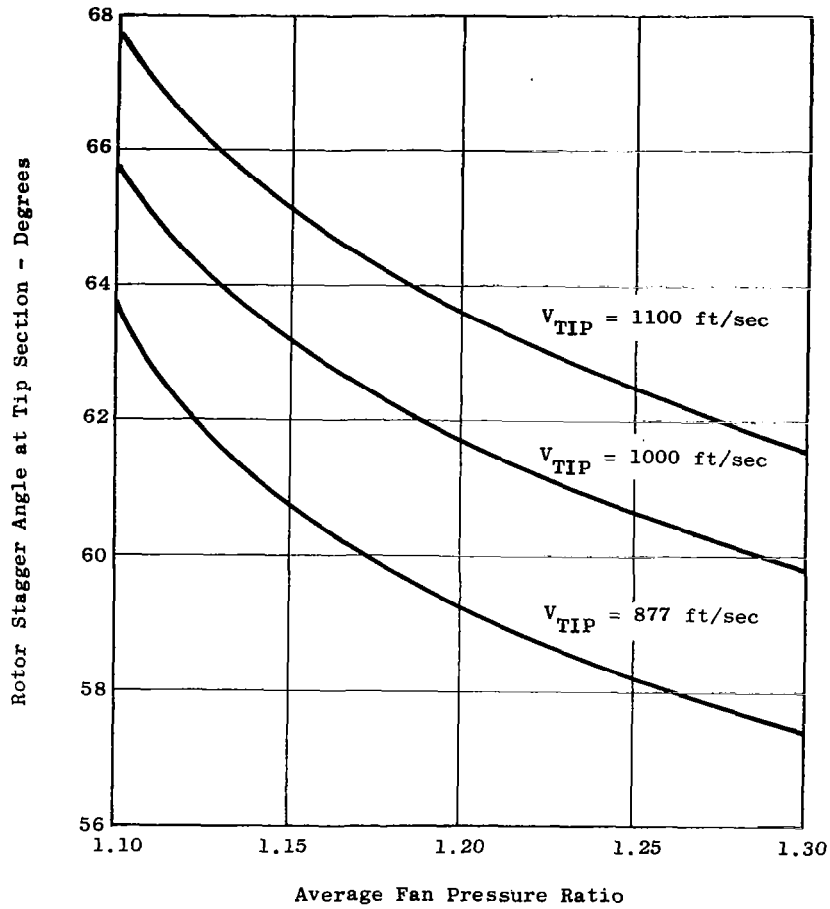

Figure 36c. IGV-Rotor Fan Characteristics - Tip Section.

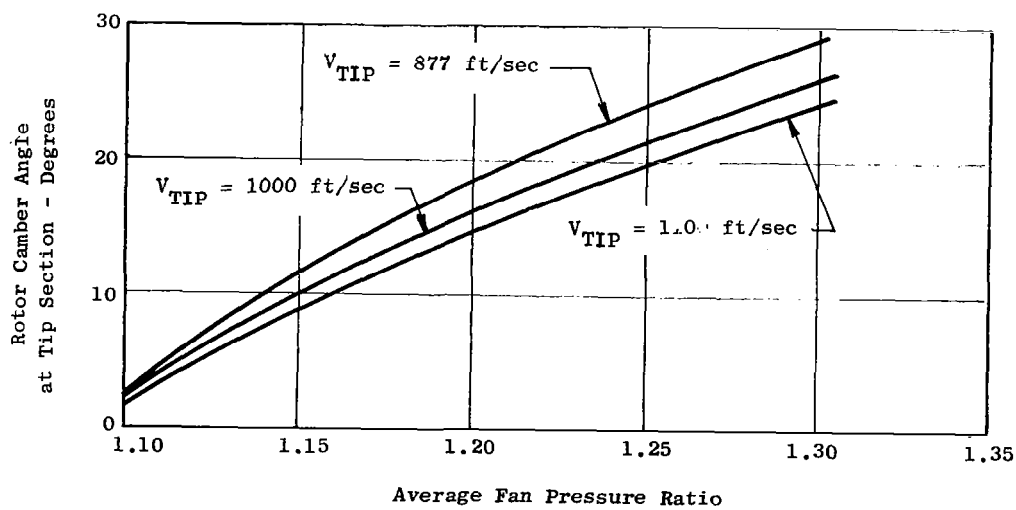

Figure 36d. IGV-Rotor Fan Characteristics - Tip Section.

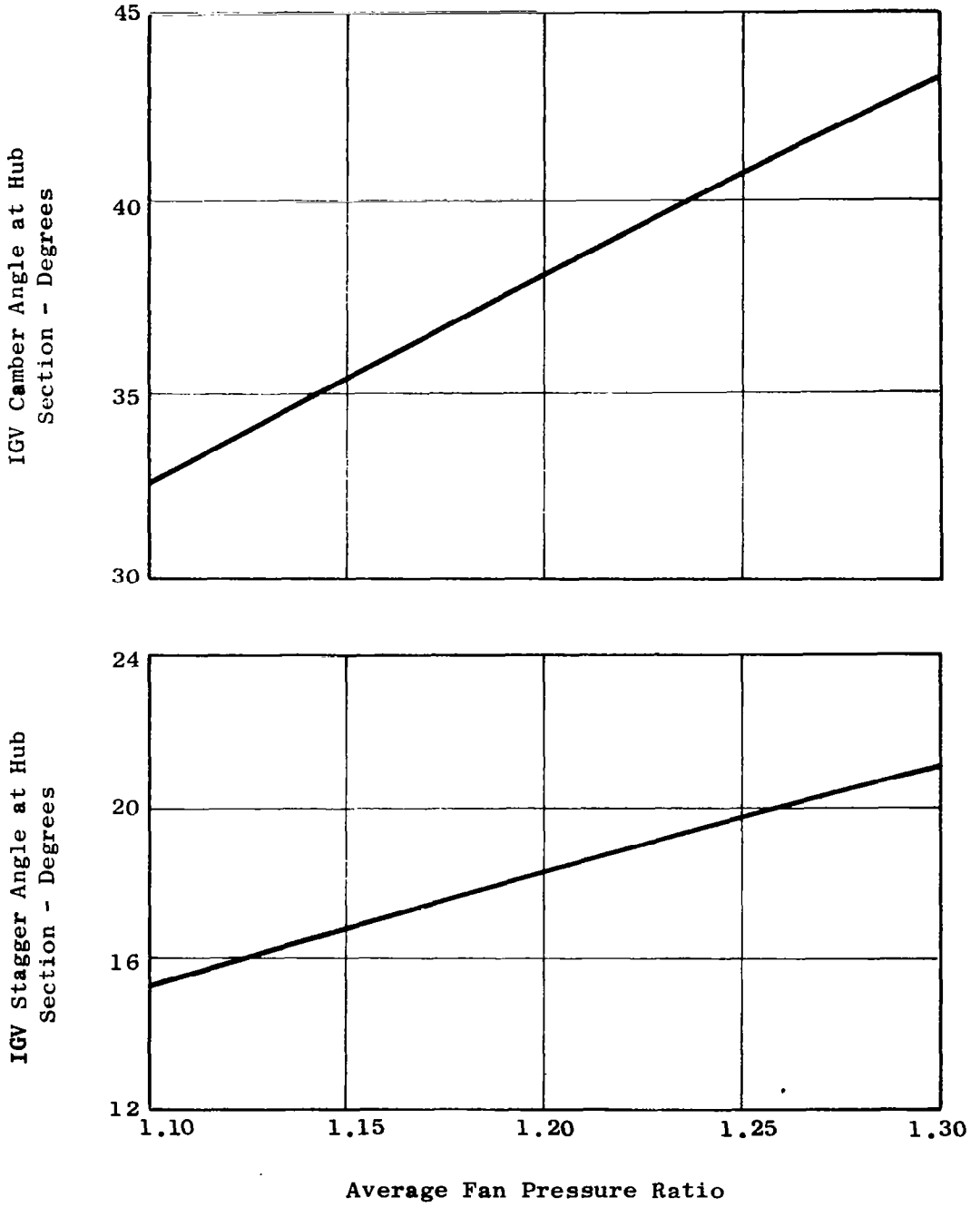

Figure 37a. Inlet Guide Vane Geometry - Hub Section.

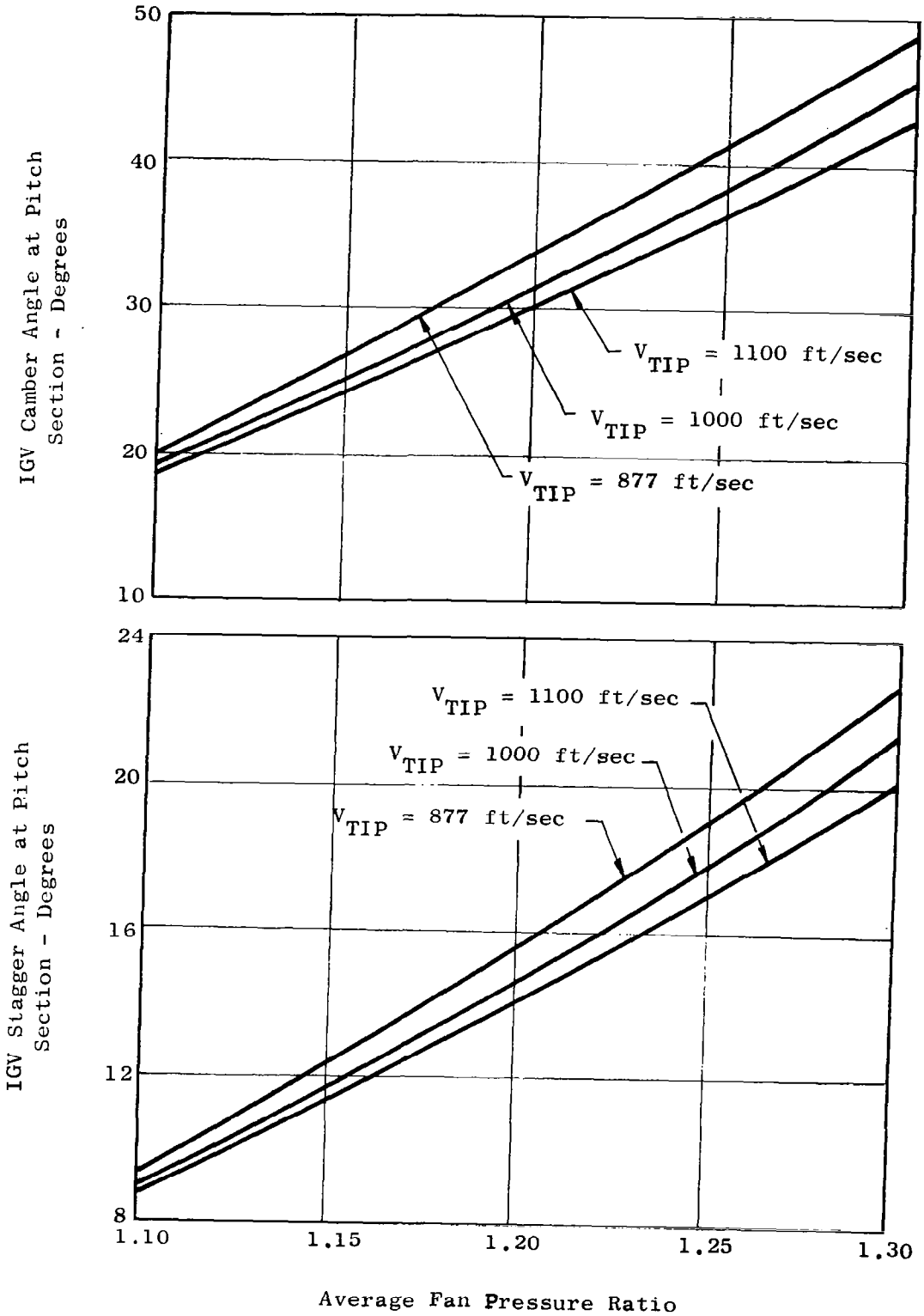

Figure 37b. Inlet Guide Vane Geometry - Pitch Section.

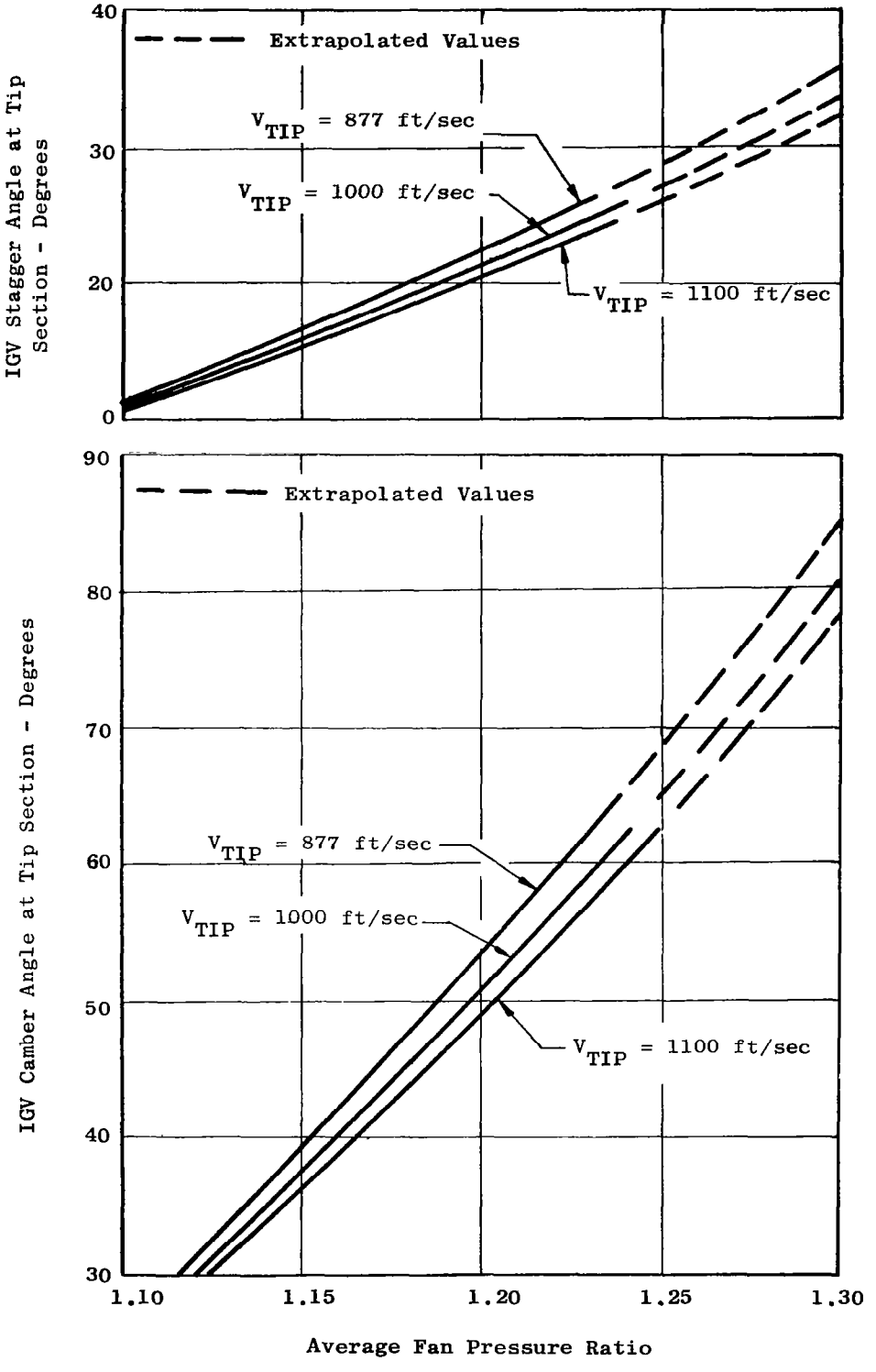

Figure 37c. Inlet Guide Vane Geometry - Tip Section.

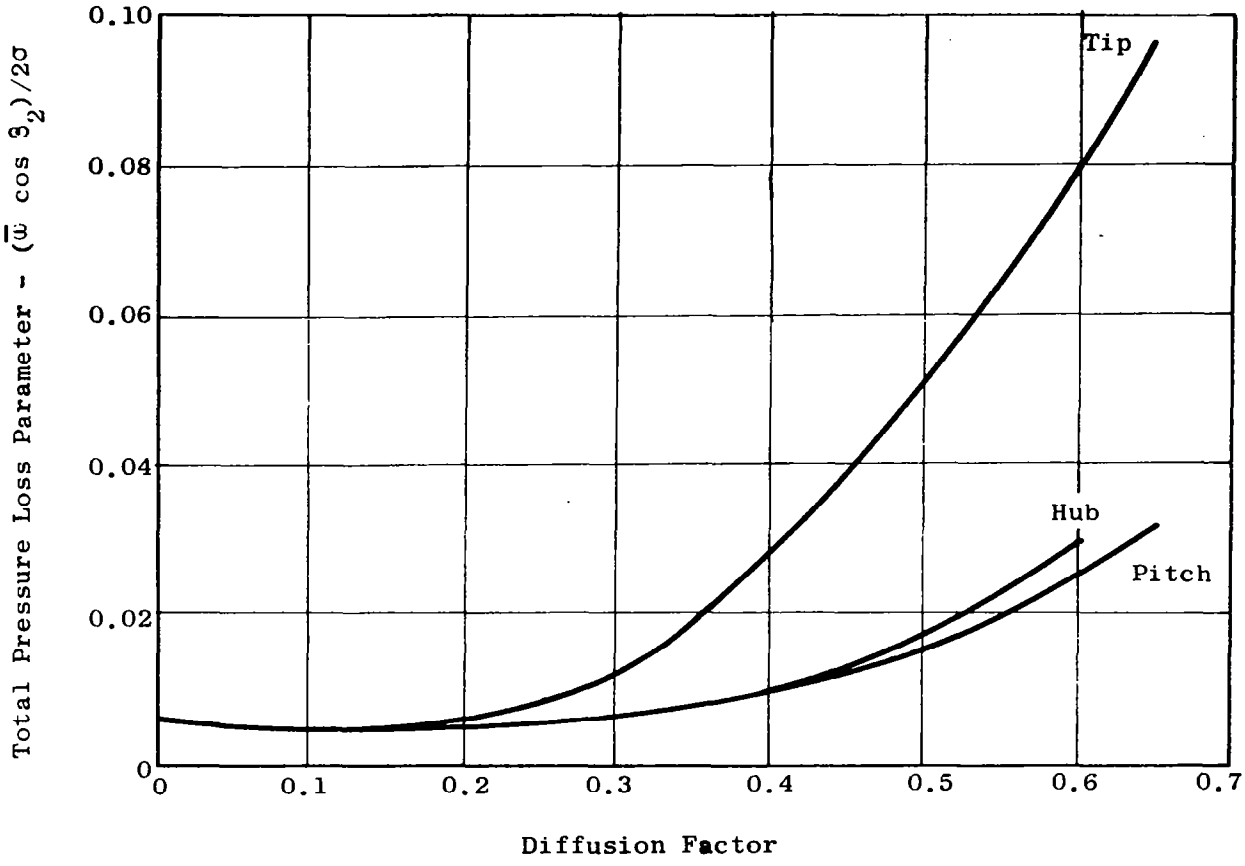

Figure 38. Conventional Fan Characteristics.

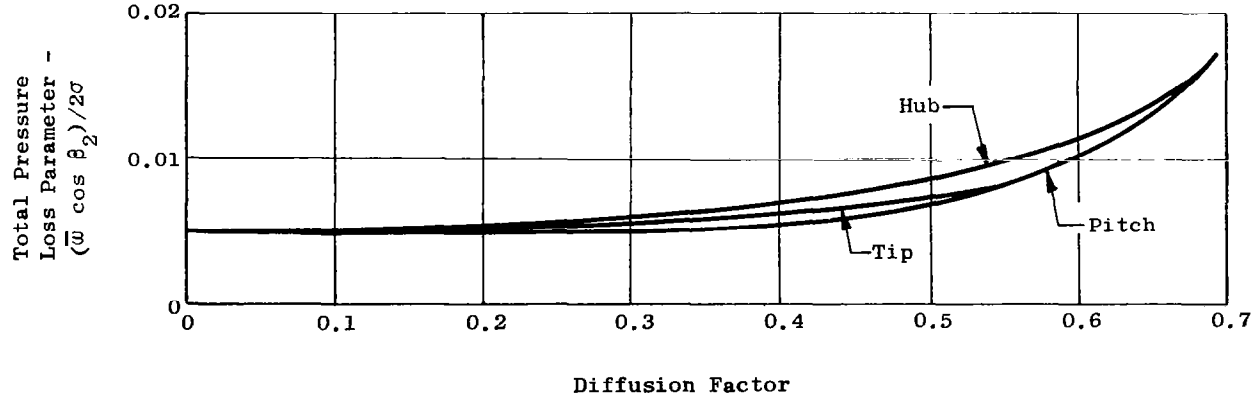

Figure 39. Conventional Fan Characteristics.

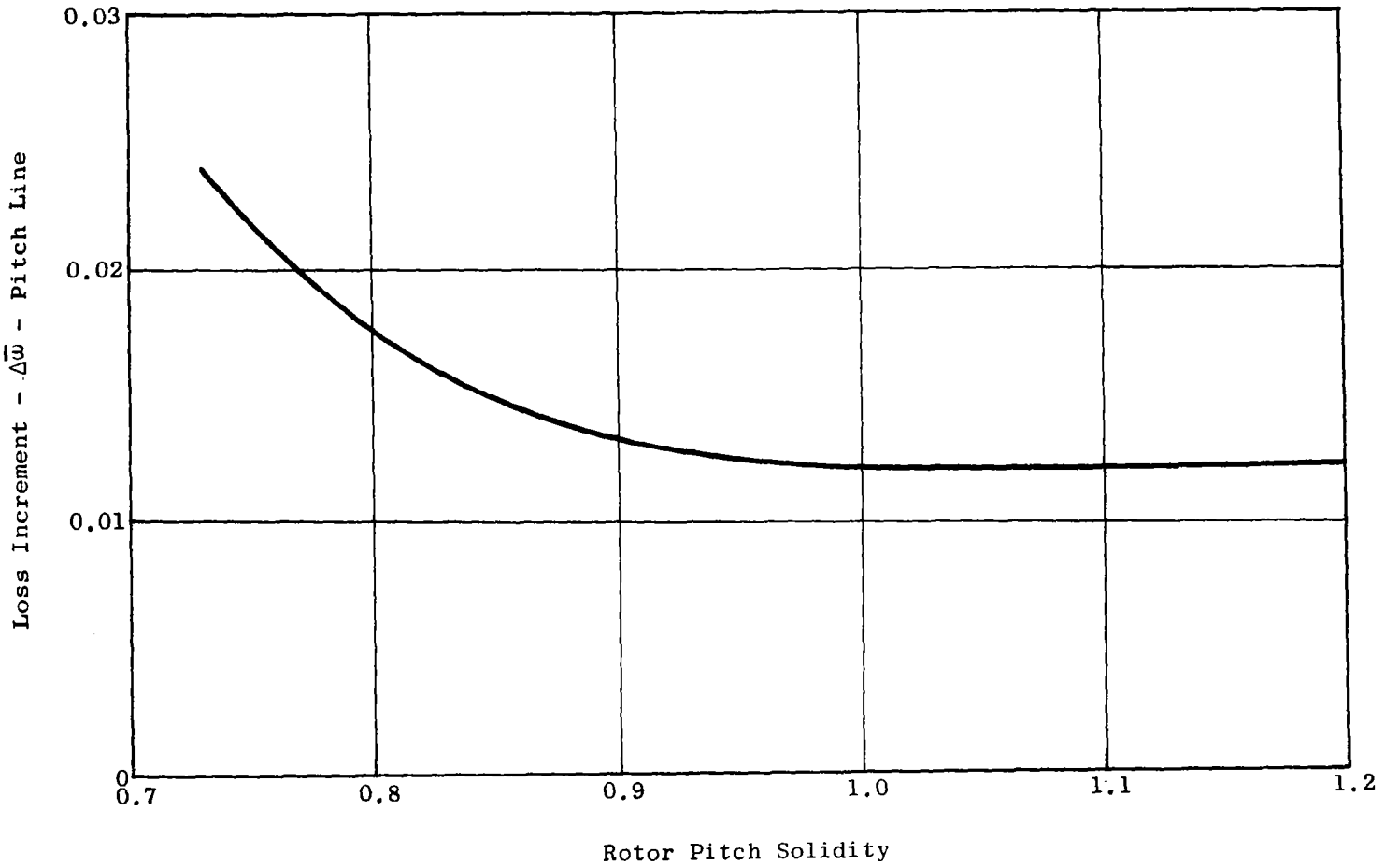

Figure 40. Conventional Fan Characteristics.

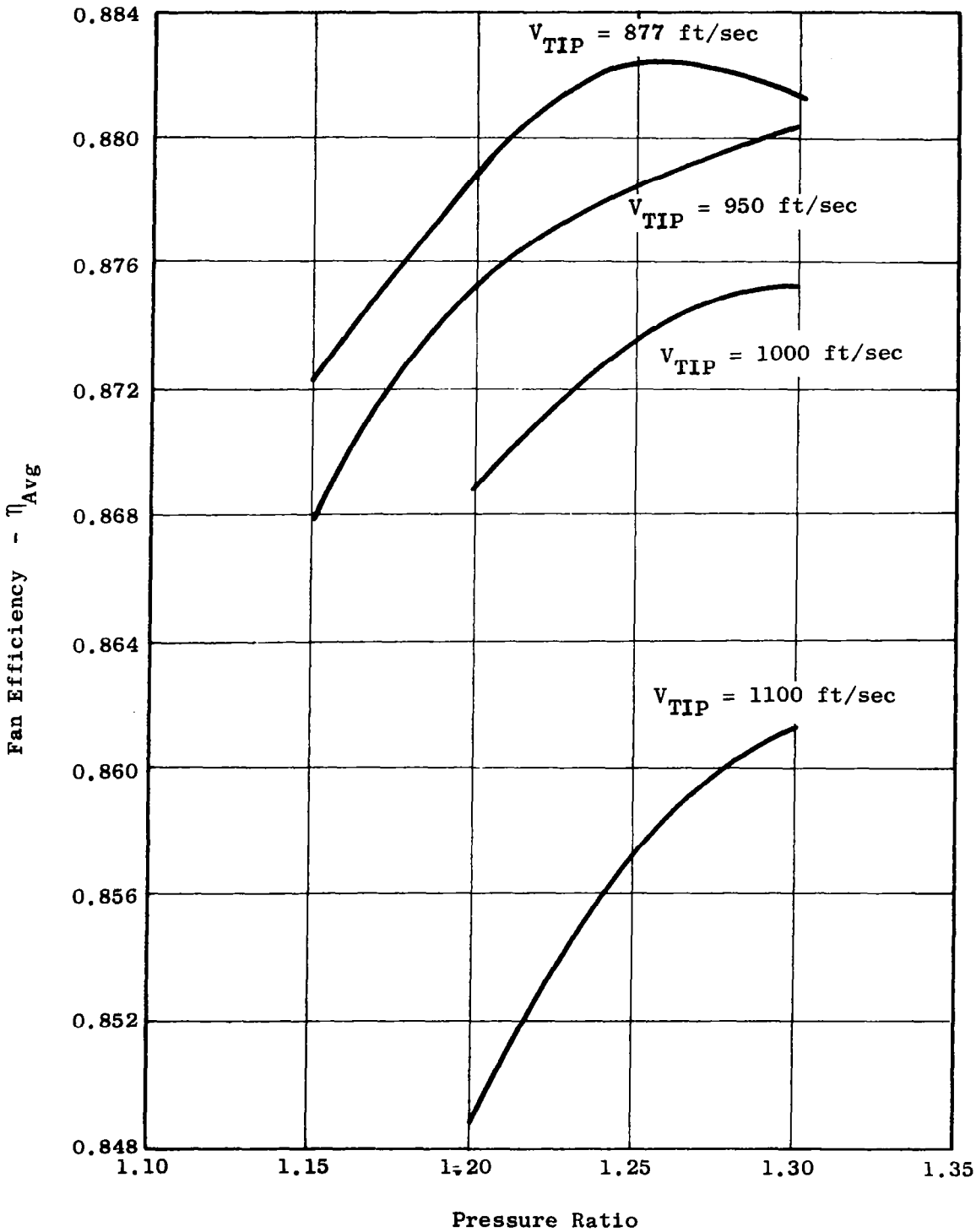

Figure 41. Conventional Fan Characteristics With Uniform Loading.

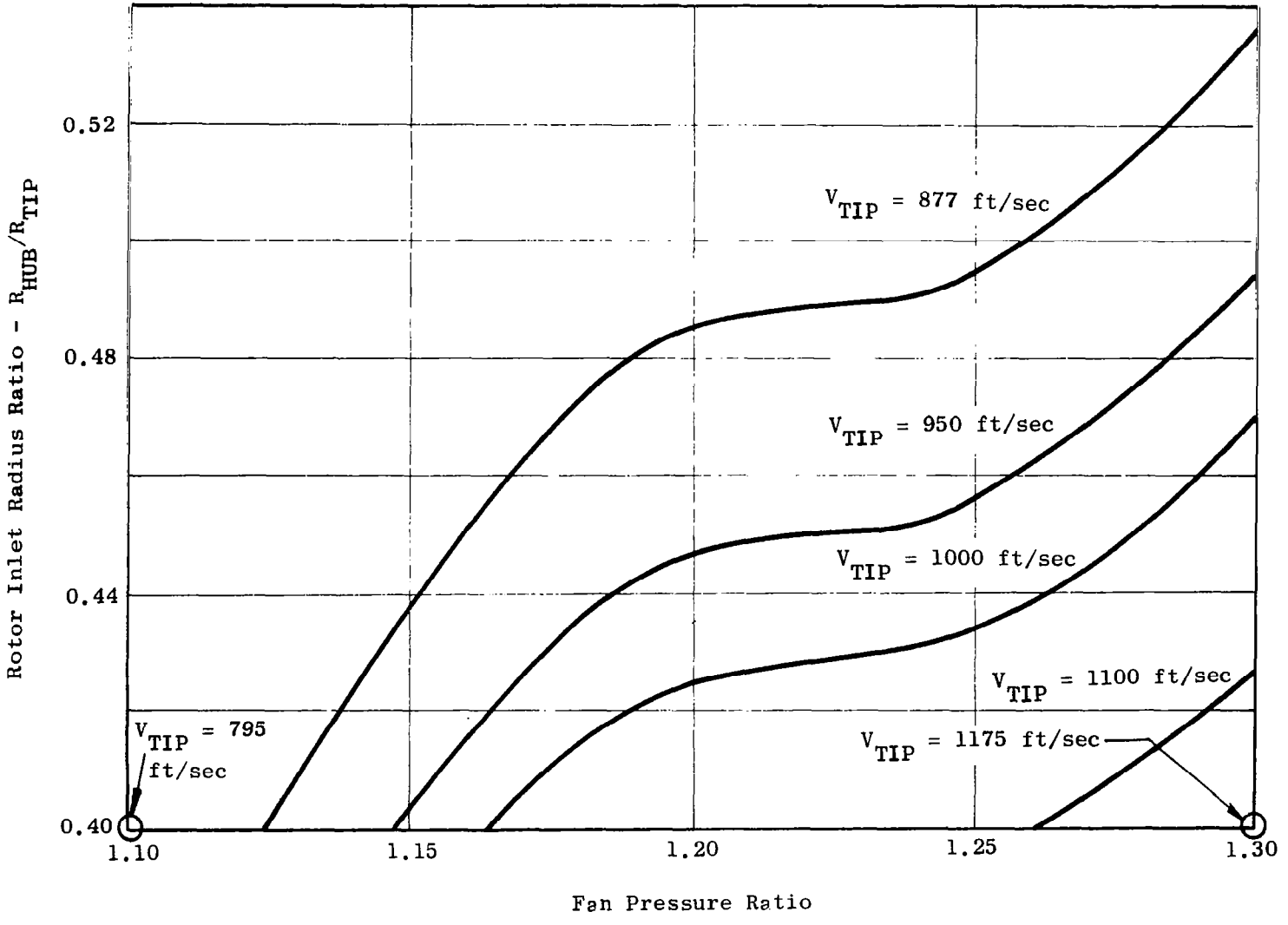

Figure 42. Conventional Fan Characteristics With Uniform Loading.

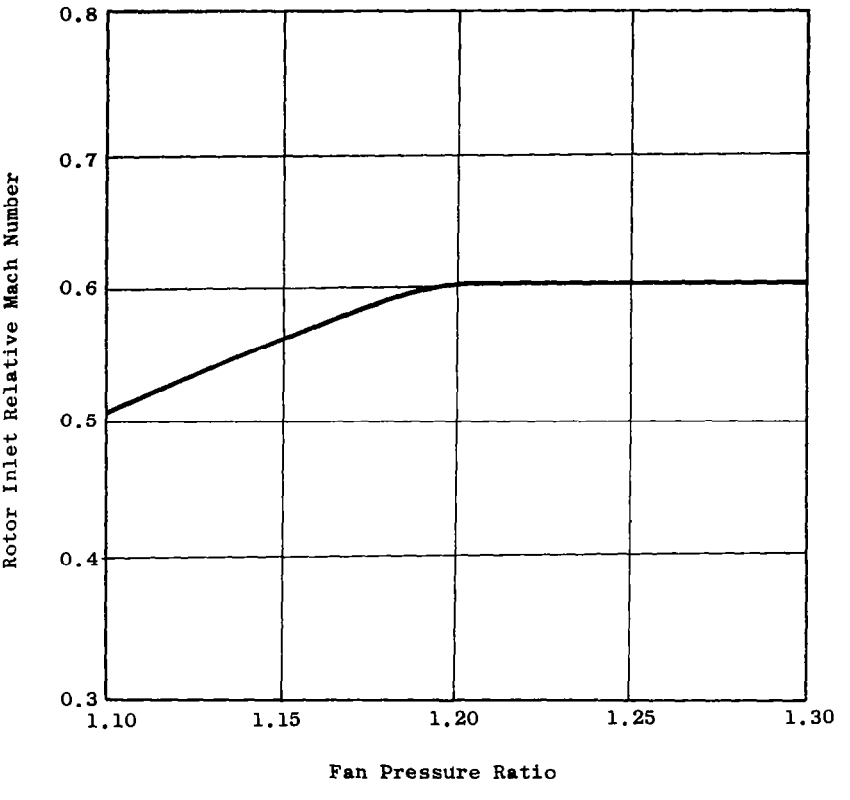

Fan 43a. Conventional Fan Characteristics With Uniform Loading - Hub Section.

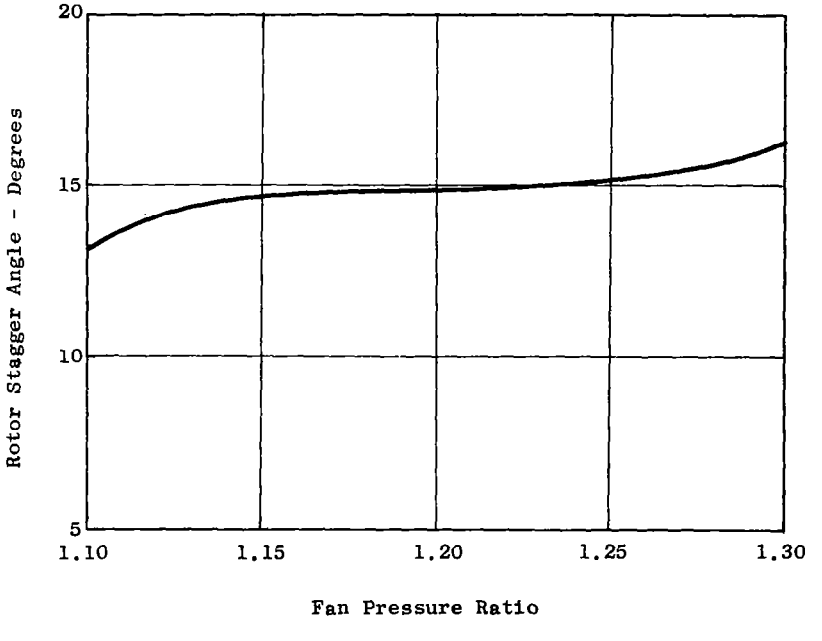

Figure 43b. Conventional Fan Characteristics With Uniform Loading - Hub Section.

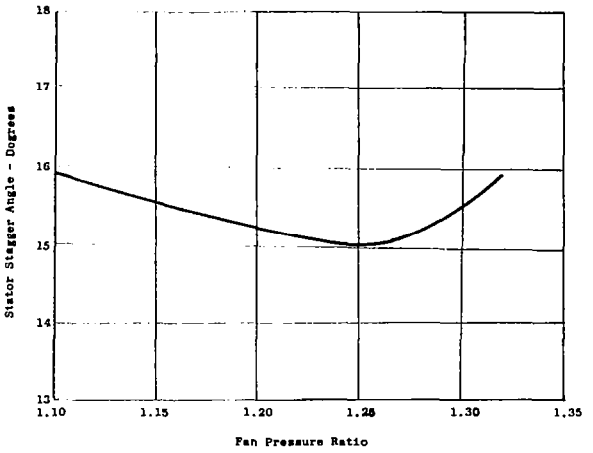

Figure 43c. Conventional Fan Characteristics With Uniform Loading - Hub Section.

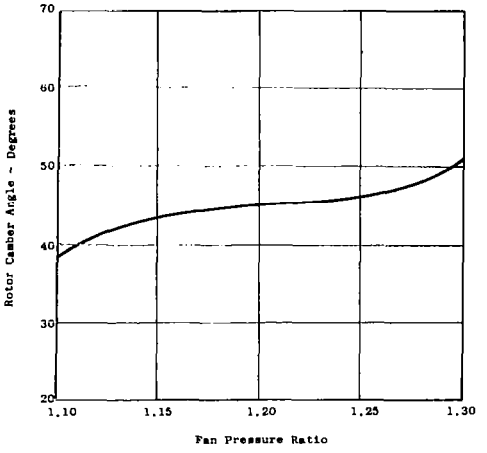

Figure 43d. Conventional Fan Characteristics With Uniform Loading - Hub Section.

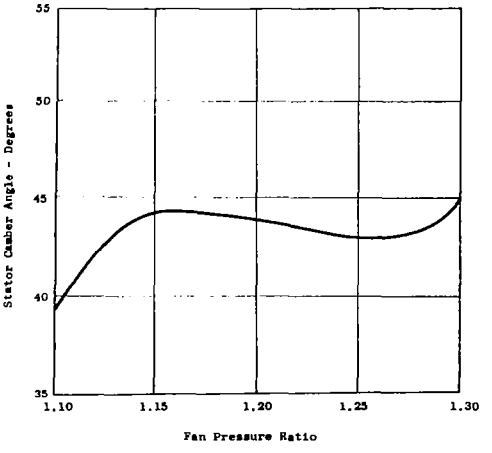

Figure 43e. Conventional Fan Characteristics With Uniform Loading - Hub Section.

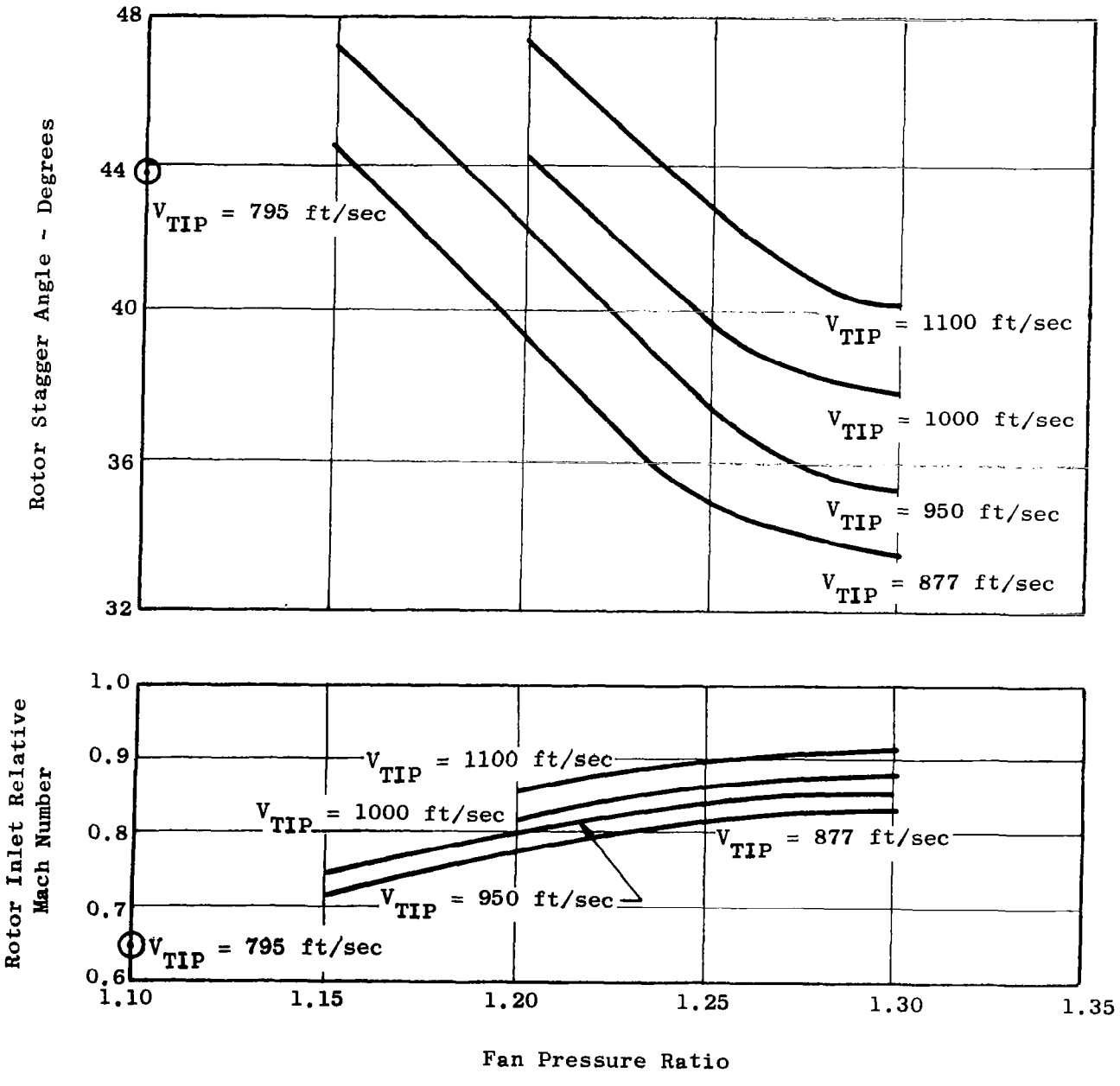

Figure 44a. Conventional Fan Characteristics With Uniform Loading - Pitch Section.

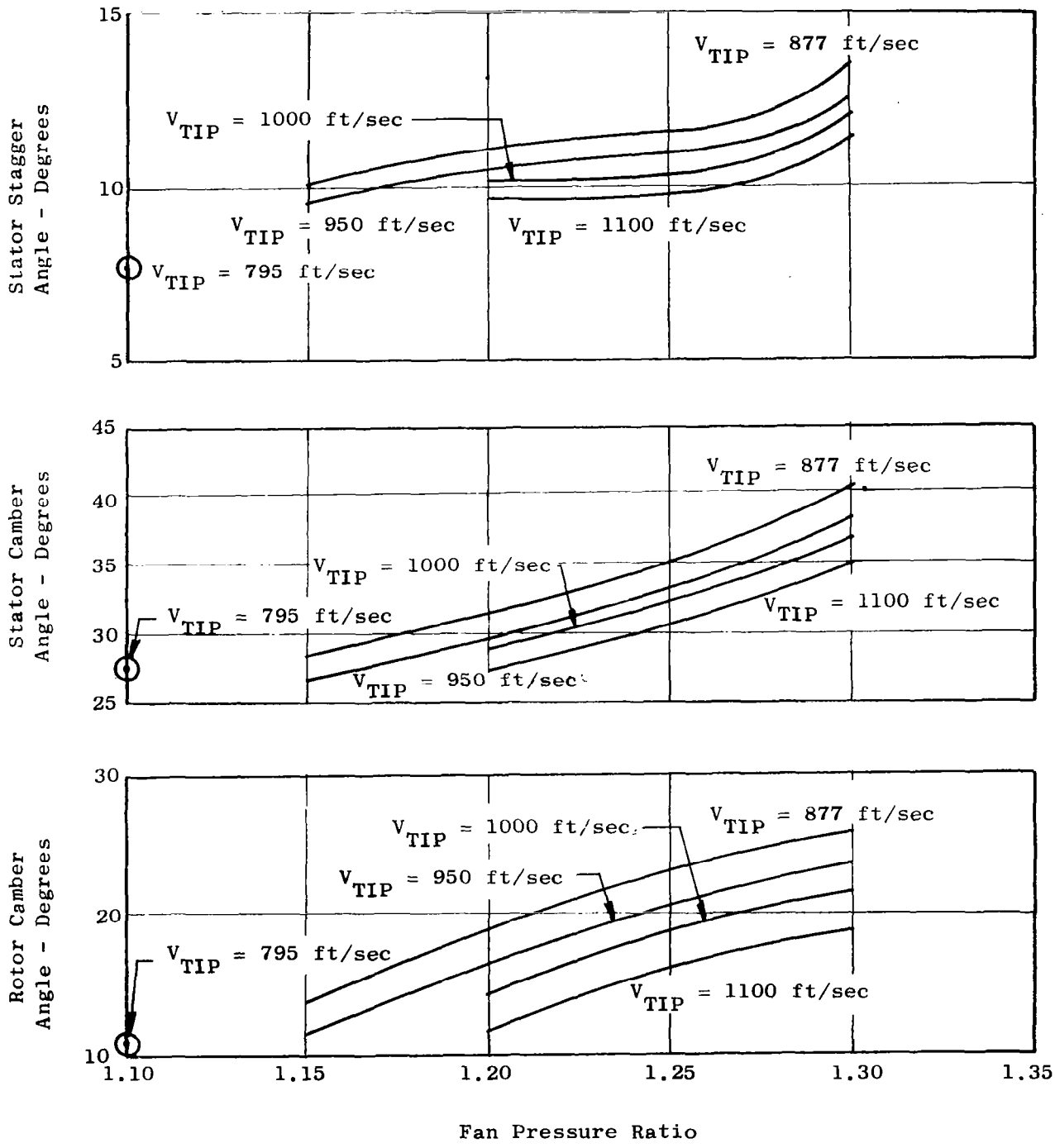

Figure 44b. Conventional Fan Characteristics With Uniform Loading - Pitch Section.

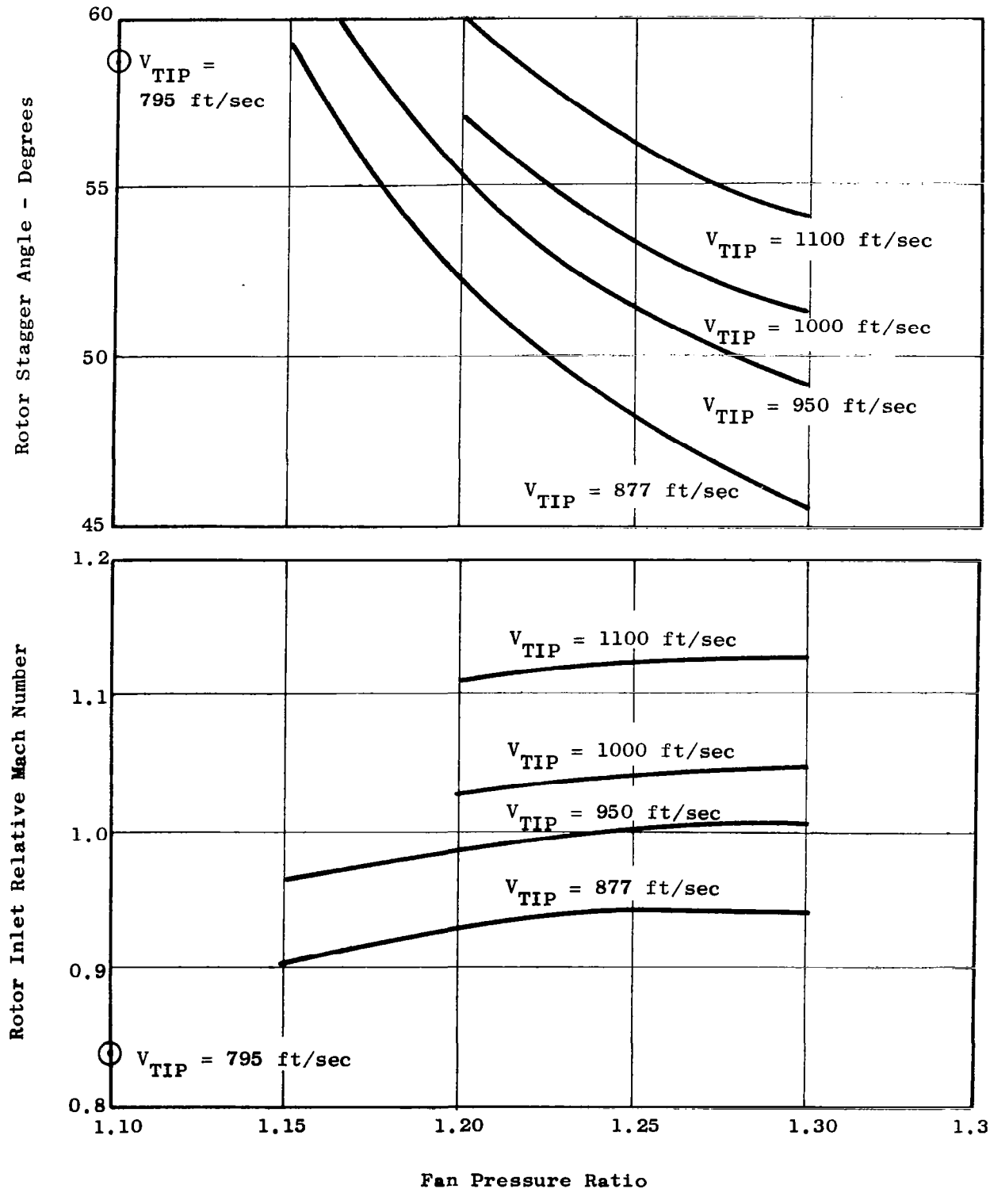

Figure 45a. Conventional Fan Characteristics With Uniform Loading - Tip Section.

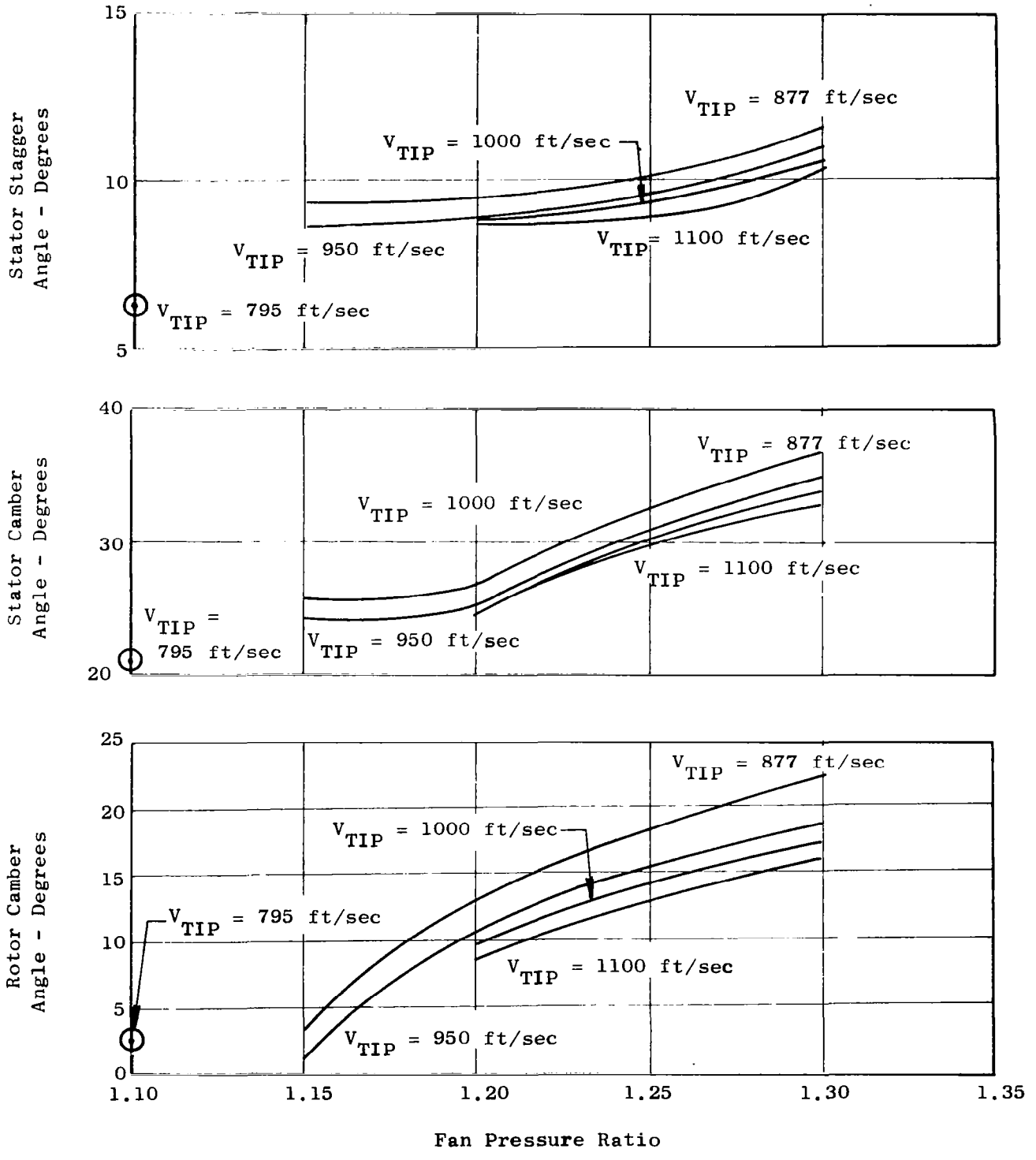

Figure 45b. Conventional Fan Characteristics With Uniform Loading - Tip Section.

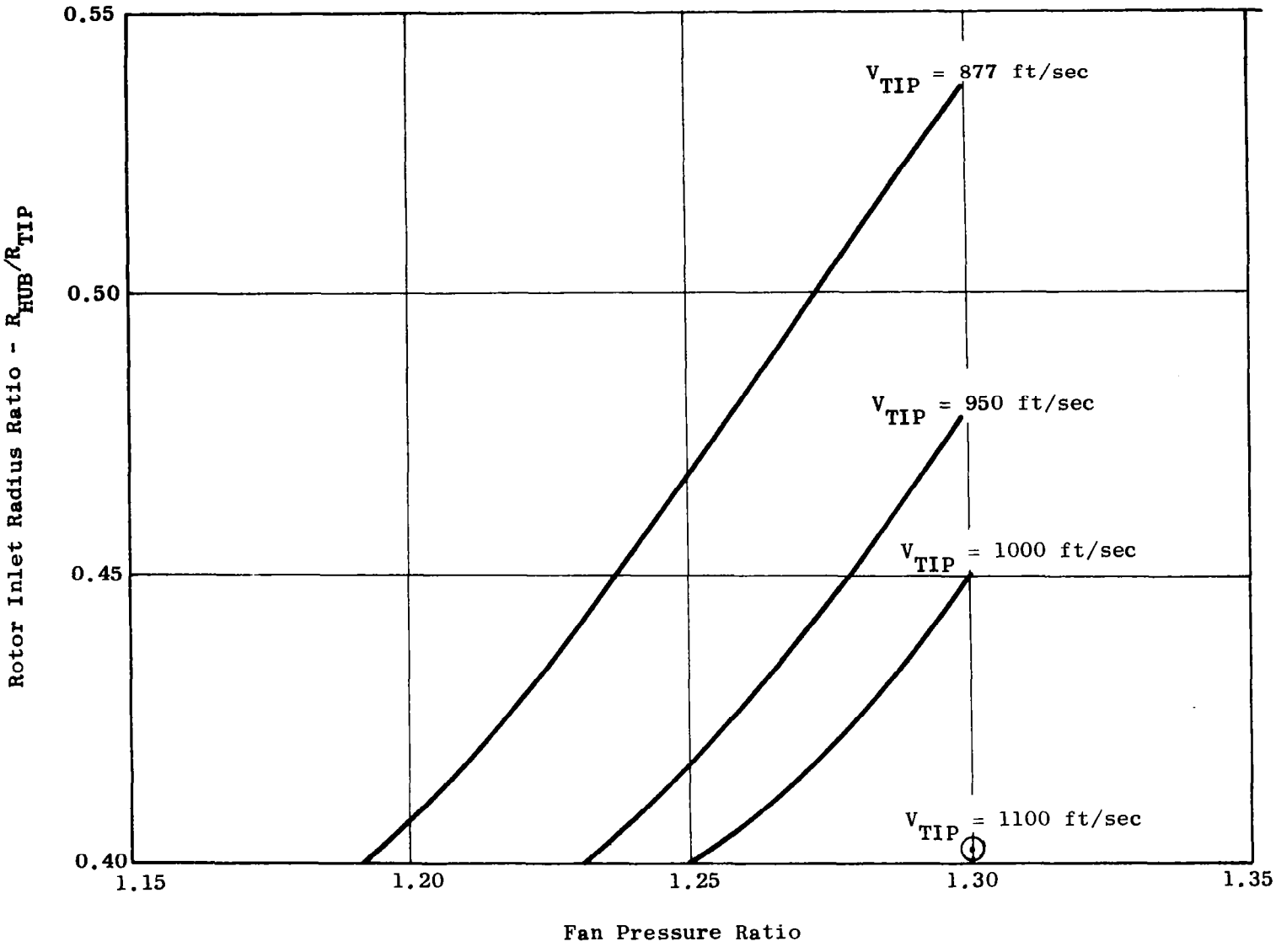

Figure 46. Conventional Fan Characteristics With Non-Uniform Loading.

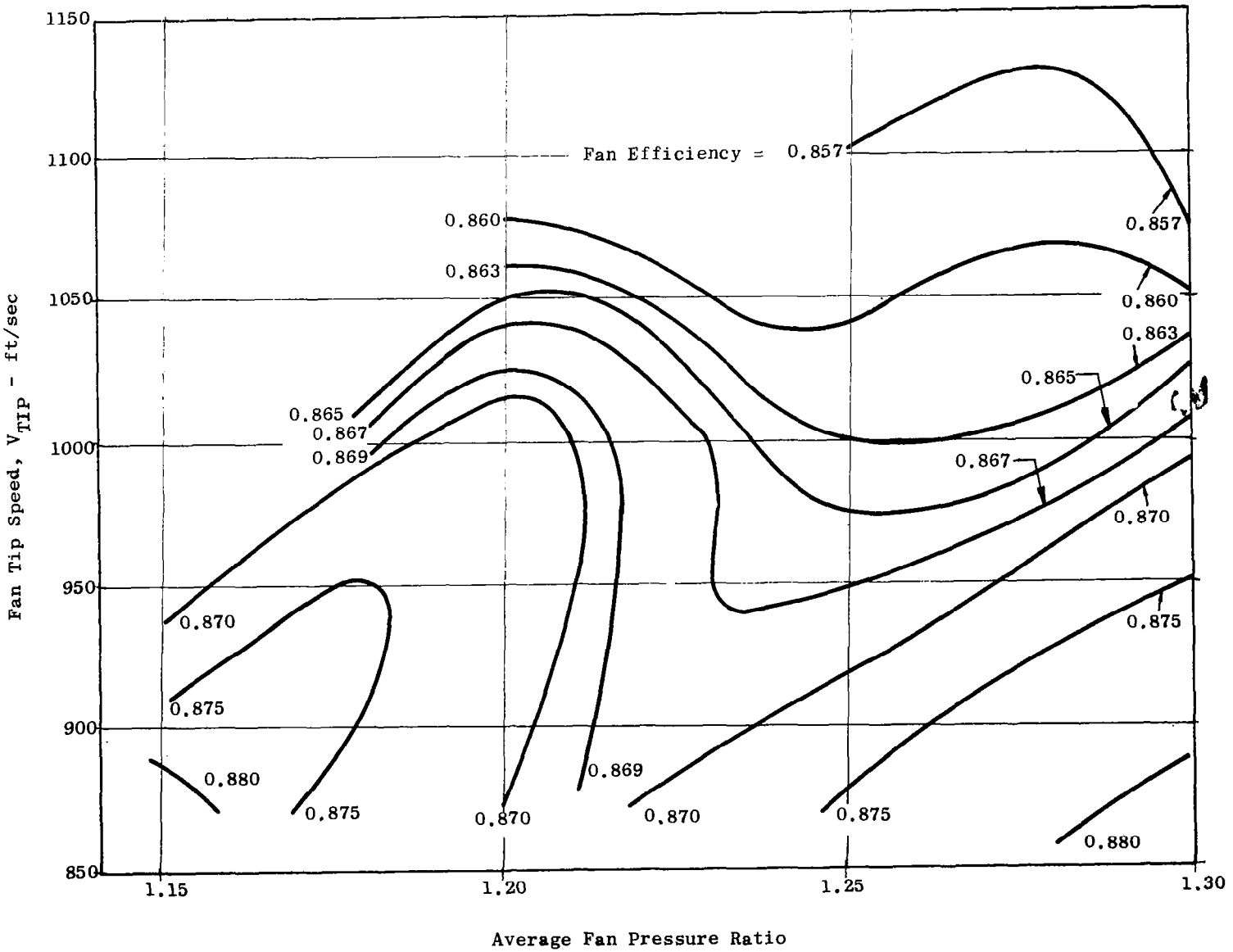

Figure 47. Conventional Fan Efficiency Trends With Non-Uniform Loading.

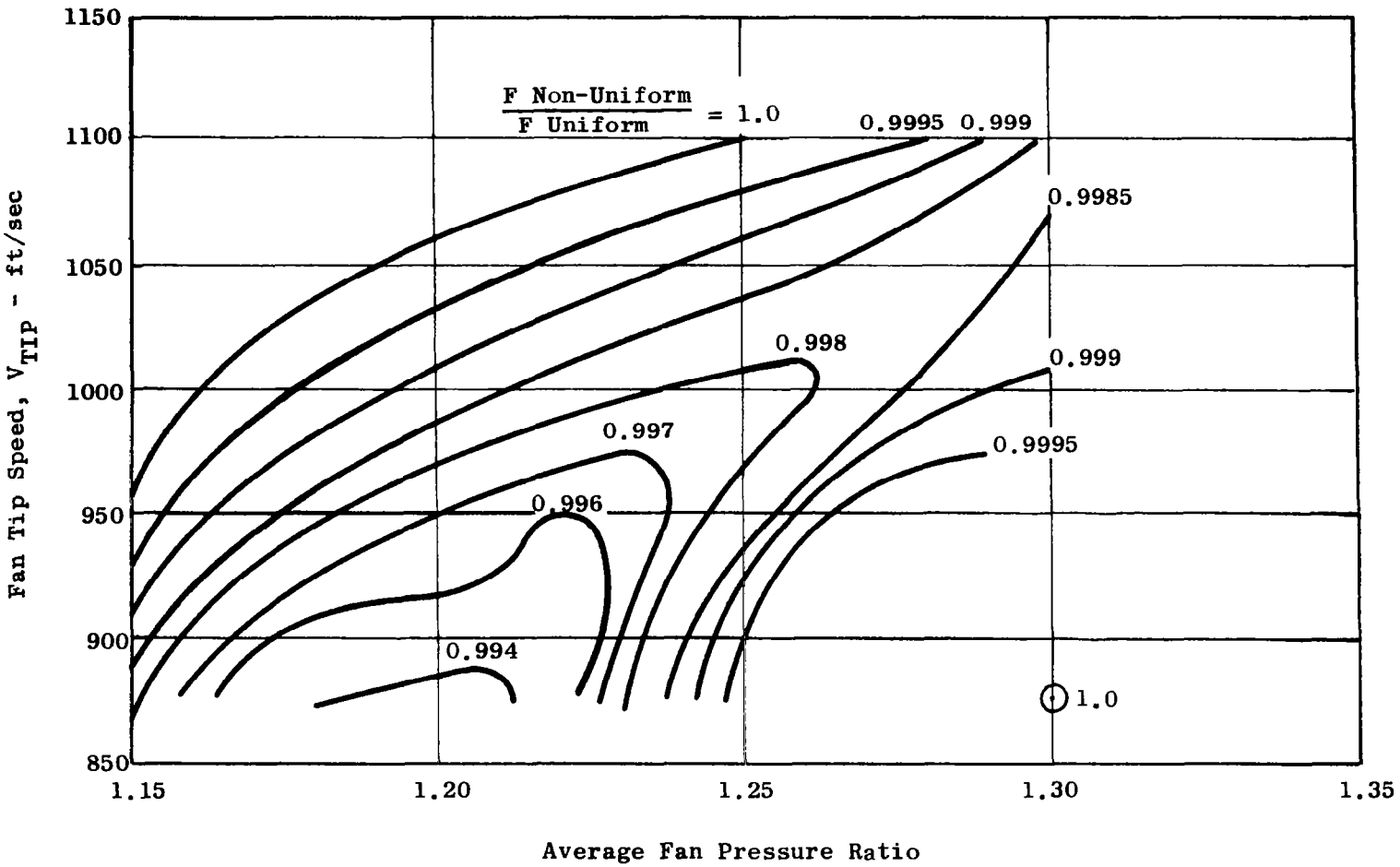

Figure 48. Conventional Fan Thrust Losses Due to Non-Uniform Loading.

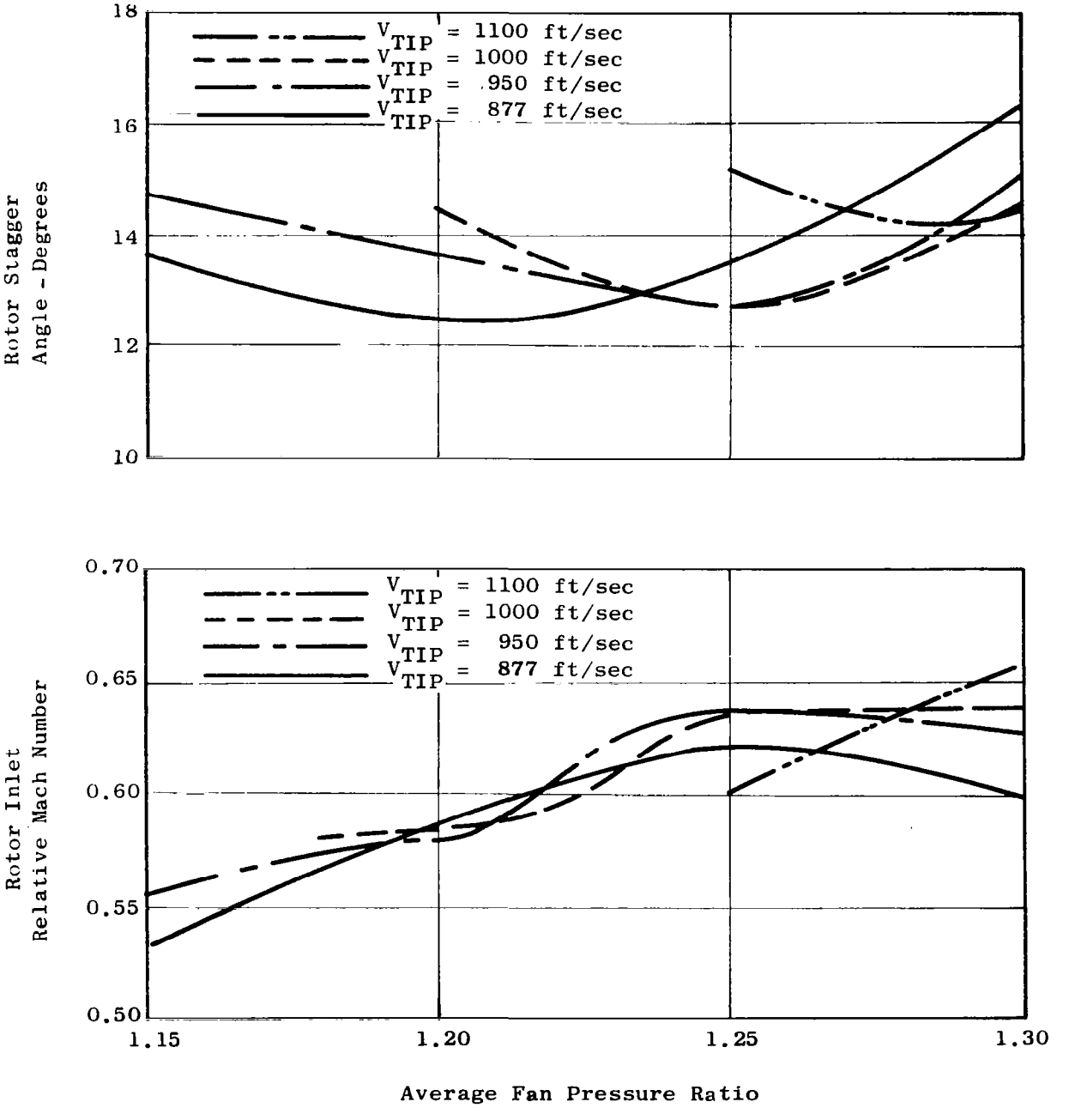

Figure 49a. Conventional Fan Characteristics With Non-Uniform Loading - Hub Section.

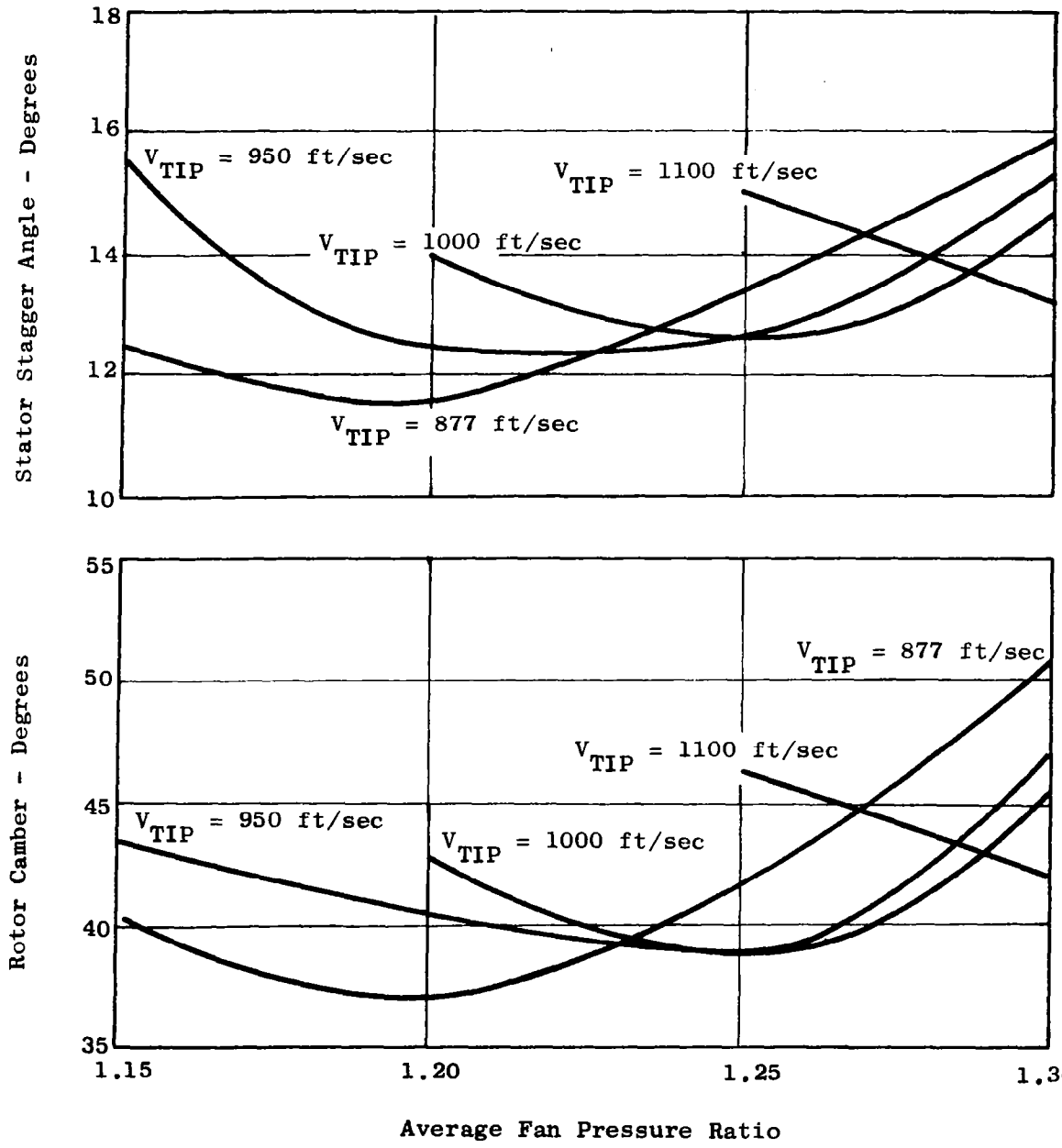

Figure 49b. Conventional Fan Characteristics With Non-Uniform Loading - Hub Section.

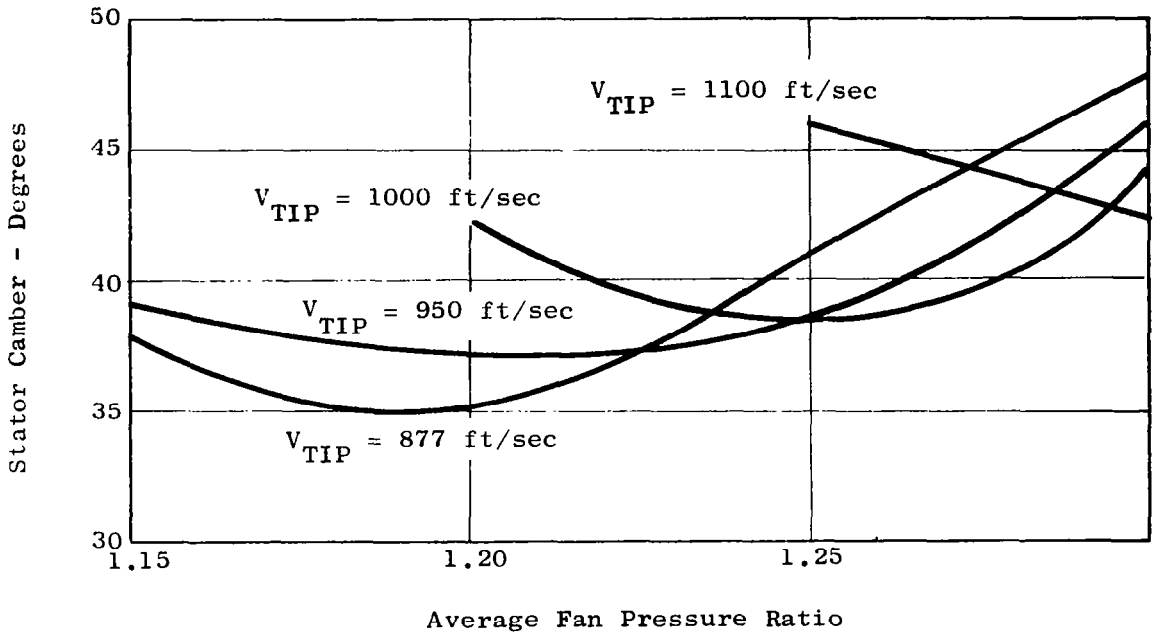

Figure 49c. Conventional Fan Characteristics With Non-Uniform Loading - Hub Section.

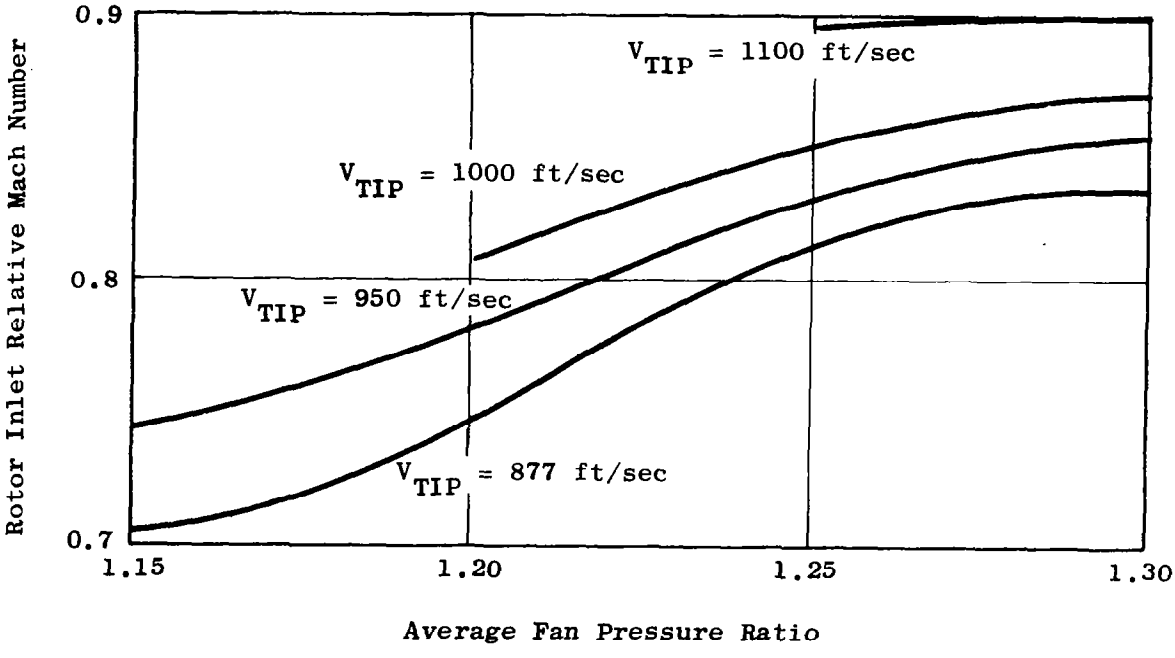

Figure 50a. Conventional Fan Characteristics With Non-Uniform Loading - Pitch Section.

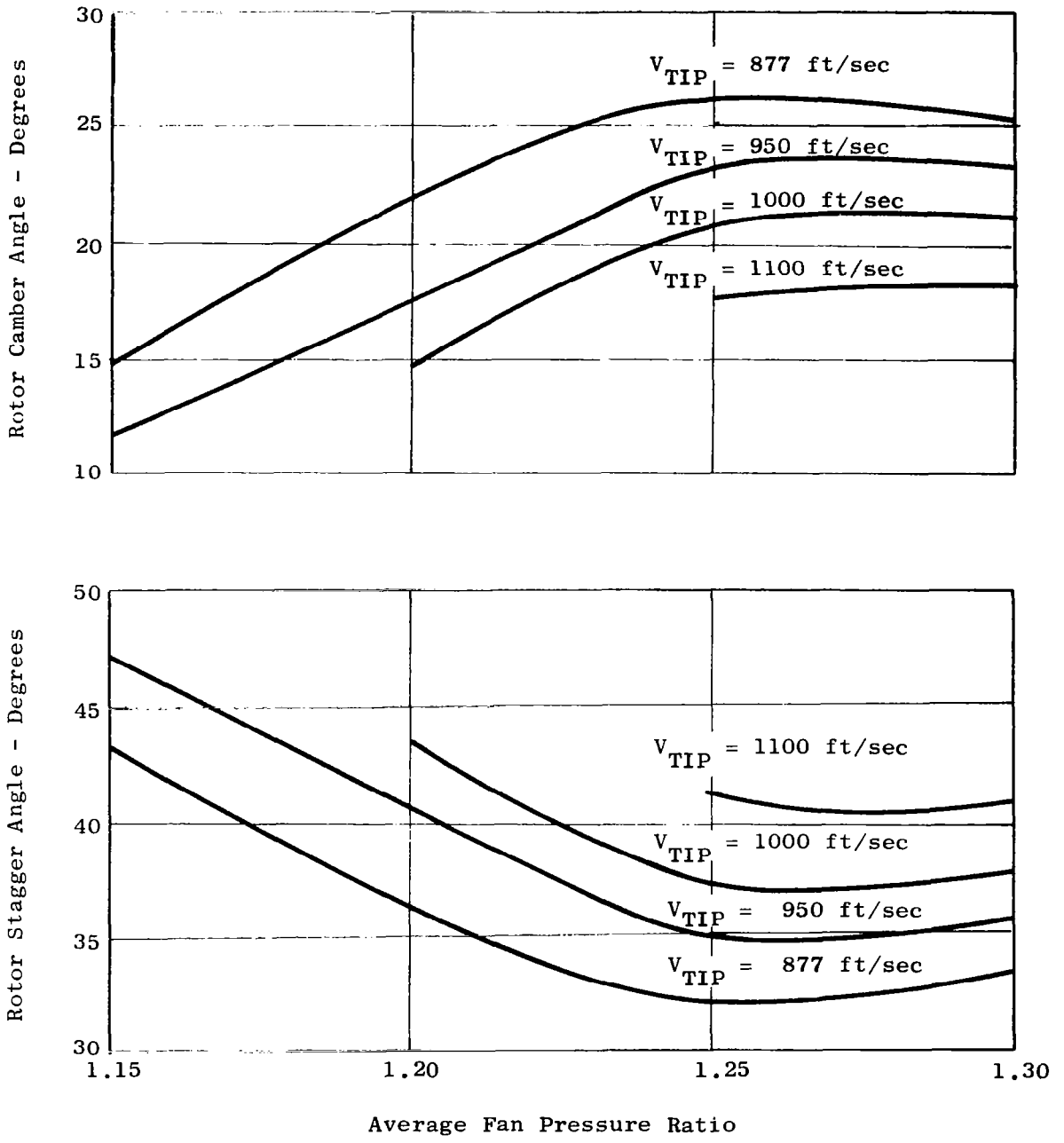

Figure 50b. Conventional Fan Characteristics With Non-Uniform Loading - Pitch Section.

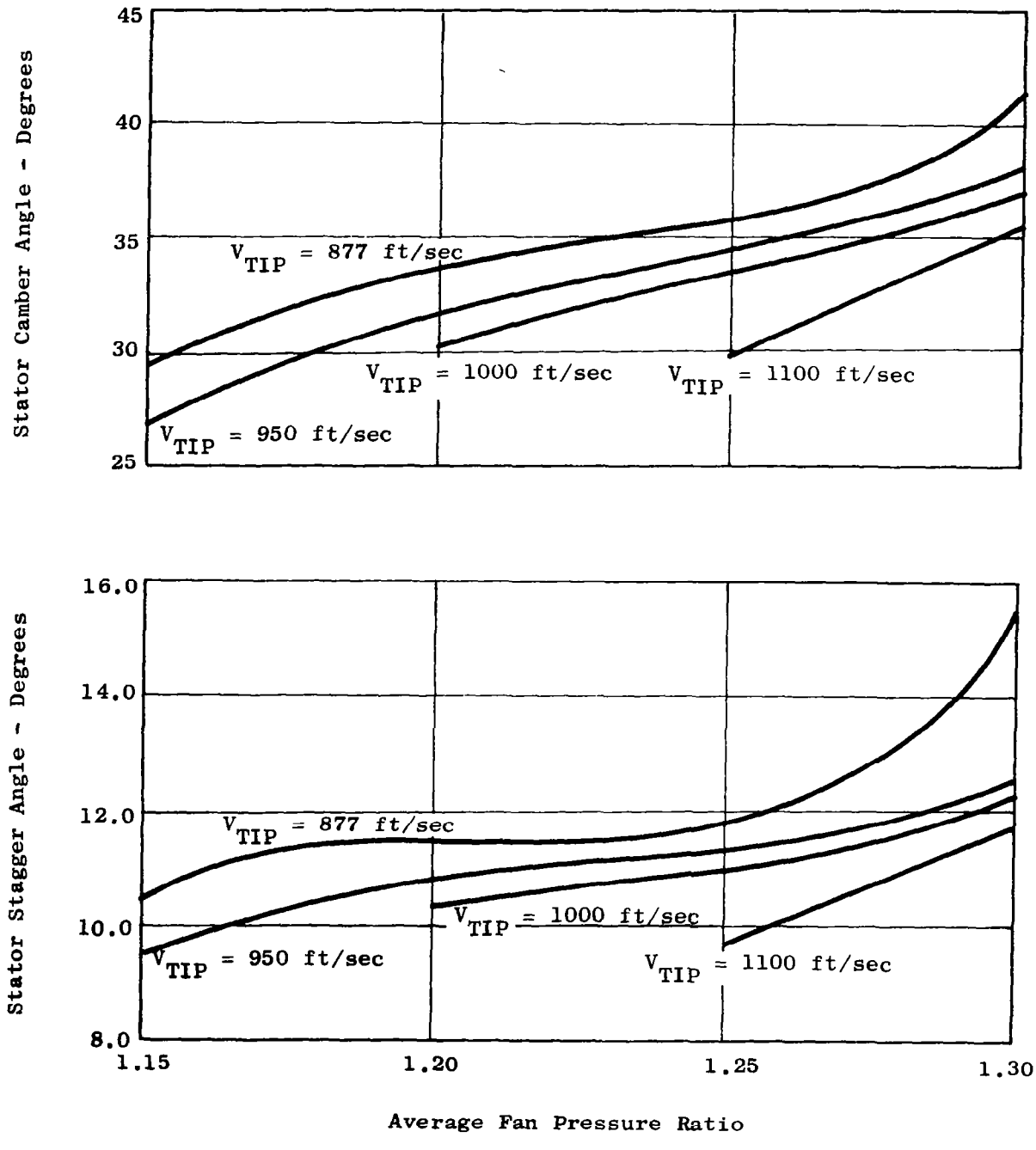

Figure 50c. Conventional Fan Characteristics With Non-Uniform Loading - Pitch Section.

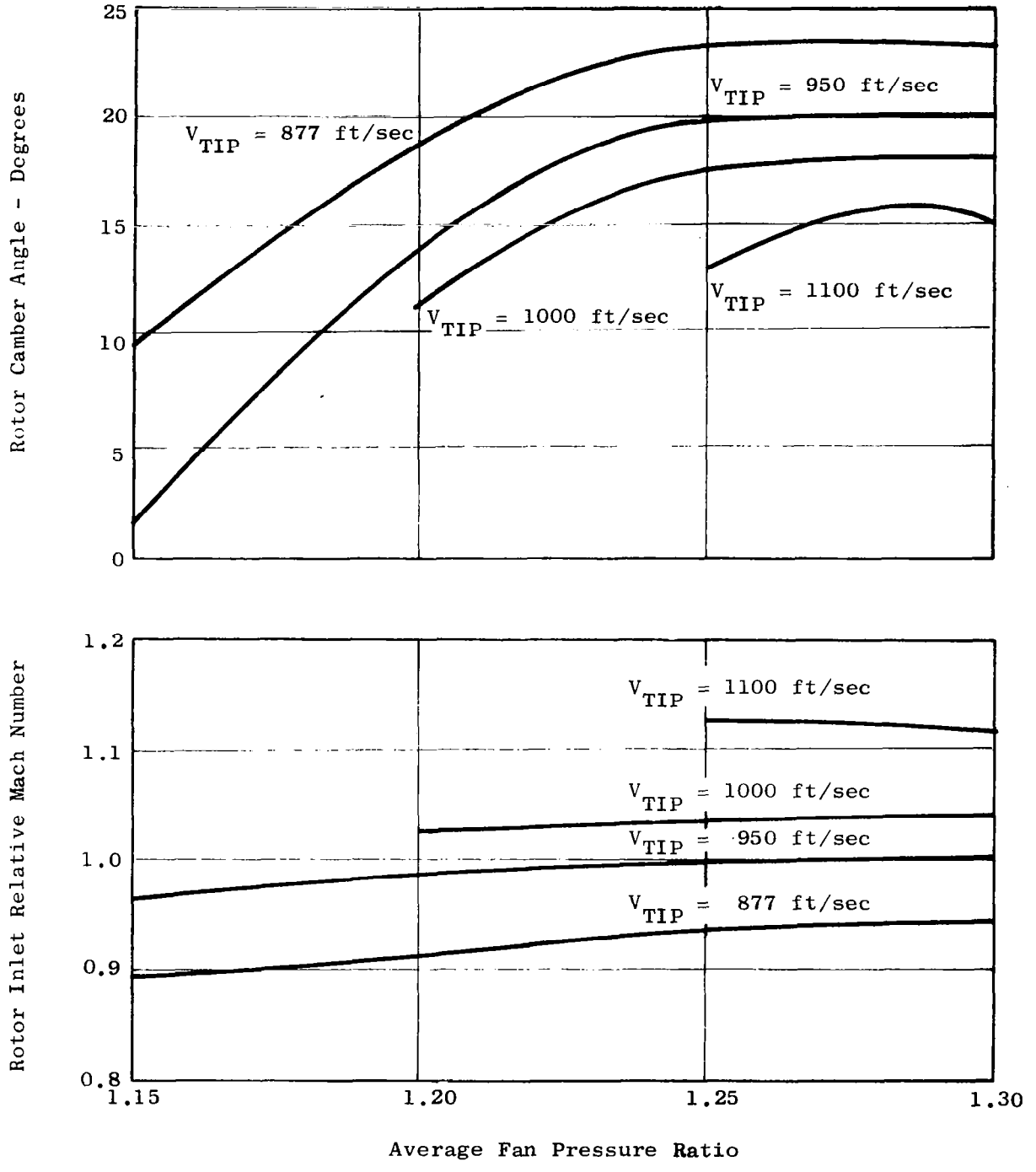

Figure 51a. Conventional Fan Characteristics With Non-Uniform Loading - Tip Section.

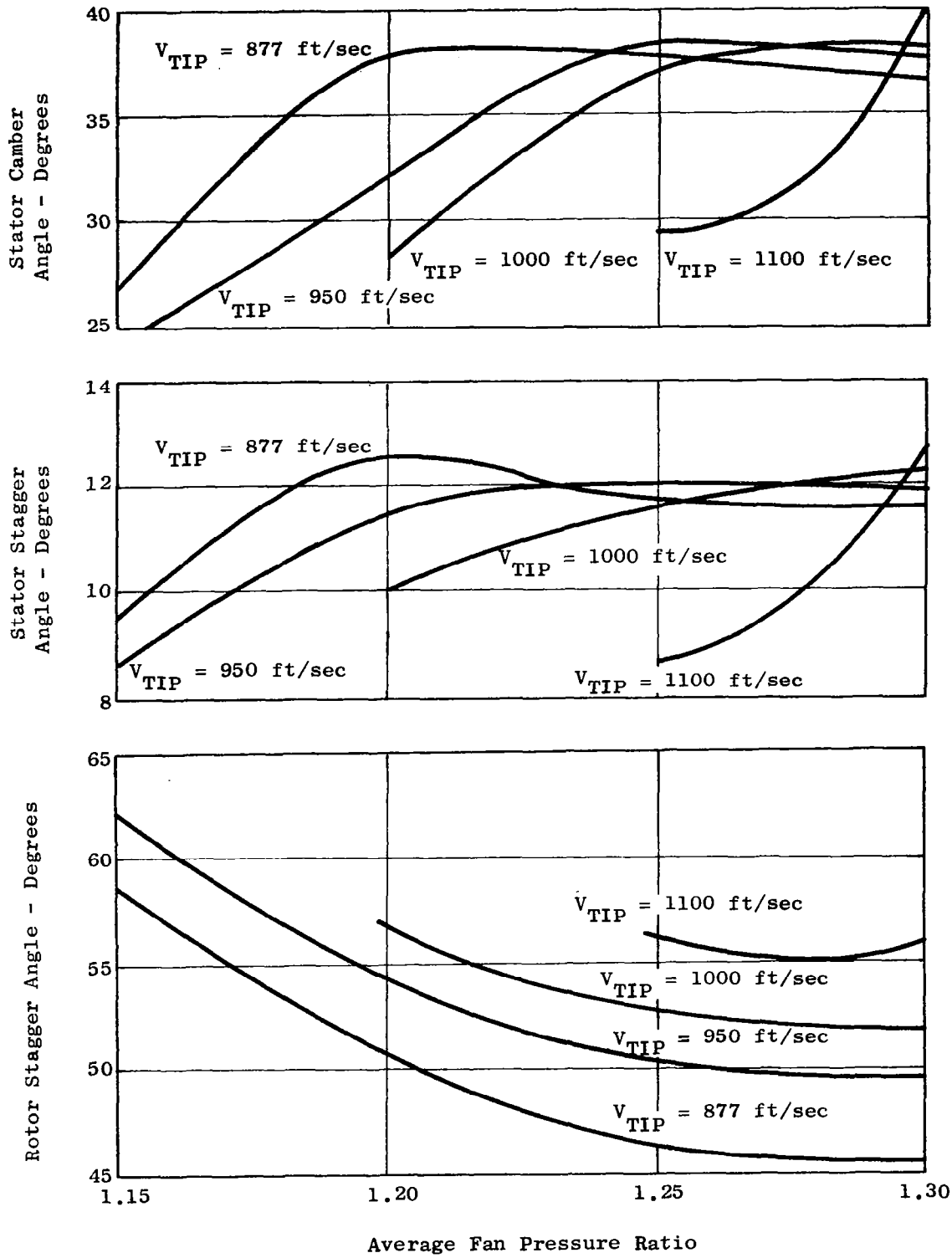

Figure 51b. Conventional Fan Characteristics With Non-Uniform Loading - Tip Section.

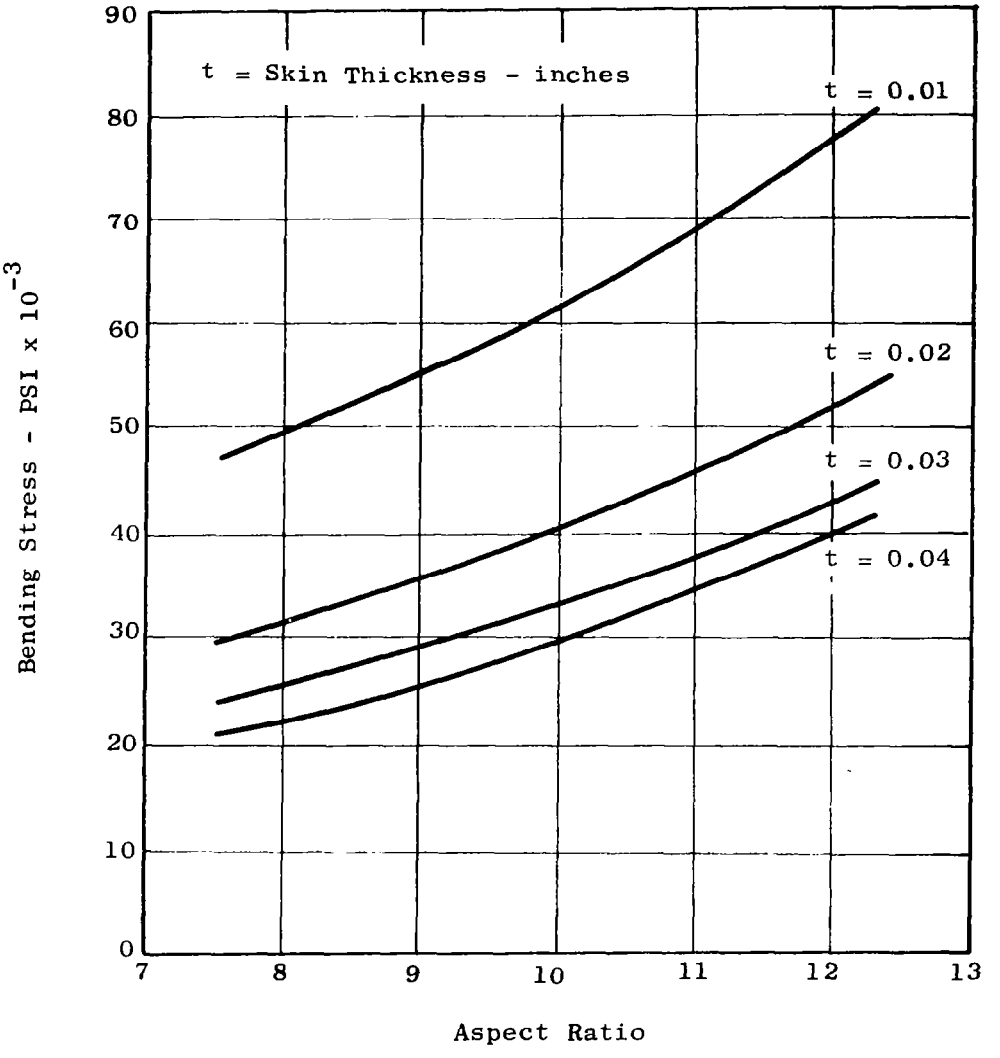

Figure 52. Bending Stress Versus Inlet Guide Vane Aspect Ratio.

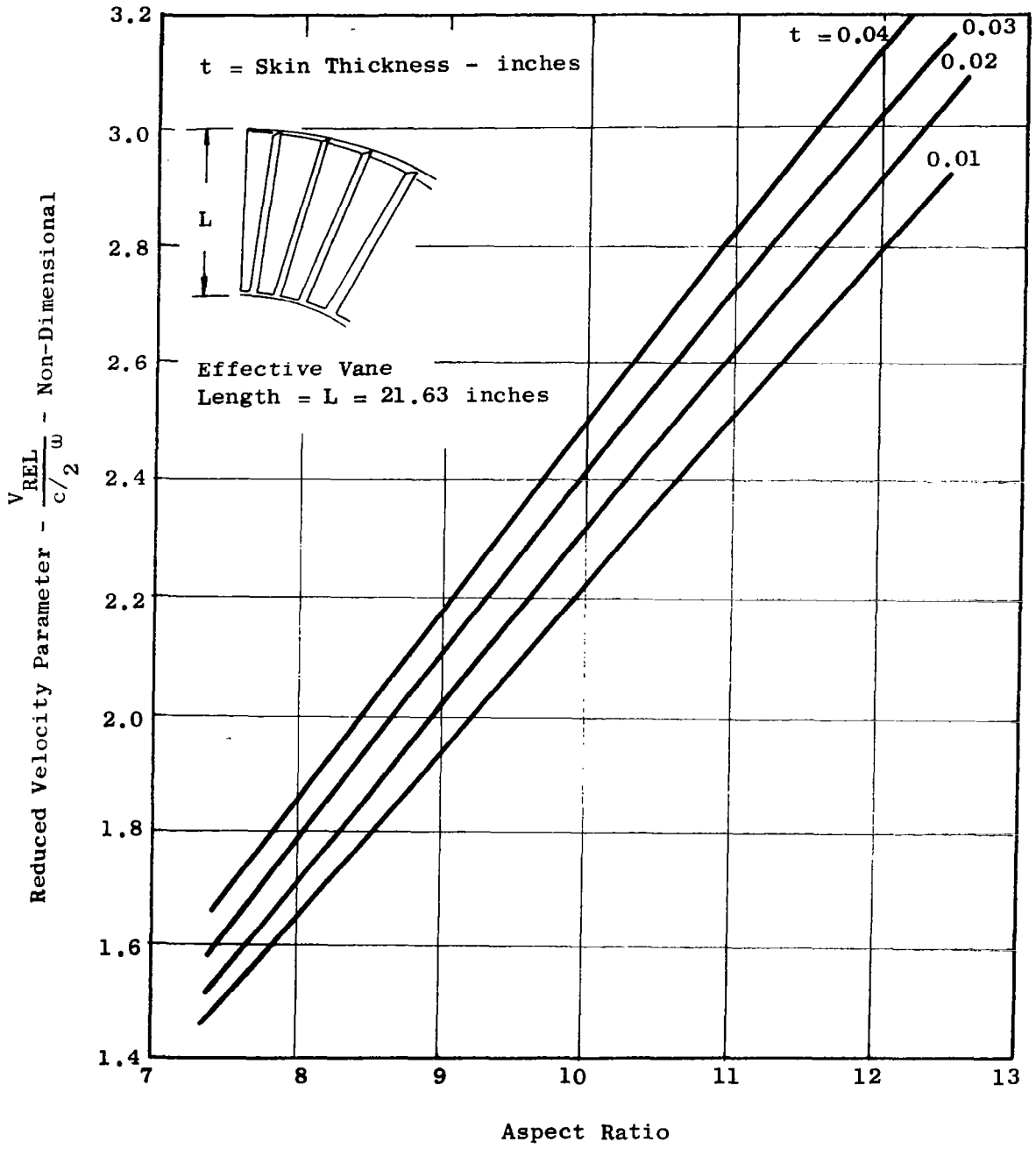

Figure 53a. Reduced Velocity Parameter Versus Inlet Guide Vane Aspect Ratio.

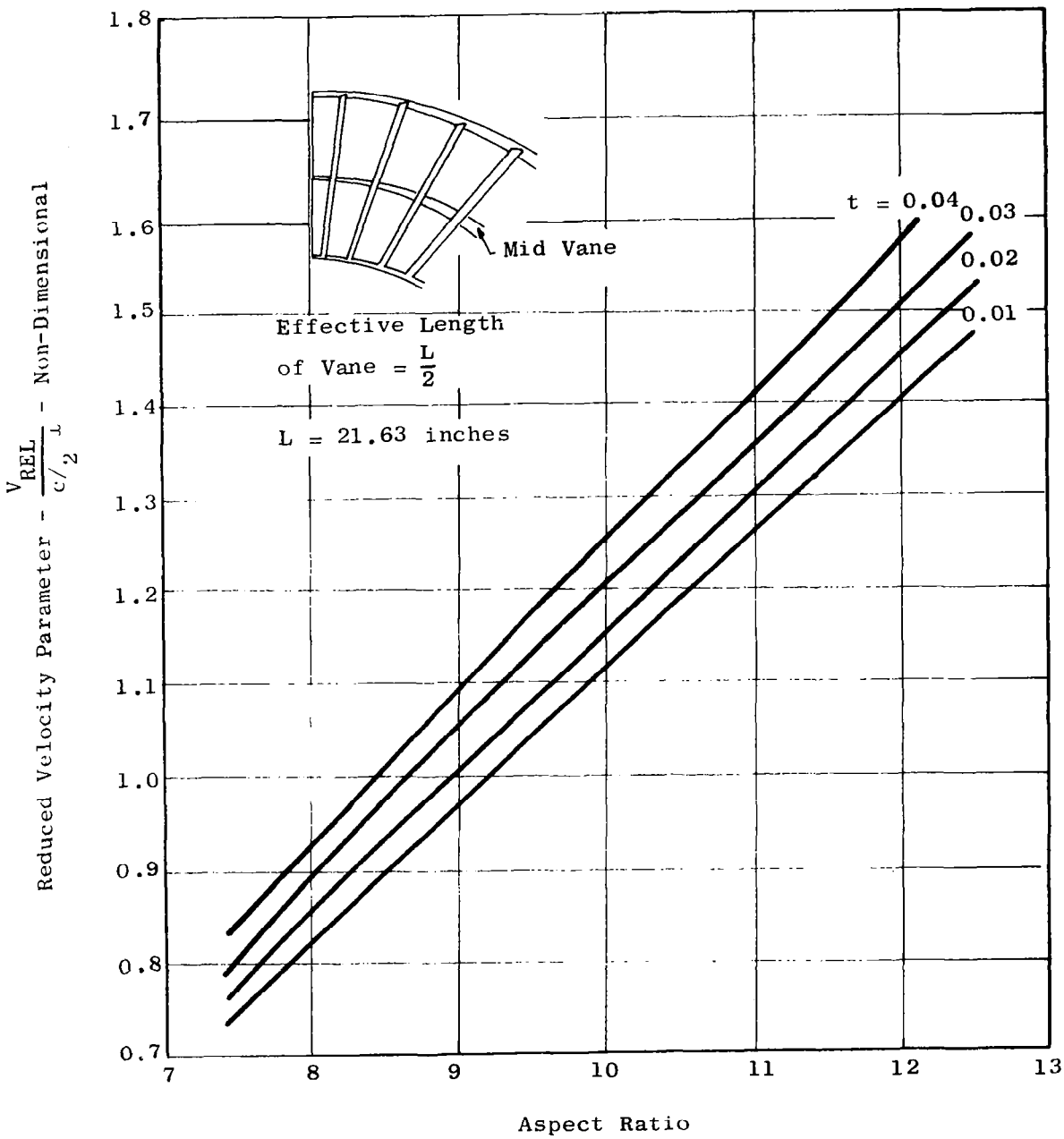

Figure 53b. Reduced Velocity Parameter Versus Inlet Guide Vane Aspect Ratio.

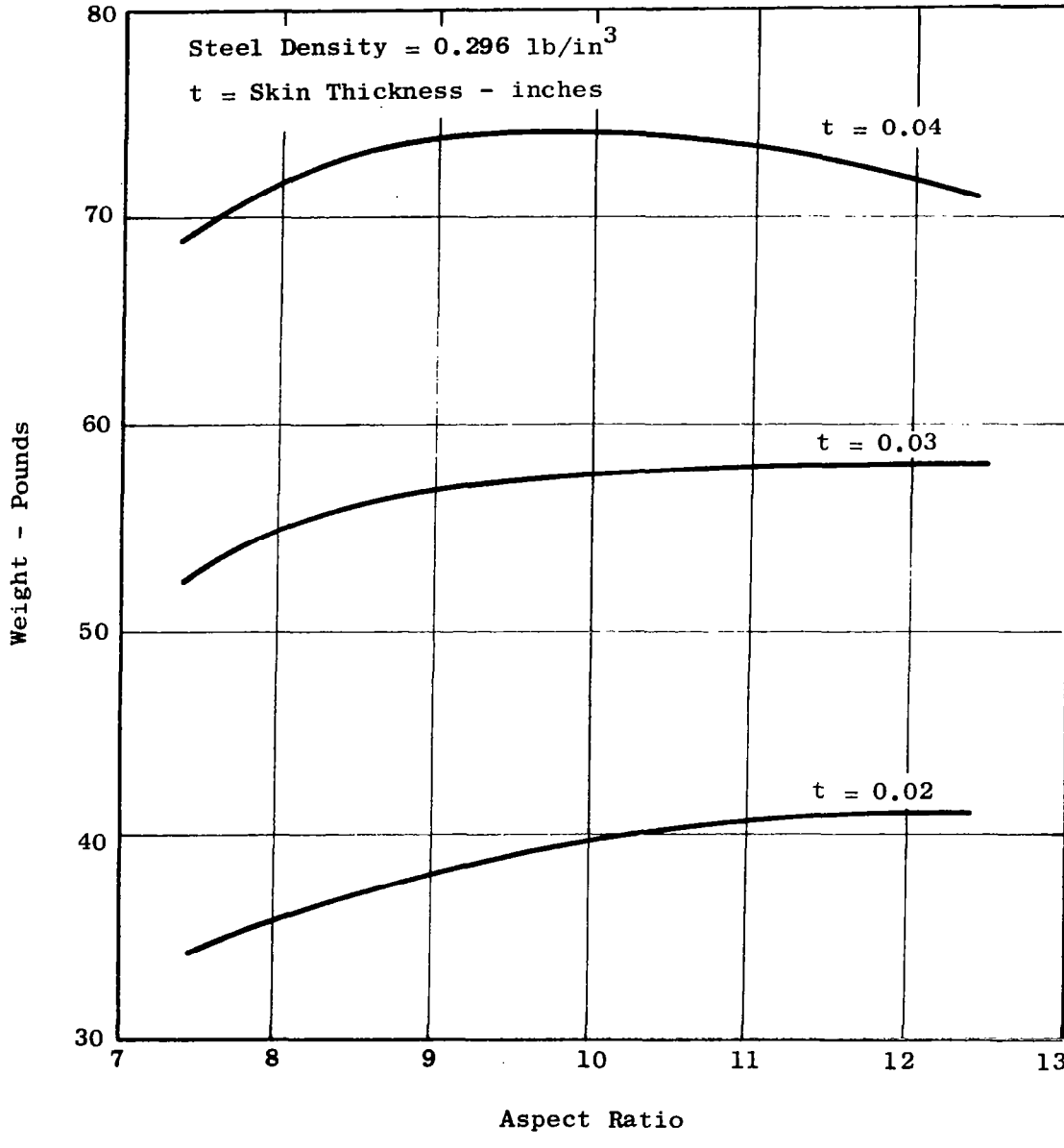

Figure 54. Inlet Guide Vane Weight Versus Aspect Ratio.

θ_S = Strut Rotation = 0.0178 radians

δ_H = Vertical Deflection of Hub = -0.050

δ_R = Rotor Tip Deflection Due to Hub Rotation θ_H = 0.060

δ_{F_3} = Frame Deflection at 3:00 = 0.0747

δ_{F_g} = Frame Deflection at 9:00 = -0.6225

Rotor Tip Deflection Due to θ_S = 0.561

δ_G = Rotor Tip Deflection Due to Gyro = -0.12

δ = Required Clearance = 0.376

Required Clearance for Steady State Only = 0.090 inches

Combined Required Clearance = 0.466 inches

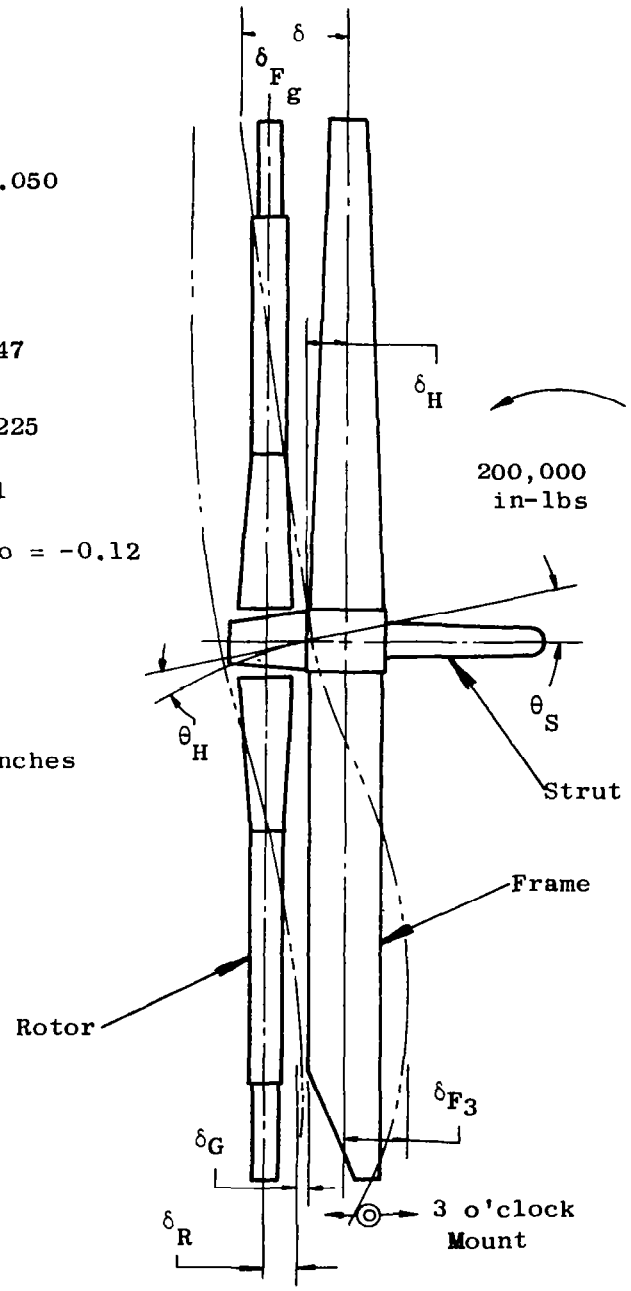

Figure 55. Relative Frame-Rotor Deflections.

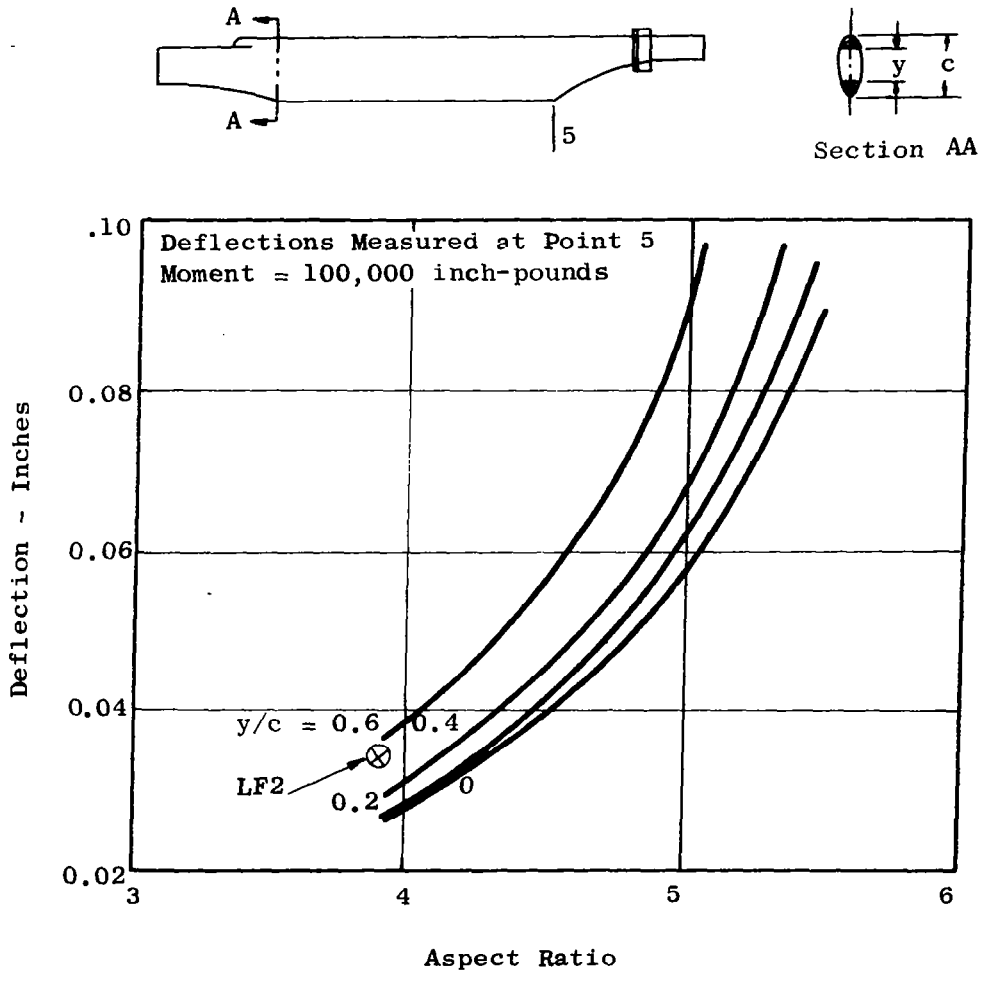

Figure 56. Minor Strut Deflections Versus Aspect Ratio.

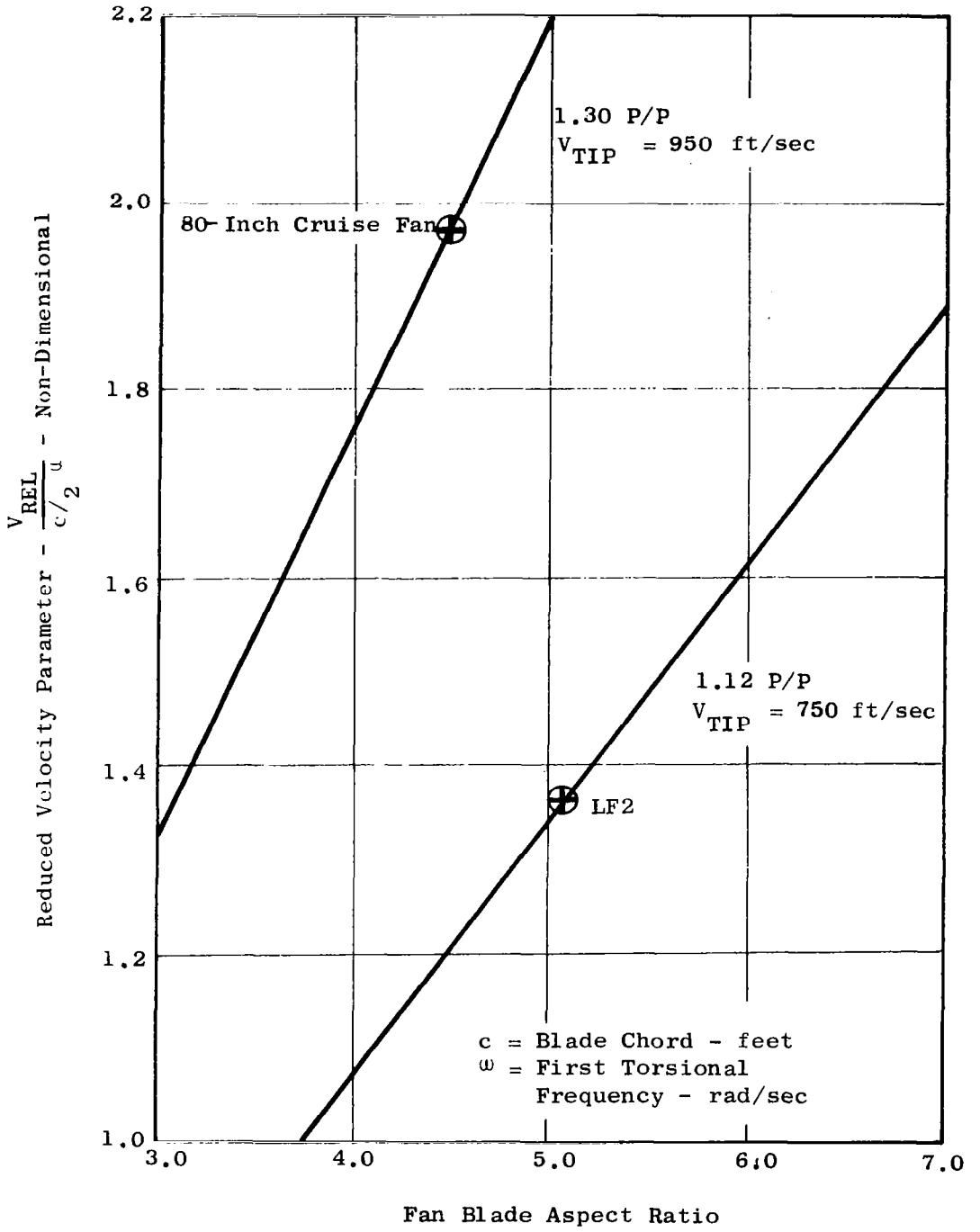

Figure 57. Reduced Velocity Parameter Versus Aspect Ratio.

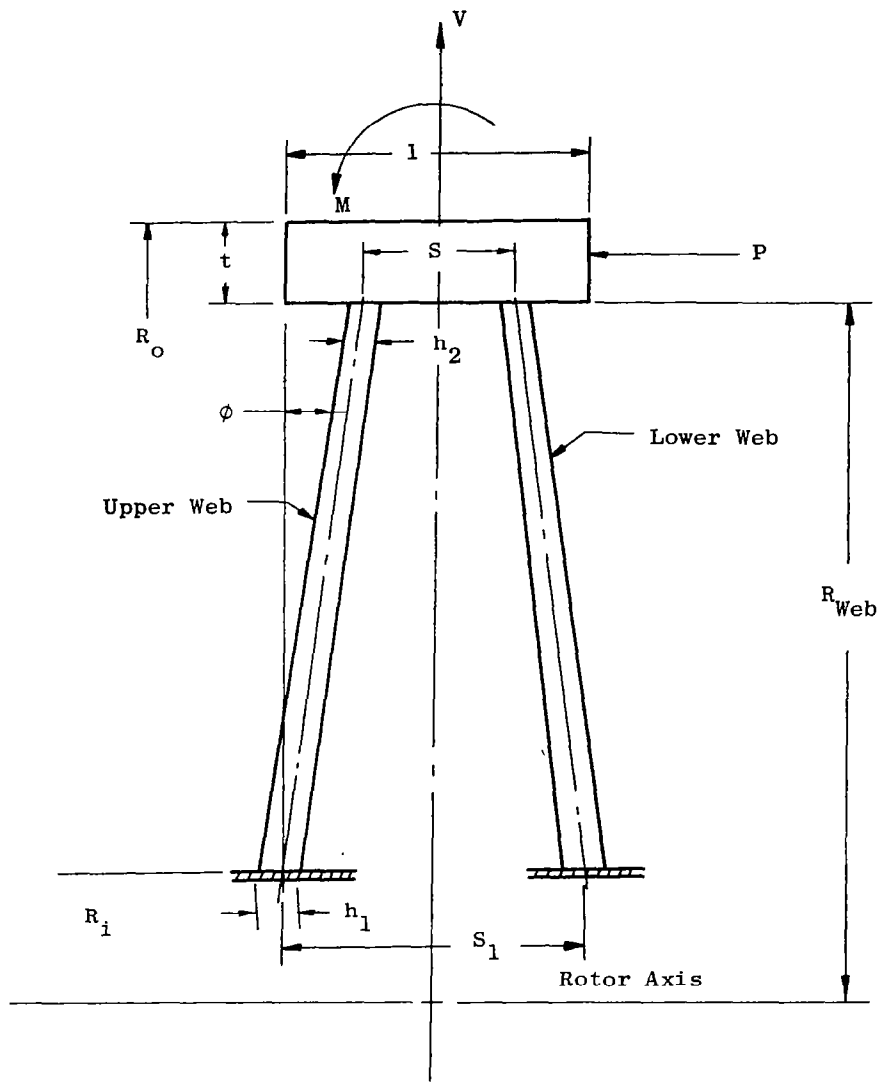

1.	R_i	- Web Root Radius - Inches
2.	R_o	- Rim Outer Radius - Inches
3.	l	- Rim Width - Inches
4.	S_1	- Distance Between Webs at Hub - Inches
5.	S_2	- Distance Between Webs at Tip - Inches
6.	t	- Rim Thickness - Inches
7.	h_1	- Web Thickness at Root - Inches
8.	h_2	- Web Thickness at Tip - Inches
9.	ϕ	- Web Inclination Angle - Degrees
10.	R_{Web}	- Web Tip Radius
11.	P	- Axial Load on Disk - Pounds
12.	M	- Moment on Disk - Inch-Pounds
13.	V	- Radial Load on Disk - Pounds
14.	W	- Rotor Speed - RPM

Figure 58. Disk Configuration and Nomenclature.

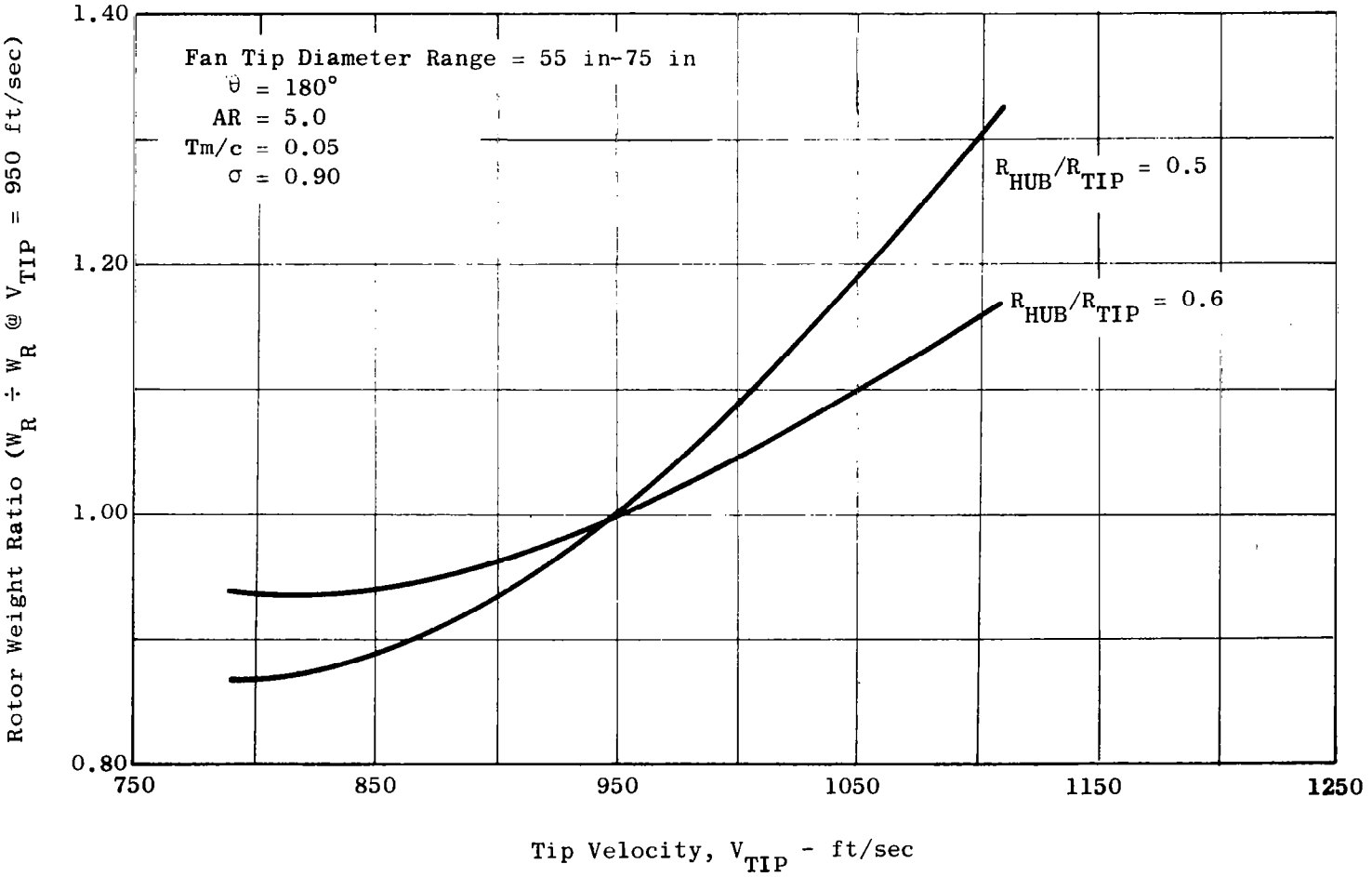

Figure 59. Rotor Weight Versus Fan Tip Velocity.

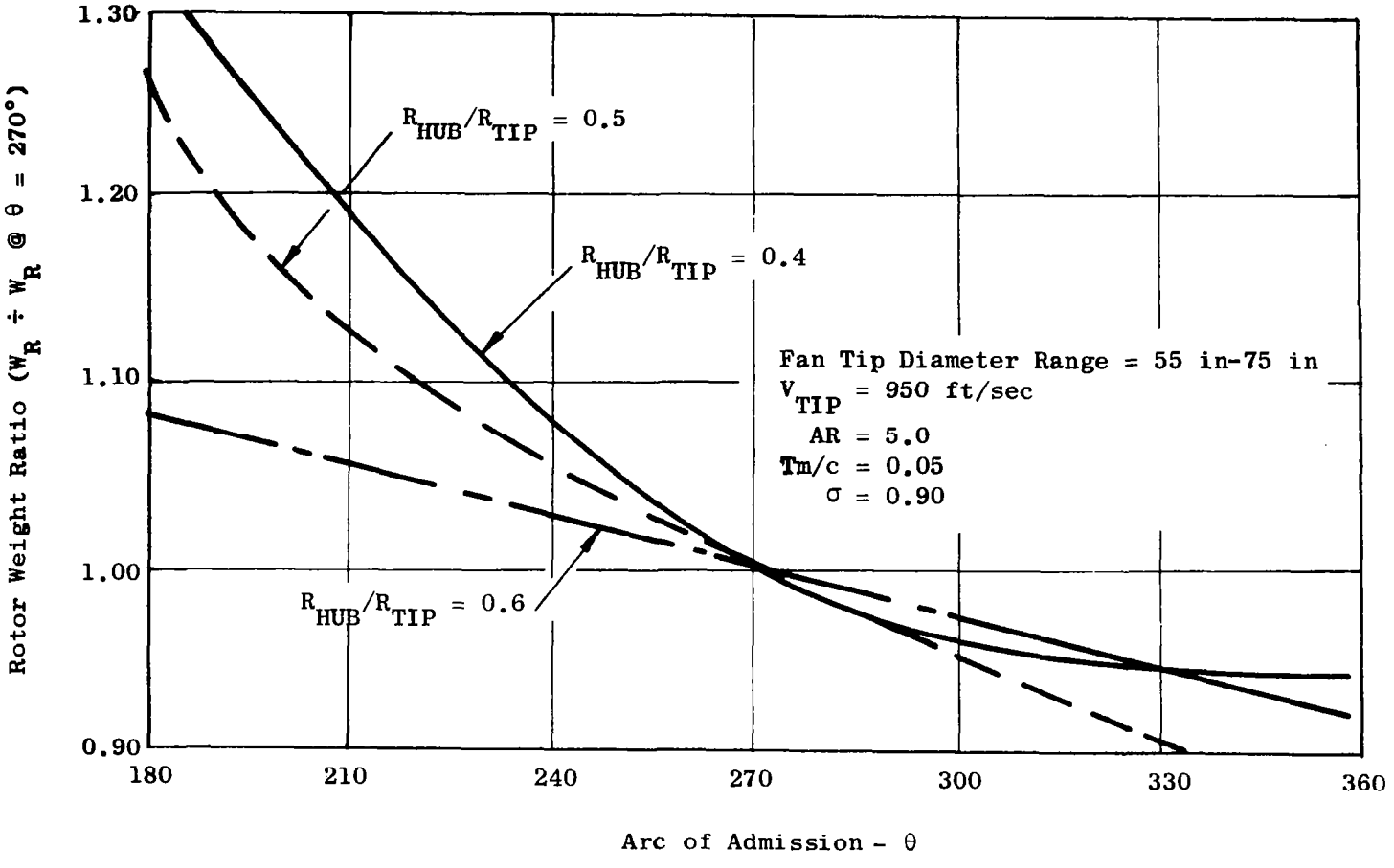

Figure 60. Rotor Weight Versus Turbine Arc of Admission.

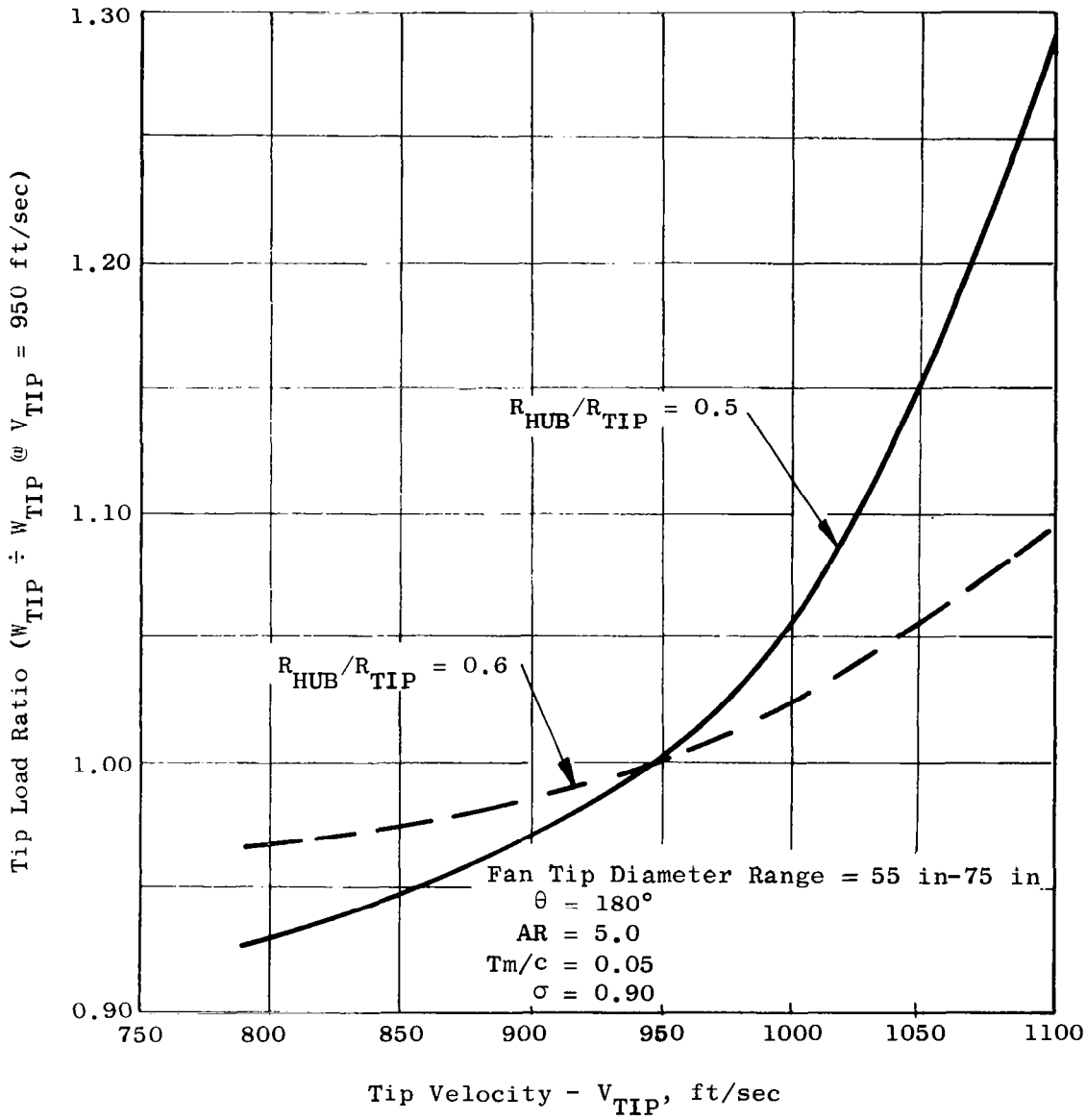

Figure 61. Tip Load Per Blade Versus Fan Tip Velocity.

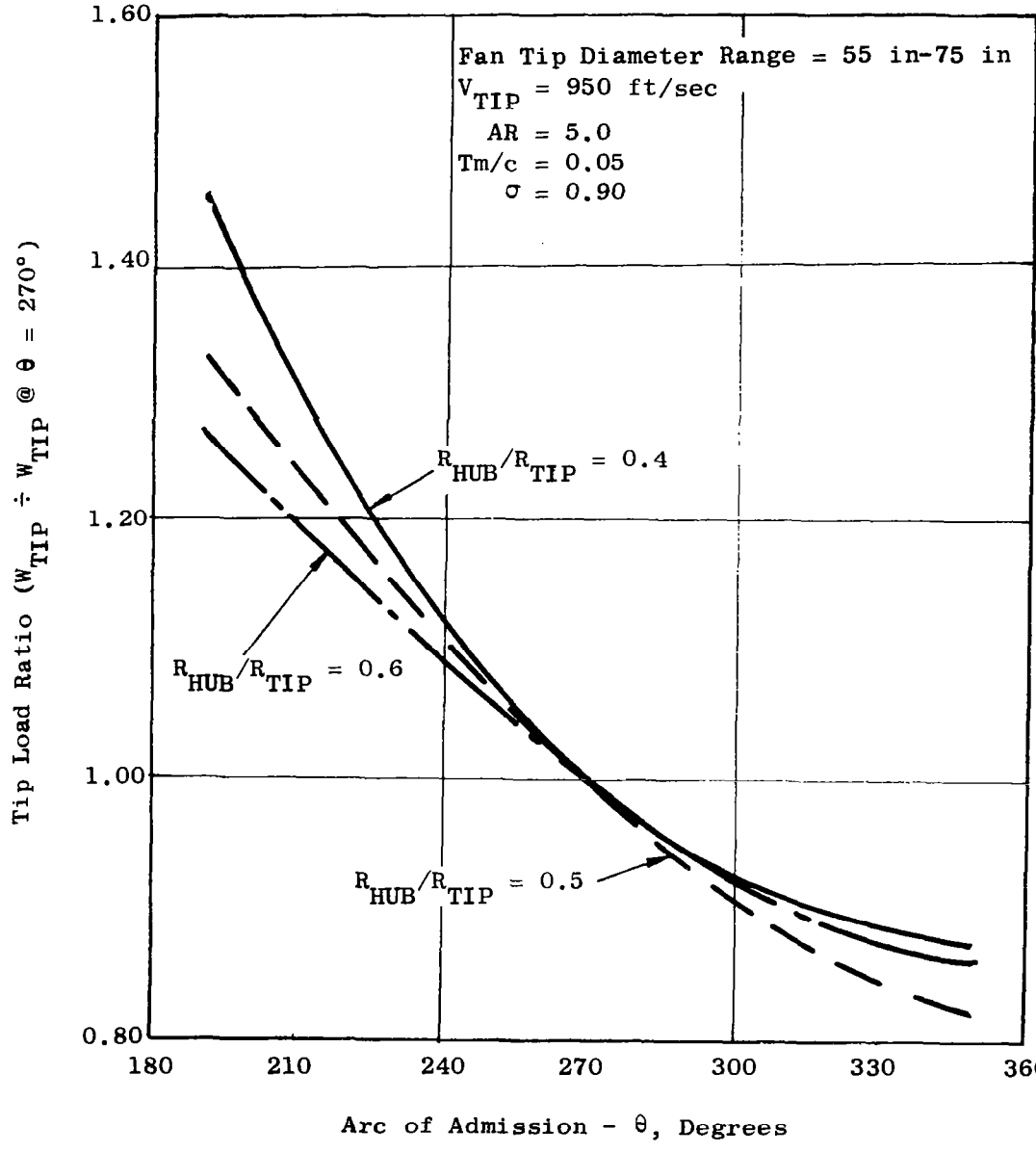

Figure 62. Tip Load Per Blade Versus Turbine Arc of Admission.

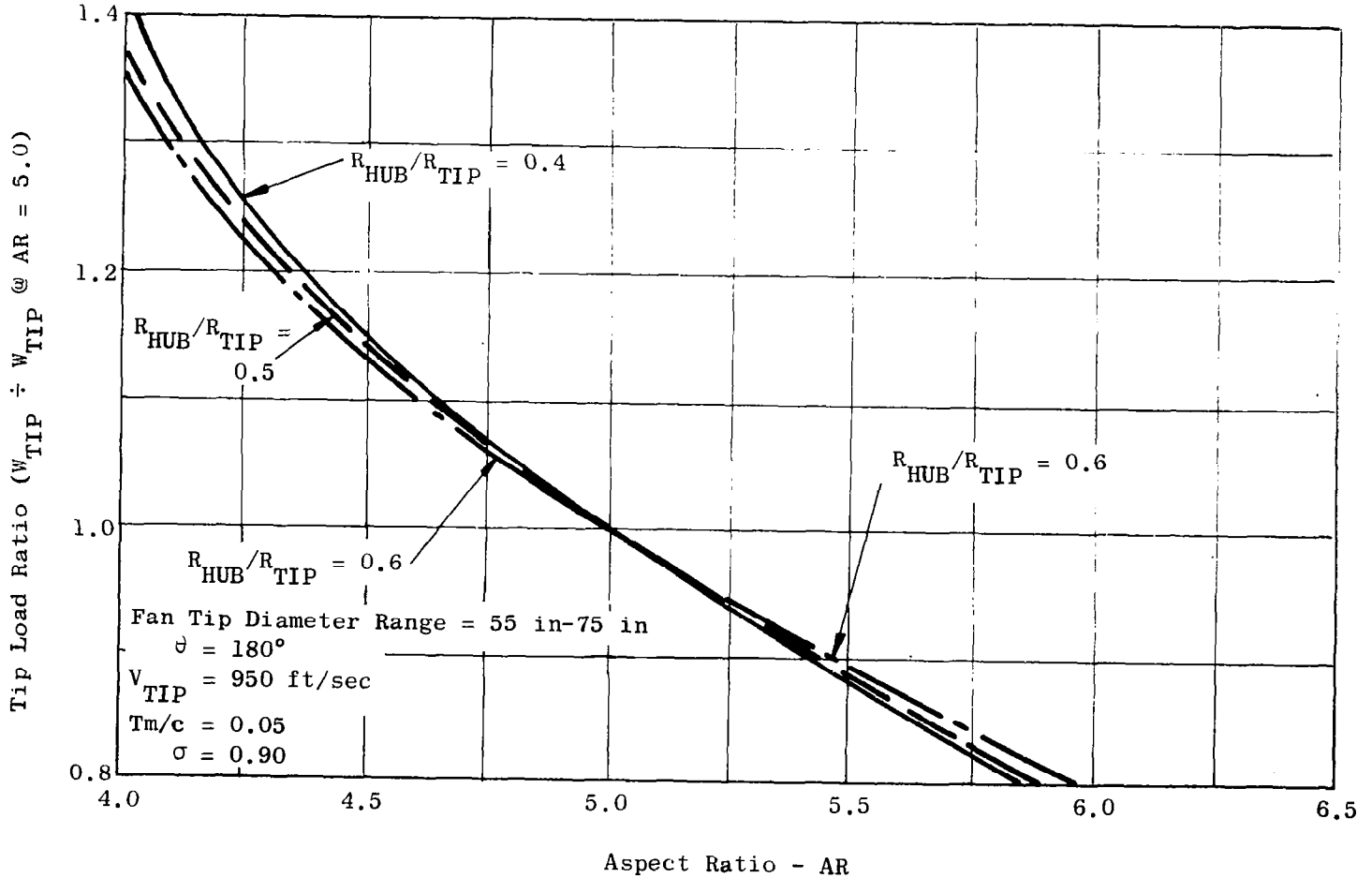

Figure 63. Tip Load Per Blade Versus Fan Aspect Ratio.

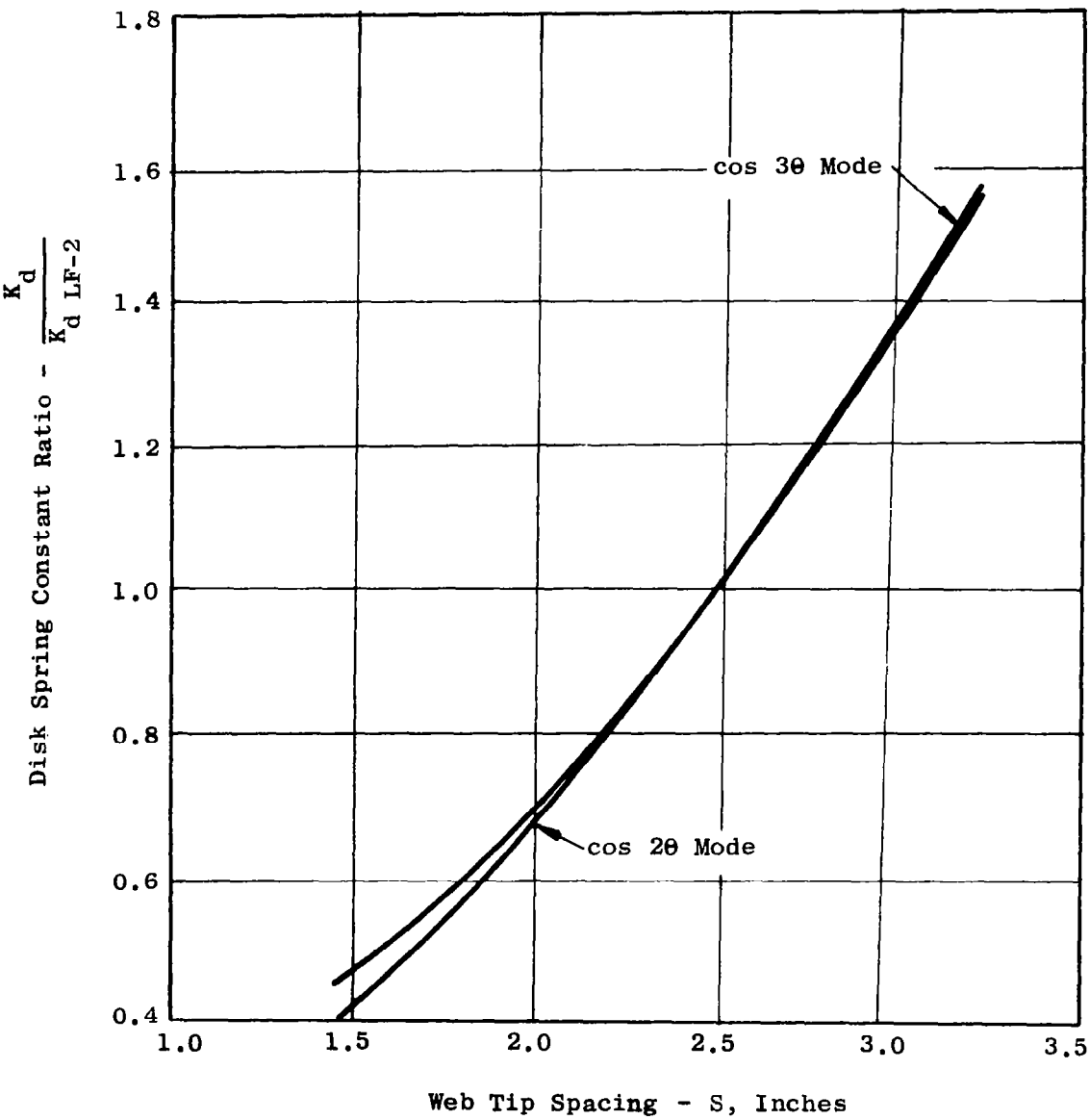

Figure 64. Disk Spring Constant Ratio Versus Web-Tip Spacing.

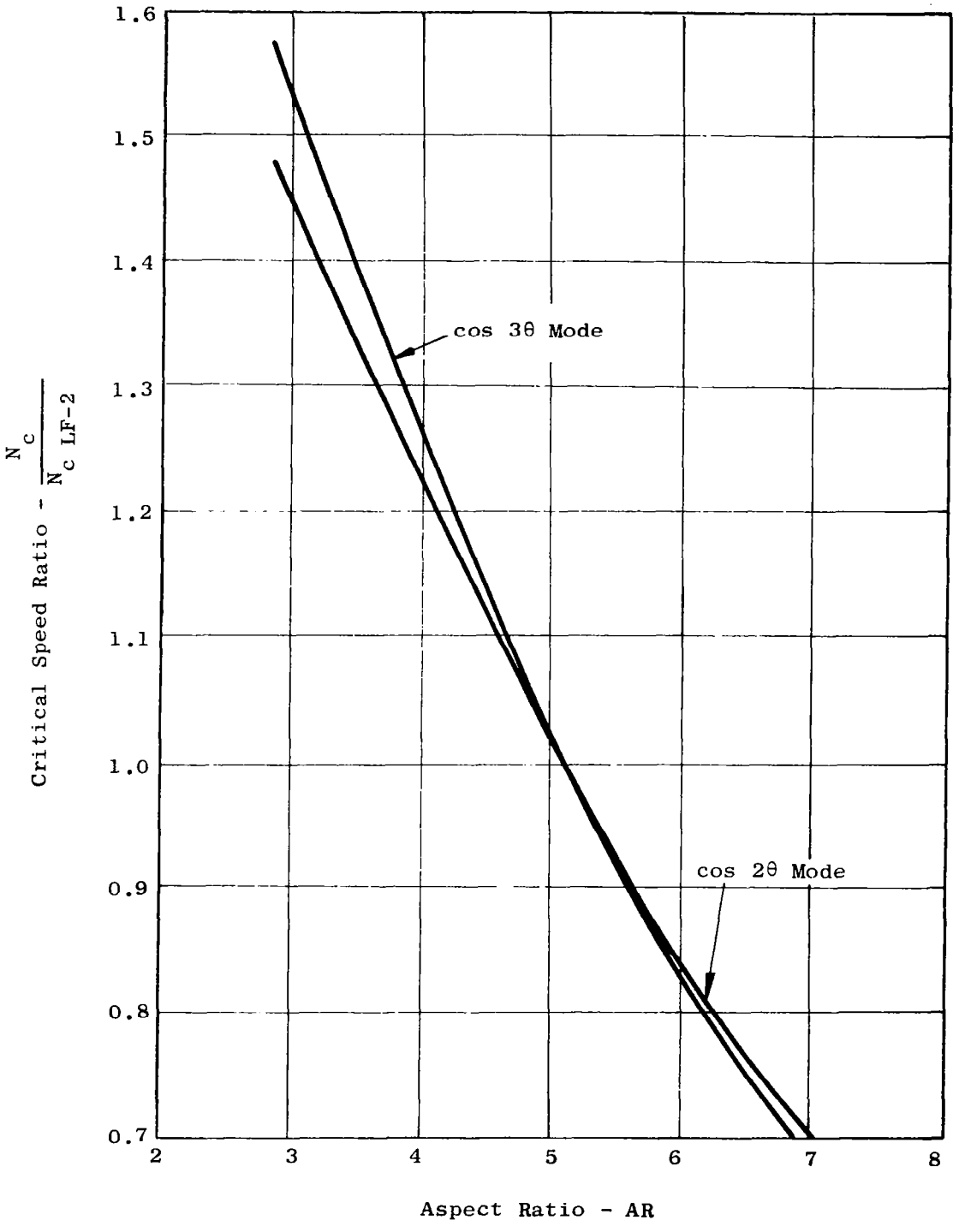

Figure 65. Critical Speed Ratio Versus Aspect Ratio.

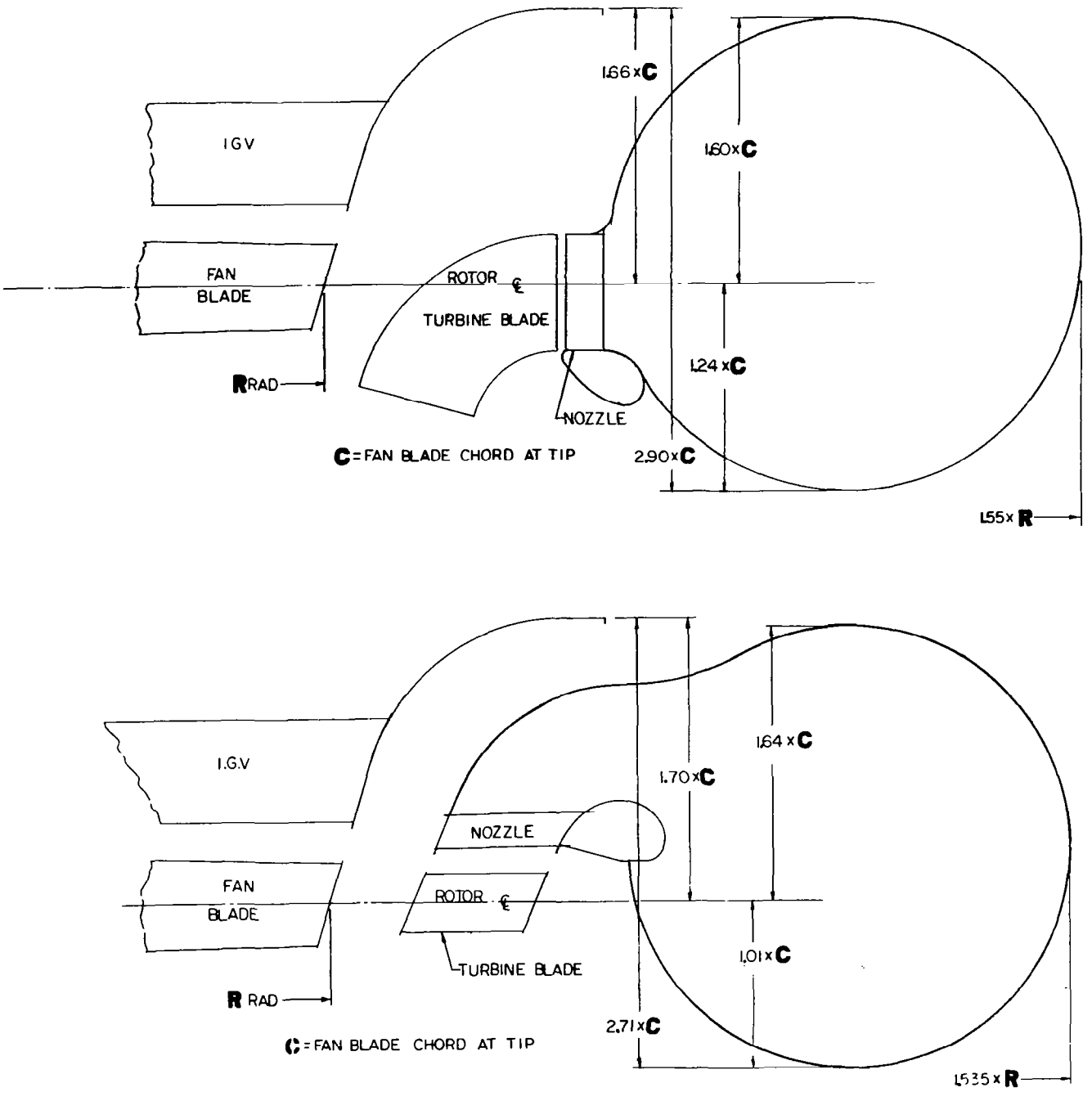

Figure 66a. Radial and Axial Turbine Installation Comparison on the IGV Fan Section at Maximum Scroll Diameter.

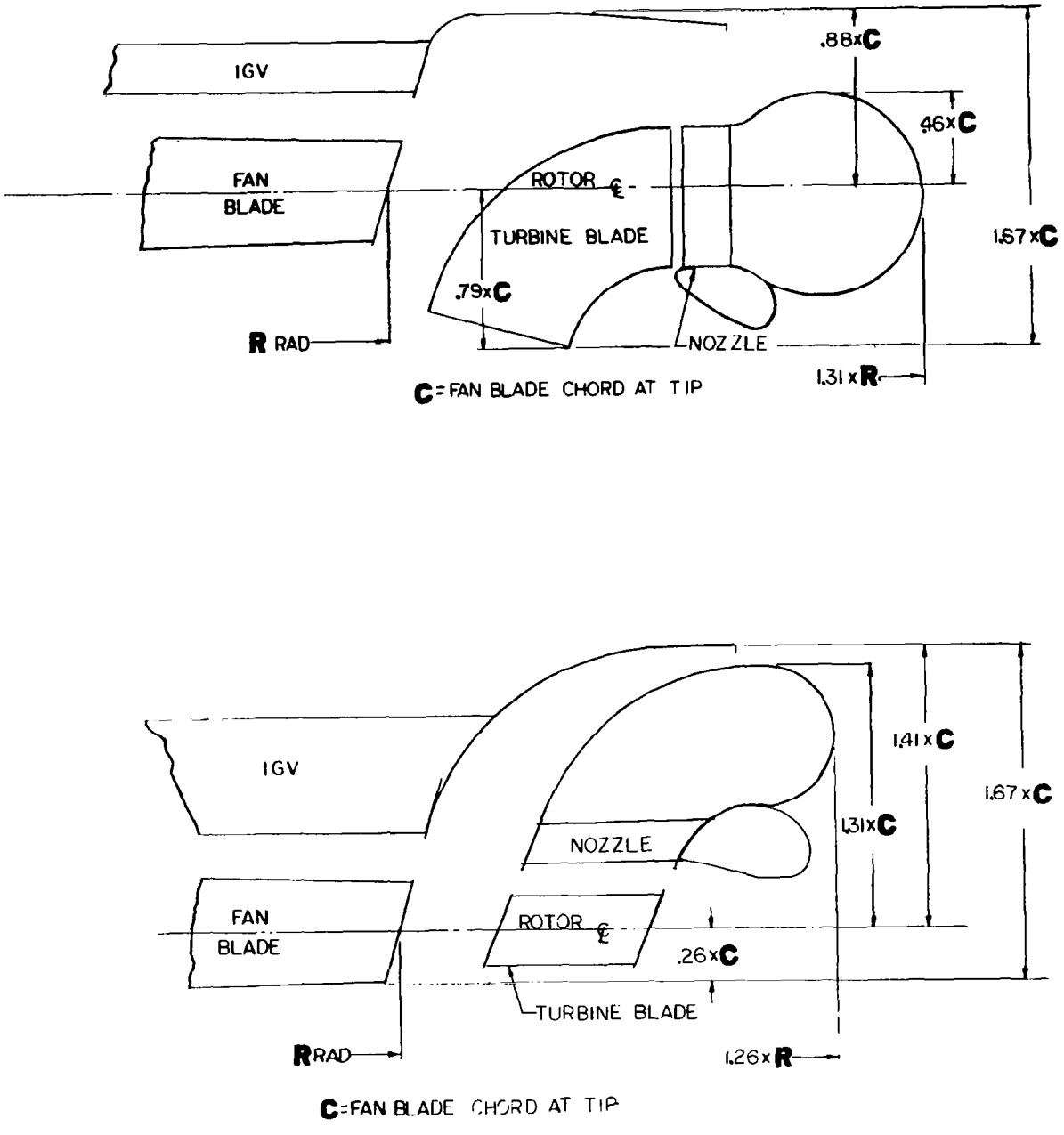

Figure 66b. Radial and Axial Turbine Installation Comparison on the IGV Fan Section at Minimum Scroll Diameter.

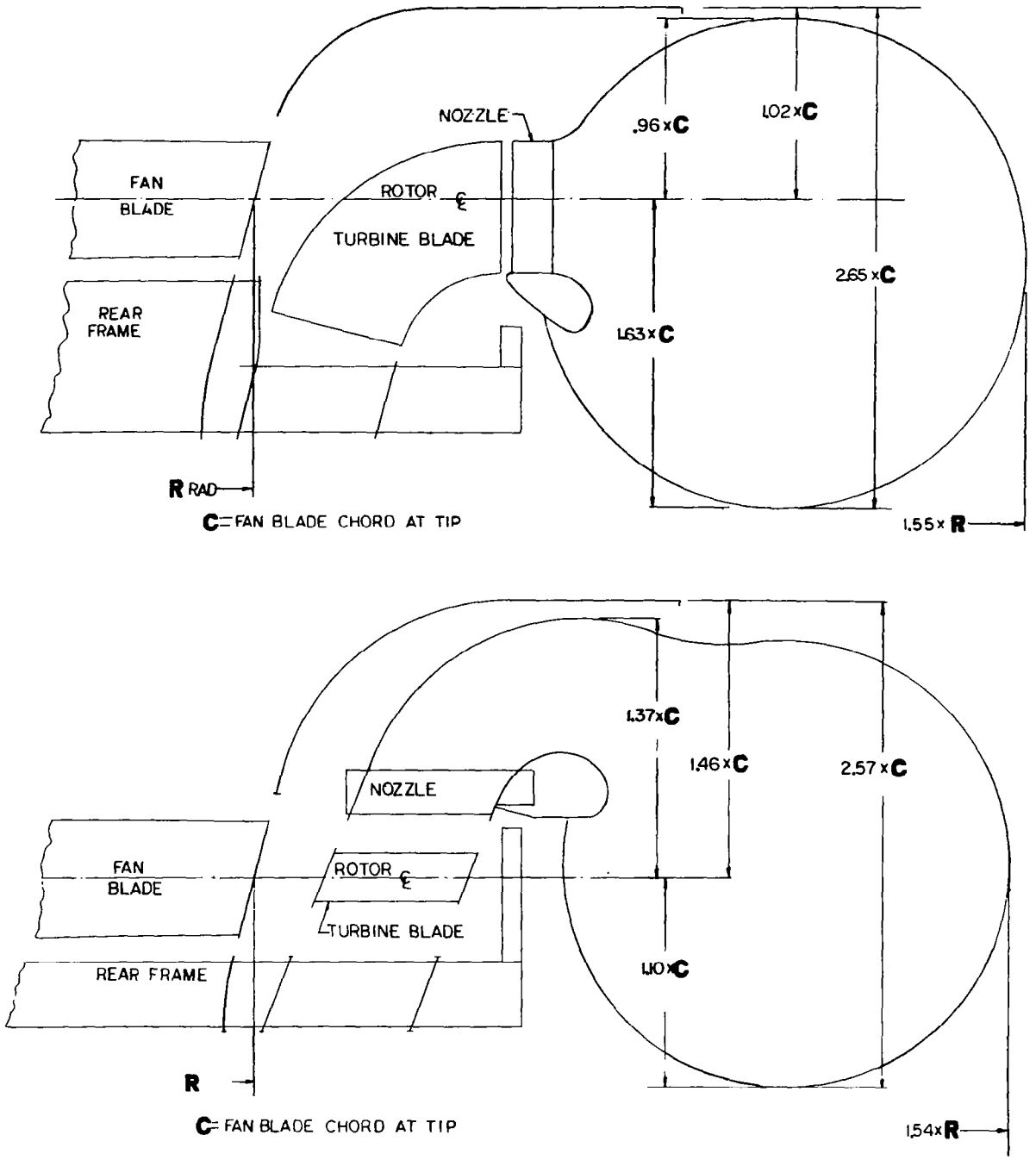

Figure 67a. Radial and Axial Turbine Installation Comparison on a Conventional Fan Section at Maximum Scroll Diameter.

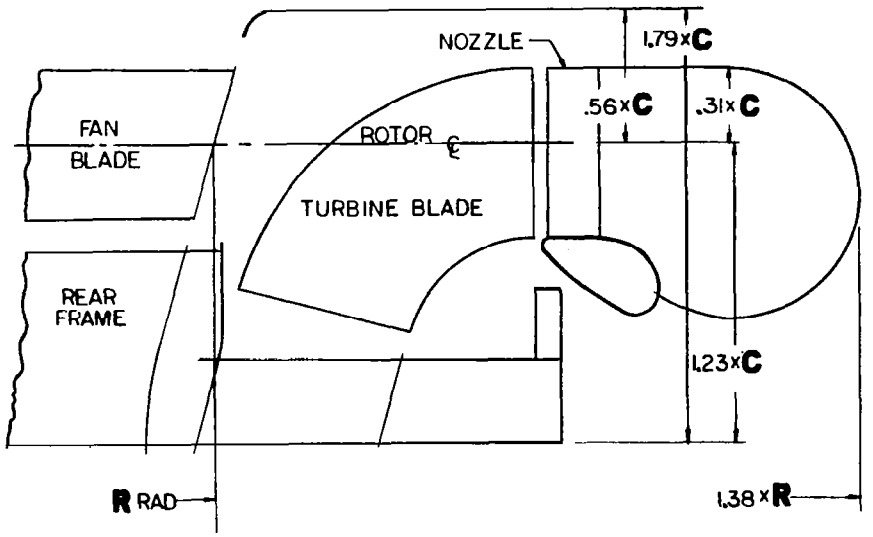

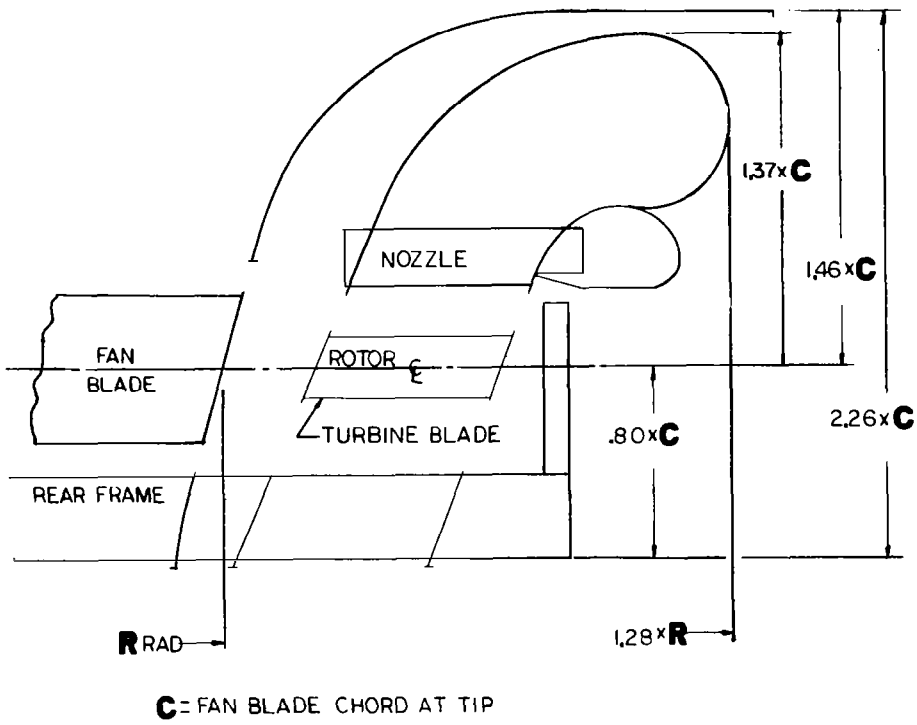

Figure 67b. Radial and Axial Turbine Installation Comparison on a Conventional Fan Section at Minimum Scroll Diameter.

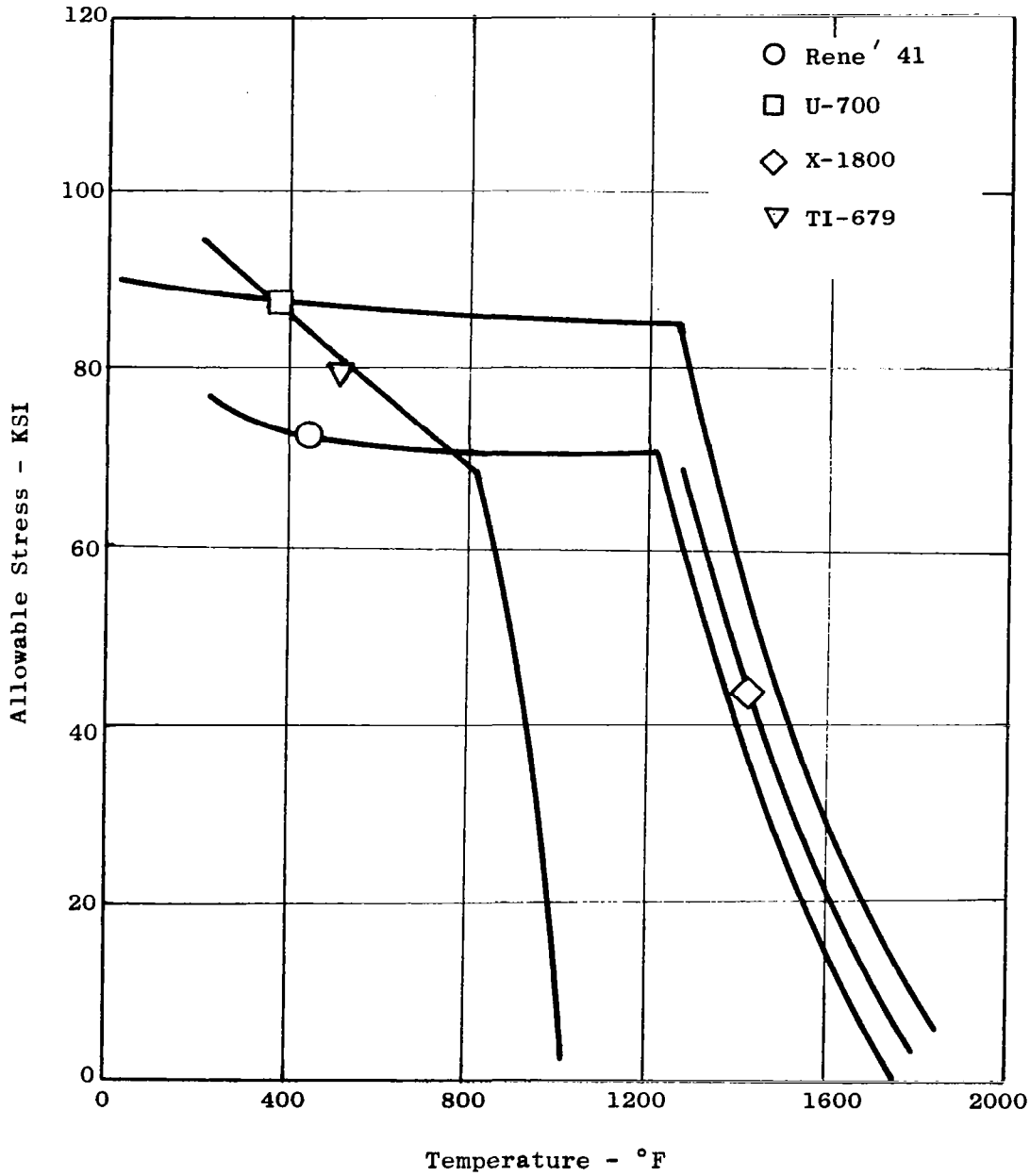

Figure 68. Material Properties - 0.02 Percent Yield, 100-Hour 0.2 Percent Creep.

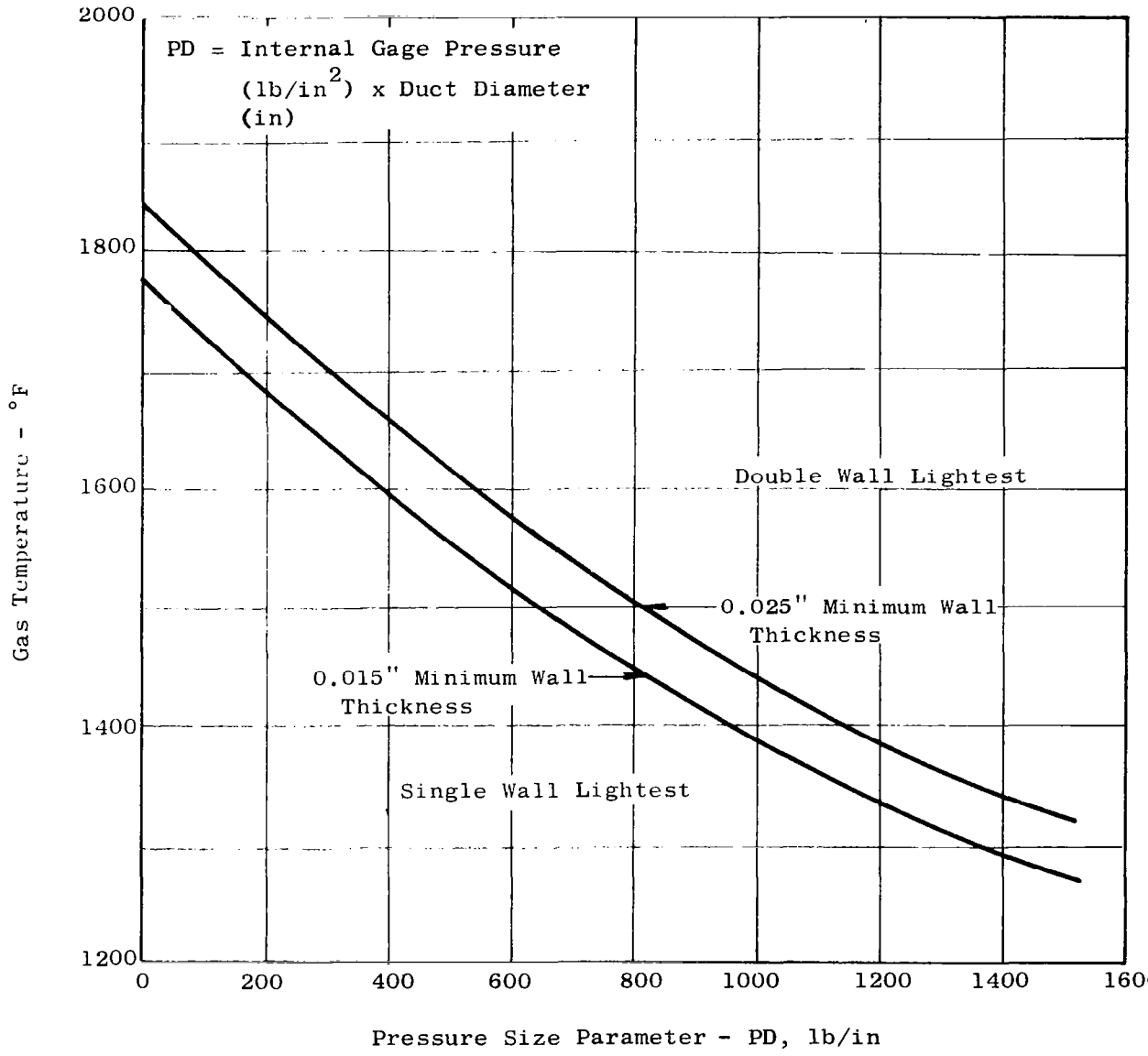

Figure 69. Gas Temperature at Which Single Wall and Double Wall Duct Weights are Equal.

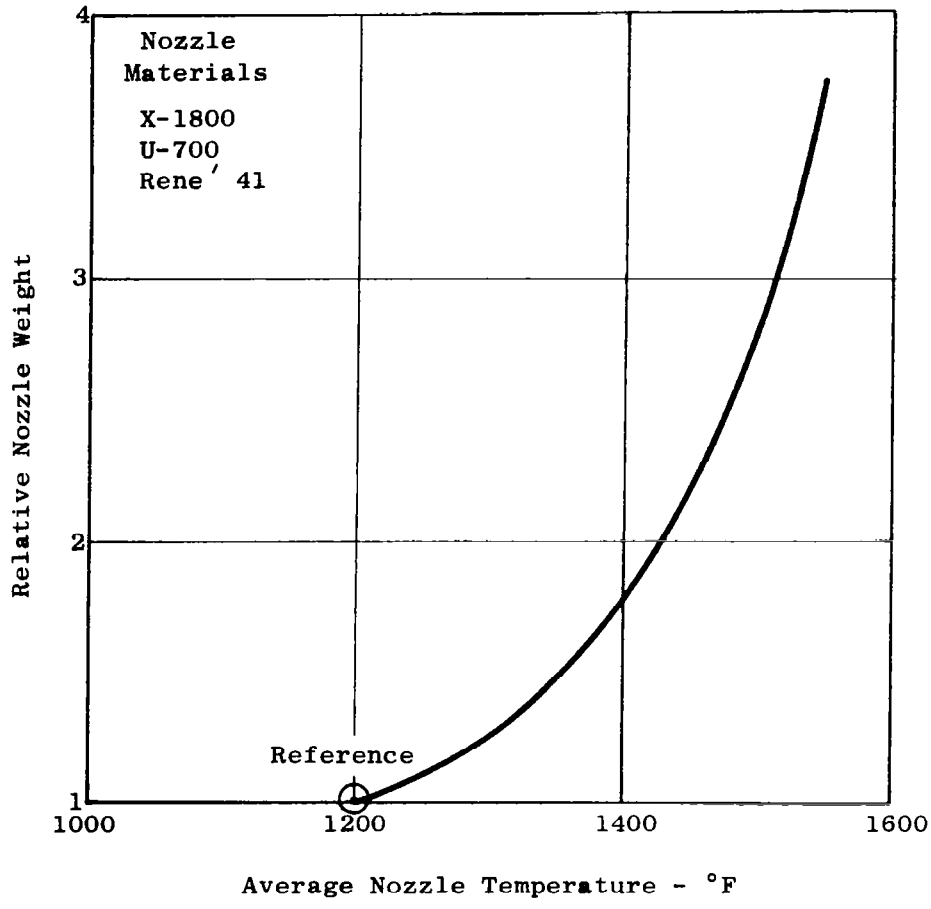

Figure 70. Effect of Temperature on Relative Weight of Nozzle Partitions.

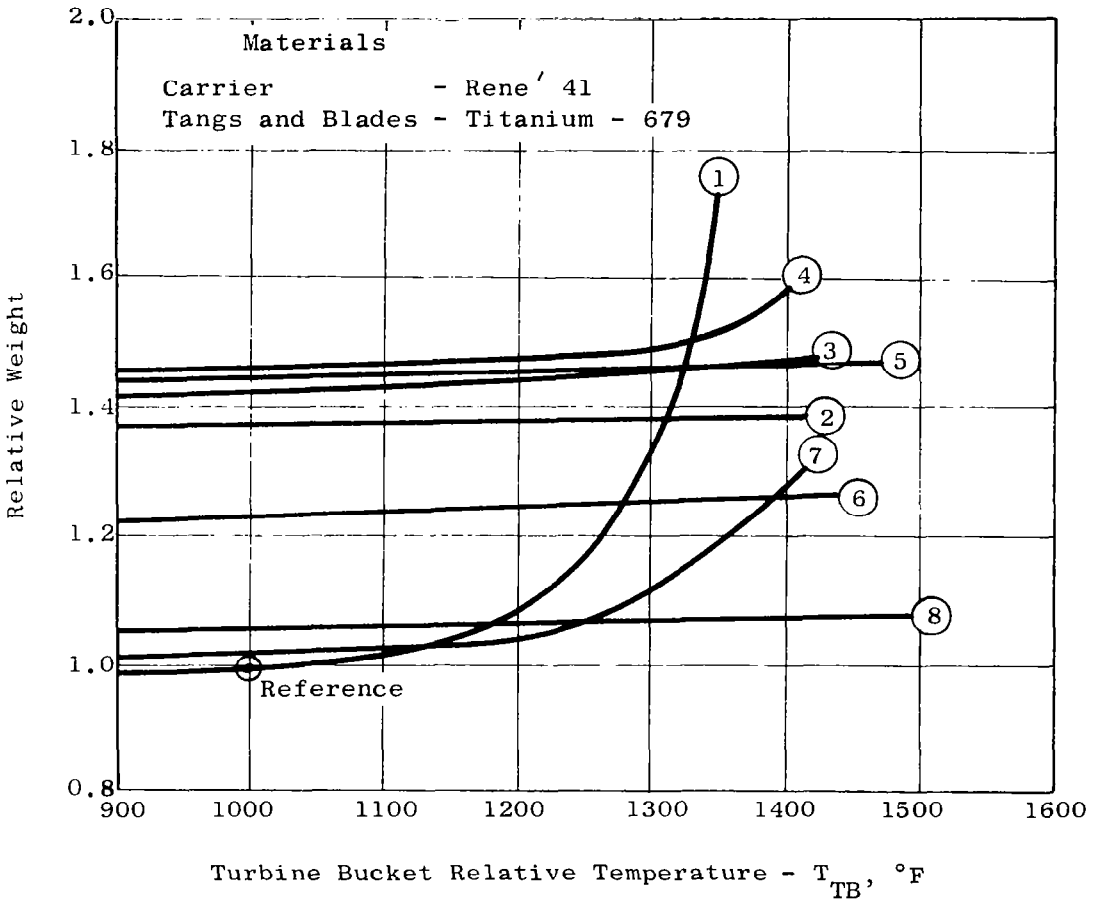

Figure 71. Effect of Cooling on Relative Weight of Bucket and Carrier Assembly (Material properties are based on 1000-hour life; weights calculated using the results of heat transfer study).

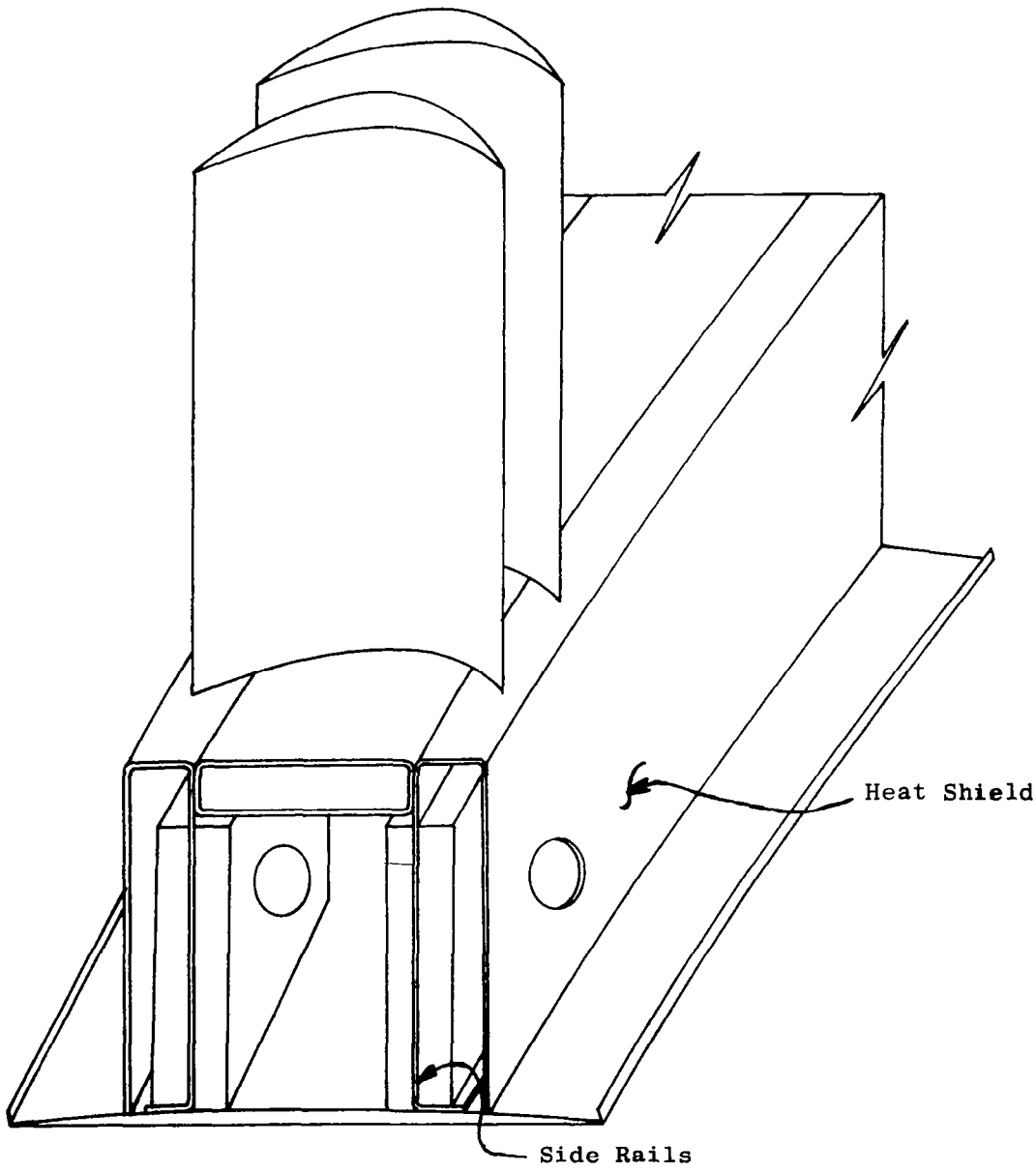

Figure 72. Bucket Carrier With Shielded Side Rails.

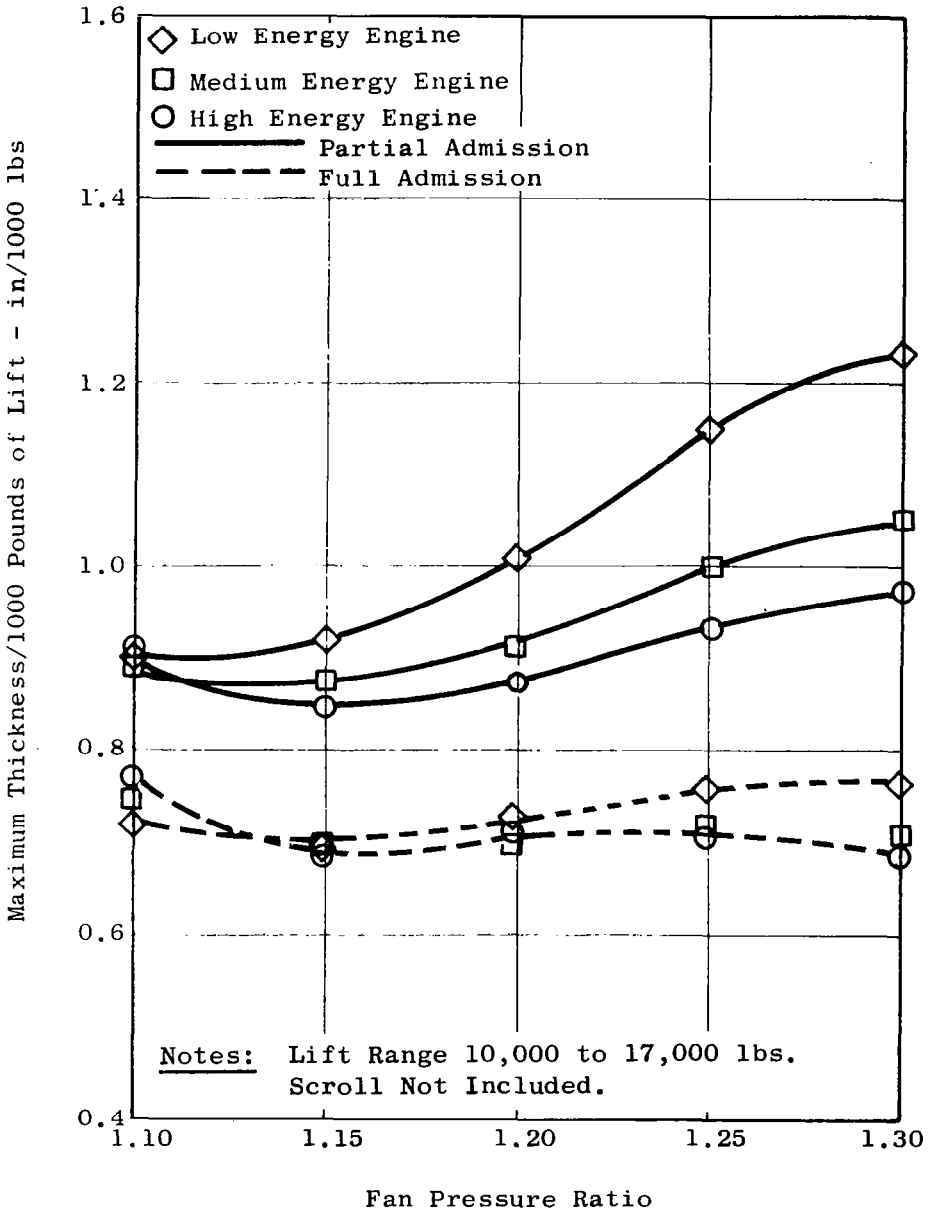

Figure 73. Maximum Fan Thickness Versus Fan Pressure Ratio for Conventional Fan.

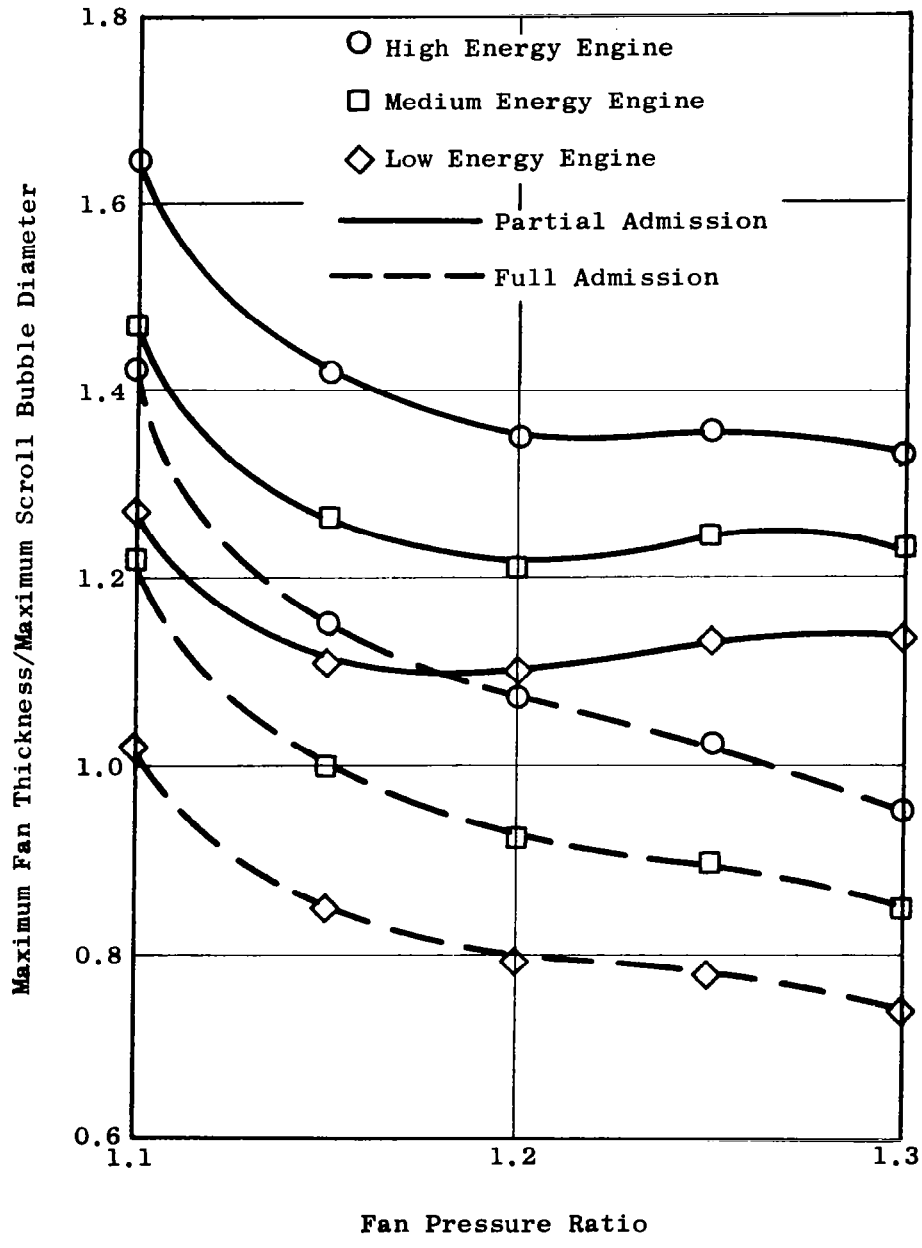

Figure 74. Fan to Scroll Bubble Thickness Ratio for Conventional Fan.

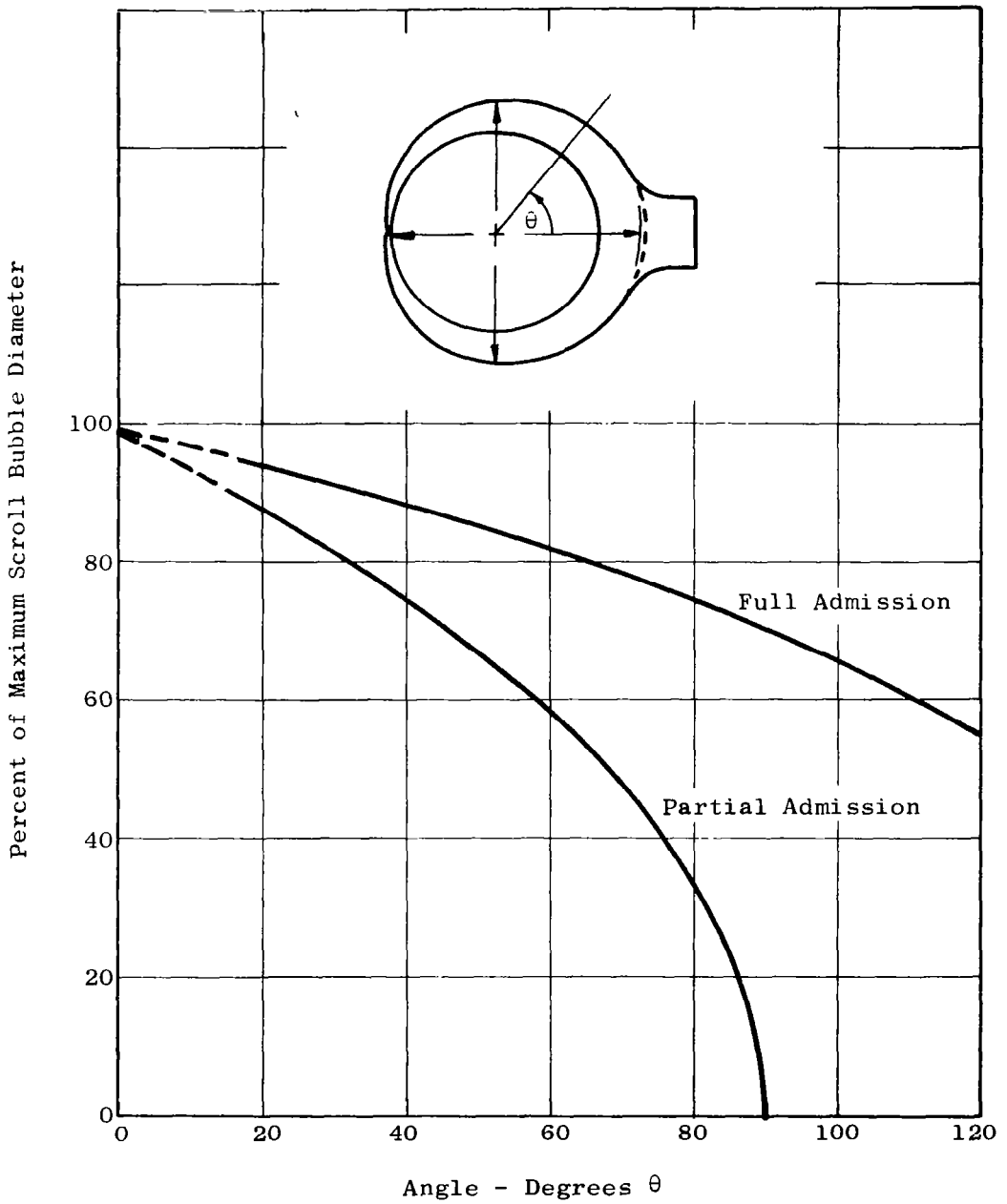

Figure 75. Scroll Bubble Diameter Decrease Versus Angle.

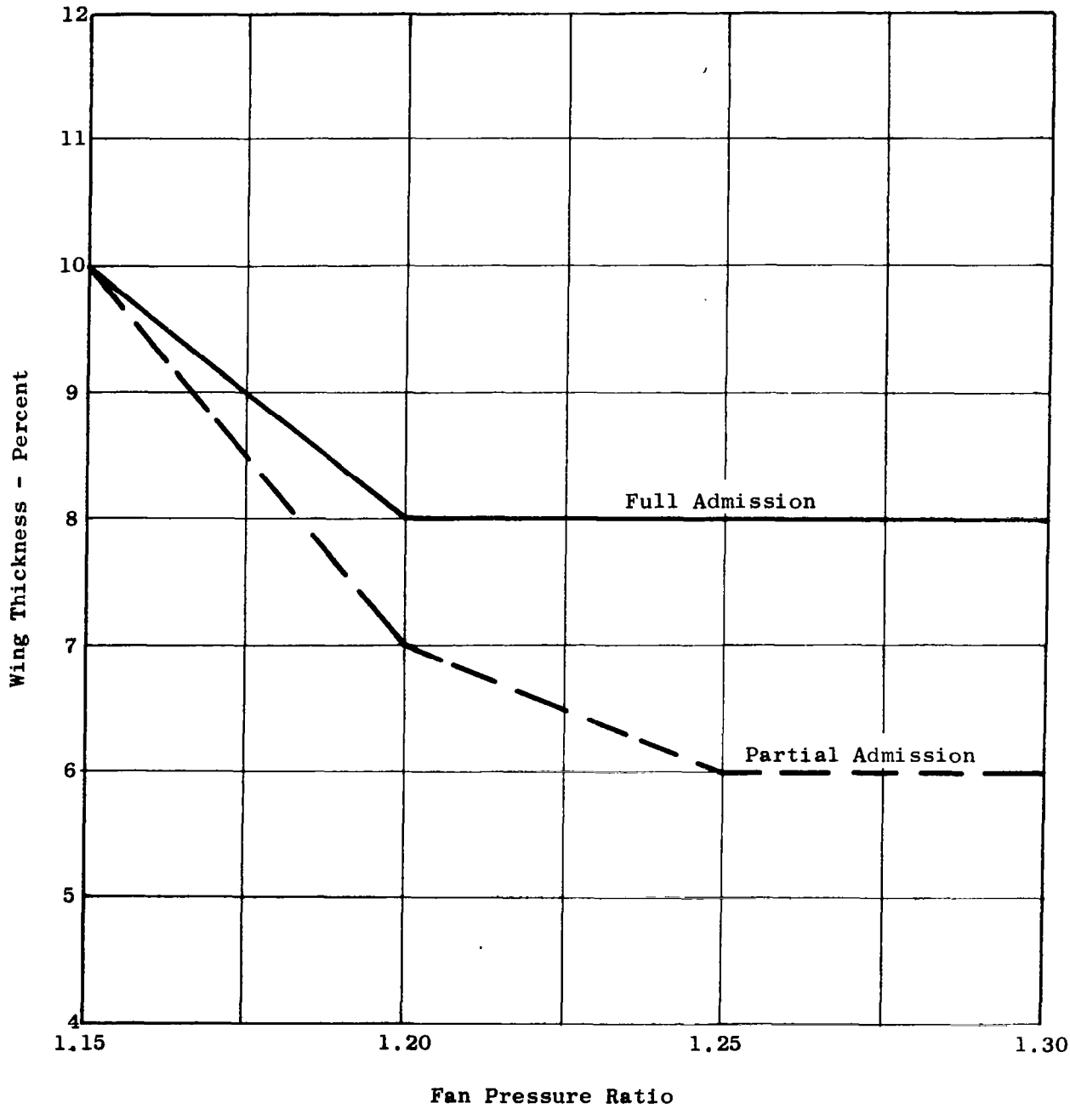

Figure 76. Delta Wing Thickness Versus Fan Pressure Ratio for Conventional Fan.

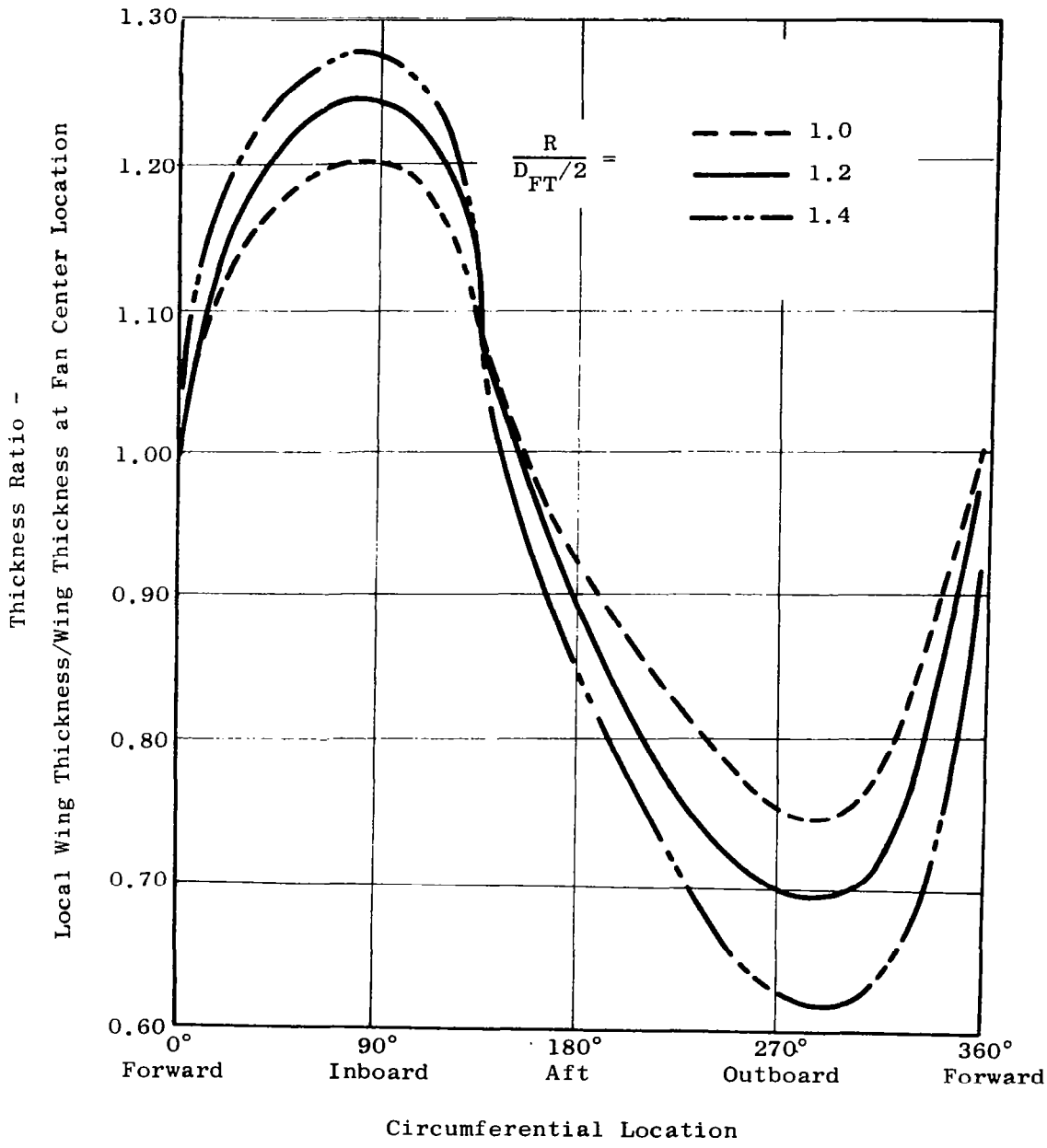

Figure 77. Wing Thickness Distribution for Delta Wing.

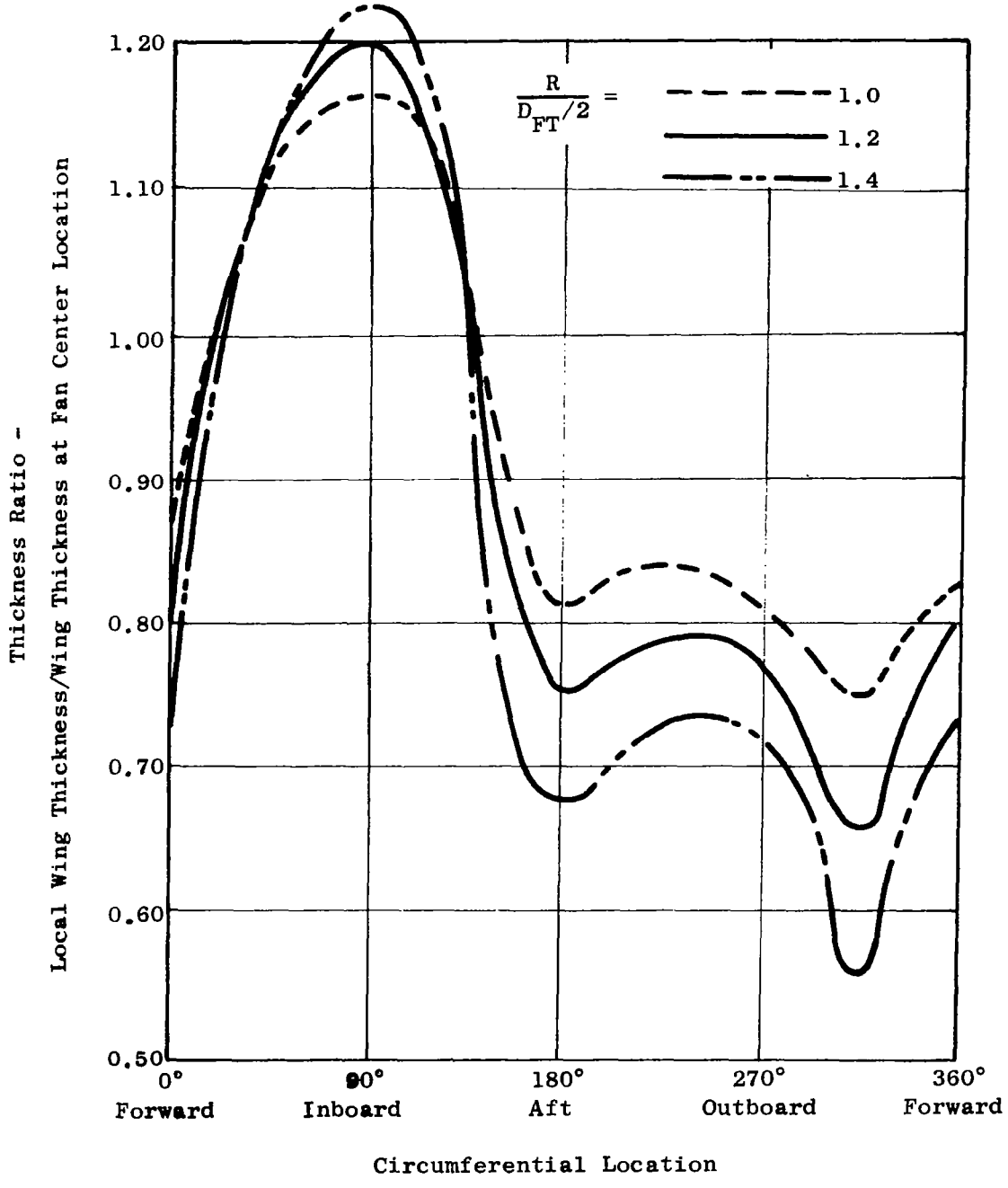

Figure 78. Wing Thickness Distribution for LFX Wing.

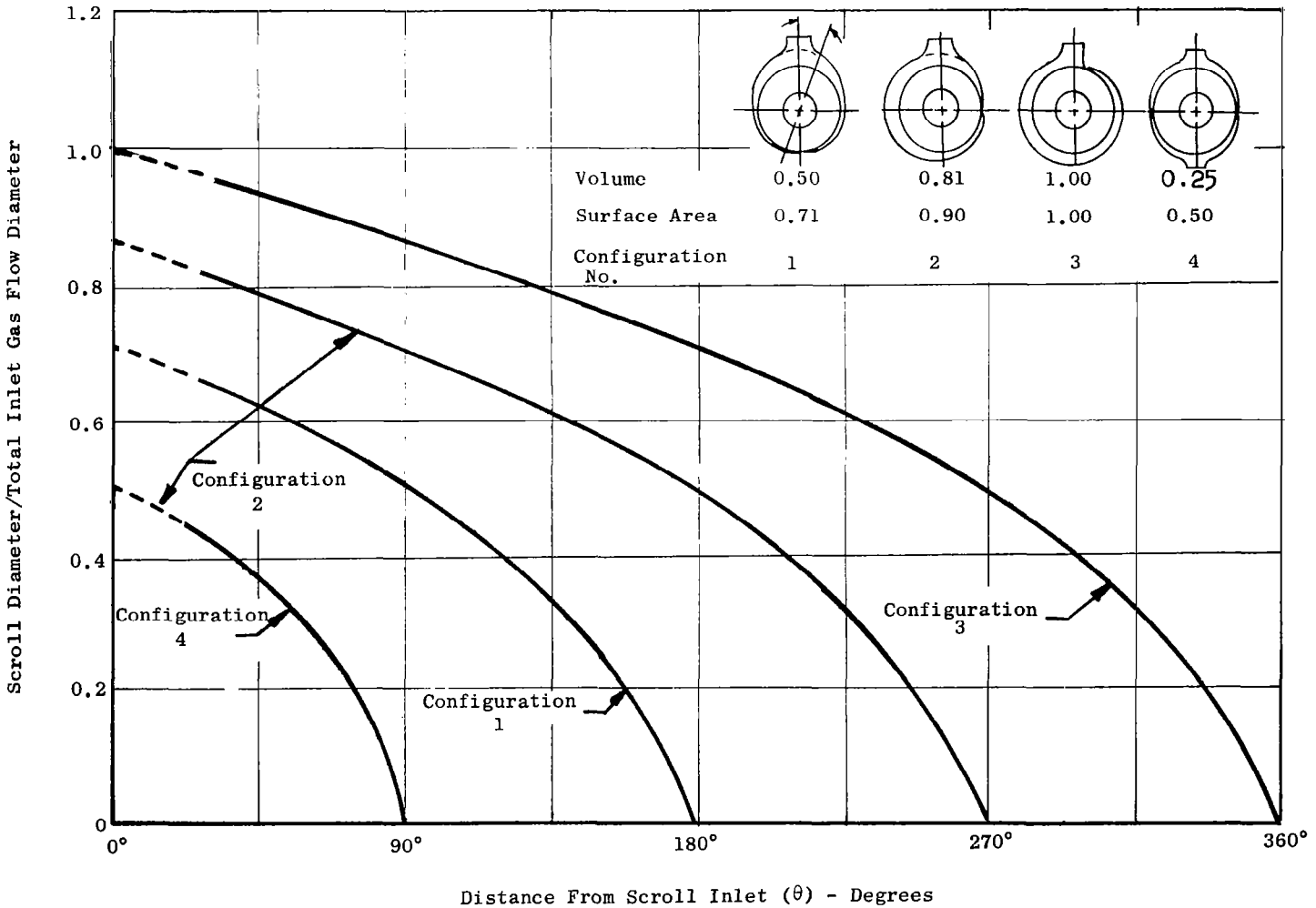

Figure 79. Effect of Scroll Configuration on Scroll Volume and Surface Area.

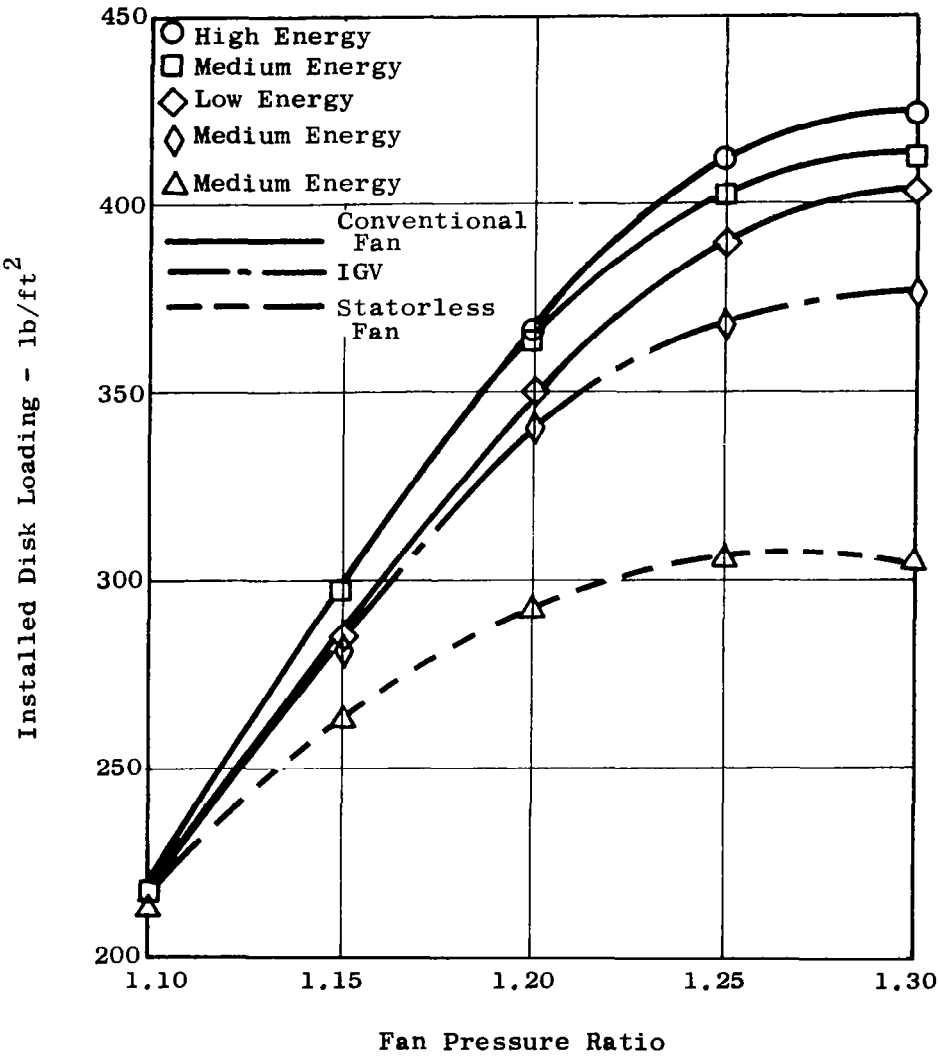

Figure 80. Installed Disk Loading Versus Fan Pressure Ratio - Full Admission.

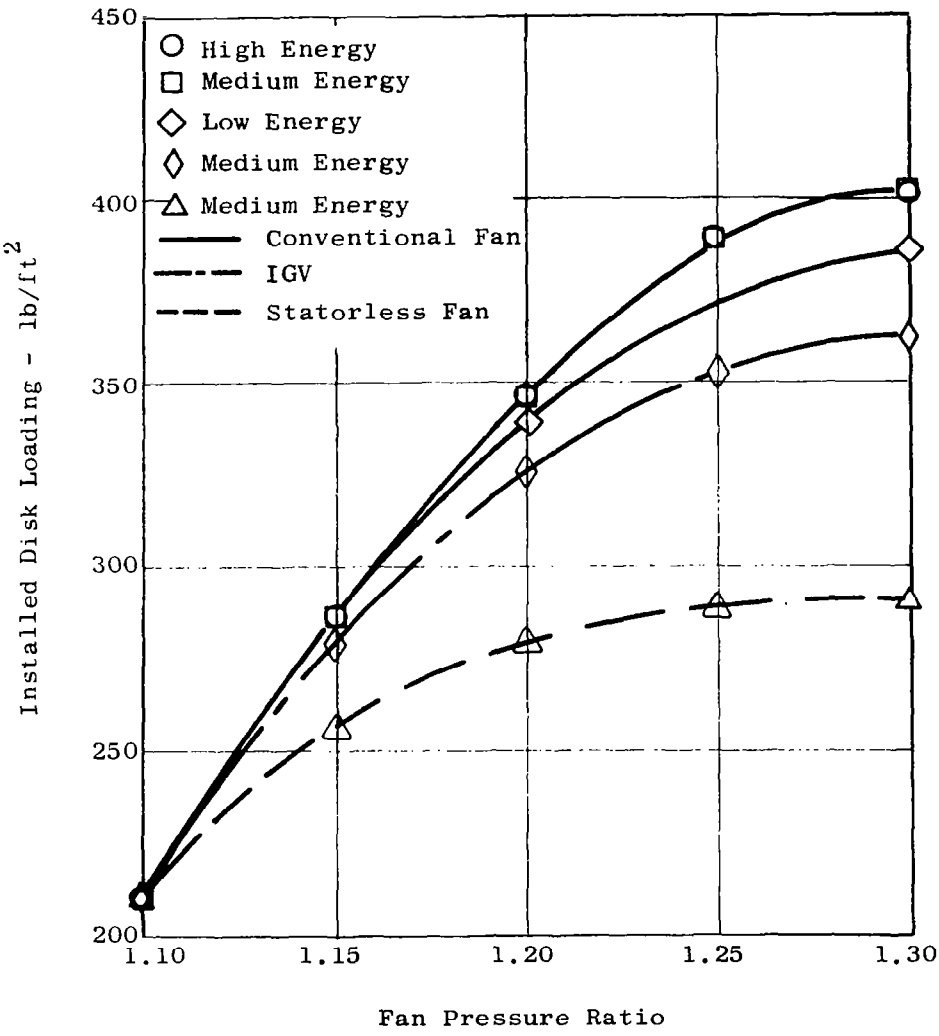

Figure 81. Installed Disk Loading Versus Fan Pressure Ratio - Partial Admission.

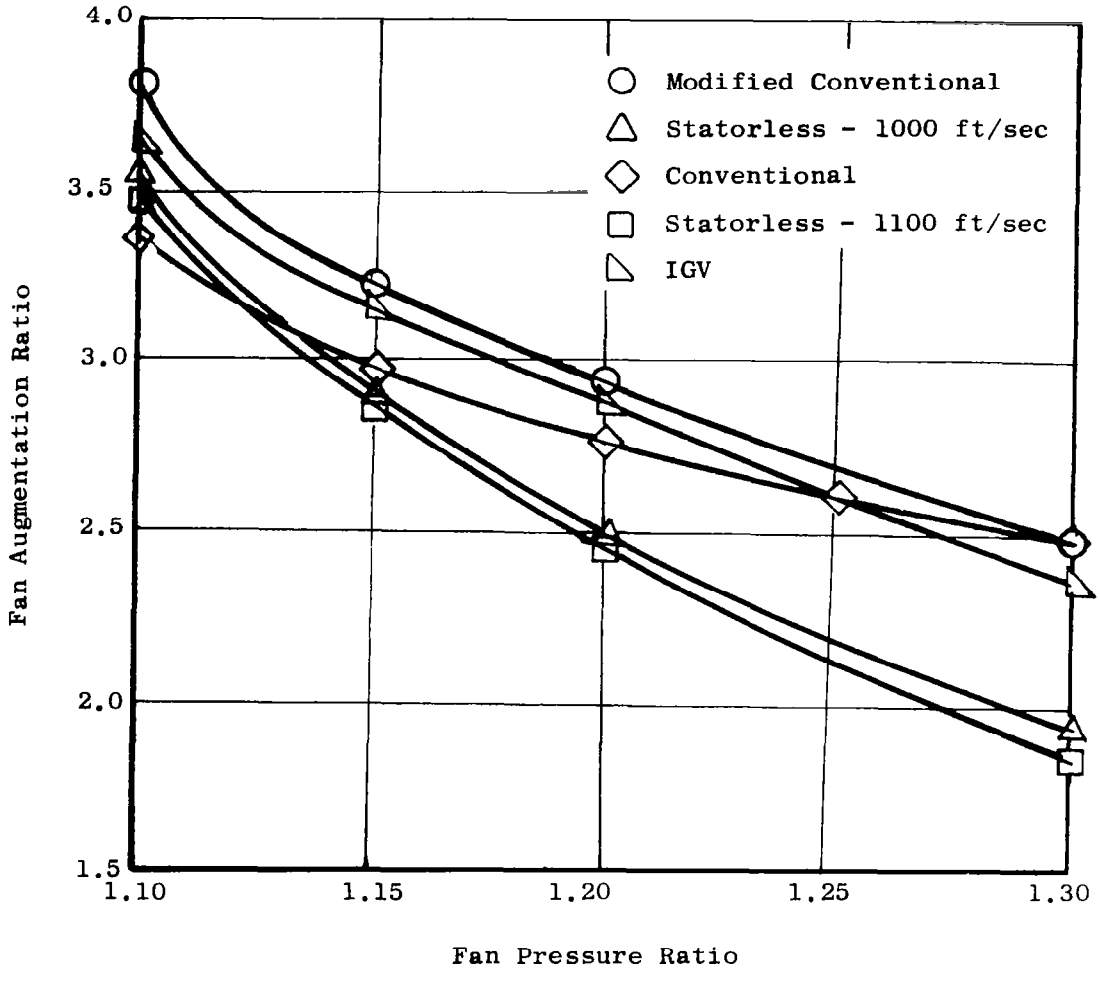

Figure 82. Augmentation Ratio Versus Fan Pressure Ratio.

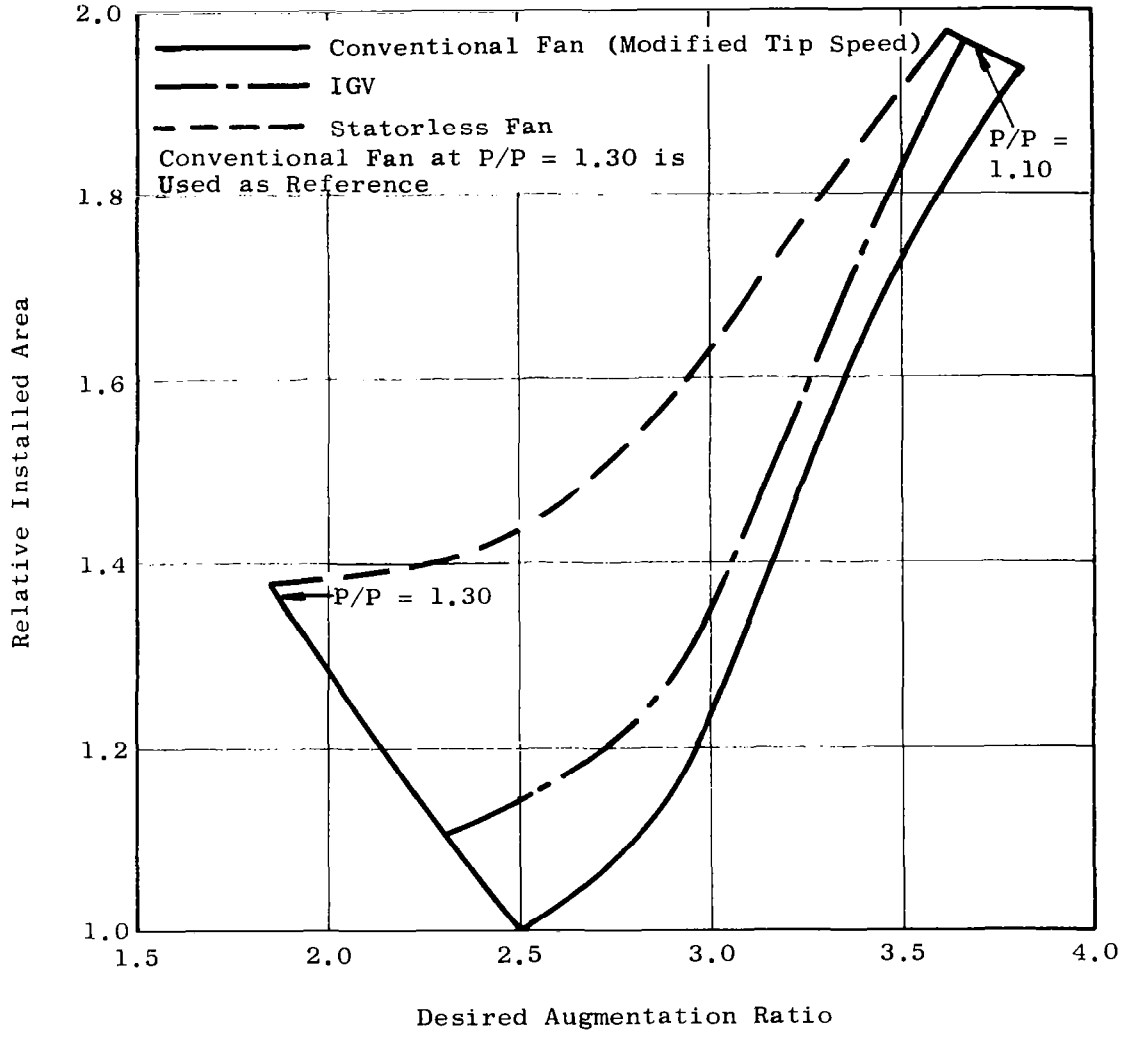

Figure 83. Relative Fan Size Versus Augmentation Ratio.

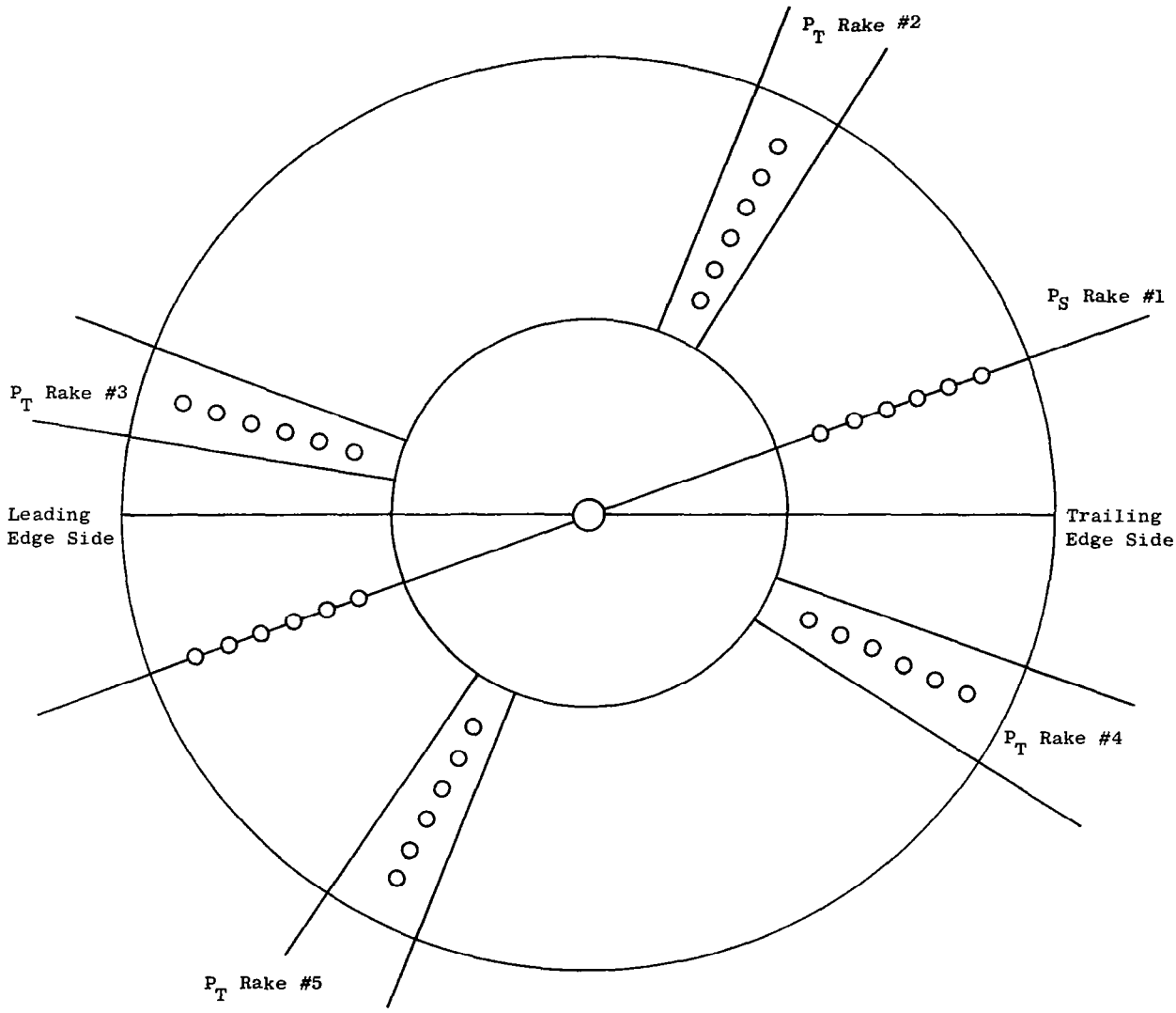

Figure 84. Pressure Instrumentation View - Bottom of Wing.

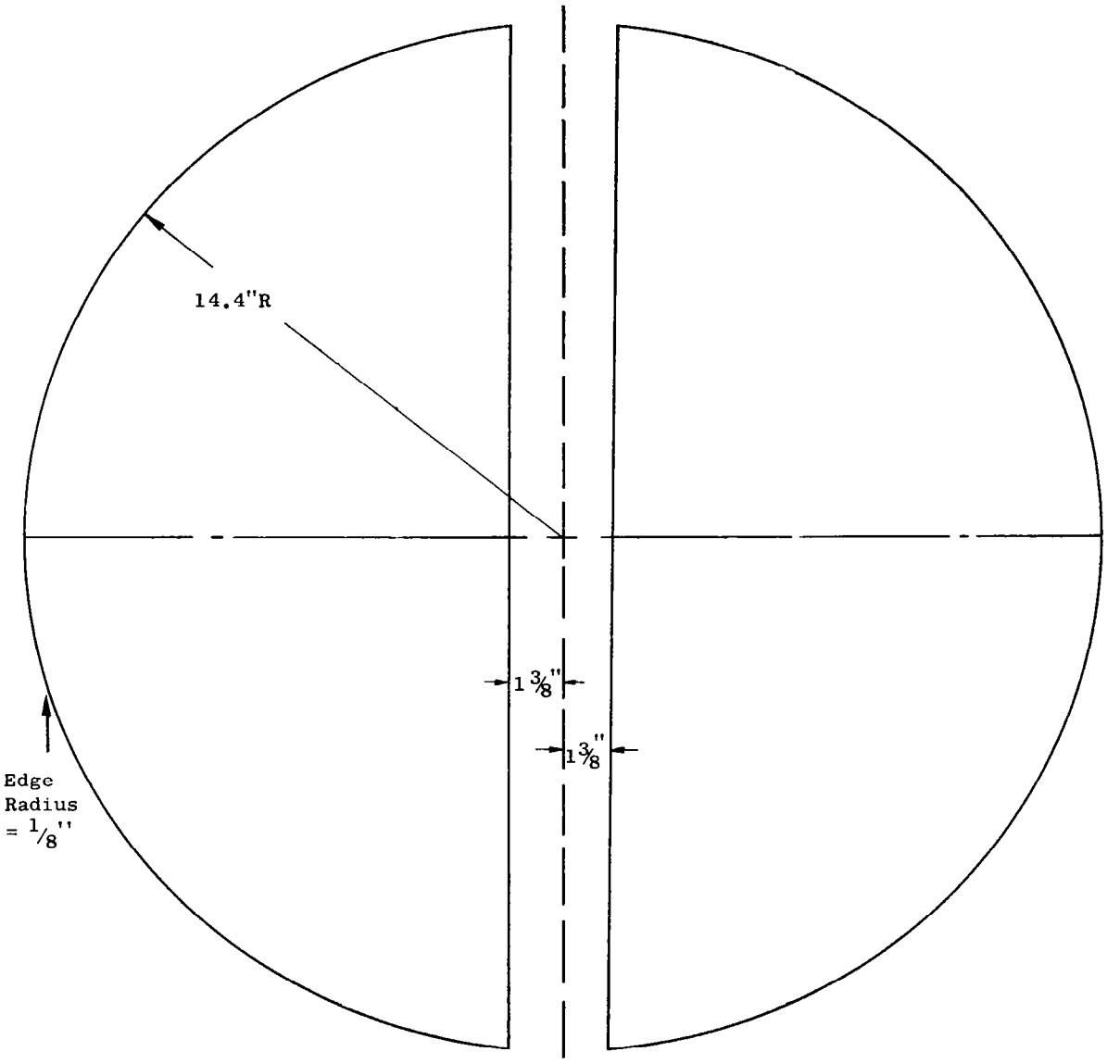

Figure 85. Basic Test Scoop.

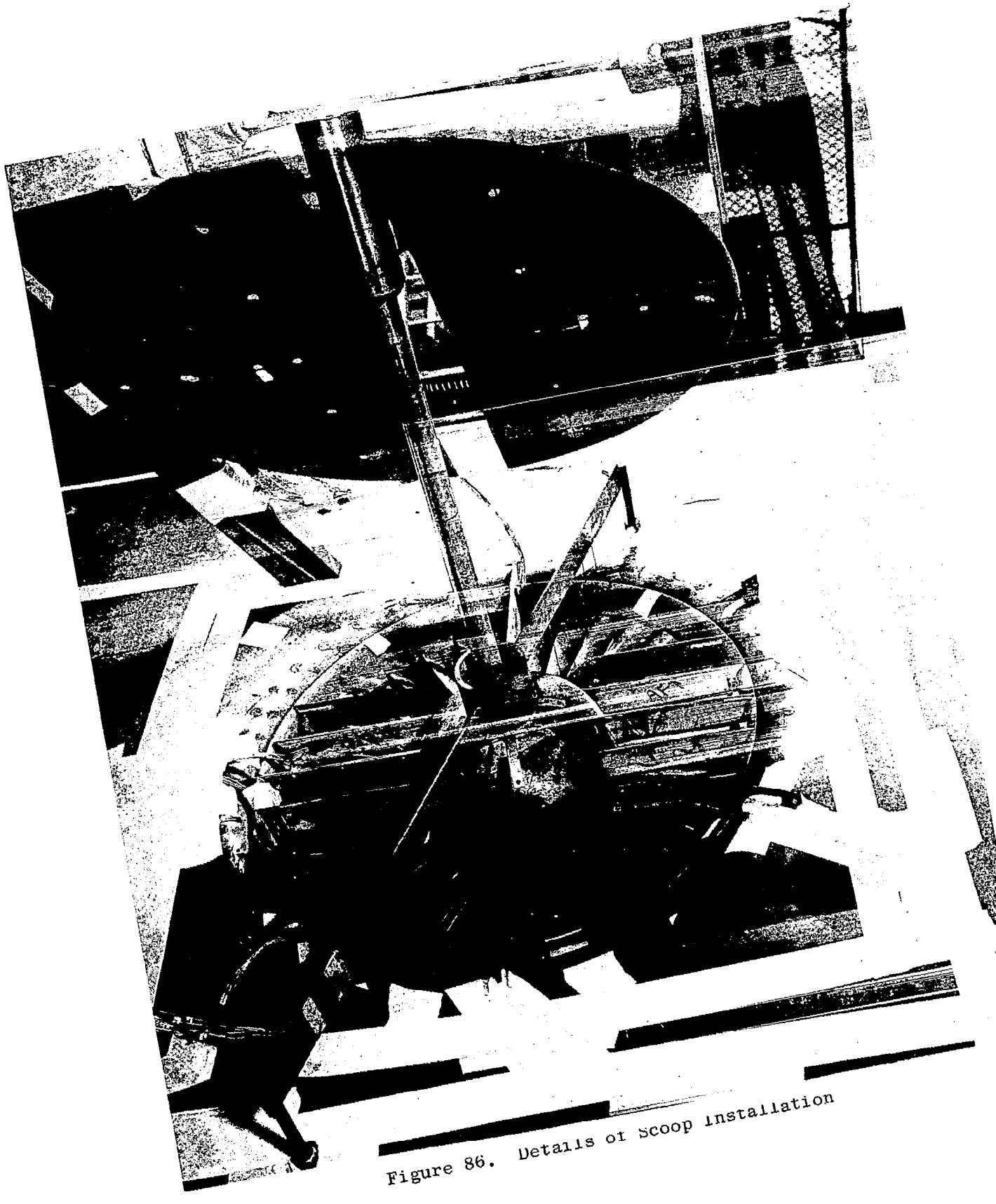

Figure 86. Details of Scoop Installation

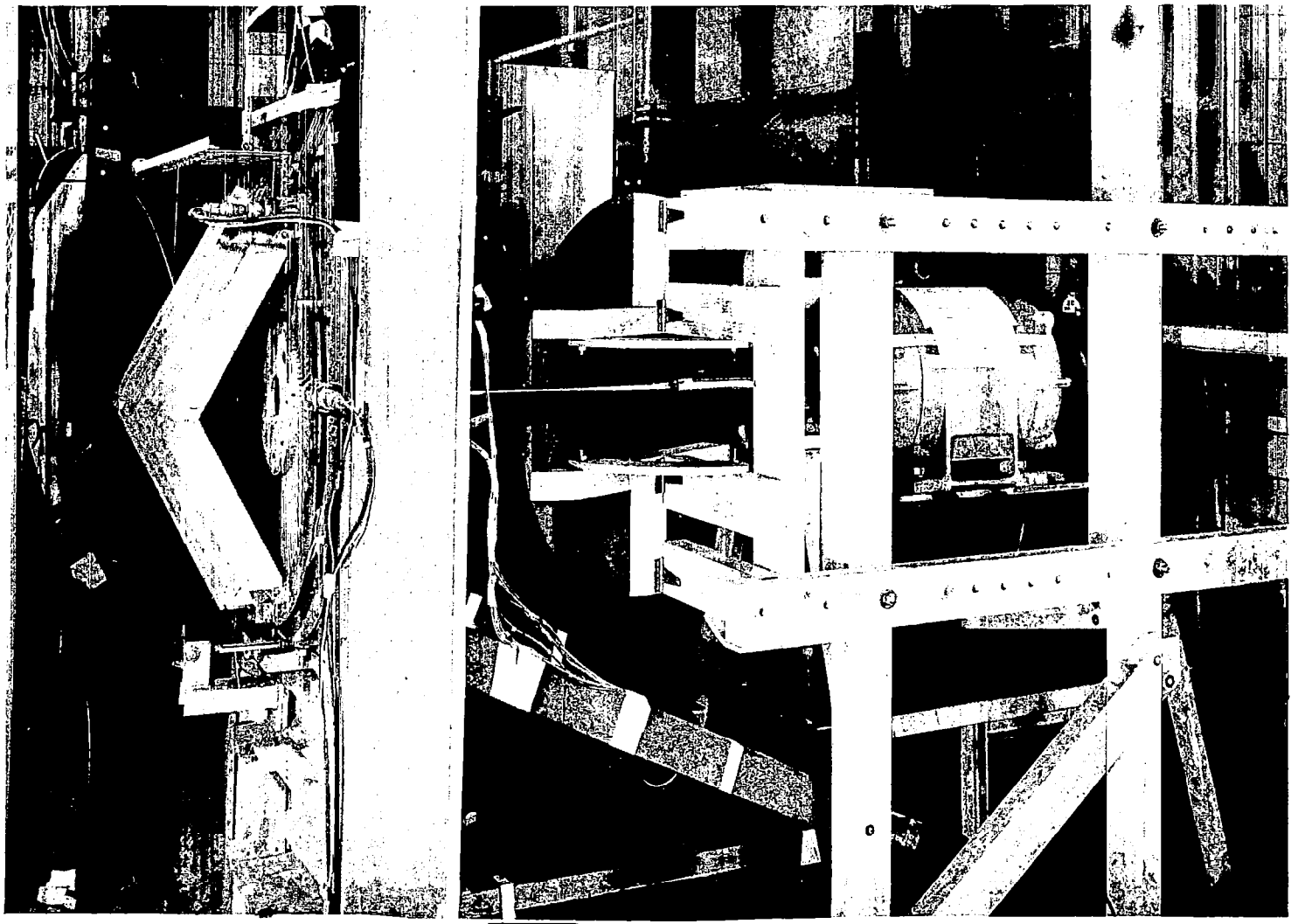

Figure 87. Overall View of Test Setup.

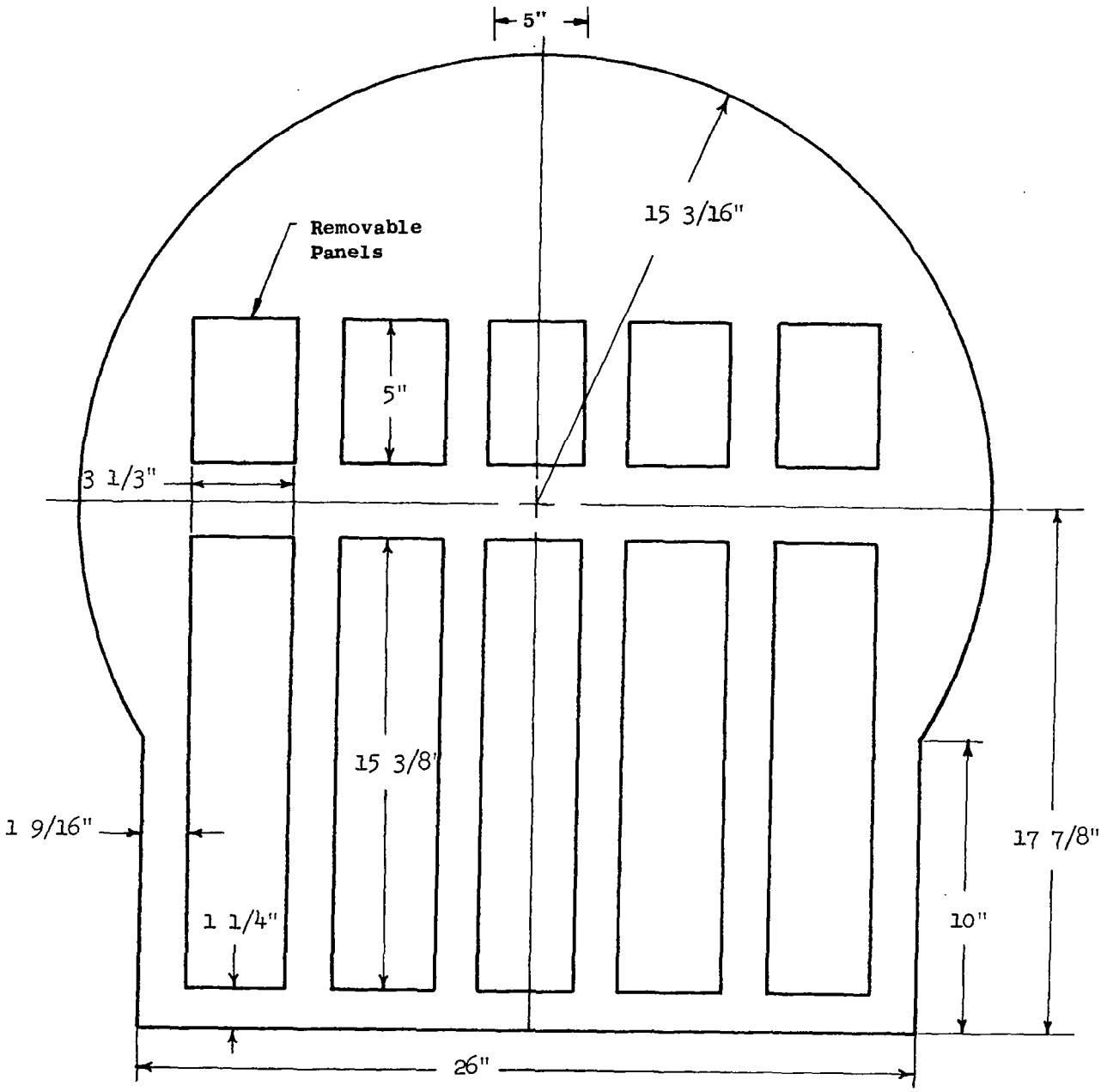

Figure 88. Final Scoop Configuration.

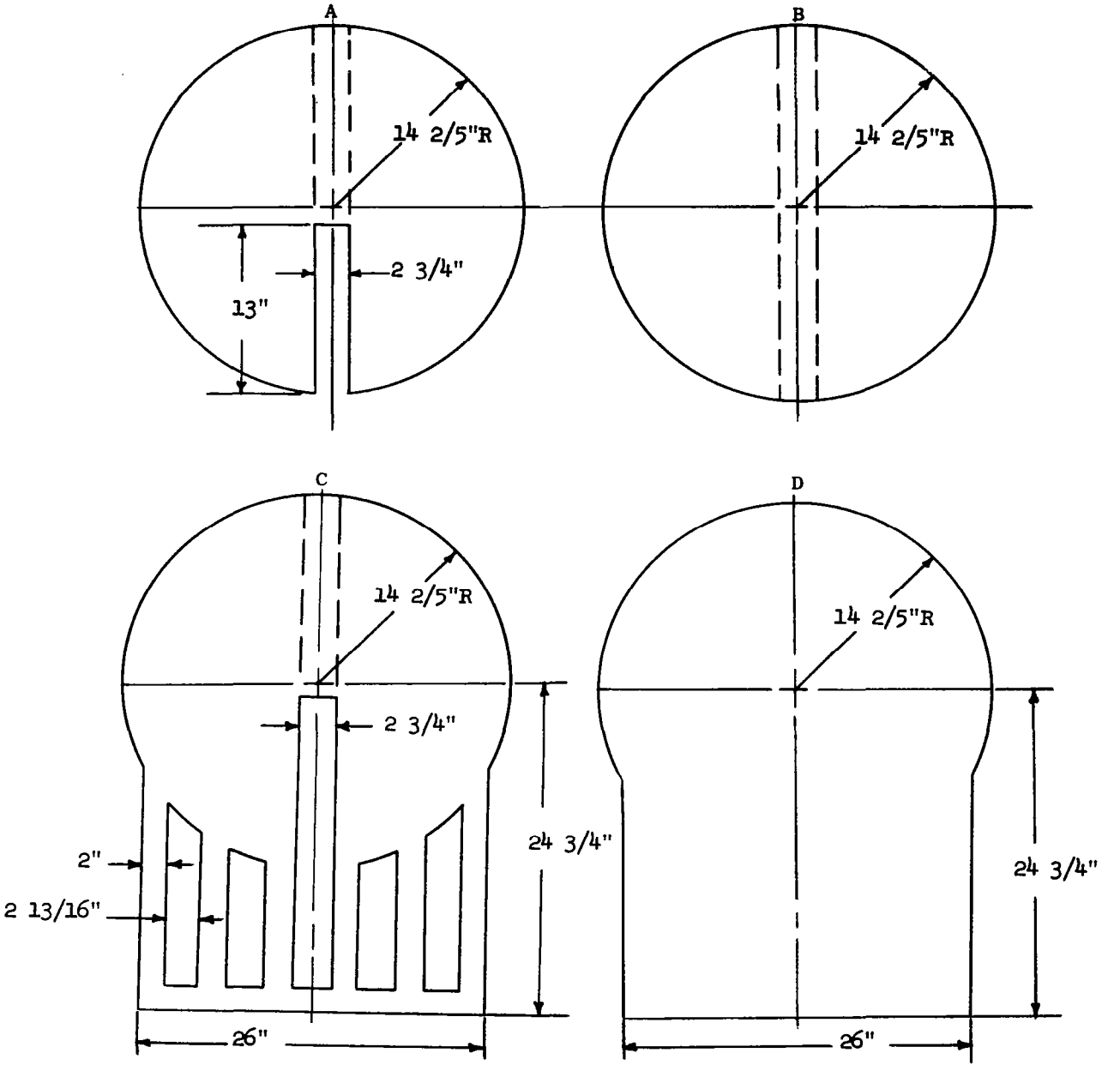

Figure 89. Scoop Configuration Variations.

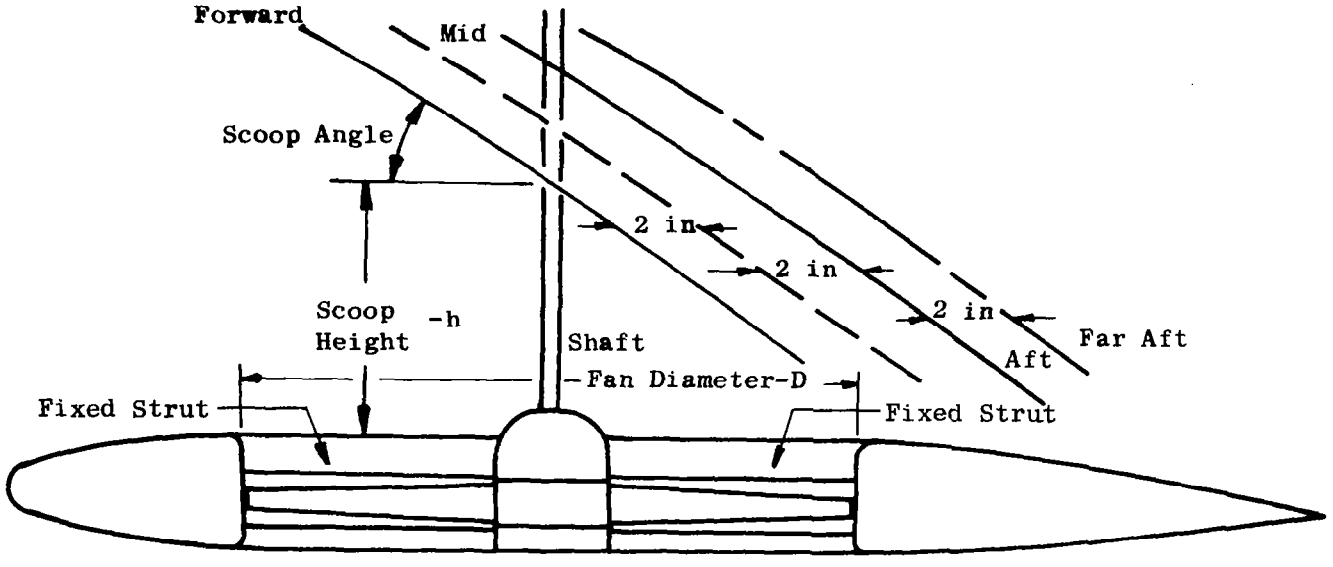

Figure 90. Scoop Chordwise Positions.

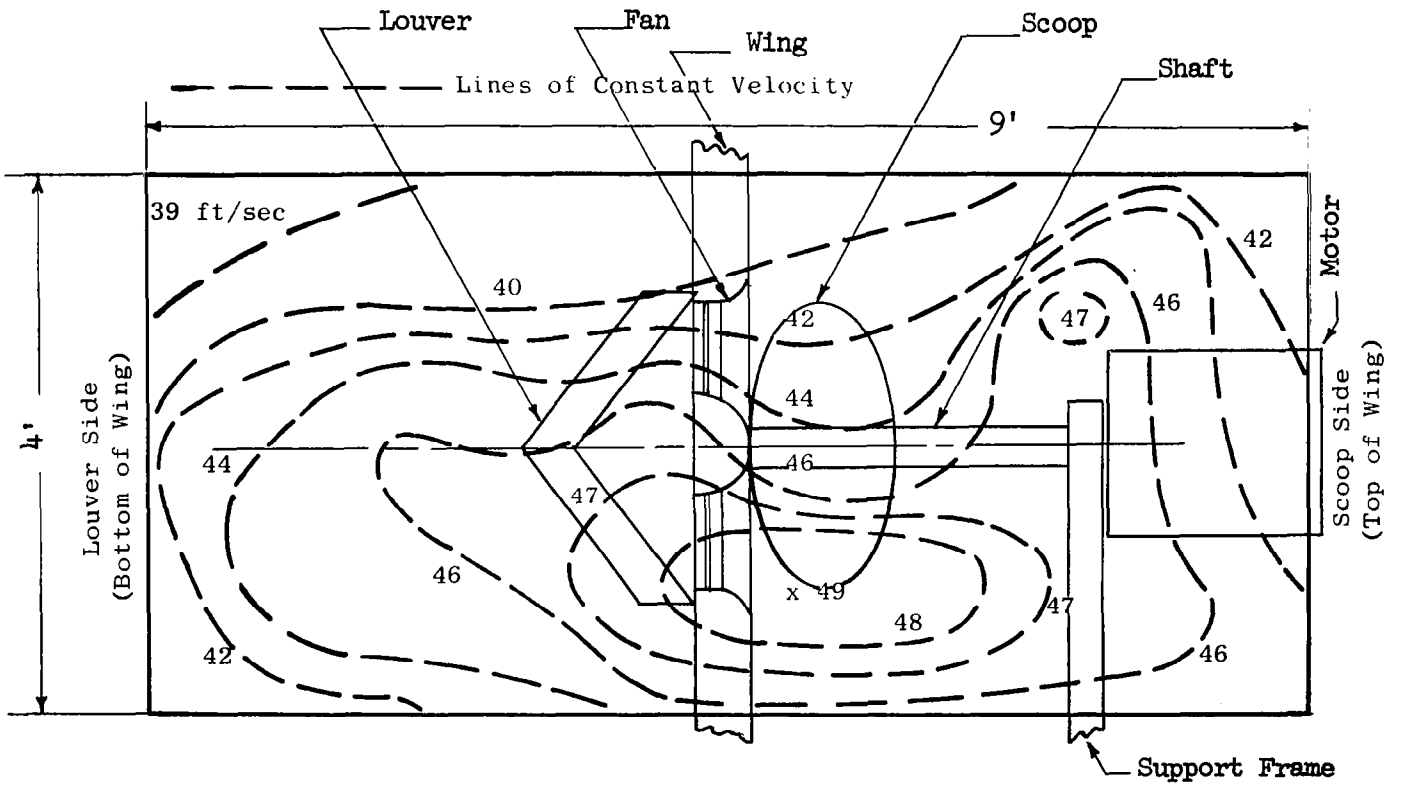

Figure 91. Low Cross-Flow Velocity Pattern in the Wind Tunnel Discharge.

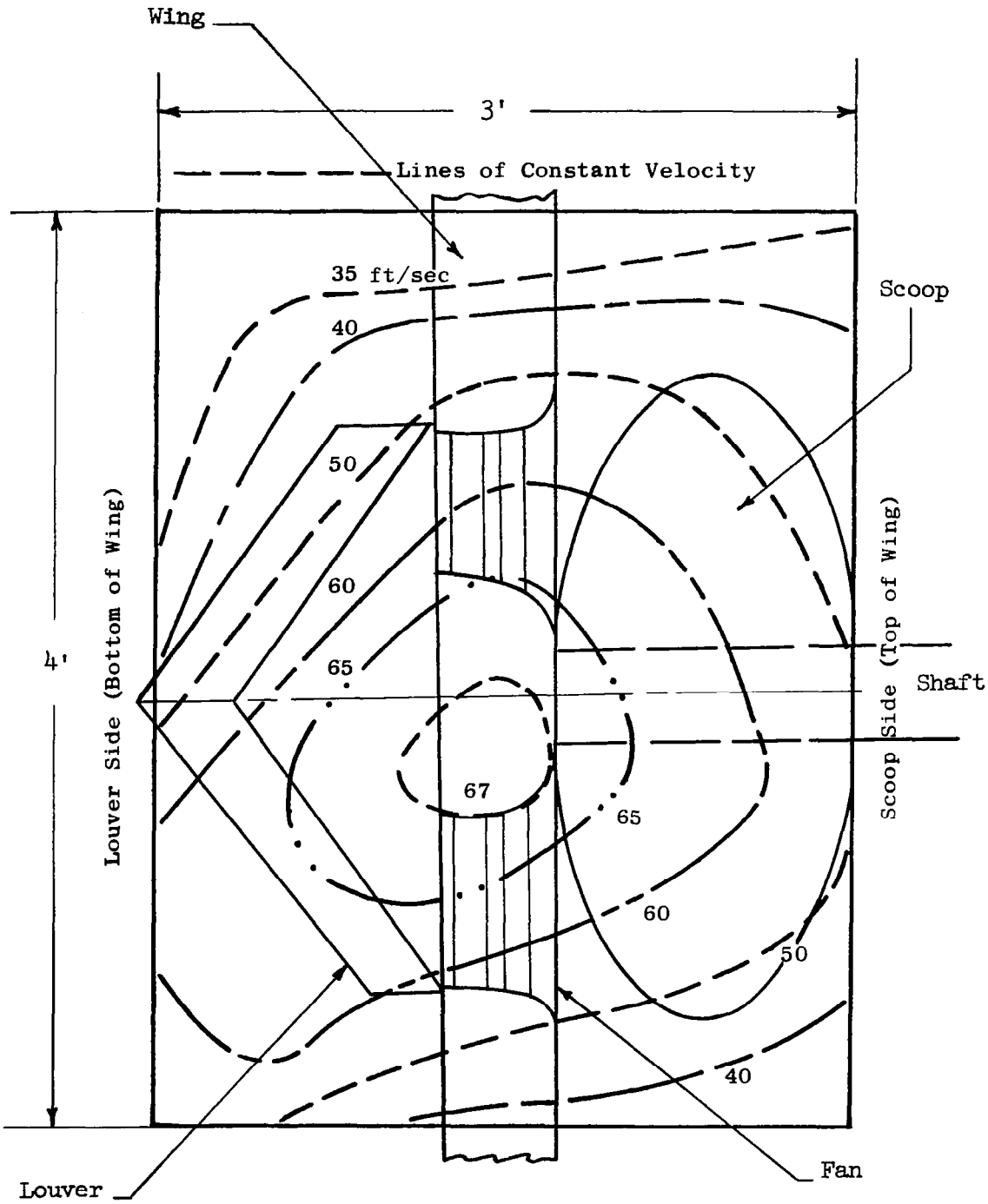

Figure 92. High Cross-Flow Velocity Pattern in the Wind Tunnel Discharge.

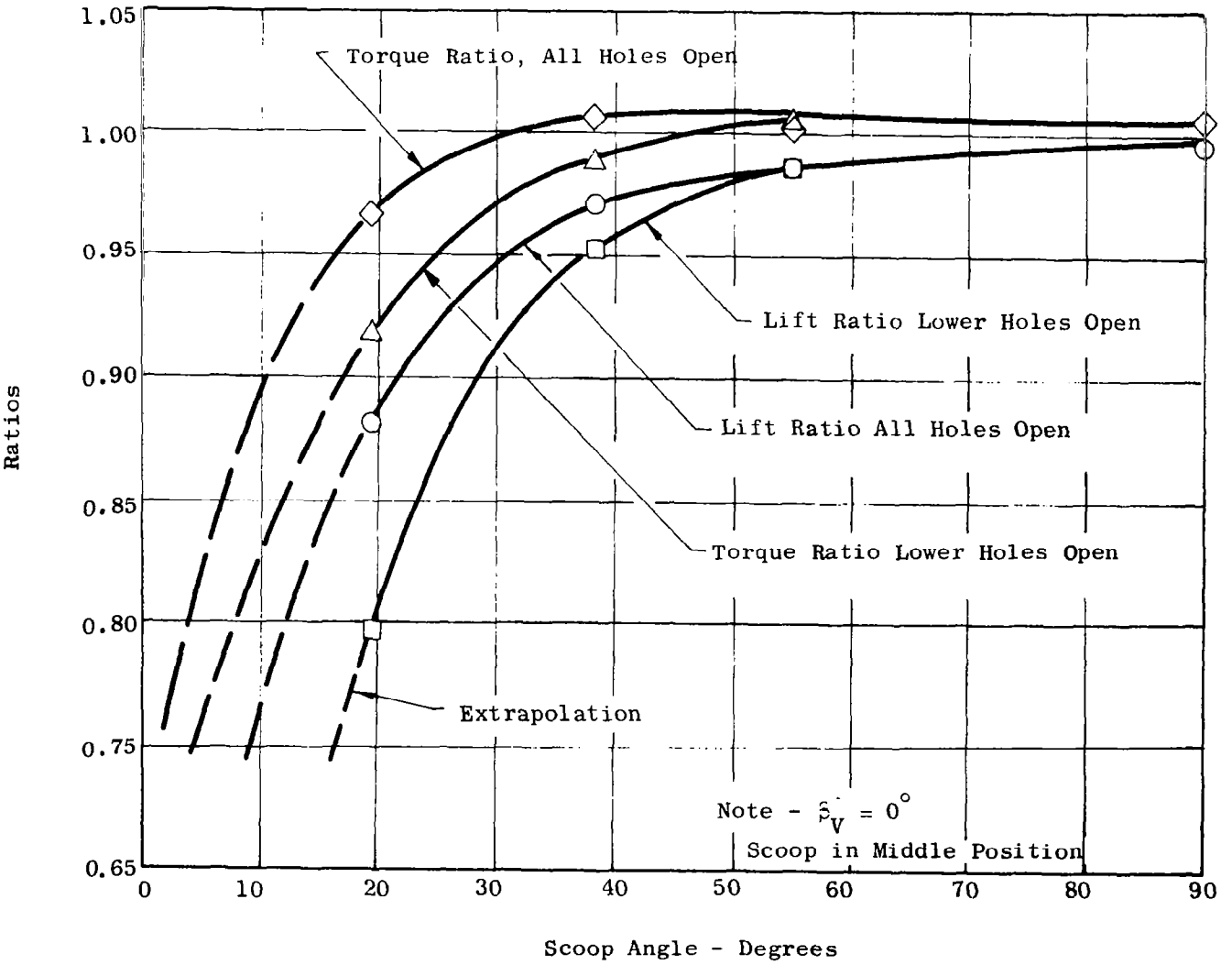

Figure 93. Final Scoop Configuration Static Performance.

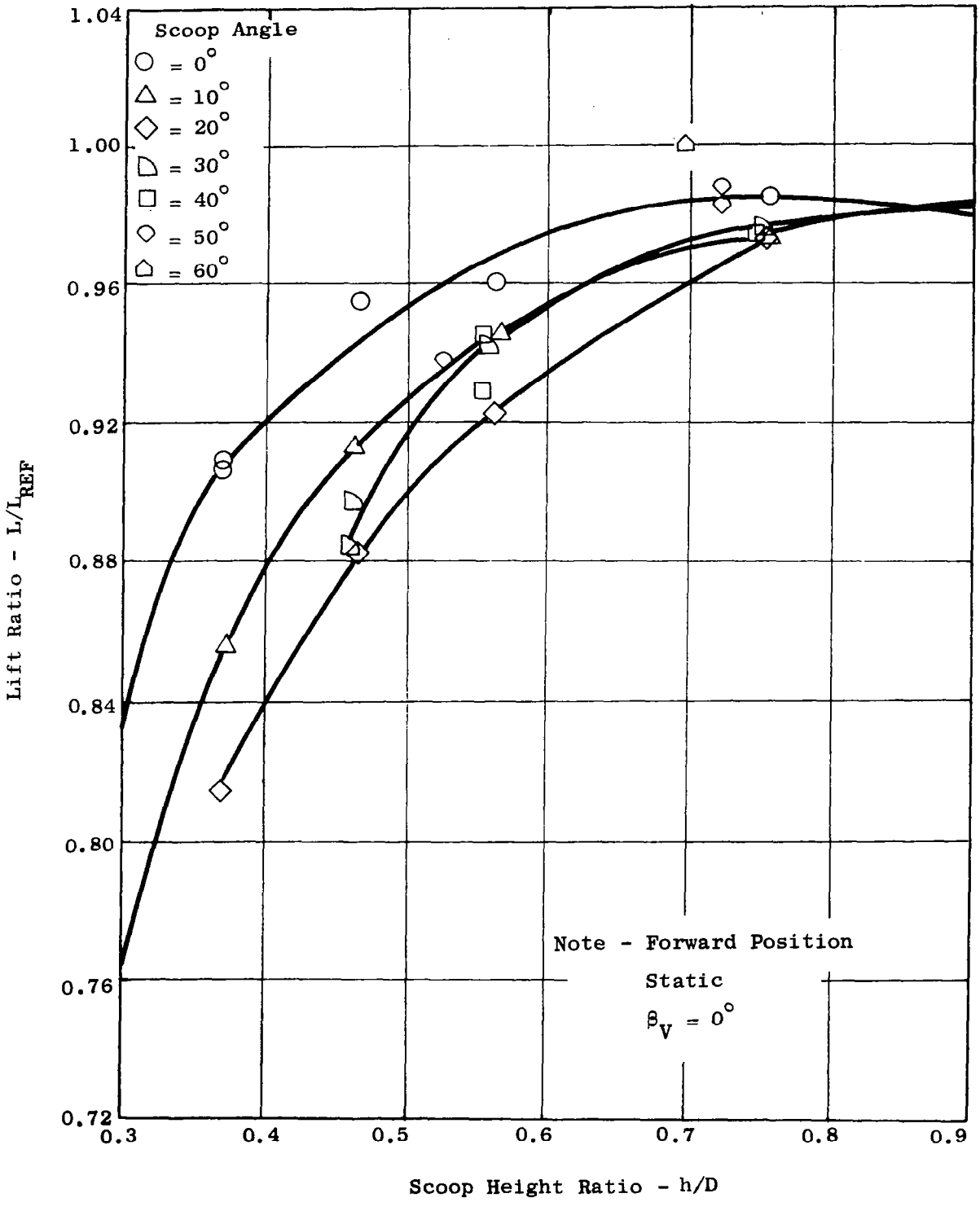

Figure 94. Basic Scoop Performance.

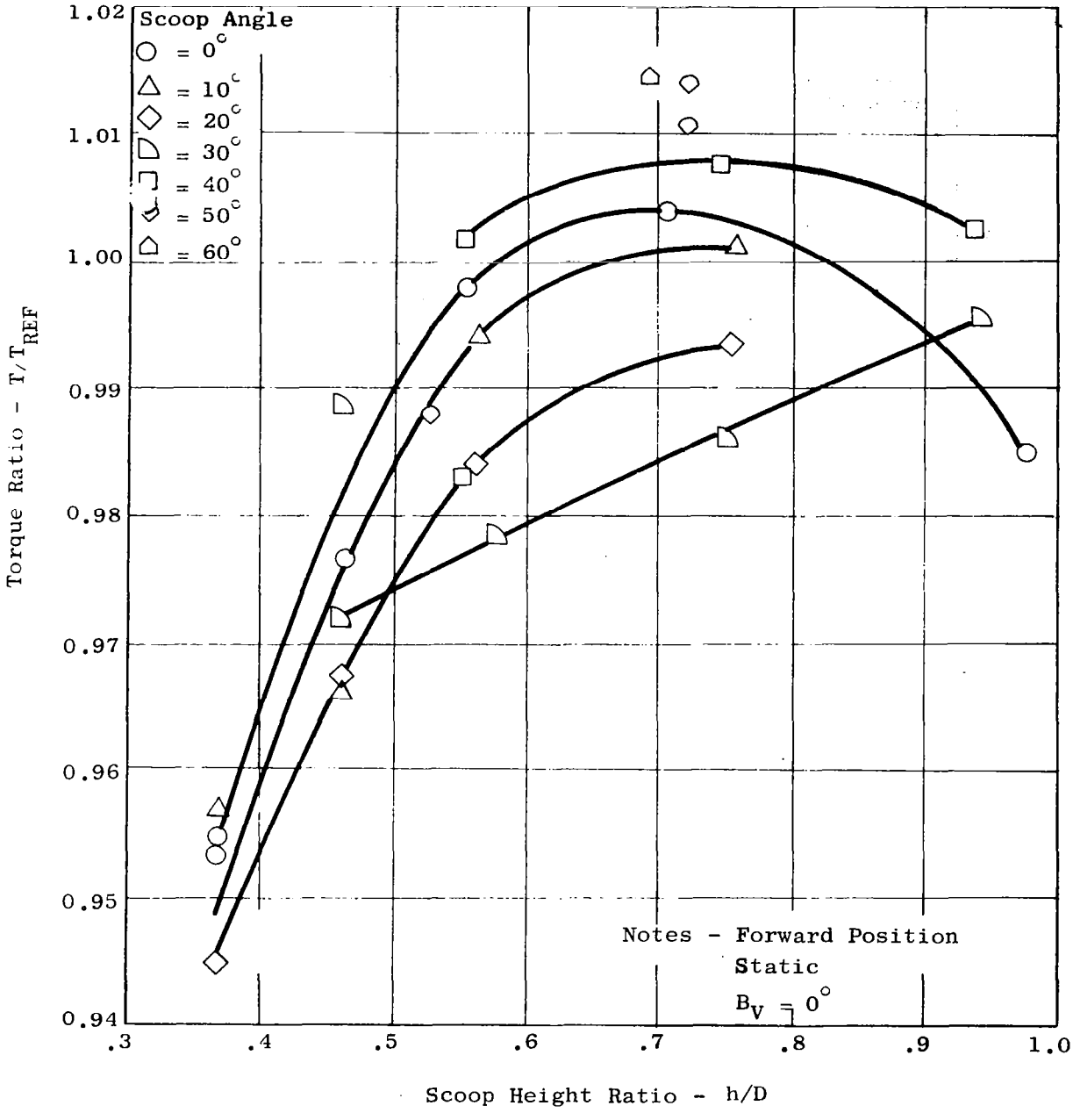

Figure 95. Basic Scoop Performance.

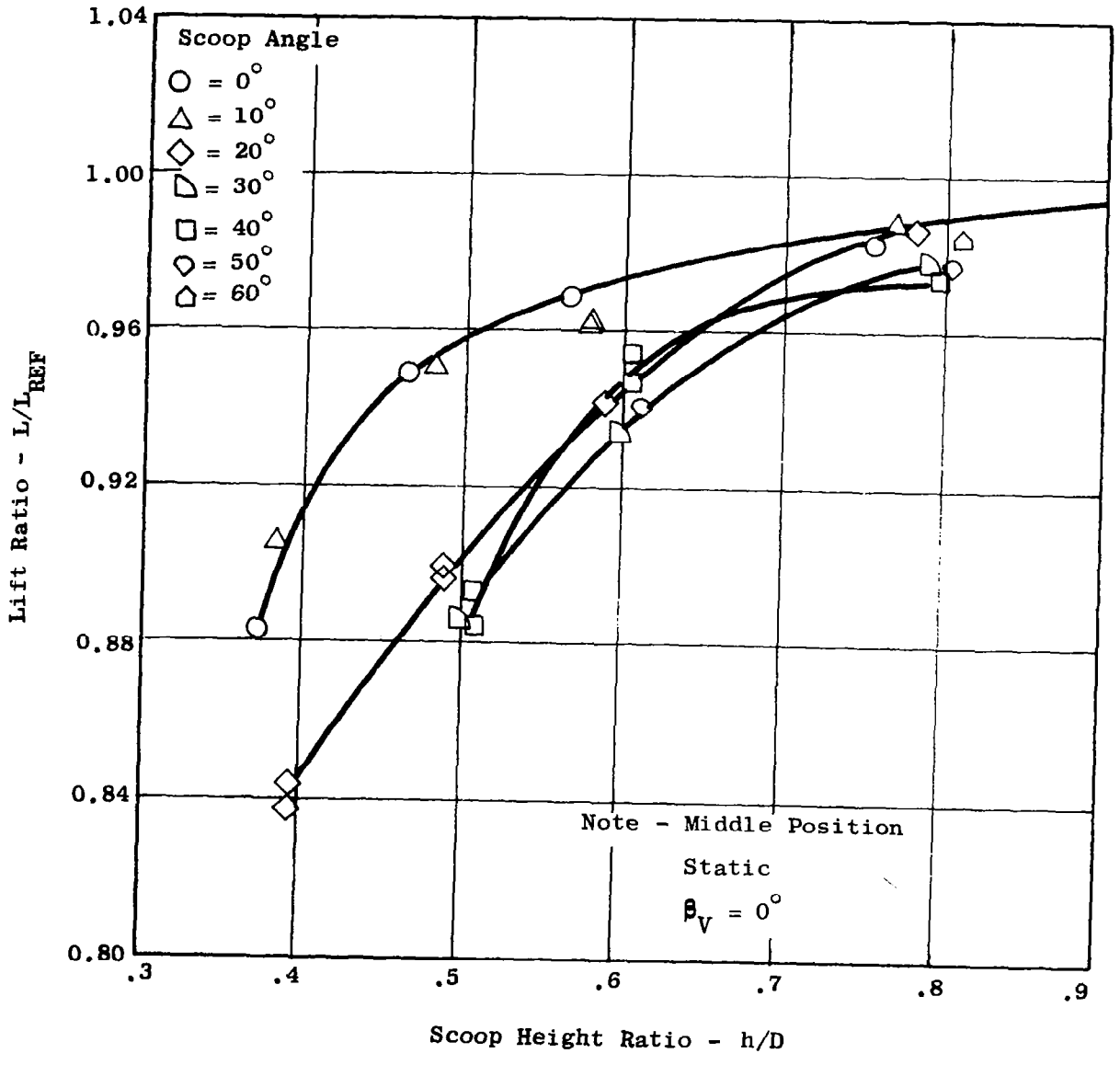

Figure 96. Basic Scoop Performance.

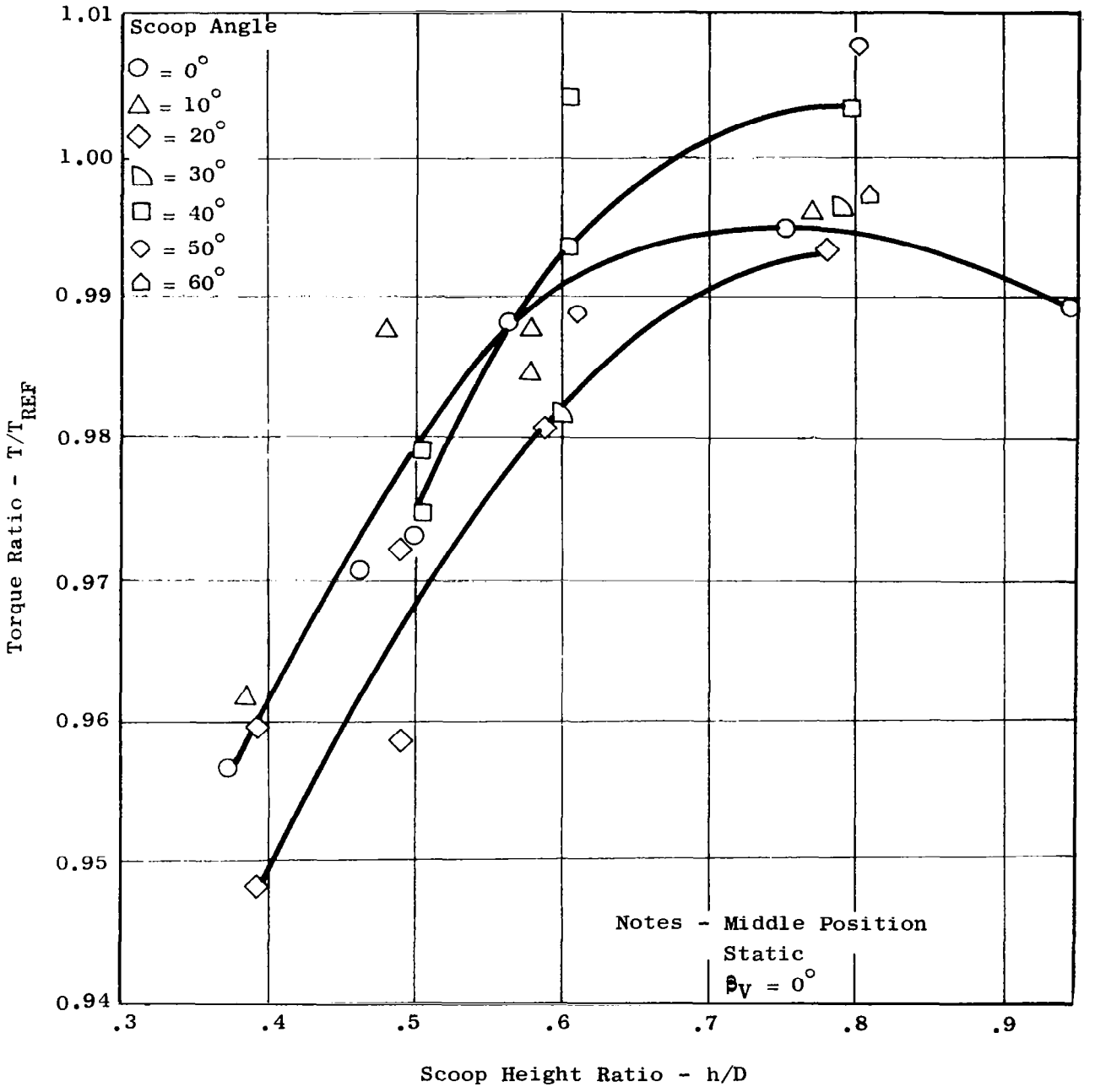

Figure 97. Basic Scoop Performance.

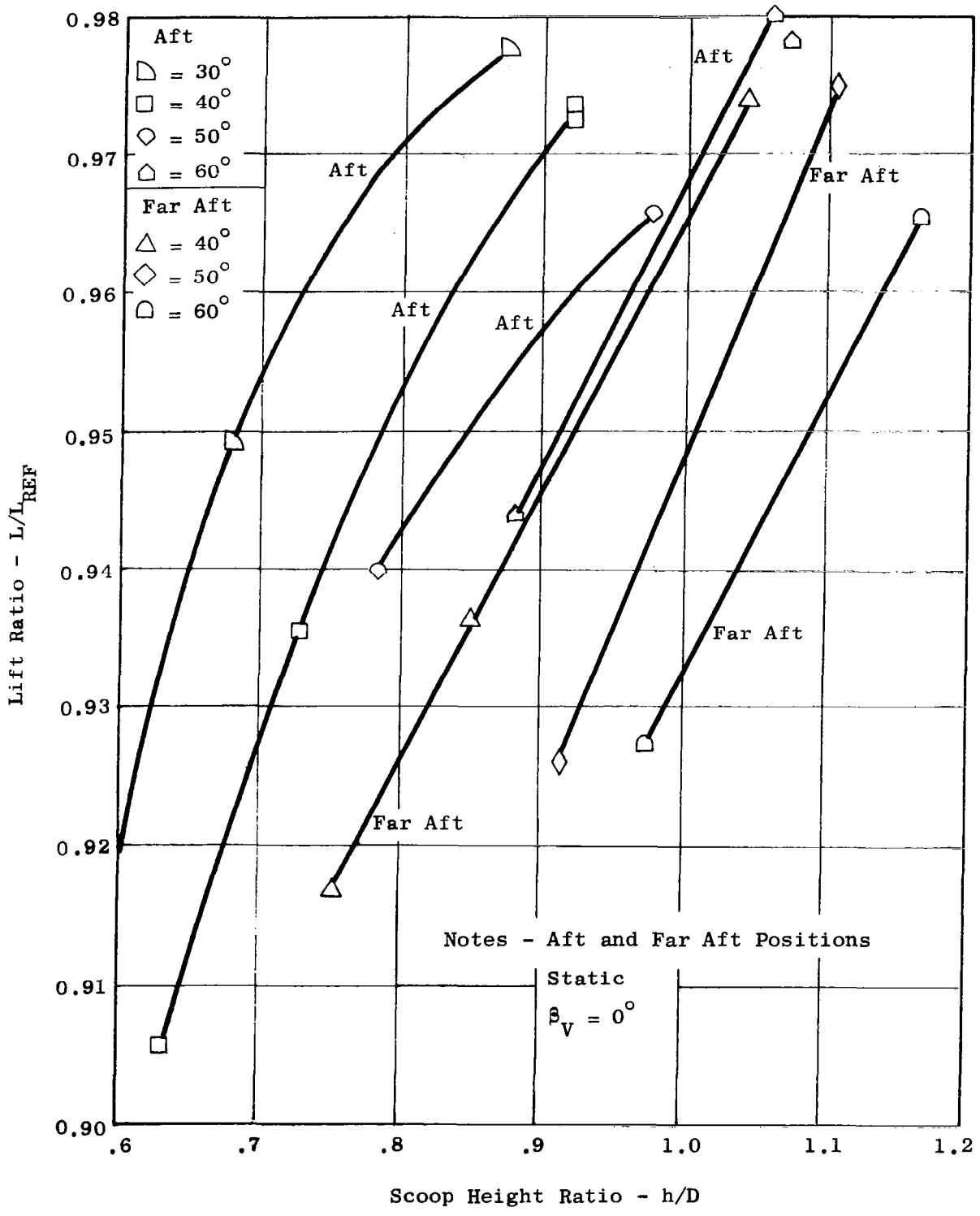

Figure 98. Basic Scoop Performance.

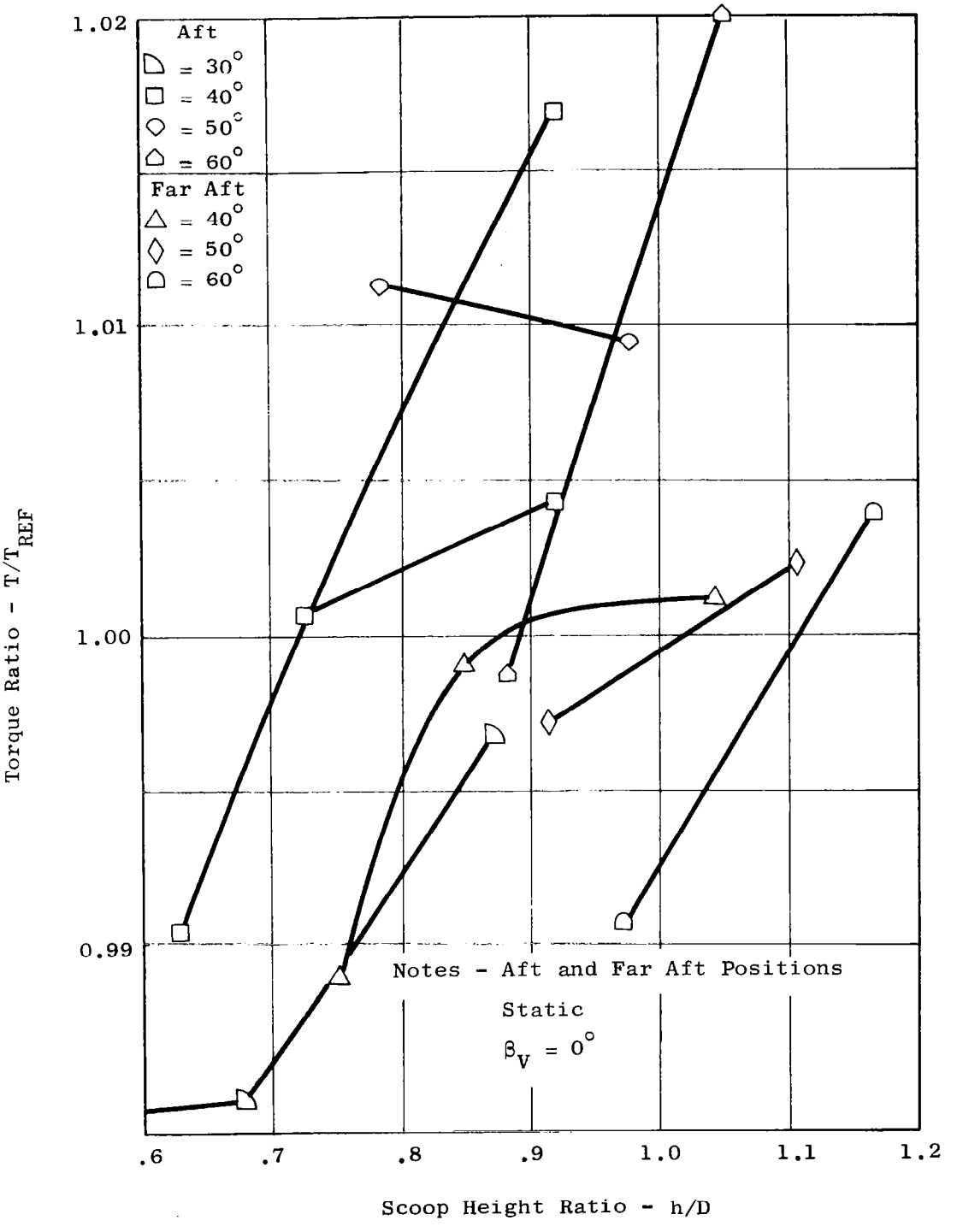

Figure 99. Basic Scoop Performance.

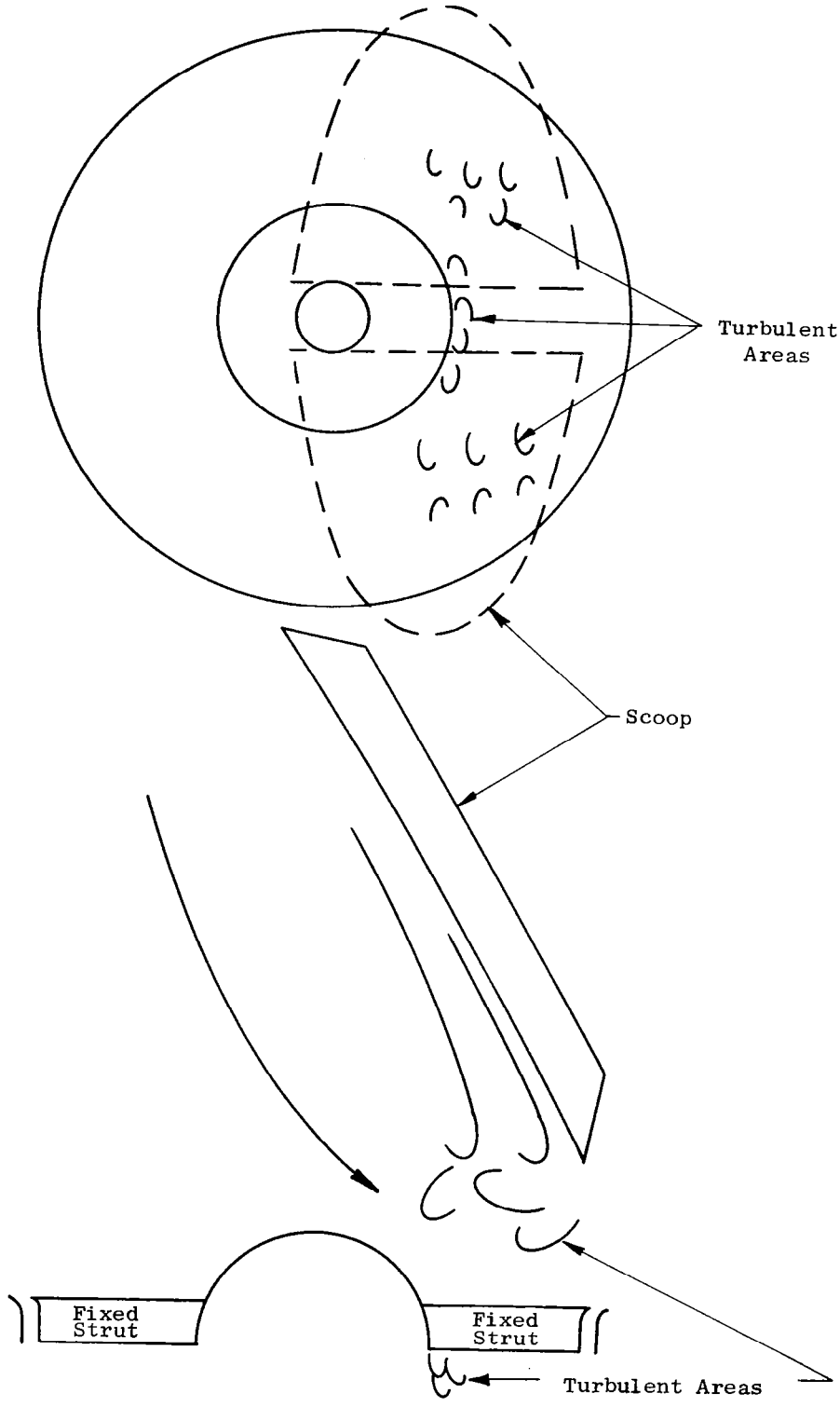

Figure 100. Turbulent Flow Areas.

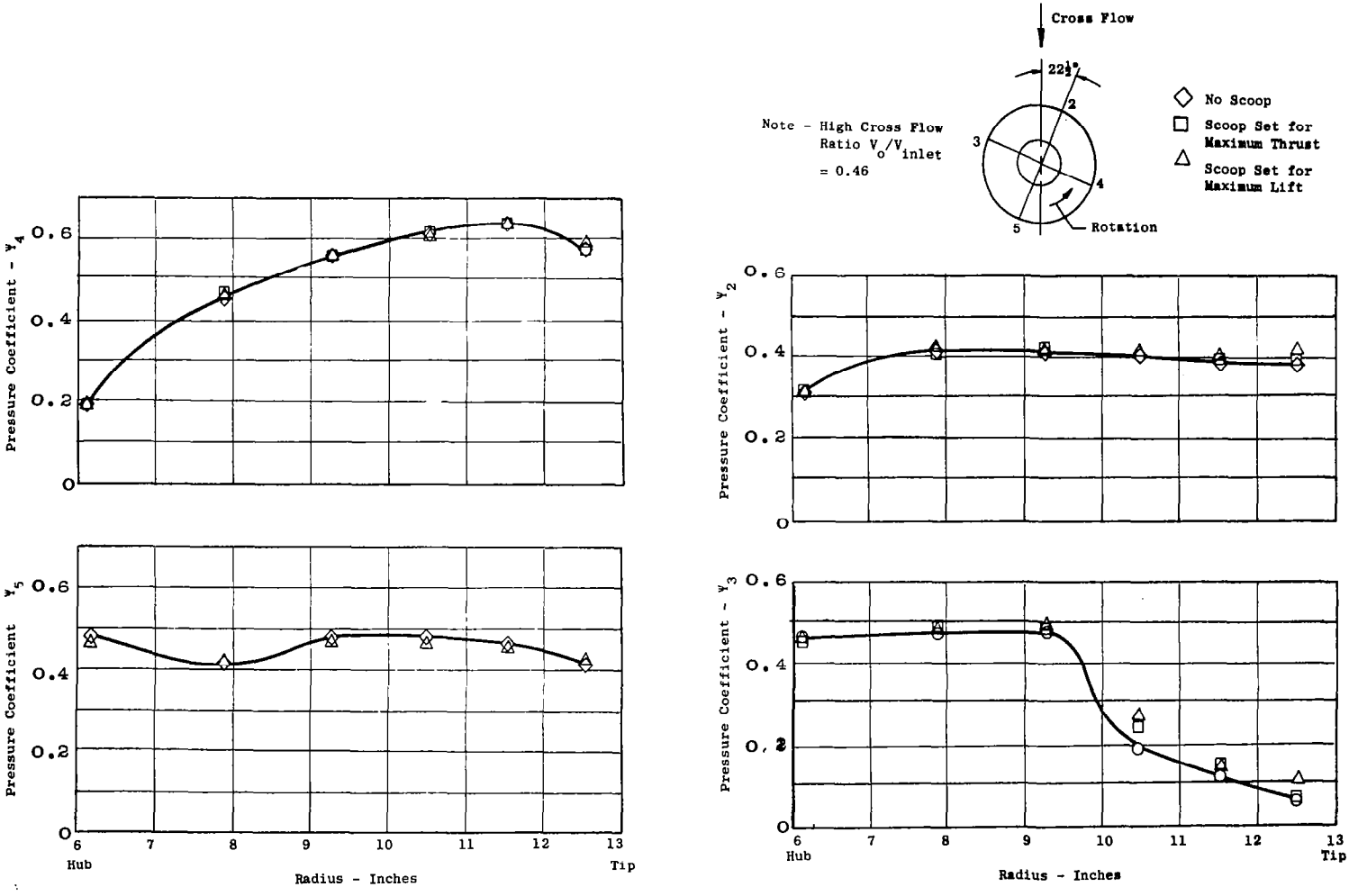

Figure 101. Rotor Discharge Pressure Coefficient Versus Radius.

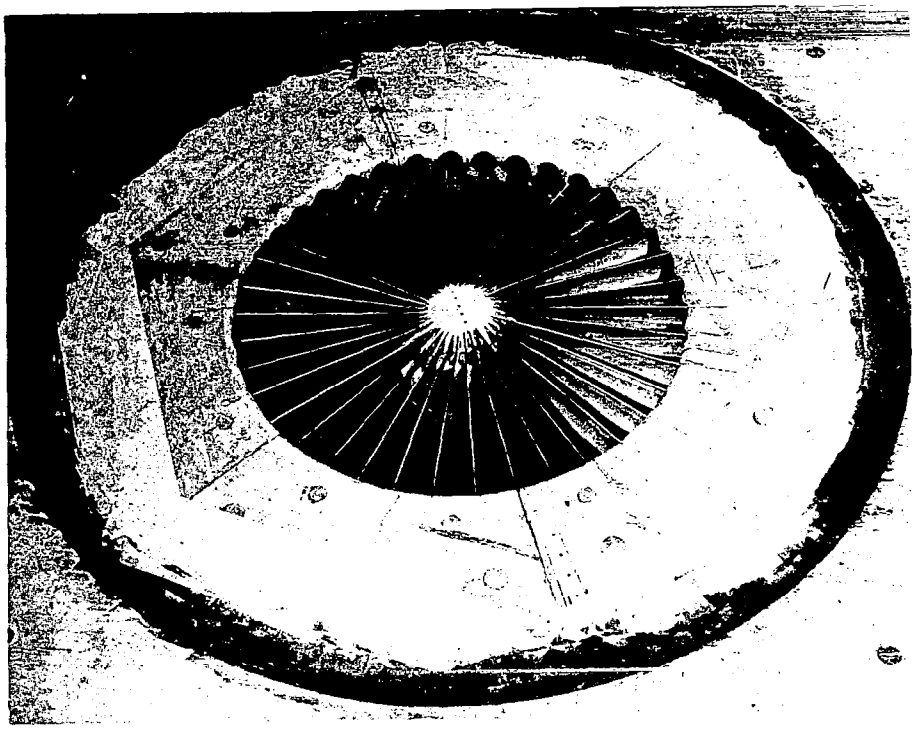

Figure 102. Inlet Suck Down Test - IGV Inlet.

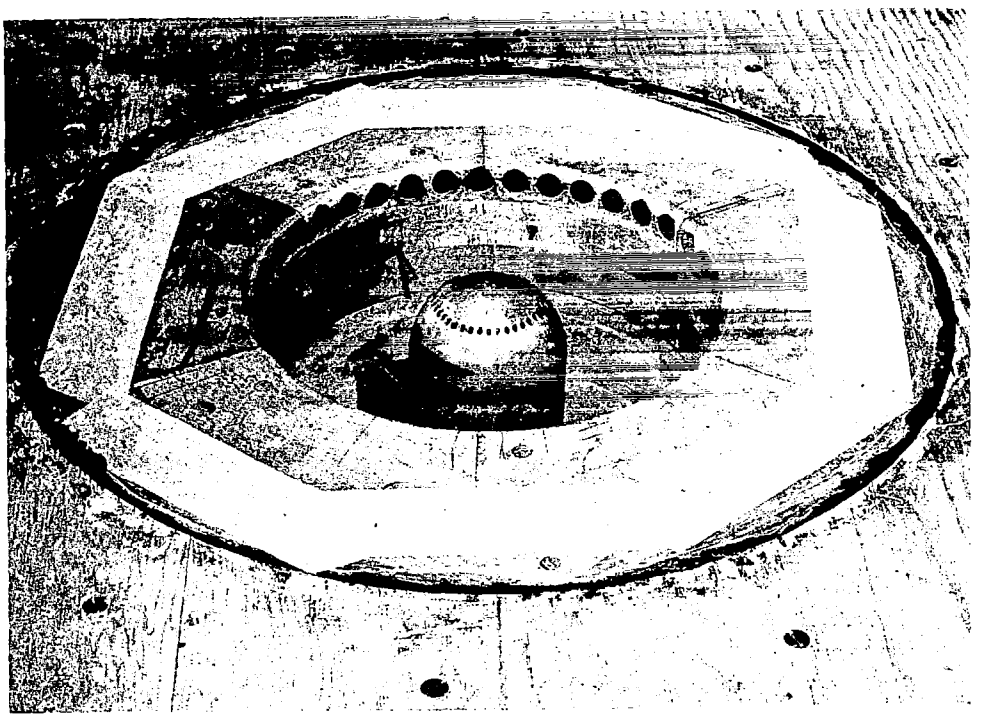

Figure 103. Inlet Suck Down Test - Simple Inlet.

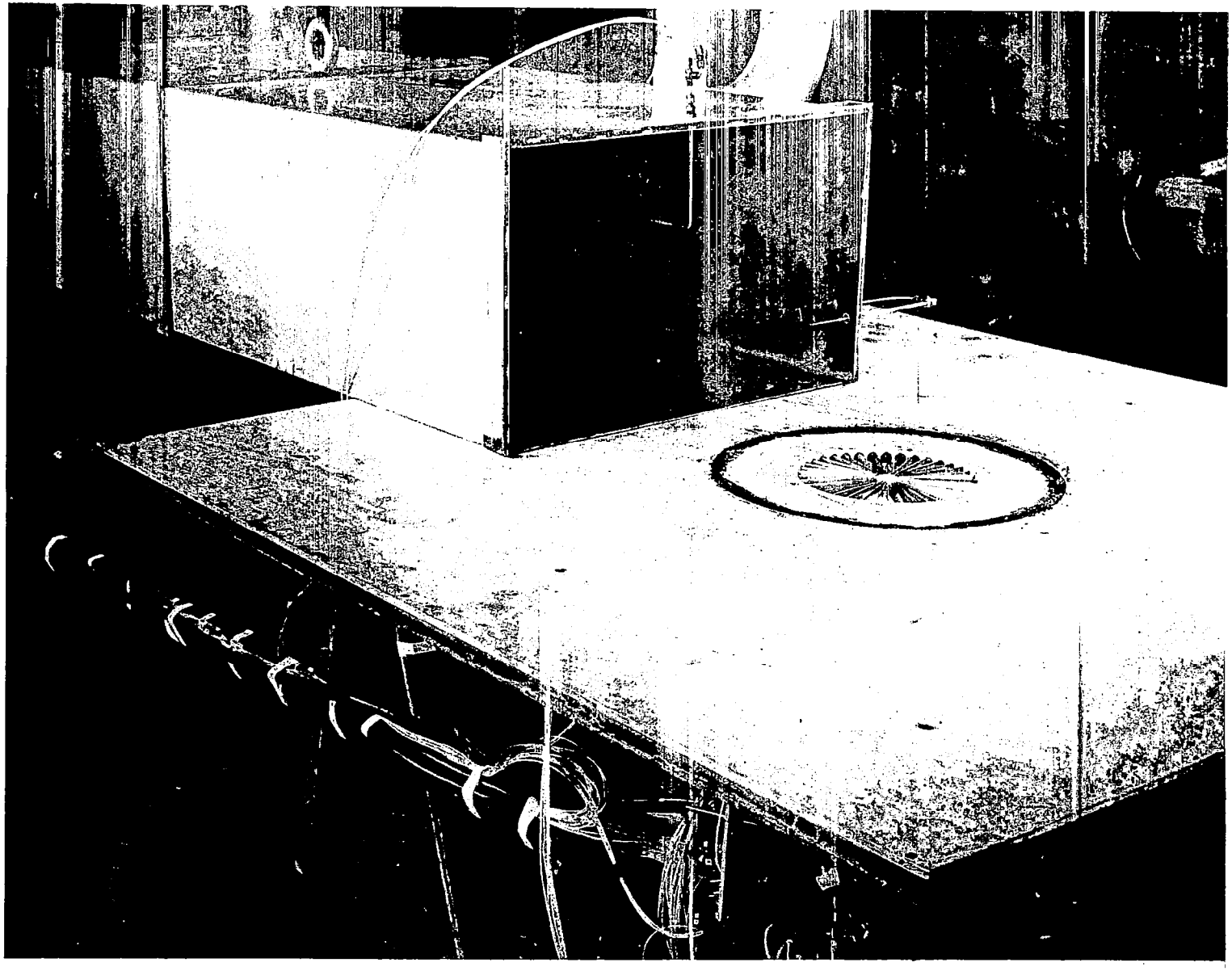

Figure 104. Inlet Suck Down Test Setup - IGV Inlet.

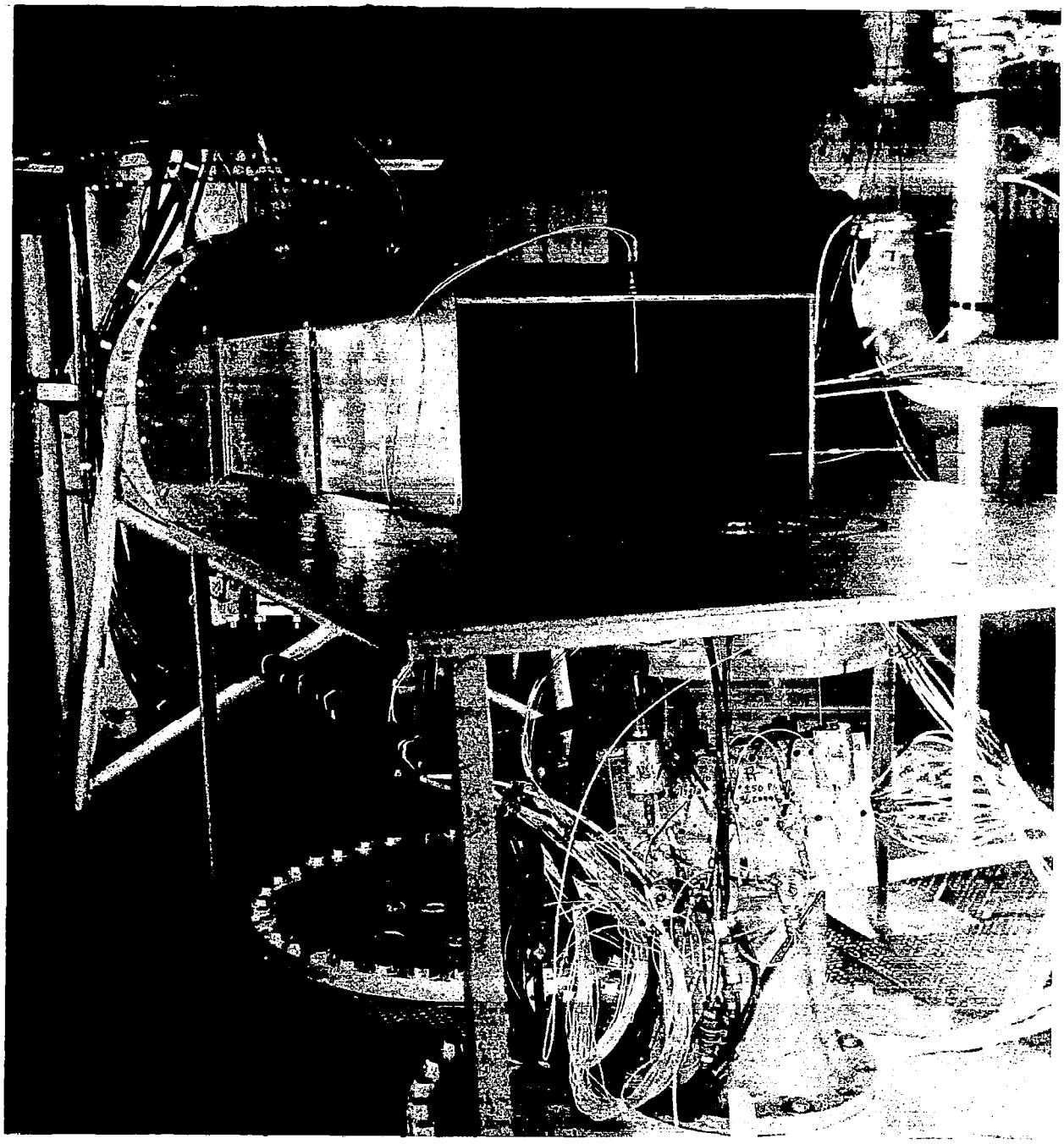

Figure 105. Inlet Suck Down Test Setup - Simple Inlet.

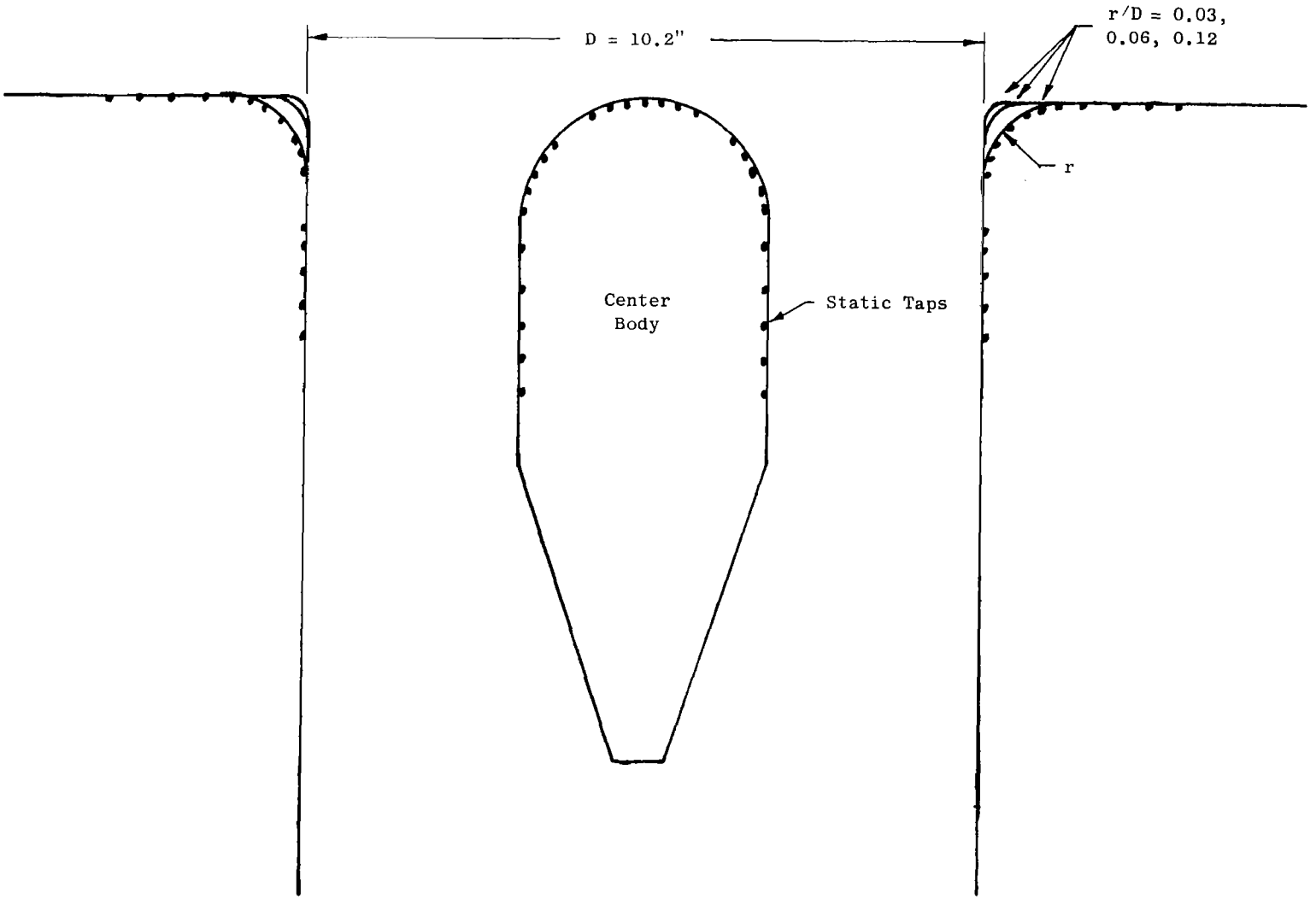

Figure 106. Static Pressure Tap Distribution.

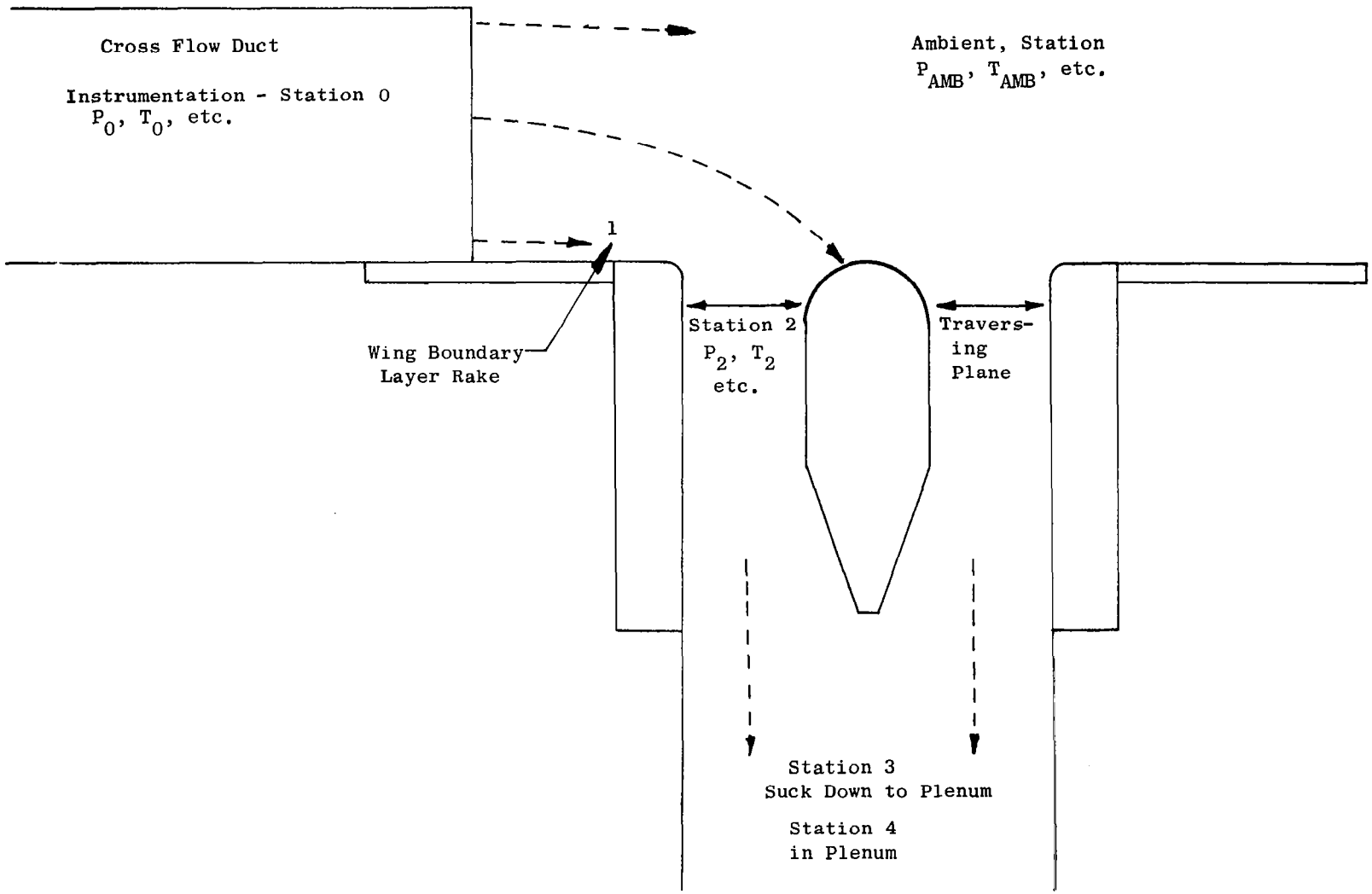

Figure 107. Measurement Station Designations.

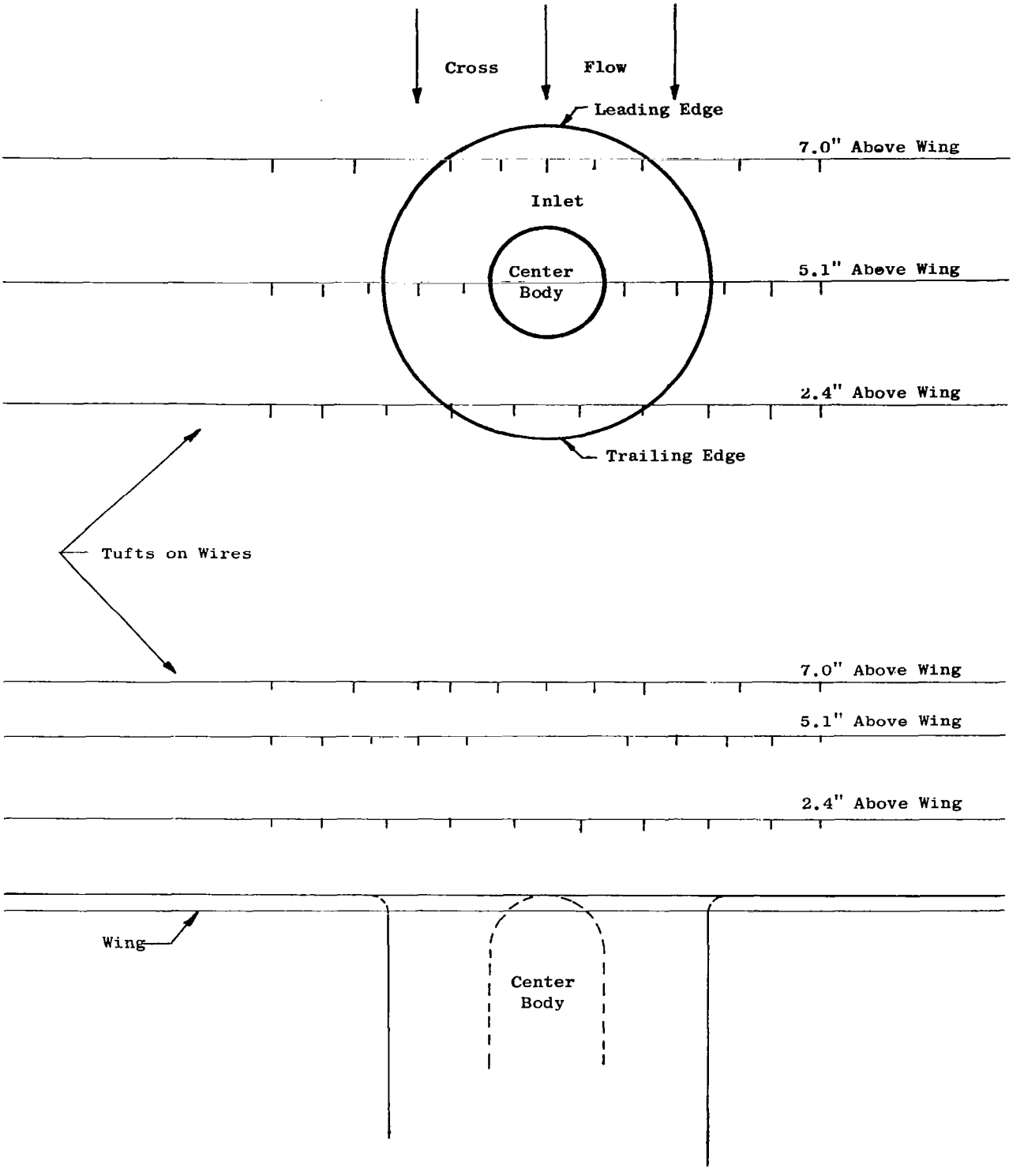

Figure 108. Tuft Locations.

Notes: Lines of Constant P_2/P_0

V_2 = 599.4 V_0 = 270 ft/sec

r/D = 0.12

Without IGV

⊙ Data Point

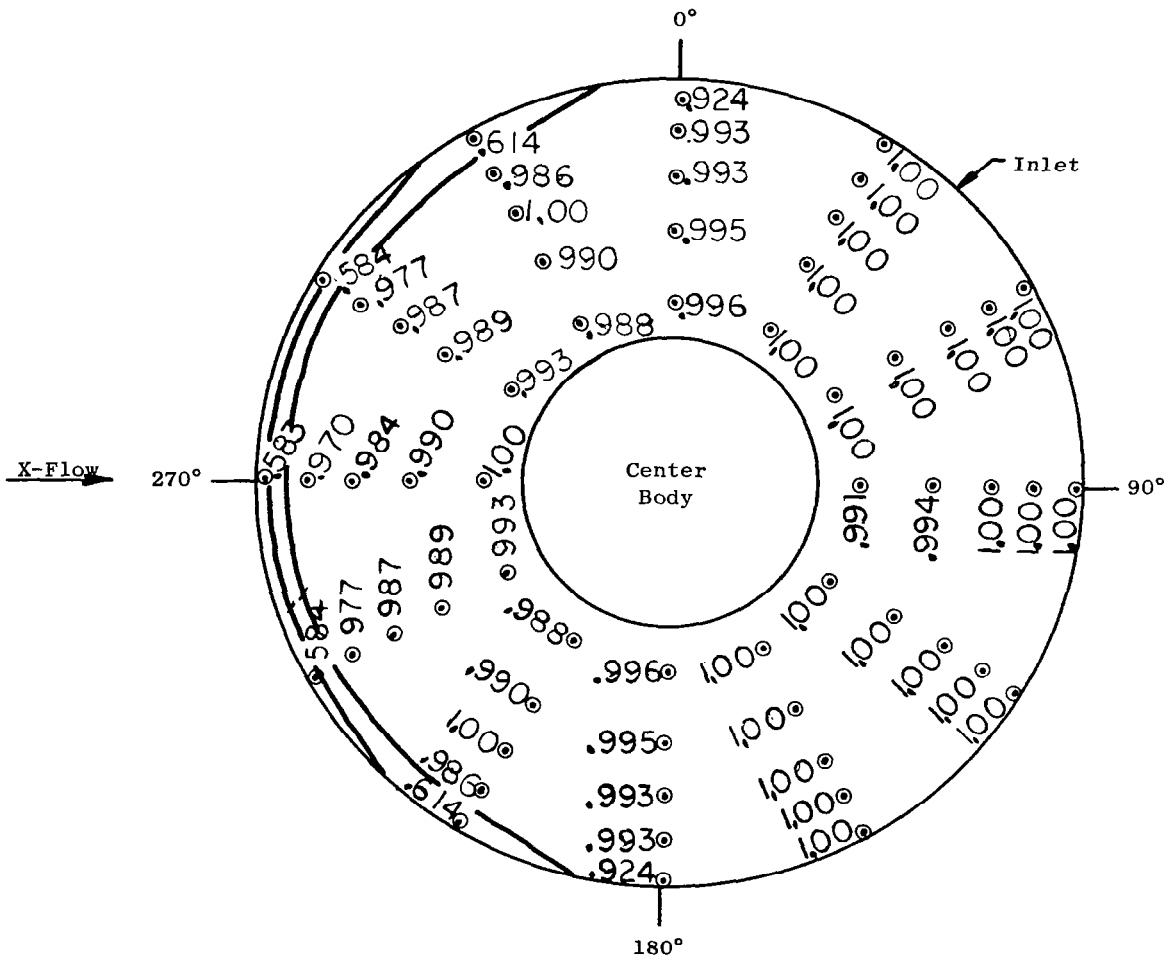

Figure 109. Total Pressure Recovery Profiles.

Notes: Lines of Constant P_2/P_0

V_2 = 599.4 V_0 = 270 ft/sec

r/D = 0.06

Without IGV

⊙ Data Point

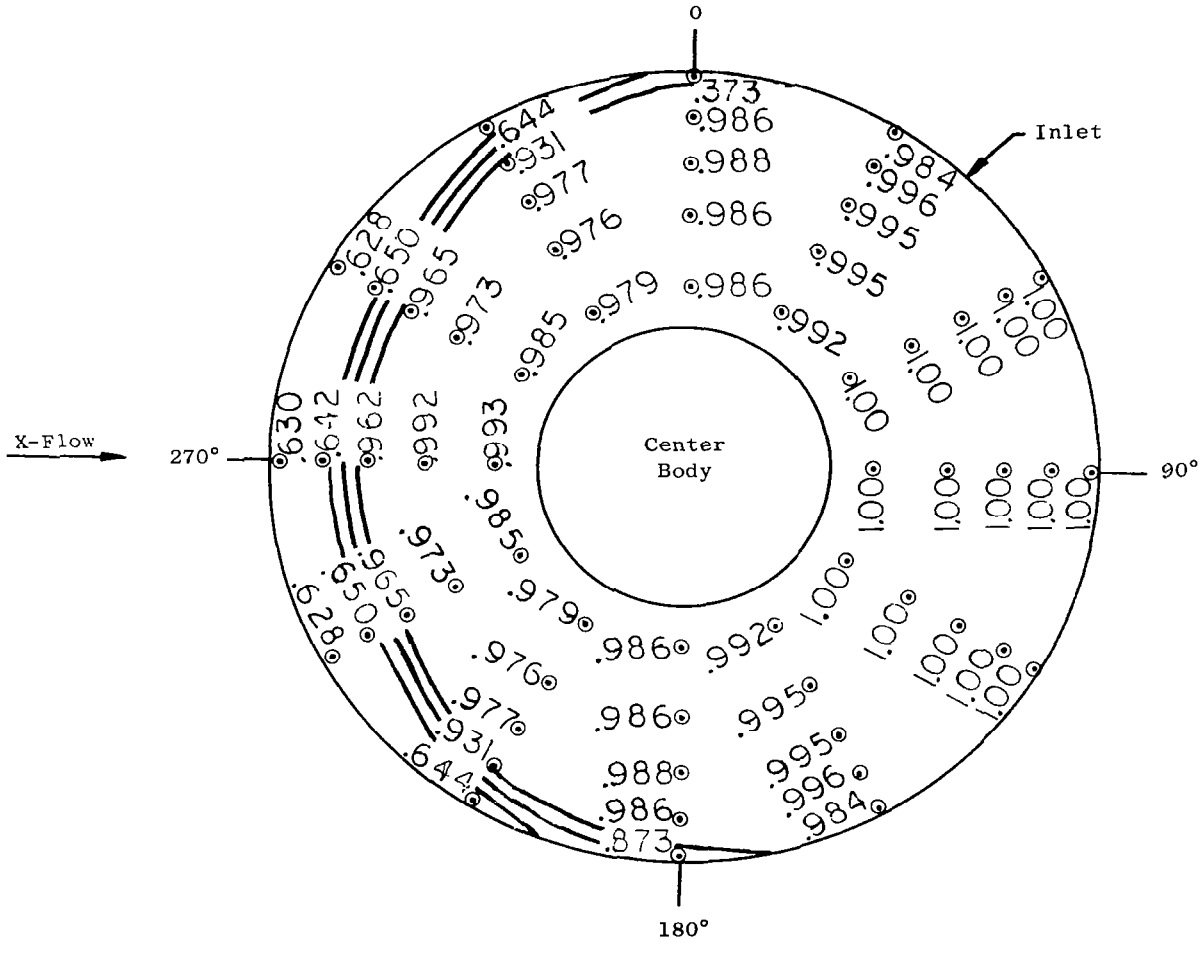

Figure 110. Total Pressure Recovery Profiles.

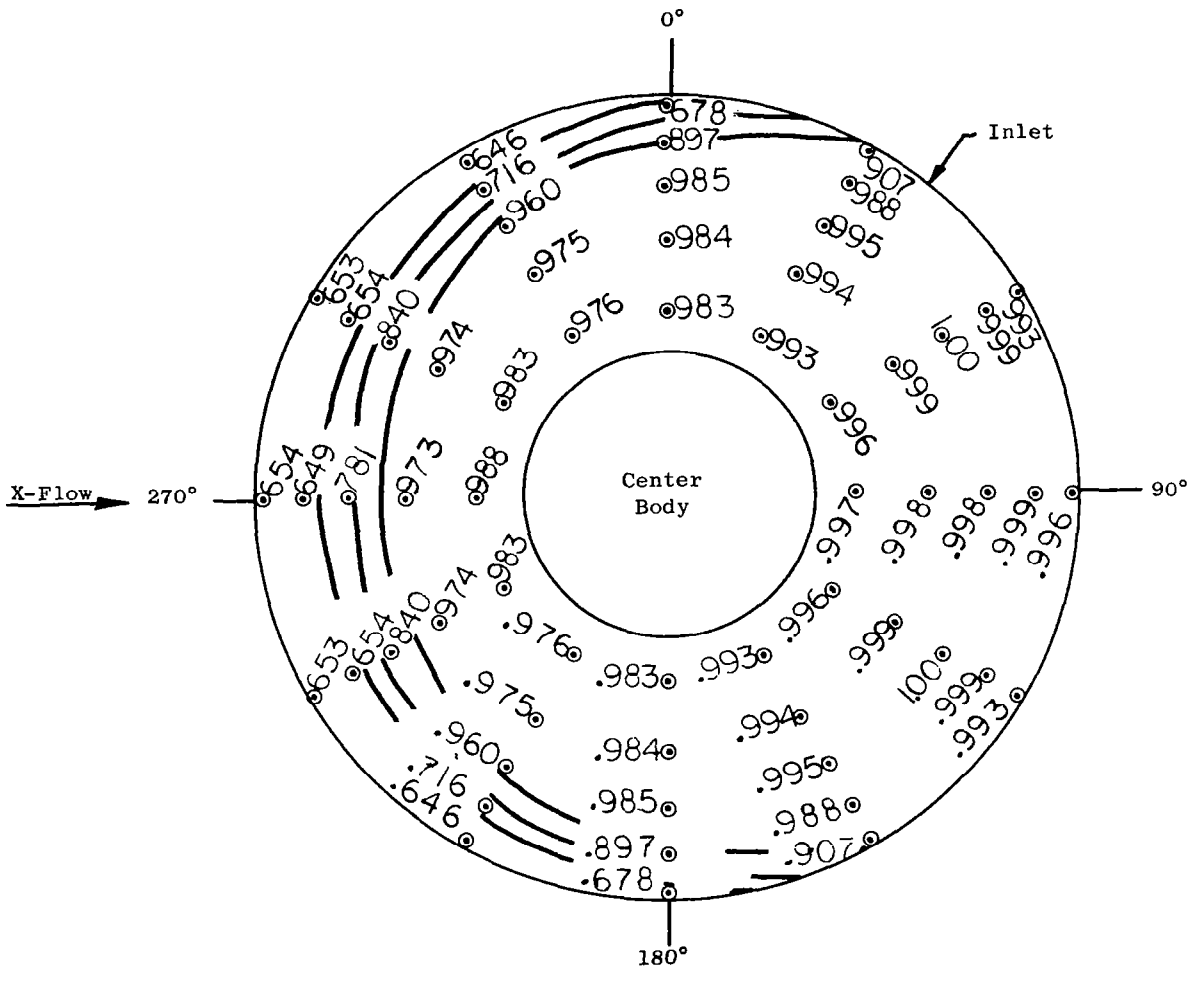

Figure 111. Total Pressure Recovery Profiles.

Notes: Lines of Constant P_2/P_0

V_2 = 599.4 V_0 = 270 ft/sec

r/D = 0.12

With IGV

⊙ Data Point

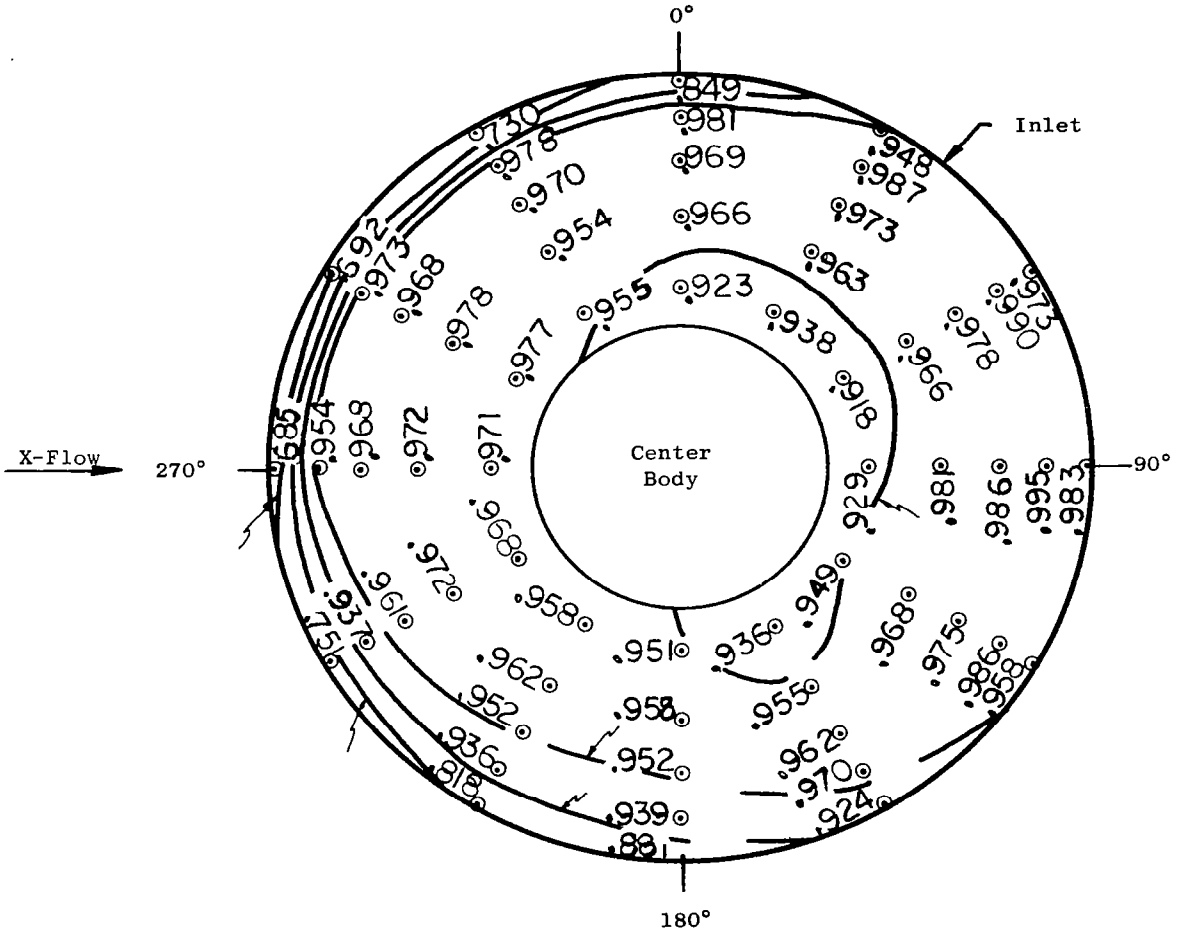

Figure 112. Total Pressure Recovery Profiles.

Notes: Lines of Constant P_2/P_0

V_2 = 599.4 V_0 = 270 ft/sec

r/D = 0.06

With IGV

⊙ Data Point

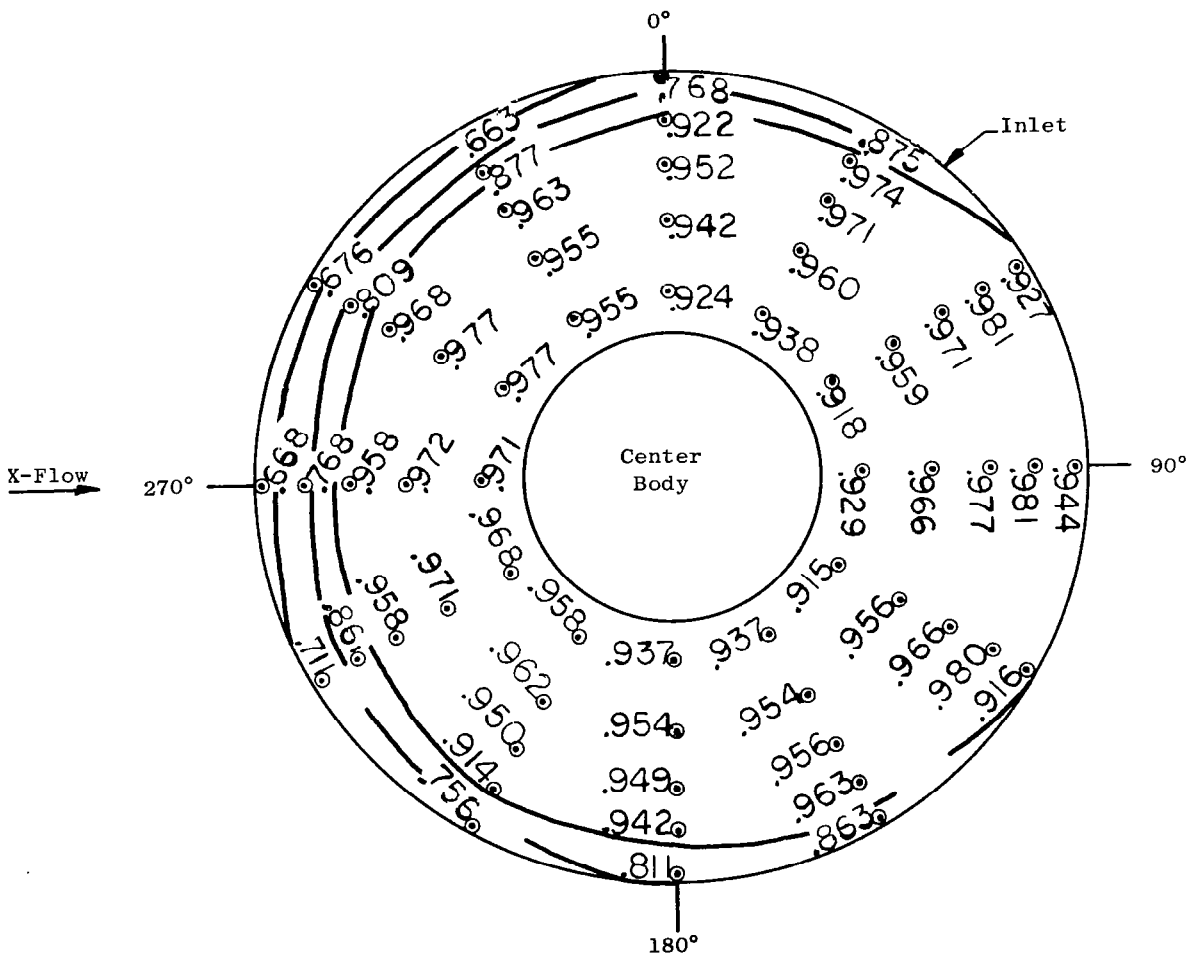

Figure 113. Total Pressure Recovery Profiles.

Notes: Lines of Constant P_2/P_0

V_2 = 599.4 V_0 = 270 ft/sec

r/D = 0.03

With IGV

⊙ Data Point

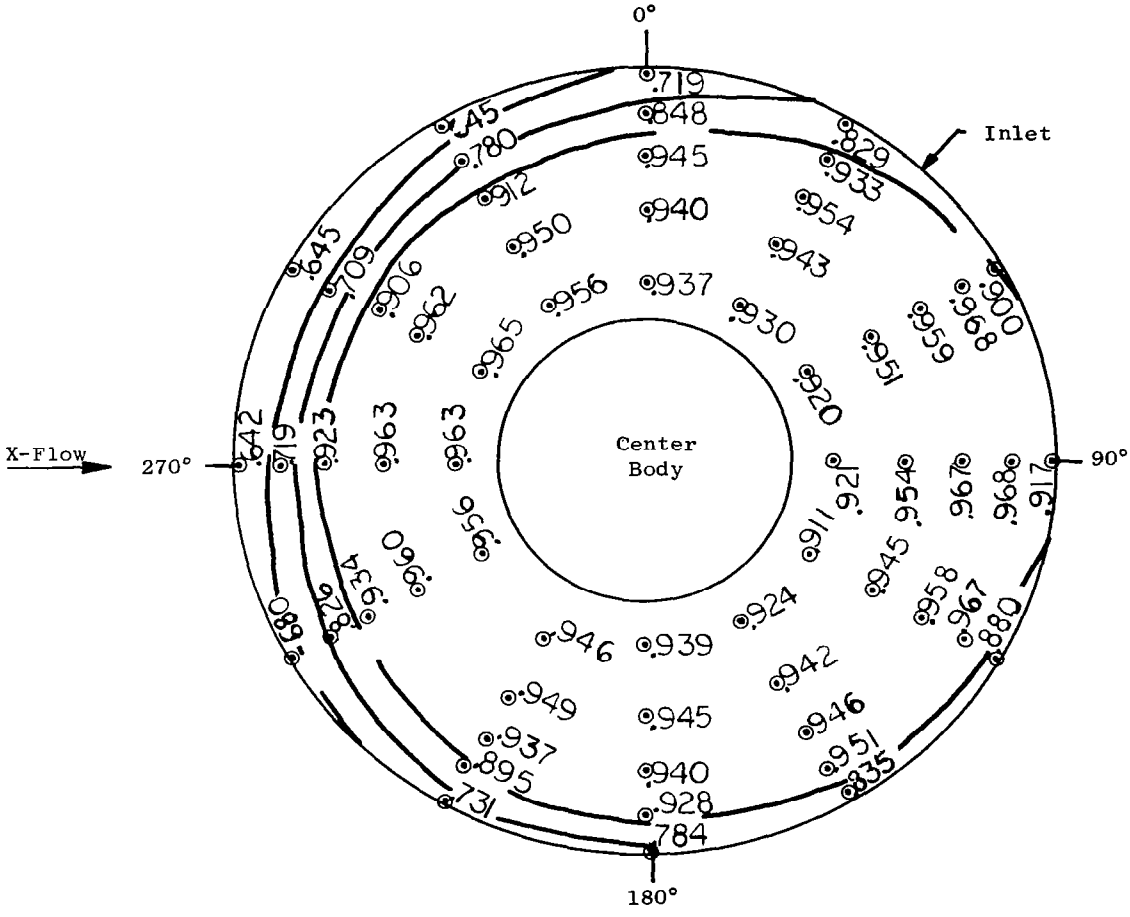

Figure 114. Total Pressure Recovery Profiles.

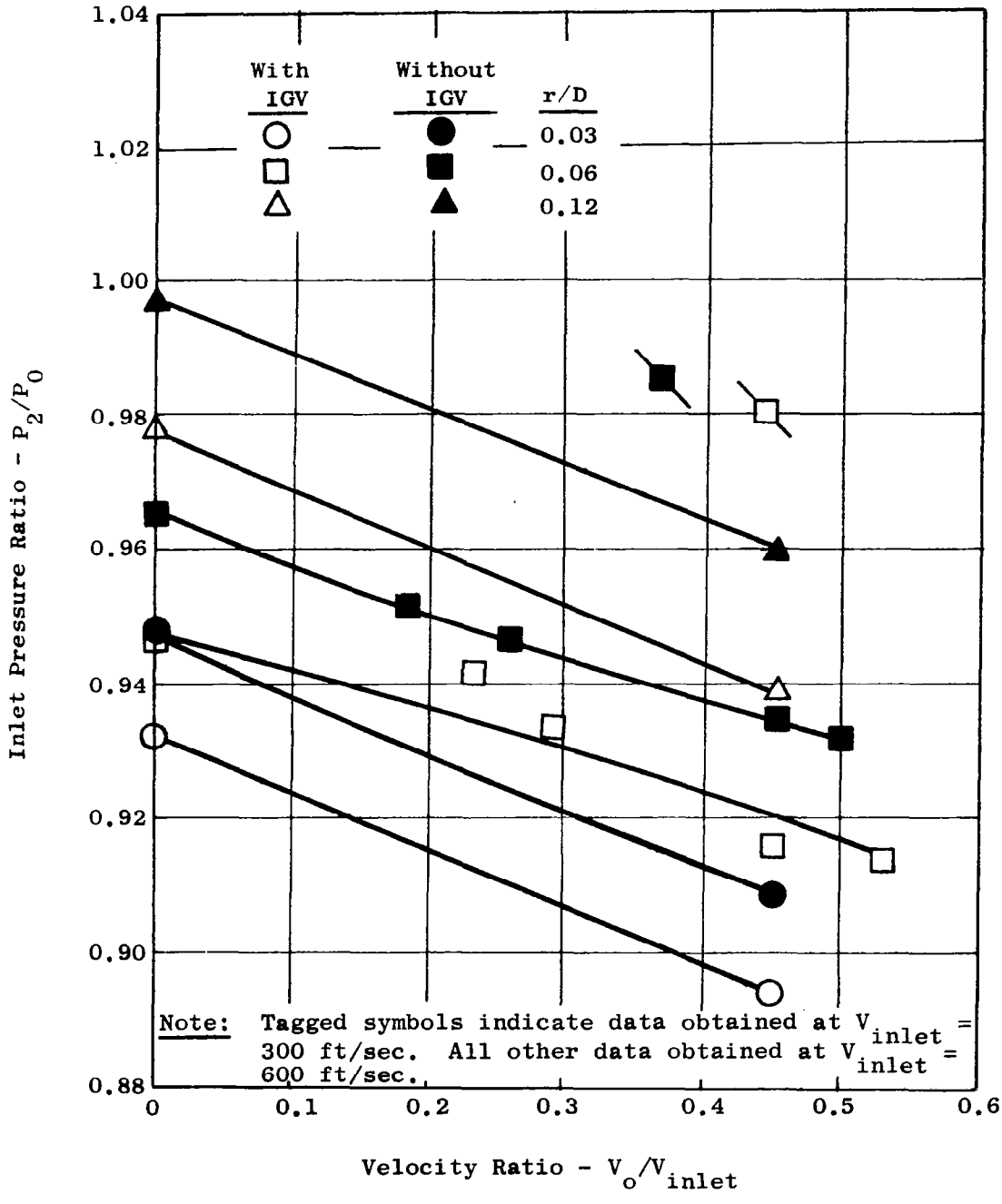

Figure 115. Inlet Total Pressure Recovery Versus Velocity Ratio.

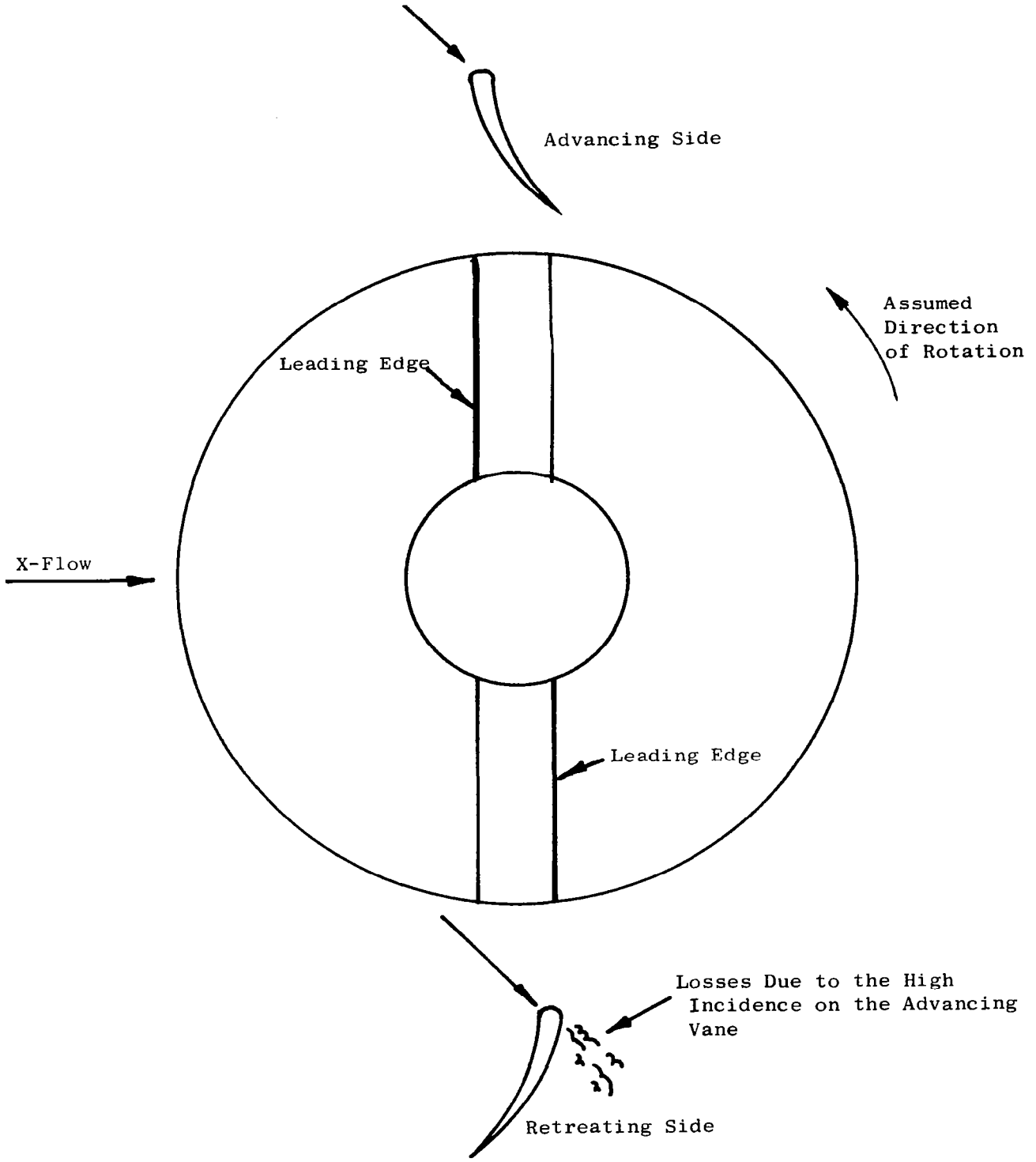

Figure 116. Advancing and Retreating Side Relationship.

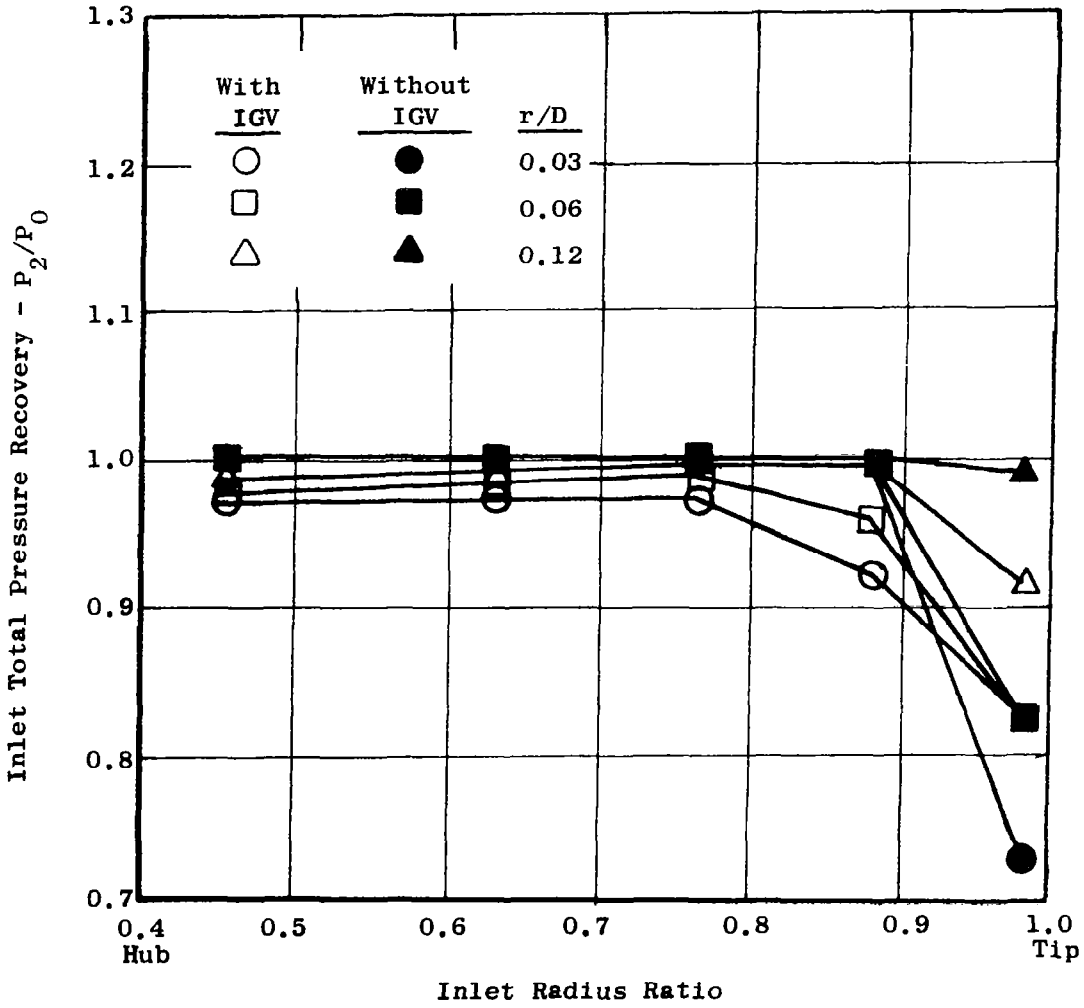

Figure 117. Radial Total Pressure Recovery Without Cross Flow.

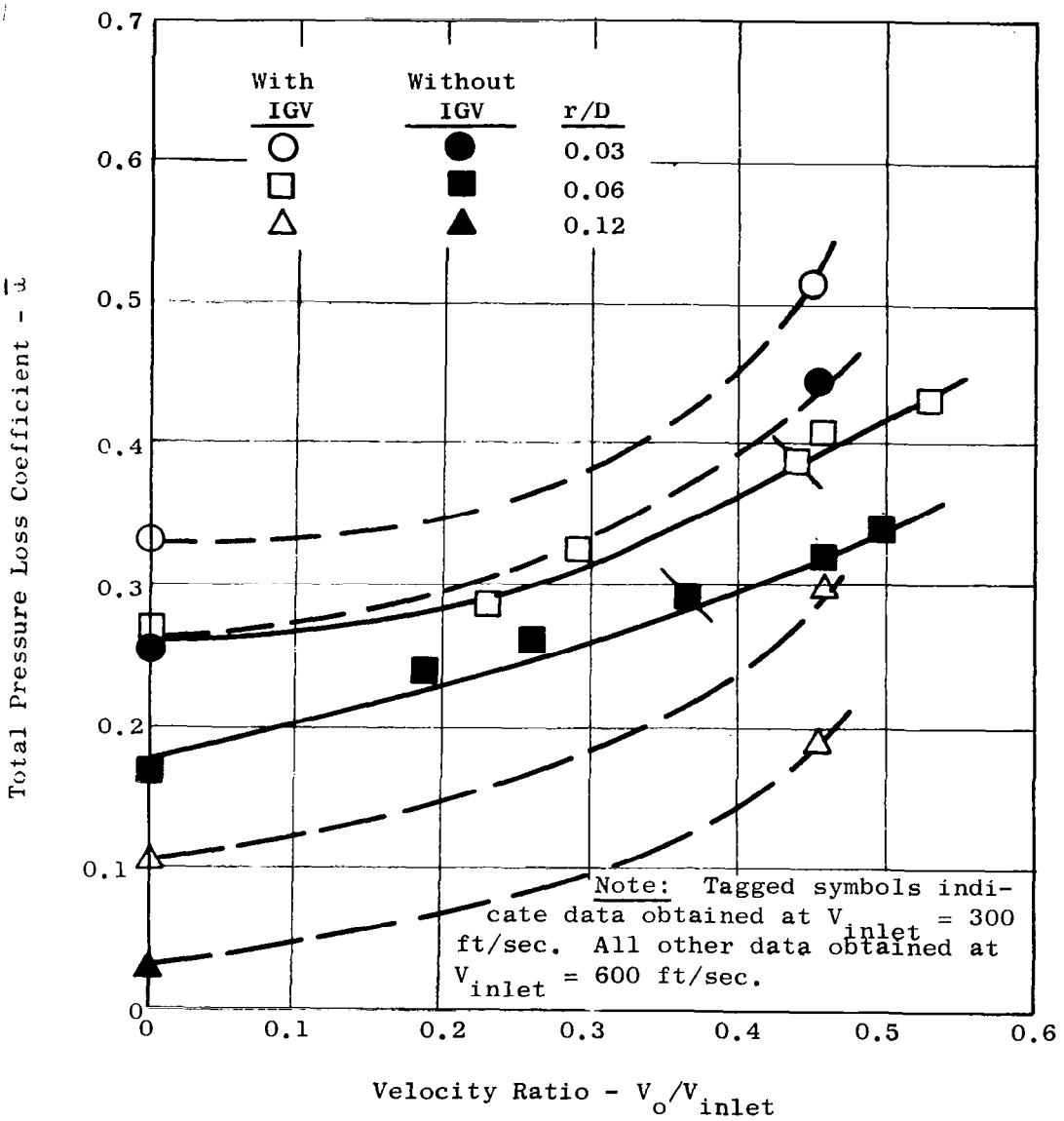

Figure 118. Inlet Total Pressure Loss Versus Velocity Ratio.

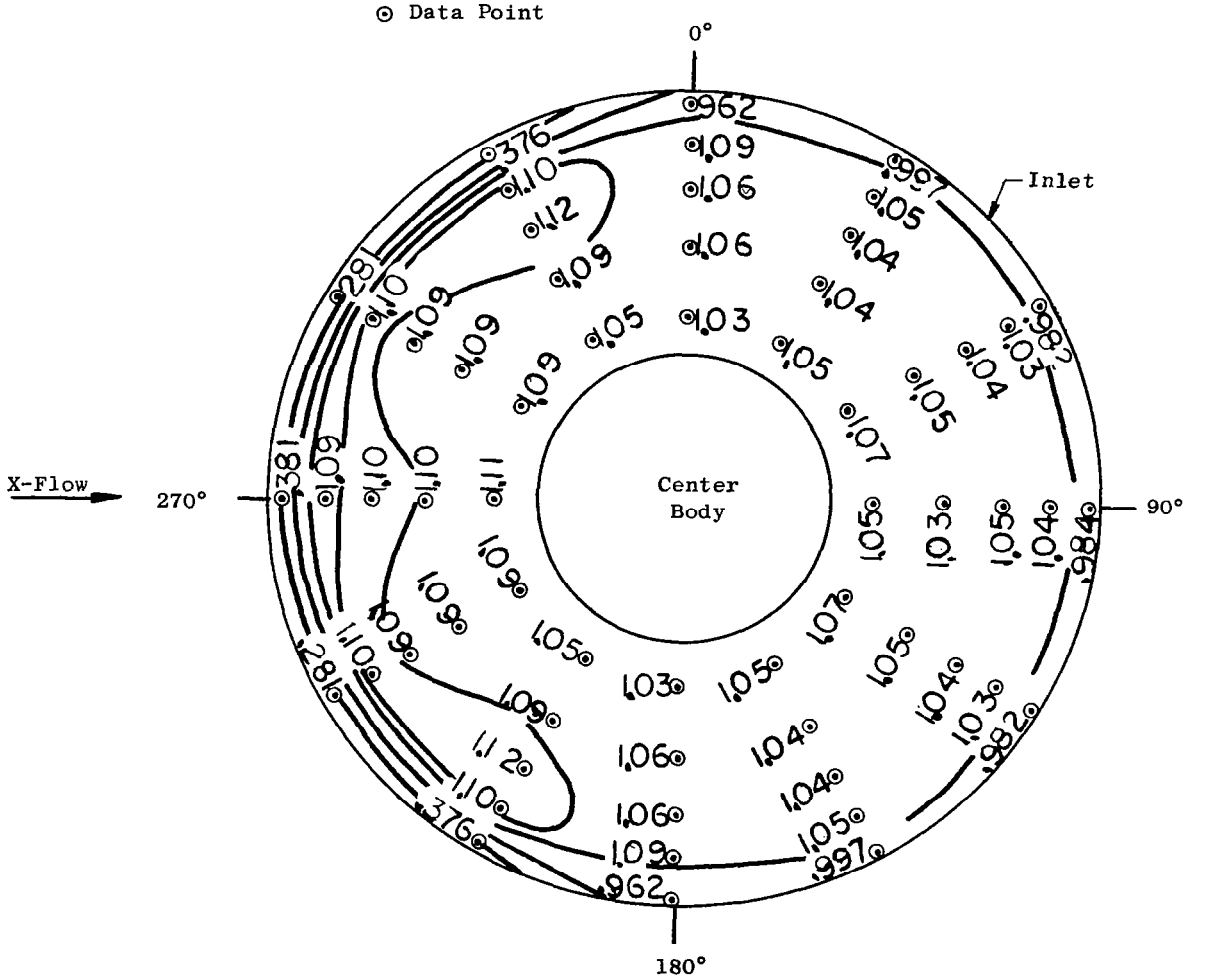

Figure 119. Weight Flow Profiles.

Notes: Lines of Constant $W_A/W_{A_{AVG}}$

V_2 = 599.4 V_0 = 270 ft/sec

r/D = 0.06

Without IGV

$W_{A_{AVG}}$ = 18.75 lb/sec

⊙ Data Point

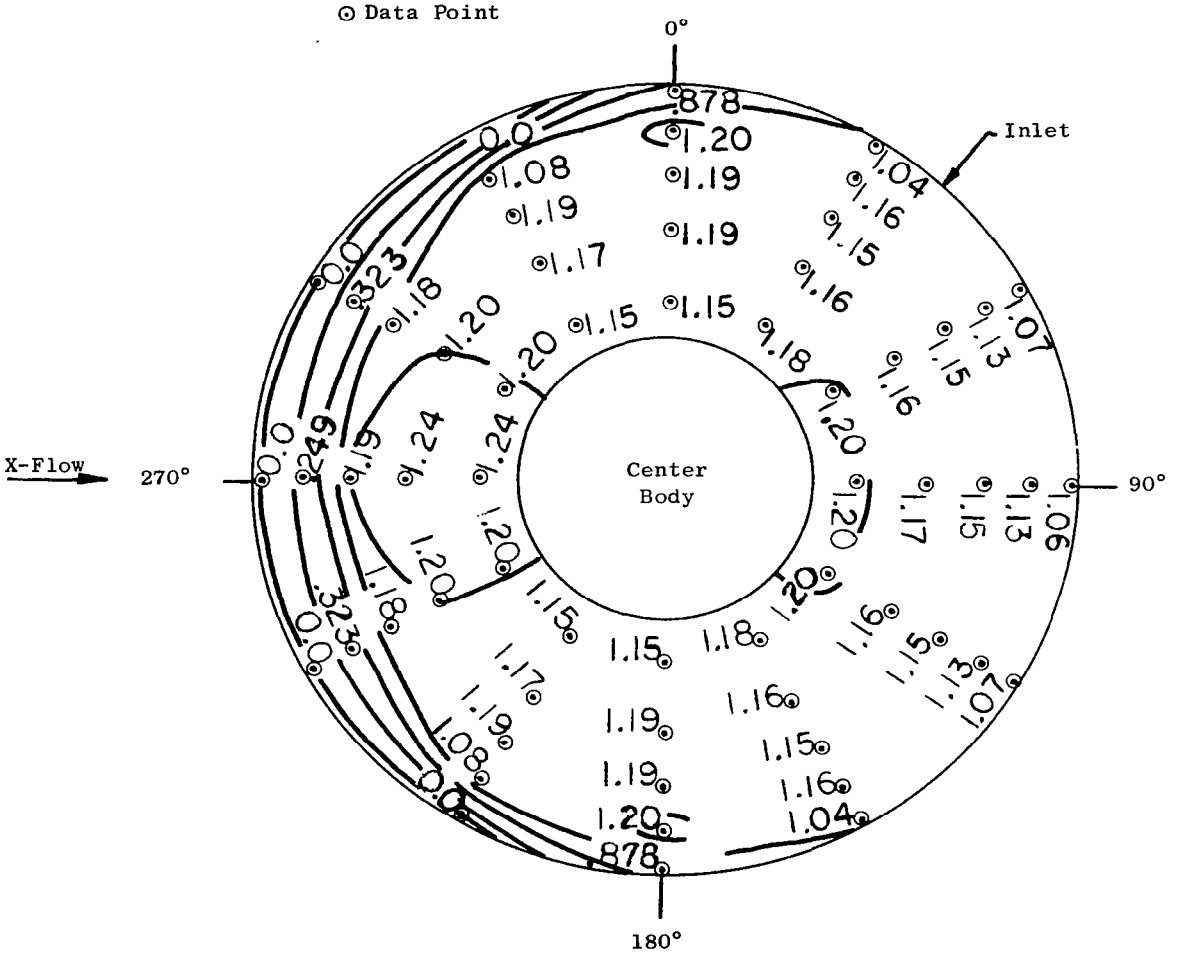

Figure 120. Weight Flow Profiles.

Notes: Lines of Constant $W_A/W_{A_{AVG}}$

V_2 = 599.4 V_0 = 270 ft/sec

r/D = 0.03

Without IGV

$W_{A_{AVG}}$ = 18.75 lb/sec

⊙ Data Point

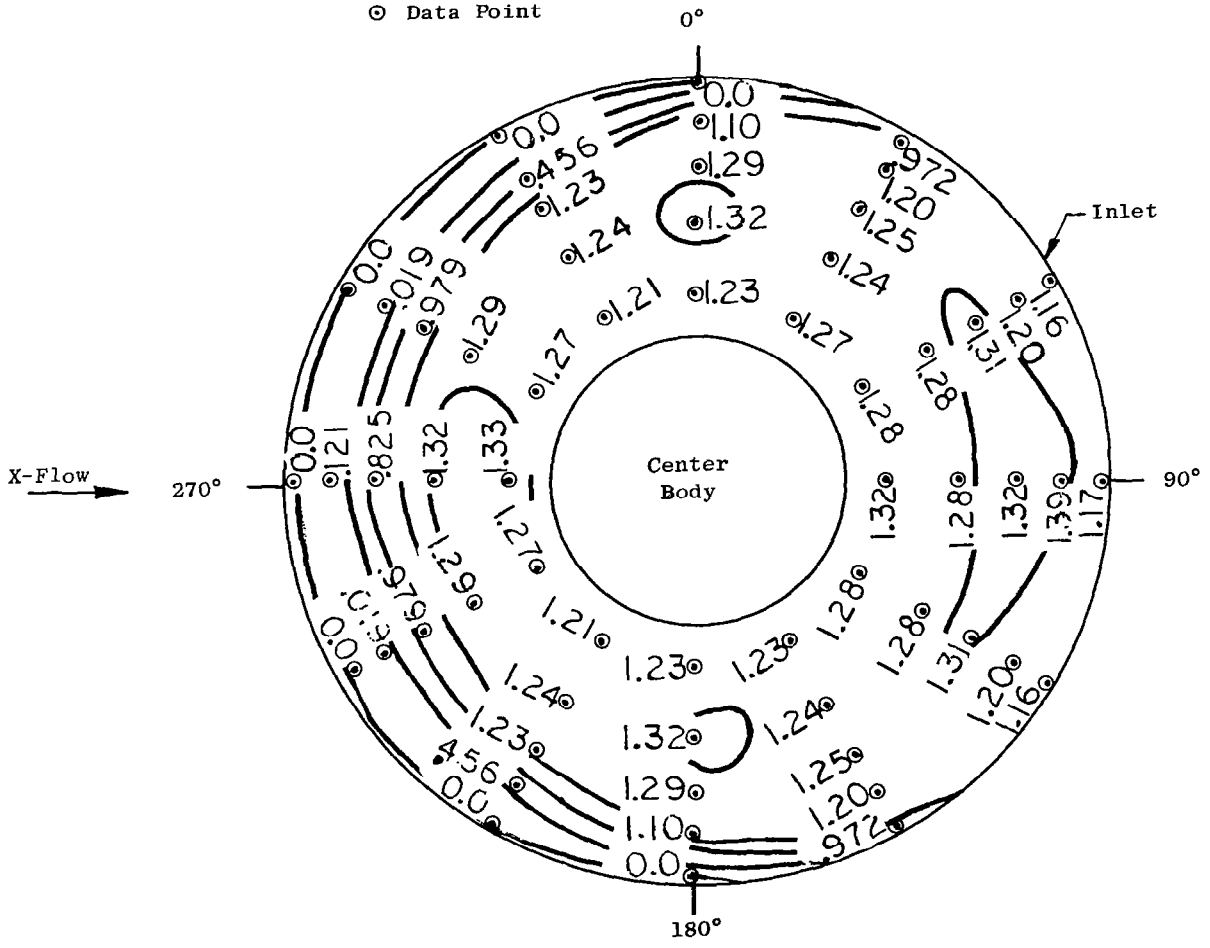

Figure 121. Weight Flow Profiles

Notes: Lines of Constant $W_A/W_{A_{AVG}}$

V_2 = 599.4 V_0 = 270 ft/sec

r/D = 0.12

With IGV

$W_{A_{AVG}}$ = 18.75 lb/sec

⊙ Data Point

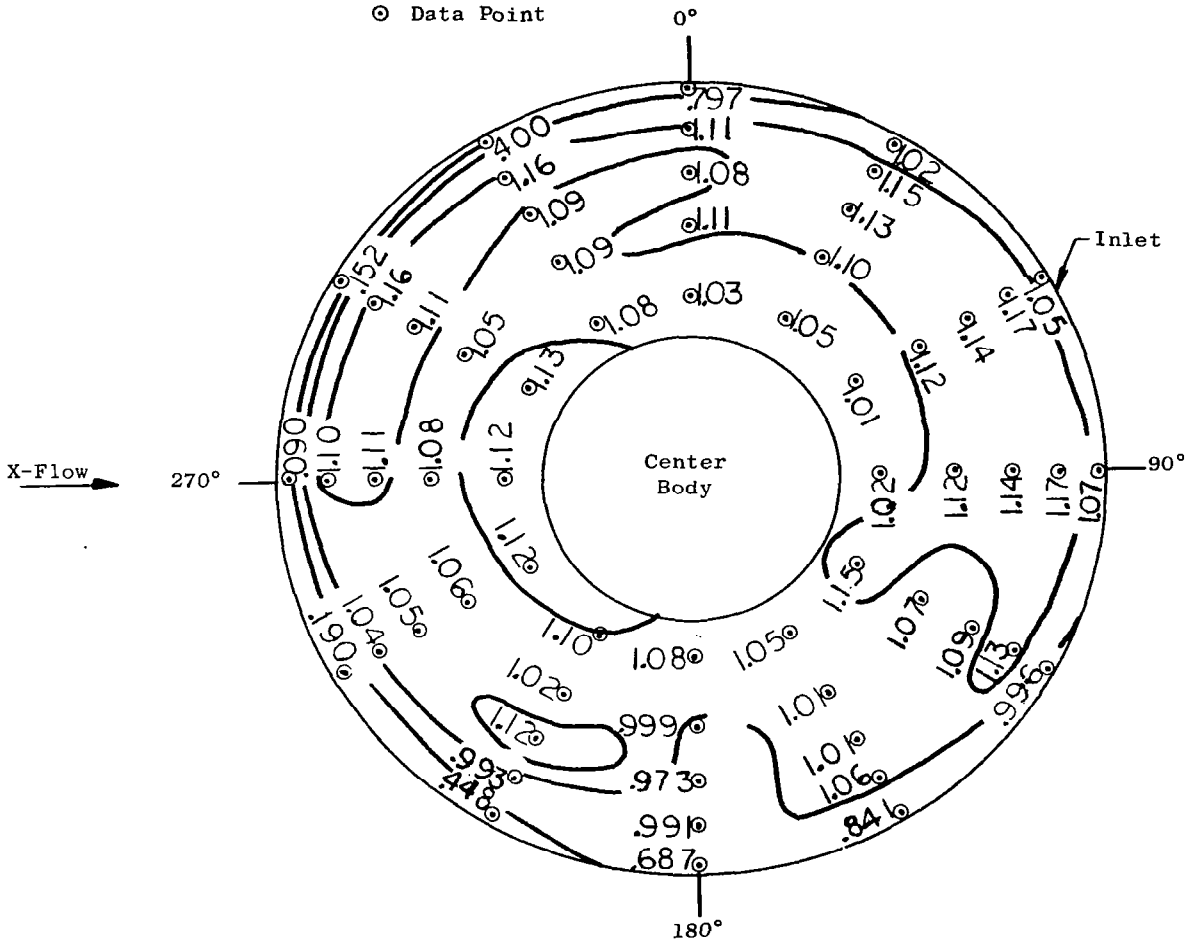

Figure 122. Weight Flow Profiles.

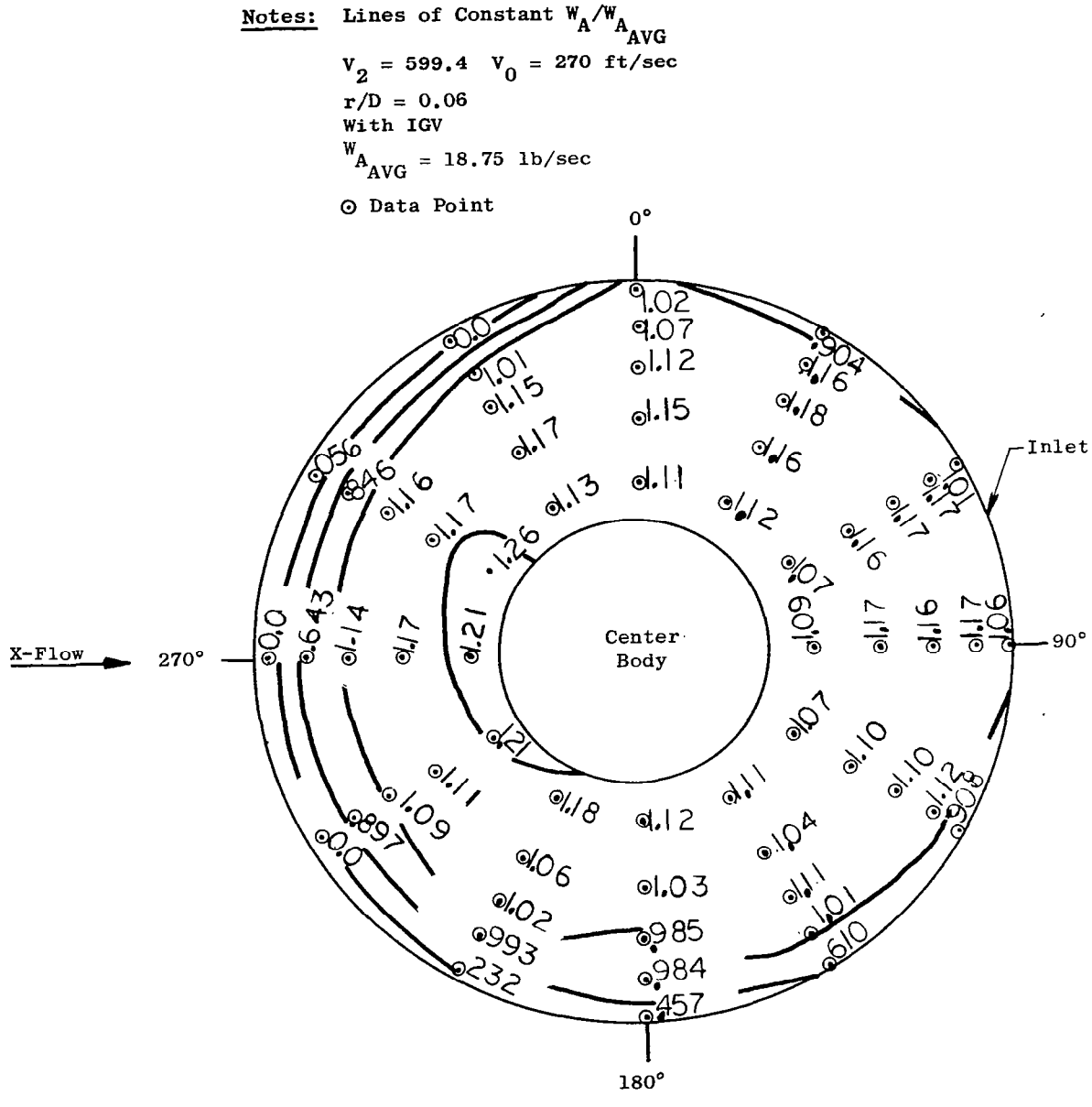

Figure 123. Weight Flow Profiles.

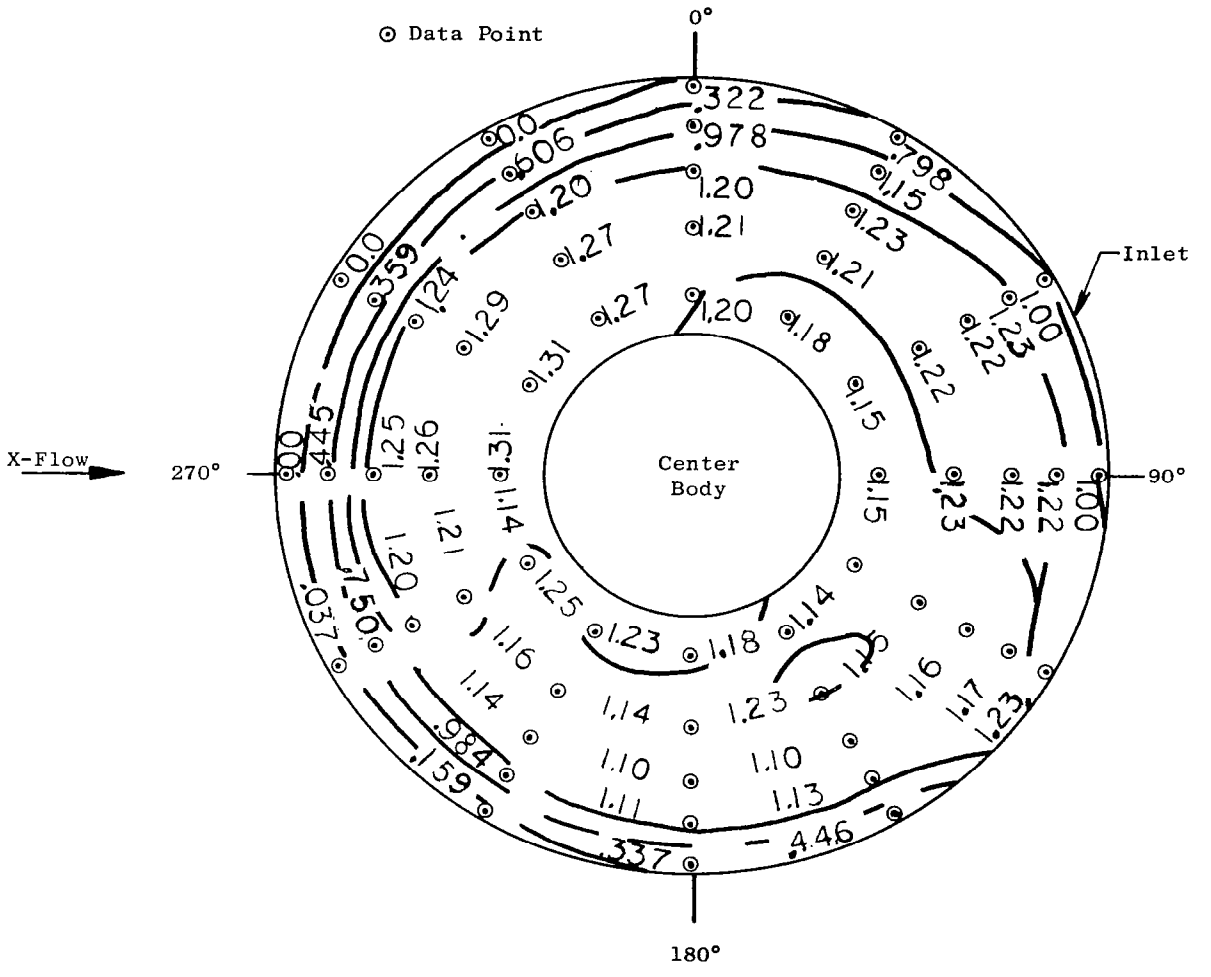

Figure 124. Weight Flow Profiles.

Notes: Lines of Constant M_2 (Axial Component)

V_2 = 599.4 V_0 = 270 ft/sec

r/D = 0.12

Without IGV

⊙ Data Point

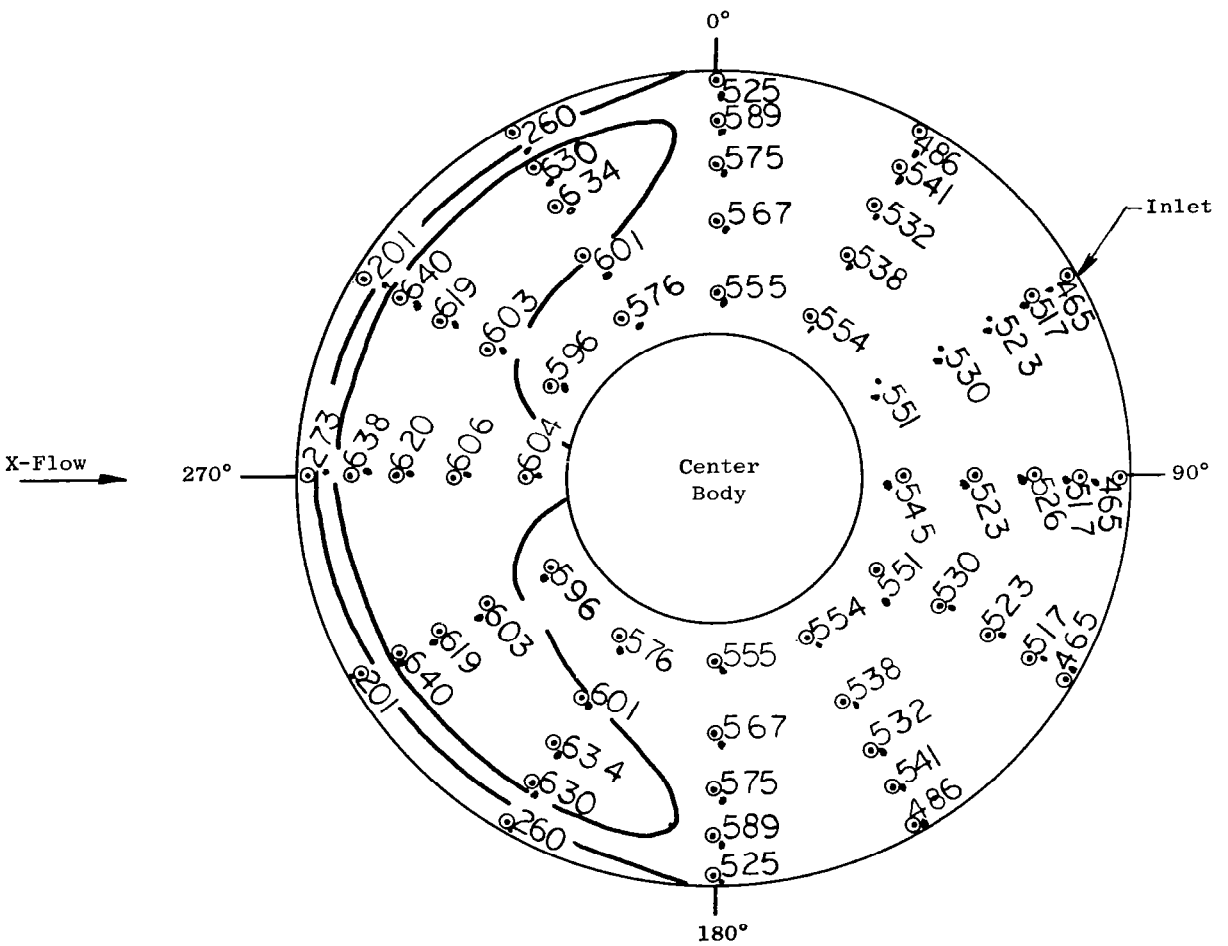

Figure 125. Axial Mach Number Profiles.

Notes: Lines of Constant M_2 (Axial Component)

V_2 = 599.4 V_0 = 270 ft/sec

r/D = 0.06

Without IGV

⊙ Data Point

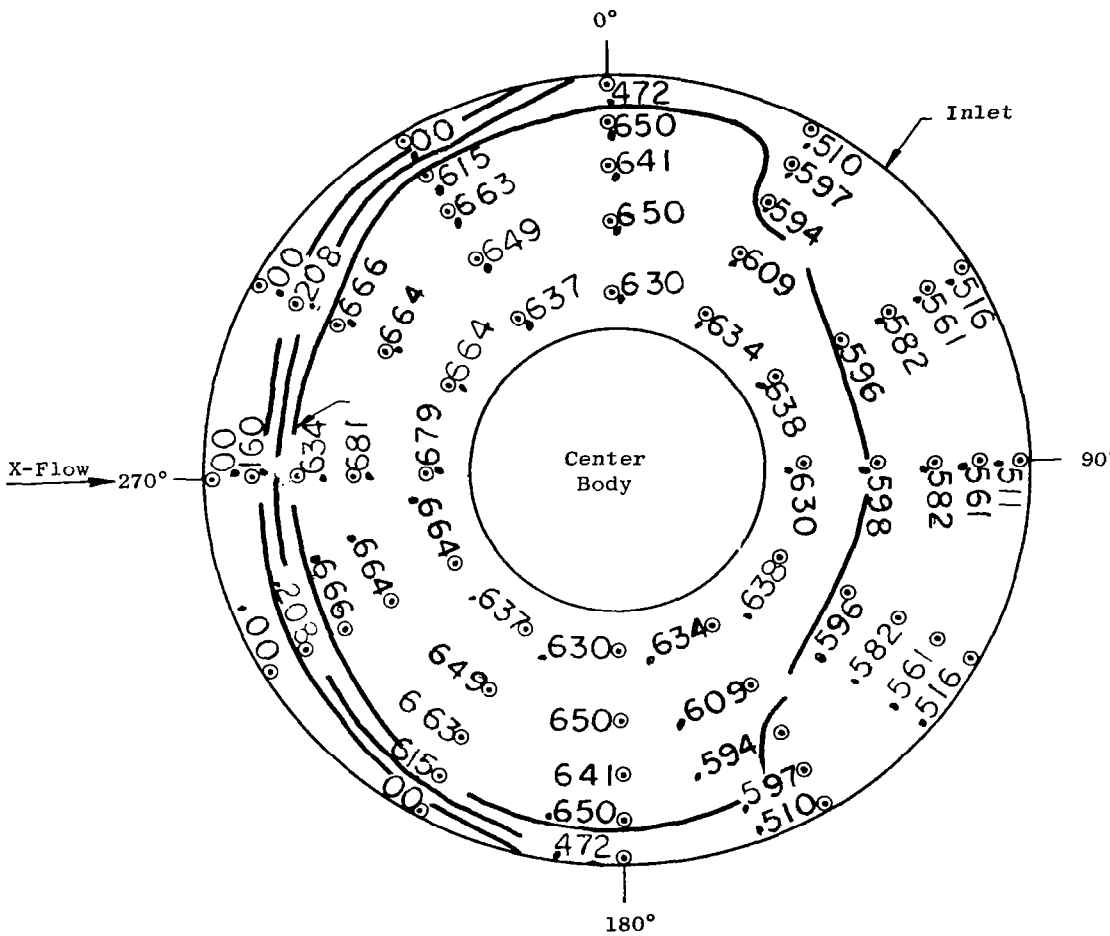

Figure 126. Axial Mach Number Profiles.

Notes: Lines of Constant M_2 (Axial Component)

V_2= 599.4 V_0 = 270 ft/sec

r/D = 0.03

Without IGV

⊙ Data Point

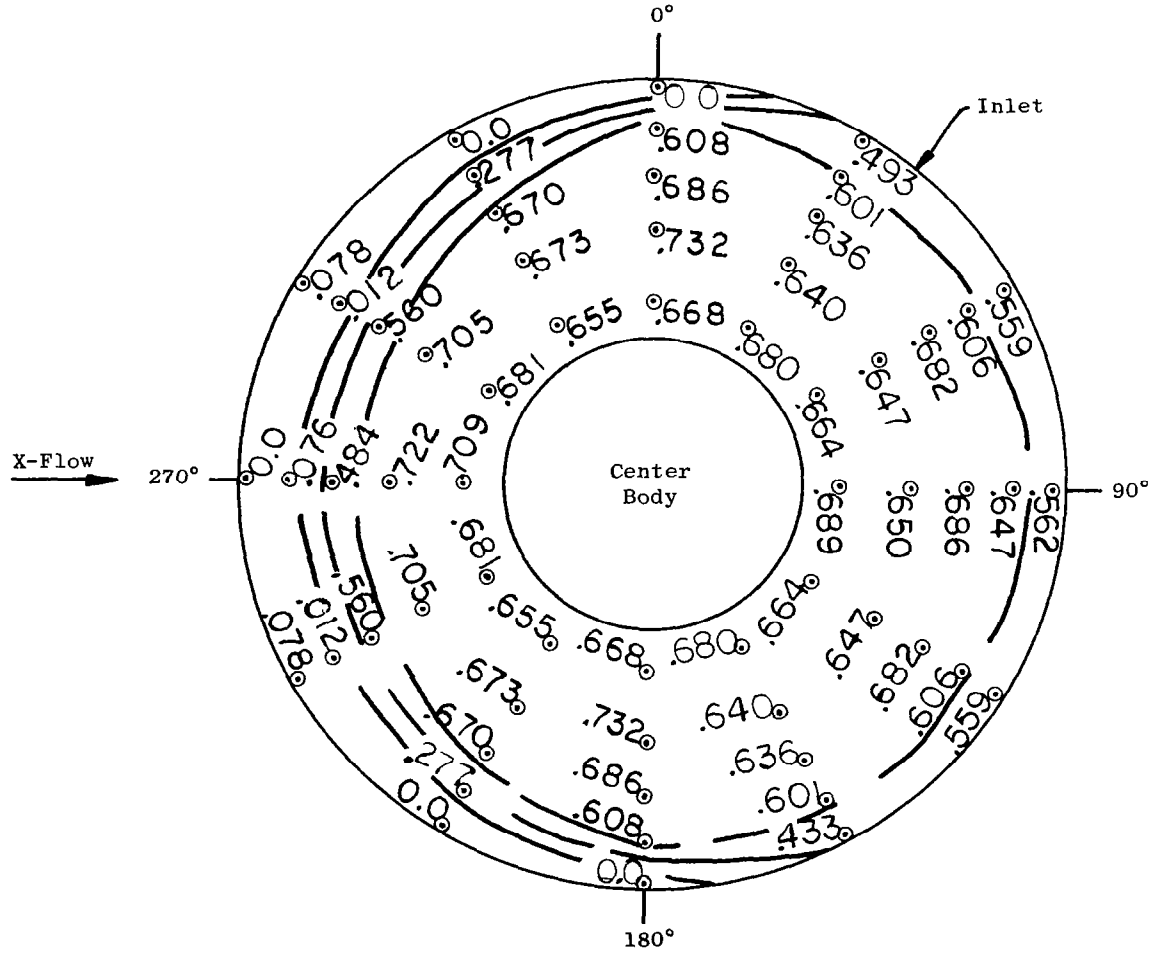

Figure 127. Axial Mach Number Profiles.

Notes: Lines of Constant M_2 (Axial Component)

V_2 = 599.4 V_θ = 270 ft/sec

r/D = 0.12

With IGV

⊙ Data Point

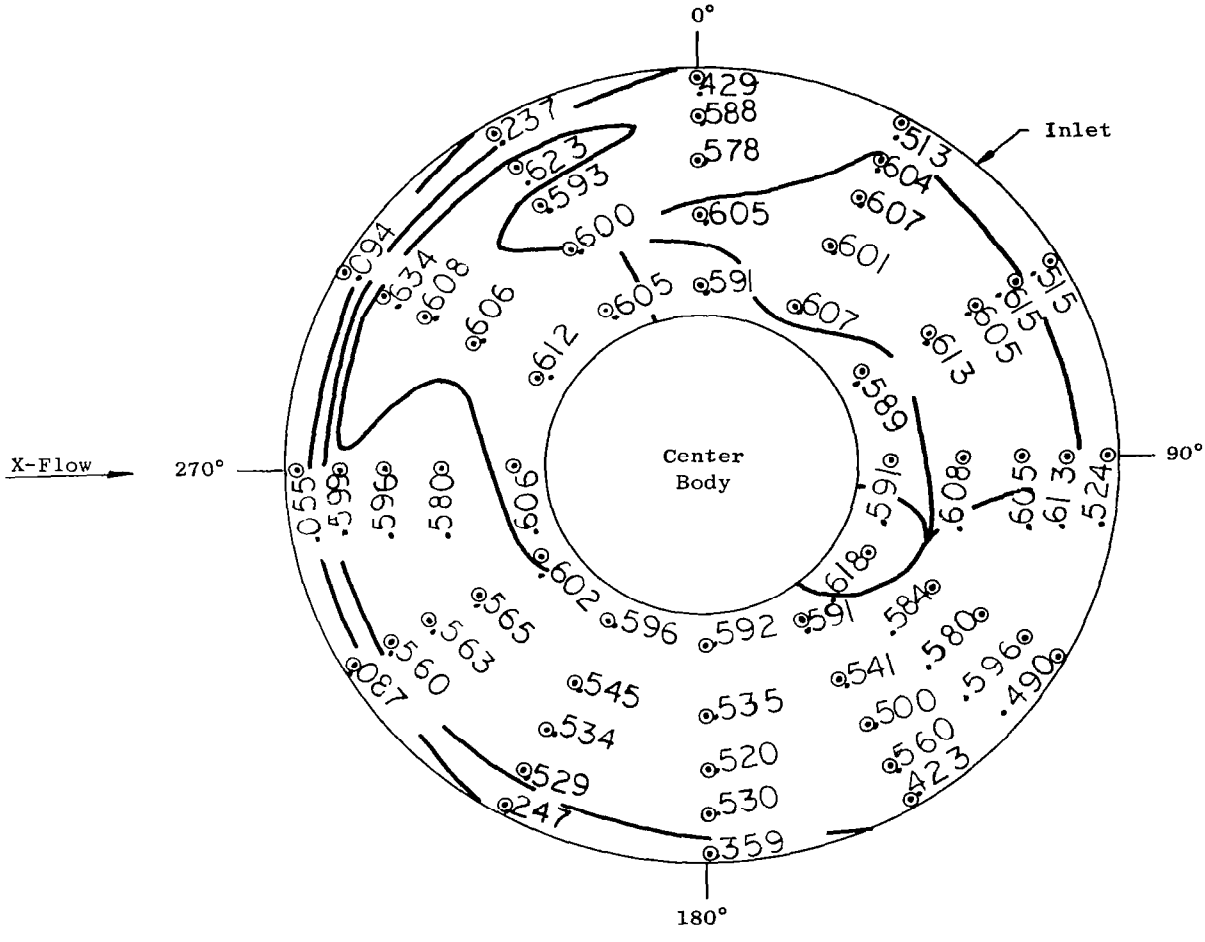

Figure 128. Axial Mach Number Profiles.

Notes: Lines of Constant M_2 (Axial Component)

V_2 = 599.4 V_0 = 270 ft/sec

r/D = 0.06

With IGV

⊙ Data Point

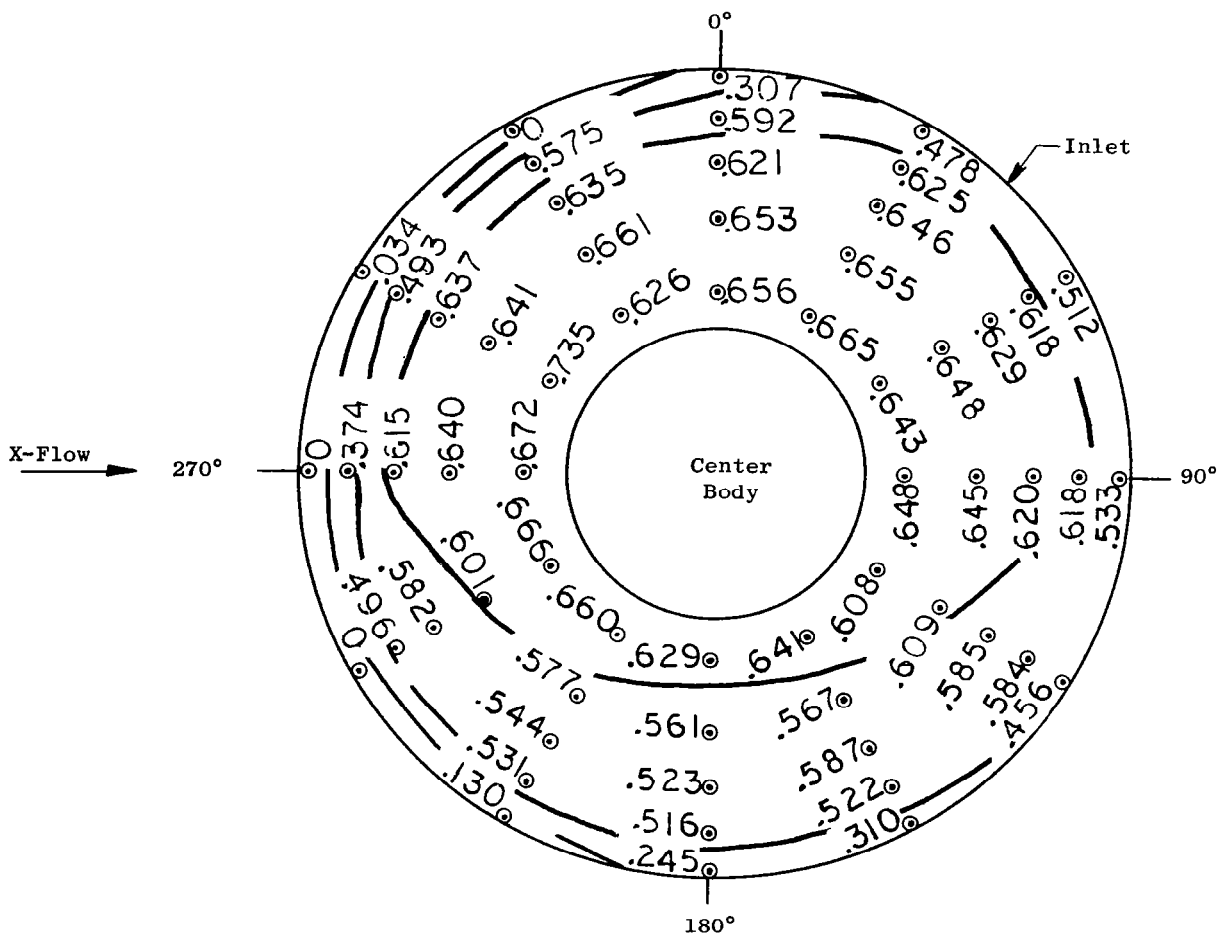

Figure 129. Axial Mach Number Profiles.

Notes: Lines of Constant M_2 (Axial Component)

V_2 = 599.4 V_0 = 270 ft/sec

r/D = 0.03

With IGV

⊙ Data Point

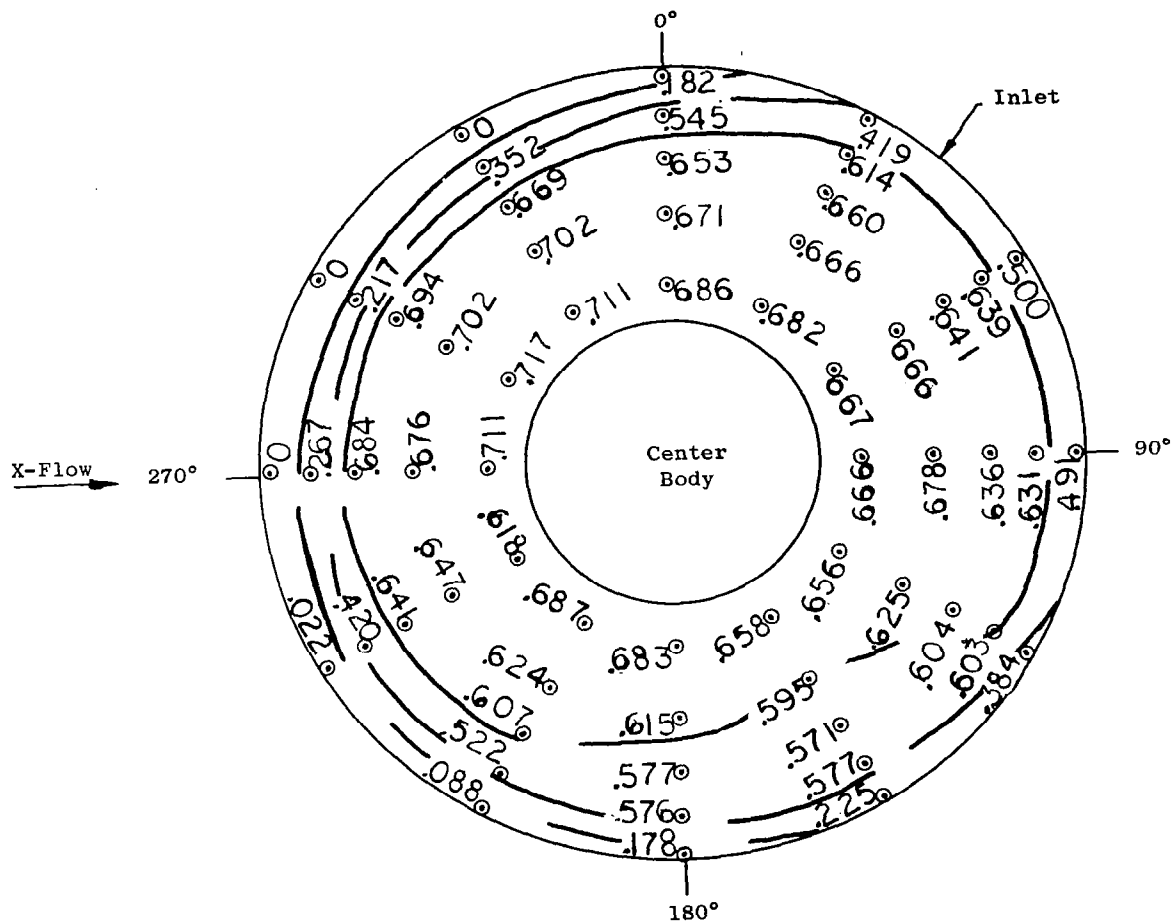

Figure 130. Axial Mach Number Profiles.

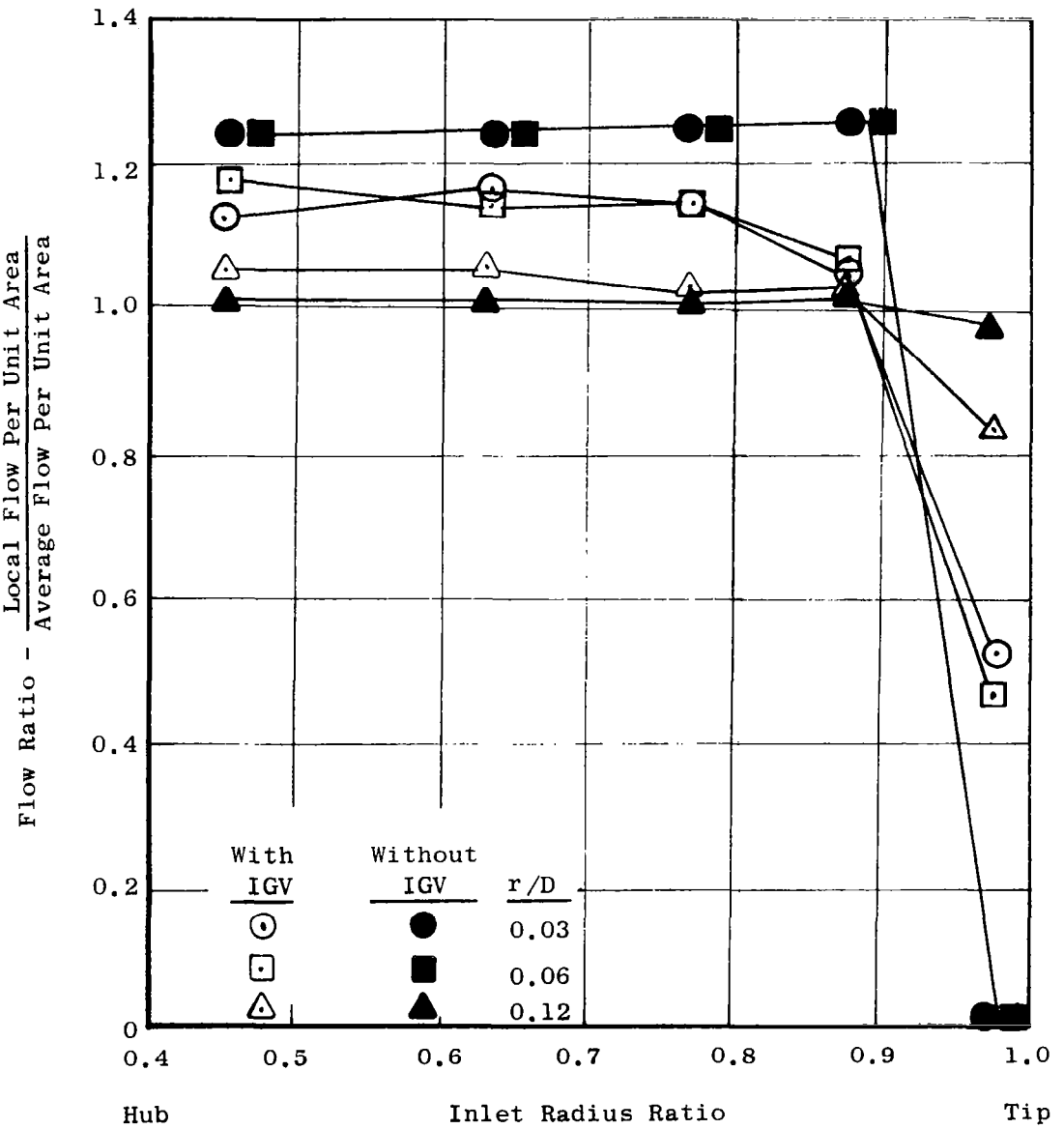

Figure 131. Radial Flow Distribution Without Cross Flow.

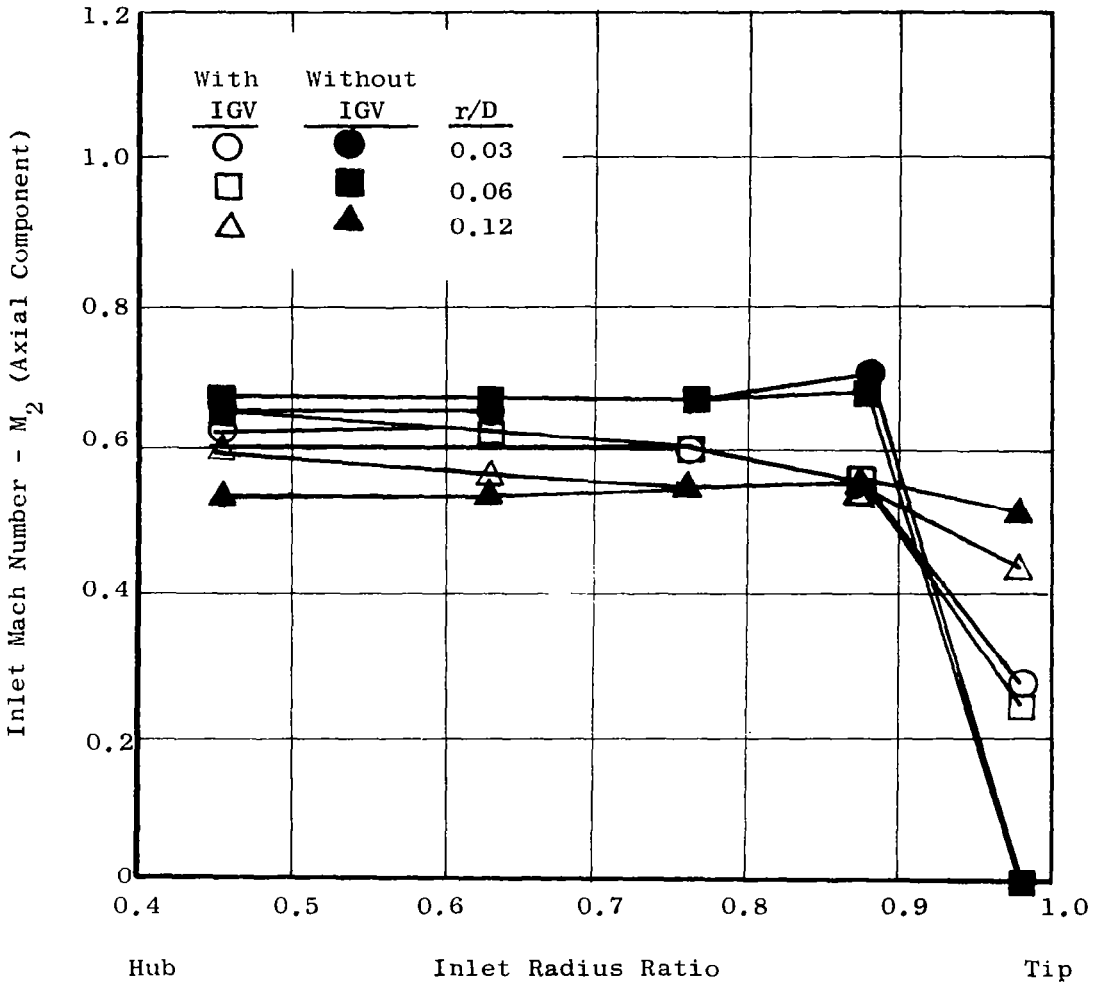

Figure 132. Radial Mach Number Distribution Without Cross Flow.

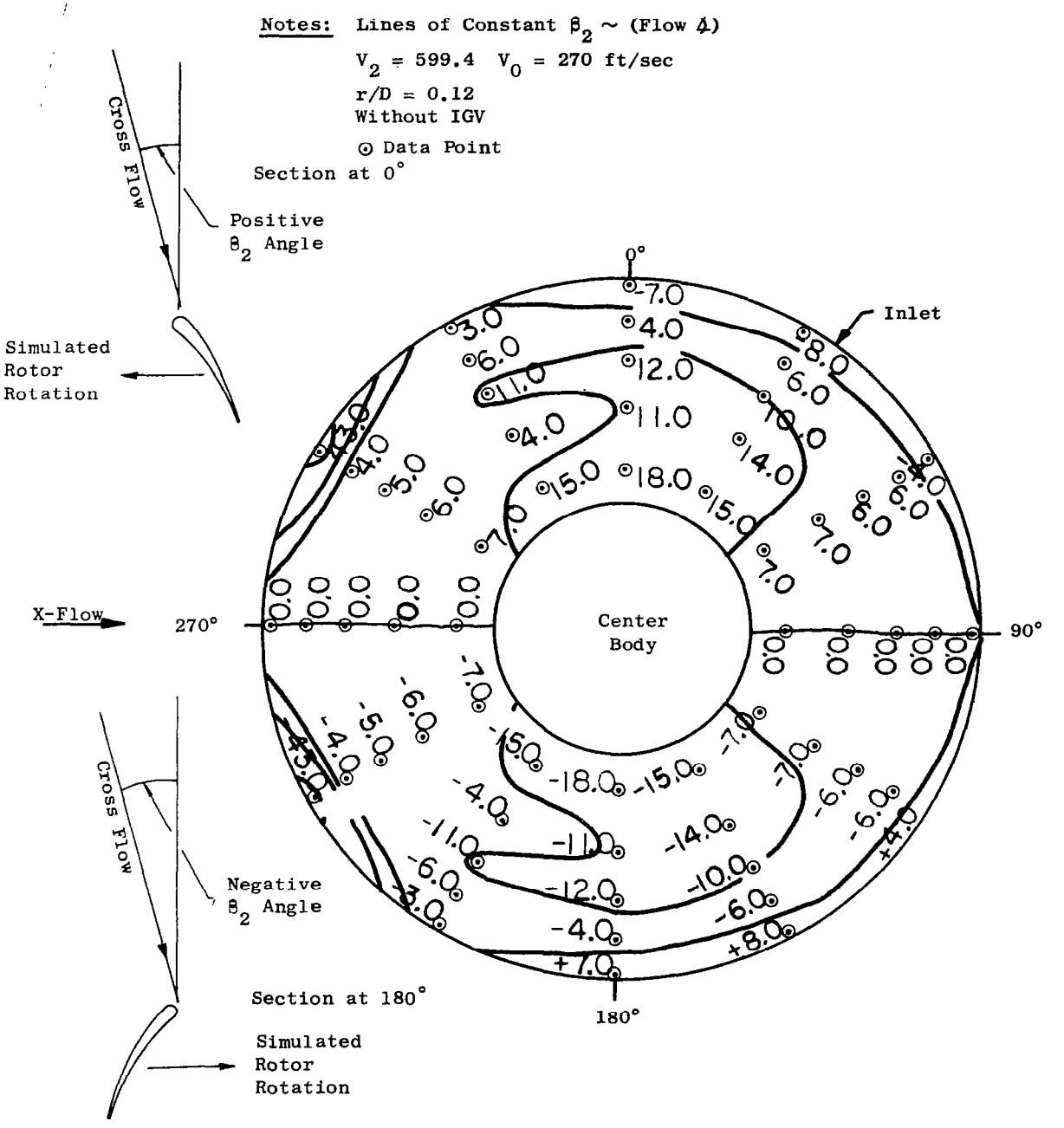

Figure 133. Flow Angle Profiles.

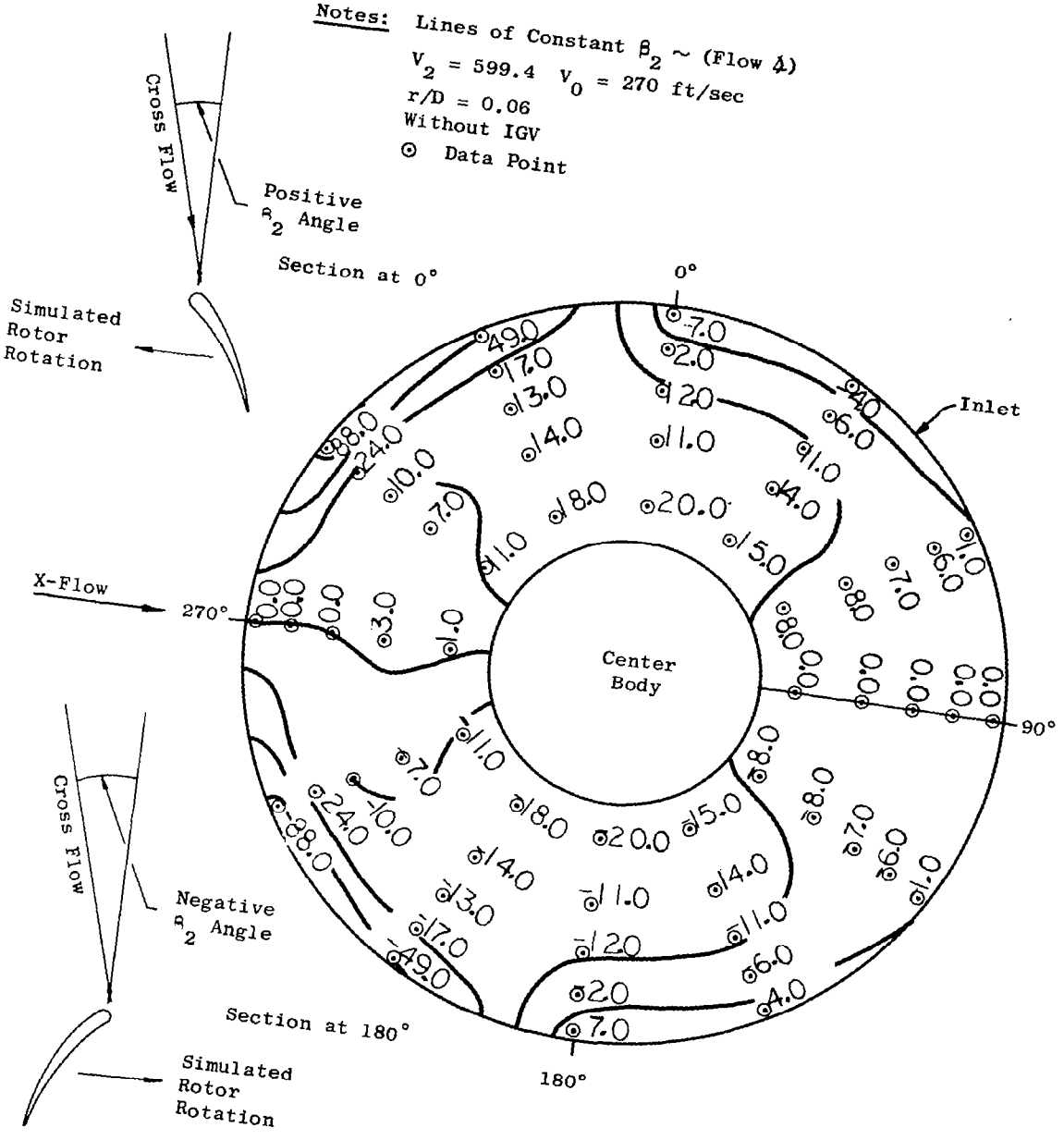

Figure 134. Flow Angle Profiles.

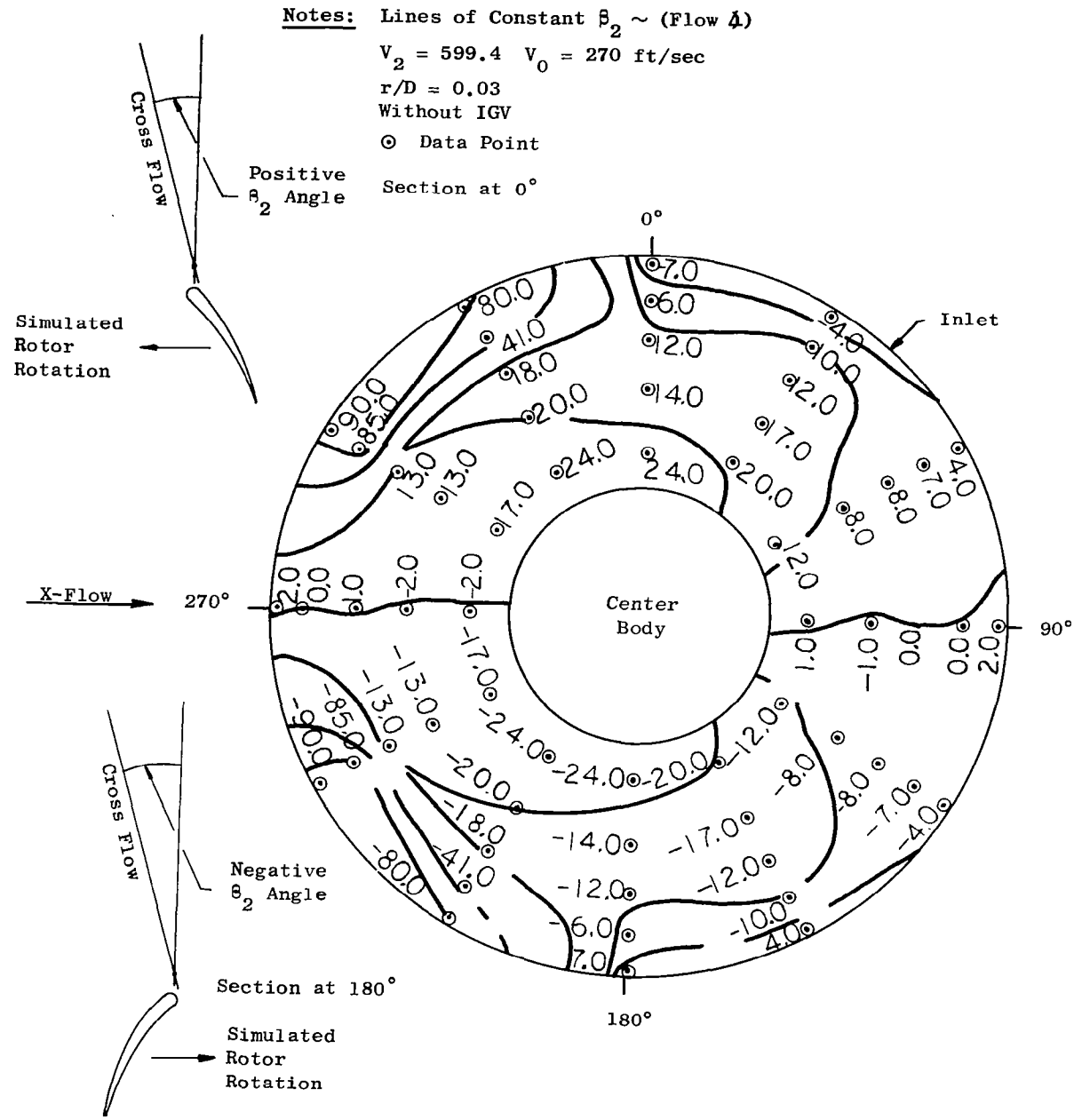

Figure 135. Flow Angle Profiles.

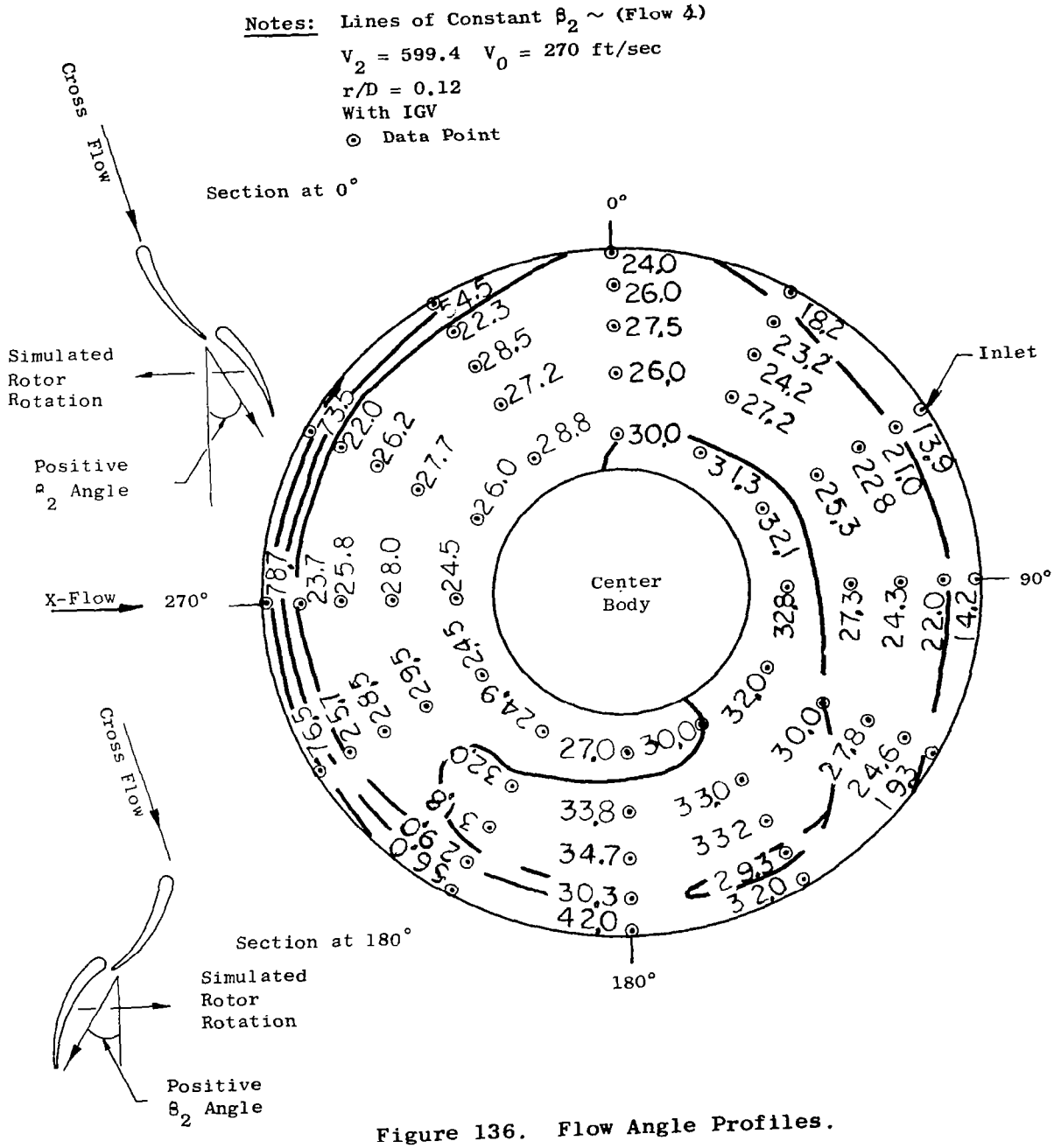

Figure 136. Flow Angle Profiles.

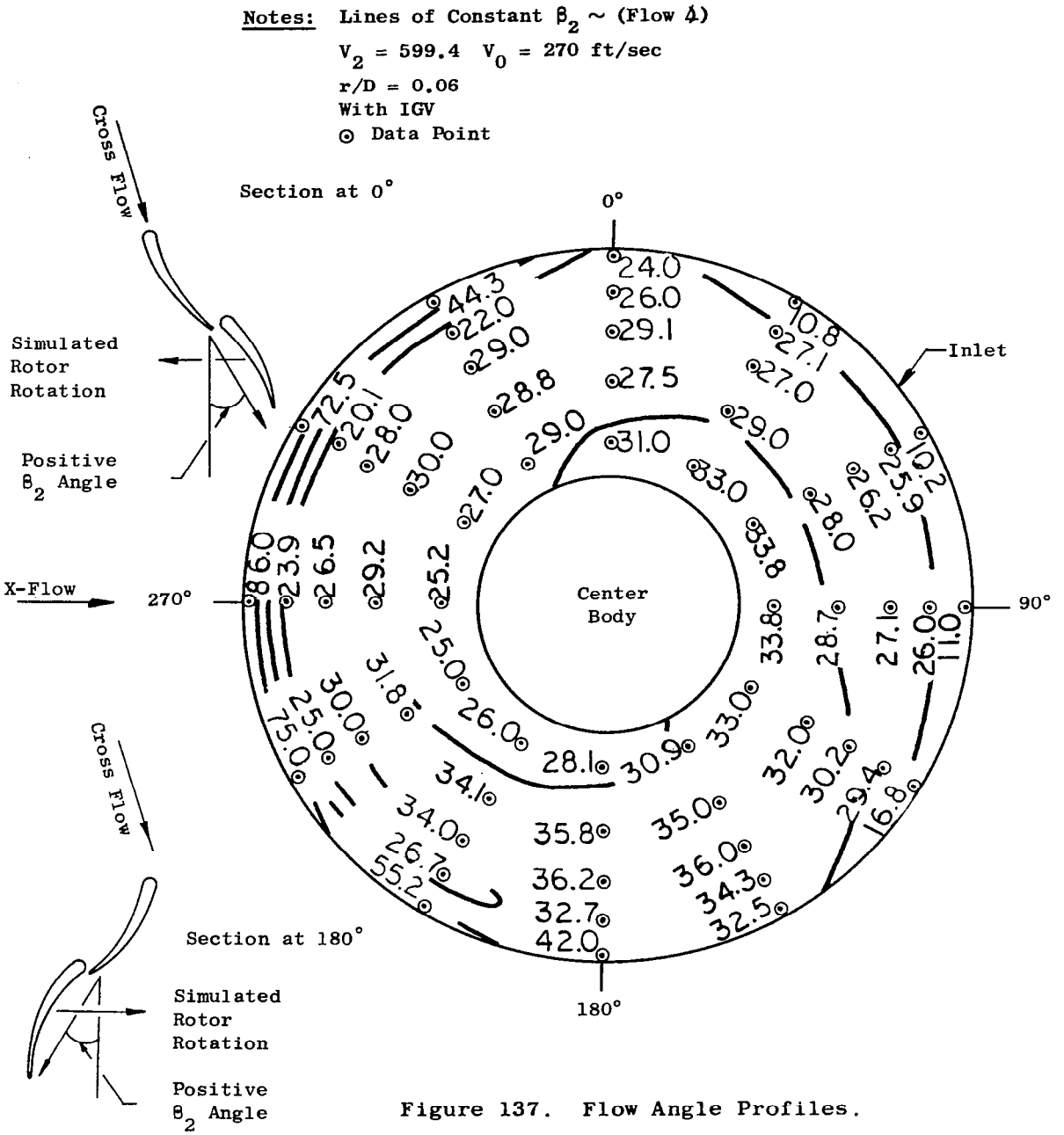

Figure 137. Flow Angle Profiles.

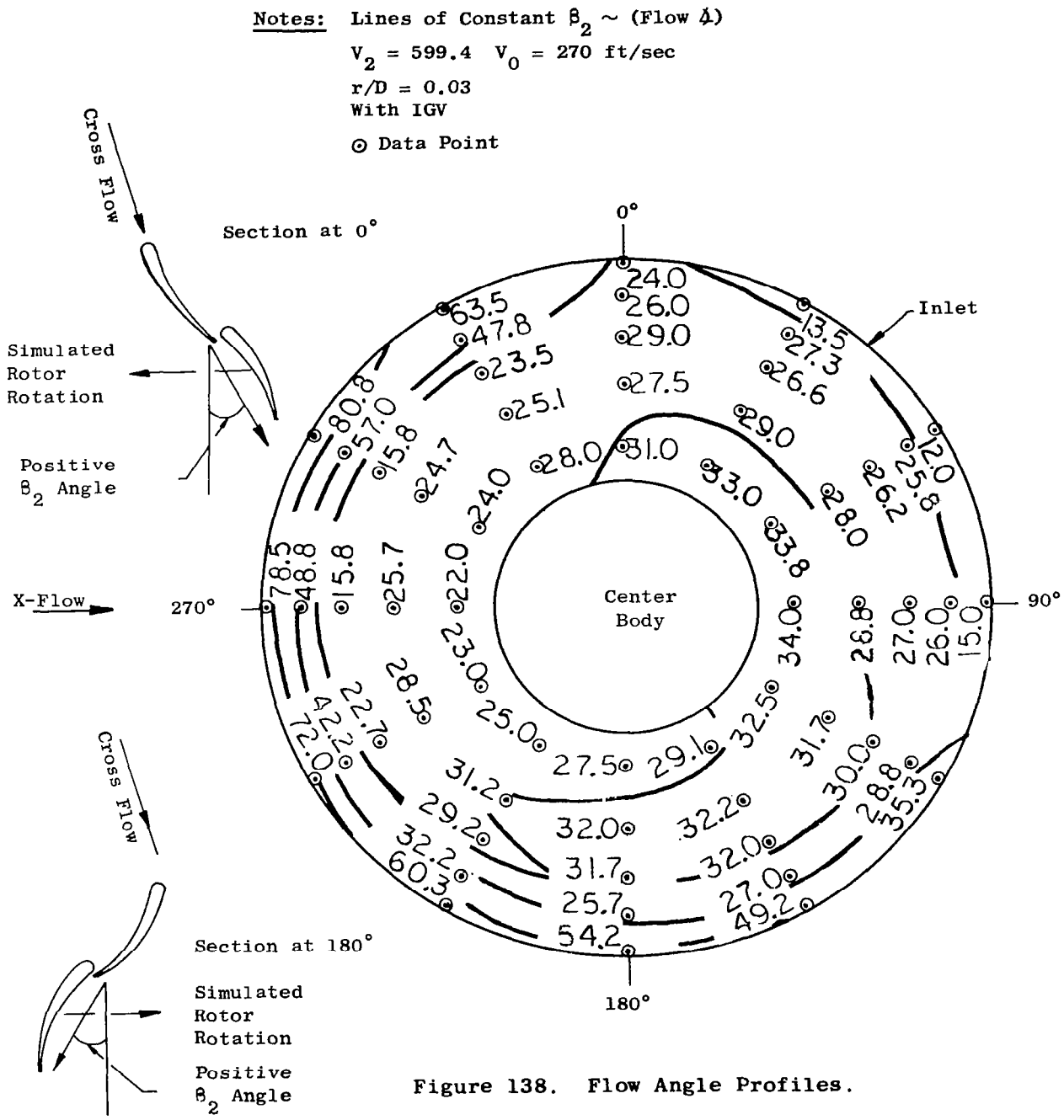

Figure 138. Flow Angle Profiles.

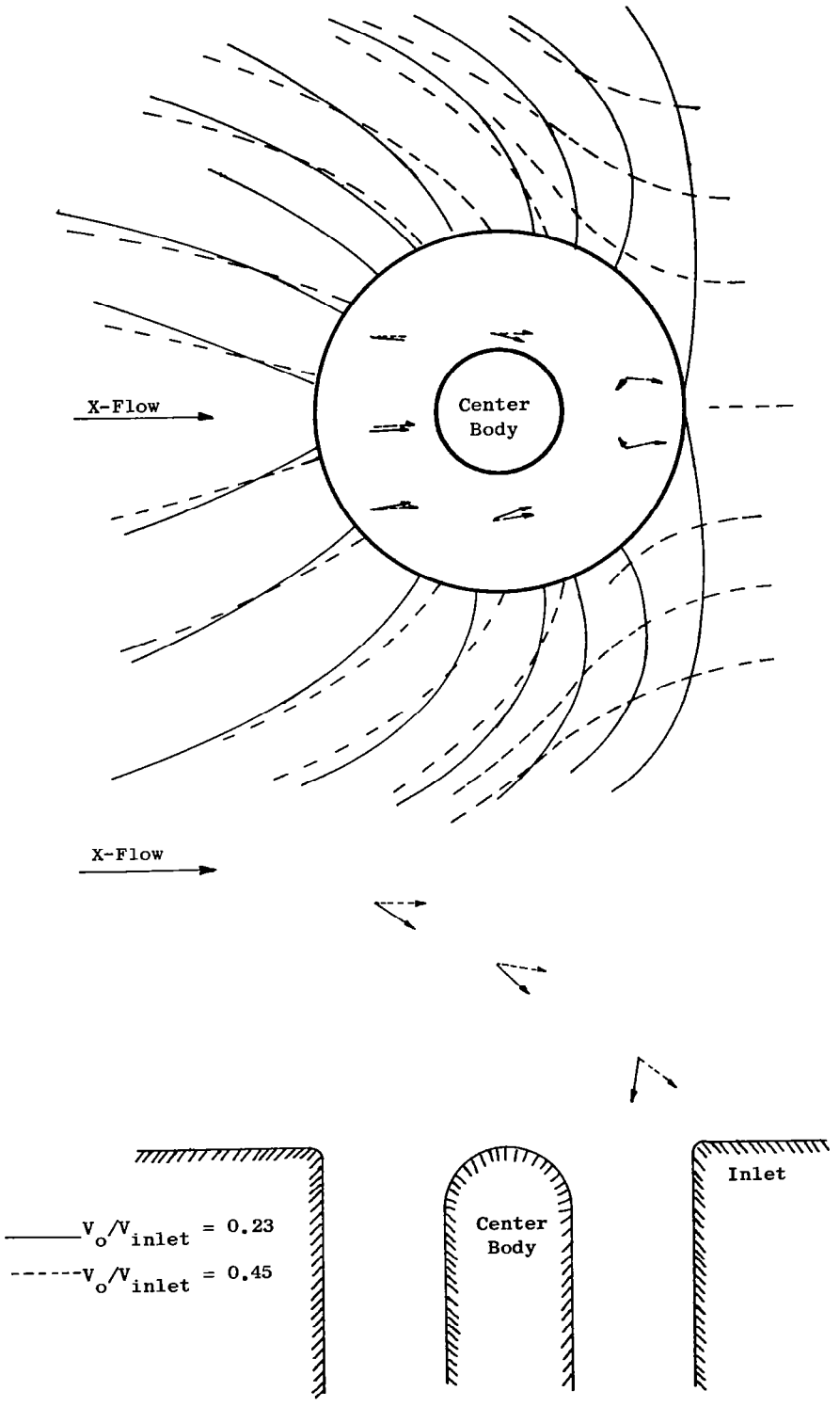

Figure 139. Flow Visualization.

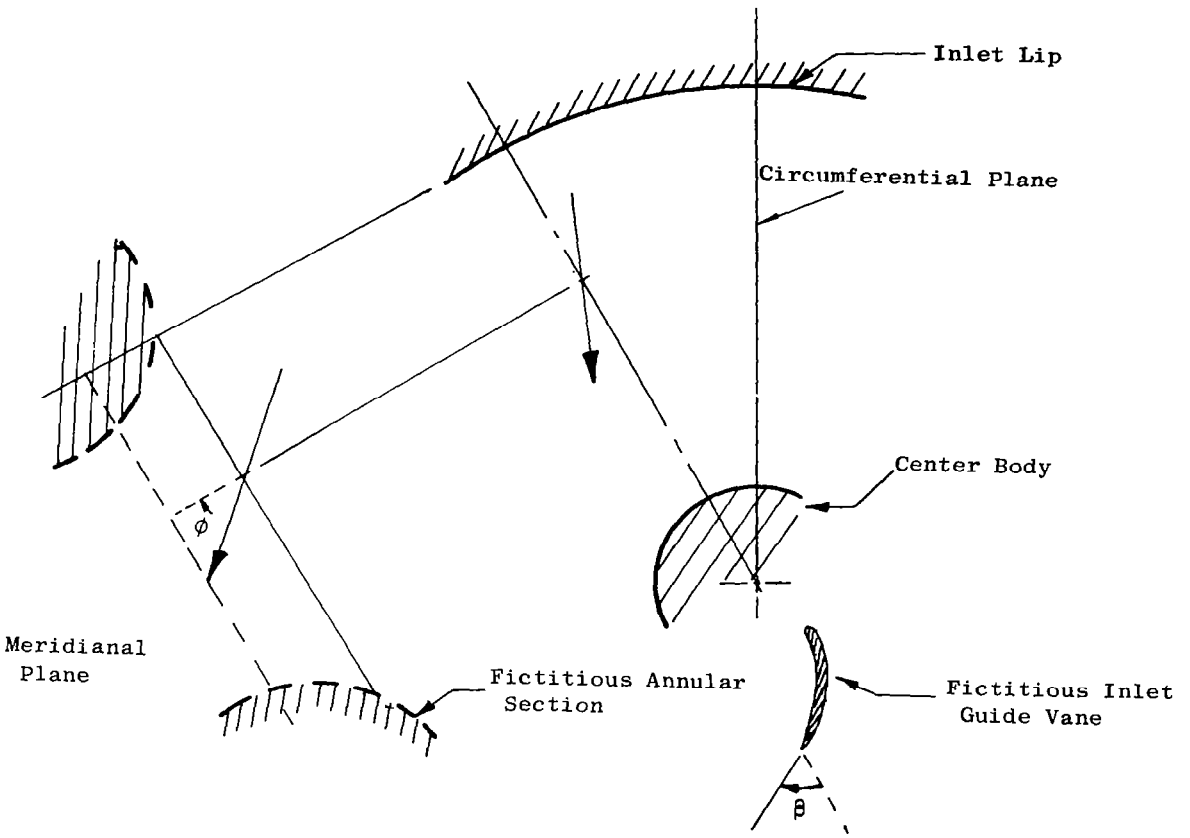

Figure 140. Cross Flow Model.

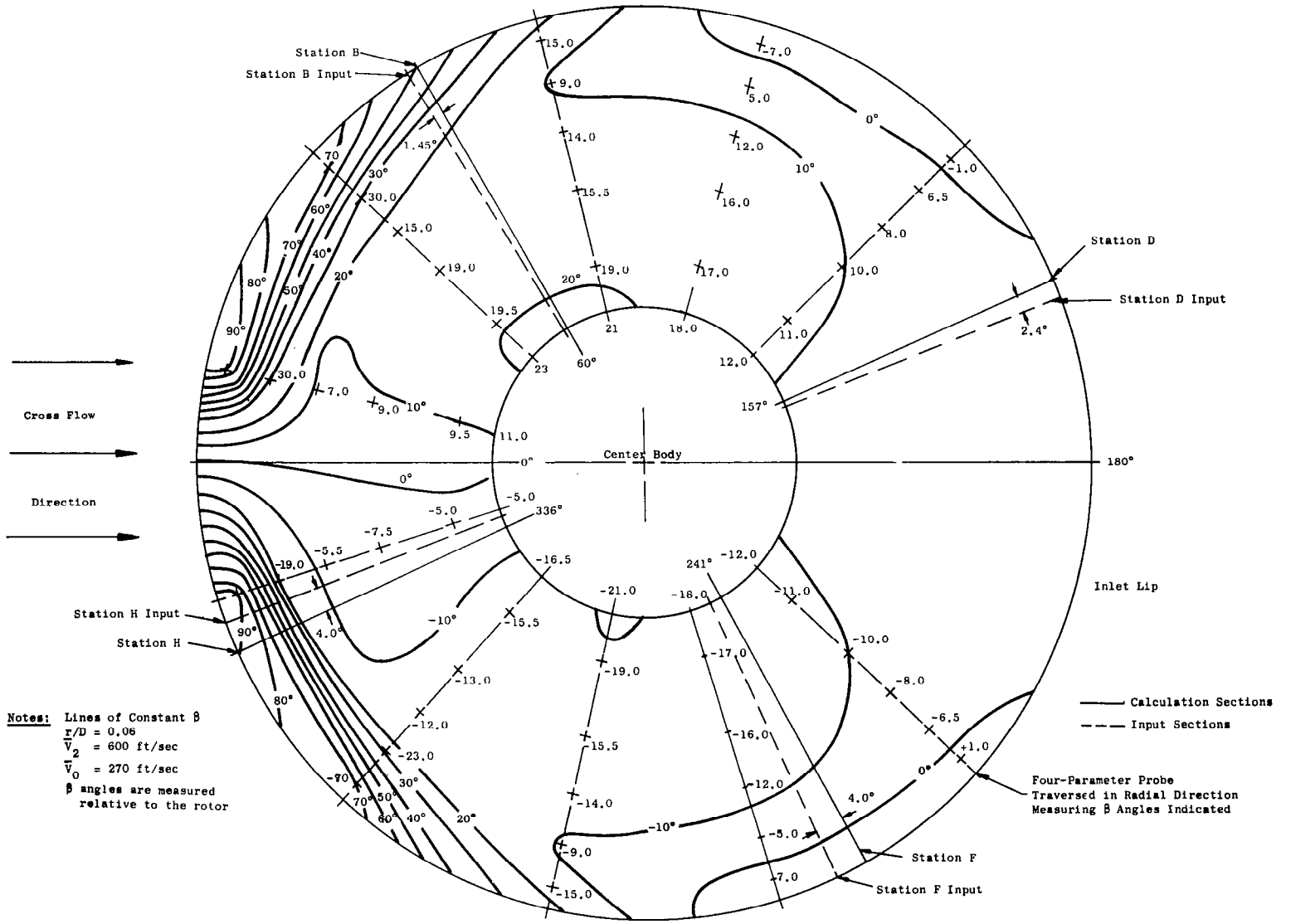

Figure 141. Top View of Inlet Showing Input Sections and Swirl Angles.

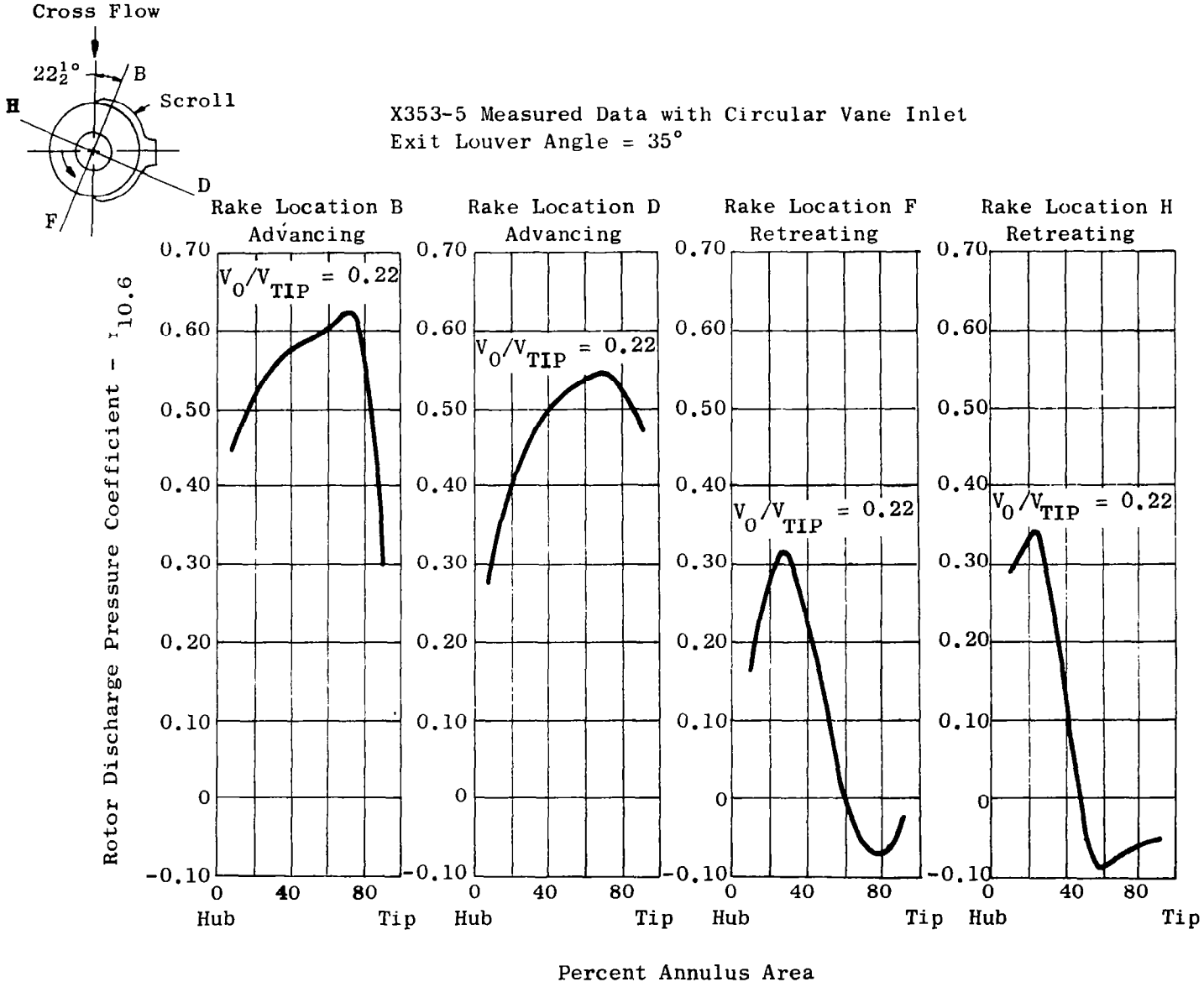

Figure 142. Pressure Coefficient Versus Percent Annulus Area.

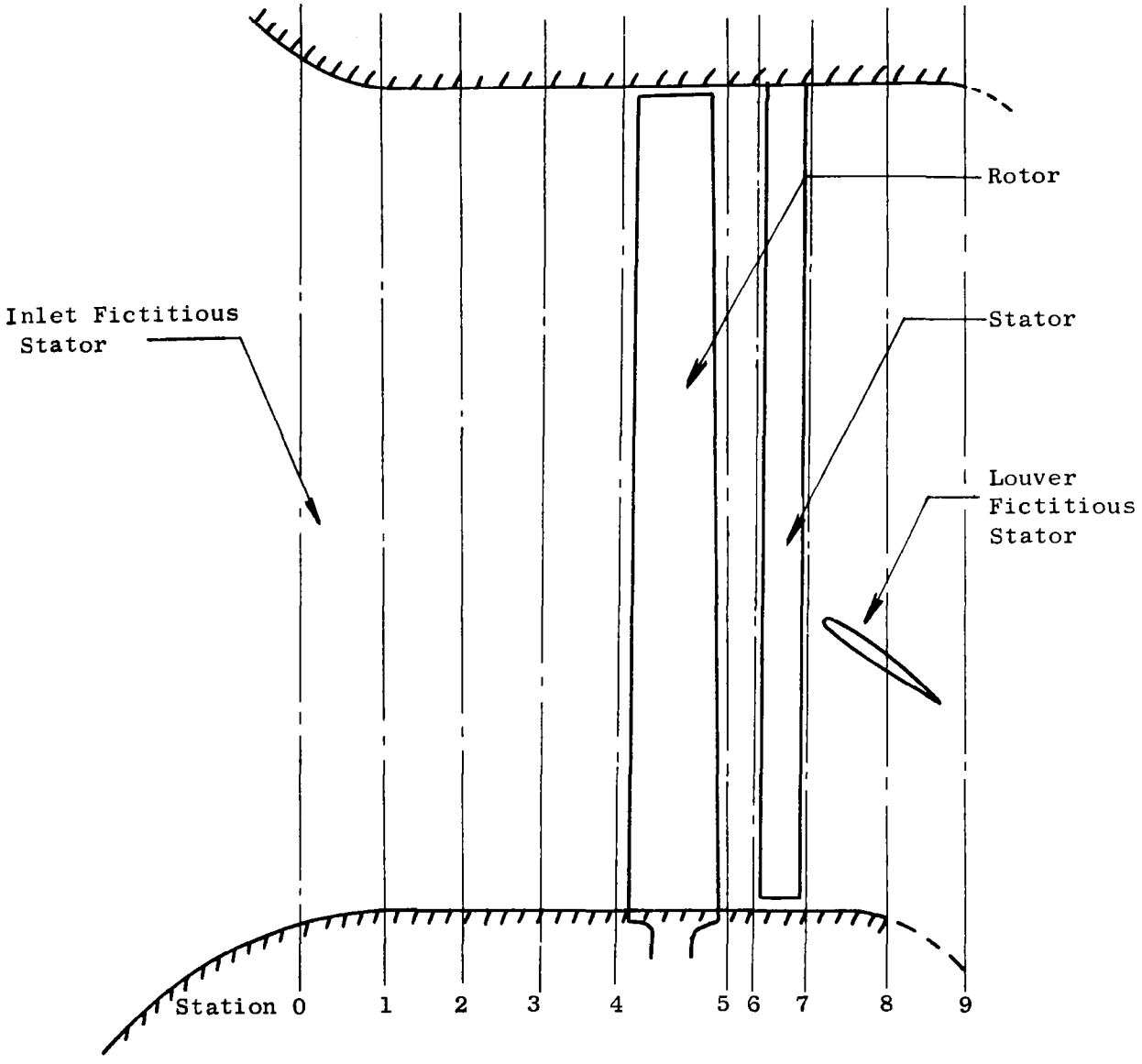

Figure 143. Schematic of Station Locations for the X353-5 Calculation.

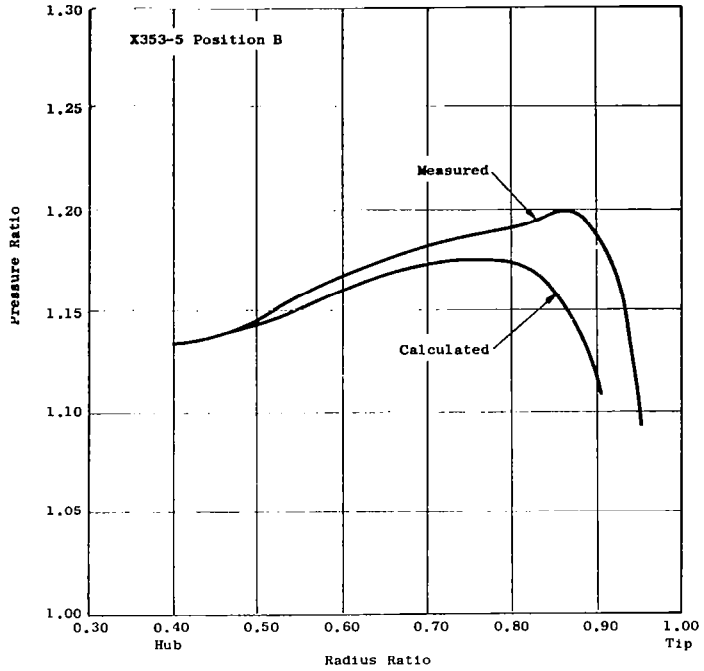

Figure 144. X353-5 Pressure Ratio Versus Radius Ratio.

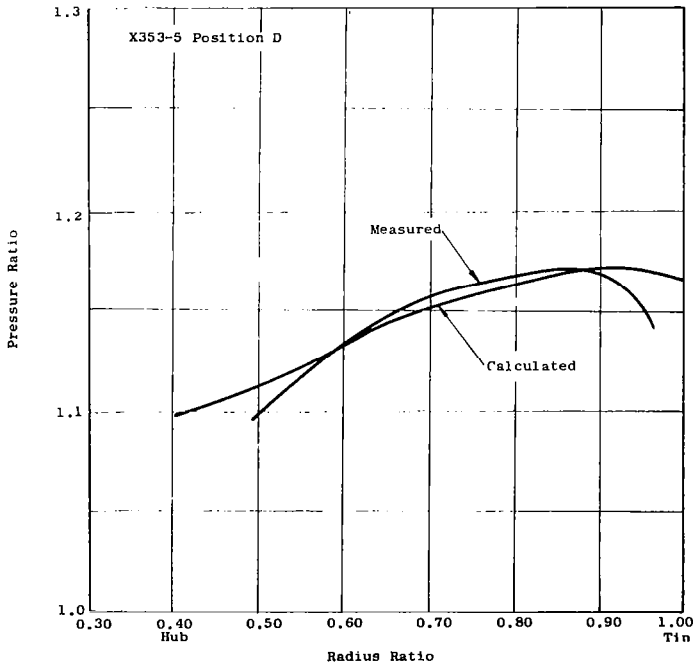

Figure 145. X353-5 Pressure Ratio Versus Radius Ratio.

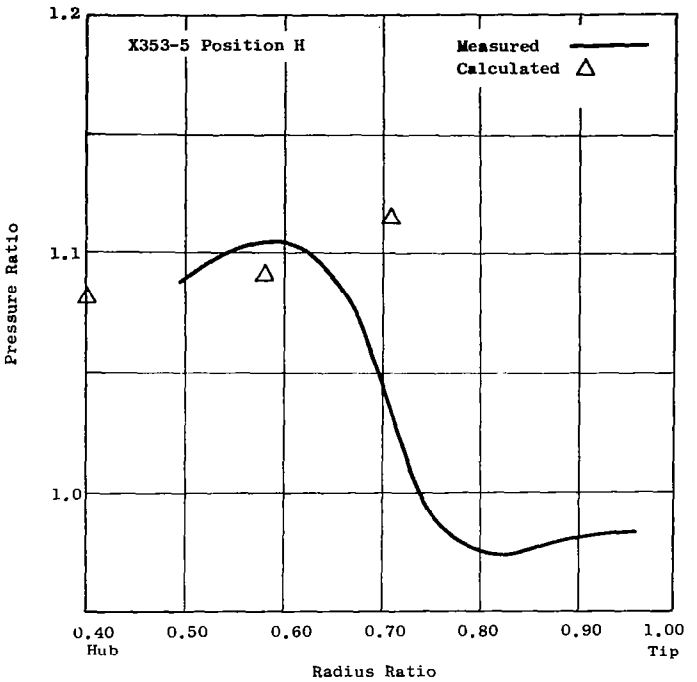

Figure 146. X353-5 Pressure Ratio Versus Radius Rati

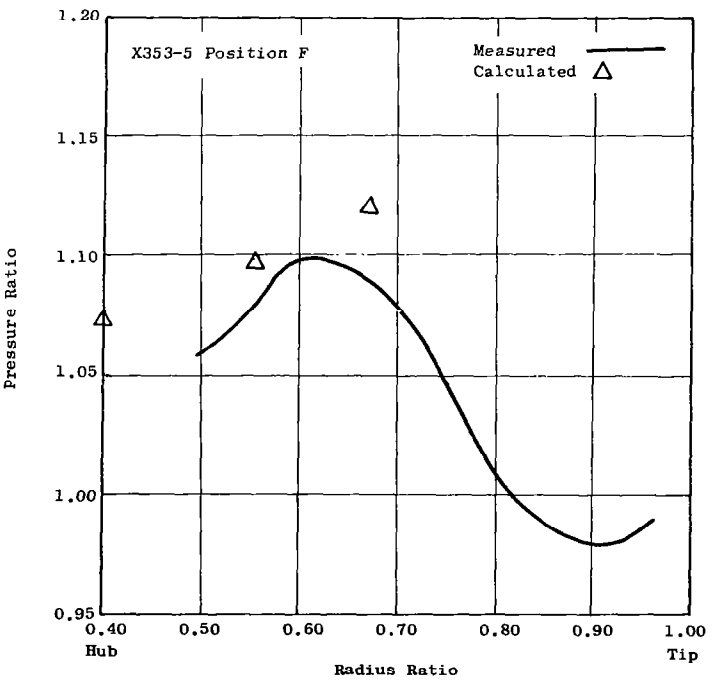

Figure 147. X353-5 Pressure Ratio Versus Radius Ratio.

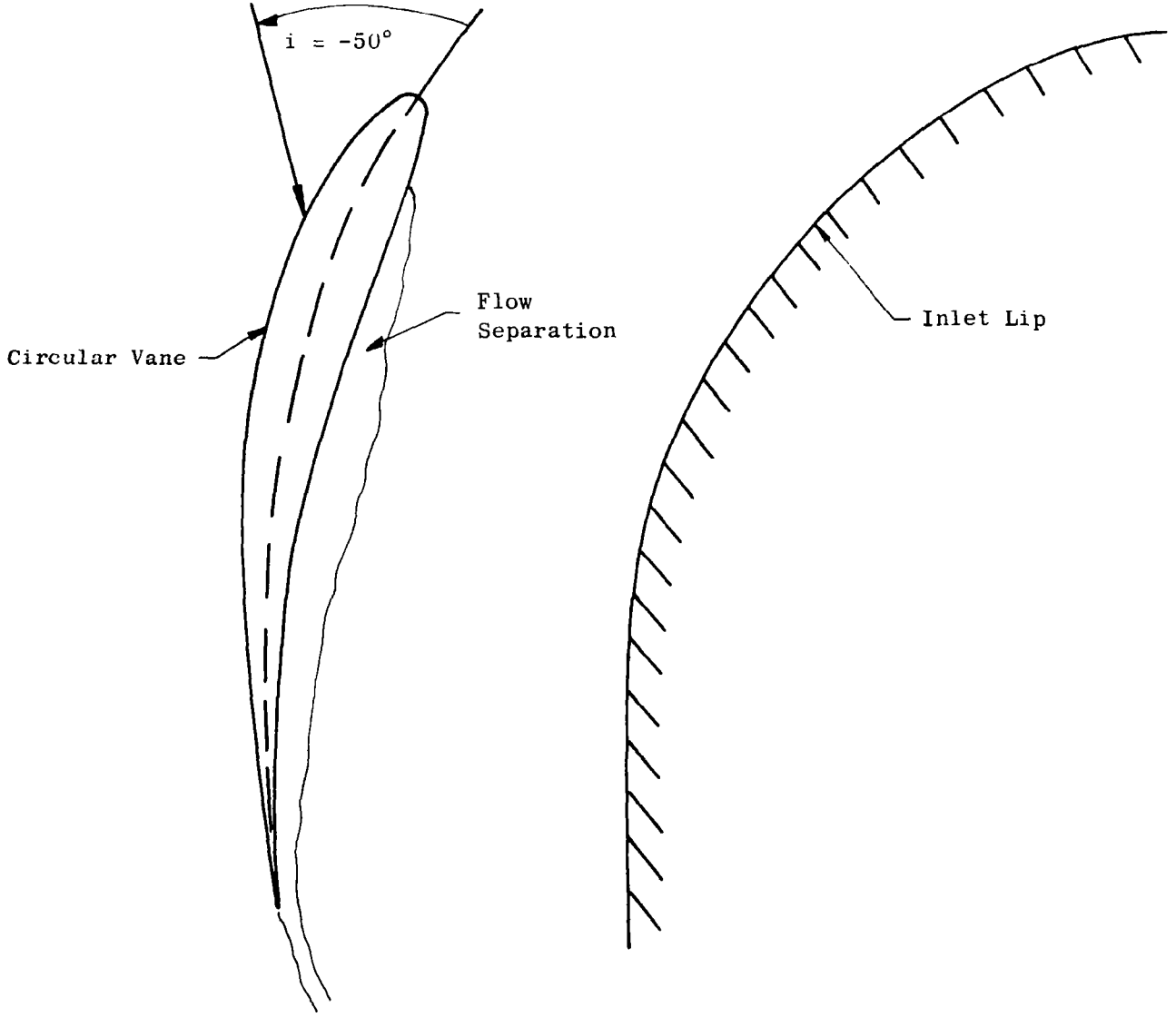

Figure 148. X353-5 Section D, Inlet Circular Vane Separation Leading to High Total Pressure Loss at the Tip Region.

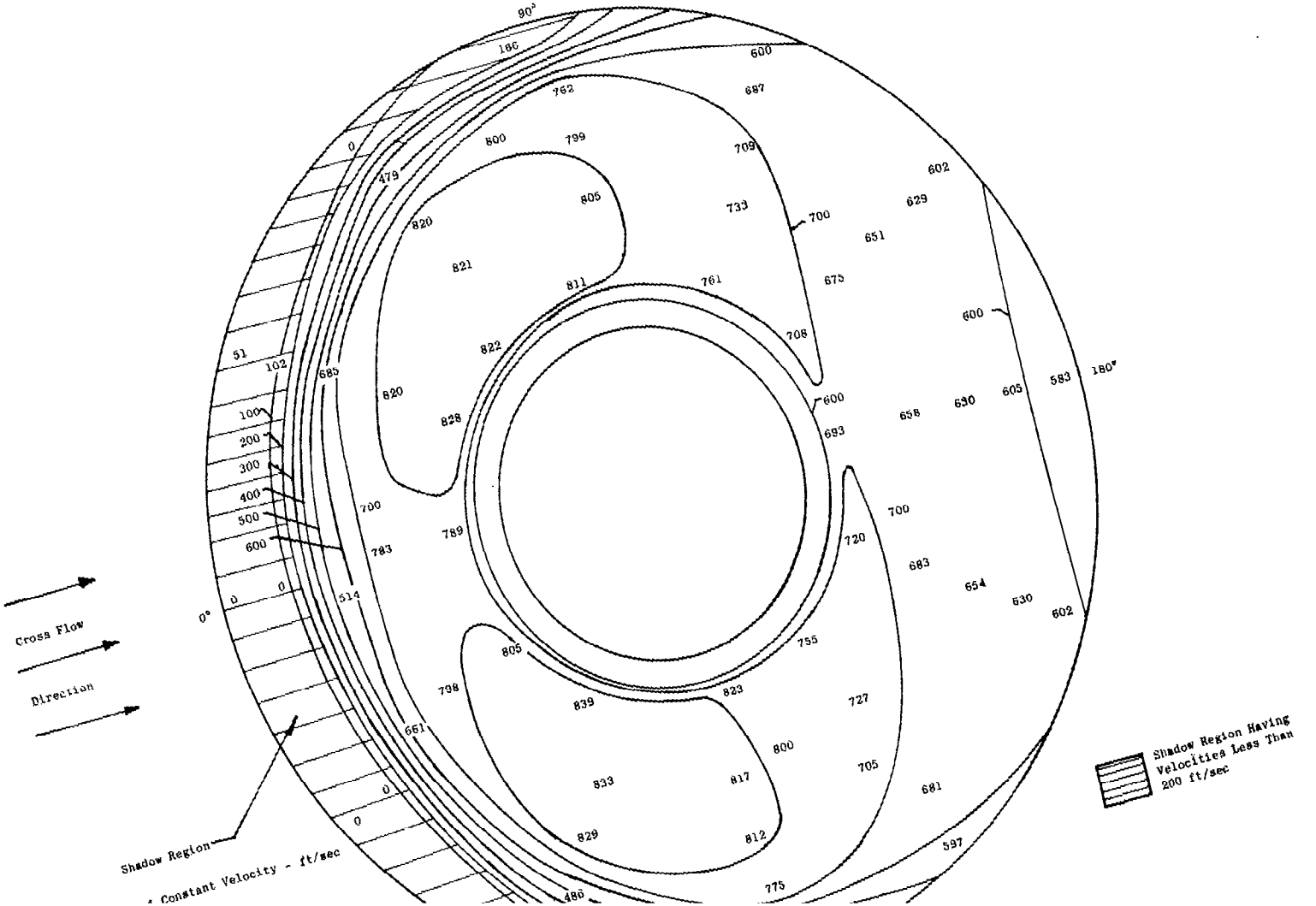
90°
180°
0°
Cross Flow Direction
Shadow Region
Constant Velocity - ft/sec
Shadow Region Having Velocities Less Than 200 ft/sec

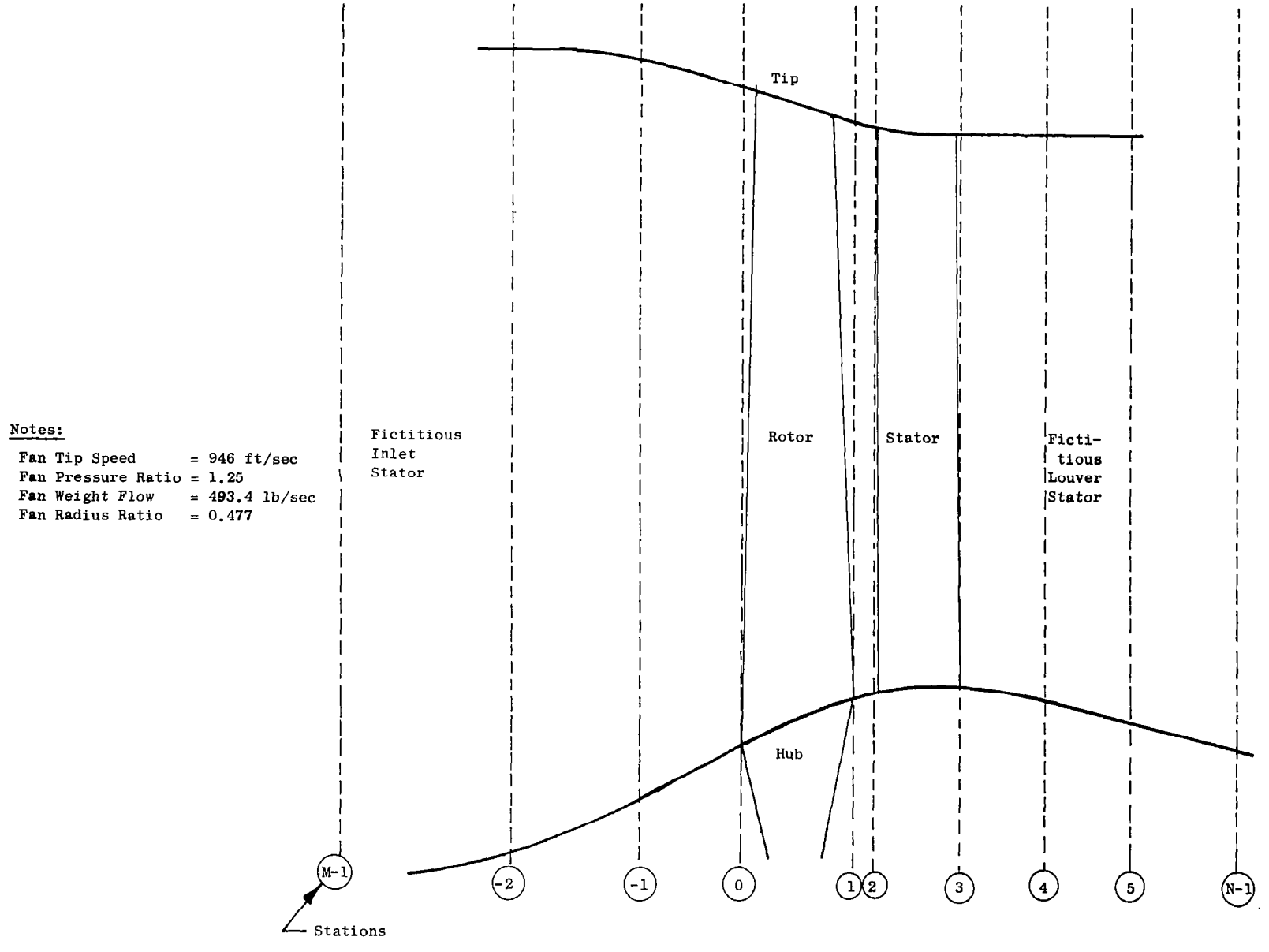

Figure 150. Schematic of Station Locations for the LFX Calculation.

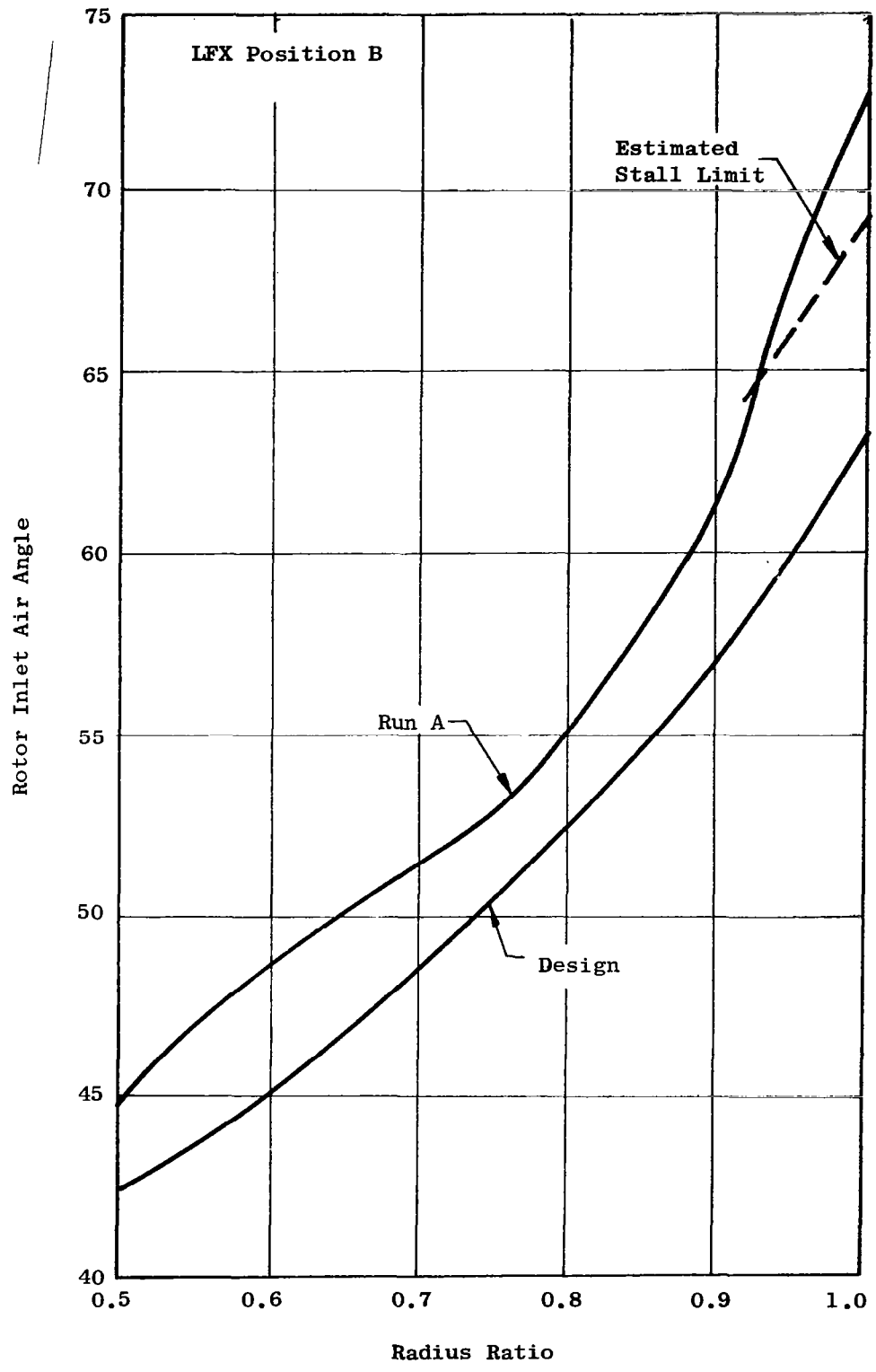

Figure 151. LFX Rotor Inlet Air Angle Versus Radius Ratio.

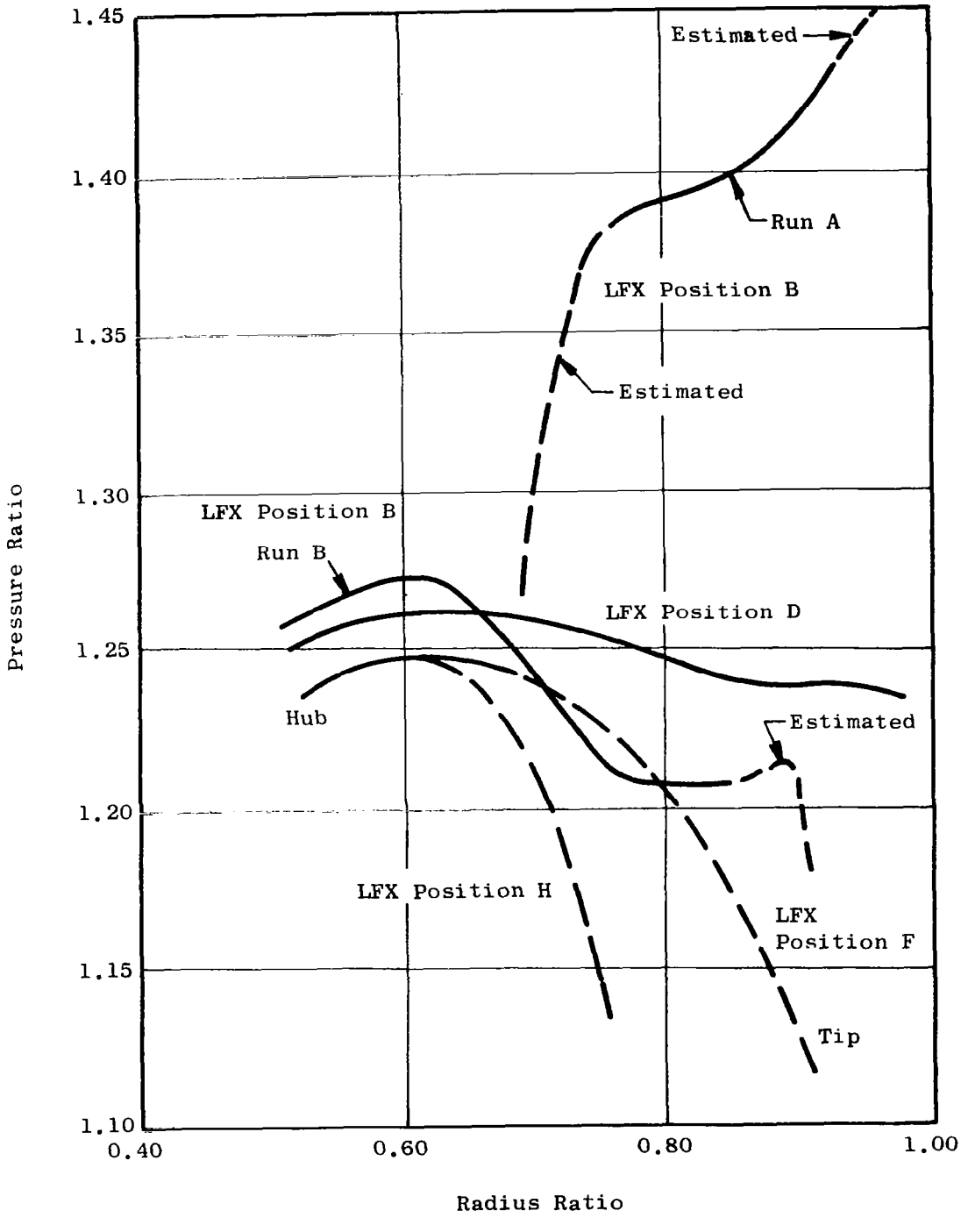

Figure 152. LFX Pressure Ratio Versus Radius Ratio.

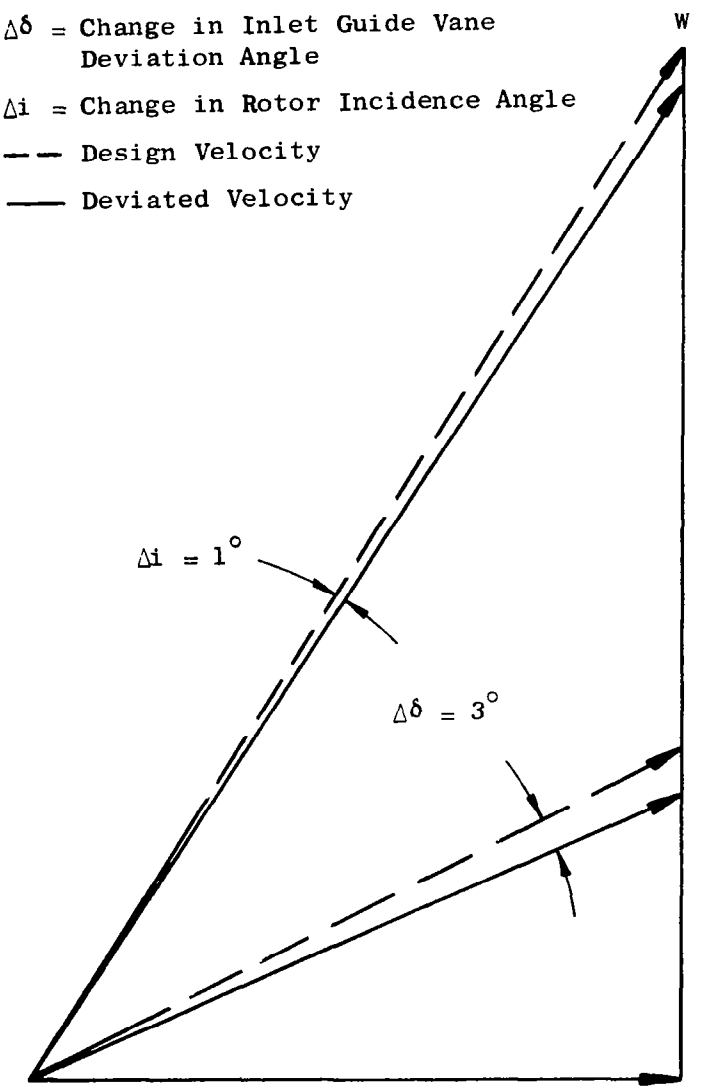

Figure 153. Inlet Guide Vane-Rotor, Effect of Increased Inlet Guide Vane Deviation on Rotor Incidence.

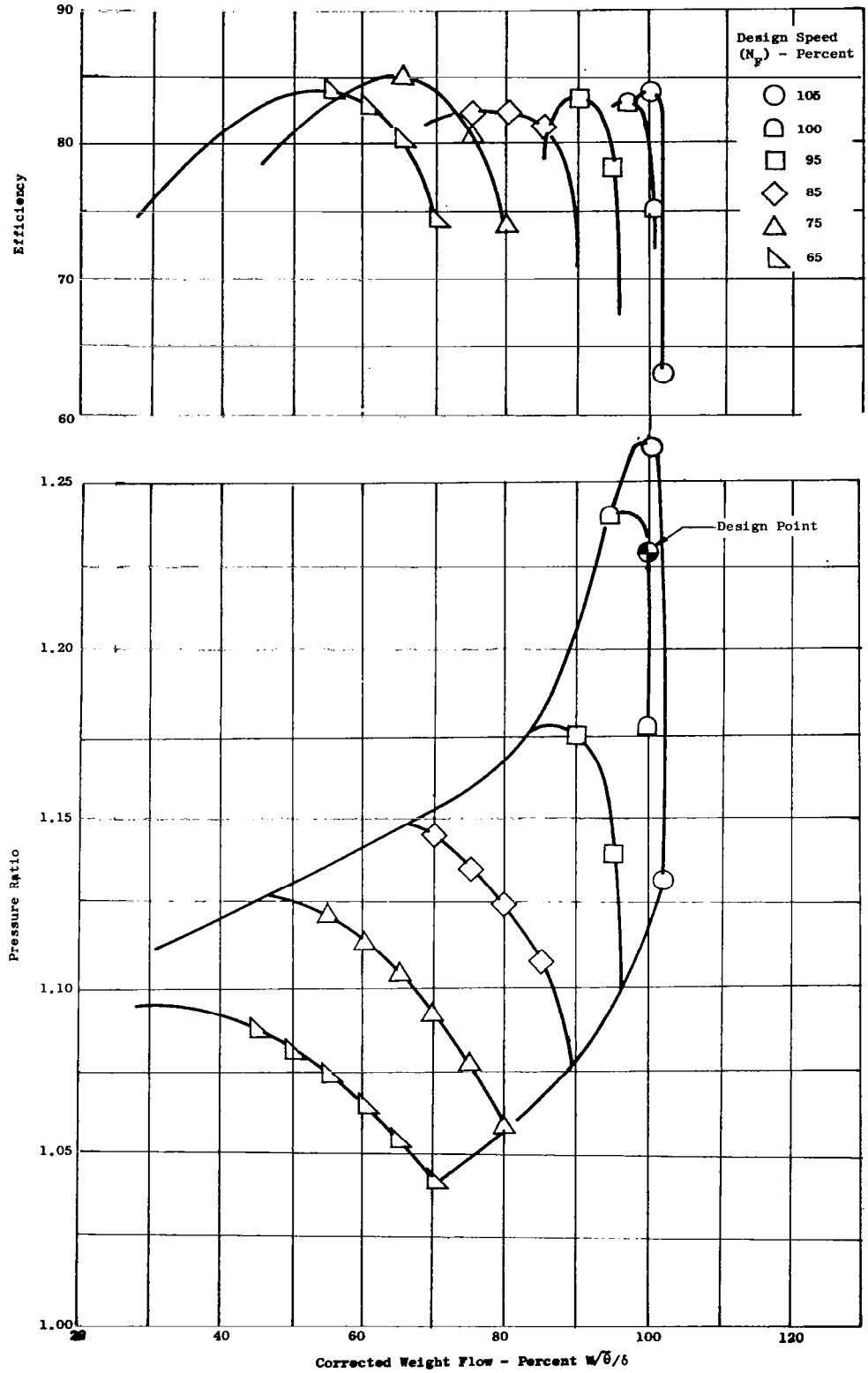

Figure 154. Predicted IGV-Rotor Lift Fan Map.

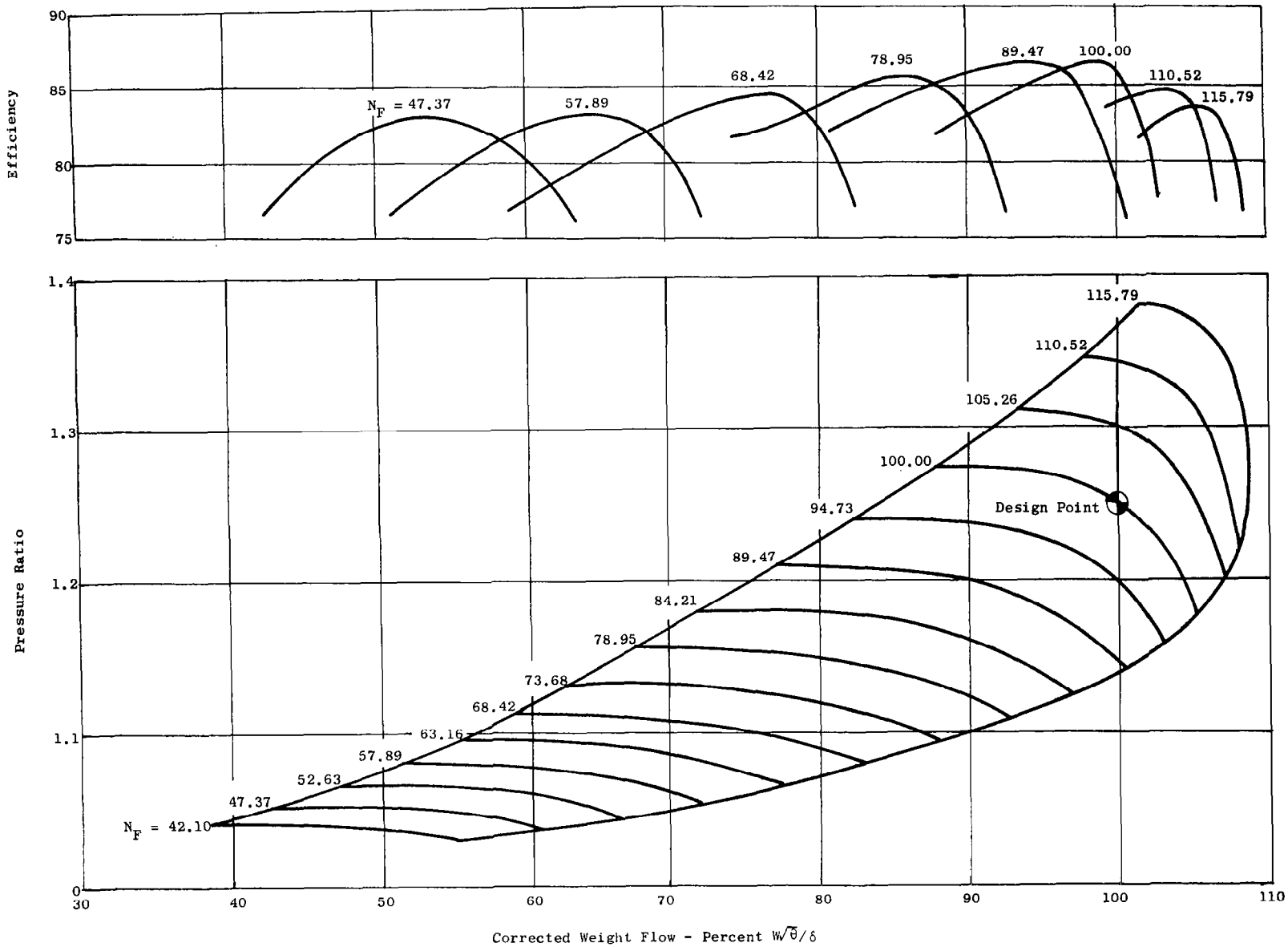

Figure 155. Predicted 1.25 Pressure Ratio Rotor-Stator Lift Fan Map.

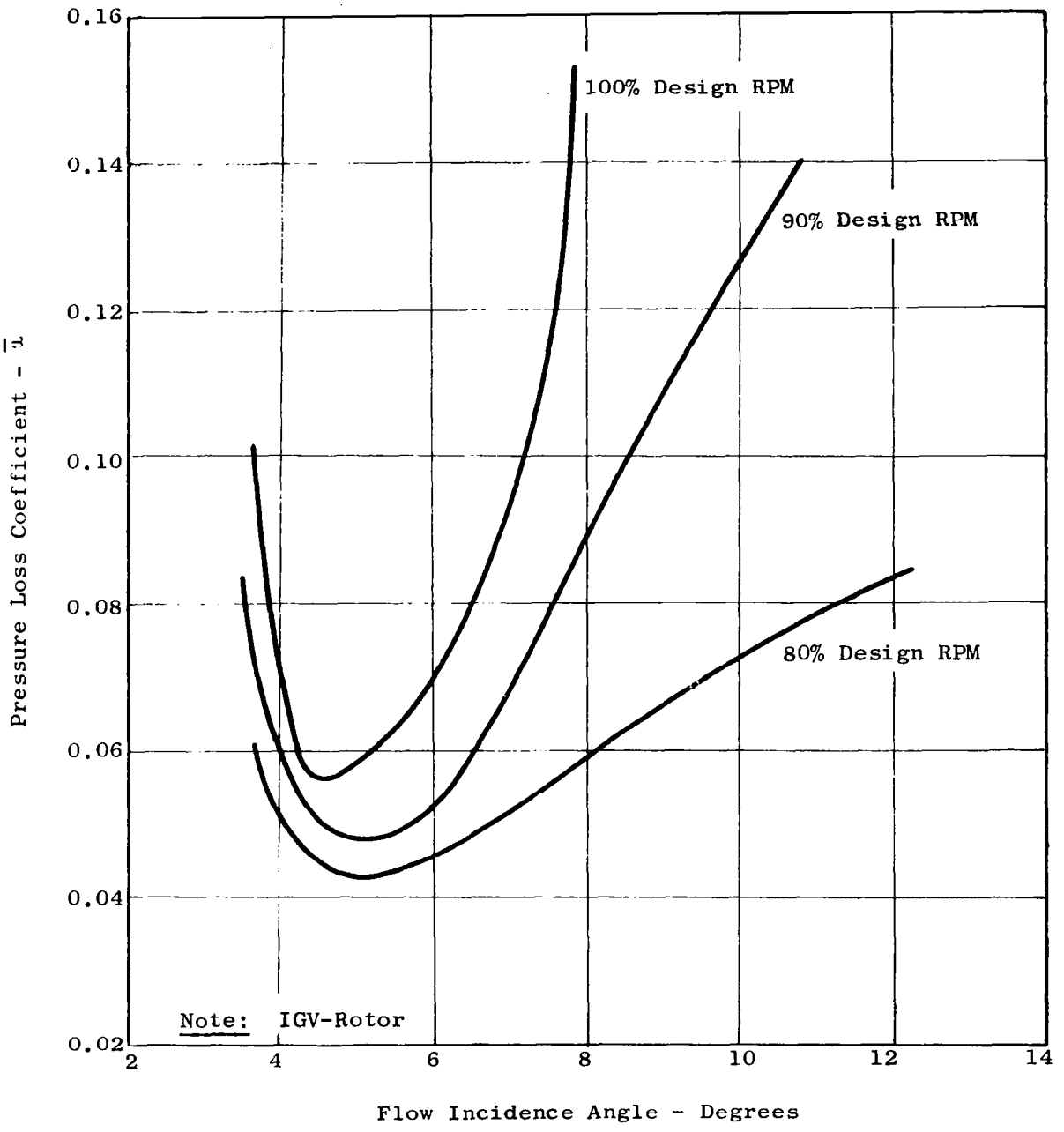

Figure 156. Relative Total Pressure Loss Coefficient Versus Incidence Angle.

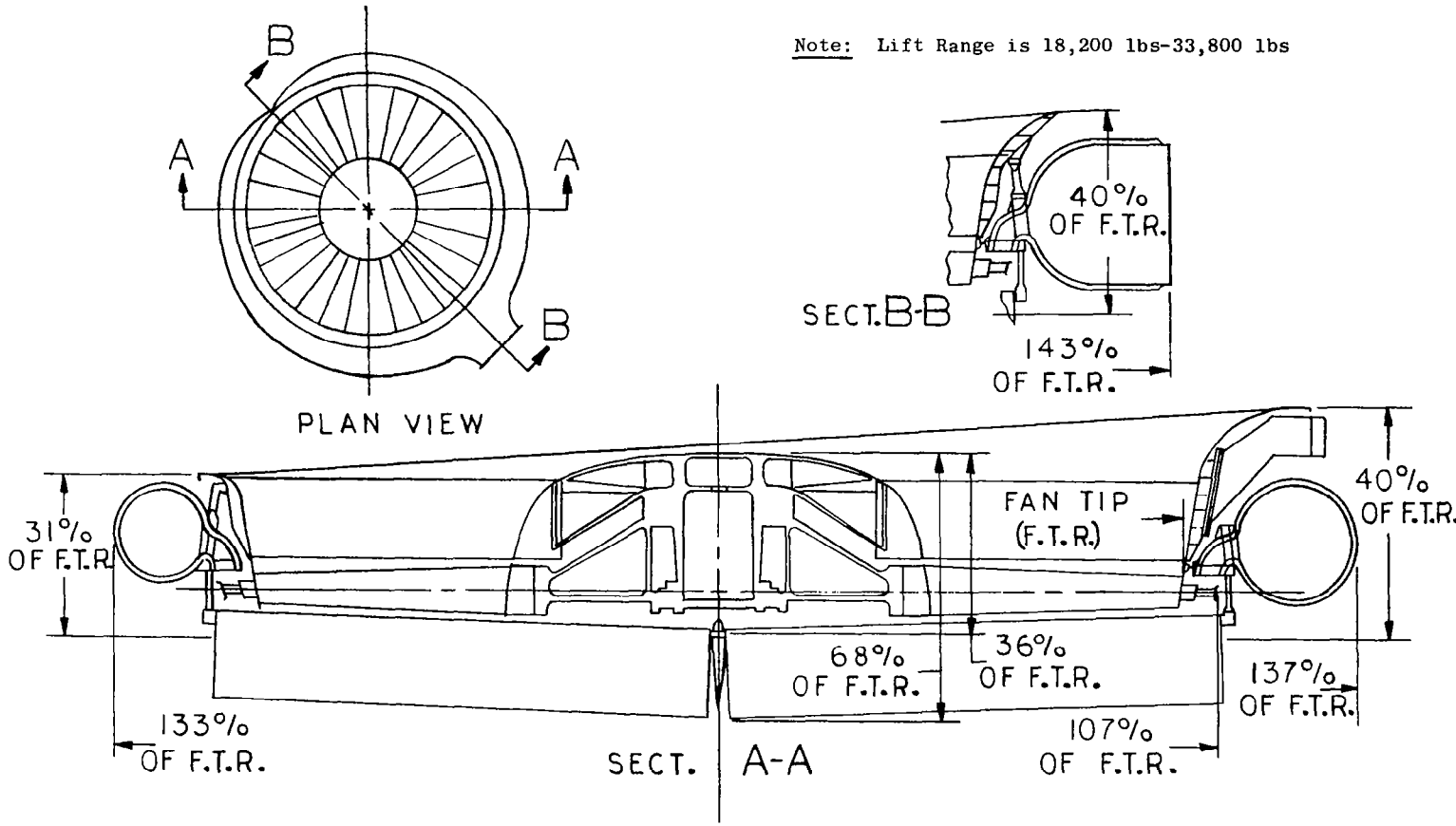

Figure 157. Large Inlet Guide Vane Fan.

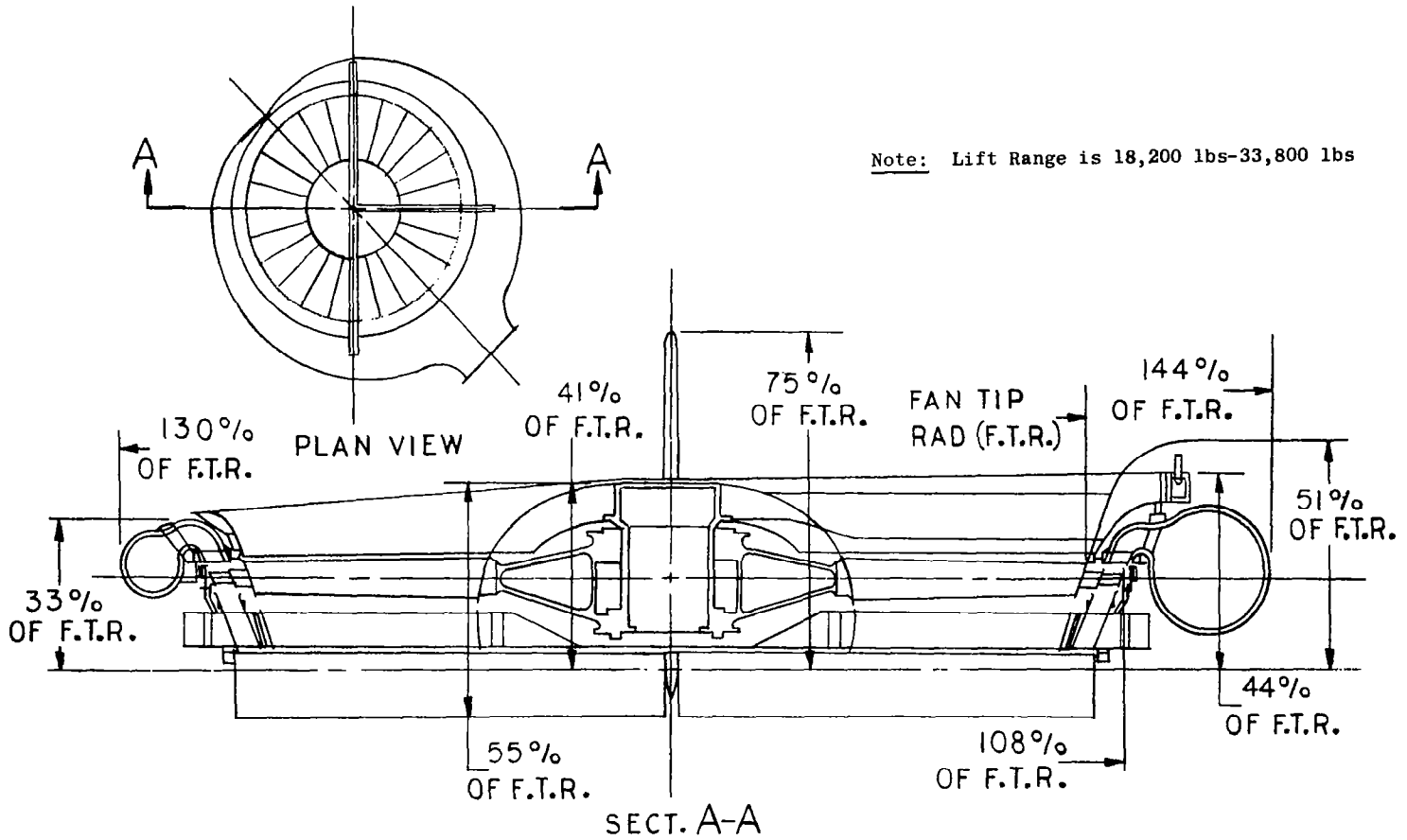

Figure 158. Large Conventional Fan.

Note: Lift Range is 9,500 lbs-17,700 lbs

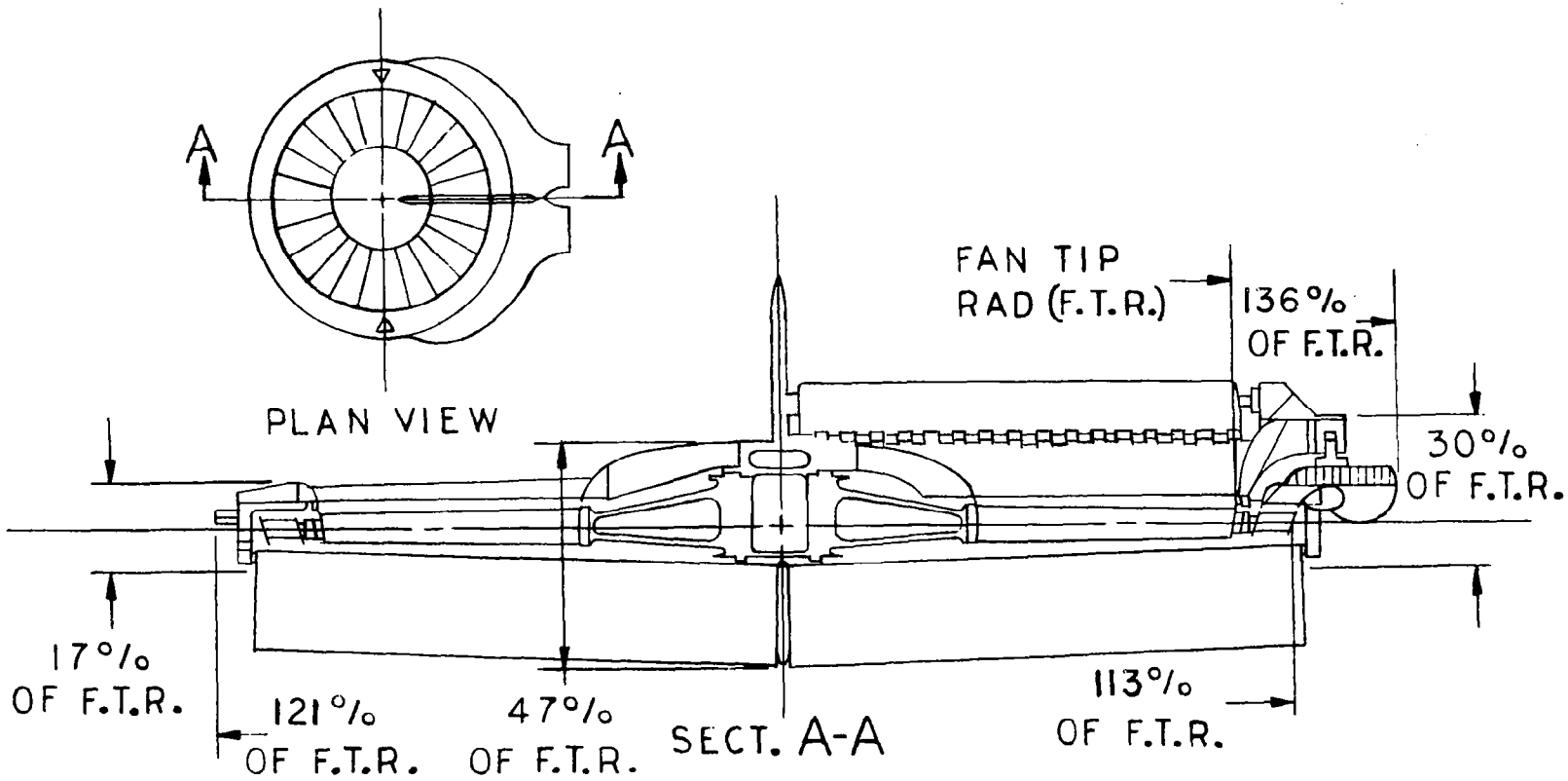

Figure 159. Small Inlet Guide Vane Fan.

Note: Lift Range is 9,500 lbs-17,700 lbs

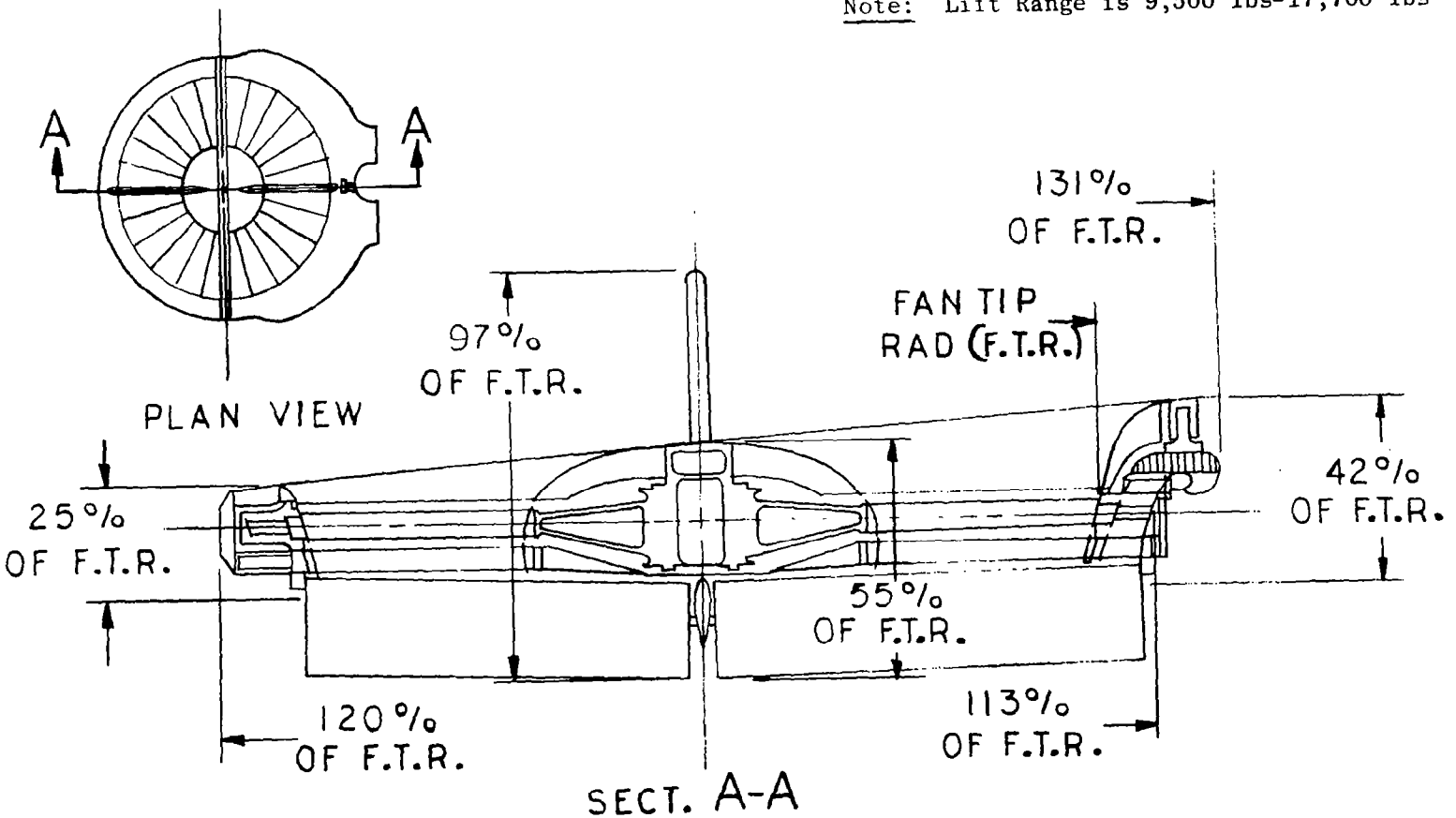

Figure 160. Small Conventional Fan.

Note: Lift Range is 9,500 lbs-17,700 lbs

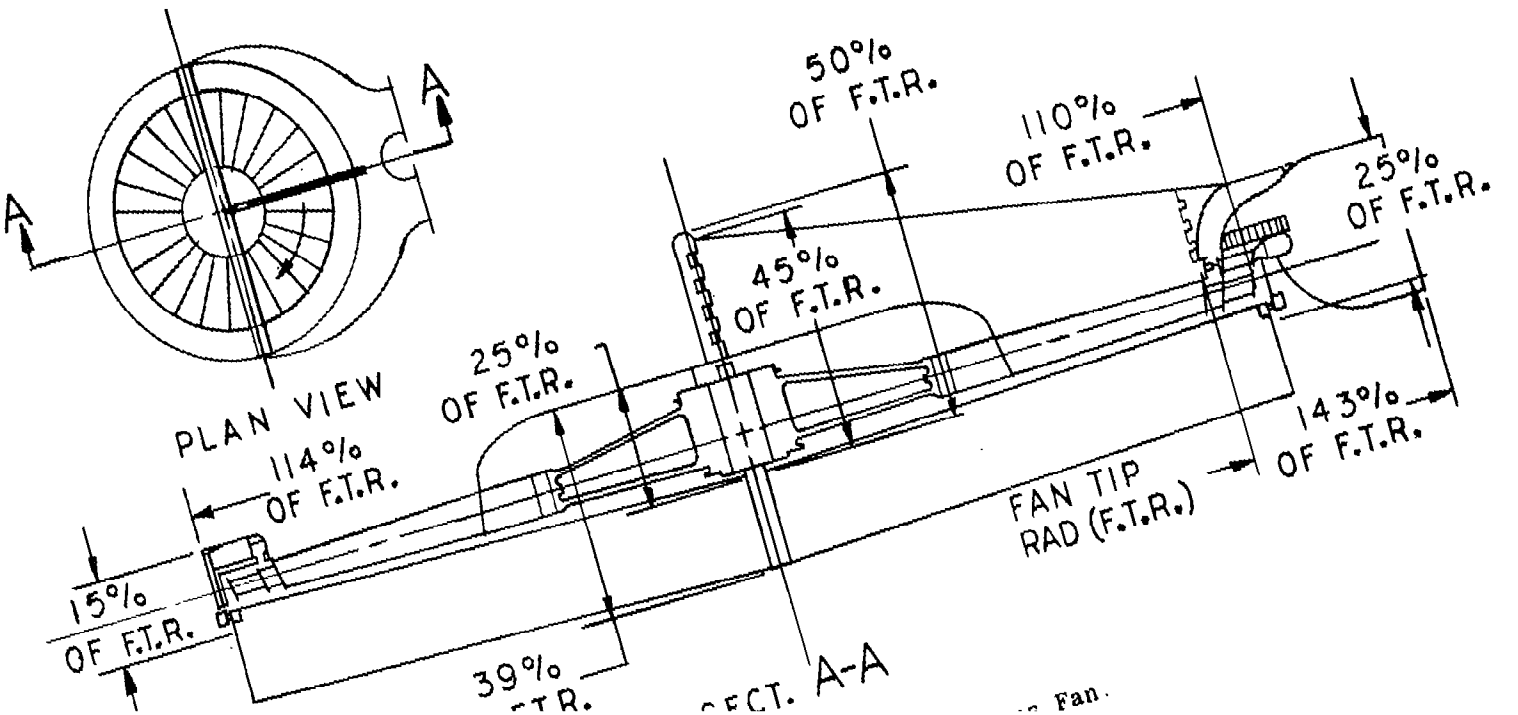

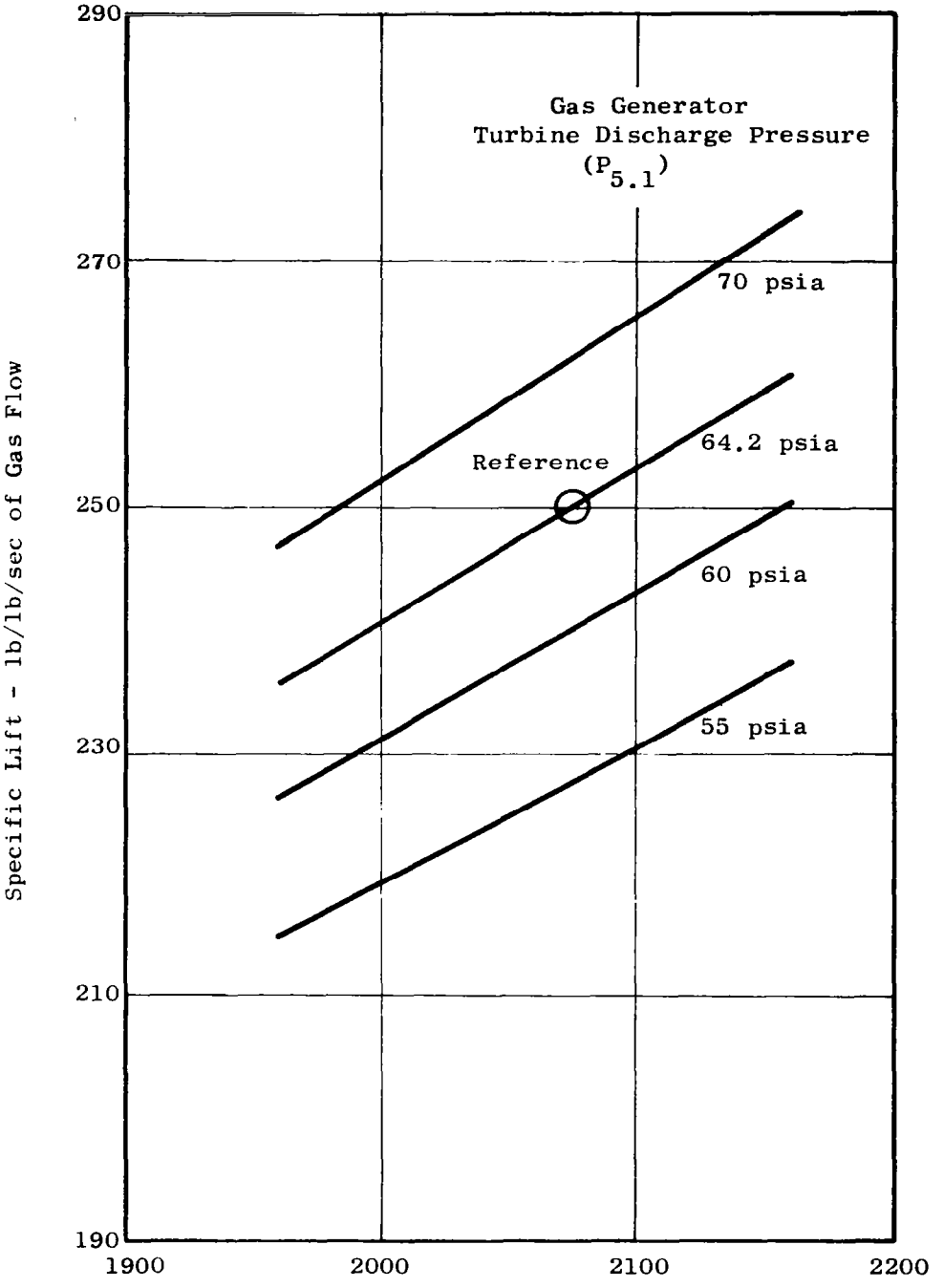

Figure 162. Specific Lift Versus Gas Generator Discharge Conditions for Large Fans.

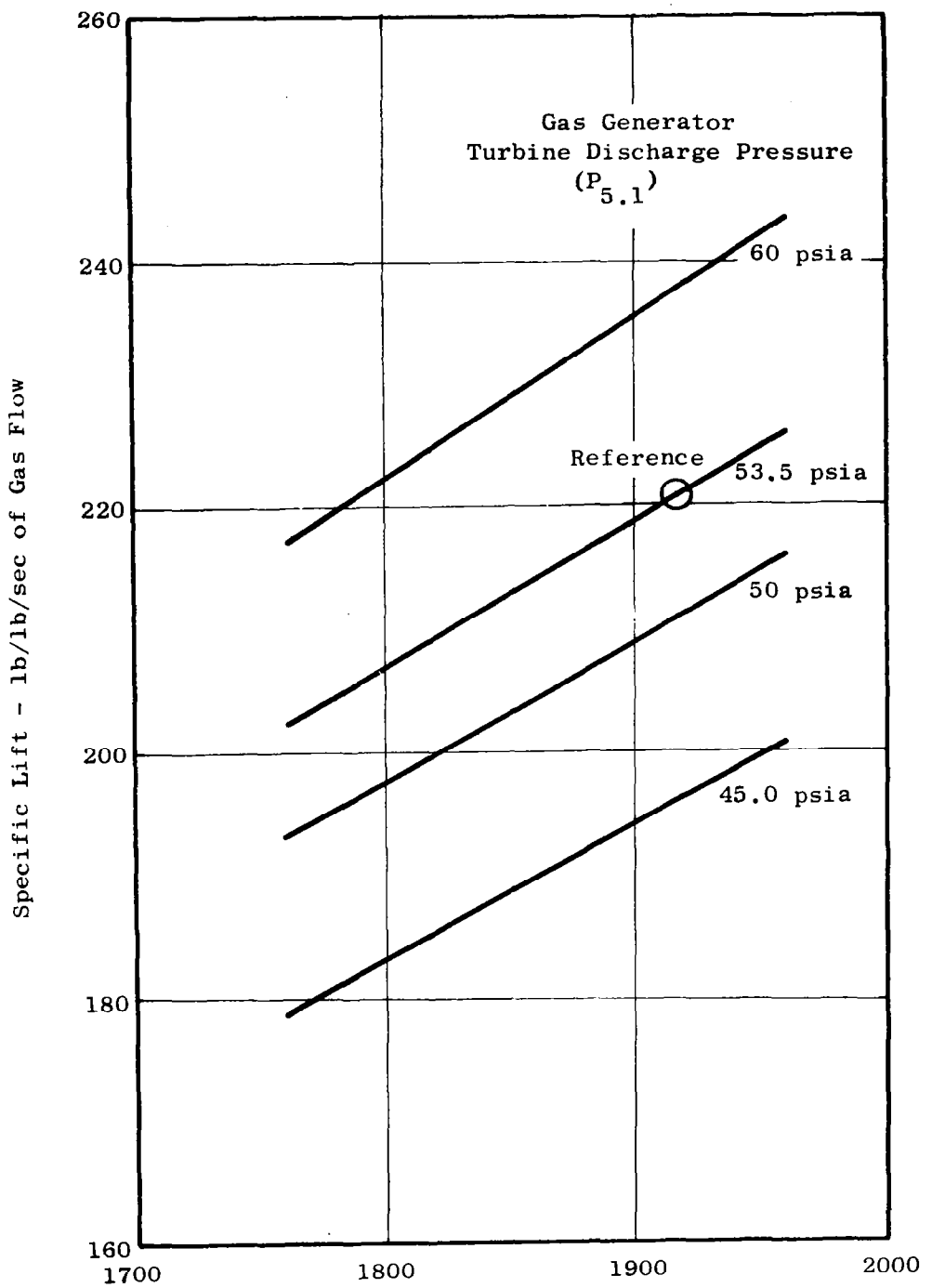

Figure 163. Specific Lift Versus Gas Generator Discharge Conditions for Small Fans.

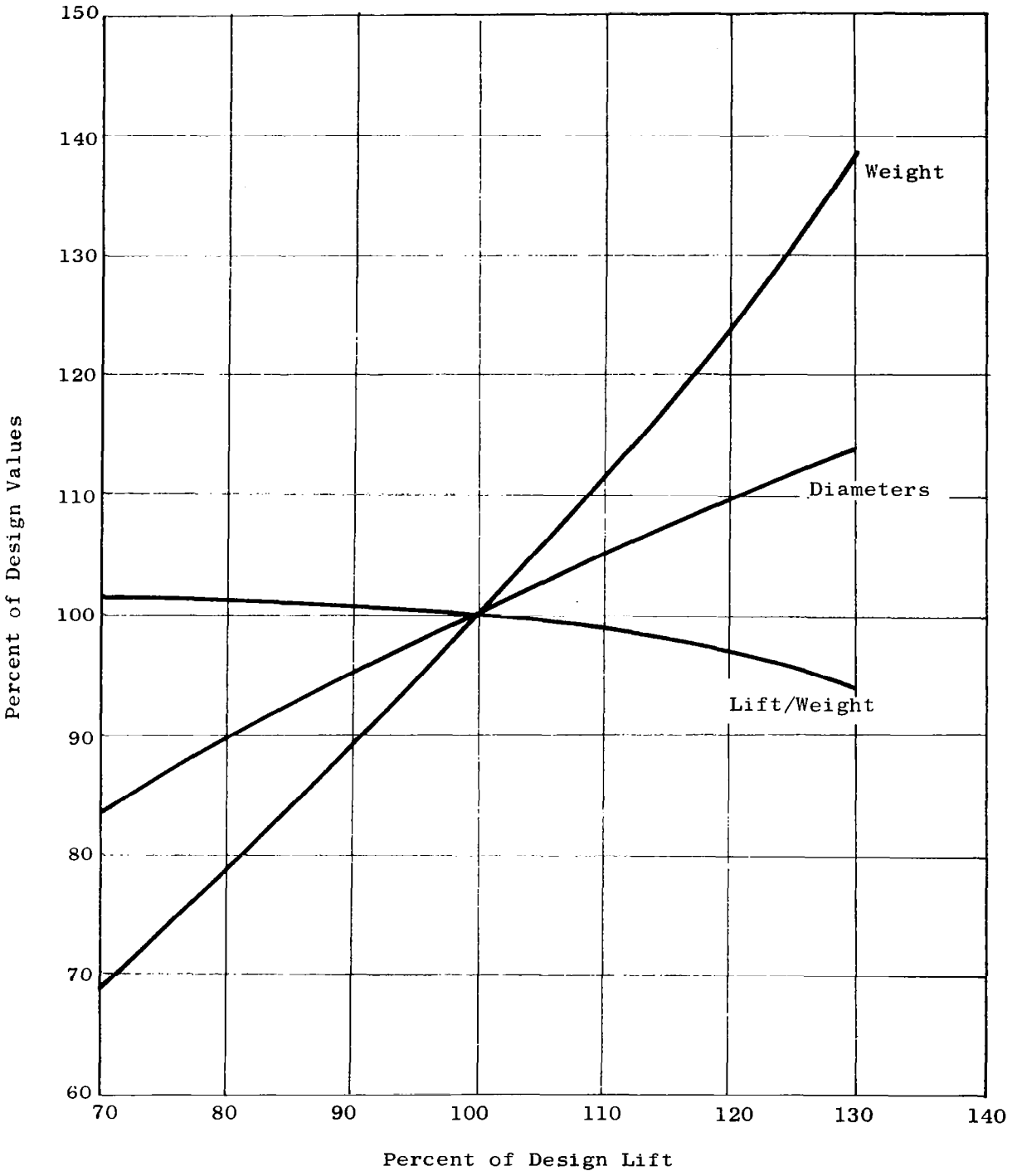

Figure 164. Scaling Factors for Large Fans.

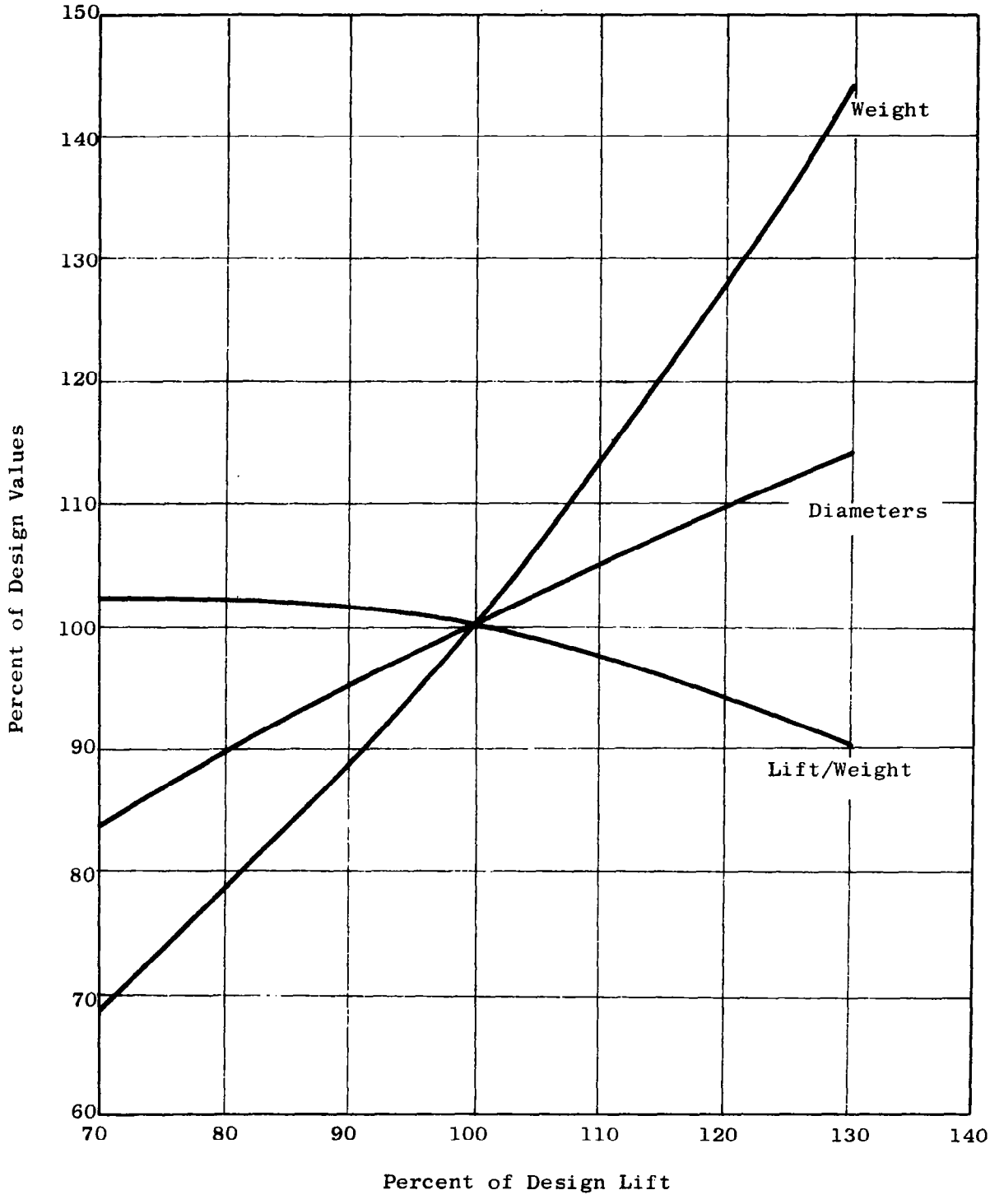

Figure 165. Scaling Factors for Small Fans.

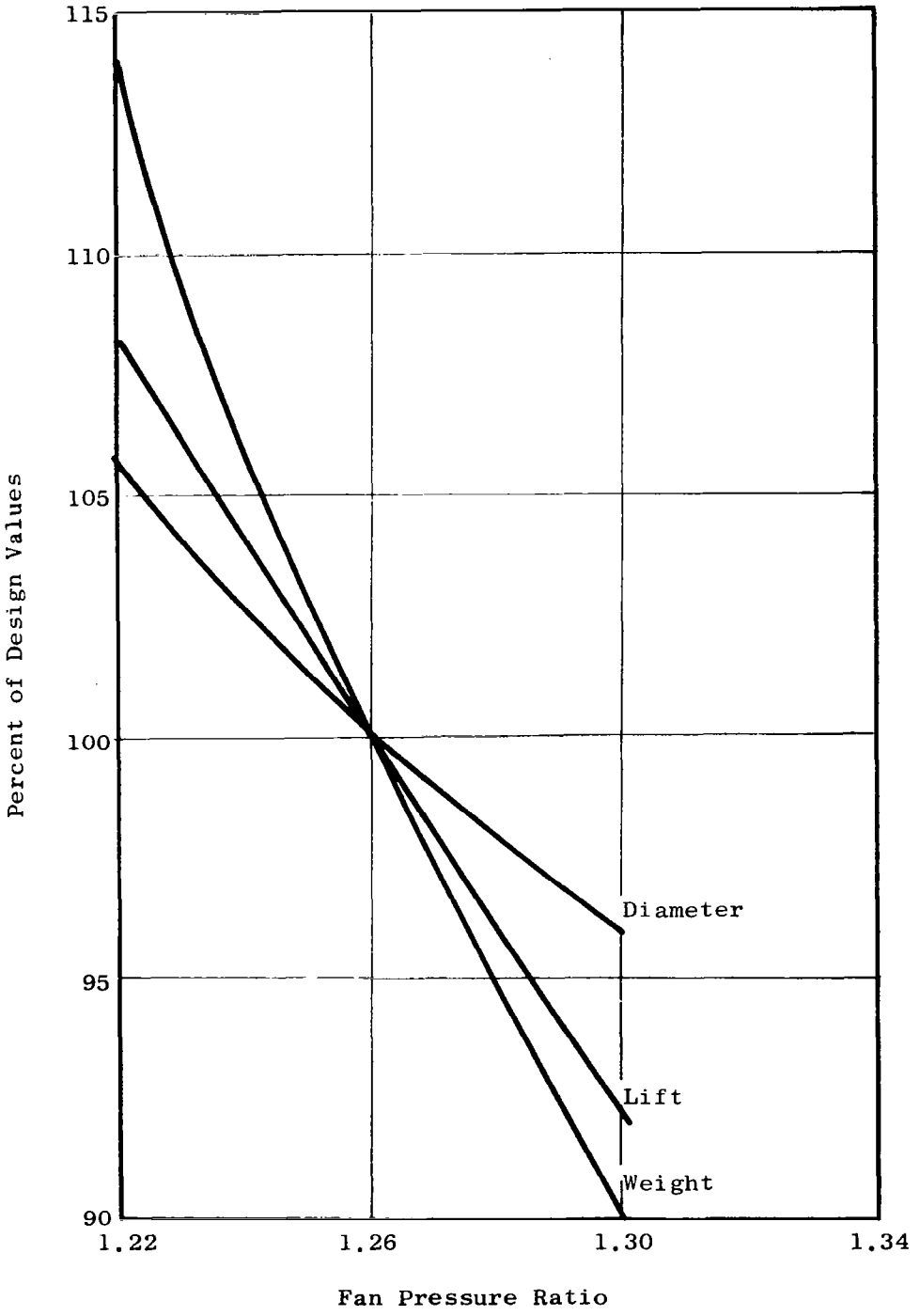

Figure 166. Scaling Factors for Large IGV Fans.

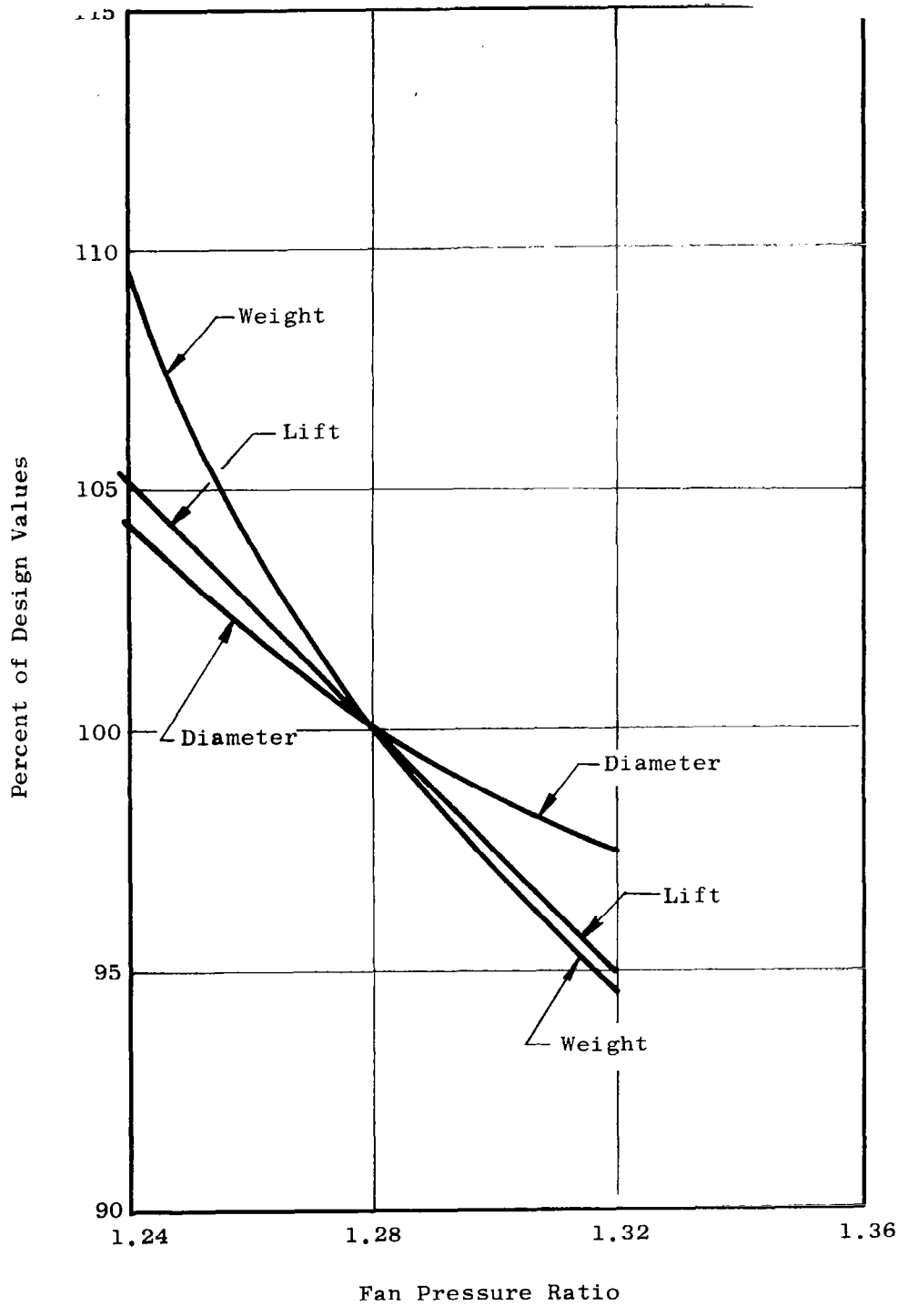

Figure 167. Scaling Factors for Large Conventional Fans.

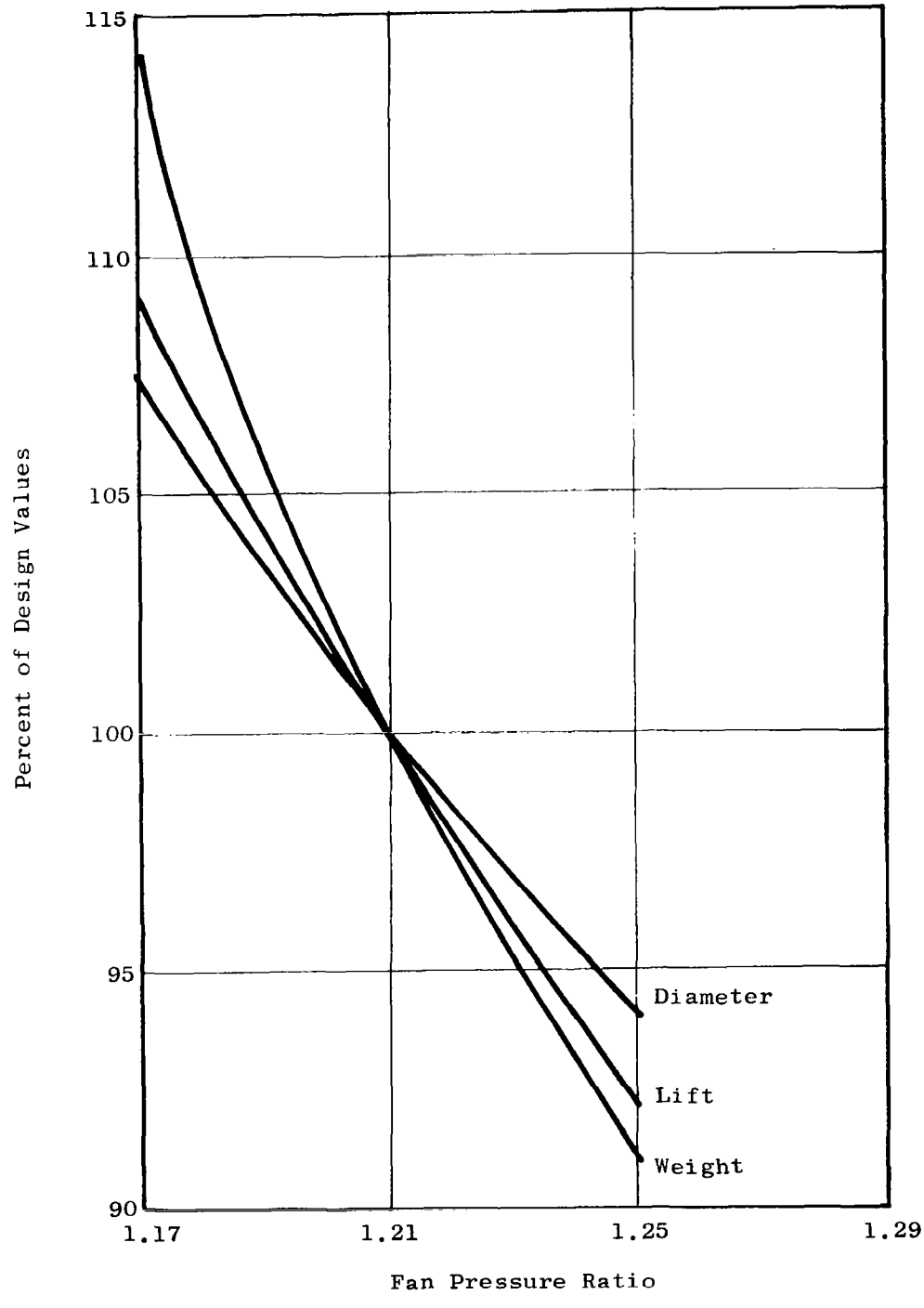

Figure 168. Scaling Factors for Small IGV Fans.

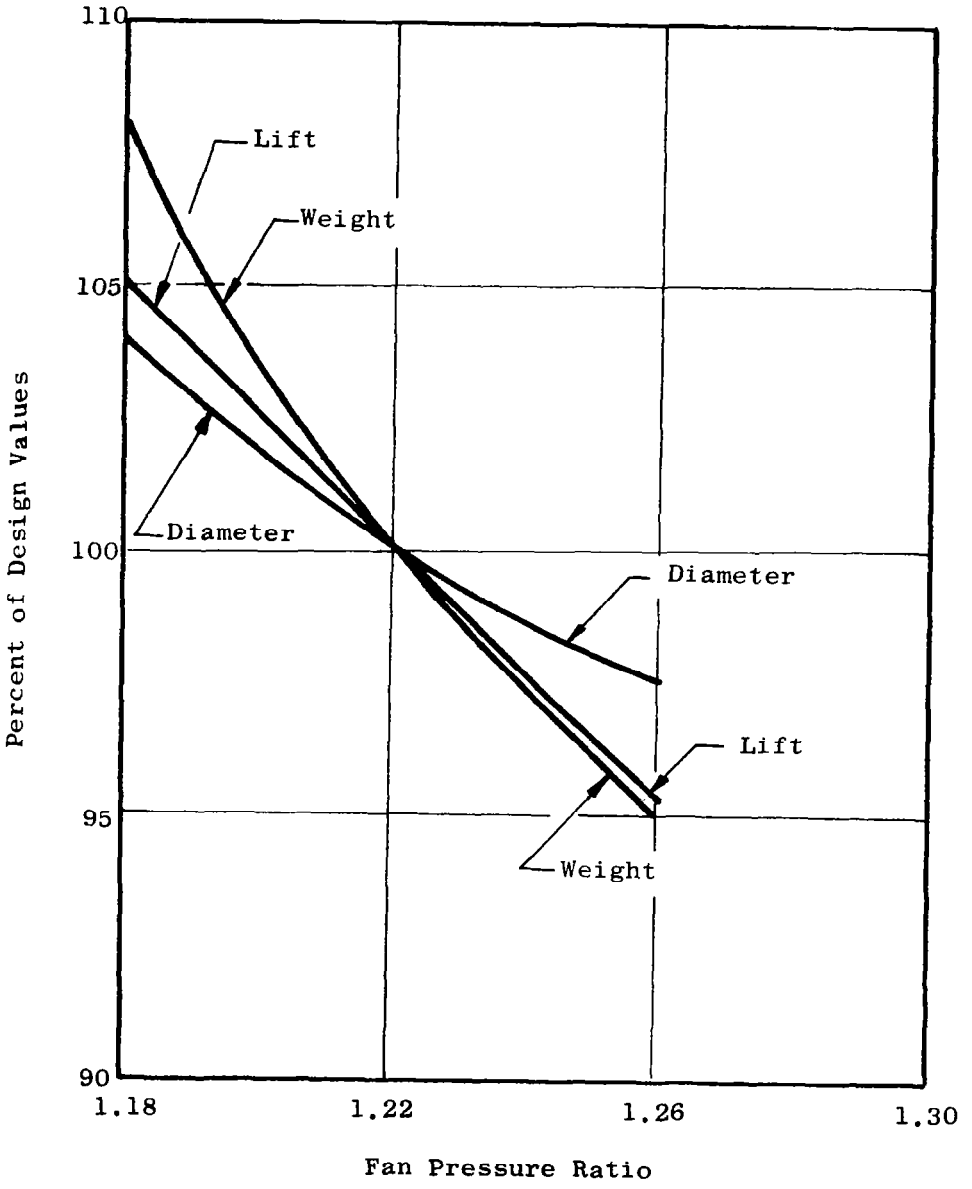

Figure 169. Scaling Factors for Small Conventional Fans.

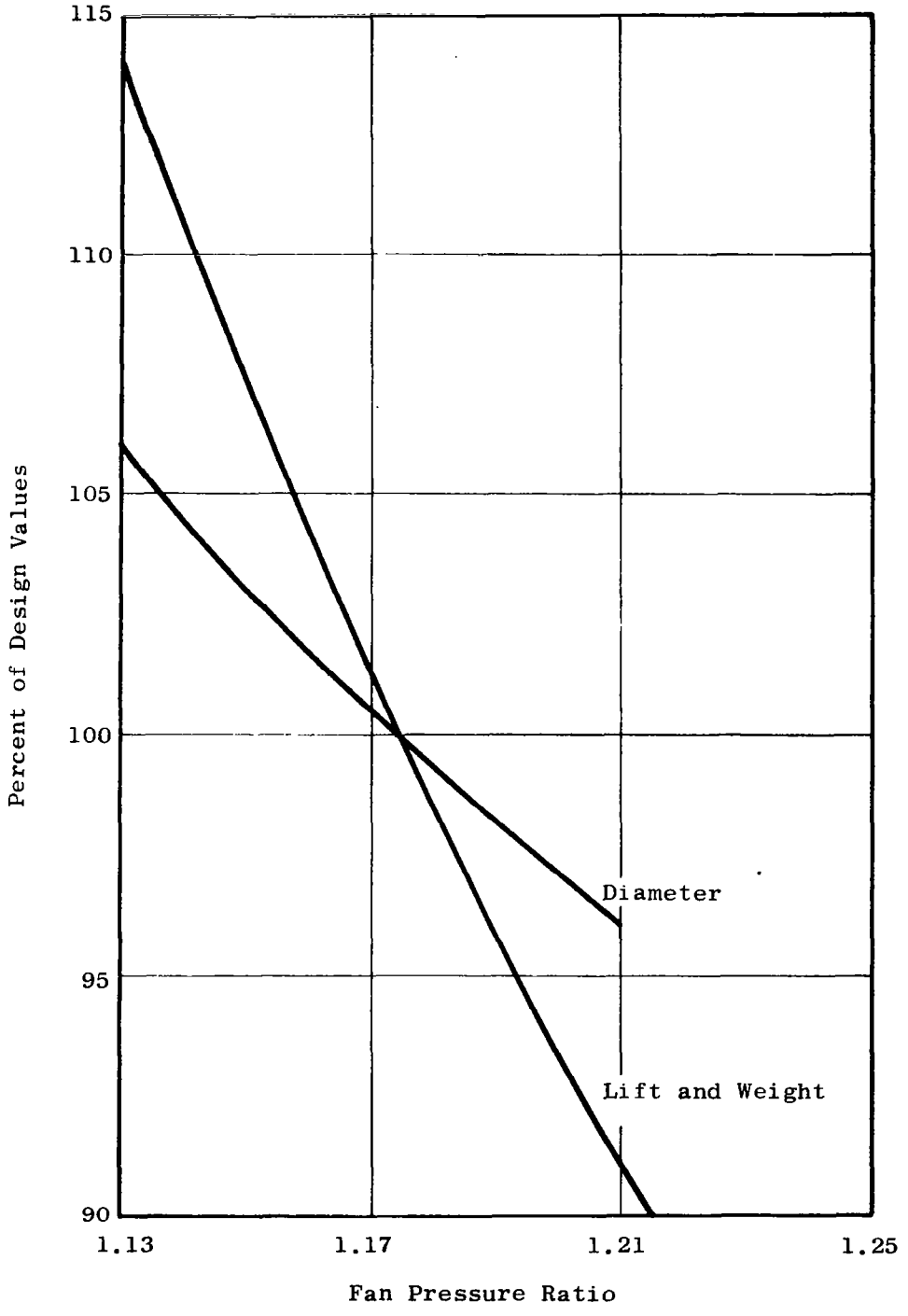

Figure 170. Scaling Factors for Small Statorless Fans.

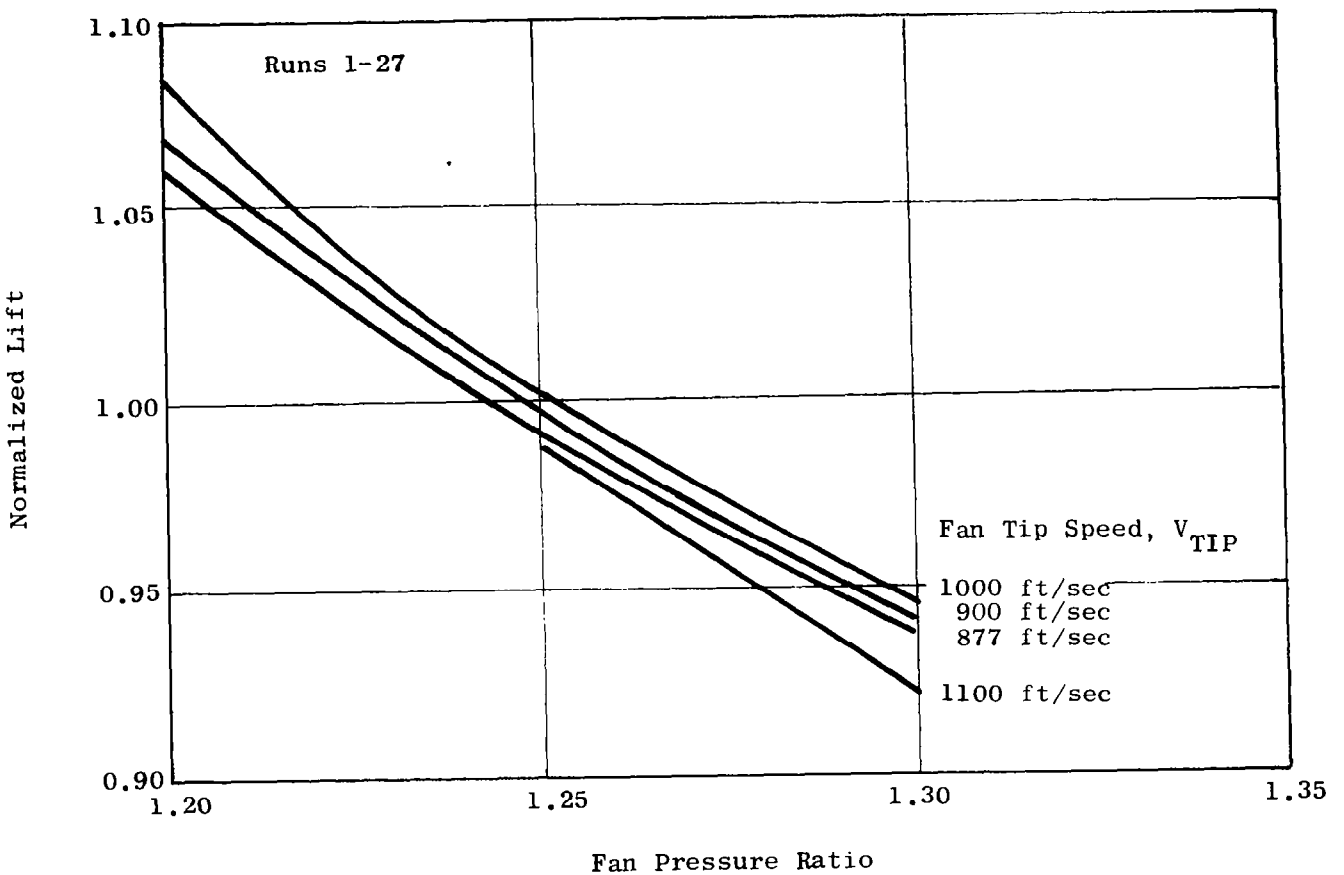

Figure 171. Small Conventional Fan Optimization.

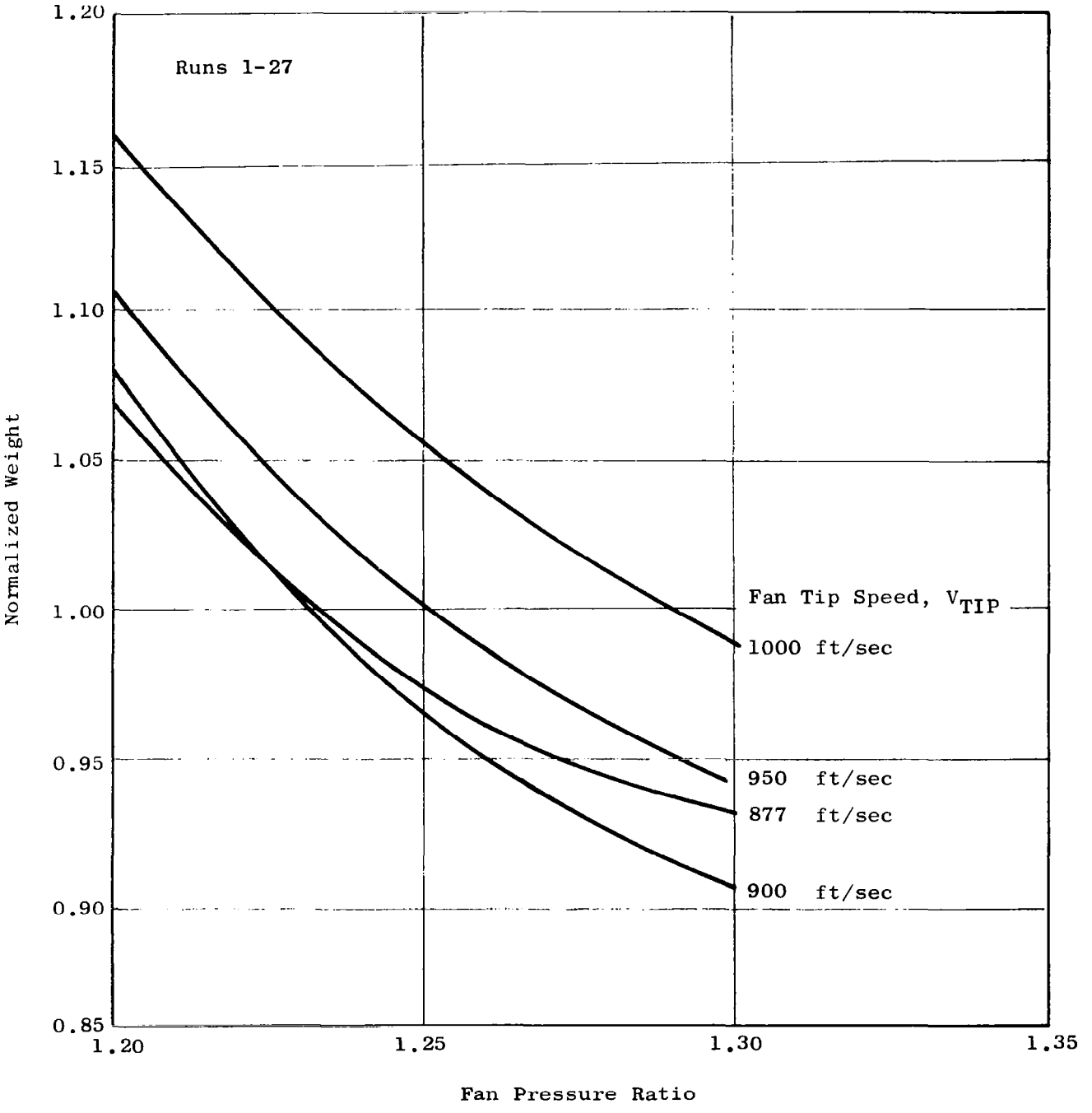

Figure 172. Small Conventional Fan Optimization.

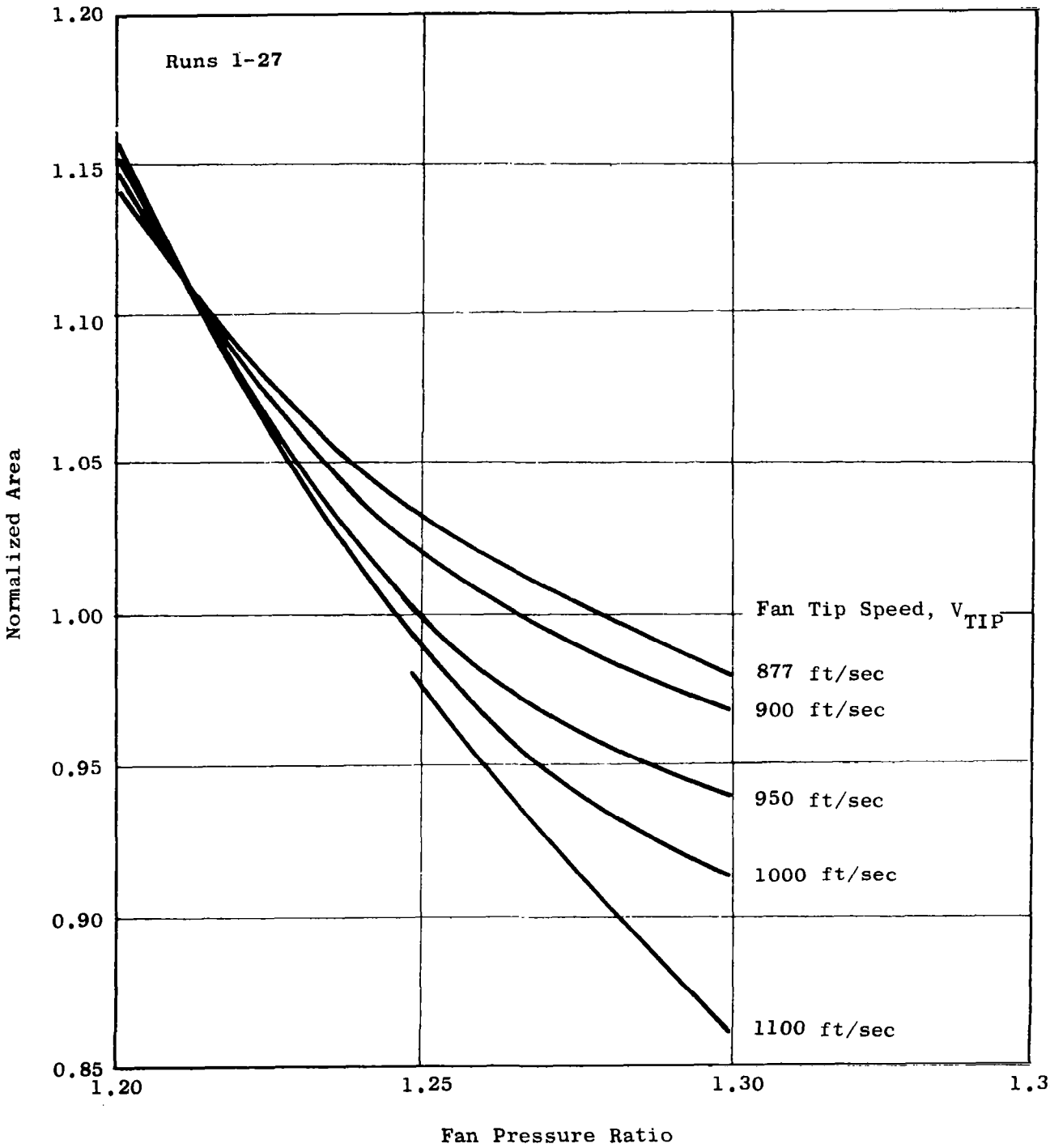

Figure 173. Small Conventional Fan Optimization.

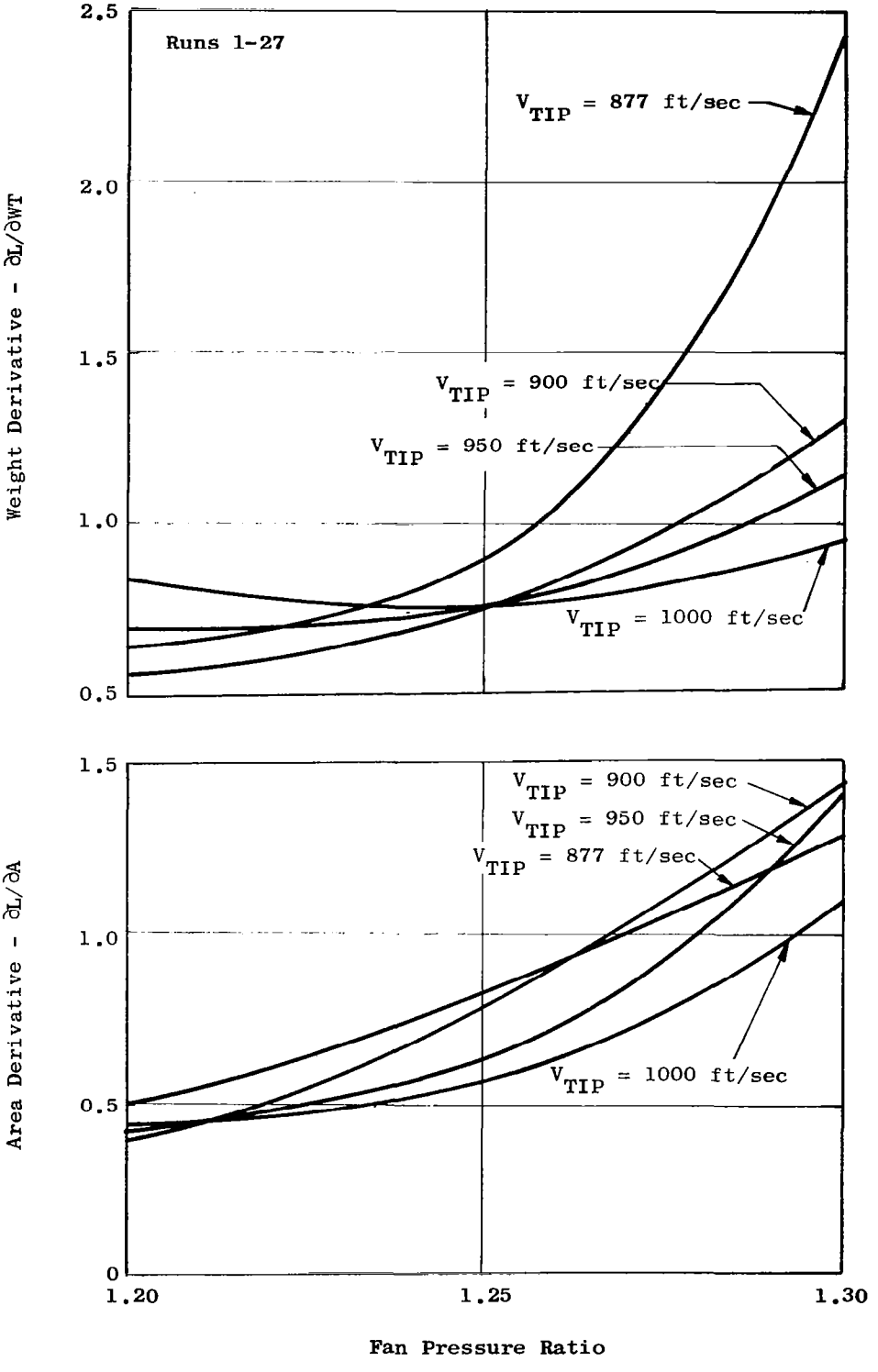

Figure 174. Small Conventional Fan Optimization.

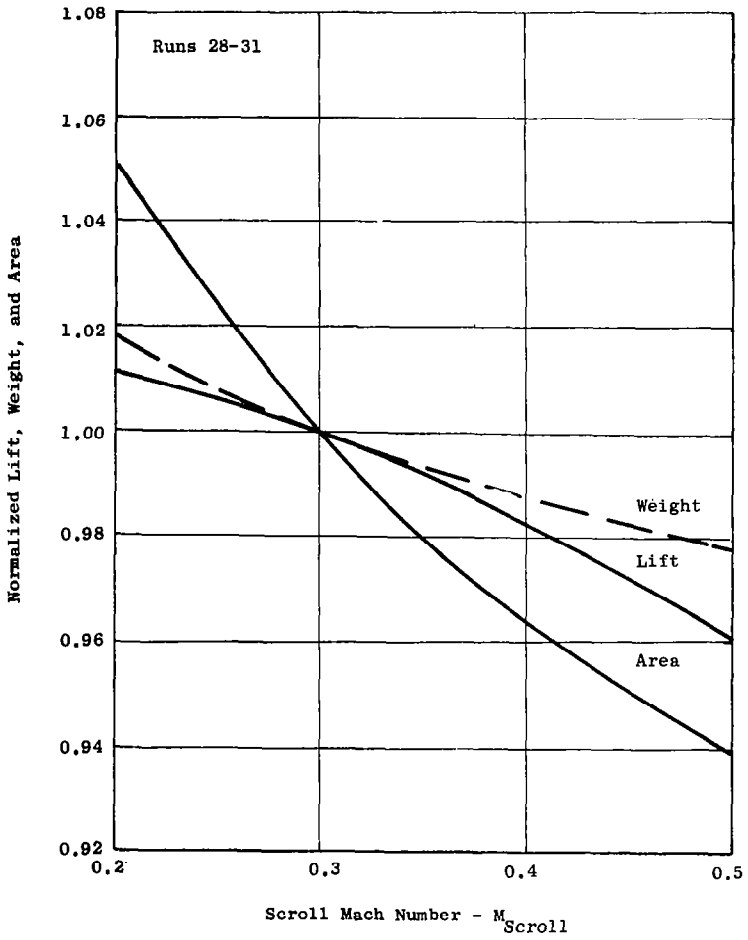

Figure 175. Small Conventional Fan Optimization.

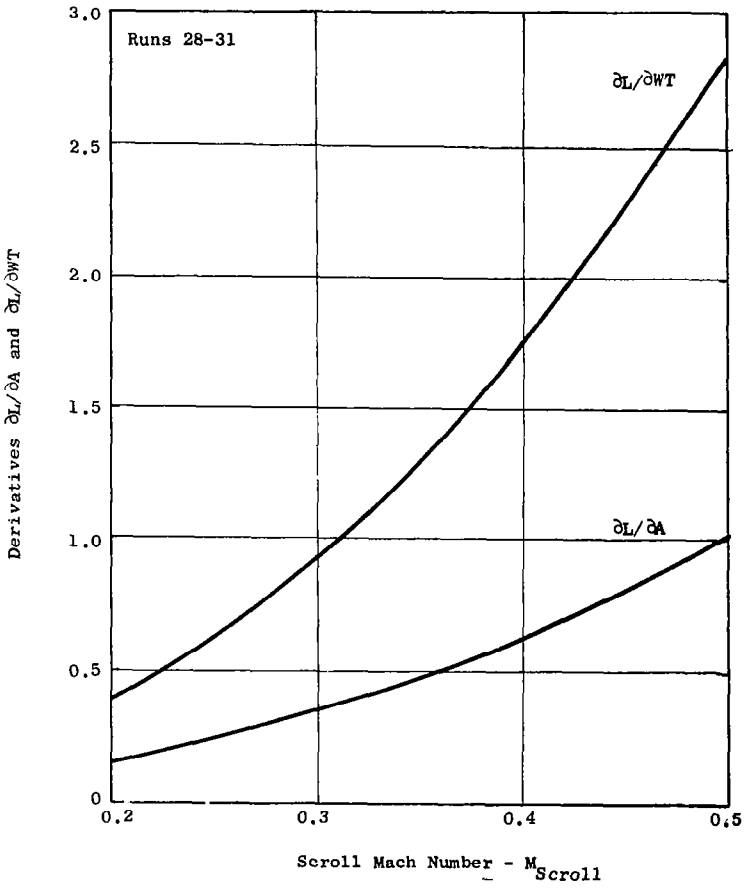

Figure 176. Small Conventional Fan Optimization.

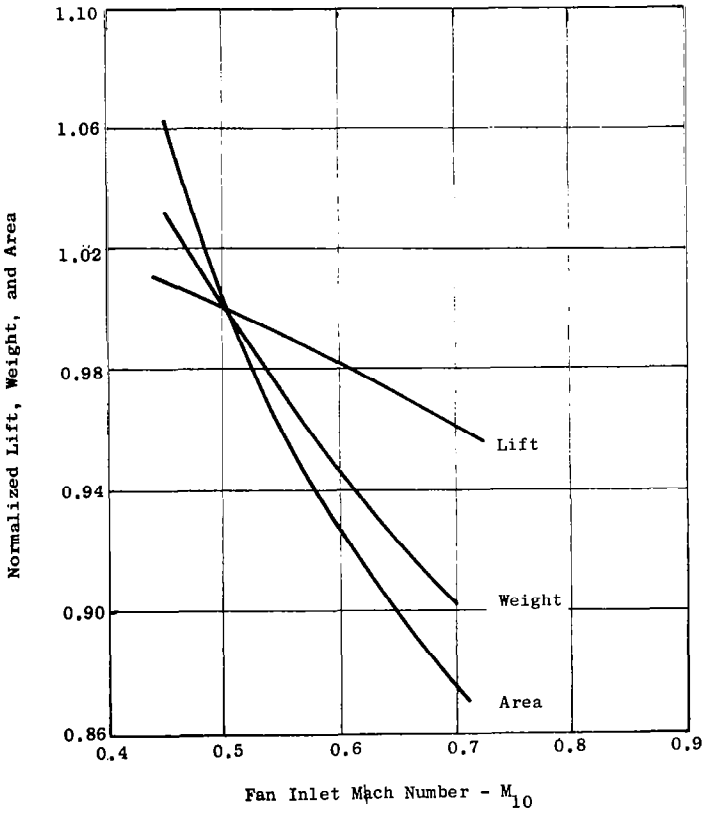

Figure 177. Small Conventional Fan Optimization.

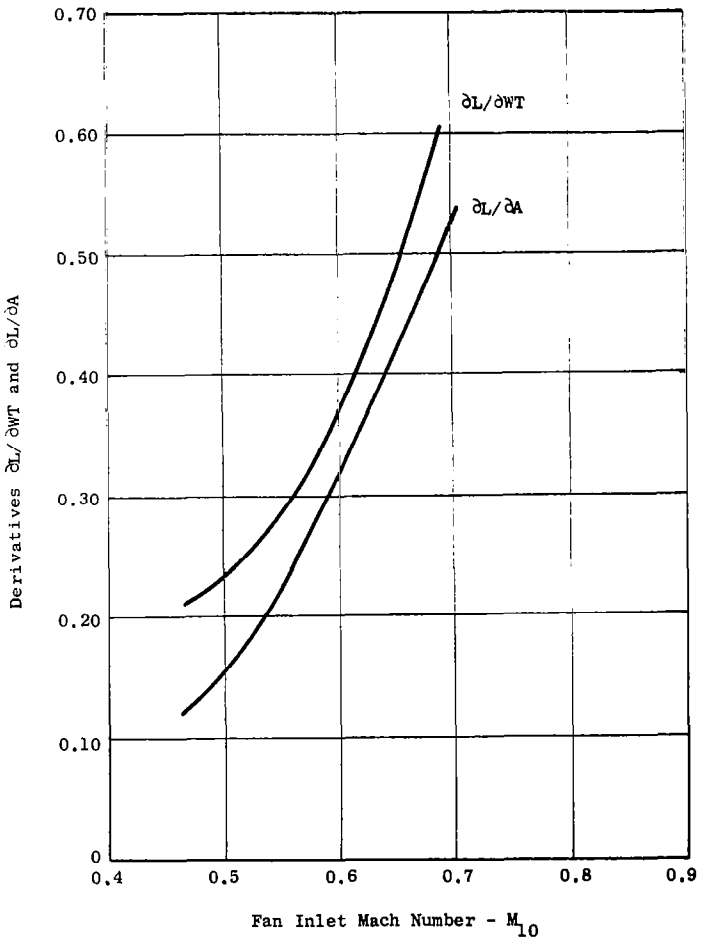

Figure 178. Small Conventional Fan Optimization

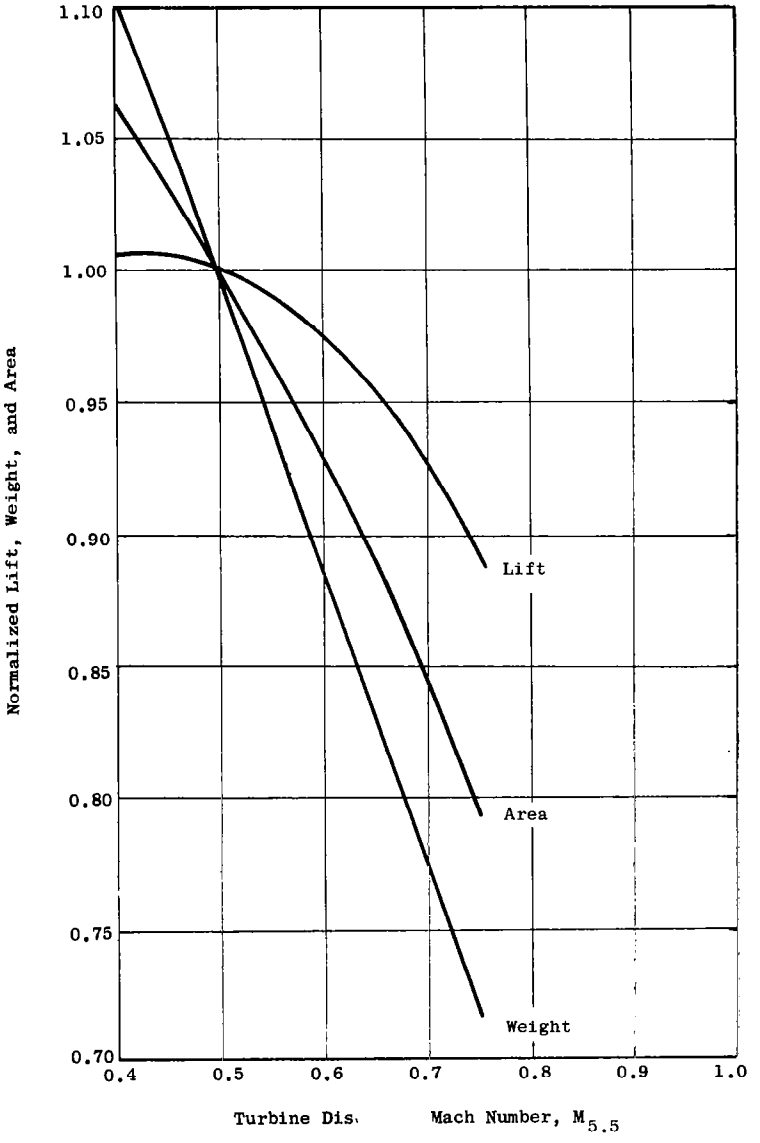

Figure 179. Small Conventional Fan Optimization.

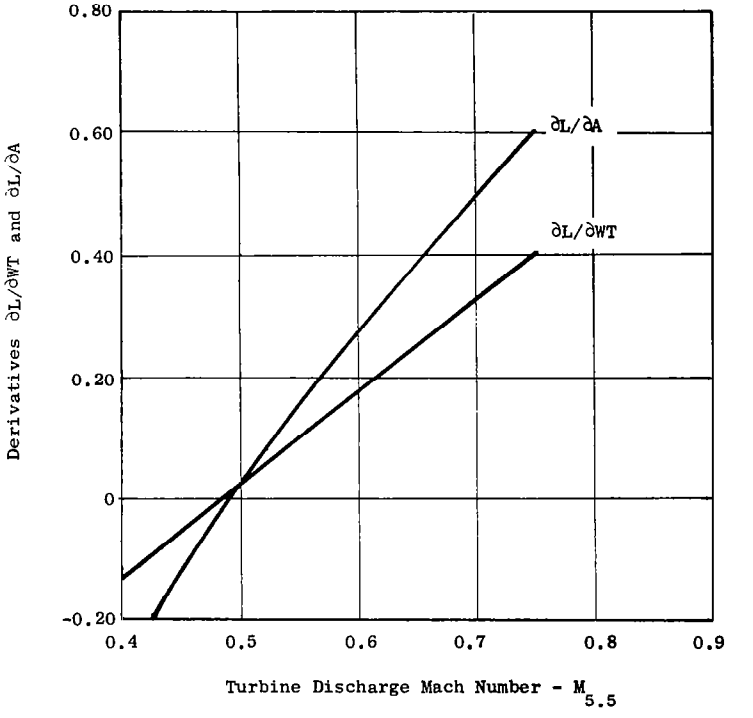

Figure 180. Small Conventional Fan Optimization.

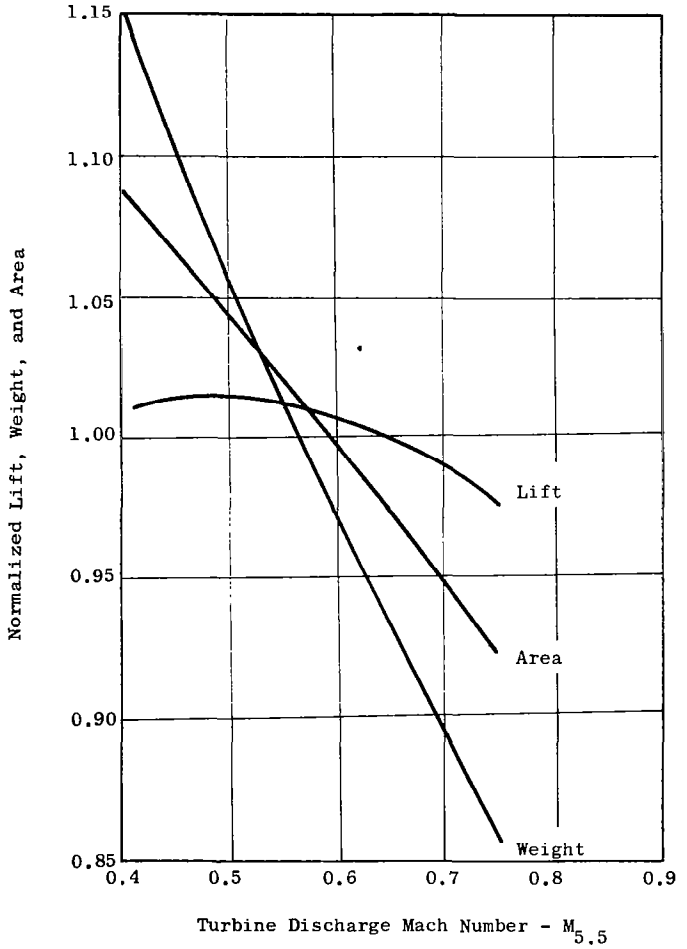

Figure 181. Small Conventional Fan Optimization.

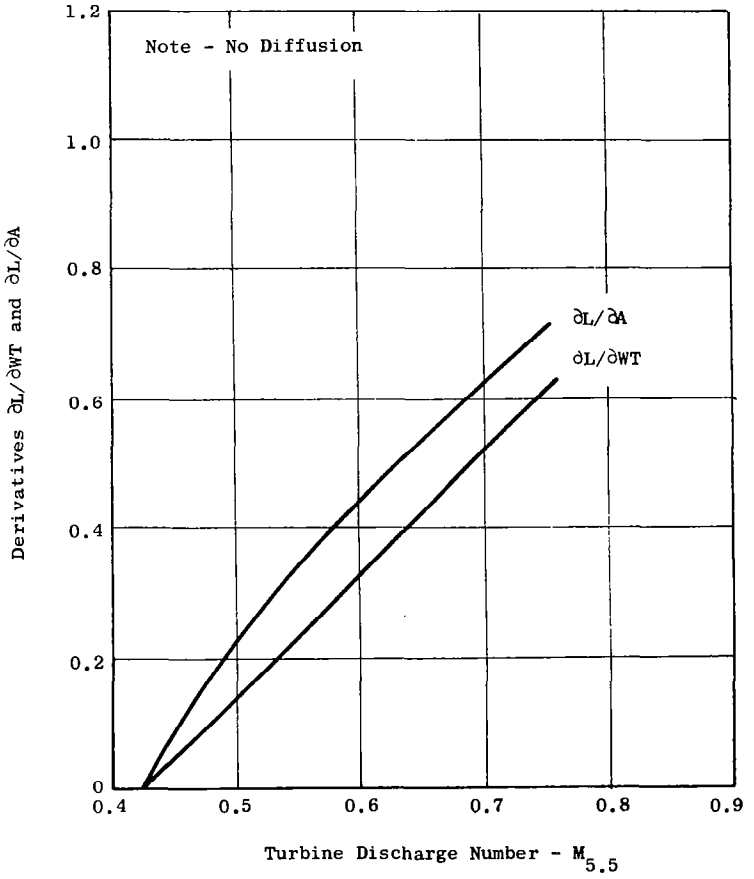

Figure 182. Small Conventional Fan Optimization.

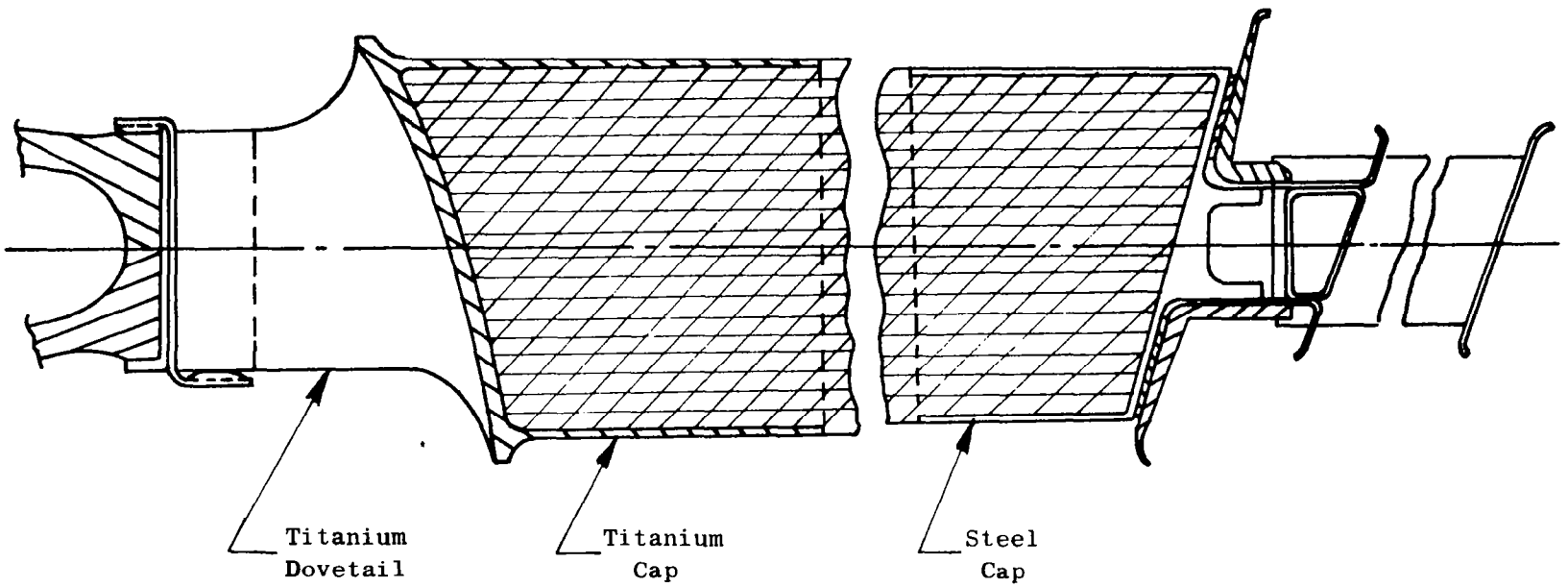

Figure 183. Bonded Blade Design.

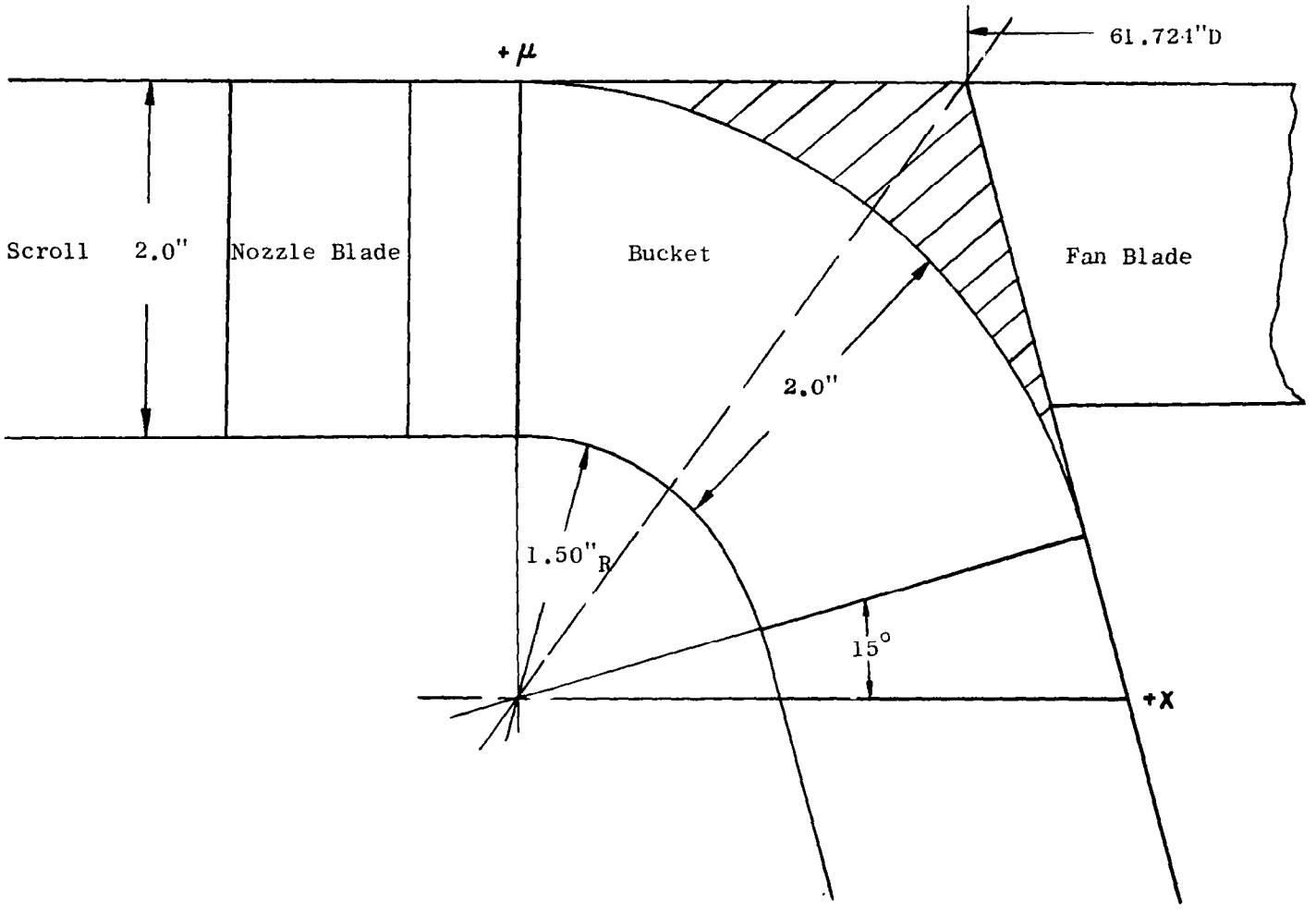

Figure 184. Radial Flow Tip Turbine.

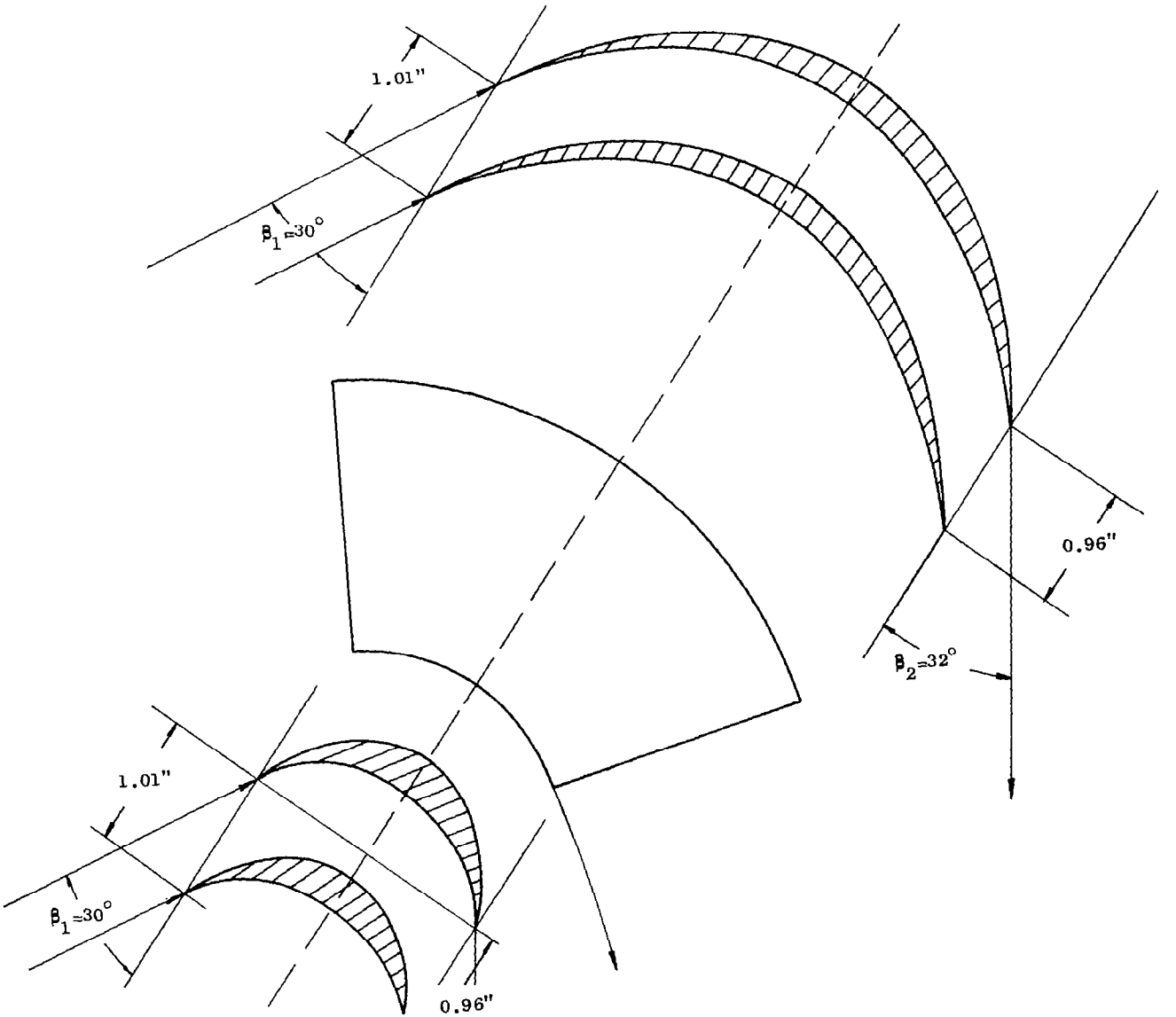

Figure 185. Radial Flow Tip Turbine.

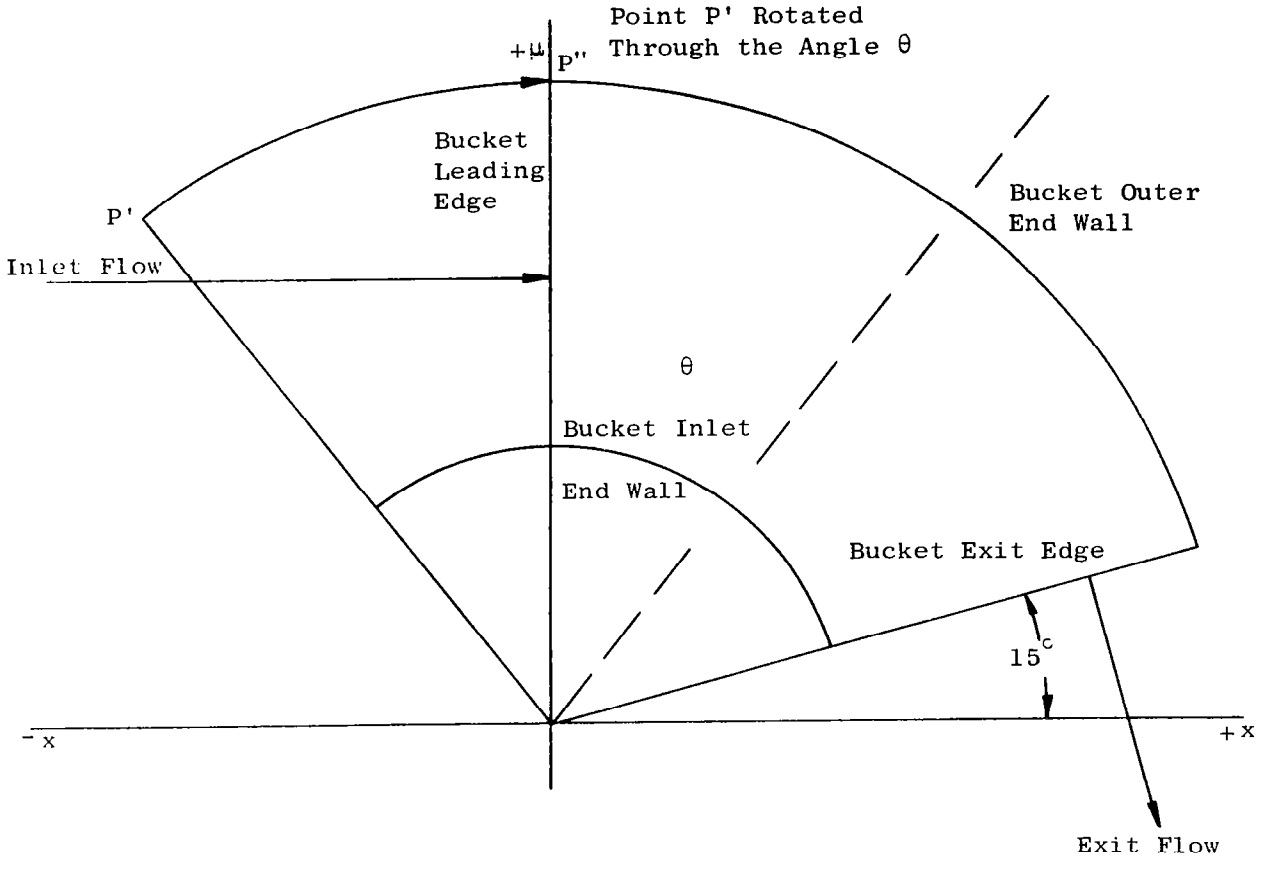

θ is the Angle of Rotation About the 'z' Axis in the Positive 'x' Direction

Figure 186. Rotation of Conical Surface About the 'z' Axis.

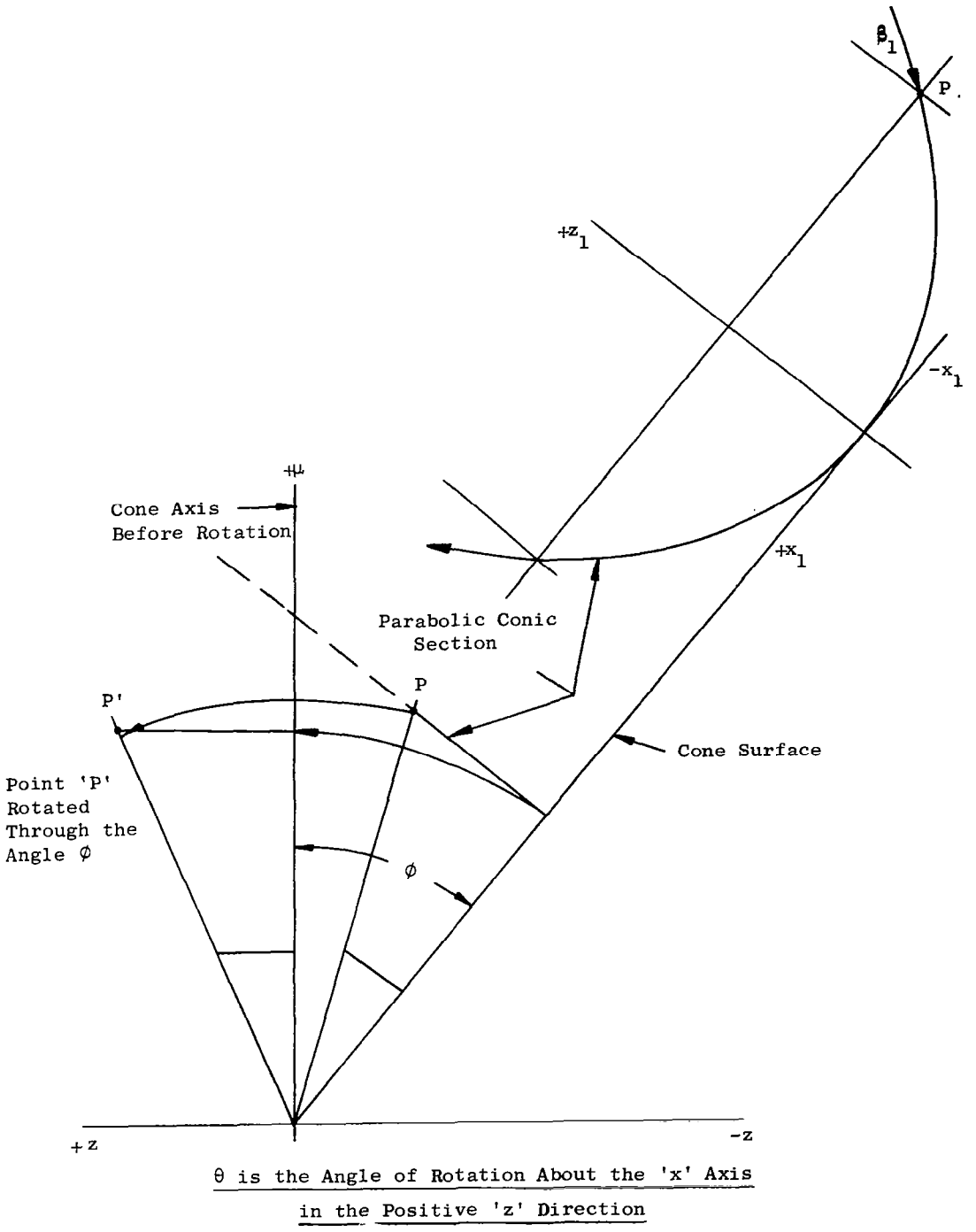

Figure 187. Rotation of Conical Surface About the 'x' Axis.

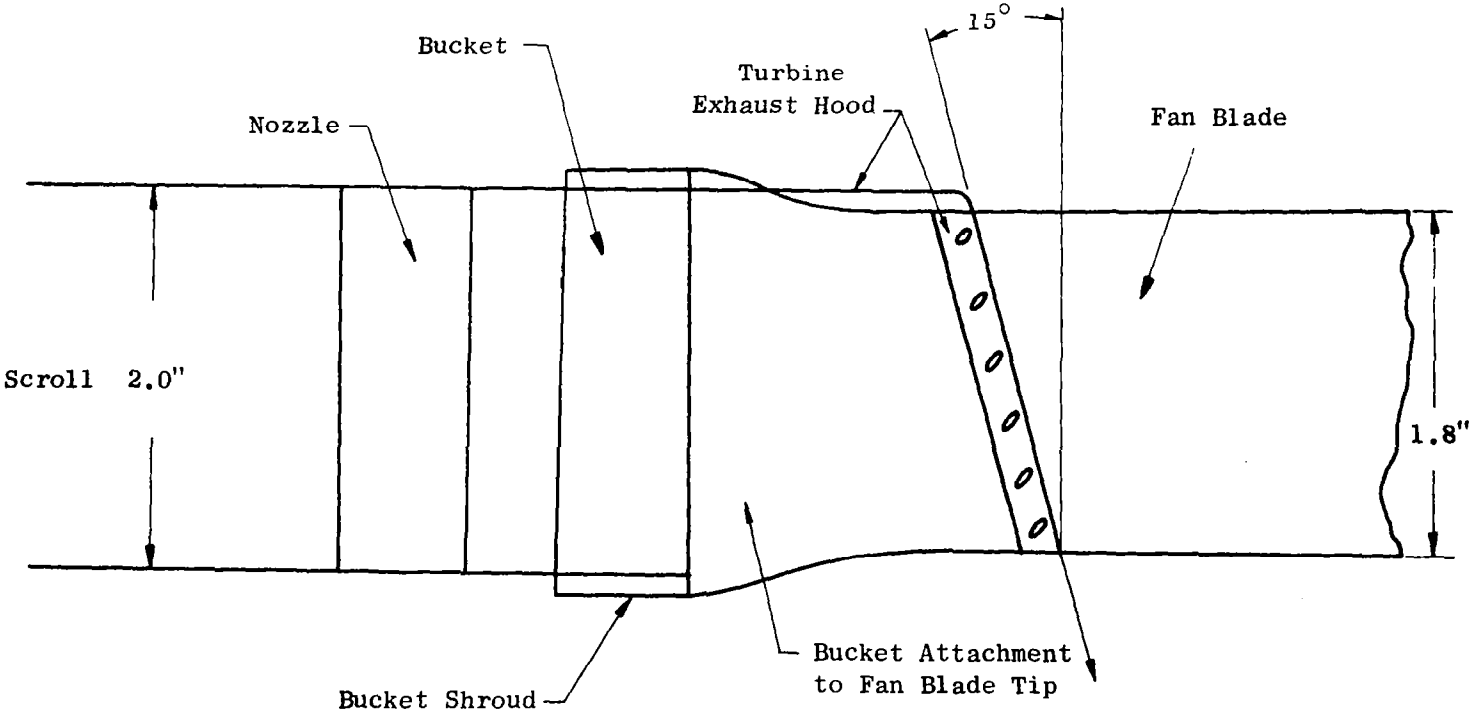

Figure 188. Radial Flow Tip Turbine Design Number 2.